SHAPING THE FUTURE OF TUNNELLING
Innovation, Sustainability and Safety

PROCEEDINGS OF THE SOUTHEASTERN EUROPE TUNNELLING CONFERENCE (SETC-2025)

Papers on Technical Subjects Related to Tunnelling and Underground Space Planning and Engineering

EDITED BY
DEJAN DIVAC, SANJA ZLATANIĆ, VESNA TRIPKOVIĆ,
SLOBODAN RADOVANOVIĆ AND NIKOLA MILIVOJEVIĆ

ITA TUNNELLING AWARDS 2025

SETC-2025 BELGRADE

ITA TUNNELLING AWARDS & SOUTHEASTERN EUROPE TUNNELLING CONFERENCE

ASSOCIATION INTERNATIONALE DES TUNNELS ET DE L'ESPACE SOUTERRAIN
AITES | ITA
INTERNATIONAL TUNNELLING AND UNDERGROUND SPACE ASSOCIATION

ITA SERBIA
Serbian Association for
Tunnels and Underground Structures

PROCEEDINGS OF THE SOUTHEASTERN EUROPE TUNNELLING CONFERENCE (SETC-2025)

1–3 October 2025, Belgrade, Serbia

Edited by

Dejan Divac
ITA Serbia President, Serbia
Jaroslav Černi Water institute

Sanja Zlatanić
ITA-AITES Vice President, USA

Vesna Tripković
Jaroslav Černi Water Institute

Slobodan Radovanović
Jaroslav Černi Water Institute

Nikola Milivojević
Jaroslav Černi Water Institute

ITA SERBIA
Serbian Association for
Tunnels and Underground Structures

Publisher:

Serbian Association for Tunnels and Underground Structures (ITA Serbia)
https://about.ita-aites.org/members/member-nations/192-serbia

Jaroslav Černi Water Institute
office@jcerni.rs

Editors:

Prof. Dr Dejan Divac
Ms Sanja Zlatanić
Dr Vesna Tripković
Dr Slobodan Radovanović
Dr Nikola Milivojević

Graphic design:

Miloš Djoković

ISBN-978-86-82565-56-7

SHAPING THE FUTURE OF TUNNELLING

Innovation, Sustainability and Safety

Shaping the Future of Tunnelling – Innovation, Sustainability and Safety contains the contributions presented at the ITA Awards & SETC-2025, held in Belgrade, Serbia, from 1 to 3 October 2025.

The papers cover a wide range of topics in the fields of tunnelling and underground engineering, including:

1. Advanced construction techniques
2. Use of new materials and machinery
3. Geological investigation and prediction
4. Numerical modelling
5. Instrumentation and monitoring/testing and inspection
6. Digital and information technology in design and construction
7. Strategic planning
8. Operational safety
9. Impact of climate change on tunnel infrastructure

Shaping the Future of Tunnelling – Innovation, Sustainability and Safety aims to provide a useful resource for everyone engaged in tunnelling and underground engineering, from students and young researchers to experienced professionals and engineers.

PREFACE

The ITA Tunnelling Awards and the Southeastern Europe Tunnelling Conference (SETC-2025) were held from the 1st to the 3rd of October 2025 in Belgrade, Serbia.

The Serbian Association for Tunnels and Underground Structures (ITA Serbia) was honoured and proud to host this outstanding event of the international tunnelling community. Bringing together hundreds of distinguished experts, researchers, and industry leaders from across the globe, the event served as a dynamic platform for sharing knowledge, presenting innovations, and advancing scientific and technical excellence in the field of tunnelling and underground construction.

Serbia, with Belgrade as its dynamic capital, is experiencing a period of intensive infrastructure development, particularly in the domain of underground construction and sustainable urban mobility. Landmark projects such as the Belgrade Metro, tunnel connections, and urban underground infrastructure systems are transforming the city's transport network and enhancing its connectivity and sustainability. These projects demonstrate Serbia's growing expertise in modern tunnelling technologies, geotechnical engineering, and integrated urban planning, positioning Belgrade as a regional hub for innovation and progress in underground construction.

The conference proceedings encompass a diverse range of nine thematic areas, reflecting the multidisciplinary nature and technological depth of modern tunnelling. Topics include advanced construction techniques, the use of new materials and machinery, geological investigation and prediction, numerical modelling, instrumentation, monitoring, testing and inspection, the application of digital and information technologies in design and construction, strategic planning, operational safety, and the impact of climate change on tunnel infrastructure. Together, these themes highlight the conference's focus on innovation, sustainability, and resilience in underground construction.

It is our sincere expectation that these proceedings will contribute meaningfully to the professional and scientific community, providing valuable insights for engineers, researchers, and decision-makers engaged in the development of underground infrastructure. The knowledge and experiences shared during SETC-2025 aim to foster innovation, collaboration, and sustainable practices, encouraging the continued advancement of tunnelling and underground construction in the years ahead.

Belgrade, October 2025

Prof. Dr Dejan Divac

Chair of the ITA Awards & SETC-2025 Organising and Scientific Committee
President of the ITA Serbia

ACKNOWLEDGEMENT

The Editors would like to thank and express their sincere gratitude to all members of the Scientific Committee for their effort and the valuable time devoted to reviewing the abstracts and manuscripts.

The SETC-2025 Organizing Committee, Scientific Committee, and Editors wish to express their sincere gratitude to the conference sponsors and exhibitors for their generous support and valuable contribution to the success of this Event.

ORGANIZING COMMITTEE

Chair: Dejan Divac (ITA Serbia)
Vice-Chair: Sanja Zlatanic
(ITA-AITES Executive Council, USA)

ITA Serbia:

Vesna Tripković, Serbia
Marijana Miletić-Radić, Serbia
Slobodan Radovanović, Serbia
Nikola Milivojević, Serbia
Ivana Mićević, Serbia

ITA-AITES:

Andrea Pigorini, ITA President, Italy
Helen Roth, ITA Executive Director
Sonia Salles, ITA Secretariat, France
Ioannis Fikiris, ITA ExCo - Greece
Soren Degn Eskesen, ITA Past President, Denmark
Monika Mitew-Czajewska, ITA past ExCo, Poland
Jenny Yan, ITA Past President, China
Gerard Seingre, ITA ExCo, Switzerland
Anne Brissaud, ITA Secretariat, France
Nick Chittenden, ITA ExCo, UK
Mike Rispin, UCA Past President, USA
Shani Wallis, ITA Media, UK
Rick Lovat, ITA ExCo, Canada
Gerhard Wehrmeyer, ITAtech, Germany

SCIENTIFIC COMMITTEE

Chairman: Prof. Dr. Dejan Divac, ITA Serbia President, Serbia

Co-Chairs:

Ms Sanja Zlatanić, ITA-AITES Vice President, USA
Dr Vesna Tripković, Serbia
Dr Nikola Milivojević, Serbia
Dr Slobodan Radovanović, Serbia

Members of the International Scientific Committee:

Prof. Dr Andreas Benardos, Greece
Prof. Dr Boban Stojanović, Serbia
Dr Cane Čekerevac, Switzerland
Prof. Dr Igor Jemcov, Serbia
Mr Ioannis Fikiris, ITA-AITES Vice President, Greece
Prof. Dr Jamal Rostami, USA
Prof. Dr Jelena Ninić, UK
Prof. Dr Jenny Yan, China
Prof. Dr Jurij Karlovsek, Slovenia/Australia
Prof. Dr Monika Mitew-Czajewska, Poland
Dr Neil Bar, Saint Vincent and the Grenadines
Dr Nikola Mirković, Serbia
Dr Petre Ene, Romania
Prof. Dr Rusanov Vladimir, Russia
Prof. Dr Srdjan Kostić, Serbia
Prof. Dr Vassilis Marinos, Greece
Prof. Dr Zvonko Tomanović, Montenegro
Prof. Dr Zlatko Zafirovski, North Macedonia

TABLE OF CONTENTS

INSTRUMENTATION AND MONITORING/TESTING AND INSPECTION

DIGITAL AND INFORMATION TECHNOLOGY IN DESIGN AND CONSTRUCTION

STRATEGIC PLANNING

OPERATIONAL SAFETY

IMPACT OF CLIMATE CHANGE ON TUNNEL INFRASTRUCTURE

SETC-2025
BELGRADE

TOPIC 1

ADVANCED CONSTRUCTION TECHNIQUES

Southeastern Europe Tunnelling Conference (SETC-2025)
1-3 October 2025, Belgrade, Serbia

DOI:10.5937/SETC25001B

Gained Experience from the ongoing construction of the line-cross of the Metrolines U2 x U5 and following considerations of the new designed U5 Extension in Vienna

Dietmar Bach[a], Helmut Schweiger[b], Andreas Rohrmoser[b] and Dejan Eybl[b]*

[a] IGT Geotechnik und Tunnelbau ZT GmbH; d.bach@igt-engineering.com
[b] Wiener Linien GmbH & Co KG; helmut.schweiger@wienerlinien.at

Abstract: The U2xU5 line interchange (a new U5 line from Rathaus to Hernals and a U2 extension from Rathaus southwards to the Wienerberg area) is identified as one of the priority projects for strengthening high-capacity public transport services in Vienna within the Mobility Master Plan for STEP 2025.

In total, the U2xU5 line interchange comprises approximately ten kilometers of subway tunnel and twelve new stations. This will create six new high-capacity public transport hubs with transfer options to the subway or S-Bahn.

The U2xU5 1st construction section is a foundational phase for Vienna's new subway lines. It involves crucial work at Rathaus station (interchange for U2 and U5), the initial segment of the new U5 to Frankhplatz, and the conversion of an existing U2 stretch to become the new automatic U5. Concurrently, the U2 begins its southern extension with stations like Neubaugasse and Pilgramgasse, laying the groundwork for the larger network.

Due to challenging, water-saturated ground, we developed an innovative tunneling concept: a pilot tunnel to pre-dewater the ground for the main station tubes. Further optimizations included construction logistics and design, including raising the station alignment for better lifecycle costs. In addition, the interaction between the applied construction methods, the prevailling geotechnical and geological conditions, and the existing surface structure must be systematically considered. This project underscores how crucial early, interdisciplinary planning is for success, informing future U-Bahn expansions.

The second construction section (Frankhplatz-Hernals) heavily integrates lessons from earlier phases, particularly the successful pilot tunnel method, which is crucial for stations like Michelbeuern and Elterleinplatz with challenging ground. Line tunnels will feature both cyclic (using steel fiber inner shells where dry) and continuous tunneling. Significant technical challenges include large cross-sections at Währinger Gürtel (protected by a pre-constructed jet-grouting arch to minimize settlement) and Leo-Slezak-Gasse. At Leo-Slezak-Gasse, where large cross-sections are shallow, our strategy involves two pilot tunnels, micro-pile supports, a reinforced concrete outer shell, and careful, partial-excavation tunneling with short ring closures for safe and low-settlement advancement through the Miocene.

Keywords: Metro; urban area; soft soil; pilot tunnel; grouting

1. Line-Cross U2xU5

With the extension of U2 and the construction of U5, Vienna is currently realizing its largest and most important public transport infrastructure project. It essentially comprises the extension of the U2 line and the reconstruction and construction of the U5 line. Implementation is divided into two phases of construction, with the currently ongoing first phase subdivided into three major sections.

The first section concerns the U2 main line between Karlsplatz and Rathaus, which is being comprehensively modernized and prepared for fully automated operation. The second section covers

*Corresponding author: d.bach@igt-engineering.com (D. Bach).

the new U5 line: in its initial stage, it takes over the former U2 section between Karlsplatz and the new interchange station Rathaus and will be extended to the temporary terminus at Frankhplatz. The third and longest section involves the southern extension of U2 from Rathaus station to Matzleinsdorfer Platz, built largely using a tunnel boring machine (TBM).

The second phase of construction connects to Frankhplatz station and extends to Hernals, with intermediate stations at Arne-Karlsson-Park, Michelbeuern, Elterleinplatz, and Hernals, as well as three technical structures and one depot facility. The longest tunnel section, from Hernals to the Währinger Gürtel technical structure, will be constructed with a TBM, while the section from Währinger Gürtel to the existing network will be excavated using the cyclic tunneling method. In total, about 4.5 km of new metro tunnels will be built, creating high-capacity transfer opportunities to other metro lines, suburban rail (S-Bahn), and tram lines.

Fig. 1. Future routes of the U2 and U5 (Source: Stadt Wien, Generelle Planung, 2023).

Both in the planning process and during construction, optimization approaches are continuously identified and integrated into project development in cooperation with Wiener Linien. For instance, the tunnel lining of the running tunnels at U5/2 Frankhplatz station was built in steel fiber reinforced concrete. At U2/21 Neubaugasse station, an innovative tunneling concept adapted to the complex inner-city conditions was applied.

Both optimizations form essential elements of the second construction phase, which is already being planned accordingly.

2. Geological Conditions

The alignment lies within the Vienna Basin. Miocene sediments of the Paratethys Sea (Pannonian, Sarmatian) are overlain by Pleistocene terrace deposits and by recent alluvial gravels of the Alserbach (both Quaternary sediments).

Below the Quaternary, the Miocene sediments of the Vienna Basin appear, primarily Pannonian deposits dominated by silts and clays, transitioning into the sandy and locally gravelly sediments of the Sarmatian.

The following geological layers are expected along the relevant sections:

- Fill, topsoil
- Quaternary: recent deposits of the Alserbach
- Quaternary: deposits of the Pleistocene terraces (city terrace, slope, Arsenal terrace)
- Miocene: deposits of the Vienna Basin (Lower Pannonian, Sarmatian)

3. Station U5/2 Frankhplatz

3.1. Overview

The U5/2 Frankhplatz section connects to the existing U2 line after Rathaus station and runs 634 m along Landesgerichtsstraße and Garnisongasse to the end of the construction lot.

U5 will be Vienna's first fully automated metro line. Glass platform screen doors with automatically controlled sliding and swing doors will ensure precise, safe boarding and alighting.

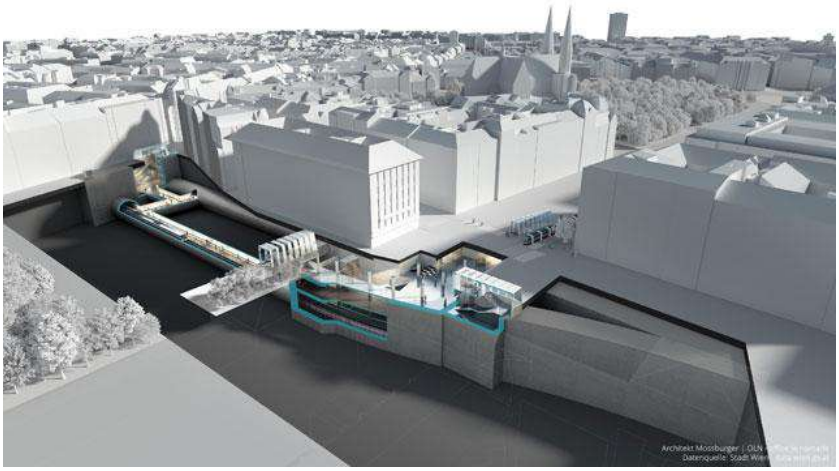

Fig. 2. General overview of the Frankhplatz station (Source: Wiener Linien).

3.2. Optimization of the tunnel lining with steel fiber reinforced concrete

As part of Vienna's metro network expansion, Wiener Linien and the planners are pursuing measures to improve sustainability and resource efficiency. One such step was the optimization of the tunnel lining. By using steel fibers instead of conventional reinforcement steel, the total amount of steel required can be reduced. This improves sustainability, increases cost-effectiveness, and reduces construction time.

During the works of the first construction phase at U5/2 Frankhplatz, a suitable opportunity arose to produce experimental tunnel lining blocks in steel fiber reinforced concrete, with and without polypropylene fibers. Since the running tunnels in this section will serve only as emergency escape routes until the extension of U5 (second construction phase), they are currently not in operational use.

The production of these blocks required intensive coordination between all project stakeholders during construction. A comprehensive monitoring program accompanies the works to provide insights into material behavior and realistic design parameters. These "test blocks" are therefore generating valuable

experience and practical knowledge for durability and implementation, forming a sound basis for the planning and tendering of the second construction phase.

Comparable linings had already been produced in steel fiber reinforced concrete during the construction of the U3 Zippererstraße station in 1999. Core samples and laboratory testing from that project have provided important conclusions on long-term performance, useful for current and future planning.

4. Station U2/21 Neubaugasse

4.1. Overview

The future U2 station "Neubaugasse" will be one of the busiest transfer hubs in the Vienna metro system, connecting the existing U3 line running longitudinally under Mariahilfer Straße with the new U2 line crossing it. Mariahilfer Straße is one of Vienna's most prominent shopping streets, featuring major retail centers and very high pedestrian volumes in a densely built-up residential area.

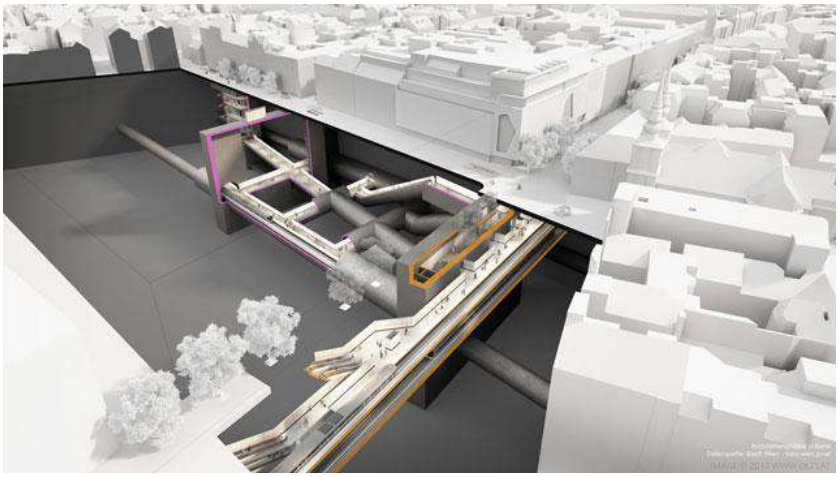

Fig. 3. General overview of the Neubaugasse station (Source: Wiener Linien).

4.2. Optimization of the tunneling concept

Based on a detailed 3D subsurface model prepared by MA29, it could not be ruled out during the design phase that tunneling in the silty-clayey Miocene soils (Vienna Marl) would encounter sand lenses extending several tens of meters, potentially containing groundwater.

As the U2/21 section lies within a very densely built urban area, full groundwater relief from the surface using wells was not feasible. Consequently, an innovative tunneling concept was developed and implemented for driving the two station tunnels.

Before excavation of the main station and running tunnels, pilot tunnels with an excavation area of approximately 20 m² were driven in the crown zone. Their primary function was to provide controlled groundwater relief within a smaller excavation profile compared to the station tunnels (~95 m²). At the same time, the pilot tunnels offered additional significant advantages for subsequent tunneling in the inner-city environment.

To ensure both rapid ring closure during excavation of the pilot tunnels and a controlled removal of their primary lining when enlarging to the full station and running tunnels, steel fiber reinforced shotcrete with a thickness of ≥15 cm was applied as support. This material provided the required

strength and flexibility for advancing the tunnel cross-section. Excavation proceeded in full-face with round lengths of 1.0–1.3 m. Where pre-support was required, lattice girders could be installed.

Only after completing appropriate drainage boreholes from the pilot tunnels was excavation of the full cross-section of the station and running tunnels undertaken.

Fig. 4. Pilot tunnel within the excavation profile of the station tunnel (Source: IGT Geotechnik und Tunnelbau).

After completion of the pilot heading, radial drainage and vacuum wells were installed within its standard cross-section to ensure reliable advance groundwater relief. To avoid interfering with the excavation of the station and running tunnels, the supply and discharge of water from these drainage boreholes was routed towards the Mariahilfer Straße shaft.

Fig. 5. Radially arranged drainage measures in the pilot tunnel (Source: IGT Geotechnik und Tunnelbau).

In addition to their primary function – providing safe groundwater relief through a smaller excavation profile compared to the significantly larger station cross-section (~95 m²) – the pilot tunnels offered a range of project-specific and technical advantages:

- Targeted and anticipatory groundwater relief and pre-drainage
- Reduced risk when encountering pressurized sand lenses
- Optimized excavation of the station tunnel
- Supplementary geological investigation

5. U5 second construction section

5.1. General

The second construction stage of Line U5 introduces five new stations: Frankhplatz, Arne-Karlsson-Park, Michelbeuern, Elterleinplatz, and Hernals.

From Frankhplatz, the line runs northwest to Arne-Karlsson-Park, providing a major interchange with seven tram lines. Skirting the General Hospital in a broad left curve, the alignment continues south to Michelbeuern, connecting to the existing U6. Turning westward, the line reaches Elterleinplatz, serving the district center of Hernals and connecting to tram services.

The final section runs beneath Hernalser Hauptstraße, terminating at Hernals station with interchange to S-Bahn line S45, trams, and buses. An operations and stabling facility directly adjoins the station, marking the end of this construction stage.

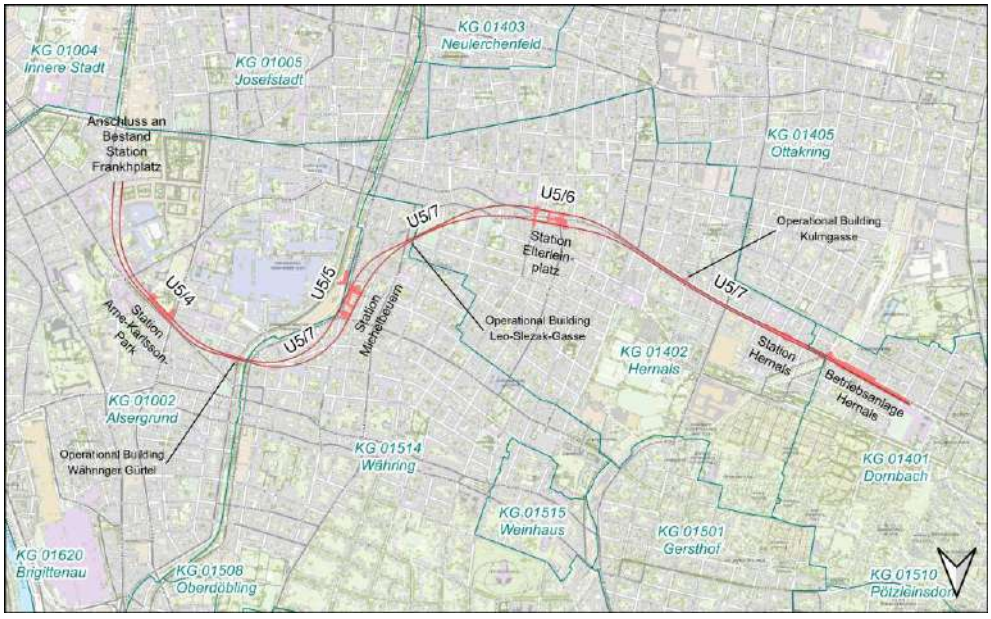

Fig. 6. Overall Site Plan U5 second section (Source: IGT Geotechnik und Tunnelbau).

5.2. Geotechnical Challenges

5.2.1. General

Experience from earlier sections will be applied, particularly at Michelbeuern and Elterleinplatz stations. However, additional challenges arise, especially regarding Miocene groundwater management in Sarmatian sands near Hernals, the 2.7 km TBM drive in variable geology, and cyclic tunneling for large cross-sections at crossover structures.

5.2.2. Groundwater Management

Due to construction depths predominantly within Miocene layers, dewatering from the surface is planned, as commonly applied in Vienna. Between Frankhplatz and Elterleinplatz, the Miocene is silt-dominated; beyond Elterleinplatz toward Hernals, sandy deposits increasingly prevail.

In Hernals, sand layers up to 10 m thick are strongly water-bearing and pressurized. Lowering groundwater below excavation level is therefore essential. Initial short pumping tests proved insufficient, necessitating large-scale relief.

A long-term pumping test (July 2025, duration 11 weeks) with six wells and four monitoring points investigated well design, screen sizes, filter gravels, and redundancy. Results indicated that sufficient groundwater relief is possible with wells at 15–20 m spacing, large diameters, and total pumping rates of ~10 l/s. Resulting settlements were only in the millimeter range and not structurally significant.

5.2.3. Closed-form construction – mechanized tunneling

Blocks and boulders:

In the area of the Kulmgasse operations building, sandy sediments from the Sarmatian era predominate; during the detailed investigations at the base of the TBM drives, gravel and stones were also found. Therefore, the density of the exploratory boreholes was increased from approx. 80 m to 40 m despite structural limitations.

A specific horizon of blocks could not be proven, so an irregular occurrence must be assumed. Blocks in the cross-section therefore cannot be ruled out; one such block was encountered about 10 m below the invert. This finding must in any case be taken into account in the cutter head design.

Fig. 7. Block approx. 10 m below tunnel invert (Source: Porr Bau GmbH, 2021).

Sticking Potential of the Miocene

Between the Elterleinplatz and Michelbeuern stations, the TBM alignment runs through Miocene geological strata, which consist predominantly of clayey silt. Due to the higher plasticity, a certain impact on the already very high sticking potential is to be expected.

Varying Ground Conditions

The alignment runs through varying ground conditions, particularly in the area between the Währinger Gürtel operations building and the Michelbeuern station. This area is characterized by very heterogeneous layers (from clayey silt to sandy gravel) as well as by fluctuating groundwater levels. These changing geological conditions pose a challenge for tunneling in EPB mode, so conditioning tests were carried out.

In conclusion, the tests showed that the extremely strong sticking tendencies of the "Vienna Clay" can be reduced to a certain extent by using suitable conditioning agents in the closed EPB (Earth Pressure Balance) mode. Furthermore, sufficiently stable and flowable earth paste masses can be produced in the tests, confirming the fundamental suitability of the chosen tunneling machine (EPB shield). However, achieving the required consistency sometimes necessitates considerable quantities of additives, foaming agents, and the use of polymers.

5.2.4. Closed-form construction – conventional tunneling

Three track-changing facilities are planned for the second construction stage, two of which are located mostly beneath existing buildings and will therefore be built using the closed-form construction method. Each of these two track changes is combined with an emergency exit and an operations building. The drives will be initiated from a shaft constructed using the open-cut method.

For this purpose, separate large-scale cross-sections will be excavated from the shafts. Due to the required length of the track changes and the variable track spacing, several different cross-section types are necessary. The resulting largest cross-section of the widened areas has an excavation area of approximately 133 m².

Conventionally excavated tunnels of this dimension in inner-city unconsolidated rock require special solutions to both stabilize the cavity during tunneling and to minimize the impact on existing buildings. The first track change passes under residential buildings, listed monuments, and a district heating tunnel. The overburden in this area is between 9 m and 10 m. Special attention is being paid to the district heating tunnel, whose invert at the critical point slightly intersects the crown of the cross-section. Fig. 8 shows the existing surface buildings (green), the existing underground structures of the district heating collector (blue), the planned shaft for the Währinger Gürtel operations building (purple), and the subsequent jet-grouting arch of the cross-section (grey).

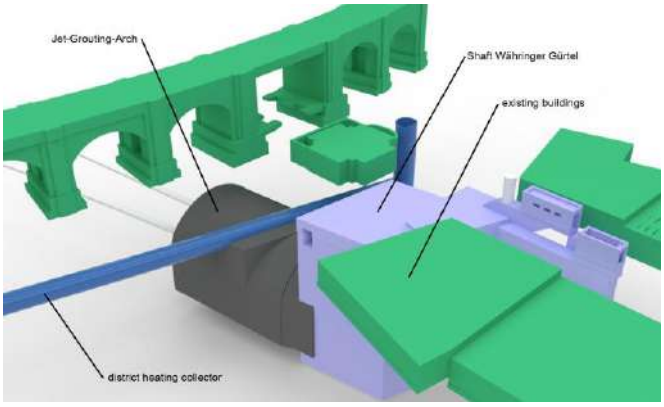

Fig. 8. Overview of the Währinger Gürtel area (Source: IGT Geotechnik und Tunnelbau).

The geological strata projected for this area (alluvial fans and quartz gravel) are well-suited for the creation of jet-grouting (DSV) columns. Furthermore, surface access is available over the entire length of the track change, divided into several phases. These conditions allow for a jet-grouting arch to be created in advance to secure the cavity of the track change before excavation work begins and to transfer the resulting rock loads into the stiff quartz gravel. Calculations have shown that the chosen concept can achieve a settlement-friendly and safe conventional tunneling of the track change cross-sections.

The second track change, which will also be built using the closed-form construction method, has an overburden of about 13 m to the top of the ground (GOK), although some buildings directly above the facility have basements with a depth of about 5 m below GOK. A particularly critical structure is one built with a two-story underground garage and two upper floors. The remaining distance between the outer crown edge of the large cross-section and the underside of the single foundations is about 3.8 m. The entire conventionally excavated part of the track change will be driven in silty-clayey Miocene or Sarmatian strata, using the innovative tunneling concept shown in Fig. 9.

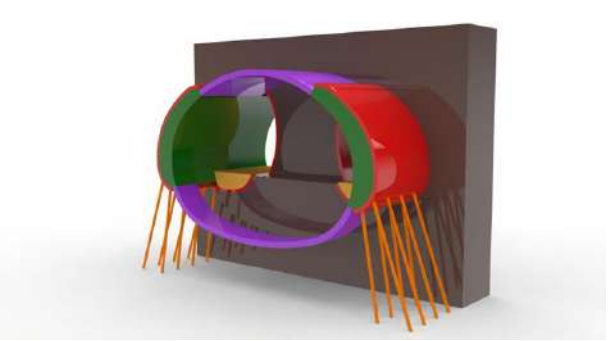

Fig. 9. Tunneling concept cross-section Leo-Slezak-Gasse (Source: IGT Geotechnik und Tunnelbau).

Initially, two pilot tunnels (red) are driven along the haunches of the widened cross-sections. In these tunnels, cast-in-place concrete slabs (green) are constructed, founded on micropiles (orange). The cast-in-place concrete slabs serve as a support for the subsequently constructed crown and invert arch (purple) and also provide longitudinal bracing. Calculations have also shown that the chosen concept enables a geotechnically safe and robust construction of the large cross-section.

6. Conclusion

With the sections of the second construction stage currently under construction and in planning, the Vienna subway network continues to grow and develop.

However, the completion of the U5 construction work does not mark the end of Vienna's subway expansion. With the extension of the U2 by approximately 4.0 km and the U1 by approximately 2.5 km, further challenging projects are in the pipeline, where past and future experiences will play a decisive role.

References

IGT Geotechnik und Tunnelbau. Available online: https://igt-engineering.com/. (accessed: 2025)

Planungsteam U5NEU2, Magistratsabteilung 18 Stadtentwicklung und Stadtplanung, 2021. Generelle Planung Abschnitt Frankhplatz – Elterleinplatz.

Planungsgemeinschaft Folgeauftrag Generelles Projekt U5-U2-U1, Magistratsabteilung 18 Stadtentwicklung und Stadtplanung, 2023. Generelle Planung Abschnitt Elterleinplatz – Hernals.

Wiener Linien, (n.d.). General overview of the Neubaugasse station. Available online: https://www.wien.gv.at/verkehr/planung-linie-u5

Southeastern Europe Tunnelling Conference (SETC-2025)
1-3 October 2025, Belgrade, Serbia

DOI: 10.5937/SETC25002D

Soil fixing technologies used in the construction of cross passages in the Moscow metro

Andrey A. Dolev[a], Elena E. Deplani[a], Dmitry S. Konyukhov[a,b], Valerij P. Kivluk[a]*

[a] JSC Mosinzhproekt, 125252, Khodynsky boulevard 10, Moscow, Russia; gidrotehnik@inbox.ru
[b] Russian Technological University MIREA, 119454, Vernadsky Avenue 78, RTU MIREA, Moscow, Russia

Abstract: In the city of Moscow, the construction of the subway is proceeding at a high pace. Over the past few years, almost 200 km of main line tunnels and more than 100 stations have been built. At the same time, it was necessary to overcome many technological difficulties associated with the construction of cross passages both between the main line tunnels and between them and the tunnel structures. The city of Moscow is located on a plain of fluvioglacial genesis, characterized by a marmorate, steep, lenticular interlayer of sandy, water-saturated and clay soils, as well as the presence of water-saturated fractured limestones. Main line tunnels and shafts are usually arranged in a mechanized way, which ensures the required predictability and quality of work. Failures have to be built in a mining way. In limestones saturated with cracks and cavities and water-saturated sandy soils, especially if they have the property of quicksand, the breakdown device is possible only under the protection of an array of fixed soil having the necessary strength and anti-filtration properties. At the same time, high-quality soil consolidation in such geological and hydrogeological conditions is a significant difficulty, especially with short construction time. During the construction process, various technologies were used to fix soils in Moscow: cementation, micro-cement impregnation, jet grouting, impregnation with organic resins capable of polymerization, as well as soil freezing. At the same time, radically different substances were used for fixation purposes. Each of the listed technologies has its advantages and disadvantages both in the nomenclature of the soils to be fixed, and in the availability of the equipment used, the availability of the substances used for fixing, the qualifications of the maintenance personnel, the time required for the work on fixing and the subsequent set of necessary strength. All of these technologies were applied in the production of construction works at different sites in accordance with the geological conditions and advantages of each technology, the quality of the fixed soil, the size of the array compared with the design values, and the manufacturability of the method were monitored. As a result, the limits of applicability of each technology were confirmed, reliability and degree of risk were determined, and environmental aspects were identified. Based on the experience of work in the construction of an array of fixed soil during the construction of buildings by mining, preferences were revealed when choosing the method of fixing, materials, and the method with the least risks with the best physical and mechanical characteristics of the fixed soil was recommended.

Keywords: antifiltration curtain; breakdowns; quicksand soils; soil anchoring; tunnel structures

1. Introduction

The construction of the Moscow metro is proceeding at a high pace – it is planned to open 3 stations in 2025, 11 stations in 2024, 14 stations in 2023, 69 stations in 2022, 12 stations in 2021, etc. Almost 200 km of subway tunnels have been built. Due to such a large volume of construction of metro facilities, many organizational, technological and technical difficulties have been overcome. This publication examines the technical and technological aspects related to the construction of cross passages, both between tunnels and between tunnels and tunnel structures. The special features of these works are the difficult soil and hydrogeological conditions.

The Moscow region is located on the Russian Plain of fluvioglacial genesis, far from mountain-forming sites. The geological structure of the region is characterized by multiple layers of sedimentary rocks formed by weathering and the transport of small particles over long distances or the separation of

*Corresponding author: gidrotehnik@inbox.ru (A. Dolev).

accumulated sedimentary rocks by watercourses. Thus, the geological section of the Moscow region is represented by clay and sandy soils in a mottled interlayer. The underlying rocks are limestones of varying degrees of weathering. The variegated layering of sandy and clay soils, together with the flat nature of the terrain and regular rains, ensures the presence of groundwater at several horizons, which, in turn, ensures the pressurized nature of groundwater in some water-bearing soils. But a special place in the geological structure is occupied by the fragmentary presence of watered fine sands with clay aggregate, the so-called 'drift sand'. This type of soil is characterized by a special property – liquefaction under the influence of vibration. In its natural state, the specified soil is dense, water-saturated, and capable of successfully withstanding various types of loads, except for vibration. Under the influence of vibration (or when a watercourse is formed from this soil, for example, with a hole in the structure), this type of soil loses its structural strength and turns into a suspension under pressure in the ground column. Another feature of the geological structure of the Moscow region, which is a consequence of the rainy climate and the anthropological impact, are gullies filled with bulk soils. At the same time, bulk soils often represent the buried remains of substandard building materials and/or buried organic inclusions.

The ancient character of the fluvioglacial plain is emphasized by the presence of places where previous sediments were washed away by water, as a result of which the soil layers become especially mottled, precipitous, and lenticular (Fig. 1).

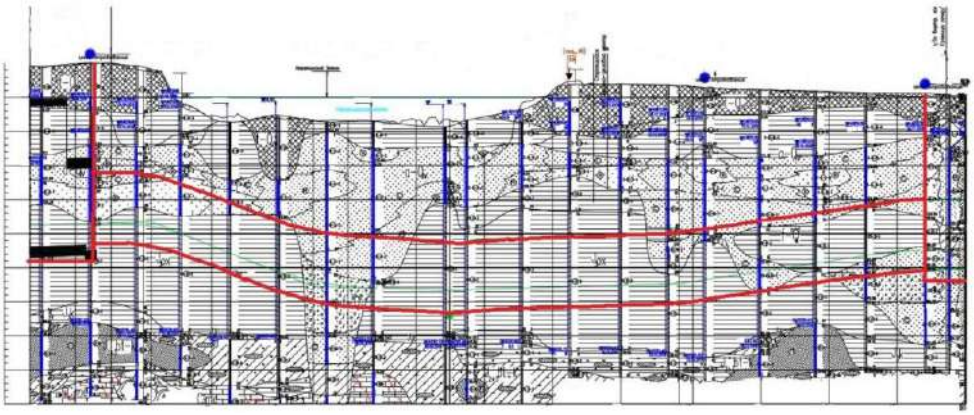

Fig. 1. Typical structure of the soil stratum of the Moscow region.

The described nature of the hydrogeological features of the ground conditions of the Moscow region dictates the specifics of the difficulties of building the Moscow Metro. Most stations are designed and built by subsurface method to allow the development of a relatively shallow excavation and, consequently, reduce capital costs. This is also more convenient for passengers – there is no need to spend extra time getting down/up from the surface to the platform. Usually, tunnels tend to be located in layers of cohesive soil. But this does not always happen due to the periodic presence of volumes of sandy soils along the tunnel route, usually shallow and water-saturated, i.e. having the properties of quicksand. Tunnels are built by means of mechanized tunnelling complexes (TBM), their construction is characterized by high speed and quality. In accordance with regulatory requirements, it is necessary to periodically arrange cross passages and near tunnel structures between tunnels, where drainage and ventilation installations are placed. Due to the fact that they require access to the surface, they must be positioned along the tunnel route in such a way that they do not fall into the footprint of existing buildings and have minimal impact on it. Thus, there is no rational choice of engineering, geological and hydrogeological conditions.

Cross passages both between interstation tunnels and between tunnels and tunnel structures built in vertical boots have to be arranged in a mining manner. This often occurs in water-saturated soils – fine sandy, even with clay aggregate (i.e. in quicksand), or, less often, in fractured and porous limestones. In any case, with a pressure level of groundwater, frequently several tens of meters. For the construction

of buildings by mining in such geological conditions, it is imperative to arrange an array of fixed soil. A typical tunnel structure is shown in Fig. 2.

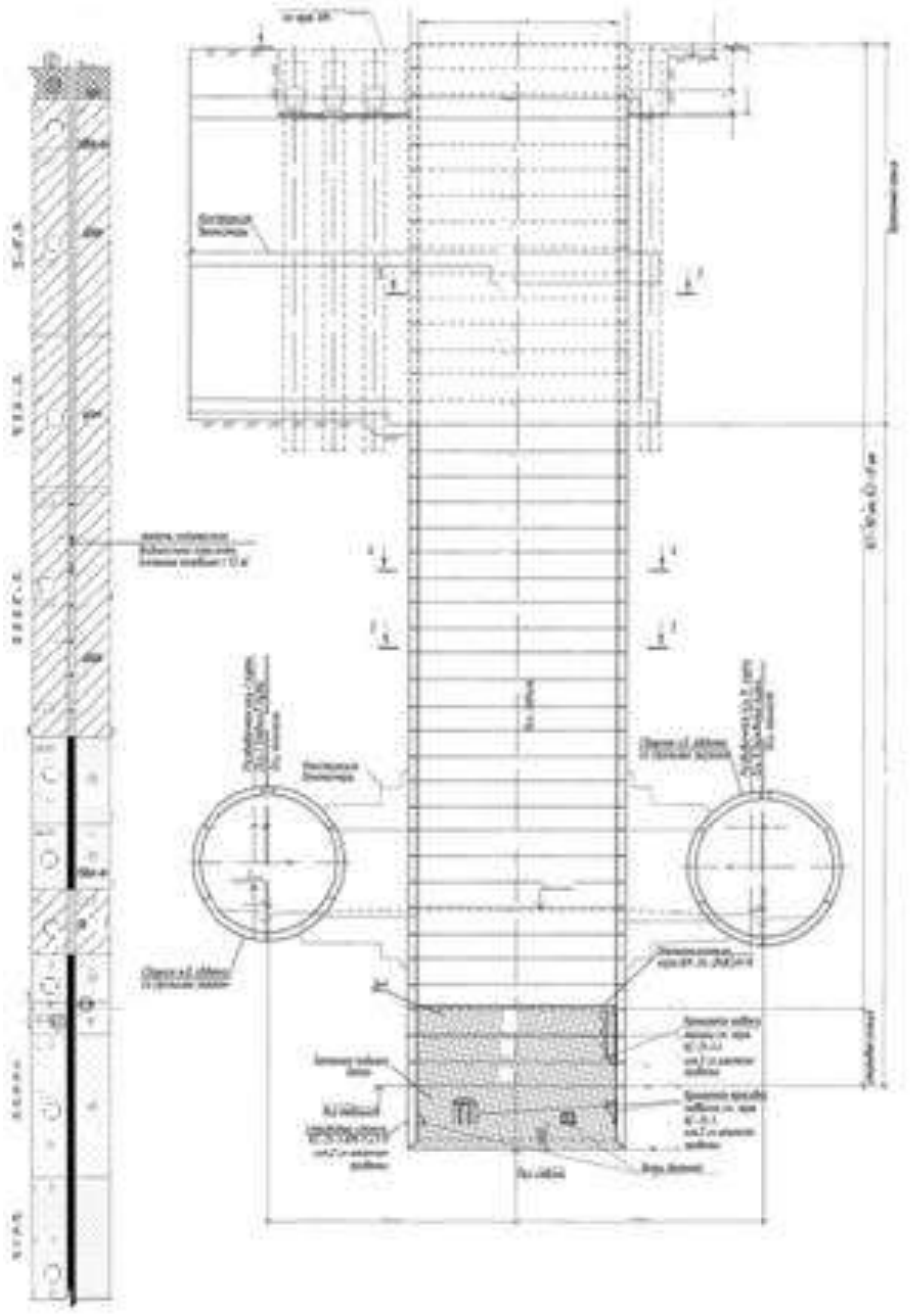

Fig. 2. A typical tunnel structure arranged in a vertical shaft traversed by a mechanized method (as well as main line tunnels).

The analysis of the possibility of solving the problem of soil consolidation consisted of a review of the positive practices of such work by contractors and an analysis of literary sources. Thus, Sokolovich (1980) described proven technologies for fixing soils using silicate solutions, organic resins, cement and cement-clay compositions. Rzhanitsyn (1986) developed technological approaches to soil consolidation and added the accumulated experience. Subsequently, when microcements appeared, soil stabilisation using them was developed by Garkavi et al. (2020), Ibragimov et al. (2016) have brought certainty to the limits of applicability. Guo et al. (2020) supplemented the description of methods for stabilisation sandy soils with polymer solutions, Shuplik and Nikolaev (2016) contributed to the introduction of artificial soil freezing.

2. Materials and methodology

When mining operations are carried out, as a rule, a borehole screen is first arranged to provide soil support in the arched part of the mine. After that, the lining of the tunnel or vertical boot is opened, the soil is worked out (usually first the upper ledge, then the lower one) and after each approach, temporary lifting frames are installed with temporary lining of the exposed soil (usually boards). Then, the next capture is developed and so, cyclically, the entire soil is extracted for the entire length of the stroke in the breakdown. Thereafter, reinforcement frames, formwork, and concrete permanent lining of the fault line are arranged.

All these works can be done only if:

- water supply in volumes that allow the work described earlier to be carried out with proper quality, especially concreting (water supply in volumes up to 5 m^3/hour);
- the strength of the soil must be sufficient to withstand the pressure of groundwater and mountain pressure.

In the presence of rocky and semi-horizontal soils, for example, fractured aquiferous limestone, the strength of the soil is sufficient for the development of traps. However, in the presence of sandy, water-saturated soils, it is necessary to consolidate the surrounding soil mass.

The criterion for satisfactory fixation of the surrounding soil mass, both according to the established practice of mining operations and according to the calculation justification, is mainly the strength of the fixed soil of 5-7 MPa with a thickness of at least 2.5-3 m. It should be borne in mind that the development of the soil is carried out with pneumatic jackhammers and the level of vibration loads at the excavation site is quite high. It is also necessary to take into account the creation of anti-filtration properties of a fixed ground mass, ideally not allowing groundwater to pass through completely or, in real conditions, ensuring an influx of water into an open passage of no more than 5 m^3/hour.

The comparison methodology was to identify the advantages and disadvantages of using certain methods to create an array of fixed soil with antifiltration properties relative to the nomenclature of soils to be fixed (fractured limestones, sands of various sizes, sands with clay filling), availability of equipment and the fixed substance (scarcity, price), the qualifications of maintenance personnel, the required time, the size of the anchoring array (actually achieved relative to the design values), environmental aspects (residues of unreacted substances, the duration of the fixed array's existence).

However, technologies capable of creating an array of water-saturated soil that has the properties of antifiltration protection and the necessary strength (at least 5 MPa) are limited in number. The set of these technologies, as well as the advantages and disadvantages of each of them, are presented in Table 1.

Table 1. Advantages and disadvantages of the adopted technologies of soil fixation

Soil consolidation technology	Advantages	Disadvantages
Grouting works	• Relative ease of work execution; • Availability and simplicity of equipment; • Availability and low cost of materials.	• Can be used only in coarse and gravelly sands without fine aggregate; • Can be used only in semi-horizontal (rocky) soils with sufficient crack opening width; • It takes time to gain strength; • Fixed array remains as such forever (environmental interference)
Micro-cement impregnation	• The possibility of application in gravelly, coarse, medium-sized and small sands with fine (but not clay) aggregate; • Possibility of application in semi-horizontal (rocky) soils, even with very small crack opening width; • Gentle method – there is no physical impact on the surrounding soil.	• Highly qualified staff is required; • Complexity and non-proliferation of equipment (pumps with strictly controlled pressure/volume supply); • Often the presence of residual water occurrences in the fixed soil; • It takes time to gain strength.
Jet grouting	• Physical mixing of the soil with the hardening compound, higher uniformity and quality of the fixed soil; • Greater reliability of the fastening process; • The use of cheap general construction cement; • The prevalence of equipment; • High-quality fixing of the boundary of sandy and clay soils.	• The risks of delamination of the soil – concrete mixture and, as a result, the risks of lowering the quality; • Difficulties in organizing a pilot site for testing injection parameters; • The effect of high pressure on surrounding building structures; • The complexity of application in rocky (semi-horizontal) fractured soils; • There are great difficulties with the uniformity of the fixed soil in quicksand soils.
Impregnation with organic resins capable of polymerization	• The possibility of application in any sandy soil without restrictions on the size of its particles; • Greater reliability of the fastening process; • Gentle method – there is no physical impact on the surrounding soil; • The prevalence of equipment; • High-quality fixing of the boundary of sandy and clay soils.	• Risks of non-reaction (polymerization of not the entire volume of resin), with a decrease in the quality of fixation; • Difficulties in organizing a pilot site for testing injection parameters; • The use of expensive hardening materials; • Ecological contamination of the fixed soil with polymerization products and organic resins.
Ground freezing	• Guaranteed uniformity and continuity of the fixed soil; • Gentle fixing of the soil without changing the type and format of its natural composition; • Absolute ecological cleanliness.	• The time required for soil freezing is long enough (30-40 days) for brine freezing; • Limited number of enterprises producing 'dry ice' and liquid nitrogen on the required scale; • The construction site is cluttered with equipment and pipelines for the entire duration of the soil freezing work.

3. Results and discussion

It should be noted that cementation with ordinary cement is performed only in rocky and semi-rocky soils, as a rule, in limestones with a sufficiently large crack opening width. For this purpose, ordinary general construction cement with a grinding fineness of about 3000 cm^2/g is used, and 95 % of the

grains of such cement should be less than 100 microns. If there are not only cracks in the rock, but also cavities or hollows, then sand is added to the slurry to reduce cement consumption by up to 2/3 by volume, depending on the absorption of the injection material by the cavity. Conversely, if the fracturing of the rock is expressed by small cracks, then up to 10 % finely ground cement with a grinding fineness of about 9,000 cm^2/g is added to the cement slurry to seal even small cracks.

If the creation of an array of fixed soil is carried out using microcement, then impregnation technology is used. Injection into the soil is carried out by a cement-water suspension, while water is a transport system and its flow transports microcement particles into the pores of the soil at a distance of 0.3 to 0.6 m from the injector (depending on the type of sandy soil and the presence of clay aggregate). Unfortunately, in the case of this technology, it is impossible to achieve complete waterproofness of the fixed soil due to the heterogeneity of the natural composition of the soil and, as a result, the deposition of more microcement grains in the volume of soil with relatively greater permeability. As a result, when drilling a cross-passage in a body of such soil, there are almost always spot water occurrences that form in a chaotic manner. The total water inflow from these water events is nevertheless acceptable for failure concreting work.

In the past, at the initial stages of the construction of the Moscow Metro, jet grouting technology was used to create blocks of fixed soil. After gaining relevant work experience, this technology, which was quite common, was gradually abandoned due to the identification of numerous problems with its implementation in quicksand soils (fine water-saturated sands with clay aggregate). The issues were the lack of continuity of the solidified soil. Quicksand soil is characterized by almost instantaneous liquefaction under the action of vibration. And the jet grouting erosion jet seems to create just such a vibration, at least near the working body of the monitor. As a result, stable erosion does not occur, and the soil is not secured in the required quality. It is necessary to combat this phenomenon by repeatedly installing each jet element in the same place. Nevertheless, the creation of an block of stabilized soil was carried out mainly from the daytime surface using: jet-1 (cement-water suspension only), jet-2 (air jet and cement-water suspension), jet-3 (water jet, air jet and cement-water suspension jet). Sometimes a preliminary washout was used. But, in addition, there was also the creation of a block of stabilized soil horizontally from a tunnel or boot using jet-1. When working from the surface, where the geological conditions were particularly difficult, jet grouting was used, followed by impregnation with microcement. This increased the quality of the stabilized soil, reduced the heterogeneity of water occurrences and increased the strength of the ground concrete. The impregnation was carried out through injection tubes, which were lowered into the ground concrete immediately after the manufacture of the jet element. Micro-cement impregnation was carried out after setting the soil-concrete and gaining the necessary strength.

To a first approximation, the most technologically advanced and most reliable way would be to stabilize the soil by impregnation with organic resins capable of polymerization. Indeed, these substances do not have a solid fraction in their composition, which means that in the presence of a pressure gradient they can easily penetrate even the smallest pores of sand with clay filler and, polymerizing, create high-quality solidified soil blocks even at large distances from the injector. Unfortunately, objective reality has made its own adjustments, and the use of organic resins has been reduced to a very small scale due to their very high price and a rather poorly predictable percentage of polymerization under field conditions with temperature variability, soil acidity, etc. In addition, both unreacted resin and polymerization reaction products, decomposing over time, pollute the soil and groundwater for many years.

The technology of soil freezing to create a block of stabilized soil was in demand at the very beginning of the construction of the Moscow metro. In those days, only brine freezing with $CaCl_2$ aqueous brine was used, pre-cooled in the heat exchanger of a refrigerating machine to minus 25 °C. Heat extraction in this way from a soil mass saturated with water occurs rather slowly. In addition, the movement of groundwater, which contributes to the constant removal of cold and the influx of heat, can further prolong this process, and at different horizons in different ways. The use of ‘dry ice’ with a lower gas formation temperature, up to minus 78 °C, significantly accelerates the process of soil freezing and reduces the impact of groundwater movement. However, the CO_2 released in the case of improperly

arranged ventilation and inappropriate attitude towards this phenomenon on the part of construction workers can lead to death if it displaces oxygen to the surface on the lower marks of the shaft and the opened cross passages. The use of a refrigerant, liquid nitrogen, with an even lower temperature, down to minus 196 °C, can further accelerate the process of soil freezing. However, there is limited experience in its use in the Moscow region due to technological difficulties.

4. Conclusion

Thus, numerous technologies in soil and hydrogeological conditions of varying degrees of complexity have been tested for ground stabilization in the construction of buildings, including those with tunnel structures, during the construction of the Moscow Metro. The limits of applicability of each technology are revealed, reliability and degree of risk are determined, environmental aspects are revealed.

Based on the experience of constructing blocks of stabilized soil during the construction of cross-passages by mining during the construction of the Moscow Metro, the following conclusions can be drawn:

1. The installation of cross-passages is a very risky and particularly responsible stage in the construction of the subway, excessive water leakage (as well as the release of quicksand masses) in which it threatens the loss of both tunnel structures and sections of interstation tunnels.
2. The making of a block of stabilized soil with anti-filtration protection properties around the cross-passage under construction minimizes the risks of excessive water occurrence and their consequences.
3. Currently, many technologies are known and tested in practice to create a block of stabilized soil with anti-filtration protection properties. Their areas of applicability, advantages, and disadvantages have been identified.
4. As the practice of the work shows (the authors tracked the effectiveness and reliability of each individual technology for fixing the soil mass according to key indicators such as guaranteed continuity, properties of anti-filtration protection, nomenclature of types of soil to be stabilized, changes in natural composition, environmental aspects, compliance of the actual size of the stabilization with design values), according to the authors, as well as a combination of such fundamental characteristics as durability and overall reliability of stabilization, the best method of stabilization soils in the construction of cross-passages is the method of water-saturated soils freezing.

References

Garkavi, M.S., Nefedieva, A.K., Nefediev, A.P., 2020. Качественные особенности инъекционных микроцементов. In Construction Materials Science: Present and future: Proceedings of the First All-Russian Scientific Conference dedicated to the 90th anniversary of the outstanding materials scientist, Academician of the Russian Academy of Natural Sciences Yuri Mikhailovich Bazhenov, Moscow, October 01-02, 2020; National Research Moscow State University of Civil Engineering: Moscow, Russia, pp. 313-318.

Guo, C., Hu, D., Wang, F., 2020. Diffusion behaviour of polymer solutions during anchoring of sandy and gravelly soils. *Soil mechanics and foundation engineering*, 6, 6.

Ibragimov, M.N., Semkin, V.V., Shaposhnikov, A.V., 2016. Fixing of soils with micro-cement solutions. *Soil mechanics and foundation engineering*, 6, 26-31.

Rzhanitsyn, B.A., 1986. Chemical stabilization of soils in construction; Stroyizdat: Moscow, Russia, pp. 1-264.

Shuplik, M.N., Nikolaev, P.V., 2016. Investigation of the parameters of the heat exchange process during the freezing of rocks using solid carbon dioxide. *Mining Information and Analytical Bulletin (Scientific and Technical Journal)*, 1, 42-49.

Sokolovich, V.E., 1980. Chemical stabilization of soils; Stroyizdat: Moscow, Russia, pp. 1-119.

Southeastern Europe Tunnelling Conference (SETC-2025)
1-3 October 2025, Belgrade, Serbia

DOI: 10.5937/SETC25003U

Analysis of primary NATM support under limited anchor capacity: implications for steel ribs and lattice girders

Milan Uljarević[a], Andrija Rašeta[b] and Dragan Bojović[c]*

[a] CRBC Serbia, Novi Sad, Serbia; umilan89@gmail.com
[b] University of Novi Sad, Faculty of Technical Science, Civil engineering, Novi Sad, Serbia; araseta@gmail.com
[c] IMS, Belgrade, Serbia; dragan.bojovic@institutims.rs

Abstract: In the conventional application of the New Austrian Tunneling Method (NATM), the primary tunnel support is designed as a composite system consisting of shotcrete, systematically installed rock bolts, and auxiliary elements such as lattice girders and steel ribs. Official guidelines typically classify steel elements as temporary supports, meant to stabilize the excavation face until the shotcrete and anchoring system become structurally active. However, field experience shows that anchors in weak or heavily fractured ground conditions often fail to mobilize their full capacity, particularly when their embedment does not extend beyond the plasticized zone around the excavation. This paper analyzes the structural behavior of the primary NATM support system in cases where anchors do not perform as intended. Using a shell-based numerical model with point support representation, the study investigates how local ground-structure interaction changes when anchors lose stiffness and how structural responsibility may shift toward steel ribs and lattice girders. Practical site observations are used to illustrate common deviations from design assumptions such as the installation of multiple ribs without proper contact with the rock mass or reliance on rigid steel elements in zones where shotcrete alone could suffice. Special attention is given to the anchorage mechanism, the conditions under which steel ribs begin to act as primary load-bearing components, and the consequences of poor shotcrete encapsulation (e.g., shadow zones). The study emphasizes that the structural contribution of steel elements in NATM should be re-evaluated when anchors are compromised, and that this redefinition must account for ground conditions, construction sequence, and time-dependent concrete performance. The paper proposes practical guidelines for the rational integration of steel supports in NATM lining systems when conventional anchoring is unreliable, aiming to improve both safety and efficiency in tunnel design and execution.

Keywords: lattice girders; steel ribs; NATM; primary lining; tunnel

1. Introduction

The New Austrian Tunneling Method (NATM) is founded on the principle that the surrounding ground mass should actively participate in the overall load-bearing system, with controlled deformations ensuring both stability and economy. In its conventional application, the primary lining typically consists of shotcrete, systematically installed rock bolts, and auxiliary elements such as lattice girders or steel ribs. Official guidelines, such as those of the Austrian Society for Geomechanics (2010) and the U.S. Department of Transportation Federal Highway Administration (2009), generally classify these steel elements as temporary supports intended to stabilize the excavation until the shotcrete and anchoring system becomes fully effective.

However, practical tunneling experience has repeatedly shown that this assumption does not always hold true. In weak or heavily fractured ground, rock bolts often fail to develop their full anchoring capacity, particularly when their embedment remains within the plasticized zone around the excavation (Nilsson and Holmgren, 1999). When this occurs, the intended composite support mechanism is compromised, and structural responsibility may shift toward the shotcrete shell and the embedded steel elements. Representative cases include the Boggo Road Busway tunnel in Brisbane (Nye and Alt,

*Corresponding author: umilan89@gmail.com (M. Uljarević).

2010), where thick shotcrete and lattice girders were relied upon as both initial and permanent lining due to settlement control requirements, and Collotta et al. (2010) study of steel ribs embedded in shotcrete linings, which demonstrated sustained stress redistribution arising from creep and shrinkage effects. Similar observations have been reported in urban tunneling projects in Central Europe, where insufficient anchor mobilization led to premature reliance on rigid steel ribs for stability.

Despite these findings, the structural contribution of lattice girders and steel ribs in NATM linings remains insufficiently quantified. Current design practice rarely accounts for their long-term stiffness contribution, the effects of poor concrete encapsulation (e.g., shadow zones), or the influence of joint behavior and spacing between elements. This research gap becomes particularly critical in cases where anchors cannot be mobilized, such as when excavation is advanced under pipe umbrellas or in heavily fractured rock masses.

The present study addresses this gap by analyzing the behavior of the NATM primary lining under conditions of limited anchor capacity. Through numerical modeling, field observations, and comparative laboratory testing of lattice girders and steel ribs, the study seeks to clarify the circumstances under which these steel elements transition from temporary stabilizers into structurally relevant components of the permanent support. By doing so, it aims to provide practical recommendations for integrating lattice girders and steel ribs into the design of NATM support systems, particularly in weak or fractured ground conditions where conventional anchoring is unreliable.

2. General principle of the New Austrian Tunneling Method (NATM)

The New Austrian Tunneling Method (NATM) is based on the fundamental concept that the surrounding ground is not merely a source of loading but also acts as a structural component of the tunnel support system. This method leverages the self-supporting capacity of the rock or soil mass, aiming to mobilize the ground's strength through controlled deformation and timely installation of support measures (Figure 1 (a) (Chapman et al., 2010) and (b) (Australian Tunnelling Society, 2024)).

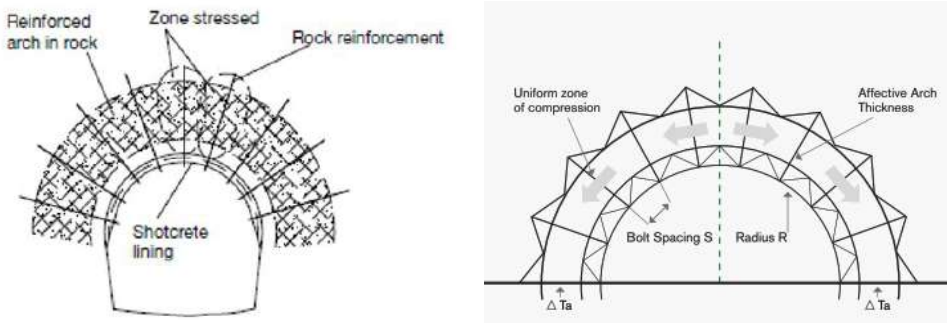

(**a**) (**b**)

Fig. 1. Principle of NATM ground-structure interaction (a) (Chapman et al., 2010); (b) (Australian Tunnelling Society, 2024).

Unlike traditional tunneling methods that rely on rigid predesigned support systems, NATM emphasizes a flexible, observational approach. Excavation and installation of support elements are continuously adapted to in-situ ground conditions and project-specific requirements. Ground response - primarily measured in the form of displacements of the initial lining is monitored in real time to verify the stability of the opening and to optimize both the excavation sequence and the type and timing of support installation.

Typical NATM support systems consist of (Austrian society of geomechanics, 2010):

Shotcrete, Rock bolts or systematic anchors, with additional elements such as steel ribs and lattice girders used to provide early structural integrity and to preserve the excavation geometry prior to full shotcrete hardening.

For a long time, especially in the initial period, this procedure encountered resistance. The opponents argued that a tiny layer of shotcrete and anchoring might counteract subsurface pressure. It was most likely because the static analysis of shotcrete and anchors had to be performed in the same way as steel and concrete structures at the time. By activating the load-bearing vault of soil or rock that encloses the underground opening, it becomes part of the overall load-bearing system. This single approach is essentially based on semi-empirical design, in-situ measurements, and corrections. The development of NATM has substantially enhanced the cost efficiency of tunneling projects and had favorable effects on infrastructure development as well. (Kovačević, 2014). NATM is based on the concept that the ground around the tunnel not only acts as a load but also as a load-bearing element. The typical support elements in NATM are shotcrete and rock dowels. Steel ribs or lattice girders provide limited early support prior to the shotcrete hardening and ensure proper profile geometry. If ground conditions require support at or ahead of the excavation face, face dowels, shotcrete, spiles, or pipe canopies are installed. The excavation cross-section is subdivided into the top heading, bench, and invert depending on both ground conditions and logistical requirements (i.e. to facilitate the use of standard plant and machinery). (Austrian society of geomechanics, 2010)

3. Lattice girders and Steel Ribs in NATM primary support

Lattice girders are structural elements made of steel reinforcing bars, interconnected into a three-dimensional shape, most commonly triangular to achieve the desired stiffness and geometric stability. They are pre-bent to match the tunnel profile and installed immediately behind the excavation face, before the shotcrete has developed sufficient load-bearing capacity. According to the *Technical Manual for Design and Construction of Road Tunnels - Civil Elements* (U.S. Department of Transportation), although lattice girders have relatively small cross-sectional areas compared to the thickness of the shotcrete lining and thus do not independently provide substantial bearing capacity, they fulfill several essential support functions (U.S. Department of Transportation Federal Highway Administration, 2009):

Provide immediate support to unstable rock blocks that tend to fall out;

- Offer a precise geometric template for shotcrete application;
- Serve as carriers for welded mesh reinforcement, when used;
- Act as rigid anchors for preliminary support measures such as forepoling.

In the conventional application of the New Austrian Tunneling Method (NATM), lattice girders and steel ribs are typically defined as temporary support elements, intended to provide early stabilization immediately after excavation. According to the Austrian Society for Geomechanics (ÖGG), these components serve a short-term role in controlling deformations and ensuring safety until the shotcrete and systematic anchoring are fully activated. *"Steel ribs and lattice girders are considered temporary support elements within the NATM framework, aimed at immediate stabilization during early excavation phases."* (based on ÖGG guidelines). This interpretation has been widely adopted in both academic literature and engineering practice. Nevertheless, the extent to which these elements contribute to the structural behavior of the primary lining system remains an ongoing subject of discussion, particularly in contexts where they are retained in the final lining or assumed to contribute to composite action with the surrounding shotcrete (Austrian Society of geomechanics, 2010).

3.1. Opposite attitude

However, several recent studies and design approaches challenge this strict classification. For instance, Nye and Alt (2010) report the use of steel ribs in combination with thick shotcrete layers (up to 350 mm) as part of a support system classified as both initial and permanent lining, especially in geologically sensitive urban tunneling conditions. Similarly, Collotta et al. (2010) present a detailed investigation into the long-term stress redistribution in shotcrete tunnel linings with embedded steel ribs. The study models the ribs as integral parts of the composite lining, highlighting their sustained structural interaction with the surrounding shotcrete due to creep and shrinkage effects and dominant influence in the composite system (Collotta et al., 2010).

These findings indicate that, under certain conditions, lattice girders and steel ribs may contribute beyond their originally intended temporary function. Nevertheless, the actual structural impact depends on several critical factors: the mechanical connection of rib segments, the manner of their base support (often acting as temporary foundations), the spacing between elements, and the quality of shotcrete placement around the steel frame. These aspects are frequently neglected in simplified models, leading to under or overestimation of the system's stiffness and stability.

4. Research background and objectives

This research focuses on the application of lattice girders and steel ribs in tunnel construction, particularly when using the New Austrian Tunneling Method (NATM). Although the technical literature often defines these elements as temporary support components, in practice it is common to see multiple lattice girders installed in a single excavation step, regardless of the rock stability. There are also frequent cases where these elements are placed at large spacing intervals (as illustrated in Figure 2), clearly indicating that they are not functioning as temporary supports but rather as part of the shotcrete lining.

A growing concern is the increasing use of steel ribs that are not properly included in structural analyses. Key factors such as staged construction, ground-structure interaction, shotcrete confinement, and the mechanical behavior of rib segment joints are often ignored. These ribs are sometimes modeled as part of the reinforcement within the concrete lining, yet their spacing and influence on the overall load-bearing capacity are rarely evaluated in detail.

The main goal of this research is to reliably determine the actual contribution of lattice girders and steel ribs to the long-term structural performance of the primary tunnel support. The central question is: under what conditions can these elements be considered relevant to the tunnel lining's permanent load-bearing capacity, and how can their role be properly integrated into design analyses according to specific geological conditions?

4.1. Practical challenges observed on construction sites

In recent years, tunneling practice has increasingly diverged from standard design assumptions. It is becoming common to install multiple lattice girders within a single excavation step, regardless of actual ground stability. In many cases, lattice girders and steel ribs are placed without proper contact or bearing on the surrounding rock, effectively eliminating their intended structural function. Moreover, these elements are often not included in structural calculations, with important factors such as joint detailing, load transfer, and construction staging being overlooked. A critical issue is also the frequent discontinuity in the shotcrete lining at the locations of large steel elements, where poor embedding and lack of confinement reduce the composite action and compromise the support system's stiffness.

(**a**) (**b**)

Fig. 2. (a) Primary support without anchors and propiate temporary foundations; (b) Installing multiple steel ribs in the stable ground with no stiff support on the ground.

4.2. Configuration examples and setup observations

As part of a broader investigation into the structural role of steel elements in NATM primary lining, several configurations of lattice girders, steel ribs, and conventional reinforcement were prepared and tested in order to illustrate typical integration approaches used in tunnel support systems. These configurations were intended not only to demonstrate the geometric variability and potential implications of steel elements embedded in shotcrete, especially in conditions where anchoring systems underperform or cannot be fully mobilized due to poor ground quality, but also to directly compare their structural efficiency.

Figures 3a, 3b, and 3c show representative stages of the preparation and testing process, including the arrangement of lattice girders and steel ribs in moulds, shotcrete application, and subsequent laboratory testing of full-scale specimens.

(a) **(b)** **(c)**

Fig. 3. (a) Lattice girder, steel ribs and reinforcement in the moulds; (b) Shotcrete aplication; (c) Labaratory testing.

The experimental results indicated that specimens reinforced only with conventionally placed reinforcement bars achieved the most favorable performance (Table 1), both in terms of stiffness and ultimate load-bearing capacity. In contrast, configurations with large lattice girders or massive steel ribs often exhibited reduced composite action due to incomplete shotcrete encapsulation and the presence of shadow zones, as confirmed by visual inspection. These outcomes suggest that while lattice girders and ribs can provide immediate stabilization and geometric control during construction, their long-term contribution to the structural capacity of the lining is limited compared to well-detailed conventional reinforcement.

Table 1. Testing results of concrete beams with different types of reinforcing

Type heading	Shape heading	Maximum force kN	Deflection mm	Sample collapse
T70-1	1-piece lat. girder	196	5.72	Yes
T70-2	2-piece lat. girder	110	4.38	Yes
T190-1	1-piece lat. girder	200	3.43	No
T190-2	2-piece lat. girder	199	17.46	No
HEB140-1	1-piece steel rib	197	4.56	No
HEB140-2	2-piece steel rib	120	11.93	Yes
HEA200-1	1-piece steel rib	196	4.44	No
HEA200-2	2-piece steel rib	83	11.69	Yes
RB-1	reinforcement bars-1-piece	200	3.89	No
RB-2	reinforcement bars-overlap	200	3.02	No

4.3. Visual inspection

Following the preparation and casting of concrete specimens with integrated steel components, a detailed visual inspection was carried out on cross-sections of the hardened shotcrete. The objective was to assess the quality of concrete placement and the degree of encapsulation around the steel elements.

The inspection revealed that large-profile steel ribs, particularly those with closed geometries or dense configurations, frequently acted as barriers to uniform shotcrete application. In several cross-sections, unfilled zones were observed along the sides and beneath the horizontal flanges of the ribs, indicating incomplete encapsulation of the steel elements by the shotcrete. These localized voids, commonly referred to as *shadow zones*, compromise the composite behavior of the lining by reducing stiffness and creating potential weak points in the support system.

By contrast, in specimens reinforced only with conventionally placed reinforcement bars, the shotcrete demonstrated excellent continuity and full encapsulation of the reinforcement. The absence of shadow zones resulted in more homogeneous stiffness across the section, which directly translated into higher load-bearing capacity and better overall performance, as confirmed by laboratory testing.

This comparative outcome clearly explains why specimens with conventional reinforcement achieved the best results, while those with lattice girders or heavy steel ribs underperformed due to difficulties in ensuring proper shotcrete confinement and structural integration.

(**a**) (**b**)

Fig. 4. (a) Steel rib HEA 200 sample; (b) Reinforcement sample.

5. Numerical modeling of the primary lining concrete shell

To better understand the behavior of the composite tunnel lining system consisting of a reinforced concrete shell supported by anchors, a detailed finite element model was developed using *Autodesk Robot Structural Analysis 2025*. The primary lining was represented as a continuous shell structure, simulating the shotcrete layer applied in NATM tunneling. This model was not intended as a direct

complement to the experimental tests but rather served as an independent tool for illustrating the structural interaction between the concrete shell and the anchoring system.

In the model, anchors were idealized as fixed point supports, assuming full load transfer and no relative displacement with respect to the surrounding ground. This reflects the theoretical condition in which the anchor heads are embedded deeply enough into the surrounding rock mass - beyond the plastic zone to act as effective restraints for the lining. The geometry of the model was simplified and assumed an idealized, smooth concrete shell without surface irregularities such as peaks or depressions. Anchors were modeled as the only fixed support points to the shell structure, simulating full fixity and perfect load transfer.

However, to achieve such an effect in real conditions, it is essential to define the extent of the plasticized zone around the tunnel excavation, particularly in weak or fractured ground. Anchors must be designed with sufficient length to extend beyond this plastic zone (see Figure 5), thus ensuring that the reactive zone into which they transfer load has not lost its mechanical integrity. If anchors are embedded only within the plastified ground, their stiffness and support capacity are significantly reduced, resulting in deformation and loss of control over lining stability.

The deformation field of the shell under uniform ground loading is shown in Figure 5a. The results indicate non-uniform displacement patterns, with pronounced local warping near anchorage points. These deformation modes deviate significantly from the smooth, parabolic curvature assumed in simplified arch models, and reveal the complex behavior of reinforced shotcrete linings under localized support.

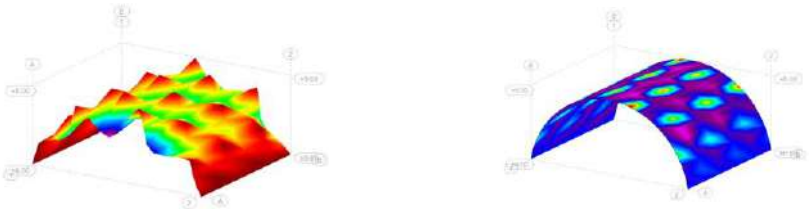

(**a**) (**b**)

Fig. 5. (a) Defomed shape of tunnel primary lining with anchors; (b) Bending moments of tunnel primary lining with anchors.

These findings align with the observations of Nilsson and Holmgren (1999), who emphasized the influence of anchor placement relative to surface geometry. When bolts are placed in depressions, the system develops high tensile stresses and loses global stiffness due to localized deconfinement. In contrast, bolts placed on geometric peaks lead to improved load transfer and higher overall capacity. This effect is especially relevant in thinner linings where surface irregularities strongly influence structural performance.

The bending moment distribution over the shell surface, shown in Figure 5b, further reveals stress concentrations around anchorage zones. These peaks result from local stiffening effects introduced by the concentrated support, and must be considered in design to avoid punching failure, excessive cracking, or deterioration of the lining system over time.

In summary, although the presented numerical model assumes ideal conditions perfect fixity, smooth surface geometry, and no anchorage deformation it provides important insight into stress behavior and the need for realistic representation of ground–lining interaction. For anchors to serve as true structural supports in NATM linings, their design must be based on geotechnical definition of the plasticized zone and anchorage beyond this zone, ensuring proper load transfer and effective integration with the concrete shell.

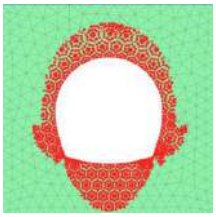

Fig. 6. Determination of plastic zone by Plaxis 2D.

5.1. Time-Dependent Behavior of Shotcrete and its Structural Implications

While the numerical model considers the concrete shell as an already stiff structural body supported by fully mobilized anchors, this assumption is only valid if shotcrete reaches sufficient strength within a short time frame. According to EN 14487-1:2005+A1:2007, structural shotcrete must achieve 100% of its design compressive strength within 24 hours when an appropriate accelerator is used.

Figure 7 shows a typical strength development curve of shotcrete (C25/30) with an alkali-free accelerator. As can be seen, the concrete reaches approximately 70-80% of its design strength within the first 8-12 hours. This rapid gain in stiffness implies that, unless the installation of steel ribs and anchoring systems is completed in significantly less time, the shotcrete itself begins to act as the primary structural element relatively early in the construction sequence.

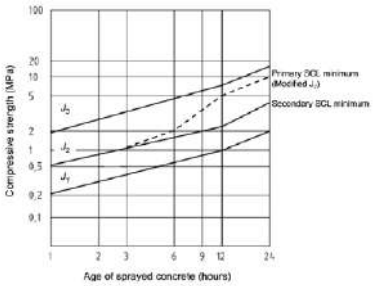

Fig. 7. Compressive strength development of C25/30 shotcrete with alkali-free accelerator over the first 24 hours (adapted from EN 14487-1 and manufacturer data).

This finding is particularly relevant in cases where steel elements are intended to serve only as temporary supports. If the shotcrete is properly applied and adequately reinforced, it can absorb and redistribute loads efficiently even before full anchor mobilization, reducing the need for rigid steel components in many situations.

6. Validation

To validate the findings of the numerical simulations, field monitoring from the Iriški Venac (Serbia) tunnel was used, executed in a zone of severely fractured siltstones (alevrolites) and claystones, characterized by unfavorable geotechnical conditions and very high deformation rates.

The monitoring results (Figure 8) show that even after the installation of two successive anchor series (6 m and 8 m), the tunnel deformations continued almost linearly and could not be stabilized. The anchors, although installed according to design specifications, did not provide sufficient restraint capacity because their embedment remained within the plastified zone of the ground. Consequently, the intended interaction between the shotcrete lining and the anchoring system was not achieved.

Convergence stabilization occurred only after the closure of the invert and the formation of a continuous circular reinforced concrete lining that provided a rigid support ring to the entire tunnel contour. This

observation is fully consistent with the numerical model assumptions: once the anchors lose effectiveness in highly fractured ground, structural responsibility shifts to the concrete shell, and overall stability is restored only when a closed ring effect is established.

It is important to emphasize that sufficiently stiff steel ribs or lattice girders, if properly connected into a closed circular frame either immediately after excavation or with adequately secured temporary footings can significantly enhance the load-bearing capacity of the primary support. In such cases, the rigid ring action can be mobilized earlier, reducing deformation rates and providing a more reliable transfer of loads to the surrounding ground. However, when ribs or girders are discontinuous, poorly supported, or left without proper closure, their contribution remains marginal and deformation control relies almost exclusively on the shotcrete shell.

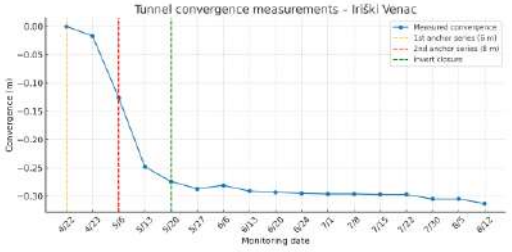

Fig. 8. Time-Convergence diagram in the tunnel Iriski Venac (testing profile).

7. Conclusion

One of the persistent dilemmas in tunneling engineering concerns the true structural contribution of lattice girders and steel ribs in NATM primary linings. The most recognized international guidelines consistently classify these elements as *temporary supports*, intended to maintain excavation stability only until the shotcrete lining and anchoring system has become structurally effective.

The Austrian Society for Geomechanics (2010) clearly states: *"The typical support elements in NATM are shotcrete and rock dowels. Steel ribs or lattice girders provide limited early support before the shotcrete hardens and ensure correct profile geometry."*

Similarly, the U.S. Department of Transportation Federal Highway Administration (2009) notes that while lattice girders have small cross-sectional areas relative to the shotcrete thickness, they fulfill several essential functions:

- providing immediate support to unstable rock blocks prone to falling out,
- offering a precise geometric template for shotcrete application,
- serving as carriers for welded mesh reinforcement, and
- acting as rigid anchors for preliminary measures such as forepoling.

Finally, Wittke et al. (2002) emphasize the time-dependent interaction between steel ribs and shotcrete: *"Immediately after the steel set is installed and covered with shotcrete, when the shotcrete still has a very low Young's modulus, it is mostly the steel set that carries the loads resulting from rock mass pressure. With the hardening of the shotcrete over time, the strength and bearing capacity of the shotcrete membrane increases. Finally, when the shotcrete has fully hardened, the normal stiffness of the steel sets can be neglected compared to that of the shotcrete membrane."*

These authoritative references consistently underline the temporary role of steel ribs and lattice girders. Moreover, practical evidence often confirms that their presence may even reduce the effective stiffness of the lining at the contact zones, as illustrated in Figure 4a, where massive steel ribs prevent proper shotcrete encapsulation and create shadow zones.

Yet, field experience and monitoring in extremely unfavorable ground conditions demonstrate that this interpretation is not universally valid. When tunneling advances through severely fractured or incoherent ground, the installation of sufficiently stiff steel ribs, arranged at short spacing and connected into a closed circular frame, can significantly enhance stability. Under such circumstances, rigid frames provide immediate load-bearing continuity around the excavation contour and may serve as the decisive element preventing excessive deformations until the shotcrete gains sufficient strength.

The contrasting examples shown in Figures 2a and 2b further highlight this ambiguity: in one case multiple ribs are installed in stable ground where they provide no structural benefit, while in another case stiff ribs become essential in controlling deformation in weak rock. Similar contradictory findings can be observed in many tunneling projects worldwide, underlining the necessity of case-specific evaluation rather than universal classification.

This study, therefore, concludes that:

In standard NATM applications and competent ground conditions, lattice girders and steel ribs should be regarded as temporary stabilizers, with negligible long-term contribution once the shotcrete shell has hardened.

In exceptionally poor geological conditions, where anchors cannot mobilize their capacity and shotcrete alone is insufficient, rigid and continuous steel frames may transition into elements of primary structural relevance, particularly when integrated into a closed ring action.

- the decisive factors governing their effectiveness are:
- proper closure of the ring (invert included),
- adequate stiffness and joint continuity, and
- quality of shotcrete encapsulation.

Finally, this research underlines the need for systematic investigation to establish clear thresholds for when lattice girders and steel ribs meaningfully contribute to the structural capacity of the lining. Only through an integrated approach combining laboratory testing, numerical modeling, and field observations can reliable criteria be developed for their rational use. Such criteria are essential to eliminate current uncertainties in tunneling practice and to ensure reliable and economical NATM designs.

References

Australian Tunnelling Society, 2024. Tunnel design guideline, (2nd edition). ISBN 978-1-925627-48-0

Austrian Society of geomechanics, 2010. *NATM – The Austrian Practice of Conventional Tunneling, Austrian society of geomechanics*, ISBN 978-3-200-01989-8

Collotta, T., Barbieri G., Mapell, M., 2010. Shotcrete tunnel linings with steel ribs: Stress redistribution dueto creep and shrinkage effects, Taylor & Francis Group, ISBN 978-0-415-47589-1

Chapman, D., Metje, N., Stark, A., 2010. Introduction to tunnel design, Spon press, ISBN 0-203-89515-0

Kovačević, J., 2014., Savremeno građenje u podzemlju, AGM Knjiga, ISBN 978-86-86363-45-9

Nye, E. J., Alt, D., 2010. Shotcrete application on the Boggo Road Busway driven tunnel, Taylor & Francis Group, ISBN 978-0-415-47589-1

U.S. Department of Transportation Federal Highway Administration, 2009. Technical Manual for Design and Construction of Road Tunnels — Civil Elements, Publication No. FHWA-NHI-10-034

Nilsson, U., Holmgren, J., 1999. *Design of steel fibre reinforced shotcrete linings In Nordic Concrete*

Wittke, W., Pierau, B., Erichsen, C., 2002. New Austrian Tunnelling Method (NATM) – Stability Analyses and Design (Geotechnik in Forschung und Praxis, WBI-Print 5). Verlag Glückauf, Essen. ISBN 3-7739-1305-2.

Southeastern Europe Tunnelling Conference (SETC-2025)
1-3 October 2025, Belgrade, Serbia

DOI: 10.5937/SETC25004D

Adaptation of tunnelling technical solutions to urban conditions: Case study Sava - Danube slope Tunnel

Nikola Divac[a], Slobodan Radovanović[a], Jovan Šaponjić[a], Uroš Mirković[a], Nikola Mirković[a] and Dejan Divac[a]*

[a] Jaroslav Černi Water Institute, Belgrade, Serbia; nikola.divac@jcerni.rs, jovan.saponjic@jcerni.rs, uros.mirkovic@jcerni.rs, slobodan.radovanovic@jcerni.rs, dejan.divac@jcerni.rs.

Abstract: Tunnelling in urban conditions is often met with demanding criteria for surface settlement control, the limitation which is arising from the fact that most of the urban area is occupied by structures which are sensitive to deformations, such as buildings, roads, communal infrastructure etc. Another important necessity in any project is to deliver the project in shortest amount of time possible. Temporary occupation of public areas for construction sites and traffic congestions alleviate social pressure which further emphasizes these requirements. If planned correctly, TBM technology promises to deliver on these requirements more readily than conventional tunnelling techniques. In this paper a Case study of Belgrade's double tube traffic tunnels is presented, in which project design went through significant conceptual transition, led by the designer's idea to change the technology of excavation from conventional to TBM, as well as to adjust the project in multiple ways to accommodate for this major turn of tides. Most notable historic background of the project is presented. Geotechnical profile of tunnels and data are shown and calculations for both TBM and conventional variants are presented and discussed.

Keywords: shield TBM; urban tunnelling; numerical modelling; sensitivity analysis; ground settlement; structural response

1. Introduction

The construction of tunnels in urban areas is the only way to transfer traffic underground in order to reduce congestion and pollution in cities that face increasing growth of population. Geological conditions affect the behavior of the tunnel during construction, as well as the impact of construction on surrounding structures and the environment. Major difficulty in urban tunneling is to minimize the impact of construction on surrounding structures and the environment, to avoid damaging the buildings and infrastructure. In modern tunnel construction, various structural and technological measures are applied for ensuring safety of operations during tunnel construction and to reduce the ground disturbance. Contractor, Designer and Investor get to choose between conventional construction methods such as NATM or ADECO-RS, and Tunnel Boring Machine (TBM method). At an increasing rate, especially in urban environments choice is made to use TBM method due to its undeniable advantages over conventional construction methods as a more reliable option which allows for safer operations and improved control over soil disturbance.

A project development of Belgrade traffic tunnels connecting Sava and Danube slope is examined and discussed as an example of mutual influence of tunnelling technology choice and design solution. A name "tunnel connection of Sava and Danube banks" describes the purpose of the project, which is to relieve traffic on main streets (Kneza Milosa and Takovska) in the city core that currently serve as a connection between New Belgrade, a major part of the city on the left bank of Sava river and Karaburma and other city districts both South and North of the Danube river. Urban plans call for two tunnel tubes, each with two traffic lanes. City core plan is shown from the orthophoto plan view in Fig. 1.

*Corresponding author: nikola.divac@jcerni.rs (N. Divac).

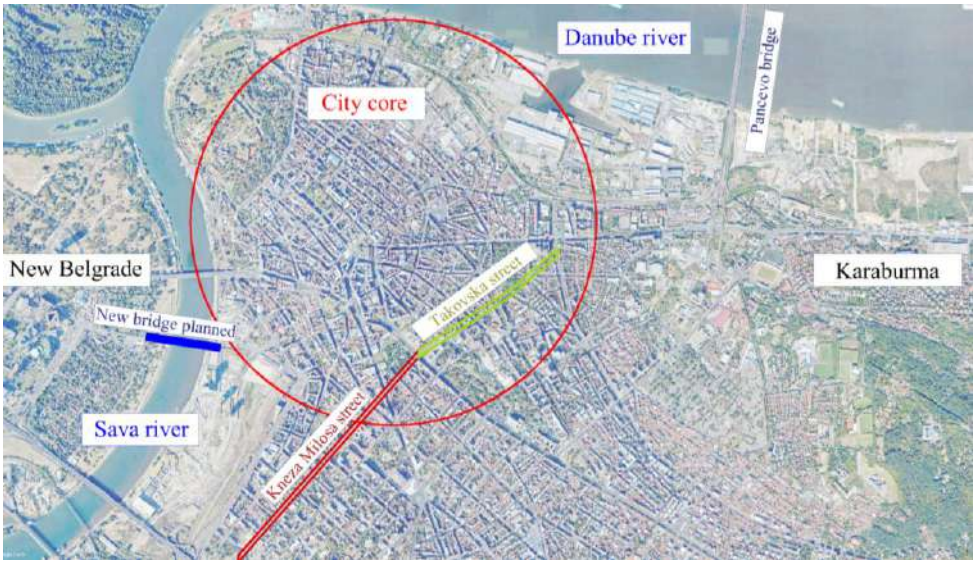

Fig. 1. Belgrade city core disposition.

Currently, the project is in transitioning state, awaiting annex of the contract between Government of Serbia and contractor PowerChina which would set up the project for both the new tunnel trajectory and TBM tunnelling technology instead of existing contract which planned a solution based on conventional tunnelling approach.

The sequence of events and prime motivators for this course change of the project are shown in following order:

- Project history – most notable moments in the long-lasting background of the project are described.
- Geotechnical conditions – objectively most influential factor when deciding on tunnelling technology.
- Conventional tunneling analysis showcase – detailed 3D FEM analysis of variant solutions that greatly influenced the adoption of TBM solution.
- TBM proposal – derived from two most recent documents, a Study which formally initialized the idea and set up an organizational pathway towards TBM-based solution agreement, and Technical Design which serves as a baseline document for the forthcoming contract annex.

2. Project history

A substantial history can be traced back to the development of the idea of the traffic tunnel beneath the heart of Belgrade in the era after World War 2. First geological investigations and even tunnel excavation works took place in 1950s. This infamous tunneling attempt was stopped early after only a few dozen meters had been breached, as observations on the surface indicated too much deformation that threatened to collapse the existing buildings above the tunnel (Stepanovic and Perić, 1961).

During 1960s more investigation works and more than one geotechnical study was conducted as an attempt to restart the construction works. These studies often criticized results of the studies which predated them, most likely due to severity in the atmosphere imposed by the failure of the first tunneling attempt. One of the interesting notations from the critics in these reports emphasized importance to reduce ground disturbance and even stated as the fact that the tunneling in most critical zones must be done with the shield technology. Nevertheless, ambition to construct a single tunnel tube, soon to be followed by another one, still existed. Moreover, the plans suggested that a third tunnel should be built

to accommodate tram traffic. None of these plans came to fruition and the project was abandoned during the nation's prosperous decades of 1970s and 1980s, likely as the result of common opinion between the experts in the field of tunneling from the time, being that the project risk was too high. Succeeding decade of 1990s was marked by wars and nation's decline during which little infrastructure was developed, while 2010s transitional years saw the idea of the tunnel only as a distant memory with no real effort put into its materialization.

Fig. 2. Portal zone of the tunnel from 1950s (Source: Kaldrma, 2023).

In recent history of 2010s, the idea is brought back to the table by the City authorities, and with a fresh start the decision was made in 2015 for the city planners to analyze the variant solutions of the tunnel trajectory and portal position on the Danube slope side (Figure 3), with more or less fixed location of the portal on the Sava slope side, which through further project development, proved to have become a prerequisite governed by the trajectory of the new bridge connecting left and right bank of Sava river (Krstić and Mihajlović, 2015).

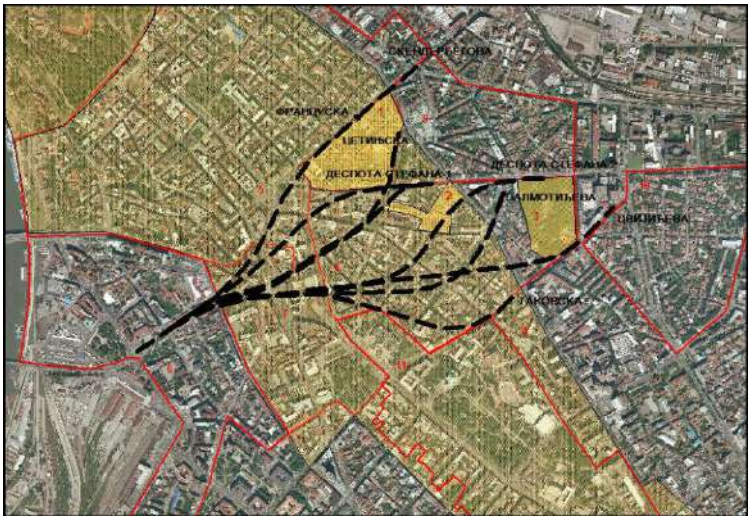

Fig. 3. Tunnel variant solutions (Source: (Krstić and Mihajlović, 2015).

From eleven proposals, the solution was adopted which differentiated somewhat from the one proposed several decades ago. For once, a portal on Danube slope side was put further away. Secondly, the tram idea was put away and solutions called only for two tunnels, each with two traffic lanes.

Conceptual Design was at first trusted to Ces-Cowi consortium (2016) and subsequently to GEOPUT (2022). As an aftermath of the proposed technical solutions, a minor position adjustment of portal on Sava slope was examined. A working group was formed and strategic decision was made which moved the portal slightly closer to the river, thus avoiding substantial expropriation obligations and costs. The secondary strategic move was to formally consider development of the project in conjunction with another important project – namely replacement of old Sava Bridge that is of cruical importance in connecting New Belgrade on one side of the river and the tunnel connection on the other side.

Based on the existing Conceptual Design and the strategic decisions made by the Working Group, a contract between Government of Serbia and PowerChina corporation as a design and build type of contract has been made.

Further development of the project, in the form of another Conceptual Design, is showcased more closely in section 4 and latest advancements in section 5 as a Study and Technical project that pose to adapt the design towards TBM construction.

3. Geotechnical conditions

Geotechnical investigation works were carried out on several occasions, dating back to 1950s attempt at the project. Latest works were carried out as part of the active contract agreement between Serbia Government and PowerChina Corporation (2023). Contractor assigned Jaroslav Cerni Water Institute for execution of investigation works and delivery of geological study (JCWI, 2023). Geological study consists of, among others, reports on geotechnical conditions from which some of the results will be interpreted in this chapter.

Majority of soil is composed of uneven layers of marly sediments mostly in loose form with some of the layers had hardened into marlstones. This implies to all possible tunnel trajectories, though depending on proposed trajectories, appearance of very porous Miocene limestones may happen sporadically on the tunnel path. Quaternary deposits occurrence is present only in portal zones. For tunneling phase, the focus is set on marly-clayey soil type. Ranges of soil physical and mechanical properties are shown in Table 1 and geotechnical profile in Figure 4. These properties come as the interpretation of laboratory and in situ investigations published in the Geological Study. Mohr-Coulomb failure criterion is used and Modulus of elasticity for both load and unload-reload stress path are extracted to be further used in numerical analysis as main input data necessary to define Hardening Soil constitutive model. All properties are for the drained conditions. Other parameters such as Poisson's ratio ν, Coefficient of earth lateral pressure K_0, constitutive model specific parameters such as reference pressure p_{ref}, stiffness/stress power factor *m* are also important for proper interpretation of the problem. The scope of this work though, is mainly to present the most important influencing factors, results and methodology that played part in decision making throughout the project.

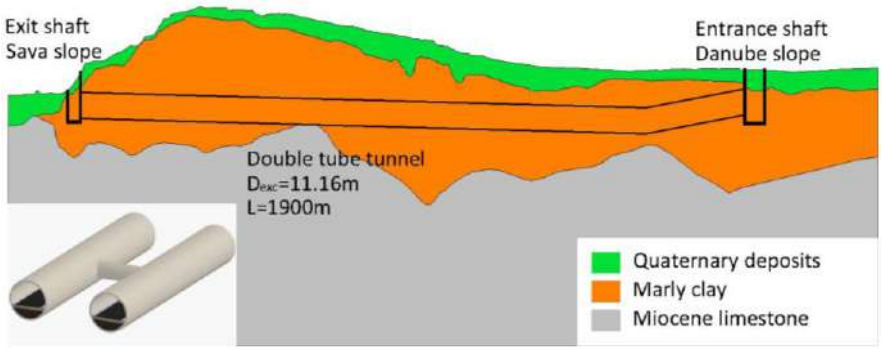

Fig. 4. Simplified presentation of geotechnical profile for one of the solutions. The profile shown in the Figure corresponds to the latest trajectory proposed for the TBM tunnel.

Table 1. Range of mechanical properties for each type of soil in drained conditions.

Soil type	Marly clay	Quaternary deposits	Limestone
c (kPa)	5-100	0-10	200-500
φ (°)	18-30	30-35	30-35
E (kPa)	20-100	100-500	100-500
E_{ur} (kPa)	50-300	400-1500	300-1500
Permeability	Low	Medium-High	High

4. Conventional tunnelling analysis showcase

A Conceptual Design (JCWI, 2023) mentioned in the last paragraph of chapter 2 took the existing premises of conventional tunnelling approach. In this endeavour, 6 structural types (with additional subtypes) were analysed in various soil conditions using 3D Finite Element Analysis. Each structural type implied using different reinforcement type, excavation and reinforcement installation sequences. All structural types and subtypes are shown in Fig. 5.

4.1. Finite element model

All structural types but type 6 were tested in multiple conditions that varied both mechanical characteristics of the soil and overburden and water level above tunnel. Structural type 6 was analysed after the fact, being the most complicated and rigorous tunnelling sequence, with the idea to analyse the best-case scenario in terms of safety and surface settlement reduction regardless of efficiency of excavation, which in case of sequential excavation of type 6 is quite poor.

Soil is modelled with Hardening Soil constitutive model. Terrain surface is simplified as flat. Dimensions of the model are L x W x H(varied) = 140 x 100 x (70-100) m. One soil material is used for the whole volume of the model, the one which mostly represents Marly-Clayey soil, though by varying parameters in the analysis within the specified range does allow for perceiving a wide palette of possible ground conditions and soil varieties.

Table 2. Varied parameters in numerical analysis of different structural types.

	Varied Hardening Soil parameters				
Parameter set	Modulus at 50% of peak triaxial strength	Oedometer Modulus	Unload-Reload Modulus	Cohesion	Friction angle
	E_{50}^{ref} (kPa)	E_{oed}^{ref} (kPa)	E_{ur}^{ref} (kPa)	c'$_{ref}$ (kPa)	φ (°)
1	20 000	20 000	60 000	10	20
2	40 000	40 000	120 000	20	25
3	60 000	60 000	180 000	40	27
4	100 000	100 000	300 000	70	30
	Varied overburden [water level] height measured from top of the tunnel (m)				
1	10m overburden [-20, 7m water level over top of the tunnel]				
2	25m overburden [-20, 13, 20m water level over top of the tunnel]				
3	40m overburden [-20, 20, 33m water level over top of the tunnel]				

Type 1 – Sprayed concrete 30cm, Steel braces IPB200 at 1m, Radial steel anchors d=32mm L=6m, Fiberglass anchors at the face L=12m. Used only for tunneling in rock conditions.

Type 2 – Sprayed concrete 30cm, Steel braces IPB200 at 1m, Grouted Steel pipe umbrella arch Ø114 (t=6mm) L=12m, Fiberglass anchors at the face L=12m. Used only for tunneling in rock conditions.

Type 3 – Sprayed concrete with 30cm or 40 cm thickness, Temporary invert for upper bank excavation, Steel braces IPB200 at 1m, Grouted Steel pipe umbrella arch Ø88 or Ø250 (t=6mm) L=14m, Fiberglass anchors at the face L=12m

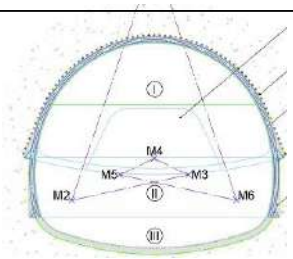

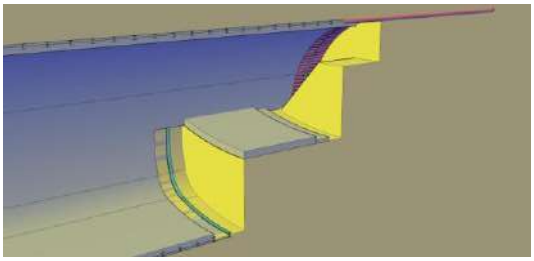

Type 4 – Sprayed concrete 30cm or 40cm, Steel braces IPB200 at 1m, Grouted Steel pipe umbrella arch Ø300 or Ø600 (t=6mm) L=16m, Fiberglass anchors at the face L=12m

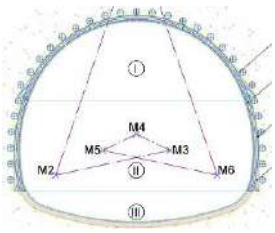

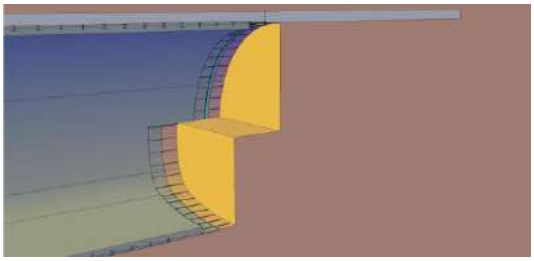

Type 5 – Sprayed concrete 30cm or 40cm, Steel braces IPB200 at 1m, Grouted Steel pipe umbrella arch Ø300 or Ø600 (t=6mm) L=16m, Fiberglass anchors at the face L=12m. Similar to Type 4, except that pipes encircle the excavation face completely and bigger piles of Ø600 are analyzed as well.

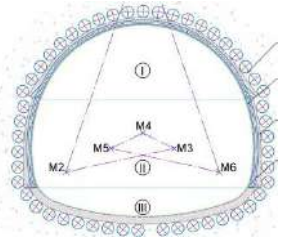

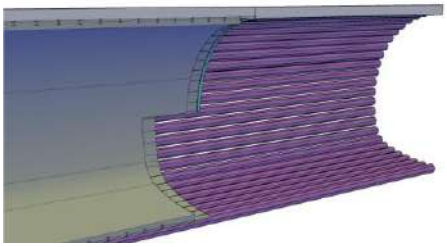

Type 6 – Sprayed concrete 40cm, Steel braces IPB200 at 1m, Grouted Steel pipe umbrella arch Ø250 (t=6mm) L=12m, Fiberglass anchors at the face L=12m, 6 excavation steps in a sequence.

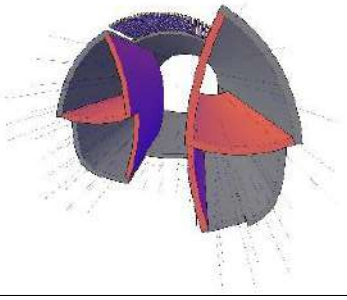

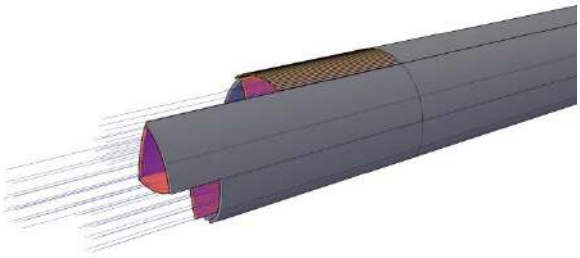

Fig. 5. Structural types parametrically analyzed in the design.

Numerical models consider one tube and are mostly modelled as symmetrical models. Structural elements are all modelled in following manner:

- Sprayed concrete – plate elements
- Fiberglass face anchors – linear beam elements
- Steel braces – linear beam elements
- Radial Anchors – linear beam elements
- Pipe umbrella – linear beam elements or combination of 3D elements (grouted pipe interior) and plate elements (steel pipe wall)

Calculation steps are designed in a way that realistically represents sequencing of operations during tunnelling, i.e. activation and deactivation of each structural element in conjunction with volume excavation (deactivation). Analysis was done with Plaxis 3D software. Detailed modelling and procedure will not be explained thoroughly since the purpose of the model showcasing in this article is only to present results in a manner which gives better perspective on broader picture of project development.

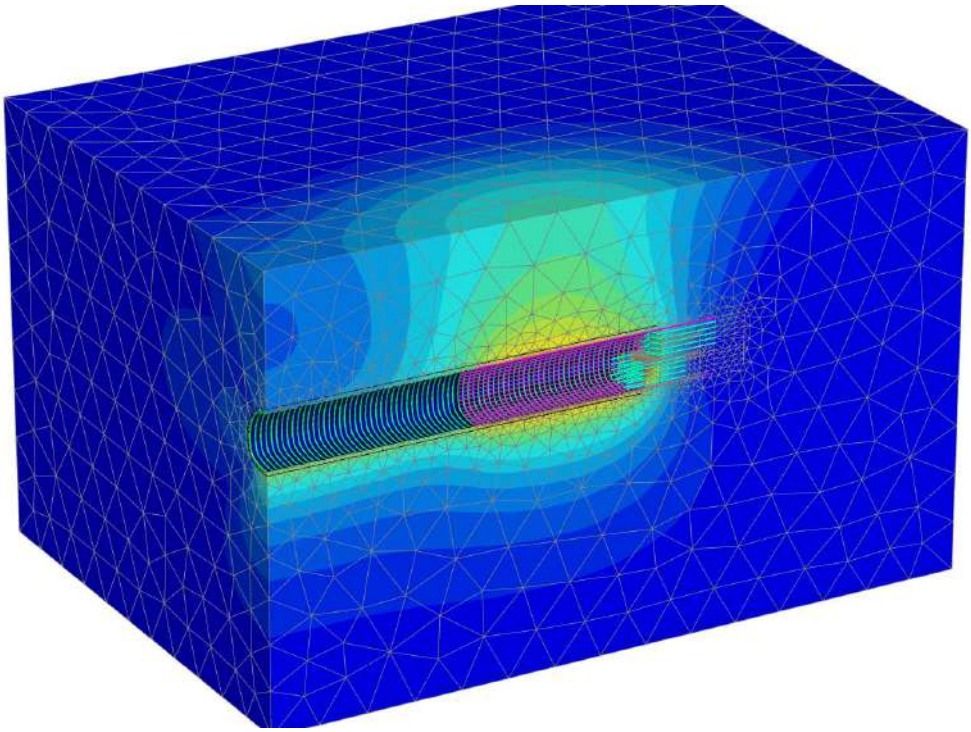

Fig. 6. 3D Numerical model of structural type 5 showing total deformations in the model.

4.2. Analysis results

In Table 3 the surface settlement and structural type dependency is shown for:

- Overburden height of 40m
- No groundwater
- Soil parameter set 2

Table 3. Settlement dependency on structural type used in calculations.

Structural type	Maximum surface settlement (mm)
3a	56
3b	49
4	47
5a	44
5b	37
6	30

The most rigorous method of tunnelling show significantly increased the safety of excavation and excavation volume loss, resulting in lesser surface settlements. One of the most influential factors on surface settlement is of course strength of the soil. Results of settlements shown for parameter set 2 are agreeable to a degree, given the proper choice of excavation sequence and structure.

In Table 4 is shown how different overburden and parameter set influences settlement, for a given structural type (type 3a) and no groundwater conditions.

Table 4. Settlement dependency on parameter set and overburden used in calculations.

Parameter set	Overburden (m)	Maximum surface settlement (mm)
1	25	166
	40	151
	10	124
2	25	67
	10	59
	40	56
3	25	39
	10	37
	40	34
4	25	23
	40	20
	10	20

The results are further greatly influenced by groundwater level which has been considered in numerical models through coupled seepage analysis with the assumption that steady state draining conditions are formed on face surface of the tunnel. Surface settlement dependency on groundwater conditions is shown through Table 5.

Table 5. Settlement dependency on groundwater conditions.

Parameter set	Water level height from top of the tunnel	Structural type	Maximum surface settlement (mm)
2	20	5 (liner 40cm, pipes 300mm)	119
	13		82
	below tunnel		47
2	20	5 (liner 40cm, pipes 300mm)	65
	13		47
	below tunnel		28
3	20	5 (liner 40cm, pipes 600mm)	62
	13		45
	below tunnel		25
4	20	5 (liner 40cm, pipes 300mm)	35
	13		25
	below tunnel		18

While resulting settlements vary greatly on adopted parameters, such parametrically generated models give broad impression on project's possible outcomes and are very representable for the whole project in which soil material can mostly be generalized as one soil type with different ranges of mechanical properties.

Ground movement has been used for this purpose as the main indicator for quality of tunneling solutions in urban areas. In different conditions, i.e., where no threat exists to damage the urban infrastructure such information provides little value. Considering the unsuccessful historical attempts, very dense urban conditions along tunnel trajectories, complexity of proposed solutions and possible outcomes of the analysis which suggest likeliness that significant further expenses and effort should be put in ensuring that no damage is dealt to the existing infrastructure, the decisions and actions were made to convert the tunneling technology to TBM.

5. TBM proposal and analysis showcase

Similar approach to NATM analysis was adopted for TBM. In this manner, soil parameters were adopted and are shown in Table 6. It can be noted that parameter sets coincide with previously used sets with addition of parameter set with even lower properties and exclusion of parameter set with highest properties.

Table 6. Settlement dependency on groundwater conditions.

	Varied Hardening Soil parameters				
Parameter set	Modulus at 50% of peak triaxial strength	Oedometer Modulus	Unload-Reload Modulus	Cohesion	Friction angle
	E_{50}^{ref} (kPa)	E_{oed}^{ref} (kPa)	E_{ur}^{ref} (kPa)	c'_{ref} (kPa)	φ (°)
1	10 000	10 000	30 000	1	20
2	20 000	20 000	60 000	10	20
3	40 000	40 000	120 000	20	25
4	60 000	60 000	180 000	40	27
	Varied overburden [water level] height measured from top of the tunnel (m)				
1	10m overburden [-20, 7m water level over top of the tunnel]				
2	25m overburden [-20, 13, 20m water level over top of the tunnel]				
3	40m overburden [-20, 20, 33m water level over top of the tunnel]				

Pressure balance TBM technology relies on actively keeping soil in balance by exerting pressure both on face of the excavation through pressure chamber of the cutterhead and by injecting grout inside the annular gap between the erected concrete structure and soil surrounding the structure. Grouting operation takes place immediately behind the shield, as the machine moves and "reveals" latest erected segmental ring behind the steel shield of the machine. If needed, additional pressure can be applied through holes on the shield with bentonite medium to further help in keeping the soil in balance and reduce the volume loss of the excavation. These actions act in conjunction with other processes that also need to be precisely controlled, such as torque application, hydraulic pistons advancement rate, screw conveyer extraction rate etc.

Applying the right actions in right amount at the same time is the task of the TBM machine and TBM operator, one that can be extremely complex and sensitive to error if soil conditions are challenging and urban tunnelling requirements rigorous. If done properly though, TBM technology promises to achieve better results in controlling volume loss during excavation and thus provide better alternative for tunnelling in urban areas.

Numerical (or analytical, for that matter) modelling of such complex processes often requires certain assumptions to be made. Depending on the required output of the analysis, these assumptions can lead

to results which can be both conservative and non-conservative at the same time, i.e. calculations which lead to overestimated volume loss often underestimate forces in the structure. As so, few modelling assumptions have been made in an endeavour to simulate TBM tunnelling process for the design of this project. It is shown how some of these assumptions can achieve results which represent somewhat conservative application of TBM tunnelling from the standpoint of surface settlements. The model is briefly described prior to presentation of the results in order to supplement the manner in which the realistic problem of TBM tunnelling sequence is interpreted in the model.

Firstly, pressure on the face of the excavation is achieved with surface load. This parameter was varied through parametric analysis and is always active on the face of the tunnel excavation, as shown on Figure 7.

Secondly, gap between tail shield external diameter and excavation diameter is achieved by radial contraction of the shield as the shield advances through sequences (each step being equal to length of segmental ring). This is achieved with gradual application of tangential contraction on plate elements that are used as shield structure (Figure 7). Interface elements are used on surface elements of the shield. This allows for different displacements on nodes which coincide on both surface elements and soil elements so that no bogus tension forces are induced, neither in shield nor in soil elements.

Lastly, grouting pressure is induced in a single step behind the tail of the shield as radial pressure. With this, assumption is made that pressure as such has effect on surface settlements while it is in fluid form and while pressure in fluid exists. This pressure is parametrically varied along with face pressure. As soon as advancement is made and the next calculation step is started, the pressure is removed and it is assumed that the grout has hardened enough so that its strength is greater than the properties of the soil, which in the case of the project is very likely considering ranges of possible properties of the soil and hardening time of two component grout.

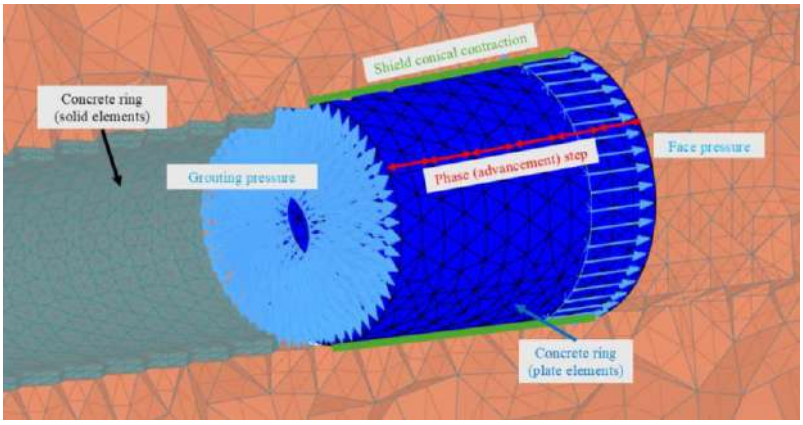

Fig. 7. TBM numerical model components.

All models, unlike in NATM analysis, consist of two tunnel tubes. Each tube advances for amount of 20 steps, which equals 40 meters in terms of length. This makes each calculation take 40 advancements steps, since tunnels start one after the other rather than at the same time.

Presented as a chart on Figure 8 are maximum surface settlements for different soil conditions and pressure/grout pressures. Results are shown for overburden of 40m and with no groundwater present above tunnel. First three columns for each soil parameter set represent results of surface settlements for conicity of the shield modelled as per manufacturers specification. Fourth, fifth and sixth column represent results of surface settlements in which conicity is zero i.e. if no convergence is allowed to happen either by the use of bentonite or actually designing the shield with zero conicity and no overcut.

Machines are generally not designed with zero clearance since this clearance is necessary for the machine to turn efficiently.

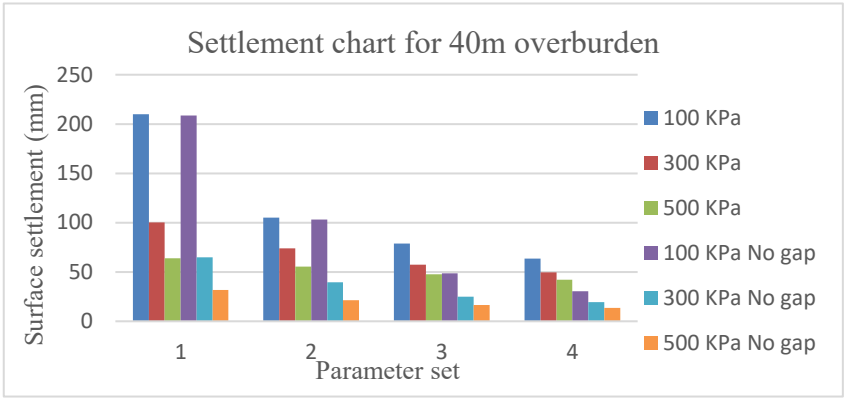

Fig. 8. Surface settlements for different soil conditions and face/grouting pressure.

It can be observed that with pressure increase, the settlements decrease significantly, especially in the case of very weak soil. However, for the case of models with specified conicity of the shield, at certain point there is little improvement with increasing soil pressure as the settlement converges to approximately 50 mm, which basically represents convergence that happens because of the shield conicity and the fact that bentonite injection effect is not modelled and for this reason the soil collapses onto the shield because it does not have enough bearing capacity. In real scenario such collapsing effect should be controlled by allowing bentonite muck or clay shock material to be injected through designated openings on the shield. If assumption is made so that the bentonite injection process is achieved in full effect, results of models with no conicity would present a good simulation of the effect and influence it has on surface settlements.

Results obtained from TBM analysis further influence the opinion that for the given conditions, the TBM method is superior to conventional method of construction.

6. Conclusion

The design and construction of tunnels in urban areas is complex and requires detailed and studious analysis that should define adequate technical solutions that will enable the safe and successful implementation of the tunnel construction project.

Risks in urban tunneling are often governed by ground settlements. In order to minimize these risks, TBM technology offers substantial advantages when dealing with weak soil conditions.

The development of the tunnel project presented in this paper began more than several decades ago. The project underwent a large number of changes that primarily related to the traffic solutions of the route and access zones and fitting into the traffic solution of the City of Belgrade. However, the essential issue with this project is the construction technology, which was obviously wrongly selected and considered in previous studies and analyses. This was to be expected at the time when the development of the project began, because the knowledge and construction practice at that time in Serbia did not recognize the application of mechanized TBM methods in the construction of tunnels. Nowadays, the advantage of TBM technology is undeniable and the further realization of the project will take place using TBM. It is expected that by the end of 2025 works on the construction of the launch shaft will begin and that the beginning of the construction of the tunnel should start at the beginning of 2027. The tunnel connection project is one of the largest infrastructure projects in the City of Belgrade.

References

Jaroslav Černi Water Institute (JCWI), 2023. Project of the tunnel connection from Karađorđeva Street to the Danube Slope with access roads, park areas and infrastructure, Study and technical documentation under a commercial construction contract, Edition A: Geological study, Belgrade, Serbia (in Serbian)

Kaldrma, Podzemni bulevar ispod centra Beograda, 19. jan. 2023. Available online: https://kaldrma.rs/podzemni-bulevar-ispod-centra-beograda/. (accessed on 2025)

Predrag Krstic, Dragan Mihajlovic, 2015. Analiza varijantnih resenja tunelske veze Savske i Dunavkse padine.

Stepanović, B., Perić, J., 1961. Inzenjerskogeoloski uslovi izbijanja bazisnog tunela ispod Terazija – Beograd.

Southeastern Europe Tunnelling Conference (SETC-2025)
1-3 October 2025, Belgrade, Serbia

DOI: 10.5937/SETC25005K

An innovative technical solution for the inclusion of a diaphragm wall into the construction system for the building of underground structures in an open pit

Tengiz Kobidze[a] and Dmitry S. Konyukhov[a,b]*

[a] JSC Mosinzhproekt, 125252, Khodynsky boulevard 10, Moscow, Russia; gidrotehnik@inbox.ru
[b] Russian Technological University MIREA, 119454, Vernadsky Avenue 78, RTU MIREA, Moscow, Russia

Abstract: For the Russian holding company Mosinzhproekt JSC, which is equipped with highly qualified personnel, an appropriate scientific and technical base and performs the functions of a general contractor and customer for the construction of the Moscow Metro, innovative marketing as a methodological basis for the development and implementation of innovations is a significant part of its activities. This is evidenced by the experience of the holding's team of authors, who, based on an innovative marketing study of the Moscow Metro construction market, identified a target market segment and a construction system with the potential for innovative segment development if the system is equipped with the missing reliable and maintainable external waterproofing. To solve this problem, an innovation strategy was developed based on the modernization method of the target construction system, which is characterized by relatively low financial costs in developing and promoting innovations to the construction market and, as a result, an original waterproofing system with double-sided adhesion, adapted to the specific conditions of construction and operation of the construction system to be modernized, for the device reliable and maintainable external waterproofing under specified conditions. The industrial testing of the upgraded innovative construction system was carried out at the Moscow Metro facility under construction. The results of the work carried out can be considered an example of creating an effective model for the development and promotion of marketing innovations in the construction market, with low financial and time costs.

Keywords: innovative marketing; subway; target market segment; wall in the ground; pit hollows; waterproofing

1. Introduction

The article considers the solution of a set of problems that arise in the development and market promotion of innovations in the field of waterproofing of underground structures built of monolithic reinforced concrete in cut-and-cover and semi-closed pits. These issues include:

- the absence of a waterproofing system that provides the required adhesive bond to the external insulated surface of the structural parts of the lining of these structures, characterized by the lack of access to perform waterproofing work using traditional waterproofing materials;
- the absence of regulations and requirements in the regulatory framework governing the use of waterproofing of this type in the construction of tunnels and subways;
- the lack of information in the technical literature on the use of waterproofing materials of this type in the construction of tunnels and subways in cut-and-cover and semi-closed excavation pits;
- difficulties associated with overcoming barriers that arise in the development and promotion of innovations in the construction market due to:
- inertia of the construction industry and, in particular, the conservatism of construction and design organizations;
- high financial costs associated with the development and promotion of innovations in the construction market;
- the lack of a methodological basis for conducting work that helps to overcome problems that arise at the stages of development and entry of innovations into the construction market.

*Corresponding author: gidrotehnik@inbox.ru (T. Kobidze).

The problems outlined in the first two paragraphs arose due to the lack of the ability of traditional waterproofing materials to provide continuous adhesive bond to concrete poured on the surface of the waterproofing coating pre-laid on the concrete base (secondary adhesion). This leads to a lack of adhesive bond of the waterproofing to the outer surface of the moulded tray structures and walls without hollows for backfilling the soil, in violation of regulatory requirements (Organization standard, 2013; Code specification, 2022; Code specification, 2023), leading to a loss of reliability, waterproofness, and maintainability of waterproofing and protected structures. Therefore, in order to eliminate this long-standing issue, the authors had to solve the problem of finding, developing and justifying the effectiveness of waterproofing materials that were free from this disadvantage of traditional materials.

A review of domestic and foreign scientific, technical and regulatory literature revealed only one scientifically sound source (Holter, 2015), indicating the presence of the desired type of waterproofing material produced on the basis of sprayed ethylene vinyl acetate polymer used in the construction of transport tunnels built by mining (closed) method. Studies conducted by the authors (Kobidze, et al., 2016) in order to adapt this material to the construction of underground structures in cut-and-cover and semi-closed pits have shown that the material is of high quality and capable of adhesive bond both to a pre-prepared concrete base and to the surface of concrete poured onto the surface of the waterproofing coating (double-sided adhesion) with a tear-off strength of more than 0.5 MPa, according to the requirements (Code specification, 2022). As a result, a reliable three-layer composite waterproof enclosing structure of the 'sandwich' type is formed (Shilin et al., 2003), consisting of two layers of monolithic concrete and a waterproofing layer.

This type of enclosing structure is formed during the construction of the wall parts of the lining of underground structures in an open excavation pit without hollows for backfilling the soil, characterized by a tendency to mutual displacement of two layers of concrete structures, which are a diaphragm wall and a wall structure built close to it. At the same time, the amount of precipitation of the structure under certain operating conditions can be 5 cm (Code specification, 2019). The results of laboratory tests of the shear patterns of these structures at the specified parameters showed the inability of the waterproofing layer made of ethylene vinyl acetate with a hardness of 80 on the Shore A scale and an elongation of 80-140 % to maintain integrity and adhesive bond to both layers of the concrete structure. This pointed to:

- the unsuitability of the material for the construction of such structures and the limited use of it in the construction of underground structures in cut-and-cover and semi-closed pits;
- the need to continue work to develop a waterproofing material with double-sided adhesion, devoid of this drawback (Kobidze and Konyukhov, 2021).

2. Methods and materials

In the methodological justification of the planned work, the choice fell on an infrequently used separate area in modern marketing related to the development and promotion of innovations (innovative marketing), the object of which is not the market of goods, but the innovation market with subjects, one of which is the state. Therefore, the use of this method is particularly effective in the context of the activities of state-owned companies, for example, Mosinzhproekt Holding, which performs the function of managing the construction of the Moscow Metro in the implementation of the priorities of the state innovation program. These factors, supported by the relevant competence and administrative resources of the company, create favourable conditions for successfully overcoming the inertia of the construction industry and financial barriers in the development and promotion of innovations in the metro construction market.

As a result of the conducted marketing research, it has been established that the construction of subway station and pier structures from monolithic reinforced concrete of shallow laying is a promising target segment of the increased capacity of the innovative metro construction market, which is characterized by the presence of a competitive environment due to the distinctive features of building systems used for the construction of underground structures (Fig. 1).

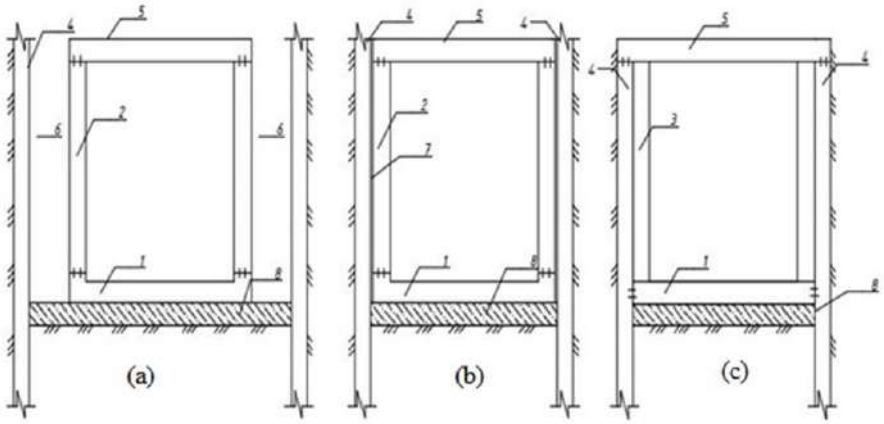

Fig. 1. Types of methods for the construction of underground structures made of monolithic reinforced concrete: (a) – cut-and-cover method with hollows for backfilling the soil; (b) – cut-and-cover method without hollows for backfilling the soil; (c) semi-closed construction method with a load-bearing diaphragm wall; 1 – tray (foundation) plate; 2 – load–bearing wall; 3 – pressure wall; 4 – excavation enclosure; 5 – coating plate; 6 – hollows for backfilling the soil; 7 – plane of mutual displacement of the walls; 8 – concrete preparation.

The construction of structures in the target segment is carried out in a cut-and-cover or semi-closed excavation. Construction in a cut-and-cover pit involves the installation of external waterproofing for structures under construction. This ensures the required waterproofing and anticorrosive protection of the enclosing structures from the effects of groundwater and reliable operation of the waterproofing coating in the 'on-hold' mode. Therefore, the method of constructing underground structures in a semi-enclosed excavation, where the load-bearing wall structure 'diaphragm wall' is protected by waterproofing from the inside, was identified as an unpromising object for innovative research.

Underground structures in a cut-and-cover pit are built regardless of the presence or absence of hollows for backfilling the soil. In the case of hollows, waterproofing is applied directly to the outer surface of the permanent wall structure, and in the absence of hollows, to the inner surface of the temporary diaphragm wall structure, which in this case acts as a protective layer of waterproofing. All other things being equal, the hollows construction method has undoubted technical, economic and competitive advantages due to (Table 1):

- the absence of labour-intensive and resource-intensive excavation work related to excavation, transportation to the dump and backfilling of soil into the hollows;
- there is no need to install a protective layer of waterproofing against damage when performing backfilling work;
- reducing the construction time of an underground structure in the absence of listed works in the construction chain.

In addition to the above, after the completion of backfilling work, expensive diaphragm walls structures used as temporary geotechnical structures for fencing the excavation pit lose their original function, turning into a useless structure buried in the ground. At the same time, the diaphragm wall also acquires a negative function, becoming an enclosing structure of stagnant wall drainage with increased hydrostatic pressure, formed as a result of filling the hollows with compacted sand and its saturation with groundwater and topsoil, which, as a rule, contains pollutants that increase the aggressiveness of the backfilling soil.

Under the given conditions, the possibility of direct contact of contaminated groundwater with overpressure and waterproofing coating of walls increases the risk of reducing the durability of the material and, in case of damage, the corrosion resistance of reinforced concrete of the protected structure and the occurrence of active (pressure) leaks in transport structures. As a result, the operational reliability of structures decreases and the operating costs for eliminating these defects increase.

Table 1. Comparison of the cost of additional work during the construction of an enclosing wall structure of an underground structure erected in an open pit with pit hollows and without pit hollows.

Name of the works	The cost of the work according to the estimate, in the price level for March 2023, in rubles	
	A pit with pit hollows	A pit without pit hollows
Excavation of the ground in the excavation with relocation and disposal	2 587,94	408,04
Installation of the leveling wall of the excavation enclosure (diaphragm walls)		3 977,30
Waterproofing protection with extruded polystyrene foam boards	1 394,16	
Backfilling of pit hollows at the walls of the excavation	4 513,56	
Total	8 495,66	4 385,34
Saving for every 1 m^2 of wall erected without pit hollows	8 495,66-4 385,34= 4110,32 руб./m^2 = 48%	

Currently, contrary to the above analysis, the dominant application in the practice of metro construction is a cut-and-cover method with hollows for backfilling the soil.

Such an illogical situation is based on an unresolved long-standing technical problem, in particular, the main condition for the installation of traditional waterproofing materials (bitumen polymer surfaced rolls, polymer compositions based on polyurea and methyl methacrylate resin) used in accordance with regulatory standards in the field of metro engineering (Code specification, 2022; Code specification, 2023; Organization standard, 2013), is the availability of access to the insulated surface of the protected structure. This condition exists only when waterproofing the external insulated surface of walls with hollows for backfilling the soil and coating plates, and is absent when waterproofing tray plates and walls erected without hollows for backfilling the soil (see Fig. 1).

In the absence of hollows, the wall structure of the underground structure is built close to the diaphragm wall (enclosure of the excavation). Therefore, for the external insulated surface of the erected wall, as well as for the tray plate, there is no access to perform waterproofing work. As a result, under these conditions, traditional materials are adhesive fixed to the accessible surface of the excavation fence (diaphragm walls) before the walls of the structure are erected and for concrete preparation – before concreting the tray plate.

The lack of adhesion to the wall and to the tray plate deprives waterproofing of reliability and maintainability, and the method of constructing structures without hollows for backfilling loses market competitiveness, since in the case of even single local damage to the waterproofing, uncontrolled migration of water occurs under the entire area of the waterproofing coating, in violation of the requirement (Code specification, 2022), leading to flooding the protected wall and the tray plate, to the loss of waterproofing and anti-corrosion protection by the structures, the restoration of which is achieved by a device behind the wall and a tray plate of unacceptably expensive veil waterproofing using injectable polymer compounds. Therefore, the elimination of the described problem is an urgent problem that needs to be solved.

3. Discussion

The results of the marketing analysis revealed the following:

1. A potentially promising object for the development of an innovative marketing construction product of the target segment, competitive in the innovative metro construction market, is a construction system based on the construction of underground structures in an open pit without hollows for backfilling, which differs from the competitive construction systems of the segment by better technical and economic indicators and short construction time.

2. The reasons for the low competitiveness of the specified construction system of the target market segment at the time of the innovation work were:

- lack of technology for reliable and maintainable external waterproofing for constructed structures;
- lack of a regulatory framework for the installation of reliable and maintainable waterproofing for structures of the type in question.

These reasons created an insurmountable barrier to the advancement of the construction system to the market.

Based on the above, a strategy for innovative work has been developed, including solving the following tasks:
1. Organization of scientific research on a conceptual basis, according to which the waterproofing coating should exhibit:

- adhesive bond not only to the accessible surface of the excavation fence and concrete preparation (concrete base), but also to the inaccessible surface of the monolithic wall of the structure, erected close to the waterproofing coating of the excavation fence and the tray plate (the ability of waterproofing to double-sided adhesive bond);
- resistance to abrasion and loss of integrity of the waterproofing layer and its adhesive bond to both structures under the conditions of the expected mutual displacement of the excavation fence and the wall structure with a draft of the structure from 2-2.5 cm (established by the results of long-term observations) to the possible permissible maximum values of 5 cm (Code specification, 2019).

2. Amendments to the regulatory framework in the field of metro construction, fixing the requirements for the rules of design and installation of reliable and maintainable waterproofing for structures erected in an open pit without hollows for backfilling.

4. Results

The implementation of innovative research and development activities has yielded the following results. The most effective type of waterproofing material suitable for solving the tasks has been selected and modified. These are sprayable compositions based on a thermoplastic elastomer with double-sided adhesion, modified by fibre reinforcement of the front layer of the coating (2 mm) from a non-woven geotextile fabric with a density of 250 g/m^2, impregnated with a sprayable waterproofing compound.
It is confirmed that the material in question, applied, like traditional technology, to a concrete base and a diaphragm by a high-performance mechanical method of airless spraying, according to the conceptual version, provides adhesive adhesion (at least 0.5 MPa) according to the requirements (Code specification, 2022; Organization standard, 2013), not only with a concrete base, but also with an inaccessible outer surface of the tray plate and wall, erected without hollows for backfilling the soil, laid on waterproofing by monolithic concreting. As a result, particularly reliable, three-layer waterproof sandwich-type enclosing structures are formed (Shilin, et al., 2003), consisting of a protective layer of waterproofing in the form of concrete preparation and a diaphragm wall, a layer of protected structure (tray, permanent load-bearing wall) and a waterproofing membrane located between them with double-sided adhesion to reinforced front layer (Fig. 2 and Fig. 3) (Kobidze et al., 2016; Kobidze et al., 2023). The operational reliability of these structures in conditions of high hydrostatic pressure is ensured by the joint operation of three components of the following structures:

- reliable protective waterproofing layers made of reinforced concrete, located on the side of the impact of groundwater, sensing the hydrostatic pressure of the waters, ensuring the operation of the waterproofing layer in a favourable ‘pressure’ mode;
- protected structures as pressure structures designed to withstand expected hydrostatic pressures (Code specification, 2022);
- a waterproofing layer trapped between two concrete structures, due to its two-way adhesion, ensures the solidity, water resistance and reliable functioning of the entire structure.

In the case of residual high humidity of the concrete base, they are coated with a thin (3 mm) protective waterproof and anti-corrosion layer of polymer cement composition.

The test results confirmed the high elasticity of the specified material and its ability to develop reversible elastic deformations under tension with a recovery coefficient of at least 90 % of the original length of the sample and a relaxation time of 15 minutes after the cessation of external forces (Table 2).

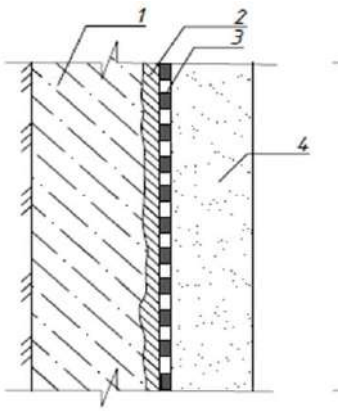

Fig. 2. Monolithic wall structure, erected without hollows for backfilling the soil, with external waterproofing with double-sided adhesion: 1 – a diaphragm wall (enclosure of the excavation); 2 – levelling layer (reinforced fine-grained concrete, monolithic reinforced concrete); 3 – sprayed seamless waterproofing made of thermoplastic elastomer 6-8 mm with a front layer of 2 mm reinforced with geotextile cloth; 4 – tunnel lining wall made of monolithic reinforced concrete, erected without hollows for backfilling the soil.

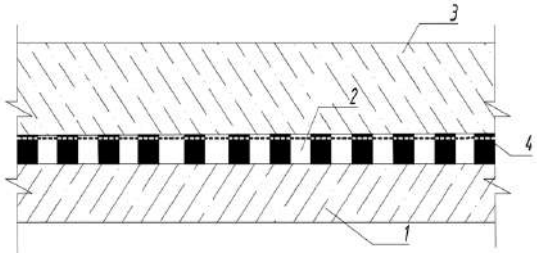

Fig. 3. Tray plate with external waterproofing with double-sided adhesion: 1 – reinforced concrete preparation; 2 – sprayable seamless waterproofing made of thermoplastic elastomer 6-8 mm with a front layer of 2 mm reinforced with geotextile cloth; 3 – tray plate.

The ability to double-sided adhesive adhesion of the specified type of waterproofing material has been confirmed (above the regulatory requirement of at least 0.5 MPa) both with a concrete base (primary adhesion) and with the surface of concrete laid by monolithic concreting on a ready-made waterproofing coating (secondary adhesion).

The test results confirmed the high elasticity of the material and its ability to develop reversible elastic deformations under tension with a recovery coefficient of at least 90% and a relaxation time of 15 minutes after the cessation of external forces (Table 2).

Table 2. Elongation and elastic deformations of thermoplastic elastomer waterproofing material.

№	Parameters	Relative lengthening, %	Восстановление
1	Before the trials	1900	≥ 90
2	After thermal aging (T= +70 °C)	1970	≥ 90

The high resistance of the 6-8 mm thick waterproofing layer to deformation loads (while maintaining integrity and double-sided adhesion) was confirmed when the concrete layer of the sample imitating the wall structure of the structure was shifted by the maximum allowable value for testing equipment of 8.3 cm (Fig. 4).

(a)

(b)

Fig. 4. Testing of a layer of sprayed waterproofing with double-sided adhesion, laid between two wall structures, for shear resistance: (a) Sample during shear tests; (b) Sample after testing.

As can be seen from Table 3 and Fig. 4, the pressure value when the sample is shifted by the specified 8.3 cm is only 0.020 MPa with a waterproofing layer with double-sided adhesion of more than 0.5 MPa. This contributed to the fact that the plane of deformation of the waterproofing layer during the shear load passed through the middle of the waterproofing coating, which at the same time retained its integrity, bilateral adhesion and thickness in the uncoated area between adjacent concrete layers of the test sample.

Table 3. Testing of a sample of a wall structure with a waterproofing layer with double-sided shear adhesion (the test surface area of the sample is 24200 mm^2).

№	Load time, s	Load, N	Deformation (displacement), mm	Shear pressure, MPa
1	31	207	5.0	0.008262037
2	61	257	10.0	0.010257698
3	121	318	20.0	0.012692405
4	181	378	30.0	0.015087198
5	241	442	40.0	0.017641645
6	301	487	50.0	0.01943774
7	361	503	60.0	0.020076351
8	421	505	70.0	0.020156178
9	480	507	80.0	0.020236004
10	494	513	83.0	0.020475483

According to the ratio of the Shore hardness scale A, due to the reinforcement of the 2-millimeter face layer of the waterproofing coating with a non-woven geotextile cloth with a density of 200-250 g/m2, the material of the initially soft category acquires an average hardness, which makes it possible to seamlessly perform general construction work on concreting the foundation plate under construction site conditions.

The national standard regulating the rules of work during the construction of the subway (Code specification, 2022), at the suggestion of the authors, has been amended to include requirements for the rules of design and installation of reliable and maintainable waterproofing for structures erected in an cut-and-cover pit without hollows for backfilling (Kobidze and Konyukhov, 2022).

5. Conclusion

As a result of the conducted research:

- by modifying the initial thermoplastic sprayed composition, a type of innovative waterproofing materials with double-sided adhesion has been developed, eliminating the contradiction between the regulatory rules for the design and installation of waterproofing for underground structures erected in an cut-and-cover pit. On this basis, the national standard for metro construction (Code specification, 2022) has been amended accordingly;
- a simple, technological and innovative method and design solution have been developed based on the use of sprayed waterproofing with double-sided adhesion for reliable waterproofing of structural parts of monolithic reinforced concrete lining of underground structures characterized by lack of access to an external insulated surface for waterproofing work.

Through marketing research:

- the area of construction of underground structures made of monolithic reinforced concrete in an open pit has been established as a target segment of increased capacity for the innovative metro construction market;
- the choice of an open method of constructing underground structures without hollows for backfilling soil as an object for innovative development from among the target segment's construction systems based on modernization, characterized by reduced capital and indirect financial costs at the stages of development and promotion of innovations in the construction market.

A marketing innovation has been developed in the form of an open-pit construction system for backfilling the soil, created on the basis of system modernization by replacing unreliable traditional waterproofing systems with one-sided adhesion with a developed sprayable waterproofing with two-sided adhesion, fully adapted to the specific conditions of construction and operation of these structures, which gave them an undoubted competitive advantage over others the construction systems of the target segment.

The effectiveness of a model for the development and promotion of marketing innovations in the construction market with low financial and time resources has been tested and demonstrated, implemented under the auspices of a state-owned construction company focused on addressing the priorities of the state program for the innovative development of the country's construction industry.

For the first time, pilot industrial application of innovative structural and technological solutions for the construction of sandwich-type multilayer enclosing composite structures with a waterproofing layer with double-sided adhesion was carried out at the Moscow Metro facility, where structures were built in an open pit with and without hollows for backfilling the soil (Fig. 5).

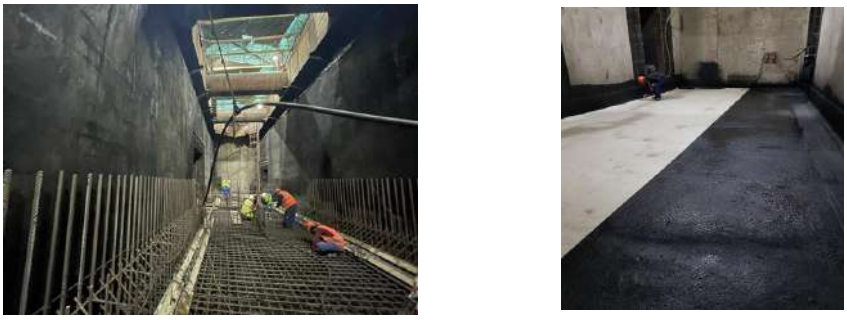

(a) **(b)**

Fig. 5. General view of the work during the installation of sprayed waterproofing with double-sided adhesion: (a) installation of a metal frame on waterproofing laid on diaphragm walls and on concrete preparation, before concreting wall structures without hollows for backfilling the soil and a tray plate; (b) installation on a primed

waterproofing base of geotextile canvases intended for subsequent spraying with a waterproofing compound to form a fibre-reinforced 2-millimeter front layer.

An inspection of the premises of the waterproofing structures after 2.5 years of operation showed that the enclosing structures are in a dry state, confirming the reliability and operability of the operated waterproofing system under specified operating conditions over the past period.

To date, the developed innovative structural and technological solutions based on sprayed waterproofing with double-sided adhesion have found application in the construction of four underground facilities of the Moscow and St. Petersburg subways with structures erected without hollows for backfilling the soil. In order to further promote innovation in the construction market, work is underway to expand the raw materials and regulatory framework of the developed waterproofing system; with the organization of events to attract potential consumers of innovations (seminars on the basis of Mosinzhproekt, field technical meetings). This purpose is also served by participation in scientific and technical conferences, publications in specialized journals, etc.

The experience of performing waterproofing works in construction conditions has shown that the customer needs to ensure stable quality indicators of the laid waterproofing coating:

- on a contractual basis, link the manufacturer of the product (supplier) and the contractor of waterproofing works as a collective responsible subject for the quality of the supplied products and the waterproofing work performed at a specific facility;
- organize strict control over the production process;
- oblige the contractor construction company to organize measures to ensure that the specified heat and humidity conditions are met, as well as to protect the waterproofing during the laying and hardening period from the 'human factor', precipitation and groundwater.

References

Code specification, 2019. SP 474.1325800.2019. Subways. The rules of inspection and monitoring of underground structures constructions. Appendix A, p. 9. https://docs.cntd.ru/document/564543321.

Code specification, 2022. SP 120.13330-2022. Subways. https://docs.cntd.ru/document/1300886470 .

Code specification, 2023. SP 122.13330.2023 Railways and highway tunnels. https://docs.cntd.ru/document/1304138944.

Holter K.G., 2015. Properties of waterproof sprayed concrete tunnel linings. A study of EVA-based sprayed membranes for waterproofing of rail and road tunnels in hard rock and cold climate. Thesis for the degree of Philosophiae Doctor. Trondheim, December 2015. Norwegian University of Science and Technology Faculty of Engineering Science and Technology. Department of Geology and Mineral Resources Engine.

Kobidze T.E., Kolobaev D.A., and Potapov G.V., 2016. Waterproofing systems for underground transportation facilities built using the diaphragm wall technology. *Metro and Tunnels*, No. 1, pp. 19-21.

Kobidze T.E., Merkin V.E., Seslavinsky A.S., Pukhov A.V., and Potapov G.V., 2016. Russian Patent 162638. Underground construction.

Kobidze T.E., and Konyukhov D.S., 2021. The causes of flooding of tunnel structures and innovative 'pre-installed' waterproofing systems to eliminate it. *Metro and Tunnels*, No. 1, pp. 18-22.

Kobidze, T.E., and Konyukhov D.S., 2022. Features of designing and installing reliable and maintainable waterproofing for underground transportation facilities. *Metro and Tunnels*, No. 3, pp. 24-27.

Kobidze, T.E., and Konyukhov D.S., 2023. Russian Patent 218662 The tray part of underground and buried structures built in an cut-and-cover manner.

Organization standard, 2013. STO NOSTROI 2.27.123.2013. Development of underground space. Waterproofing of transport tunnels and subways constructed by open method (Rules for design, production and acceptance of works). https://docs.cntd.ru/document/1200127364 .

Shilin A.A., Zaitsev M.V., Zolotarev I.A., and Lyapidevskaya O.B., 2003. Waterproofing of underground and buried structures during construction and repair. Publishing house '*Russian trademark'*: Tver, Russia, pp. 1-23.

Southeastern Europe Tunnelling Conference (SETC-2025)
1-3 October 2025, Belgrade, Serbia

DOI. 10.5937/SETC25006G

Overcoming TBM Launch Challenges in Doha's WWDT Project

K. Gaurav Singh[a], H. Vigil Fernandez[b], J.B. Stypulkowski[c] and K. Saif Al-Khayareen[c]*

[a] Parsons International, Doha, Qatar; kumargaurav.singh@parsons.com
[b] PORR-HBK-MIDMAC-JV, Doha, Qatar; hernan.vigil@porr.qa
[c] Public Works Authority (ASHGHAL), Doha, Qatar; jstypulkowski@ashghal.gov.qa

Abstract: Over the past two decades, Doha has experienced rapid growth, putting considerable pressure on the city's infrastructure, particularly its aging sewer system and wastewater treatment facilities. To address these challenges, the Public Works Authority ASHGHAL has initiated several projects involving both shallow and deep sewer tunnels, alongside the construction of new treatment plants to accommodate the demands for Doha's expanding population in the future. The scope of the Wakrah and Wukair Drainage Tunnel (WWDT) project includes a 13.3 km bored and lined tunnel, using two 5.85-meter diameter EPB TBMs, eight shafts, adits for future connections, and hydraulic structures. Due to project constraints and the delivery schedule of the TBMs on site concerning Covid-19 pandemic restrictions, the contractor had to launch a 148-meter-long Tunnel Boring Machine (TBM) inside a 15-meter diameter shaft located at a depth of 59.4 meters. This paper details how the contractor successfully managed these challenges and launched both TBMs. The TBM launch and commissioning were contractual key milestones. The approach involved partially excavating a Stub Adit/Logistics tunnel using a Sequential Excavation Method (SEM) to create space for multiple TBM sections at the base of the shaft, while some TBM gantries operated simultaneously by situating on the surface and connected via umbilical lines to the cutterhead and main shield of the TBM for commencement of the tunnelling operations.

Keywords: sewer tunnel; EPB TBM; launching challenges; tunnelling

1. Introduction

ASHGHAL is a Public Works Department (PWA) for the country and has launched several schemes in response to the growth and rapid expansion of the population, which has strained the country's infrastructure including sewerage system and treatment facilities. The PWA developed strategic plans utilizing shallow and deep sewer tunnels and new treatment works to serve the growing population in the years to come.

The Wakrah Wukair Drainage Tunnel (WWDT) project (C853/2) is primarily located within the western and southern utility corridors, an assigned buffer zone between the two utility corridors, and inside the Al Wakrah and Al Wukair Sewage Treatment Plant (STP).

The Project comprises the design, construction, testing, commissioning, and handover of the Drainage Tunnel. The Drainage Tunnel (DT) is approximately 13.3-km long with four temporary work shafts for TBMs launch and/or reception – WS07, WS08, WS09 and WS10 and four additional temporary shafts for the construction of permanent access shafts in between the TBM work shafts – AS08, AS09, AS10 and AS11 which shall all be converted to permanent access shafts.

The DT final inner diameter is 4.5 m. The lining concept consists of primary lining, which is a 300 mm thick fiber reinforced segmental concrete (C50/60), and a Secondary Corrosion Protection Lining (CPL) of 250 mm thick concrete (C35/45) with a 2.5 mm thick HDPE protective membrane. For additional information about concrete used please refer to Bernardeau et al. (2018).

*Corresponding author: kumargaurav.singh@parsons.com (K.G. Singh).

WWDT project sites are in an undeveloped area, and the ground surface levels along the approximately 13.3 km-long alignment range from approximately +5 to +25 m above the Qatar National Height Datum 95 (QNHD95). The sites are surrounded by Qatar Petroleum (QP) pipelines, overhead high-voltage transmission lines, other utility services, as well as expressways. There are no existing permanent roads to many parts of the sites. Please refer to Stypulkowski et al (2023, 2024) for omitted details.

2. Project Tunnelling Plan

The tunnelling for WWDT project has been planned for TBM 1 to start at WS10 and pass AS11 and WS09. After passing WS09, the TBM stopped at about 150m before (in flow direction) the shaft. During the interruption of tunneling, the Site Installation for TBM 1 was shifted from WS10 to WS09. After reinstallation of the tunnelling logistics, TBM 1 was launched again from WS09, passed AS10 and was received finally at AS09. AS09 was constructed as TBM Launch and Reception Shaft for TBM 2, which drove through WS08 and consecutively through AS08 and was than received at WS07.

3. Geology general overview

The project area is geologically a part of the Arabian Gulf Basin as described in detail by Cavelier et al. (1970) and Sadiq and Nasir (2002). The post Cretaceous sedimentation is a sequence of shallow marine limestone with occasional shale and evaporates in a shallow basin. The formations encountered in the Doha region comprise of Quaternary marine, aeolian and sabkha deposits. The Simsima Limestone is subdivided into four geological units in the project area: the Highly Weathered Simsima Limestone (HWSL), Weathered Simsima Limestone (WSL), Simsima Limestone (SL) and Basal Simsima Limestone (BSL). The underlying lower geological units, which include the Midra Shale (MSH), Khor Limestone (KLS), Rus Calcareous (RUS) and Rus Gypsum (RUSGYP), lay below the SL formation (Karagkounis et al. 2016).

Based on the available information, PHM-JV interpreted the geology as presented in Figure 1 and summarised below.

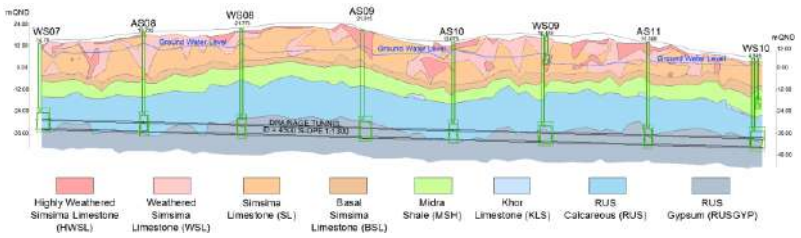

Fig 1. Interpreted geology (PHM-JV, 2022c).

4. Surface Enabling Works and Rock Grouting (Shafts)

The experience accumulated from other projects in the state of Qatar by the contractor, suggested that rock grouting (or permeation grouting) is the best option to reduce the active karstification/voids of rock formation and thus the water inflow towards the excavation, see Fig.2. Rock grouting was performed ahead of excavation using a down-the-hole hammer with a diameter of 115mm and a Tube-a-Manchete system. The mix design used was a combination of Ordinary Portland cement (OPC) between 320 kg and 420 kg, bentonite between 30 to 60 kg, and water from 800 to 900 l.

In shaft WS10, two drilling schemes were used: full-length primary-secondary grouting around the shaft perimeter, and a base plug grouted only in the last 10 m to block bottom water inflow.

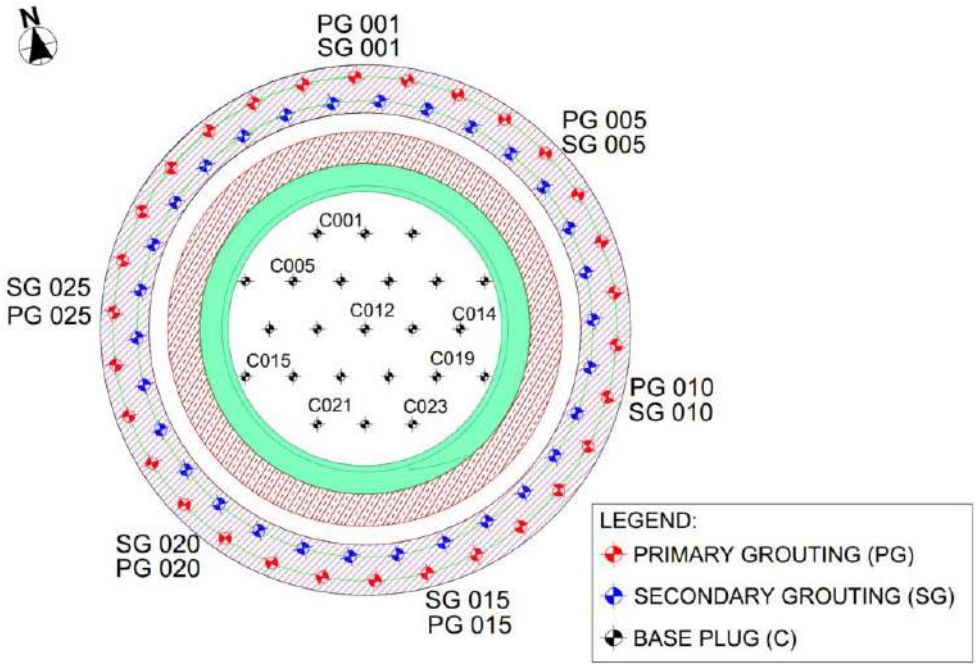

Fig 2. Rock grouting drill pattern.

For shaft AS09, only the base-plug rock grouting was required. Perimeter grouting had been completed by a previous contractor (2016-2018); after that contract was cancelled, the shaft was backfilled with lean concrete (2018). On taking over the shaft under the WWDT contract, the contractor confirmed the existing rock grouting was still fit for purpose.

A total number of 30 primary and secondary and 23 center bore holes have been drilled in WS10 with a grout consumption of 574.5 m^3, while in AS09, only 24 center bore holes have been drilled with a grout quantity of 22.3 m^3.

5. Surface Enabling Works and Rock Grouting (Launching chamber and Logistic Tunnels)

The excavation method for the TBM launching chambers and logistics tunnel is based on NATM, thus considering the groundwater conditions, the rock grouting block containing the tunnel lining inside is necessary in a similar way, as it has been described previously.

In WS10, 297 primary and secondary bore holes were drilled with a grout consumption of 1458 m3, while in AS09, 190 bore holes were drilled with a grout quantity of 590 m^3.

6. Dewatering

To mitigate the effect of water inflow in the shaft, a complementary action to the rock grouting, an integrated dewatering system consisting of dewatering wells with effective slotted casing diameter of 315 mm and French-drainage of 1 m by 1m and sump pits, permanent and temporary, was deployed in the launching shafts (WS10 and AS09), as shown in Fig. 3.

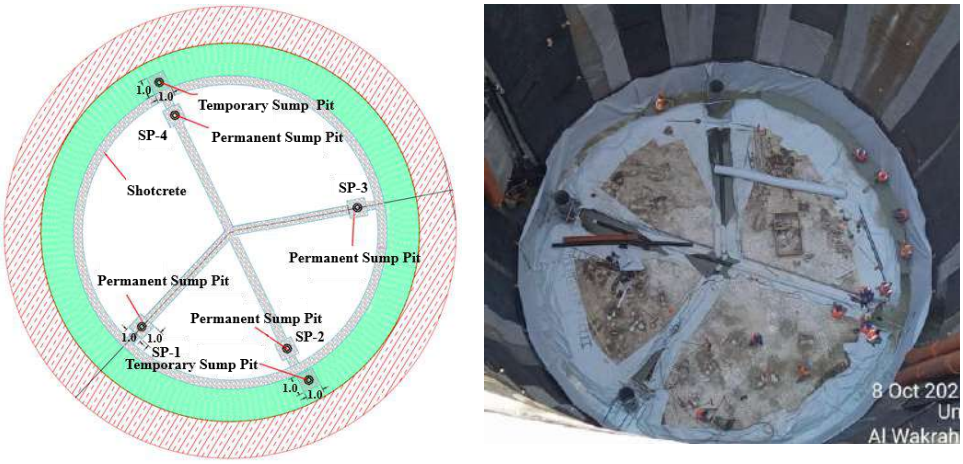

Fig 3. De-watering design and construction in shaft WS10.

The water collected from the dewatering system in each shaft was discharged into a main internal discharge line via a lay-flat hose and HDPE pipes. Extracted groundwater was discharged to the recharge wells at a depth of 450 m via a break tank through internal HDPE pipes, after maintaining the parameters stipulated in the relevant permits. During excavation of the shafts, the amount of dewatering was around 40 m^3/h, while during the TBM activities, it was around 20 m^3/h. As WS10 and AS09 shafts are two TBM launching shafts, each site has its own deep recharge wells and its associated surface facilities, in order to maintain the quality of discharge water and not to exceed the daily capacity of the recharge wells.

7. Shaft Excavation

The shaft construction consisted of excavation works and application of SCL primary support. The excavation was carried out by using conventional excavators (with more than one excavator) working in the shaft at the time, a drum cutter and hydraulic hammer. The primary support was sprayed wet shotcrete C25 distributed in a single layer of 100 mm thickness or 300 mm distributed in a double layer, reinforced with a single or double layer of wire-mesh (200 X 200 X 8mm), and installation of spot rock bolts.

8. Tunnel Excavation (NATM)

The excavation of the launching tunnel and logistics tunnel has been done by the New Austrian Tunneling Method (NATM) also known as Sequential Excavation Method (SEM). Ground conditions and geotechnical loads considered in the design of the Non TBM-Tunnel were calculated based on the data provided in the Preliminary Geotechnical Interpretative Report which showed as Strata – Rus Gypsum, ϒ [MPa] = 22.5 and Erm [MPa] = 4363.

Horizontal probe drilling along with Face mapping has been systematically done to assess the rock mass condition and its support which was based on the shotcrete (C25) with thickness between 100mm to 250mm, reinforced with two layers of wire-mesh (200 X 200 X 8mm) and rock bolts of 3m length in a pattern of 2m X 2m. Excavation was done as full circle in launch adits and by heading & benching manner in logistics tunnels, see Fig.4 and Table 1.

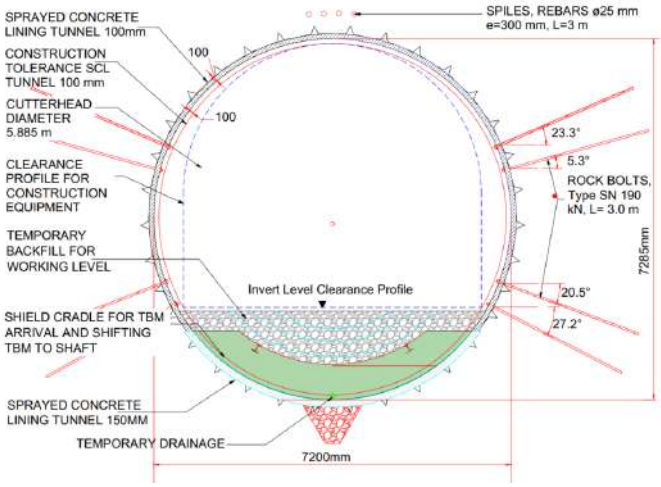

Fig 4. Launching and logistics tunnel cross sections.

Table 1. Summary of NATM tunnels.

Location	Excavation rate (m/day)	Support class	Water inflow (m^3/hr)	Maximum deformation (±mm)	Simplified geology
AS09-Logistic Tunnel	0.9	1 & 2	0.6	3.2	Rus Gypsum
AS09-Launching Tunnel	0.3	1	0.2	2.9	Rus Gypsum
WS10-Logistic Tunnel	0.5	1 & 2	0.4	2.85	Rus and Rus Gypsum
WS10-Launching Tunnel	0.7	2	0.2	2	Rus and Rus Gypsum

9. Temporary slab and thrust frame reaction installation

Once the shaft excavation was completed, the permanent drainage and waterproofing installed, the permanent slab has been poured. On top of the permanent slab, the temporary slab, which contains the cradle and base support of the thrust reaction frame, was built.

10. TBM related surface facilities

While the above-described works continued inside the shafts, at the same time, the contractor was busy installing and / or constructing the facilities at ground also, which are essential to perform tunneling works:

- Grout batching plant – cement, bentonite, retarder chemical and sodium silicate.
- Water Tanks and Cooling tower.
- Tunnel Ventilation system.
- Muck-pit and De-mucking unit.
- Segment Storage area to ensure operations of a minimum of 4 days regular production.
- Power Plant (Substation) and diesel tanks.
- Passenger Hoist – Passenger Hoist was installed for access and egress.
- Wastewater treatment Plant.
- Gantry crane capacity 60 ton.

11. TBM Umbilical launching at Shaft AS09

The TBM was launched in the shaft AS09 by using an umbilical system. Thus, after the related enabling works described in the previous sections were completed, the assembly of the TBM started with the preassembly of the drive motor, reducers, thrust cylinders, shields, segment erector and screw conveyor among other front and rear parts, Fig. 5.

The Figure below shows the assembly of the TBM parts in the shaft. Once the shield was assembled, it was pushed into the launching tunnel.

Fig 5. Assembly of the TBM in the shaft.

The following parts from backup gantry 1 and B were removed placed in shaft bottom, temporarily, for the umbilical launch. Among others, operator cabin, foam generators, B- component tank and pumps.

Water, air, and electrical connections were laid down from the surface to backup gantry 7. All the hoses between gantries 2 to 7 were connected.

Thrust reaction frame was installed, fixed and surveyed, see Fig.6.

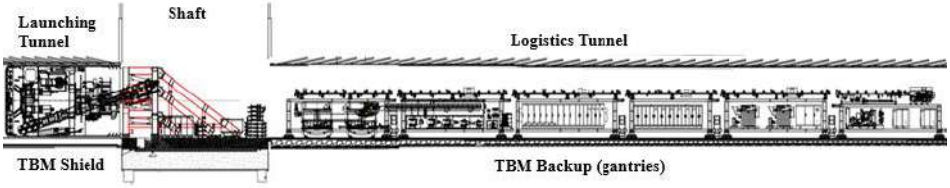

Fig 6. Final configuration of the umbilical launching shaft AS09.

Upon the installation of Thrust frame, TBM launching/initial drive started and the TBM shield advanced 90m, see Fig.7.

Fig 7. TBM and umbilical support. Rolling stock configuration.

Completion of 90 m of TBM shield advance, with umbilical, marks the end of contractually required phase 1 of the lowering and assembly works of TBM, in the shaft bottom/tunnel, see Fig.8.

TBM continued mining until there was sufficient space to install the remaining gantries until full assembly at the TBM bottom/tunnel.

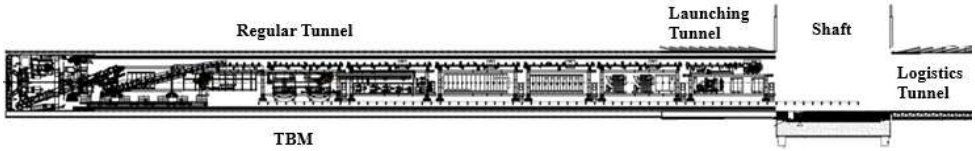

Fig 8. TBM after mining 90 m.

12. TBM super umbilical launching at Shaft WS10

The Shaft WS10 presented a specific challenge based on the geometry and site constraints, where the launching tunnel was not in the same alignment as the logistic tunnel where the backup was to be installed. In addition, the length of the logistics tunnel was not long enough to accommodate the TBM backup in one go. In this case, the logistic tunnel was 40 m out of 70 m, which was required.

After several configuration considerations, it was decided to use an unconventional umbilical configuration to assemble and launch the TBM in shaft WS10.

The TBM and its backup were split into three parts; the TBM shield in the launching tunnel, backup gantries 2 and 3 in the logistic tunnel, and backup gantries 4 to 7 connected at the surface, see Fig.9.

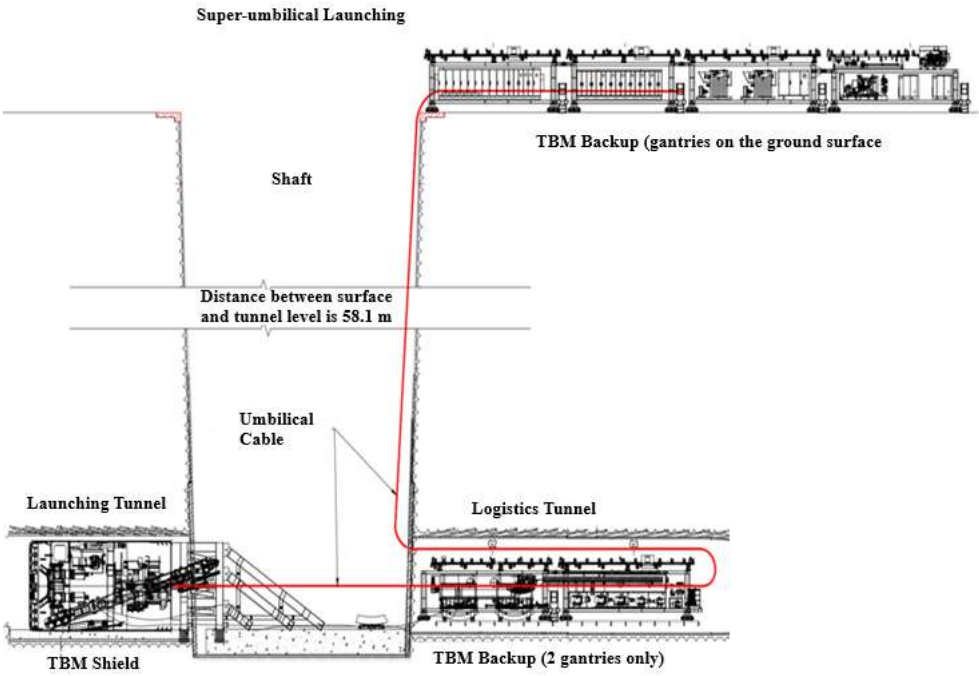

Fig 9. Super umbilical configuration in the shaft and surface.

The following assembly of the TBM and the gantries was followed:

- Lowering and assembling the TBM shield in the shaft and sliding into the launch tunnel.
- Lowering and assembling of gantry 3 and gantry 2 in the logistics tunnel.
- Lowering and assembly of the thrust frame.
- Connecting gantries 2 and 3 to the TBM shield through umbilical pipes and power cables. All other TBM backups were located at the surface level using extended power cables and hydraulic pipes running down the shaft to the TBM to be launched, see Fig.10.

Fig 10. Supraumbilical support and logistics configuration in the tunnel.

TBM was launched and mined until it reached a length of 90 m, see Fig.11. After completing 90m of tunnelling, mining stopped, all the umbilical connections were disconnected, and the thrust frame was removed from the shaft. All umbilicals were disconnected and removed from the shaft and the logistic tunnel:

- Gantry 1 and bridge were lowered from the surface, and all components for the initial drive were reinstalled towards the main machine, and also gantry 2 and gantry 3 from the logistics tunnel.
- All the backup gantries from 4 to 7 were lowered and pulled towards the TBM shield, and connections were made for the next 80 m of tunnel advance, see Fig.12. However, gantries 8 to 11 with rescue chamber and cable extensions were not connected to the main TBM, which was not essential for the initial drive.

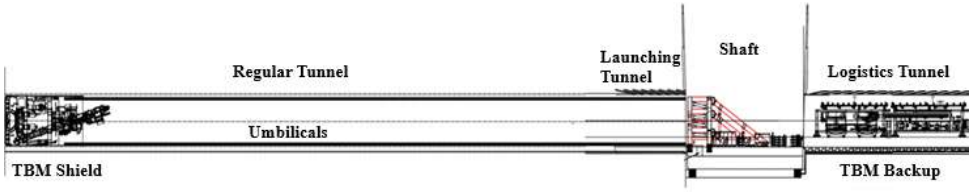

Fig 11. Mining 90 m of tunnel with super umbilical.

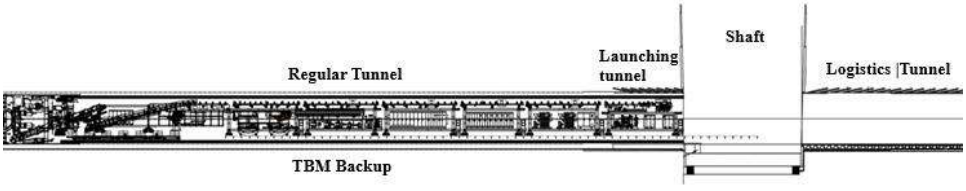

Fig 12. Removal of the umbilical and connection of the backup gantries with the TBM shield.

At this stage, see Fig.13, the excavation of the logistics tunnel to reach the final configuration with a length of 70 m restarted. Once the excavation was done, the remaining gantries were lowered and installed, considering the TBM full assembly.

Other enabling works, like the temporary concrete fill in the tunnel invert for locomotive logistics, and California switches were installed to allow the TBM to start regular mining activities.

Fig 13. Installation of California switches and final arrangement for TBM regular mining activities.

Table 2. Key dates for TBM-1.

TBM-1 - WS10-AS09	Start	Finish	Total Duration	Working days	Length (m)	Productivity Per day in rings
Lowered on	6-Jan-22	4-Feb-22	29			
Initial Drive Started	5-Feb-22	2-Mar-22	25			
WS10-AS09	26-Apr-22	5-Oct-23	542	453	7200	10.1
Best Day (Rings/Meters)			19-Jun-22 (22 / 35.2m)			
Best Week (Rings/Meters)			18 to 23-Jun-22 (113 / 181m)			
Best Month (Rings/Meters)			June 2022 (377 / 604.3m)			

Table 3. Key dates for TBM-2.

TBM-2 - AS09-WS07	Start	Finish	Total Duration	Working days	Length (m)	Productivity Per day in rings
Lowered on	2-Jan-22	27-Feb-22	56			
Initial Drive Started	28-Feb-22	22-Mar-22	22			
AS09-WS07	9-Apr-22	6-May-23	390	329	5879	11.23
Best Day (Rings/Meters)			25-Feb-23 (20 / 31.7m)			
Best Week (Rings/Meters)			22 to 27-Apr-23 (105 / 168.3m)			
Best Month (Rings/Meters)			March 2023 (356 / 569.0m)			

13. Conclusion

Constraints faced by the contractor were unprecedented. The delivery schedule of the TBMs was disturbed with Covid-19 pandemic restrictions in place. There was lack of skilled manpower availability, prolonged visa processes to enter the country were just a few of them. At the same time the contractual accountability to achieve key dates milestones were enforced. All of it pushed the contractor to develop and adopt a customized but efficient plan to launch a 148-meter-long Tunnel Boring Machine (TBM) inside a 15-meter diameter shaft located at a depth of 59.4 meters. Successful

TBM launching and completion of tunnelling works without significant delays are the testament that Umbilical launch method can be adopted as a feasible alternative. Despite having some safety concerns related to numerous pressurized hydraulic pipelines and cables hanging 60m down vertically, Umbilical Launch method is an impressive technique to launch TBMs in a confined space having limited time.

Acknowledgements

The writers acknowledge PHM for all the construction and design effort and PIL for actively managing the project.

References

Bernardeau F.G., Stypulkowski J.B., 2018. Innovative Concrete for Aggressive Ground in Qatar. in The North American Tunneling Conference (NAT), June 24-27, 2018, Washington, D.C. pp 227-235.

Cavelier, C., Salatt, A., Heuze, Y., 1970. Geological description of the Qatar Peninsula (Arabian Gulf): Explanation of the 1/100.000 geological map of Qatar. Bureau de Recherches Géologiques et Minières.

PHM-JV., 2021, C8532-PHM-GEN-TUN-MST-9 TBM Launching, PORR-HBK-MIDMAC C853/2 JV, Doha, Qatar.

PHM-JV., 2021, C8532-PHM-GEN-TUN-MST-10 Lowering and Assembly of TBM in Shafts WS10 and AS09, PORR-HBK-MIDMAC C853/2 JV, Doha, Qatar.

Sadiq, A., Nasir, S. 2002. Middle-miocene karst evolution in the state of Qatar. Arabian Gulf. Journal of Cave and Karst Studies, 64(2): 132–139.

Stypulkowski, J.B., Najder Olliver, A.M., Khalid Saif F S Al-Khayareen, 2023. Tunnelling in the Desert, Wakrah and Wukair Tunnel, Doha, Qatar, in "Expanding Underground. Knowledge and Passion to Make a Positive Impact on the World" Anagnostou, Benardos and Marinos (Eds) © 2023 The Editor(s), ISBN 978-1-003-34803-0, Open Access: www.taylorfrancis.com, CC BY-NC-ND 4.0 license, ITA-AITES WTC2023, Athens, Greece. https://doi.org/10.1201/9781003348030-118.

Stypulkowski, J.B., Khalid Saif F S Al-Khayareen, 2024. Successful Tunnelling in the Desert, Wakrah and Wukair Tunnel, Doha, Qatar. In Yan, J., Celestino, T., Thewes, M., and Eberhardt, E. (Eds.), Tunnelling for a Better Life (1st ed.). CRC Press, ITA-AITES WTC2024, Shenzhen, China. pp. 2162-2169.

SETC-2025
BELGRADE

TOPIC 2

USE OF NEW MATERIALS AND MACHINERY

Southeastern Europe Tunnelling Conference (SETC-2025)
1-3 October 2025, Belgrade, Serbia

DOI: 10.5937/SETC25007S

Next-Generation of readily biodegradable foaming agents for EPB TBMs

Mike A. Sposetti[a]*

[a]Sika Services AG, Tüffenwies 16 · 8048 Zürich · Switzerland; sposetti.mike@ch.sika.com

Abstract: The paper presents a new class of readily biodegradable foaming agents specifically engineered for EPB TBM applications. These advanced formulations incorporate enhanced biodegradable chemistries beyond traditional raw materials, delivering superior foamability, increased stability over time, and improved control of the excavated soil's rheology. Crucially, these properties are achieved without increasing the Foam Injection Rate (FIR), thereby reducing overall chemical consumption. An important advantage of this Next Generation Technology is the ability to develop a reliable Soil Conditioning Plan early in the project; this includes accurately forecasting the volume of foaming agent required per geological section, which supports effective planning and real-time consumption control throughout the excavation process. This Next Generation Technology of foaming agents offers a robust, environmentally conscious solution tailored to the demands of modern EPB TBM tunneling. It facilitates greater process control, reduces waste, improves safety, and enhances the reliability of tunnel excavation through all types of ground conditions.

Keywords: EPB TBM; foaming agents; soil conditioning; biodegradability

1. Introduction

1.1. Why is the Next Generation Technology of foaming agents needed

The application of Earth Pressure Balance Tunnel Boring Machines (EPB TBMs) has expanded significantly in recent years, particularly in projects involving cohesionless soils located below the groundwater table. Under these geotechnical conditions, the use of foaming agents with superior stability is critical to maintain chamber pressure, improve face support, and enable controlled and continuous spoil removal.

To meet these demands, foaming agents must demonstrate enhanced rheological control of the soil over time while minimizing overall foam consumption. Temporal stability of the foam has emerged as a key parameter in soil conditioning: extended foam life directly contributes to improved excavation efficiency and reduced resource utilization.

Recent developments in foam chemistry have introduced a Next Generation Technology of readily biodegradable foaming agents specifically engineered to address these challenges. These formulations exhibit increased surface tension and improved bubble stability, allowing the foam to remain functional over longer periods within the excavation chamber. This sustained performance not only enhances soil conditioning quality but also contributes to a measurable reduction in total foam volume required compared to conventional products.

As a result, higher Foam Expansion Ratios (FER) can be achieved in conjunction with lower Foam Injection Ratios (FIR), without compromising the mechanical behavior of the conditioned ground. The implementation of this Next Generation Technology contributes to a more stable and efficient

*Corresponding author: sposetti.mike@ch.sika.com (M. Sposato).

excavation process, enabling optimization of the TBM mining cycle and supporting adherence to project schedules in complex tunneling environments.

2. Basics of soil conditioning – Old Technology

2.1. Foam generation

A soil conditioner is a chemical product which is added to a soil, together with water, to improve soil physical and mechanical properties. Soil conditioning is the process to achieve this, and heavily depends from the generation of foam and the quality of the foaming system used.

The generation of foam, whether done in laboratory or in TBM, is divisible in two separate steps:

- Step 1: the surfactant is mixed with water at a certain concentration rate (Cf), creating the foaming agent.
- Step 2: the foaming agent is then mixed with air to create the foam.

The standard foams in the TBM industry are based on a surfactant, or tensioactive, called Sodium Lauryl Ether Sulfate (commercial name is SLES). As per Fig. 1, SLES is an ionic tensioactive that, when enters in contact with water, its molecules work like an emulsifier, bonding the water with its chemical structure.

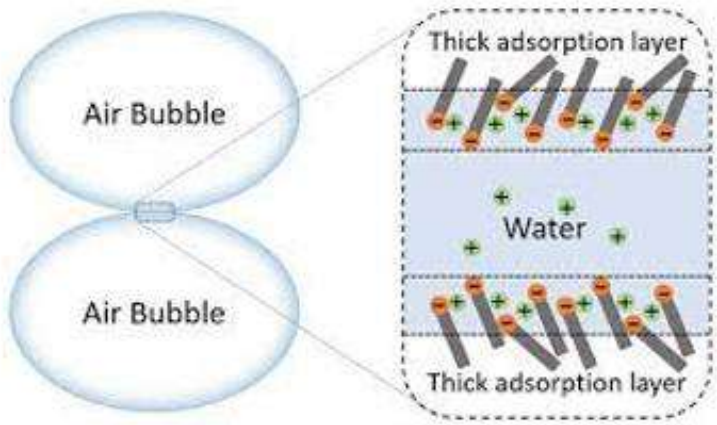

Fig. 1. Thick adsorption layers of SLES mixed with water, acting on air bubbles (Source: Peng et al., 2020).

SLES works on the surface of the bubbles favoring the stabilization of the air-liquid interface by developing the surface tension that allows the air bubbles to be generated. Initially once the foam is generated, bubbles are in small size but, with the passing of time, these tend to increase in their size in a simultaneous effect with the reduction of the surface tension applied on the external layer of the air bubbles.

The reduction of the surface tension on the external layer of the air bubble results at a certain point in the air bubble to implode, which effect is detrimental to the stability of the foam and its ability to work when mixed with a soil.

Therefore, the concept of time, which until now has not been properly addressed by the industry, is now a vital parameter that must be taken in consideration when we condition a soil in a TBM.

2.2. Foam parameters

Foams are generated and used through the control of these three essential parameters:

- Concentration (Cf), expressed in percentage as the rate of tenside inside the foaming agent; the higher the Cf, the stronger the foam from the chemical and mechanical point of view.
- Foam Expansion Rate (FER), as the ratio between the volume of air and liquid; the higher the FER, the drier the foam; FER is the indication of quality of the foam and the indication of how much air is trapped inside the bubbles; as a matter of example, a foaming agent foamed at FER 10 means that it expands its volume ten times.

Fig. 2. Example of one foam at same Cf expanded at three different FER (Source: Sposetti, 2023).

- Foam Injection Rate (FIR), expressed in percentage as the ratio between the volume of the foam and the volume of the soil; the higher the FIR, the higher the volume of the foam injected into the ground and, therefore, higher the consumption.

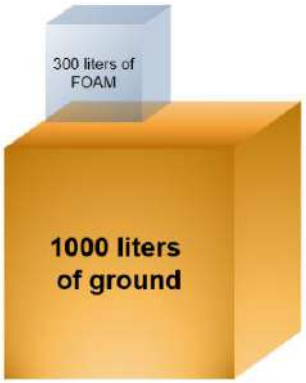

Fig. 3. Example of FIR 30%. The total volume in play is 1300 liters (Source: Sposetti, 2023).

3. Quality control

Historically, soil conditioning in Earth Pressure Balance (EPB) Tunnel Boring Machine (TBM) operations has been performed using foaming agents composed primarily of sodium lauryl ether sulfate

(SLES) and water, commonly referred to as the conventional or Old Technology. While these formulations were initially effective under basic tunneling conditions, their limitations have become increasingly apparent in modern tunneling applications, particularly those involving heterogeneous soft ground strata with variable permeability profiles.

When operating EPB TBMs through such complex geological environments, maintaining control over soil rheology and face pressure becomes critical. Under these conditions, conventional SLES-based foams demonstrate a performance plateau when the Foam Expansion Ratio (FER) exceeds approximately 10. Beyond this threshold, the foam tends to lose structural stability, leading to reduced control over conditioned soil behavior. To compensate, contractors are often required to significantly increase foam injection rates, resulting in higher material consumption and suboptimal operational efficiency.

This degradation in foam performance has been quantitatively verified through standardized laboratory tests. One such test, the Half-Life Time (HLT) test, is defined by the Specification and Guidelines for the Use of Specialist Products for Mechanized Tunnelling (TBM) in Soft Ground and Hard Rock (EFNARC, 2005). The test assesses foam drainage stability under controlled conditions by measuring the time required for 80 grams of foam, generated at a specific foaming agent concentration (Cf) and FER, to drain 40 mL of liquid through a synthetic fleece into a graduated cylinder. The foam is generated using a laboratory foam gun calibrated to replicate those used in TBM operations. A schematic representation of the HLT test is shown in Figure 4.

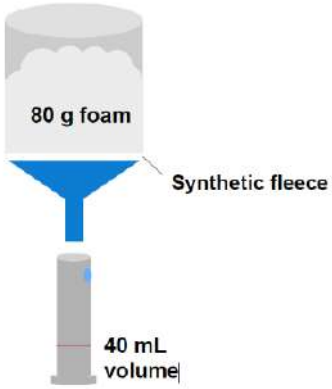

Fig. 4. Schematic diagram of the Half-Life Time test (EFNARC, 2005).

In typical tests of conventional SLES-based foaming agents, the recorded Half-Life Time ranges from 5 to 7 minutes. This limited drainage stability illustrates the inability of the Old Technology to maintain foam integrity at high FER values, reinforcing its inadequacy for advanced tunneling applications. As a result, foam utilization is constrained to a narrow operational window, limiting both its technical effectiveness and economic efficiency.

In addition to HLT testing, the Mechanical Resistance Test offers further insights into foam performance, particularly its structural resilience over time. Although not yet standardized, this test provides a practical evaluation of foam strength by measuring the time required for a water-filled ping-pong ball (approximately 18 grams) to descend vertically through a column of foam placed inside a transparent plastic cylinder. As with the HLT test, the foam is generated using a representative TBM foam gun. A schematic of the setup is shown in Figure 5.

The duration of the ball's descent serves as a proxy for the foam's internal resistance to deformation. A longer penetration time indicates a stronger foam matrix capable of better supporting the conditioned

soil. Comparative data between conventional and Next-Generation foaming technologies, presented in Figures 6 and 7, respectively, clearly illustrate the performance gap in both drainage stability and mechanical resistance.

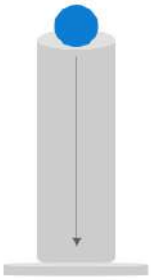

Fig. 5. Schematic diagram of the unstandardized Mechanical Resistance test (Source: Sposetti, 2023).

In summary, while SLES-based soil conditioners remain in widespread use, their limitations in modern EPB TBM operations are well-documented. Their inability to maintain stability and performance beyond FER 10 restricts their applicability in complex geologies, increases operational costs, and limits tunneling efficiency. These challenges underscore the need for advanced soil conditioning technologies capable of meeting contemporary performance standards.

4. Next Generation Technology – Sika Stabilizer-1215, 1219, 1515 TBM

Recent innovations in soil conditioning foaming agents have enabled a significant advancement in EPB TBM operations: the ability to consistently produce stable foam above the previously limiting Foam Expansion Ratio (FER) threshold of 10. This development marks the removal of what was long considered a practical upper limit, and introduces new flexibility in foam generation and management, resulting in more effective and efficient soil conditioning in varied ground conditions.

- The Next Generation Technology represents a new class of high-performance, readily biodegradable foaming agents, fully compliant with OECD biodegradability standards. These formulations offer substantially improved stability and foaming capacity while maintaining compatibility with standard TBM foaming systems. Using identical procedures for foam generation and standard operating parameters, including foaming agent concentration (Cf), FER, and Foam Injection Ratio (FIR), these agents are capable of producing highly stable foams at FER values significantly exceeding 10, without compromising performance or operational safety.
- Enhanced foam stability correlates with improved performance during TBM operation. As FER increases, the air bubbles formed within the foam exhibit a reinforced surface tension at their outer layer, maintaining structural integrity over extended periods. This prolonged stability ensures improved rheological control of the conditioned soil, enhancing face support and optimizing pressure management in the excavation chamber.

4.1. Technical and operational advantages

- Compared to conventional SLES-based foaming agents (Old Technology), the Next Generation Technology offers a broad spectrum of technical and operational benefits:
- Improved Drainage Stability: Significantly prolonged Half-Life Time (HLT) enhances foam durability during extended excavation cycles.
- High FER Compatibility: High foaming capacity enables operation at elevated FER levels without foam collapse, overcoming a key limitation of conventional agents.

- Optimized FIR Utilization: Lower FIR values can be employed to achieve desired soil rheology, reducing overall chemical consumption.
- Sustained Face Support: The high foam stability contributes to the maintenance of EPB chamber pressure, enhancing excavation control and reducing the likelihood of over-excavation or surface settlement.
- Enhanced Soil Conditioning:
  - Improved plastic deformation properties and cohesion of the excavated soil.
  - Reduced permeability, supporting better pressurization and spoil extraction.
  - Improved behavior in fine-grained soils, with reduced stickiness and clogging potential.
- Reduced Cutterhead Wear and Shield Friction: Lower internal friction and abrasiveness of the conditioned ground contributes to prolonged tool life and reduced energy consumption.
- These advantages translate into improved machine performance, reduced downtime, and lower environmental and operational costs. The enhanced rheological control, combined with the agent's biodegradable formulation, positions the Next Generation Technology as a significant step forward in the sustainable and efficient execution of mechanized tunneling projects.

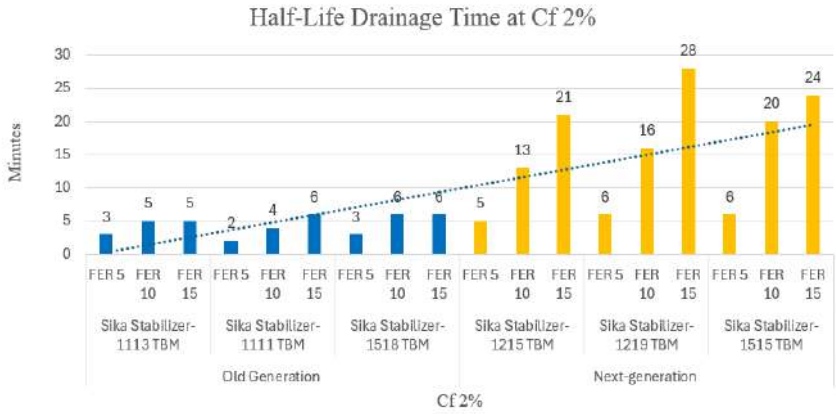

Fig. 6. Old and Next Generation Technology comparison HLT at Cf 2%.

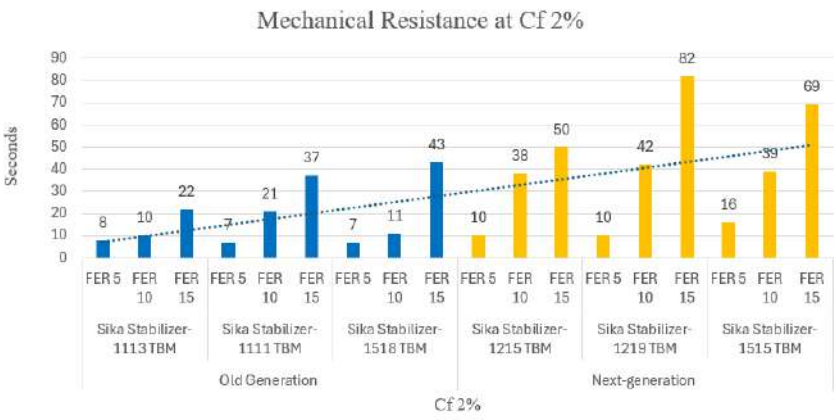

Fig. 7. Old and Next Generation Technology comparison Mechanical Resistance at Cf 2%.

5. Interpretation of results

To provide a robust and scientifically sound interpretation of laboratory test results—specifically the Half-Life Time (HLT) and Mechanical Resistance performance of Next Generation foaming agents, a comparative benchmarking framework was developed. This high-level technical evaluation includes a broad spectrum of commercially available foaming agents currently in use in the TBM industry, enabling a direct and rigorous assessment of relative performance.

This benchmarking exercise offers critical validation of the superior properties of the Next Generation Technology and underscores the growing performance gap between modern formulations and traditional SLES-based (Old Technology) foaming agents.

In 2020, the Department of Structural and Geotechnical Engineering and the Department of Chemical Engineering, Materials and Environment at *La Sapienza University of Rome* (Italy) introduced a novel classification system for foaming agents based on foam stability (Sebastiani et al., 2019). This system organizes foaming products into five classes, where Class I represents the highest level of performance in terms of foam durability and stability, and Class V denotes the weakest performing formulations.

The classification was established using HLT data at a foaming agent concentration of 2% (*Cf*) and a Foam Expansion Ratio (FER) of 10. In this work, traditional SLES-based foaming agents were plotted using HLT (Y-axis) versus FER (X-axis), as shown in Figure 8 (dark dots). These agents were predominantly clustered within Classes III to V, indicating limited drainage stability and durability.

In 2024, the same departments incorporated results from newly developed products—Sika Stabilizer-1215 TBM, Sika Stabilizer-1219 TBM, and Sika Stabilizer-1515 TBM—which belong to the Next Generation Technology. These products demonstrated significantly higher HLT values under the same testing conditions and were represented by star markers in Figure 8. Due to their distinctly superior performance, these foaming agents could not be placed within the pre-existing classification system, prompting the creation of a new, superior class beyond Class I.

It is also noteworthy that the earlier-generation Sika Stabilizer-1113 TBM, based on Old Technology, is included in the classification and falls into Class III, labeled as “Considerable Stability.”

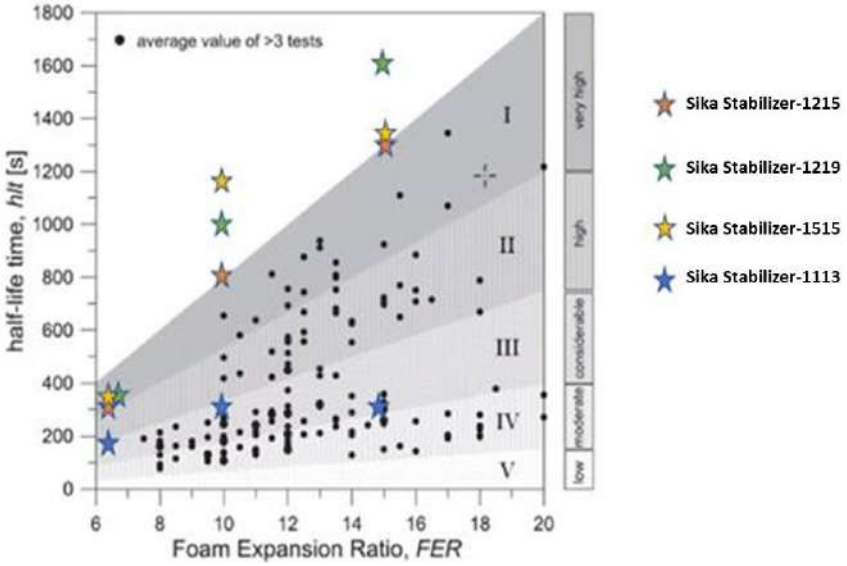

Fig. 8. Foaming products classification based on the stability of the generated foam.

To further reinforce the classification results, a second benchmarking analysis was conducted comparing HLT and Mechanical Resistance performance across four products: the Next Generation Technology (orange), Old Technology (blue), and two other commercially available foaming agents (red). Results were evaluated at three concentration levels (Cf = 1%, 2%, and 3%) with FER fixed at 10. The outcomes are presented in Figures 9 and 10, showing a clear and consistent performance advantage of the Next Generation foaming agents in both stability and mechanical integrity. Figure 9 illustrates HLT benchmarks, demonstrating significantly extended foam stability for Next Generation products at all tested concentrations. Figure 10 presents Mechanical Resistance test results, with longer penetration times indicating superior foam structural strength and cohesion.

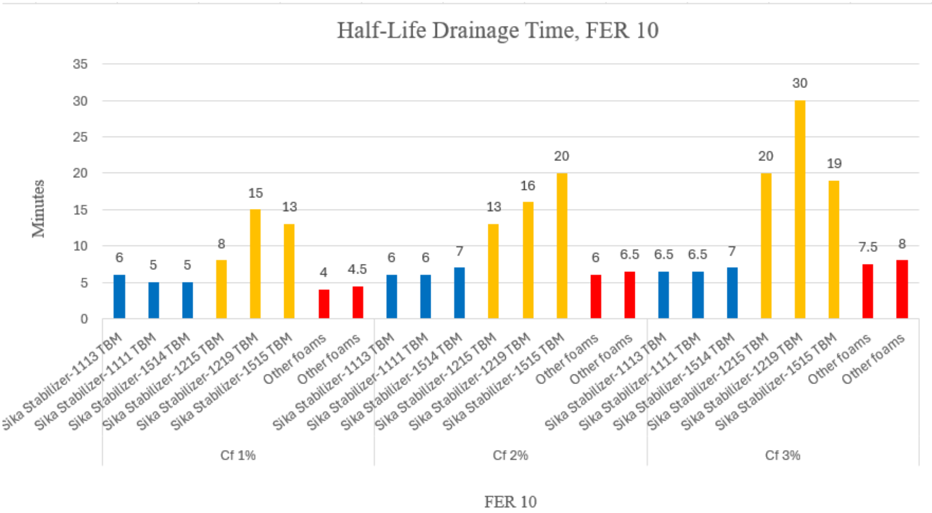

Fig. 9. Half-Life Time benchmark, FER 10.

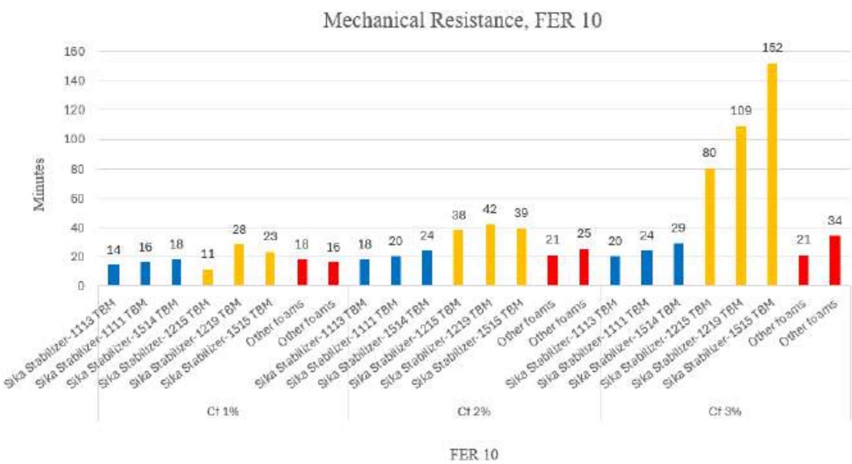

Fig. 10. Mechanical Resistance benchmark, FER 10.

5.1. Conclusions from benchmarking

The benchmarking and classification studies lead to the following key conclusions:

- The Next Generation Technology exhibits markedly higher drainage stability than all other tested foaming agents.
- Foam stability increases with FER, a behavior not observed in traditional products, which tend to destabilize beyond FER 10.
- No other foaming agents currently available in the TBM industry demonstrate comparable performance across both drainage and mechanical stability metrics.

These findings provide compelling scientific validation of the enhanced performance of Next Generation foaming agents and support their application in advanced EPB TBM operations requiring high reliability, extended stability, and optimized soil conditioning.

6. Conclusions

This study has presented and validated the performance of a newly developed class of soil conditioning agents, referred to as the Next Generation Technology, specifically engineered for use in EPB TBM operations. These advanced foaming agents represent a significant departure from traditional SLES-based formulations (Old Technology), offering substantial improvements in foam stability, rheological control, and environmental performance.

The Next Generation of foaming agents enables extended control over soil rheology, reducing the need for frequent reinjection of low-stability foams into the excavation chamber. This enhancement results in a measurable reduction in foam consumption, yielding both economic benefits and improved operational efficiency. The benefits are particularly pronounced in heterogeneous soils with variable permeability and in large-diameter TBMs (> 9 meters), where the excavation volume and stabilization demands are significantly higher.

The improved foam stability contributes to a more consistent excavation cycle, with enhanced control of face pressure, reduced risk of surface settlements, and minimized operational downtime. Additionally, the reduced quantity of active chemical agents in the excavated spoil, due to the high efficiency and lower required dosage of the Next Generation foams, represents a clear environmental advantage.

These technological improvements are especially relevant in the context of modern tunneling projects, which are trending toward increased tunnel diameters and longer excavation cycles. In such scenarios, the time factor becomes critical, as the ability of the foam to maintain stability over extended periods directly supports face pressure regulation and soil plasticity throughout the mining and ring-building phases.

From a practical perspective, the adoption of Next Generation Technology enables more predictable planning and control of the soil conditioning process. Contractors can now operate at higher Foam Expansion Ratios (FER) and lower Foam Injection Ratios (FIR), allowing for optimized foam usage and better forecasting of total conditioning costs.

In summary, the Next Generation foaming agents offer a comprehensive improvement over conventional products, supporting more sustainable, efficient, and cost-effective EPB TBM tunneling across a wide range of geological conditions.

References

EFNARC, 2005. Specification and Guidelines for the use of specialist products for mechanized Tunnelling (TBM) in Soft Ground and hard Rock".

Peng, M., Duignan, T.T., Nguyen, A.V., 2020. Significant effect of surfactant adsorption layer thickness in equilibrium foam films. *The Journal of Physical Chemistry B*, 124(25), 5301–5310. https://doi.org/10.1021/acs.jpcb.0c02883

Sebastiani, D., Vilardi, G., Bavasso, I., Di Palma, L., Miliziano, S., 2019. Classification of foam and foaming products for EPB mechanized tunnelling based on half-life time. *Tunnelling and Underground Space Technology*, Volume 92, 103044. https://doi.org/10.1016/j.tust.2019.103044.

Sposetti, M., (2023). New technology of readily biodegradable soil conditioning foaming agents. In book: Expanding Underground - Knowledge and Passion to Make a Positive Impact on the World (pp.1462-1469) Doi: 10.1201/9781003348030-174

Southeastern Europe Tunnelling Conference (SETC-2025)
1-3 October 2025, Belgrade, Serbia

DOI: 10.5937/SETC25008R

Design and construction of FRC tunnel precast segment with fibre enabled carbon footprint reduction

Benoit de Rivaz[a]*

[a] NV Bekaert, Zwevegem, Belgium; benoit.derivaz@bekaert.com

Abstract: The construction industry is a major producer of CO_2 emissions. The significant impact of the construction industry largely arises from the embodied carbon in the primary construction materials, cement and steel. In a tunnelling project, it is generally considered that 60% to 70% of embodied carbon is contained in the concrete linings of the shafts and tunnels. It is paramount, therefore that the tunnelling industry should pro-mote sustainable design. Fiber reinforcement plays a vital role in reinforcing concrete linings in underground structures and tunnels. This paper will explain how High-performance steel fiber reinforcement over rebar, combined with structural design optimization and the utilization of Supplementary Cementitious Materials (SCM) concrete mixture, the embodied carbon in the segmental lining and permanent spray concrete lining can be reduced by nearly 50%.

Over the past years the use of Fiber Reinforced Concrete (FRC) for finagling has increased dramatically. One aspect allows the boosting the use of FRC was the publication of guideline for FRC design: in 2012, the international Federation for structural concrete (fib) presented Model Code 2010 which include specification section on FRC. the Mode code 2020 just published has led to a successful and now widespread use of FRC in the final lining tunnelling with considerable benefits to owners, designers, and contractors. This paper will describe design principle and detail carbon counting from recent project around the world in Europe, Australia, North America and middle east.

Keywords: carbon counting; fibre-reinforced concrete

1. Introduction

Underground space plays a vital role in sustainable urban planning as it provides a solution to the limited surface area available. In terms of transportation, underground networks enable efficient and rapid mass transit, helping alleviate congestion and reduce carbon emissions. Moreover, underground space is essential for the infrastructure required to sustain cities, such as dense networks of pipes for delivering fresh water and sewers for wastewater treatment. Additionally, it accommodates the extensive network of cables and service stations necessary for modern communication systems. By utilizing underground space, cities can optimize their resource management and minimize their environmental impact, contributing to a more sustainable urban future. For a sustainable use of structural concrete, environmental and mechanical performances of concrete structures must have the same importance. By means of sufficiently high mechanical performances, the structural safety of a construction is ensured.

In a tunnelling project, it is generally considered that 60% to 70% of embodied carbon is contained in the concrete linings of the shafts and tunnels (Allen, 2021). It is paramount, therefore that the tunnelling industry does its utmost to significantly reduce or eliminate its use of cement in all applications – segmental linings, in-situ linings, sprayed concrete, and annulus grouts.

This is the reason why a great challenge for the coming years will be to develop solutions for low carbon lining.

*Corresponding author: benoit.derivaz@bekaert.com (Benoit de Rivaz).

Mechanical excavated tunnels (tunnels excavated with a TBM – Tunnel Boring Machine) are more and more used in Civil Engineering. In these tunnels, the lining is made by assembling precast segments used by the TBM as reacting elements in the excavation process.

The use of Fibre-Reinforced Concrete (FRC) allows to reduce or eliminate the traditional reinforcement in the precast segment production. Over the last twenty years, the use of this technology has increased. The use of Fibre Reinforced Concrete (FRC) allows several advantages, compared with traditional steel mesh or steel bar reinforcement according to fib bulletin 83 and all main recommendations published as:

Cracking control during construction phases

- Higher impact resistance
- Durability advantages at final stage
- Reduction of costs
- Sustainability advantages
- Boosting of the production process

Recent projects have demonstrated that structural ductility, durability, and sustainability are going hand in hand.

This holistic approach will be clearly a new booster for FRC tunnel lining. This paper will provide the start of the art on this issue, the key design principal and detail recent cases studies showing impact in carbon calculation saving in France, Middle East, and Australia.

2. Sustainability and Structural Requirement

For a sustainable use of structural concrete, environmental and mechanical performance of concrete structures must have the same importance. By means of sufficiently high mechanical performances, the structural safety of a construction is ensured. At the same time, a low environmental impact guarantees sustainable development, which is, in accordance with the definition by the Brundtland Commission of the United Nations, a "development that "meets the needs of the present without compromising the ability of future generations to meet their own needs" (Brundtland Commission, 1987).

FRC acts on the tensile behaviour of cracked concrete and imparts ductility to fragile material. FRC's excellent properties which overcome cracking as well as its improved durability over reinforced concrete are why we continue to develop that material and explain its economic success. Life Cycle Assessment (LCA) is a methodology for assessing environmental impacts associated with all the stages of the life cycle of a product or process. It quantifies a material impact on the environment over its entire existence, from extraction of the raw materials required for its production up to its end of life. This approach, combined with research into a low-carbon solution, will give new momentum to FRC.

3. Basic FRC Behaviour

A minimum tensile (strength) strength > 2200 MPa is recommended for final lining application considering the performance required and concrete classes.

The hooked ends ensure the desired fiber pull-out. This is the mechanism that generates the renowned concrete ductility and post-crack strength.

The tensile strength of a steel fiber has to increase in parallel with the strength of its anchorage. Only in this way can the fiber resist the forces acting upon it. Otherwise, it would snap, causing the concrete to become brittle. On the other hand, a stronger wire cannot be fully utilized with an ordinary anchor design. Therefore, the tensile strength of a fiber has to be perfectly aligned with its anchorage system and its diameter.

Wire ductility and concrete ductility are two different aspects. Dramix® 4D steel fibers create concrete ductility by the slow deformation of the hook during the pull-out process, and not by the ductility of the wire itself. The network provides by the fibre get a fundamental importance. Recommended diameter is 0.75mm and l/D= 80 to ensure a network > 10km/m^3 with 40kg/m^3. This network will play a key role in cracking control, structural ductility and allow low dispersion in the result.

Table 1. Influence of the l/D ratio on the network effect.

l/D	80/60	65/60	45/50
Length (mm)	60	60	50
Diameter (mm)	0.75	0.90	1.05
Aspect Ratio	80	65	45
Network (m/kg)	276	200	147

4. Design Principle

Model Code 2010 is the most comprehensive code on concrete structures. It covers their complete life cycle from conceptual design, dimensioning, construction, and conservation through to dismantlement. It is edited by fib Model Code 2010 and was produced through the exceptional efforts of participants in 44 countries from five continents. The fib bulletin 83 document aims to support designers, contractors and clients with guidance for the use of steel fibre-reinforced concrete, known as FRC, in precast segmental lining tunnels constructed using tunnel boring machines (TBMs) The document is intended to complement the fib Model Code 2010 (MC2010), which presents a section on the design of FRC, with the Model Code 2010 being considered as the reference basis for the design of FRC segmental lining.

Fig. 1. Design process.

The tensile behavior of the materials was characterized by performing bending tests on a notched beam. The tests were performed according to the EN 14651 European code, which is the reference standard for the CE label of steel and for ISO certification.

The compressive strength of the materials was measured by a testing cube with a side of 150 mm. For every cast made to produce every single segment, three beams were produced. In agreement with EN

14651, nominal strengths corresponding to four different crack mouth opening displacement (CMOD), namely 0.5, 1.5, 2.5 and 3.5 mm, were evaluated.

.

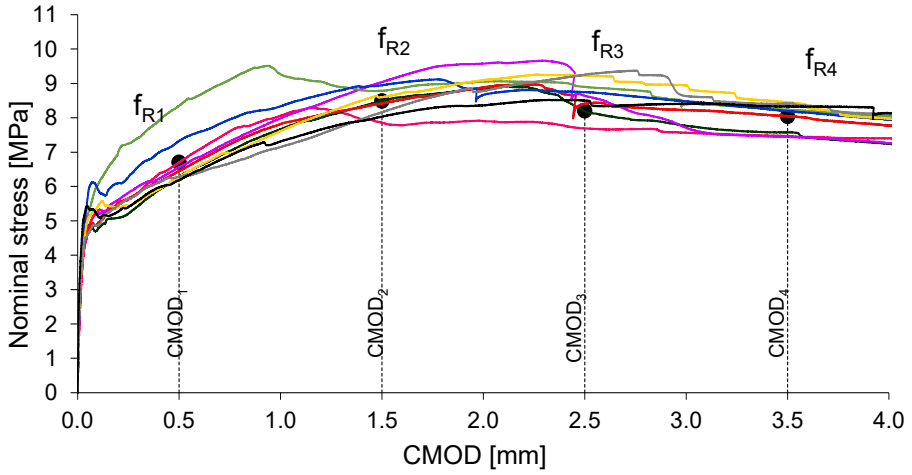

Fig. 2. Curve Load -deflection of the beam bending tests according to EN 14651. (Roma University Report).

Figure 2 and Table 2 shows a typical result of the beam tests considering 40KG fibre type Dramix® 4D 80/60BGP with significant strength values. FL is peak force, fR1 and fR3 are the stresses related to CMODs equal to 0.5 and 2.5 mm respectively. These values are the reference ones for final lining design performed according to the fib Model Code 2010 prescriptions

Table 2. Results of the beam bending tests according to EN 14651 mean and characteristic value (Roma University Report).

	f_L [Mpa]	f_{R1} [MPa]	f_{R2} [MPa]	f_{R3} [MPa]	f_{R4} [MPa]
Beam_01	4.68	6.70	7.86	7.69	7.47
Beam_02	4.90	6.28	8.49	8.20	7.58
Beam_03	4.78	6.45	8.41	8.42	8.04
Beam_04	5.15	6.56	9.04	8.64	7.44
Beam_05	5.72	7.33	8.95	8.75	8.19
Beam_06	5.03	6.27	8.60	9.23	8.45
Beam_07	5.63	7.75	10.2	8.99	8.54
Beam_08	4.60	6.28	8.16	9.25	8.40
Beam_09	5.43	6.18	8.03	8.50	8.33
Average	5.10	6.64	8.64	8.63	8.05
Characteristic	4.30	5.58	7.26	7.65	7.19

To dimension a steel fiber-reinforced concrete segment, a reference test methodology needs to be adopted for the characterization of performance. In addition to the mechanical performance, various properties of the FRC can be specified.

Since brittleness must be avoided in structural behavior, fiber reinforcement can be used as substitution (even partially) of conventional reinforcement (at ULS), only if both the following relationships are fulfilled:

- fR1k/ fLk > 0.4
- fR3k / fR1k > 0.5

Where fLk is the characteristic value of the nominal strength, corresponding to the peak load (or the highest load value in the interval 0 – 0.05 mm), determined from the EN 14651 beam test.

It is recommended to realize 12 beams per dosage and concrete mix formula.

If fibres are used as the only reinforcement for final lining, hardening post-crack behavior at section level (beam test) is allowed immediately:

- Cracking control at SLS
- Structural ductility (ULS)

The figure 2 how the typical expected result considering FRC only as reinforcement. The performance class according to Model Code 2010 in this example is C40/50 5e FRC material, which means,

- Fr1k> 5MPA
- Fr3k/fr1k> 1,3

Indeed, materials with fR1k ranging from 4.0 MPa mini to 6.0 MPa are commonly used for precast tunnel segments without any bar reinforcement, combine with a fR3k / fR1k ratio in the ranges 1.1 < fR3k / fR1k < 1.3 or1.3 < fR3k / fR1k < (class d and e respectively, according to the Model Code 2010 definition).

5. Carbon Counting

Among various construction processes, tunnel construction results in a significant amount of CO_2 emissions because almost all tunnels are lined with rein-forced concrete and utilize various high energy consuming equipment for excavation. Embodied carbon and high energy consumption can be minimized through three distinctive ways. Two main complementary approaches can be adopted to mitigate embodied carbon and reduce high energy consumption. The first method includes decreasing the overall quantity of reinforced concrete utilized through design optimization. The second approach is lowering the embodied carbon within each unit volume of the reinforced concrete by reducing the usage of Portland cement and steel rebar. This can be established by substituting Portland cement in the concrete mix low carbon binder and rebars by steel fibre. Indeed, the total mass of $C0_2$eq is what we want to minimize from environmental product declaration and by decreasing the total mass of material.

Table 3. CO_2 eq Factors from EPDs For Each Mix Design Component.

Mix Design Components	Portland Cement	Slag (GGBS)	Fly Ash	Silica Fume	Admixture	Aggregate	Rebar	Steel Fiber
CO_{2eq} Factor (kg CO_{2eq})	0.92	0.1466	0.093	0.014	1.67	0.06	1.85	0.7

An Environmental Product Declaration (EPD) is a document that transparently communicates the key environmental performance indicators of a product over its lifetime.

A third-party verification ensures that data relating to environmental aspects of Dramix® has been validated by an external organization.

This declaration is the Type III Environmental Product Declaration (EPD) based on EN 15804:2012+A1 and verified according to ISO 14025 by an ex-ternal auditor. It contains information on the impact of the declared construction materials on the environment. Their aspects were verified by

the independent body according to ISO 14025. Basically, a comparison or evaluation of EPD data is possible only if all the compared data were created according to EN 15804:2012+A1.

The environmental impact of Dramix® product (cradle to gate with options) is largely dependent on the energy intensive production of steel (half product) on which the manufacturer has only a limited influence. The carbon impact of steel production (Wire Rods) in the product stage A1 is as high as 85%. The impact of the production line largely depends on the amount of electricity consumed by manufacturing plant (0.34 kWh/kg of product). There are no significant emissions or environmental impacts in the A3 production processes alone (partly gas combustion). The production process itself does not have significant environmental impacts in the life cycle.

6. Low Carbon Precast Segment Case Studies

6.1. Grand Paris

The use of steel to replace all or a part of conventional reinforcement has been demonstrated to lower the embodied CO_2 of the segmental lining. While it is possible to significantly reduce the embodied CO_2 of a concrete mixture for segment production by replacing a portion of its cement content with alternative cementitious materials, there is little or no difference between the cementitious blends and contents required to produce fiber reinforced or conventionally reinforced concrete segments for tunnel linings.

Figure 3 shows an example reduction in CO_2 emissions on a project made possible by modification of the concrete and further reduction by being able to replace the rebar with steel fibers in a dosage that satisfied all the design requirements. On a per pound (kg) basis the embodied CO_2 of conventional rebar and steel fibers is assumed to be the same. This is a generalization assuming the wire rod that the fiber is produced from, and the rebar has similar % recycled material content and similar steel production methods. In a precast segment the reduction in carbon footprint is due to the steel fibers being more efficient in reinforcing the element. In this example the elimination of the right binder and steels fibre could conduct to a reduction of 70%.

Fig. 3. Project jobsite Grand Paris, photo credit by Eiffage Génie Civil.

The recent project for the Grand Paris Linea 16.1 has shown the following:

- From the saving in the ratio of fibers compared with steel reinforcement bars, leading to a significant reduction in CO_2 emissions during transportation. If we compare 85kg/m3 for steel reinforcement bars with the 40kg/m^3 for fibers, we get a saving on materials of more than 50%.
- By the benefit of better optimized loading for the fibers. 22 big bags of 1,100/kg per truck = 24.2 tons per load for the delivery of the fibers in comparison with 60 equivalent segments per truck = 17.85 T for the de-livery of the concrete reinforcement bars.
- From the small diameter of the fibers which helps to further limit toxic emissions from the primary steel industry, due to primary coils which do not exceed 1 mm of wire diameter. The drawing technology is low emission.
- Fewer trucks on the road and optimized waste management in a large city like Paris is an important element to take into account. From an ecological point of view, the carbon balance is therefore very positive. In this respect, Bekaert has recently obtained its EPD (Environmental Product Declaration) Type III ITB certificate number 215/2021.
- The concrete chosen for Line 16 Lot 1 fibre reinforced segments has a low carbon footprint of 170kg CO_2 equivalent/m^3 and reduces the carbon weight of the steel in the segments by 90kg equivalent CO_2/m^3 or nearly 11,000 tons equivalent CO_2 per 10km.

In terms of concrete, there will be a before and after Grand Paris Express. Until now, to design the segments, we used reinforced concrete, that is to say concrete poured around cages of massive metal reinforcements.

The graph hereunder illustrates the main impact gain in terms of carbon emission for typical precast segment ring used for a Metro tunnel.

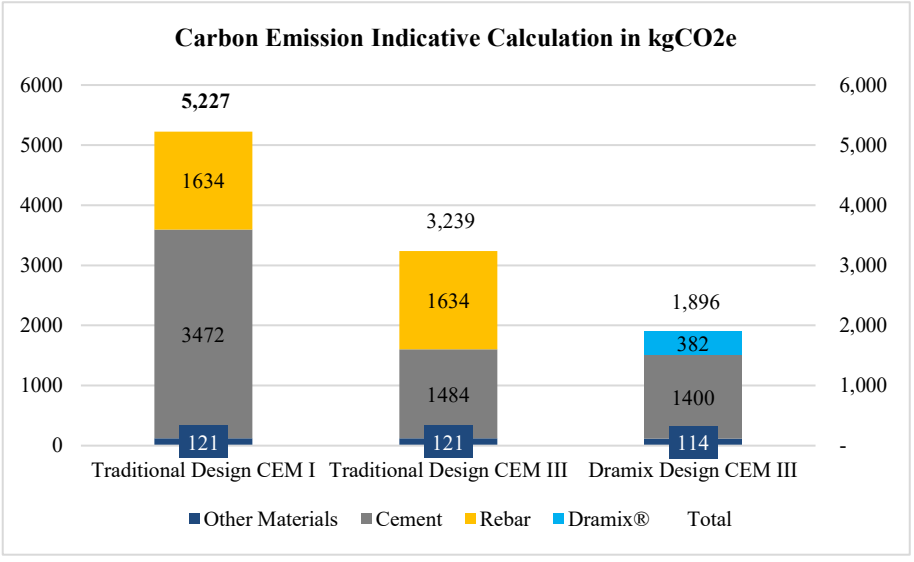

Fig. 4. Typical metro project, precast segment carbon emission counting.

This example, Fig. 4 is based on the following assumption.

- Using CEM III vs CEMI improves the CO_2 score significantly.
- As we use 60% less reinforcement (100kg rebar vs 40 kg Dramix®) and also average rebar EPD is higher than Dramix® EPD, we end up with this difference with reinforcement.
- Using FRC allows thickness reduction by 2cm mini which results in additional savings in concrete.
- Thickness 38 cm.

6.2. Middle East Journey

A paper by consultant COWI Denmark entitled 'Consultant's view of durable and sustainable concrete tunnel constructions in the Middle East" WTC 2018 Dubai provides this example how much CO_2 emission saving was reached by replacing traditional concrete and steel-reinforced with steel fiber reinforcement and adding GBBS/FA to the concrete mix. provides an example of reduction of concrete and further reduction by being able to replace the rebar with steel fibres in a dosage that satisfied all the design requirements.

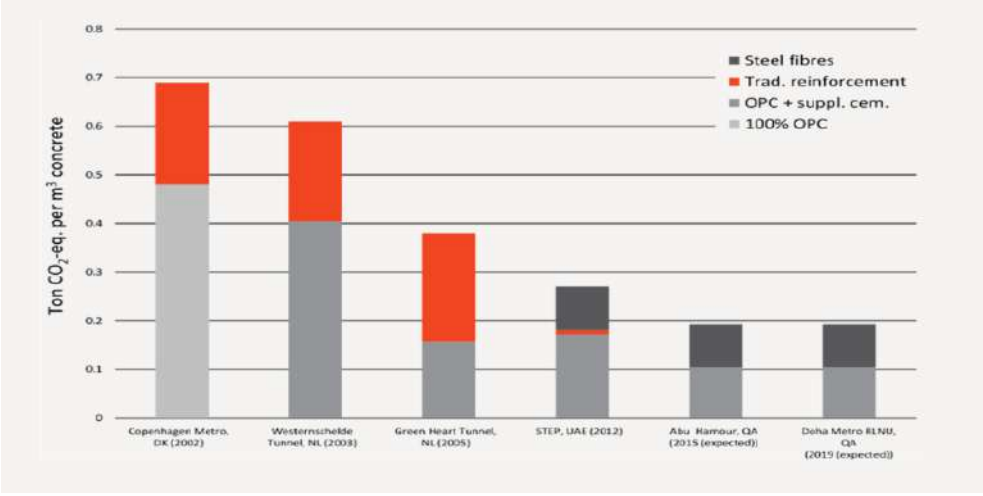

Fig. 5. Evolution of Precast segment lining (Cowi /C.Edvarsen publication WTC 2018).

This project as Doha Metro Green line has been designed with FRC using Dramix® fibre based on MC2010 to meet some specific condition:

- Very high chloride content: 10,000 - 50,000 mg/l
- High sulphate content: 100 – 5,500 mg/l
- High soil temperature: 28 - 32°C

Main advantages

- Increased resistance to chloride-induced corrosion
- Eliminated risk of stray current-induced corrosion
- Easier production/handling
- Simplified segment precasting process

This return of experience in Middle East demonstrates that by using FRC in-creased resistance to chloride-induced corrosion and reduced carbon footprint. Durability and sustainability go hand in hand.

6.3. The Montreal Metro Blue Line Extension Project

The Montreal Metro Blue Line Extension Project consists of construction of 6 kilometers of tunnel, as well as five new underground stations. This represents a good example showing that durability and sustainability goes hand in hand. Indeed, the reduction in segment thickness achieved with fibers can be primarily attributed to the concrete cover requirements of 60-75 mm on both intrados and extrados rebar to ensure the durability against corrosion when designing according to Canadian code CSA A23.1:19 (2019). In contrast, when subjected to chloride exposure, corrosion in steel fiber reinforced concrete is limited to just a few millimeters from the surface, and nonetheless, does not lead to spalling

cracks and is not regarded as a durability issue. CO_2 savings in the segments are realized by replacing rebar with steel fibers as the quantity of steel required is 50% less per m3 of concrete with fibers (40 kg/m^3 vs 80 kg/m^3). Additionally, the CO_2 equivalent factor for rebar is reported to be 1.85 vs 0.88 for fibers. The fiber reinforced segments can be reduced in thickness due to no requirement for cover like rebar. This quantity of concrete savings also lowers the carbon footprint.

The owners' design engineer, AECOM, as part of a commitment to integrating sustainability best practices, performed a study utilizing the Envision framework to evaluate alternatives to achieve a most sustainable infrastructure project. Based on the results of this study the TBM bored tunnel sections will be lined with steel fiber reinforced precast concrete segments using low-carbon Supplementary Cementitious Materials (SCM) concrete.

In the TBM tunnel sections lined with pre-cast concrete segments, high performance Dramix® steel fiber 4D80/60BGP with a dosage of 40 kg/m3 is designed as standalone reinforcement.

See the table below summarizing the results of the evaluation showing a reduction in total CO_2 equivalent by nearly 50% using SFRC with an optimized SCM concrete mix design.

Table 4. Embodied carbon in unit volume for the baseline and the optimized final mix designs.

		Baseline Concrete Mixture (OPC) with Rebar			**Optimized SCM Concrete Mixture with Steel Fiber**		
Mix Design Component	**CO_{2eq} Factor**	**Mass (kg/m^3)**	**CO_{2eq} (kg/m^3)**	**% Replacement by Mass**	**Mass (kg/m^3)**	**CO_{2eq} (kg/m^3)**	**% Replacement by Mass**
Portland Cement	0.92	475	437		346.8	319.056	
Slag	0.1466	0	-	0%	104.5	15.3	22%
Fly Ash	0.093	0	-	0%	0	0	0%
Silica Fume	0.014	0	-	0%	23.8	0.3	5%
Admixtures	1.67	4.5	7.5	1%	4.5	7.5	1%
Aggregate	0.006	1430	8.6		1430	8.6	
Steel bar	1.85	80	148		-	-	
Steel Fiber	0.92	-	-		40	36.8	
Total		**Total**	**601.1**		**Total**	**387.6**	

Table 5. Embodied carbon in unit volume for the baseline and the optimized final mix designs.

	Ring width (m)	**Tunnel length (m)**	**D_{ex} (m)**	**D_{in} (m)**	**Ring Volume (m^3)**	**Total concrete volume (m^3)**	**CO_{2eq}/m^3 (kg)**	**CO_{2eq}/1 m tunnel (ton)**	**Total CO_{2eq} (ton)**
40 cm Thick Segments	1.8	6000	9.4	8.6	20.4	67858	601.1	6.8	40,79
35 cm Thick Segments SCM w/ Fiber	1.8	6000	9.3	8.6	17.7	59046	387.6	3.8	22,886

6.4. The Forrestfield Airport Link

"The Forrestfield airport link is a "design and construct" type of project; it will deliver an 8.5 km extension of the existing PTA urban rail network in Perth, Western Australia, connecting the Midland Line, just past Bayswater Station, to Forrestfield. The twin-bored tunnels will travel underneath the Swan River, Ton-kin Highway and Perth Airport. The project will include three new stations; Recliffe Station (located underground in Redcliffe), Airport Central Station (located underground at Perth Airport to service both domestic and international terminals) and Forrestfield Station. The tunnel excavation diameter is 7,100 mm; the segmental lining has an inside diameter of 6,170 mm, and thickness of segment is 300 mm with an average length of 1,600 mm".

The segmental lining was designed to meet the project's concrete requirements of 120-year service life with a minimum water/binder ratio of 0.35. This article draws its attention to the specific concrete mix design from the design up to the construction phases of the precast segmental linings.

Several trials were performed with cast concrete beams according to standard BS EN 14651 (single trial was made with #9 concrete beams) with 35 kg/. The characteristic values of these results were more than the serviceability state 5.08 MPa at CMOD1 and 5.28 MPa at CMOD3. The results have confirmed the assumptions for the quantity reduction and the mix with 35 kg/m3 of Dramix® 4D 80/60BGP steel fibres content was adopted in project work.

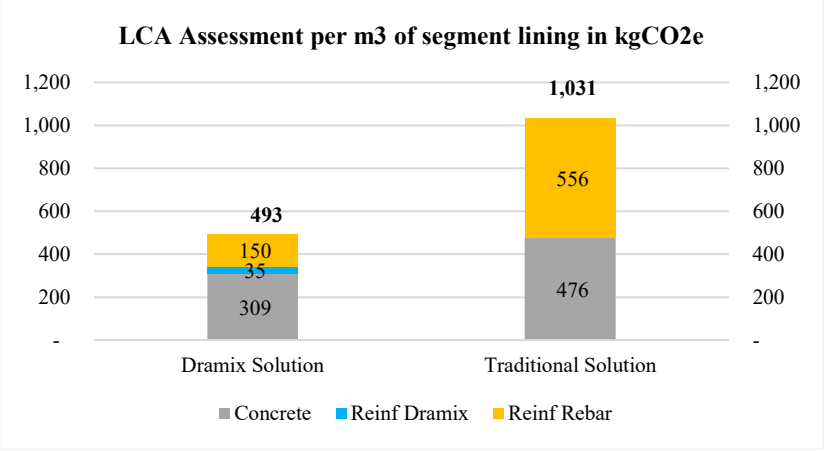

Fig. 6. One Click LCA calculation.

7. Conclusion

There has been a trend in the last years that concrete tunnel linings have increased material consumption, cost, and environmental loads. Nowadays develop and/or improve tunnel construction methodology to choose the optimal tunnel lining, including environmental footprint and cost-effectiveness. Create required knowledge to produce final lining to meet new large infra-structure projects with modern demands to functionality incl. 100-year service life and environmental impact.

The use of steel fibre reinforced concrete will highly participate in meeting low carbon lining by concrete consumption and steel reinforcement saving. If ductility-ty and durability have been the key words in the last 40 years, sustainability will be the key driver for further FRC lining development in the coming years.

Indeed, a new generation of binder combined with FRC allows new achievement:

- Provide excellent long-term durability performance exceeding that of Portland cement-based concrete.
- Excellent long-term durability performance exceeding that of Portland cement-based concretes. Extremely low embodied carbon footprint compared to conventional concretes on Port-land cement.
- Compared to reinforced concrete, fiber-reinforced concrete notably rep-resents savings of around 5,000 tons of steel for 10 kilometers of tunnels (Typical Metro Tunnel).

We all believe that tunnels should use smart and sustainable construction materials. The future of tunnelling is choosing these materials today. High Performance steel fibre could play an important role in this final lining sustainable journey.

References

Allen, C., 2021. Low Carbon Concrete/rules of the thumb. *T&T Journal*.

Brundtland Commission. 1987. Our Common Future. Report of the World Commission on Environment and Development, 1987. United Nations World Commission on Environment and Development. Published as Annex to General Assembly document A/42/427.

EN 14651. 2005. Test Method for metallic fibre concrete. Measuring the flexural tensile strength.

April 2022. *A leap forward for SFRC segmental linings in France*, Tunnel Tech.

Edvardsen, C., 2010. The consultant's view on service life design, WTC Congress, COWI A/S, Paral-lelvej

FIB. 2010. *Model Code 2010 – First complete Draft*. Bulletin 55-56.

Forrestfield airport link project in Perth, Western Australia -Precast concrete segmental lining. S.C. Scaffidi, Salini Im-pregilo S.p.A., Milano, Italia now e Build Spa &A. Anders, S. Porto & E. Torres SI-NRW JV, Redcliffe, Perth, *Western Australia published in WTC 2019*.

ITB. 2021. *EPD – Environmental Product Declaration Type III ITB No. 215/2021.*

ITA TECH. 2024. *Low Carbon Lining*. Guideline N°35.

October 2017. *Precast tunnel segments in fibre reinforced concrete fib bulletin 83*.

Verya Nasri, Medhi Bakshi, 2023. Design and Construction of FRC Tunnel Segments in North America with Fiber-Enabled Carbon Footprint Reduction. fib ACI 2023.

Southeastern Europe Tunnelling Conference (SETC-2025)
1-3 October 2025, Belgrade, Serbia

DOI: 10.5937/SETC25009Y

EPB TBM design for deep-overburden and long-distance tunnelling construction

Yin Yuefeng[a], Pang Peiyan[a], Cao Shulei[a], Yang Lin[a], Chen Ling[a]* and Zhao Qian[b]*

[a] China Railway Engineering Equipment Group Co., Ltd. (CREG), Zhengzhou City, Henan Province, China; chenling@crectbm.com, yinyuefeng@crectbm.com
[b] China Railway Engineering Equipment Group (Tianjin) Co., Ltd., Tianjin City, China
chenling@crectbm.com, yinyuefeng@crectbm.com

Abstract: This paper takes the earth pressure balance tunnel boring machine (EPB TBM) used in the Palermo-Catania (PA-CT) high-speed rail tunnel project in Sicily, Italy, as an example to analyze the numerous challenges encountered during deep-overburden and long-distance tunnelling. It conducts an in-depth analysis of key aspects such as cutter head overcutting, main drive lifting, shield structure and high thrust designs, as well as synchronous invert casting. Various innovative designs are proposed to address issues such as high ground pressure, TBM jamming due to ground convergence, wear during long-distance tunnelling, and construction efficiency. It is aimed to enhance the reliability and efficiency of EPB TBMs in deep-overburden and long-distance tunnelling, offering valuable insights for the design selection and construction of future projects.

Keywords: EPB TBM; deep-overburden and long-distance tunnel; overcutting; main drive lifting; synchronous invert casting

1. Introduction

With the growing demand for intercity transportation, regional economic development and resource exploitation in mountainous areas, the tunnel construction has gradually expanded from urban metros to intercity high-speed railways and mountain tunnels, bringing an increasing number of deep-overburden and long-distance tunnelling projects. As a commonly used underground tunnelling equipment, the EPB TBM (earth pressure balance tunnel boring machine) plays a crucial role in such projects. However, deep-overburden and long-distance tunnelling presents numerous challenges, such as high ground pressure, TBM (tunnel boring machine) jamming due to ground convergence and cutter head wear. Therefore, this raises the design requirements for the EPB TBM.

Taking the tunnel projects in Italy as an example, many tunnels have overburdens of over 100m, with some exceeding 400m, and lengths of more than 6km. These conditions require consideration of underground pressure, geological conditions, safety and excavation efficiency to ensure that the TBMs can construct safely and efficiently in deep-overburden tunnel projects (Amadini et al., 2021). This paper takes the Palermo-Catania high-speed rail tunnel project in Sicily, Italy (hereinafter referred to as "PA-CT project") as a case study and provides a detailed discussion on the design of the EPB TBM for deep-overburden and long-distance tunnelling from aspects including cutter head design, main drive lifting technology, shield structure design, thrust system design and synchronous invert casting system.

The PA-CT (Palermo-Catania) project is a twin-tube double-track high-speed rail tunnel located at the northwestern end of Sicily, Italy. In the future, it will connect three major cities, namely, Messina, Catania and Palermo. In this project, the longest section is approximately 15km, the overburden ranges from 10m to 400m, the minimum turning radius is 500m and the segment is 9000 in O.D. (outer

*Corresponding author: chenling@crectbm.com (Chen Ling); yinyuefeng@crectbm.com (Yin Yuefeng).

diameter) and 8000 in I.D. (inner diameter), 1800mm in width and adopts the 7+0 arrangement. The tunnel geology consists of clayey silt, sand layers, sandstone, argillaceous siltstone and quartzitic sandstone. The uniaxial compressive strength reaches up to 80MPa, while the geological strength index (GSI) of the rock is below 60. The maximum static ground and water pressure reaches 15bar, and during construction, the TBM faces risks such as convergence in soft rock strata (Zhu et al., 2016).

2. Targeted Designs

2.1. Special Design of the Cutter Head

2.1.1. Cutter head overcutting

For the deep-overburden and long-distance tunnel excavation, the cutter head overcutting function design is critical to accommodate various geological conditions. The combined method of heightening gauge disc cutters and reserved overcutting cutter housings is adopted to realize the flexible cutter head overcutting function. During normal excavation, the cutter head advances at its originally designed excavation diameter. When the overcutting is required, the installation height of the gauge disc cutters can be adjusted to move them outward. At the same time, additional cutters can be installed in the three reserved empty cutter housings, increasing the excavation diameter. The maximum radial overcutting range can reach up to 150mm. Furthermore, two additional hard rock copy cutters are included in the design to meet short-distance overcutting requirements in specific strata. As shown in Figure 1, the blue areas indicate the positions of the three reserved cutter housings and the pink areas represent the two hard rock copy cutters. For long-distance tunnelling, the overcutting is achieved by heightening the disc cutters and installing additional cutters in the reserved housings. This design not only enhances the adaptability of the cutter head but also ensures efficient excavation performance under varying geological conditions.

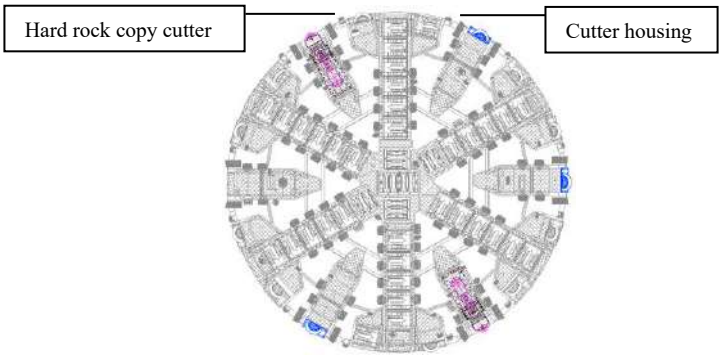

Fig. 1. Cutters for overcutting.

2.1.2. Cutter configuration and wear resistance

Based on the geological conditions, appropriate cutter types and arrangements are selected. This project involves hard rock and composite strata with upper-soft and lower-hard layers. Therefore, wear-resistant disc cutters are used and the cutter arrangement and spacing are optimized to improve rock-breaking efficiency and cutter lifespan. The dual-layer cutting structure is formed by adopting disc cutters with the cutter space of 90mm and cutter height of 185mm, and replaceable rippers with the same track and 25mm height lower than the disc cutter height. When the disc cutters are worn to a certain extent, the rippers can continue to bore, thus extending the overall cutter change interval, reducing the frequency of cutter changes, and improving construction efficiency and cost-effectiveness. In soft soil strata, the disc cutters at the front can be replaced with rippers and the number of replaceable ripper bits at the front can be adjusted according to the geological conditions of the project.

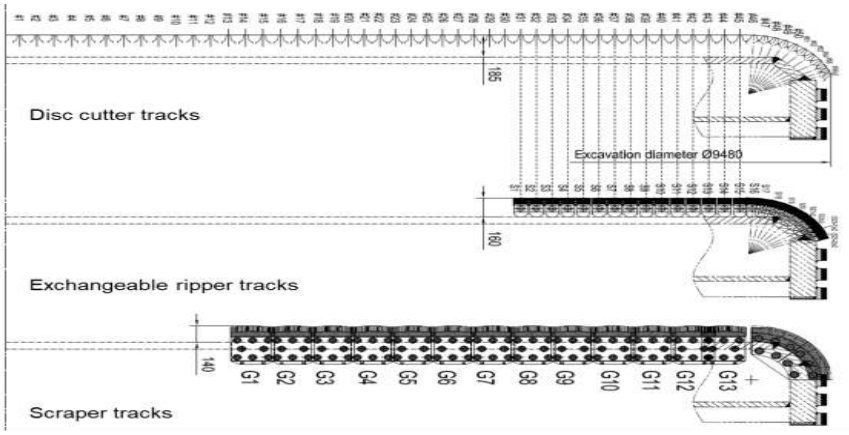

Fig. 2. Cutter track.

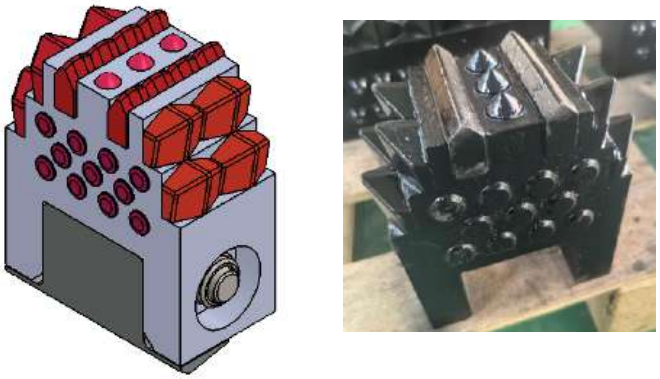

Fig. 3. Replaceable ripper bit.

2.2. Main Drive Lifting Design

To prevent TBM jamming caused by ground convergence at the tunnel crown during excavation, it is common to adopt the main drive lifting technology to achieve overcutting at the top of the cutter head. This also helps to avoid overcutting at the bottom of the cutter head, which can lead to the TBM "nosing down". While this main drive lifting technology is relatively mature in hard rock TBMs, its application in deep-overburden EPB TBMs remains undeveloped.

Unlike hard rock TBMs, the EPB TBMs advances with the excavation chamber under pressure, making the sealing between the lifting structure and the shield structure critically important. Inadequate sealing may allow the muck and slurry to flow from the excavation chamber into the inside of the shield structure, potentially leading to equipment failure and increased construction risks. Therefore, based on complying with the main drive lifting's basic functions, this project has also incorporated special sealing designs for the main drive lifting structure. Additionally, pre-reinforcement of the tunnel face is mandatory before lifting operations to create a relatively safe working environment and prevent large volumes of groundwater from entering the TBM through gaps during lifting, thereby mitigating unforeseen consequences.

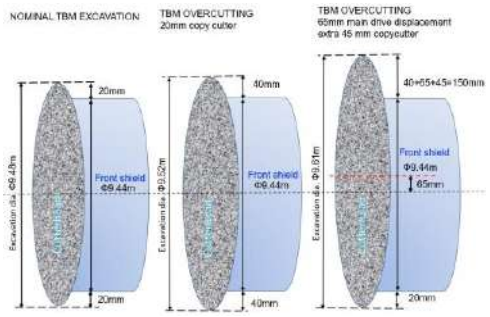

Fig. 4. Main drive lifting during overcutting.

2.3. Special Design of the Shield Structure

2.3.1. Step design of the shield structure

In deep-overburden strata, increasing the step between various parts of the shield structure (front shield, middle shield and tail shield) can help to alleviate TBM jamming caused by ground convergence. In the design of these steps, those factors such as strata characteristics, TBM dimensions and tunnelling parameters must be comprehensively considered to ensure their rationality and effectiveness. For conventional TBMs of similar diameter, the shield structure step is normally designed to be 30–35mm. After enlargement, the shield structure step can reach up to 100mm. In deep-buried strata, prolonged stoppage is not recommended, and the thrust speed should be maintained at no less than 10mm/min. For the specific construction process, the convergence rate of the strata and the minimum TBM thrust speed need to be determined based on calculations by geotechnical engineers to prevent the shield structure from jamming. In summary, a well-designed stepped configuration can significantly reduce friction between the shield structure and the strata, thus lowering the risk of TBM jamming and ensuring smooth advancement of the TBM. Additionally, the step design must be determined after considering factors such as support from the strata at the bottom of the TBM, prevention measures of backflow during tail shield grouting and TBM attitude control.

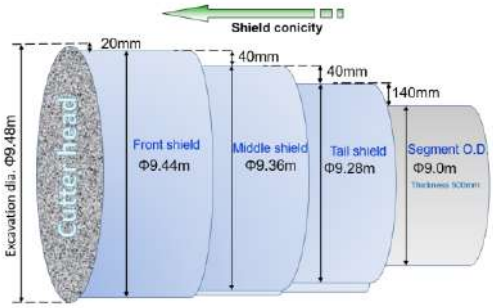

Fig. 5. Step arrangement of the shield structure.

2.3.2. Anti-roll design of the shield structure

When the shield structure has a large step and the cutter head needs to overcut, the contact area between the shield structure and the strata is reduced, which lowers the confining force exerted by the strata on the shield structure. This increases the risk of shield structure rolling. In addition to the conventional method of cutter head CW (clockwise) and CCW (anticlockwise) rotation, the fin stabilizer is also equipped to correct the rolling. This stabilizer consists of a driving component and a stabilizing component located inside the shield structure. One end of the stabilizing component is hinged to the

shield structure, and the other end is hinged to the driving component. The driving component uses a direct-drive mechanism to rotate and extend the stabilizer outward from the shield structure. The stabilizing component that contacts the strata is capable of penetrating into the earth, anchoring itself to stabilize the shield structure and thereby preventing rolling.

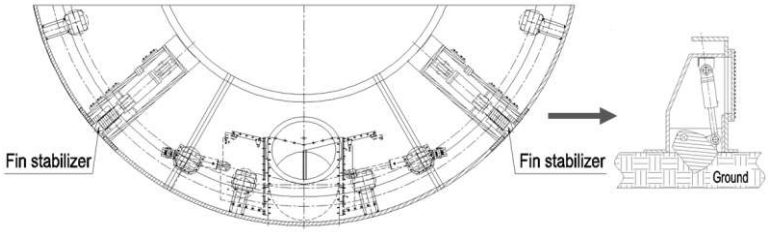

Fig. 6. Fin stabilizer.

2.3.3. Shield structure strength design

For deep-overburden tunnels, the shield structure must withstand significant strata pressure, water pressure and various loads during excavation. Therefore, it must have sufficient strength and rigidity to ensure operational stability and safety. Given that the front shield has abundant stiffeners and support structures inside it, while the tail shield is typically a circular structure without internal supports to accommodate segment erection, high-strength steel and rational structural configurations, such as sandwich structures or additional reinforcement plates, can be adopted to enhance its load-bearing capacity (DAUB, 2005). Considering that the maximum strata pressure encountered in this project may reach 15bar, a stress analysis of the tail shield under different scenarios is carried out based on the geotechnical parameters of the project. It is concluded that reinforcement steel bars are to be added inside the tail shield to meet the potential maximum earth and water pressure as well as any abnormal squeezing conditions.

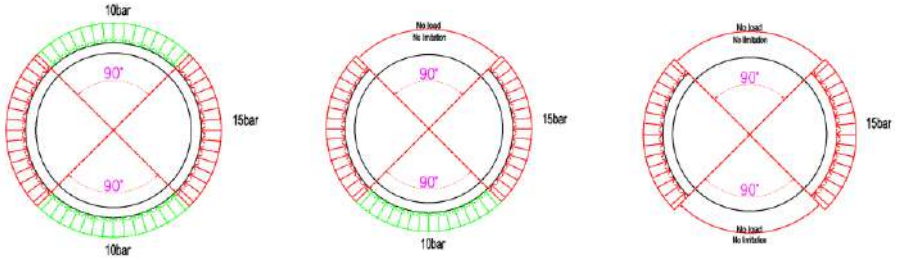

Case 1 Case 2 Case 3

Fig. 7. Stress conditions of the shield structure in the strata.

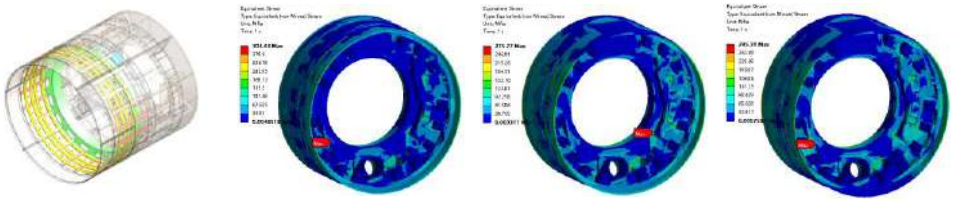

(**a**) (**b**) Case 1 (**c**) Case 2 (**d**) Case 3

Fig. 8. Stress analysis of tail shield with reinforcement plates. (a) Reinforcement schematic of the tail shield; (b) Tail shield stress analysis; (c) Tail shield stress analysis; (d) Tail shield stress analysis.

According to the stress analysis in the Fig. 8, it can be seen that the stress cloud map for case 1 shows a maximum calculated stress of 304MPa; for case 2, the maximum stress is 277MPa; and for case 3, it is 295MPa. In all cases, the maximum stress occurs at the junction between the reinforcement plates and the rear bulkhead. The plate thickness is 70mm, with a corresponding minimum yield strength of 325MPa. Therefore, the structural strength meets the requirements.

2.3.4. High-pressure breakout design of the shield structure

To prevent unexpected TBM jamming, the EPB TBM for this project is equipped with a sufficiently powerful thrust system, which can provide a thrust of 118,692kN. In addition, the machine features a high-pressure breakout capability of 550bar, which can generate a maximum thrust of 163,201kN to assist in breakout. Five rows with a total of 39 DN80 high-pressure water ports are reserved around the shield structure. The rock around the shield structure is continuously flushed by 1,000bar high-pressure water to being broken or loosened, creating an appropriate space for solving TBM jamming. This technique was first successfully applied by Seli Overseas on the Cociv Ramimero Project in Italy and has demonstrated good results.

Table 1. Configuration of the thrust system.

Item	Parameter	Unit
Cylinder specification	Φ300/240	mm
Cylinder quantity	42	pcs
Rated working pressure	400	bar
Rated thrust	118692	kN
Working pressure for breakout	550	bar
Thrust for breakout	163201	kN

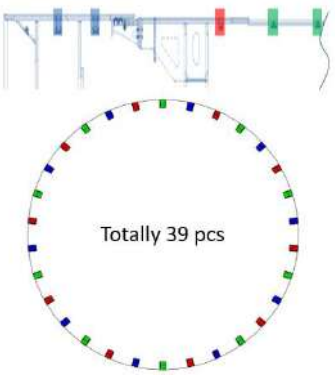

Fig. 9. Distribution of high-pressure water ports on the shield structure.

2.4. Back-up Synchronous Invert Casting System

In the traditional construction method of invert bridge casting, it is necessary to separately set up a track area, a concrete transport passage and a working platform. For tunnels with the inner diameter of being equal or greater than 8m, the height of the bridge structure usually occupies more than one-third of the tunnel's clear space, resulting in interference between material transportation and TBM advance. Moreover, invert casting can only proceed in sections after the tunnel face has been bored forwards a certain distance, leading to a non-continuous "excavation–waiting–casting" workflow. Statistics show that in traditional methods, invert construction typically is behind the tunnel face by 200–300m and requires dedicated mobile steel structures, which adds significantly to overall costs.

For long-distance tunnels with an inner diameter greater than 8m, a synchronous invert casting system based on an integrated back-up design can replace the traditional invert bridge system by using the "structural sharing + process coupling" approach. Due to the configuration of such TBMs, the back-up gantry is usually nearly 100m long, enabling the integration of the invert casting equipment directly onto the TBM back-up platform, which can satisfy the constraints of casting time and construction efficiency.

This system uses intelligent control to achieve precise coordination between excavation and casting, enabling accurate adjustment of concrete placing speed and levelling quality. It synchronously completes invert casting, levelling and curing operations, allowing excavation and casting to proceed at the same time. This reduces worksite interference, ensures timely formation of the invert structure, shortens construction periods, lowers costs and aligns with green construction principles. There are designated zones for casting cleaning, concrete placing, concrete levelling, concrete demoulding and mould transfer, concrete curing and concrete transfer on the back-up system. By optimizing the workflow, the system minimizes construction interruptions and significantly enhances the overall efficiency of both tunnel excavation and invert casting.

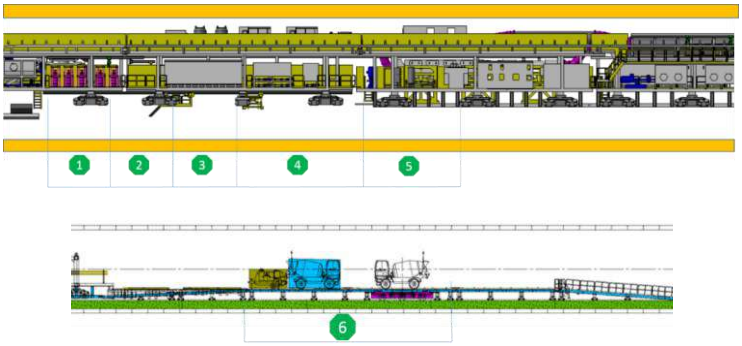

Fig. 10. Schematic diagram of simultaneous invert casting. 1-Cleaning area for concrete placing area; 2-Concrete placing area; 3-Concrete leveling area; 4-Demoulding and mould transfer area; 5-Concrete curing area; 6-Concrete transfer area.

Taking a Φ9.48m EPB TBM as an example, and assuming an average thrust speed of 60mm/min, the construction data for the system can be calculated as the following table.

Table 2. Construction data.

Item	Parameter	Item	Parameter
TBM thrust speed	60mm/min	Invert casting area	24m
Segment length	1800mm	Actual concrete placing section	6m
Segment erection	30min/ring	Embedded pipeline	6m
TBM advance speed per hour	1.8m/h		

It is evident that this synchronous invert casting system can theoretically match the TBM maximum daily advance speed of 36m, which is essentially its optimal performance, indicating that the casting efficiency can fully keep pace with advance speed and it is an efficient and cost-effective construction solution.

3. Conclusion

This paper takes the EPB TBM used in the PA-CT high-speed rail tunnel project in Sicily, Italy, as the research object. It focuses on addressing key challenges encountered during deep-overburden and long-

distance tunnelling, such as high ground pressure, TBM jamming, cutter head wear and low construction efficiency, and carries out innovative design and in-depth research in terms of cutter head, main drive, shield structure, back-up system and other aspects, forming a tailored EPB TBM solution suitable for complex deep-overburden and long-distance strata. The cutter head adopts designs such as heightening gauge disc cutters and reserved cutter housings, enabling flexible overcutting. The dual-layer cutter configuration extends the lifespan. The main drive lifting technology, together with sealing and advanced ground reinforcement, fills a technological gap in deep-overburden EPB TBM construction. The shield structure is optimized through stepped configuration, anti-roll design, enhanced structural strength, and high-pressure breakout capabilities to improve adaptability and safety. The back-up synchronous invert casting system enables the excavation and concrete placing can be implemented at the same time, significantly improving construction efficiency and reducing costs. The relevant design concepts and methods provide valuable references for TBM selection and construction in similar projects and offer important engineering application value and theoretical guidance for the advancement of deep-overburden and long-distance tunnel engineering. Future work may further integrate intelligent and information technologies to optimize system monitoring, fault diagnosis, and prediction of the TBM, thereby achieving safer and more efficient tunnel construction.

Acknowledgements

The authors would like to express their sincere gratitude to the project team of the Palermo–Catania (PA–CT) high-speed rail tunnel for their strong support and collaboration throughout the research and data collection process. The authors also appreciate the contributions of the on-site engineering staff and design team, whose practical experience and feedback greatly enriched the technical depth of this paper. Their collective efforts were instrumental in the successful development and application of the EPB TBM described in this study.

References

Amadini, F., et al., 2021. Case studies related to jammed TBM in rock. Gallerie e grandi opera sotterranee, Italy, pp. 15–25.

German Committee for Underground Construction (DAUB) – Shield Statics Working Group. 2005. Statische Berechnungen von Schildvortriebsmaschinen. *Tunnel* 7: 49.

Liu Haibo, 2021. Selection of Shield Machine for Great Depth and Long Distance Water-Carrying Tunnel Project [J]. *Haihe Water Resources*, 2021. (03):108-110+116.

Li Guang, Research and Application of Key Technologies for Small-Diameter Shield Machines in Long-Distance, Deeply Buried Tunnels. Henan Province, China Railway Engineering Equipment Group Co., Ltd., 2019-08-28.

Wang Zhenfei, 2023. Synchronous Construction Technology of Large-diameter Shield Tunnel for Single-track Railway [J]. China Railway, 2023. (03):58-62.

Zhu, Y., Xia, H., Hu, Z., 2016. An uplifting practice of shield tunnel in soft ground. *Rock and Soil Mechanics*, 37(S2), 543–551.

Southeastern Europe Tunnelling Conference (SETC-2025)
1-3 October 2025, Belgrade, Serbia

DOI: 10.5937/SETC25010S

Reducing the Carbon Footprint by Innovations in Tunnel Construction

Srđan Spasojević[a]*

[a] Geo.tunnel·konsult LLC, Belgrade, Serbia; srdjan.s@geotunnelkonsult.com

Abstract: Tunnels are a necessary transportation infrastructure element but substantially contribute to CO_2 eq. (Carbon) emissions and energy consumption. This paper is a gentle but fervent step towards minimization and better usage of resources that are the main "sustainable drivers" towards CO_2 eq. (Carbon) emission. An analysis of the carbon footprint was performed for drill and blast tunnelling near the Mratinje Dam in Montenegro. The life-cycle assessment (LCA) technique is employed to assess the environmental impacts associated with CO_2 emissions directly related to the materials production and tunnel construction activities. Two different alternatives were evaluated to identify where efforts should be focused to reduce the carbon footprint of the tunnel construction process. Different materials and approaches are examined to maximize sustainable opportunities. These examinations may help practitioners think differently and create new habits

Keywords: sustainability; tunnelling; carbon emission; resources, materials; drill and blast

1. Introduction

In 2020, the famous fictional Doomsday Clock was set to 100 seconds to midnight, and in 2023, it was set to 90 seconds to midnight (Bulletin of the Atomic Scientists, 2024). This is primarily but not exclusively due to the increased risk of nuclear escalation, but it is also influenced by continuing threats posed by the climate crisis and the breakdown of global norms and institutions needed to mitigate risks associated with advancing technologies and biological threats such as COVID-19 (Bulletin of the Atomic Scientists, 2024).

Almost 80% of global warming gas emissions by volume are carbon dioxide (CO_2). Of that 80%, approximately a third arises from sectors relevant to transportation infrastructure, including transport, cement and steel manufacture, and commercial energy consumption (Sun and Park, 2020; Hunziker, 2024). Therefore, the construction sector is responsible for 38 % of global greenhouse gas (GHG) emissions (United Nations Environment Program, 2020). There are six greenhouse gases to be accounted for: CO_2 (carbon dioxide), CH_4 (methane), N_2O (nitrous oxide), HFCs (hydrofluorocarbons), SF6 (sulphur hexafluoride), PFCs (perfluorocarbons) and NF3 (Masson-Delmotte et al., 2021). Tunnels are a vital part of transportation infrastructure and our modern societies. However, since they utilize various high energy-consuming equipment, they also substantially contribute to CO_2 eq. emissions and energy consumption, highlighting the importance of our work in reducing their environmental impact. Some research shows that more than 80% of the CO_2 emissions in the construction phase of a tunnel are attributable to the construction materials cement and steel (Nasri et al., 2023), however the CO_2 eq. emissions and energy consumption aspects concerning tunnelling are very complex, and many factors must be considered.

This study employs the life-cycle assessment (LCA) technique to assess the environmental impacts of CO_2 eq. emissions directly related to the materials production and tunnel construction activities in a specific project. Two alternatives were evaluated to identify where efforts should be focused to reduce

*Corresponding author: srdjan.s@geotunnelkonsult.co (S. Spasojević).

the tunnel construction process's carbon footprint. Different materials and approaches are examined to maximize sustainable opportunities and optimization potentials

2. CO_2 emission calculations

2.1. CO_2 emissions concerning the entire construction life cycle

Construction materials and activities in tunnel construction are significant sources of tunnel CO_2 emissions. The life-cycle assessment (LCA) technique is used to assess the environmental impacts of CO_2 eq. emissions related to all stages of a product's life (US Environmental Protection Agency, 2018). The life-cycle assessment (LCA) technique is defined by SRPS ISO 14040 (Institute of Standardization of Serbia, 2008) and SRPS ISO 14044 (Institute of Standardization of Serbia, 2009). CO_2 emissions are calculated by estimating the fuel consumed by machinery and transport equipment (diesel, electrical energy) and raw materials and then using the conversion factors to get kg CO_2 eq.

Transport and machinery equipment includes a wheel loader, waste dump truck, concrete mixer, concrete pump, lining trolley, shotcrete spraying machine, grouting pumps, drilling jumbos, power supply units, and axial flow fan.

Construction raw materials used in such analysis include cement, steel, sand, coarse aggregate, polyethene, silica fume, accelerators, plasticizers, polypropylene or steel fibers, polyester resin, etc.

The carbon emission factors are obtained from government organizations (Official Gazette of the RS, 2023), relevant international institutions (International Energy Agency (IEA), 2023), and literature. They mean the greenhouse gas emission per unit input expressed in kilograms of carbon dioxide equivalent (kg CO_2 eq).

The construction work and resource consumption analysis are done for a 1.0 m tunnel and can be applied to the entire tunnel length. The study includes and is limited to resource consumption for the following construction sequence: pre-grouting, excavation (i.e. drilling, loading, and blasting), ventilation, dewatering, scaling, spoil removal, installation of the initial lining (primary support – bolts, steel support or mesh and shotcrete), waterproofing, final (secondary) lining, and built-in parts, such as backfilling concrete, side-walk, kerbs, etc. Carriageway and subgrade works are not considered in this study.

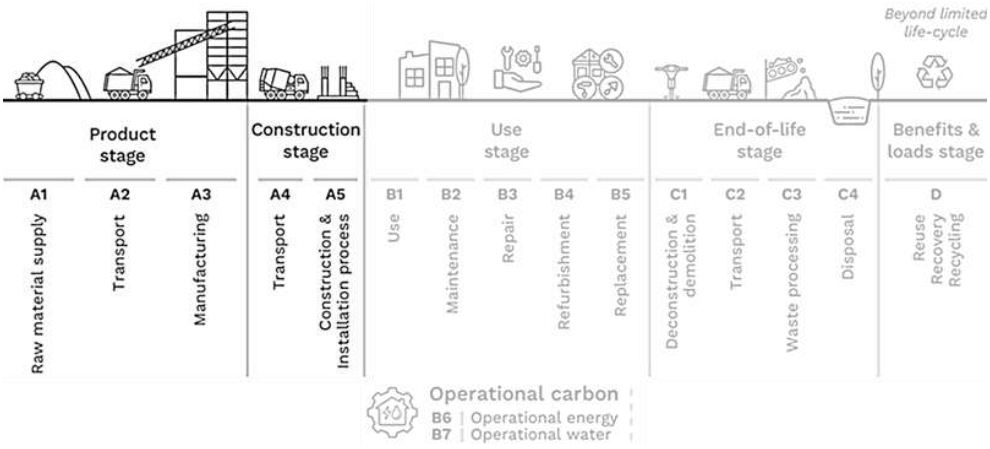

Fig. 1. Stages of a tunnel construction life-cycle according to SRSP EN 15978:2016 (Source: Institute of Standardization of Serbia, 2016), highlighting of phases considered in LCA calculations in this study.

The study is limited to the following life cycle phases: production stage (A1-A3), transportation (A4), and construction (A5) process stage, Fig. 1. The analysis does not consider the life cycle phase during usage of the object, repairing and managing (B1-B7), and the end-of-life (C1-C4), i.e., tunnel recovery or demolishing and removing materials to be recycled. The author of the final design gathered and estimated the input data for the LCA study from the basic design documentation and other working estimations from similar tunneling projects. No records were collected during construction since there were a couple of delays in executing the tunneling work. However, the actual results should be further refined as the project progresses.

2.1.1. Tunneling cross-section and load-bearing systems

The subject of this study is the tunnel No. 10 on the road from Plužine to Šćepan Polje in the Republic of Montenegro (Spasojevic, 2022, 2025). The tunnel is part of the road designed to extend straight into the mountain after the Mratinje Dam. The tunnel structure is a single-tube double-track tunnel with an approximate cross-section of 56,40 m^2 for the road infrastructure (the theoretically useful area) and a minimum service life of 50 years. The tunnel excavation is designed to be executed using the drill and blast technique.

The LCA tunnel study deals with two fundamentally different solutions for hard rock tunneling:

- two-layer tunnel lining
- single-layer load—bearing system,

A two-layer tunnel lining is designed as a double shell system. First, the outer layer is placed—the initial tunnel lining (rock support system). The initial tunnel lining consists of shotcrete, reinforcing steel wire mesh, and rock bolts (Spasojevic, 2022, 2025), Fig. 2. It is installed after the excavation and designed to provide controlled stress release and redistribution in the surrounding rock. After the initial lining is completed, the final (secondary) lining is executed. The final lining (inner layer) is made from cast-in-place reinforced concrete (Spasojevic, 2022, 2025), Fig. 3. The secondary lining is load-bearing for long-term loads.

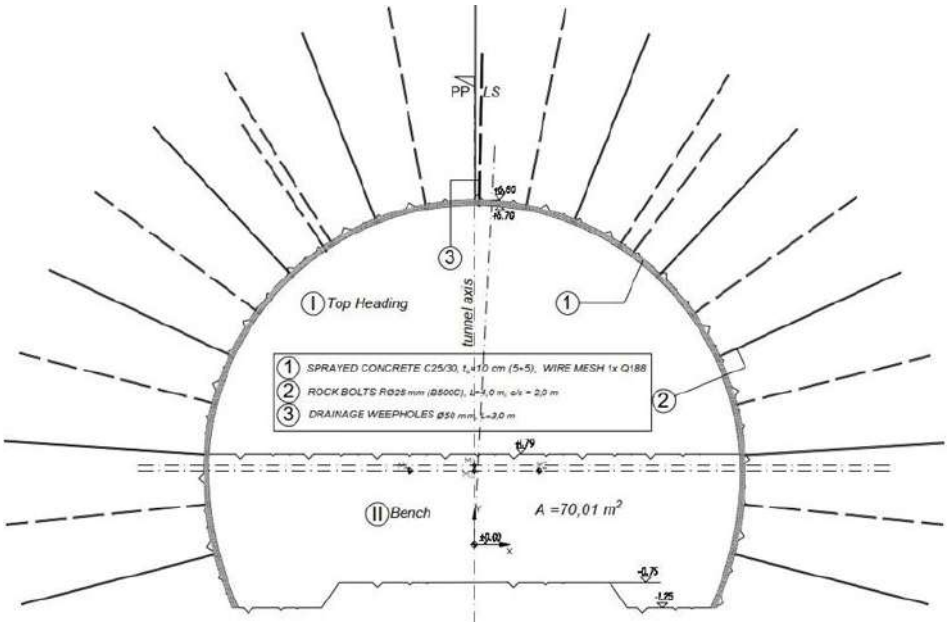

Fig. 2. Typical cross-section of the initial lining (rock support system) for a two-layer tunnel lining (Source: Spasojevic, 2022, 2025).

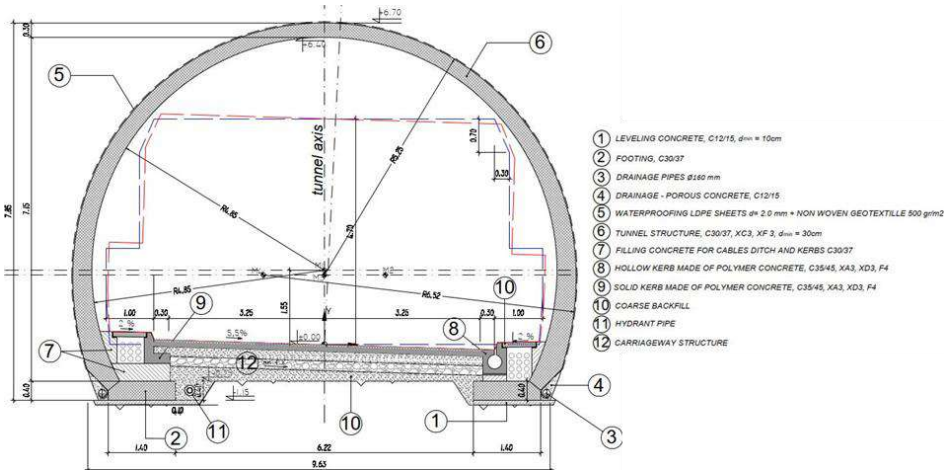

Fig. 3. Typical cross-section of the final (secondary) lining for a two-layer tunnel lining (Source: Spasojevic, 2022, 2025)

Single-layer load-bearing is similar to the initial lining of a double-shell lining, Fig. 4 and Fig. 5. The most significant difference is solving or reducing the presence of groundwater around the tunnel. Groundwater is the most important factor that leads to the decomposition of load-bearing elements of the initial rock support system in the case of a double shell system. This is solved by limiting groundwater inflow by pre-grouting the rock mass, Fig. 6. Further differences are the quality of the material properties for shotcrete and bolts. The quality of the shotcrete properties and bolts is much better. The compressive strength and durability of shotcrete are higher than those of the double-shell system. This is achieved by utilizing micro-reinforcement (fibers) and silica fumes. The rock bolts are characterized by a double protection system against corrosion, with a plastic tube and cement mortar (Spasojevic, 2022, 2025). In exceptional cases, an additional "protective" layer of shotcrete is designed to cover a single load-bearing system. This layer is not part of the load-bearing structure. It is designed with high compressive strength of C32/40 and includes polypropylene monofilament fibers (PP) to provide the required fire resistance and anti-spalling behaviour during fire or explosion accidents, Fig. 4.

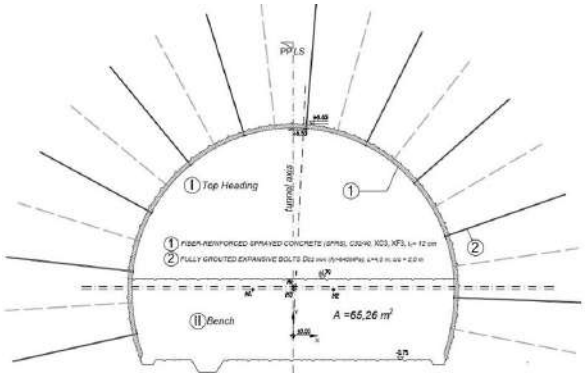

Fig. 4. Typical cross-section of the "protective" layer for the tunnel with the single-layer load-bearing lining (Source: Spasojevic, 2022, 2025).

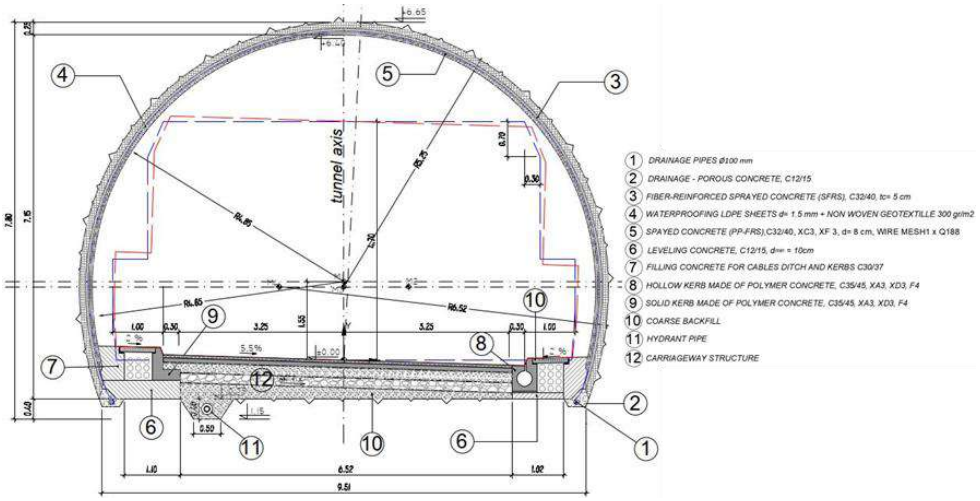

Fig. 5. Typical cross-section of the "protective" layer for the tunnel with the single-layer load-bearing lining (Source: Spasojevic, 2022, 2025).

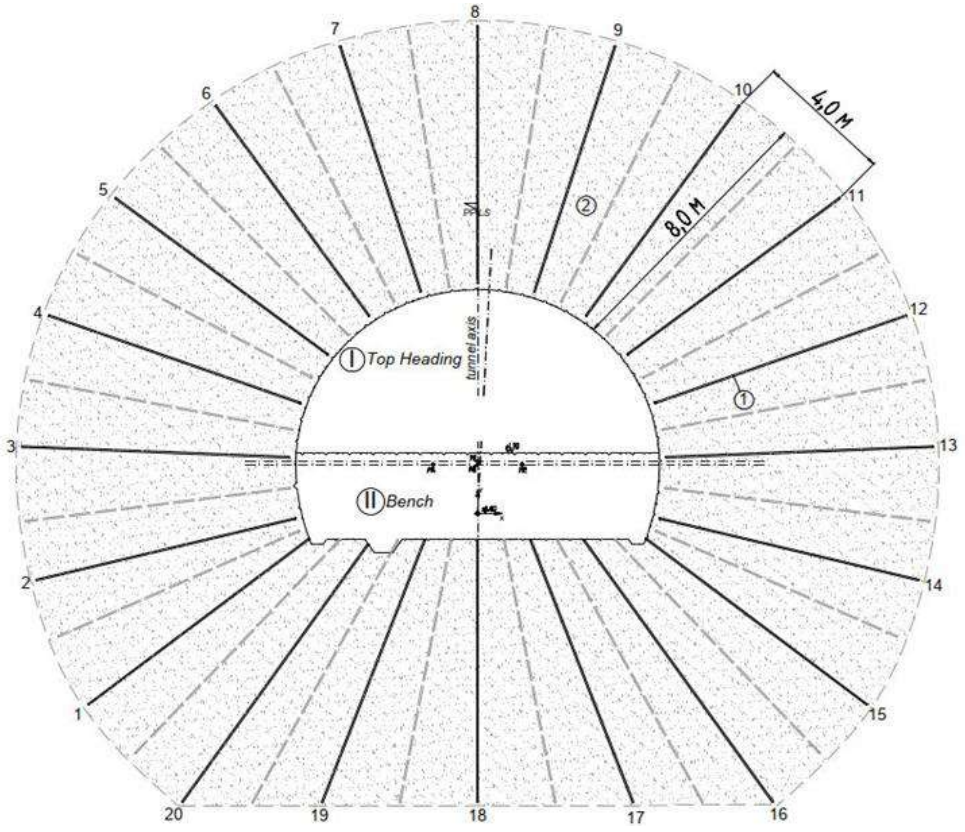

Fig. 6. Typical pre-grouting layout for the tunnel with the single-layer load-bearing lining (Source: Spasojevic, 2022, 2025).

3. Results and conclusion

The LCA tunnel study is divided into two main construction processes related to tunneling load-bearing systems or linings. The first process is related to constructing the load-bearing elements and rock support, which provide sufficient stability for the tunnel excavation. This is the initial tunnel lining for a two-lining tunnel system and rock support in the single-layer load-bearing system.

The second process is related to constructing the final (secondary) lining in a two-lining tunnel system and an additional "protective" layer of shotcrete in a single-layer load-bearing system. Fig. 7 and Fig. 8 shows CO_2 emission (kg CO_2 eq.) due to resource and raw material consumption for each defined construction process for the life cycle phases A1-A5.

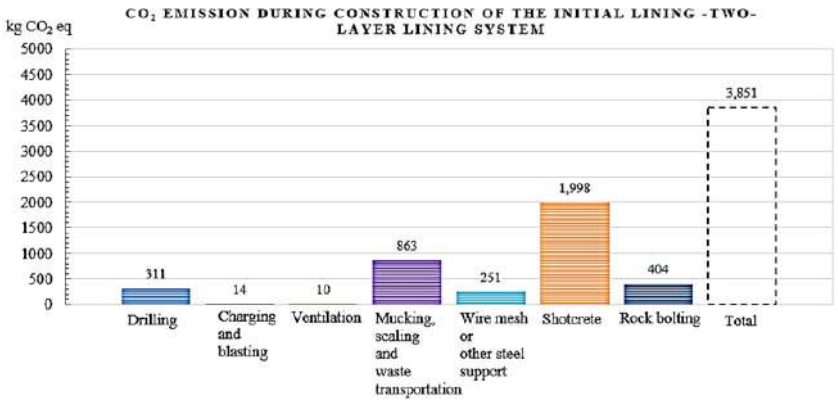

Fig. 7. Carbon emission (kg CO_2 eq) contributes to life cycle modules A1 - A3, A4, and A5 due to constructing the initial lining (primary support) in the two-lining tunnel system.

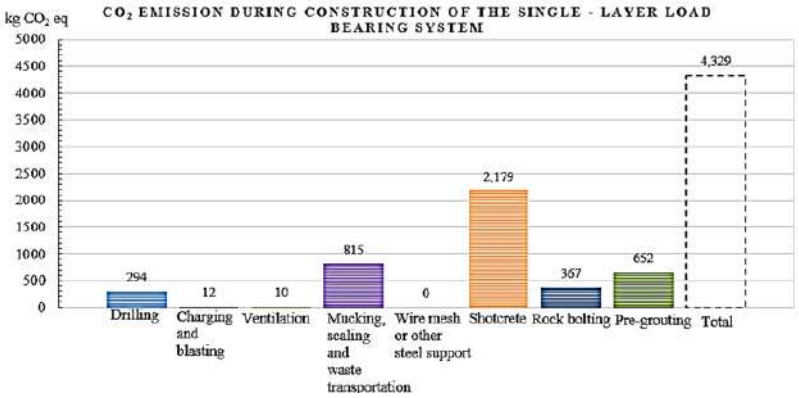

Fig. 8. Carbon emission (kg CO_2 eq) contributes to life cycle modules A1 - A3, A4, and A5 due to the construction of rock support in the single-layer load—bearing system.

Fig. 7, shows CO_2 emission due to the construction of the initial lining (primary support) for the case of a two-lining tunnel system. Fig. 8 shows CO_2 emission due to the construction of rock support in the single-layer load-bearing system.

The total CO_2 emission during the construction of the rock support in the single-layer load—bearing system is 4,329 kg CO_2 eq. The total CO_2 emission during the construction of the rock support in the initial lining (primary support) for the case of a two-lining tunnel system is 3,851kg CO2 eq. According to the estimates, the total CO_2 emission during the construction of the rock support in the single-layer

load-bearing is 12.4 % higher compared to the initial lining (primary support) for the case of a two-lining tunnel system.

Fig. 9 shows CO_2 emission due to the construction of the final (secondary) lining for the case of a two-lining tunnel system.

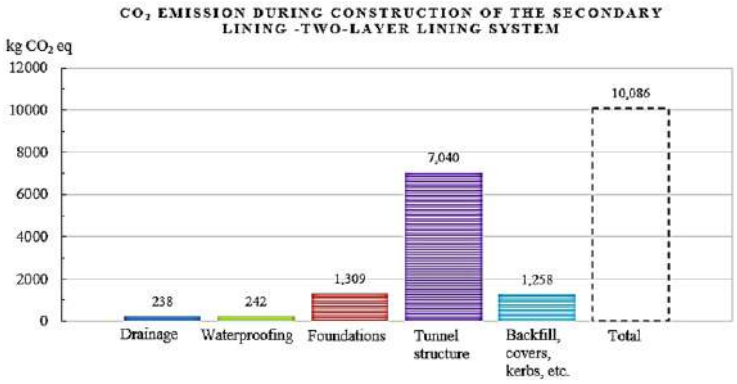

Fig. 9. Carbon emission (kg CO_2 eq) contributes to life cycle modules A1 - A3, A4, and A5 due to the construction of the final (secondary) lining for the case of a two-lining tunnel system.

Fig. 10 shows CO_2 emission due to constructing the "protective" layer for the tunnel with the single-layer load-bearing lining.

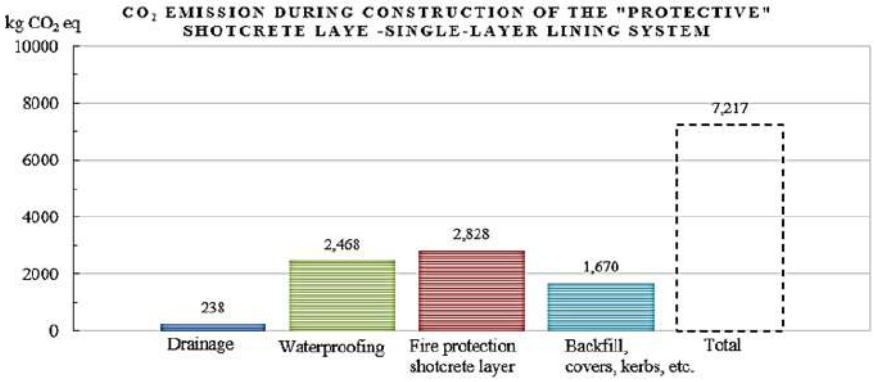

Fig. 10. Carbon emission (kg CO_2 eq) contributes to life cycle modules A1 - A3, A4, and A5 by constructing the "protective" layer of the single-layer load-bearing lining.

The total CO_2 emission during the construction of the final (secondary) lining for the case of a two-lining tunnel system is 10,086 kg CO_2 eq. The total CO_2 emission during construction of the "protective" layer for the tunnel with the single-layer load-bearing lining is 7,217 kg CO_2 eq. According to the estimates, the total CO_2 emission during the construction of the final (secondary) lining for the case of a two-lining tunnel system is 39.8 % higher compared to the case of a tunnel with a single-layer load-bearing lining. Collecting all estimations from Fig. 7 to Fig. 10, the total initial CO_2 emission of the construction of the two-lining tunnel system is 13,938 kg CO_2 eq, and for the single-layer load—bearing system is 11,546 kg CO_2 eq. The construction of the two-lining system produces 20.7 % more CO_2 emission than the single-layer load—bearing system. In rock conditions where a "protective" shotcrete layer is not required or pre-grouting works are insignificant, the total CO_2 emission drops to 8,066 kg CO_2 eq for the single-layer load-bearing lining. This is 30 % less. In this case, constructing the two-lining system produces 73 % more CO_2 emission than the single-layer load—bearing system.

The CO_2 emission distribution for the life cycle phases production stage (A1-A3), transport (A4), and construction (A5) process stage is shown below on Fig. 11.

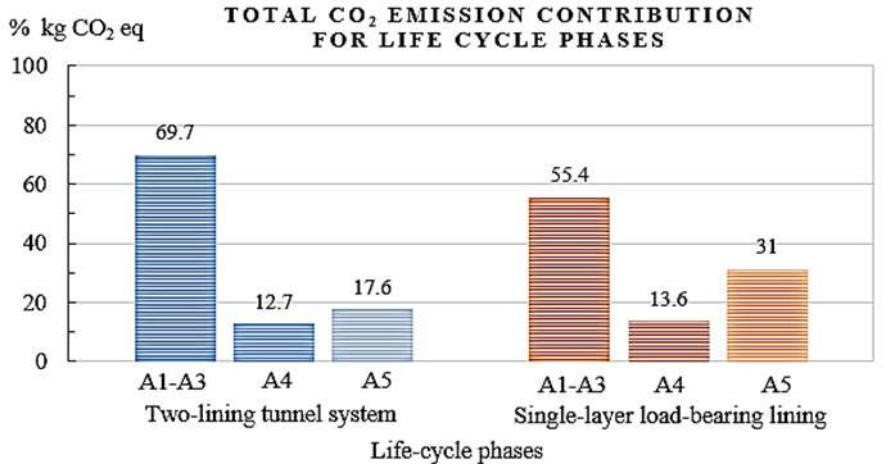

Fig. 11. The distribution of carbon emissions (in %) for life cycle phases production stage (A1-A3), transport (A4), and construction (A5) process stage related to tunnel lining systems.

The impact of life cycle phase A1-A3 dominates nearly all resource consumption in the CO_2 emission. According to Fig. 11, the carbon emission CO_2 from raw material input accounts for about 55.4-69.7%. The carbon emission CO_2 in life cycle phase A4 includes transporting all materials and products from producers and manufacturers to the construction site (Sun and Park, 2020). This phase generates similar share distributions for both tunnel lining systems. The life cycle phase "Construction" (A5) has a slightly higher impact for the single-layer load-bearing lining, 31%. This is due to increased resource consumption and activities necessary to construct an additional "protective" layer of shotcrete to cover a load-bearing system.

4. Conclusion

This paper compares the two fundamentally different tunnel lining solutions in hard rock tunnelling from a carbon footprint emission perspective.

The single-layer tunnel lining is operationally effective (time-effective) and results in cost savings (cost-effective) (Spasojevic, 2022, 2025).

Given the findings in this paper, it can be concluded that the carbon footprint emission can be reduced by at least 20.7% using single-layer load-bearing tunnel lining.

The study also reveals a very high carbon emission for a few materials and a very high contribution of the production stage (A1-A3) to all life cycle phases. Phases A1-A3 have a total share of 55-70 % of carbon footprint emissions. The influence of transport is comparable to other studies (Hopf et al. 2022). It follows that improvements in the production of raw materials are key to improving the life cycle assessment of tunnel structures. The usage of raw materials should be minimized by revising assumptions which are often conservative. Significant CO_2 reduction can be achieved by optimizing concrete mix design. This way, low-carbon or ultra-low concrete (or shotcrete) emissions of < 120 - 220 kg CO_2 eq./m^3 could be achieved. Reducing carbon related to steel is replacing steel bar reinforcement completely with structural fibers. The reduction in carbon related to grout could be by switching from a two-component system to a single-component grout with lower cement content where possible. To a certain extent, efforts should be made to equipment operation by considering and optimizing energy consumption.

This study can provide a reference for calculating carbon emissions throughout the life cycle of other tunnelling projects in hard rocks. The greatest hope is that it may help practitioners think differently and create new habits.

References

Bulletin of the Atomic Scientists. 2024. Doomsday clock.

Hopf, B.W., Hoxha, E., Scherz, M., Heichinger, H., Kreiner, H. and Passer, A., 2022. Life cycle assessment of tunnel structures: Assessment of the New Austrian Tunnelling Method using a case study. IOP Conference Series: Earth and Environmental Science 1078.

Hunziker, R., 2024. Monster Heat Hits 1/3rd of World Population. Counterpunch , April 23, 2024. Available online: https://www.counterpunch.org/2023/04/24/monster-heat-hits-1-3rd-of-world-population.

Institute of Standardization of Serbia. 2008. SRPS ISO 14040:2008 Environmental management - Life cycle assessment - Principles and framework, Belgrade, Serbia.

Institute of Standardization of Serbia. 2009. SRPS ISO 14044:2009 Environmental management - Life cycle assessment - Requirements and guidelines, Belgrade, Serbia.

Institute of Standardization of Serbia. 2016. SRPS EN 15978:2016 Sustainability of construction works - Assessment of environmental performance of buildings - Calculation method, Belgrade, Serbia.

International Energy Agency (IEA). 2023. Emissions Factors Database.

Masson-Delmotte, V, Zhai, P, Pirani, A, Connors, SL, Péan, C, Berger, S, Caud, N, Chen, Y, Goldfarb, L, Gomis, MI, Huang, M, Leitzell, K, Lonnoy, E, Matthews, JBR, Maycock, TK, Waterfield, T, Yelekçi, O, Yu, R and Zhou, B., 2021. Climate Change 2021: The Physical Science Basis. Contribution of Working Group I to the Sixth Assessment Report of the Intergovernmental Panel on Climate Change. Summary for Policymakers. Cambridge University Press, Cambridge, UK and New York, NY, USA.

Nasri, V., Bakhshi, M., Jarast, P., 2023. Carbon Footprint Reduction for Major Transit Projects. *Tunnel Business Magazine online*.

Official Gazette of the RS. 2023. The Rulebook on the Content of the National GHG Inventory and Content of the National GHG, No. 55/23, Belgrade, Serbia.

Spasojevic, S., 2022. Single-layer load-bearing tunnel lining structure in hard rock masses. *Building materials and structures*, vol 65, no. 4, pp. 167-177.

Spasojevic, S., 2025. Steps toward reducing carbon footprint in rock tunnelling. Tunnelling into a Sustainable Future – Methods and Technologies. Proceedings of the ITA-AITES World Tunnel Congress 2025 (WTC 2025), 9-15 May 2025, Stockholm, Sweden

Sun, H., Park, Y., 2020. CO2 Emission Calculation Method during Construction Process for Developing BIM-Based Performance Evaluation System. *Applied Sciences*, vol 10, no. 16, p. 5587.

United Nations Environment Programme. 2020. Global Status Report for Buildings and Construction: Towards a Zero-emission, Efficient and Resilient Buildings and Construction Sector. Executive Summary. Nairobi, Kenia.

US Environmental Protection Agency. 2018. Defining Life Cycle Assessment (LCA).

Southeastern Europe Tunnelling Conference (SETC-2025)
1-3 October 2025, Belgrade, Serbia

DOI: 10.5937/SETC25011F

Analysis of EPB TBM Torque Calculation and Component Assessment: A Case Study of Mashhad Metro Line 3

Ebrahim Farrokh[a], Davood Lotfi[b] and Mehdi Dalir[c]*

[a] Amirkabir University of Technology, Mining Engineering Department, Tehran, Iran; e-mail: e.farrokh@aut.ac.ir
[b] Tunnel Saz Machine Co., R&D Division, Tehran, Iran; d.lotfi@Tunnelsazmachine.com
[c] Tunnel Saz Machine Co., R&D Division, Tehran, Iran; m.dalir@tunnelsazmachine.com

Abstract: This paper presents a comprehensive analysis of EPB TBM torque calculations, focusing on the evaluation of eight torque components and conducting a sensitivity analysis for Mashhad Metro Line 3. The significance of accurate torque assessments in optimizing Tunnel Boring Machine (TBM) operations is highlighted. By examining the contributions of various torque components—such as those arising from soil resistance and frictional forces—the most influential parameters affecting overall cutterhead torque are identified. The findings provide insights into mitigation measures aimed at reducing TBM torque, ultimately enhancing operational efficiency during tunnelling projects. This research contributes to the understanding of cutterhead performance and offers practical recommendations for improving TBM operations.

Keywords: EPB TBM; cutterhead torque; soil mechanics; tunnelling efficiency; Mashhad Metro

1. Introduction

The construction of urban metro systems increasingly relies on mechanized tunneling methods, with EPB TBMs being a preferred choice due to their adaptability in soft-ground conditions (Farrokh and Lotfi, 2025). However, excessive cutterhead torque remains a critical challenge, leading to machine wear, delays, and increased costs. The increasing complexity of urban tunneling projects demands precise understanding of machine-ground interactions, particularly regarding cutterhead torque dynamics (Farrokh and Rouhani, 2022). Mashhad Metro Line 3 presents a unique case study where two parallel tunnels excavated with identical EPB TBMs exhibited markedly different torque behavior despite comparable machine specifications. The western tunnel segment, traversing coarse-grained soils, recorded cutterhead torque values approaching 10 MN-m—approximately 2.5 times higher than those observed in the fine-grained eastern section. This discrepancy, coupled with the uniformity of TBM specifications and operational protocols, provides a controlled setting to isolate the influence of ground conditions on torque generation. The unusually high torque values observed in the western tunnel segment led to reduced advance rates, increased cutter wear, and operational difficulties, thereby justifying a comprehensive analysis of torque components. The study is thus motivated not only by the torque difference itself but by its broader implications for TBM performance and the potential to optimize tunneling operations through targeted maitigation strategies.

While foundational models for torque estimation have been proposed (Zhang et al., 2016; Godinez et al., 2015; Zhou et al., 2018), most rely on theoretical assumptions or laboratory-scale simulations, limiting their applicability to field conditions. Recent studies have begun to bridge this gap by integrating machine learning and hybrid modeling approaches. Koohsari et al. (2023) demonstrated improved torque prediction by incorporating thrust force and geotechnical parameters. Hong et al. (2021) introduced a stage-based regression framework using LSTM networks to distinguish startup and steady-state torque behavior. Fu et al. (2022) developed a transfer learning model (TRLS-SVR) to

*Corresponding author: e.farrokh@aut.ac.ir (E. Farrokh).

enhance torque prediction across varying geological contexts. These studies underscore the complexity of torque behavior and the need for field-based validation to complement predictive models.

This research advances current knowledge by systematically evaluating eight torque components in EPB TBM operations using high-resolution field data from the Mashhad Metro Line 3. The consistent TBM specifications across tunnel sections allow for controlled comparison, while detailed geological and operational records enable correlation of torque fluctuations with soil properties and machine parameters. A sensitivity analysis identifies the most influential factors affecting torque demand, providing insight into the underlying mechanics of cutterhead resistance.

In addition to diagnostic insights, the study proposes targeted mitigation strategies to optimize TBM performance, including adjustments to cutterhead design, soil conditioning protocols, and control parameters. These findings contribute to a more granular understanding of torque mechanics and offer practical guidance for improving tunneling efficiency, reliability, and cost-effectiveness.

2. Project Overview: Mashhad Metro Line 3

Mashhad Metro Line 3 represents a critical infrastructure development in Iran's second-largest metropolitan area, comprising a 24-station alignment, 23.6 km route connecting Elahieh district in the northwest to Abuzar township in the southeast. (Fig. 1.).

Tunnel construction commenced in 2016 utilizing two identical Earth Pressure Balance Tunnel Boring Machines (EPB TBMs) with 9.4-meter diameters - among the largest TBMs deployed in Iran's urban tunnelling history. In the following sections, the geotechnical characteristics of the soil layers in the study area between chainage 4+700 and 5+700 for both western and eastern tunnels are explained.

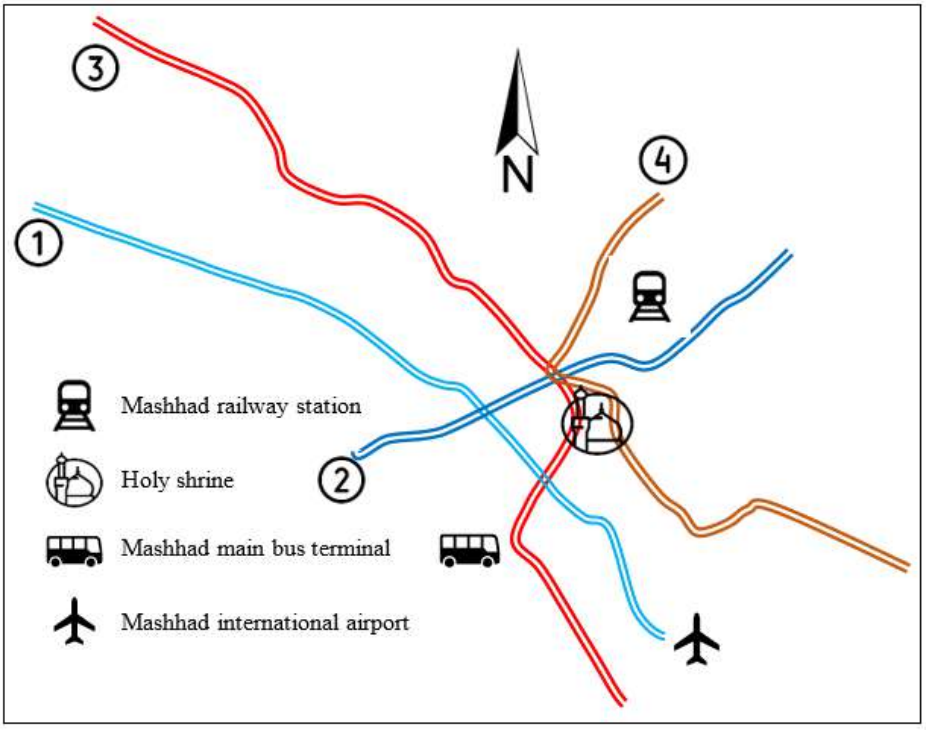

Fig. 1. Mashhad metro lines.

2.1. Western Tunnel

The western tunnel extends approximately 11,480 meters, with an overburden depth of 15–20 meters. Groundwater levels in the region range between 30–80 meters, placing the tunnel above the water table. Dominant soil unit comprises SM (Sandy Silt, often mixed with other soil types including GM (Silty Gravel). Standard Penetration Test (SPT) values are above 50 indicating very dense soil conditions. Key geotechnical properties are summarized in Table 1.

Table 1. Geotechnical data of soil units along the western tunnel route (Chainage 4700 to 5700).

Borehole	Approximate Chainage	Geological Units	Passing % (No. 200 Sieve)	Passing % (No. 4 Sieve)	Friction Angle (°)	Cohesion (kPa)
GB-31	4733	SM-GM	15-20	29-66	35	0
GB-30	5325	SM	19.1	>66	37	5
GB-29	5651	GM-SM	12.8-21.5	55-75	40	4

2.2. Eastern Tunnel

The eastern tunnel, approximately 13,800 meters long, traverses finer-grained soils with distinct geotechnical characteristics. Based on the geological cross-section, fine-grained soil units—including CL (clay) and ML (silt)—alternate with coarser-grained soils along the alignment. Toward the end of the tunnel, the proportion of CL (clayey soil) progressively increases. Key geotechnical properties are summarized in Table 2. In general, the soils encountered in the eastern tunnel are finer-grained compared to those in the western tunnel. The groundwater table is predominantly situated below the tunnel invert.

Table 2. Geotechnical data of soil units along the eastern tunnel route.

Borehole	Approximate Chainage	Geological Units	Passing % (No. 200 Sieve)	Passing % (No. 4 Sieve)	Friction Angle (°)	Cohesion (kPa)
QB-85	6048	ML-CL	>75	100	15-18	20-40
QB-86	5994	CL	>57	100	-	-
QT-87	5960	ML	>56	100	-	-

3. Analysis of cutterhead torque components based on operational data

In estimating the cutterhead torque (T) of EPB and Slurry TBMs under face pressure, eight key components are typically considered (Table 3 and Eq. 1).

Table 3. Cutterhead Torque Components.

Torque Component	Description
T1	Torque required for soil excavation
T2	Frictional torque on the cutterhead's front face
T3	Frictional torque on the cutterhead's rear face
T4	Frictional torque on the cutterhead's peripheral surface
T5	Reactive torque from cutterhead structure rotation
T6	Torque due to soil shear resistance against cutterhead openings
T7	Torque from mixing rods and cutterhead pedestals
T8	Frictional torque from the main bearing seal system

$$T = \sum_{1}^{8} T_i \tag{1}$$

Fig. 2 presents an example of the torque calculation methodology for the cutterhead.

T1: Cutting torque			
R	4.6	m	*tunnel radius*
p	0.013	m/rev	*max penetration depth*
qu	1	MPa	*The compressive strength of soil*
Fc	9811	kN	*Net cutting force*
μ	0.1		*friction coef*
Tt	2306	kNm	*Torque at the tip of the cutting tools*
Tc	138	kNm	*crushing torque*
T1	**2443.1**	kNm	*Cutting torque*
T2: Cutterhead front face friction torque within the slurry or earth mud			
R	4.6	m	*tunnel radius*
A	66.5	m^2	*tunnel area*
n	0.33		*opening ratio*
Ps	207	kPa	*effective horizontal earth pressure at cutterhead center*
T2	**2827.3**	kNm	*Resisting torque from earth mud in front of TBM*
T3: Friction torque from cutterhead reverse side			
T3	**1414**	kNm	
T4: Circumferencial Torque			
R	4.6	m	*tunnel radius*
W	0.7	m	*Cutterhead width*
μ	0.1		*friction coef btw soil and steel*
Pr	207	kPa	*average effective radial pressure*
T4	**1925.5**	kNm	*Circumferencial Torque*
T5: main bearing rotation counter torque of cutterhead dead weight			
G	1350.0	kN	*cutterhead dead weight*
R1	1.4	kN/m	*main bearing rolling radius*
μg	0.004		*coefficient of rolling friction*
Pt	8802	kN	*axial load*
T5	**57**	kNm	*Resisting torque of main bearing sealing*
T6: resisting torque across the cutterhead openings			
R	4.6	m	
Ʈ	20.7	kPa	*Muck shear strength*
A	66.5	m2	*CH area*
n	0.33		*opening ratio*
T6	**1393**	kNm	*resisting torque across the cutterhead openings*
T7: The torque required to rotate the mixing bars and cutterhead frame pedestals (struts)			
Rb	2.6	m	*the distances btw the mixing bar and shield centerline*
Rp	1.4	m	*the distances btw pedestal and shield centerline*
Db	0.1	m	*the transverse dimensions of mixing bar*
Dp	0.5	m	*the transverse dimensions of pedestal*
Lb	0.5	m	*bar length*
Lp	0.9	m	*pedestal's length*
nb	4.0		*number of bar*
np	4.0		*number of pedestals*
μ1	0.15		*friction coefficient between the bars/pedestals and muck*
s'	167	kPa	*Effective face support pressure*
T7	**520**	kNm	*The torque required to rotate the mixing bars and cutterhead frame pedestals (struts)*
T8: Sealing device friction torque			
μm	0.2		*friction coefficient between sealing and steel*
Fm	1.5	kPa	*sealing pressing force*
ni	7.0		*Seal number*
Ri	1.1		*Sealing installation radius*
T8	**16**		
Total			
T	**10595**	kNm	*Sum*

Fig. 2. Cutterhead torque calculation considering component breakdown.

T1 (excavation torque) is typically calculated based on the effort required to overcome the soil's unconfined compressive strength (q_u), as illustrated in Fig. 3. This component generally results in a

relatively low torque value. However, another contributor to the excavation torque—often overlooked—is the frictional force (Ff) acting on the tip surface of the cutters. This additional torque is referred to as Tt in this paper, also depicted in Fig. 3.

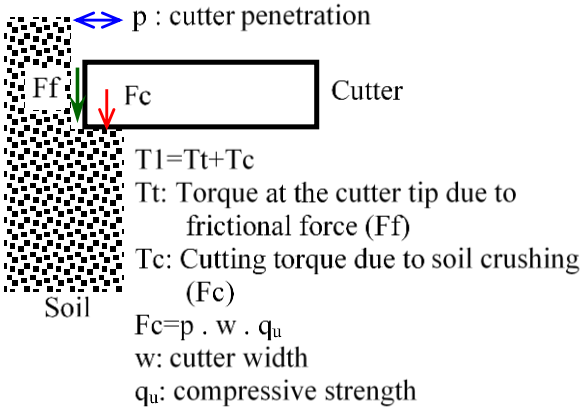

Fig. 3. Schematic of excavation force calculation for the evaluation of excavation torque.

The study of relationship between cutterhead torque and machine thrust force shows, there is a direct correlation between these two parameters (Fig. 4). Part of this direct correlation stems from frictional interaction between cutting tools' front face and high-friction tunnel face - a factor often overlooked in conventional torque estimation models. To account for this effect, the net thrust force applied to the cutting tools must first be calculated. Subsequently, the torque transferred from the cutting tools to the cutterhead can be determined by applying an appropriate dynamic friction coefficient.

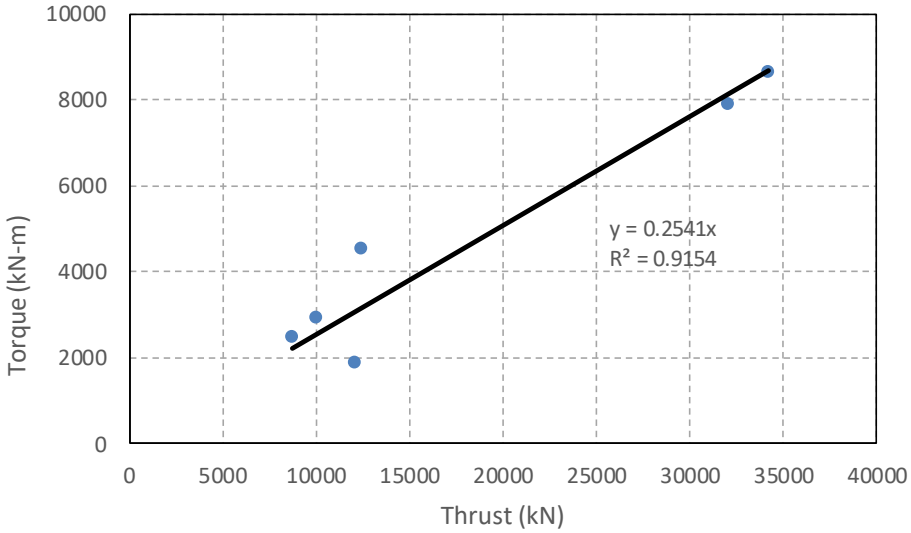

Fig. 4. Thrust-torque relationship in Mahhad metro line 3.

The surface friction torque components (T2, T3, T4, T6) are functions of both the normal pressure acting on the cutterhead surfaces and the soil-steel interface friction coefficient. While the granular soils encountered in Mashhad Line 3 would normally exhibit high friction coefficients, soil

conditioning with foam additives may substantially lower these values. Quantitative data on this reduction effect remains limited. Regarding the friction coefficients between soil and steel or soil and soil, in a study conducted by Godinez et al. (2015) to calculate the dynamic friction coefficient, they concluded that the dynamic friction coefficient can be obtained from the following equation:

$$\mu = tan(\alpha\varphi') \quad (2)$$

where:

μ: Dynamic friction coefficient between conditioned soil and the cutterhead surfaces,

φ': Effective internal friction angle of the in-situ soil

α: Correction factor to consider the shape of the surfaces in contact with the soil and the effect of soil conditioning

Based on the results of the studies by Godinez et al. (2015), the correction factor for clay, silt, and sandy soils is 0.15, 0.15, and 0.35, respectively. The internal friction angles for the soils in the tunnel studied by Godinez et al. (2015) were 33, 37, and 39 degrees, respectively, hence the dynamic friction coefficient for these three soil types was obtained as 0.087, 0.097, and 0.2, respectively. The clay and silty soil in the project studied by Godinez et al. (2015) have friction angles and adhesion values similar to the sandy and gravelly soils of Line 3 of the Mashhad Metro tunnels. Hence, the correction factor of 0.1 is considered suitable for the dynamic friction coefficient between the soil and the cutterhead surfaces in the Mashhad Metro Line 3 project.

Table 4 presents the calculated torque components and their percentage distributions (Fig. 5) for cutterheads in both eastern and western tunnel sections near the tunnel faces (chainage 4800 in the western tunnel and chainage 8000 in the eastern tunnel), along with an in-situ cutterhead rotation test conducted in the western tunnel. One note to consider is that the center cutterhead face pressure was used to calculate the torque components.

Table 4. Calculated Cutterhead Torque Components for Western & Eastern Tunnels.

Parameter	Western Tunnel			Eastern Tunnel			Rotation Test (Western Tunnel)	Avg. Rotation Test (%)	Avg. Western Tunnel (%)	Avg. Eastern Tunnel (%)
Face Pressure (bar)	1.31	1.3	0.28	0.278	0.27	0.265	0.5	-	-	-
Thrust Force (kN)	34174	32085	8756	10054	12095	12457	-	-	-	-
Torque (kN-m)	8662	7903	2489	2943	1882	4523	2000	-	-	-
Net Thrust (kN)	11973	10023	4369	5667	1125	8094	0	-	-	-
Penetration Rate (mm/rev)	16.9	17.5	16.7	17.32	17	17	0	-	-	-
T1	2993	2541	1203	1515	444	1499	0	0	33	47
T2	1736	1723	368	368	358	351	663	31	21	16
T3	868	861	184	184	179	176	331	16	10	8
T4	1567	1555	332	332	323	317	598	28	19	15
T5	39	39	14	14	14	14	19	1	0	1
T6	935	928	198	198	193	189	357	17	11	9
T7	390	387	83	83	80	79	149	7	5	4
T8	16	16	16	16	16	16	16	1	0	1
Total Torque (Tt) (kN-m)	8543	8048	2399	2711	1607	2640	2133	100	100	100
Deviation from Actual (%)	1	2	4	8	15	42	7	-	-	-

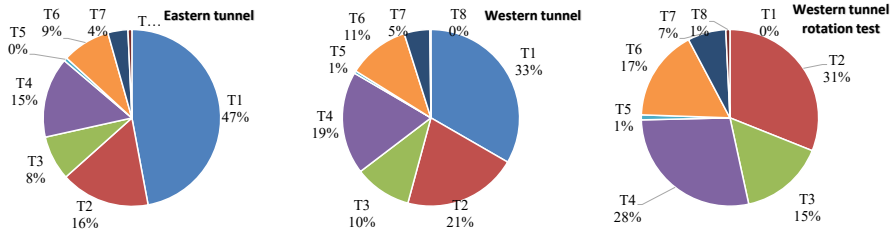

Fig. 5. Percentage distribution of the values of the cutterhead torque components in the eastern and western tunnels.

A comparative analysis of cutterhead torque in the eastern and western tunnels (Table 4 and Fig. 5) reveals:

- The western tunnel exhibits approximately 1 bar higher face pressure than the eastern tunnel (1–1.3 bar vs. 0.3 bar), resulting in increased thrust force requirements (29000–35000 kN vs. 8500–12500 kN).
- Even when comparing net thrust forces, the western tunnel requires significantly higher values. This is attributed to the presence of coarser-grained and more compact soils in the western alignment, which demand greater thrust to facilitate tool penetration and shield dragging.
- Torque-to-Thrust Ratio: 0.25–0.3 (Western) vs. 0.16–0.36 (Eastern).
- Dominant Torque Sources:
  - Excavation tools (T1 : 30–60% of total torque).
  - Friction on cutterhead surfaces (T2, T3, T4 : 40–75%).

4. Methodology

To evaluate the influence of cutterhead torque components on total torque, a sensitivity analysis was conducted. The baseline parameters in Table 5 are derived from average values observed in the western tunnel, with consideration given to adjustable parameters in cutterhead design.

Fig. 6 illustrates the percentage variation in cutterhead torque relative to the baseline under different sensitivity scenarios.

Table 5. Baseline Parameters for Sensitivity Analysis.

Parameter	Baseline Value
Face Pressure (bar)	1.3
Contact Force (Net Thrust Force) (kN)	11,000
Penetration Rate (mm/rev)	17
Friction Coefficient (μ)	0.1
Cutterhead Opening Ratio (%)	35

Key findings from sensitivity analysis are as follows:

- Most Influential Parameters (Descending Order):
  - Friction Coefficient (μ) – Highest impact on torque variation
  - Face Pressure – Directly affects frictional resistance
  - Net Thrust Force – Influences cutting and muck flow
  - Penetration Rate – Moderate effect due to soil-tool interaction
  - Cutterhead Opening Ratio – Least impact (but affects muck flow efficiency)
- Practical Implications:

− Reducing μ (e.g., via foam conditioning) significantly lowers torque.
− Optimizing face pressure minimizes unnecessary frictional losses.
− Higher opening ratios marginally improve performance but are less critical.

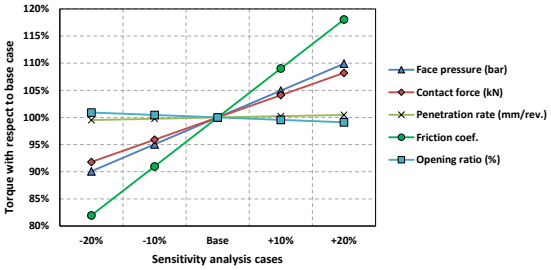

Fig. 6. Sensitivity analysis of the parameters of the cutterhead torque components.

5. Discussion

The analysis confirms that dynamic friction (μ) and face pressure dominate torque fluctuations, while mechanical parameters (thrust, penetration rate) play secondary roles. This aligns with empirical observations in EPB tunneling, where soil-conditioning efficacy directly governs torque demands. For this reason, to optimize the operation and to reduce the total torque it is recommended to prioritize friction reduction (e.g., enhanced foam injection) for torque control. To reduce the coefficient of friction between the surfaces of the cutterhead and the excavated soil mixed with foam, the following can be considered:

- Optimizing the foam injection parameters (type of foam or injection material, FIR, FER, percentage of foam concentration, arrangement of foam injection points in front of the cutterhead and near its periphery and inside the chamber, ...)
- Using coatings on the cutterhead surfaces with a lower coefficient of friction and less likelihood of adhesion.
- Using water jets in places where the likelihood of material accumulation is higher (center of the cutterhead and center of the chamber and the entrance to the screw conveyor)
- Lowering face pressure can reduce the total cutterhead torque. Adjustments to face pressure are evaluated against geotechnical stability criteria using limit state analyses. Both ultimate and service limit states should be considered to ensure that reductions in face pressure would not compromise tunnel face stability or induce ground settlement. The proposed torque reduction strategies involving face pressure optimization are contingent upon satisfying these safety thresholds and are intended to be implemented within the permissible range defined by geotechnical design standards.
- Increasing the percentage of cutterhead opening can facilitate the muck flow, reduce clogging, and lower total torque. In addition, increasing the opening area reduces the frictional forces applied to the cutterhead. Some of these factors are included in the torque calculation formulas and some are not. For example, reducing the effect of mud clogging leads to better performance of the cutting tool, the effect of which is not considered in the torque components.

Although the variation in soil composition between the eastern and western tunnel segments is a primary factor influencing cutterhead torque, other elements such as tunnel alignment, cutterhead geometry, and operational parameters also contribute. In this study, the uniformity of TBM specifications and cutting tools across both segments allowed for a controlled comparison. Operational parameters—including thrust force, penetration rate, and face pressure—were integrated into the torque component calculations and sensitivity analysis. These factors were monitored and found to be consistent, supporting the conclusion that soil contrast is the dominant driver of torque variation, while operational conditions modulate its magnitude.

6. Conclusion

The comprehensive analysis of cutterhead torque components in Mashhad Metro Line 3's eastern and western tunnels has yielded valuable insights into TBM performance across varying geotechnical conditions. Excavation torque (T1) emerged as the dominant component, accounting for 30–60% of total torque demand—particularly in the coarse, denser soils of the western tunnel. Frictional torques (T2–T4) collectively contributed 40–75%, with their magnitude strongly influenced by soil-steel friction coefficients and face pressure.

A clear linear correlation was observed between thrust force and torque, with the western tunnel requiring approximately 2.5 times higher thrust than the eastern alignment. This disparity was primarily driven by differences in soil composition and elevated face pressures. Sensitivity analysis identified friction coefficient and face pressure as the most influential parameters, with torque reductions of up to 20% achievable through targeted optimization. Recommended strategies include enhanced soil conditioning protocols, cutterhead design improvements to facilitate muck flow, and continuous monitoring of operational parameters to balance performance and tool wear.

While the study focuses on a 1 km section of Mashhad Metro Line 3, the findings are broadly transferable to EPB tunneling in similar geotechnical contexts. The torque component framework and sensitivity analysis are rooted in fundamental soil-tool interaction principles, making them applicable across projects involving both coarse- and fine-grained soils. The results reaffirm that dynamic friction and face pressure are the primary drivers of torque fluctuations, with thrust and penetration rate playing secondary roles. This aligns with established EPB tunneling practices, where soil conditioning—especially foam injection—directly governs torque demand. Accordingly, the proposed mitigation strategies are not only grounded in field data but also adaptable to site-specific conditions, offering practical guidance for optimizing cutterhead performance and excavation efficiency.

Key limitations include uncertainties in friction coefficient estimation due to reliance on back-analysis, and significant torque variability stemming from geotechnical heterogeneity. These findings underscore the critical interplay between soil properties, machine parameters, and torque demand in EPB tunnelling. For Mashhad Line 3 and similar projects, prioritizing friction reduction and adaptive face pressure control will be essential for maximizing TBM efficiency. Future research should focus on deploying real-time torque monitoring systems to refine predictive models and enhance operational decision-making.

References

Farrokh, E., Lotfi, D., 2025. Decision tree analysis of cutter selection for tunnel boring machines: A study of geological conditions and machine types in high-performing TBM projects. *Tunnelling and Underground Space Technology*, 162, 106612.

Fu, T., Zhang, T., Song, X., 2022. A novel hybrid transfer learning framework for dynamic cutterhead torque prediction of the tunnel boring machine. *Energies*, 15 (8), 2907.

Godinez, R., Yu, H., Mooney, M., Alavi, E., 2015. Earth Pressure Balance Machine Cutterhead Torque Modeling: Learning from Machine Data, RETC.

Hong, K., Li, F., Zhou, Z., Li, F., Zhu, X., 2021. A data-driven method for predicting the cutterhead torque of EPB shield machine. *Discrete Dynamics in Nature and Society*, 2021, 5980081.

Koohsari, A., Kalatehjari, R., Moosazadeh, S., Hajihassani, M., Tarafrava, M., 2023. Measurement and enhancing prediction of EPBM torque using actual machine data. *Measurement*, 223, 113780.

Rouhani, H., Farrokh, E., 2022. Study of methods of EPB TBMs torque calculation in mixed face conditions, 8th Iranian Rock Mechanics Conference.

Zhang, Q., Su, C., Qin, Q., Cai, Z., Hou, Z., Kang, Y., 2016. Modeling and prediction for the thrust on EPB TBMs under different geological conditions by considering mechanical decoupling. Science China *Technological Sciences*, 59(9), 1428–1434.

Zhou, X.P., Zhai, S.F., 2018. Estimation of the cutterhead torque for earth pressure balance TBM under mixed-face conditions, *Tunnelling and Underground Space Technology*, vol. 74, pp. 217–229.

SETC-2025
BELGRADE

TOPIC 3

GEOLOGICAL INVESTIGATION AND PREDICTION

Southeastern Europe Tunnelling Conference (SETC-2025)
1-3 October 2025, Belgrade, Serbia

DOI: 10.5937/SETC25012H

Unveiling correlations between transient tunnel deformations and in-situ geomechanical parameters derived from tunnel seismic data

Jozsef Hecht-Méndez[a], Thomas Dickmann[b], Carlos Andres Giraldo[c]*

[a] GeoSolutions Hechtm, Küssaberg, Germany; geosolutions@hechtm.de
[b] Amberg Technologies AG, Regensdorf-Watt, Switzerland; tdickmann@amberg.ch
[c] Consorcio Antioquia al Mar S.A.S., Cañasgordas, Colombia; direccion.ingenieria@tuneldeltoyo.com

Abstract: Hard rock tunnelling is a unique endeavour that requires close collaboration among various disciplines, including civil engineering, geotechnics, geology, and geophysics. In modern tunnelling projects, diverse types of data are continuously collected by instruments and personnel across these fields. Typically, these datasets are analysed within each discipline separately, and due to time constraints, comprehensive interdisciplinary evaluations are rarely conducted. Beyond standard descriptive parameters—such as those provided by rock mass classification systems and convergence measurements—seismic velocities obtained from Tunnel Seismic Prediction methods are of particular interest. Tunnel seismic is carried out during the excavation phase by placing seismic sensors and generating waves in boreholes using small explosive charges near the tunnel face. From the estimated wave velocities, geomechanical parameters such as the dynamic Young's modulus can be derived. These seismic surveys typically allow predictions up to 150 meters ahead of the tunnel face. In this work, results from approximately twenty seismic surveys conducted at the longest road tunnel ever constructed in Latin America are validated using geological face mapping. Subsequently, a detailed evaluation of the geomechanical parameters and convergence measurements collected along the same segments as the seismic data revealed breakthrough correlations between the datasets. Based on these analyses, unique look-up tables, helpful for future surveys and for risk management, were developed that integrate rock support types, elastic modulus, and maximum accumulated deformation.

Keywords: Geological uncertainty; tunnel seismic; deformation; geomechanical parameters

1. Introduction

Thanks to advancements in excavation techniques over the past two decades, hard rock tunneling projects are now executed at greater depths and involve increasingly longer tunnel alignments. Simultaneously, the proliferation of sensors, monitoring technologies, exploration methods, and digital data storage has enabled the collection of a wide variety of multi-source datasets (Apoji et al., 2023).

Among the diverse datasets typically collected across various disciplines are geological data such as face logs, probe drill logs, and discontinuity mapping; geotechnical data including deformation monitoring, convergence measurements, and both in-situ and laboratory-based strength data; geophysical data comprising tunnel seismic surveys, resistivity measurements, and borehole ground-penetrating radar (GPR); and excavation-related data such as Measurements While Drilling (MWD) and Tunnel Boring Machine (TBM) performance parameters.

During excavation, geological and geotechnical data are evaluated by site geologists and geotechnical engineers. While these analyses may often be conducted independently, in the best scenario at least one project member has interdisciplinary knowledge or background bridging both domains. A key output of this process is the rock mass classification, typically updated after each production cycle and integrated into the evolving geological model. Furthermore, monitoring networks for deformation and convergence of the tunnel surface or lining are increasingly implemented in tunnelling projects. These systems enable the collection of time-dependent data, which reflect the rock mass's response to

*Corresponding author: geosolutions@hechtm.de (J. Hecht-Méndez).

excavation. Such data serve as valuable indicators of rock mass behaviour and stress redistribution due to material removal, as well as the interaction between ground and support structures (Kaiser and Korpach, 1986).

Tunnel Seismic Prediction (TSP) is a geophysical technique specifically developed for hard rock tunnelling which helps to minimise the risks associated to poor rock mass conditions (Dickmann and Krueger, 2014). By using 4 sensors installed into the tunnel walls, seismic waves generated using explosives charges or an impact source are recorded and evaluated. The technology aims at detecting geological structures such as: fault and shear zones, fractures/jointed zones, presence of cavities, etc. It stands out due to its rapidness for data acquisition and processing, achievable prediction range (up to 150 metres or more) and high accuracy.

Each of the aforementioned techniques provides critical information for the tunnel engineer's decision-making process in areas such as excavation performance, support design, and alignment adjustments. More importantly, this geo-information is vital for mitigating geological risks. However, a common shortcoming is the limited interdisciplinary evaluation of these datasets, a gap that can be attributed to the time-consuming nature of data integration and analysis across domains.

In this work, we present an integrated analysis of geological face mappings, convergence measurements, and tunnel seismic data collected from a road tunnel project in the Colombian Andes. At the moment of this study, approximately 2,590 meters of tunnel were covered by 20 seismic campaigns. Seismic predictions were carefully compared against Rock Mass Rating (RMR) values and convergence measurements, with the aim of evaluating the consistency and predictive value of the seismic data. Moreover, despite the differing nature of the data sources, and assuming that each dataset directly or indirectly reflects the physical properties of the rock mass, an important objective of this study was to explore potential correlations between them.

2. Fundamentals

2.1. Convergence in tunneling

Convergence in tunneling refers to the radial closure of the tunnel section in time due to the stresses excerpt by the surrounding rock mass and the excavation itself. Depending on the rock mass type and condition, tunnel convergence may result in either reduction of the section or collapses (Kontogianni and Stiros, 2003). Commonly, tunnel convergence occurs near the excavation face and it can be interpreted as a response of the ground due to the gradual rearrangement of stress around the opening. Generally, it can be inferred that convergence in weak rock masses with low compressive strength tends to be greater than in competent rock masses with higher compressive strength. Moreover, the presence of large fault and intense jointing or fracturing may influence the degree of deformation (Kim et al, 2005). Consequently, it can be assumed that the elastic modulus should be rather low at zones prone to high deformation.

In modern tunneling, convergence measurements can be considered as a standard. Hence, there are a number of instruments and methods for measuring tunnel deformation, tape extensometers being the most traditional common one. Tape extensometers measure relative displacement of the tunnel periphery at fixed point locations. The main importance of measuring tunnel convergence is that it helps on understanding the rock mass behavior at the predefined geotechnical units throughout the tunnel alignment. Therefore, it contributes to the decision-making process for the most suitable and economic rock support to be used at each section.

2.2. Tunnel Seismic Prediction

TSP is a method widely used in hard rock tunneling. It relies on reflection seismic and allows to estimate the velocity of the P-waves (longitudinal waves) and S-waves (shear waves) directly from data recorded

behind the tunnel face. In its standard application 24 shot holes (or shot point when using impact sources) are prepared and blasted using small explosive charges. The shot holes are placed as close as possible to the tunnel face (Fig. 1).

Fig. 1. Standard layout when using the TSP 303 technology consisting of an array of 24 shot points and four 3-component receivers are installed as close as possible to the tunnel face.

The downtime needed for data recording can be as short as 15 to 30 minutes and results can be delivered within few hours after data acquisition. The processing involves a number of steps for preparing and evaluating the seismic data, i.e. the seismic traces, before going into a numerical modeling. By meanings of 3D velocity analyses and depth migration, zones featuring high reflections ahead of the face are illuminated (located) in space resulting in so-called reflectors. The most significant reflectors are automatically extracted by the software accompanying the system. According to their spatial position along each velocity field, each reflector has velocity values for P- and S-waves and the corresponding elastic or geomechancial parameters. The parameters dynamic Young's modulus (*Edyn*), Poisson ratio (ν), shear modulus (μ) and Bulk modulus (K) are calculated from the estimated seismic velocities assuming a representative density value for typical rock types.

Variations in the velocity values and the geomechanical parameters between consecutive reflectors form the basis for drawing conclusions about the changes in rock mass conditions ahead of the face. For instance, decreasing the value of *Edyn* is a good indicator of decreased rock stiffness due to the presence of a weakness zone. As the spatial position and orientation of each reflector is estimated, these changes are projected onto the tunnel axis. The latter is also an input to the system's software, which uses the same project coordinates. The prediction of the rock mass state is thus included in the metrics used in the project.

3. Project location and description

The Guillermo Gaviria Echeverri Tunnel and its access roads Megaproject is a road project located at the western part of the Antioquia Department, Colombia (Fig. 2). Along with several other structures, it comprises the construction of the 9.7 km tunnel, also referred to as the Toyo Tunnel. The project belongs to the Proyecto Autopistas de la Prosperidad which is part of the National Government Program Fourth Generation Roads 4G and it is executed as a public work led by the regional government. The project will connect two other key road projects, the concessions Mar 1 (Medellin – Santa Fé de

Antioquia) and Mar 2 (Cañasgordas – El Tigre), all of them aiming at connecting production centres located within the Antioquia Department, the country middle region and the Pacific and Atlantic coasts. The tunnel was built by the Antioquia al Mar Joint Venture (CAM). It comprises the excavation of a main tunnel and an escape gallery being excavated with two opposite headings (Entry and Exit Portals).

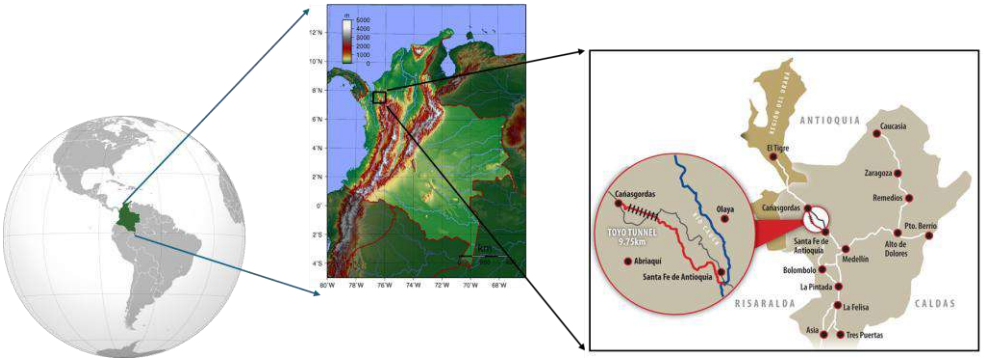

Fig. 2. Location of the Megaproject Guillermo Gaviria Echeverri Tunnel and its access roads (right: Modified from FCC Construction).

3.1. Local Geology

Local geology along the tunnel alignment comprises sedimentary and igneous rocks of two formations: Penderisco and Barroso. The first formation includes thin layers of shales, siltstone, mudstone and lydite occasionally interbedded by volcanic rock packages (basalt and diabase) while the second comprises basalts, gabbro, diabase, andesites and volcanic tuff. According to the geological forecast, a number of fault zones and intrusions are expected along the transect (Fig. 3). Likewise, predicted RMR values range between 20 and 80 indicating a high variability of the rock mass condition along the almost 10 km transept to be crossed. The overburden varies from a few meters around portal area up to about 900 m in the middle of the tunnel.

The geology after excavation along the areas where tunnel seismic results were available present two different rock mass conditions. Along the Entry Portal (EP), the Barroso Formation is found while at the Exit Portal (OP) the Penderisco Formation dominates, the boundary of both formations is located approximately at the middle of the tunnel alignment. At the EP, the geology is predominantly diabase rocks (dolerite) and basalts of moderate to high strength with moderate fracturing. At the OP, lithology is dominated by a sequence of sedimentary (siltstone, mudstone, shales) and volcanic rock (basalt). According to site geologists and face mappings, predominantly sequences of siltstone and shale are present characterised by low to moderate strength, moderate alteration, tectonised, high degree of fractures and folding evidence.

4. Methodology

4.1. Data collection

Seismic and geological results were collected in separated databases. Results coming from 17 seismic campaigns, 10 and 7 at the EP and OP, respectively, were analysed. Geological information is available in form of spreadsheet. Inputs of the spreadsheets contain information gathered from the geological face mappings after each blast. Deformation measurements were performed using 5 convergence points placed about every 15 metres along most of the alignment, only at weakness zones, e.g. rock type 4 and 5, distance was in average 5 metres. The measuring points were situated symmetrically as shown in Fig. 4. After a given blast, recordings of deformation were done daily at stations near the face. For the

remainder stations, the recordings were either weekly, biweekly or monthly, depending on the response of the rock mass to the rock support. The stop criterion was when deformations were at maximum 2 mm/d. The recordings are available in spreadsheets. Table 1 shows the main parameters obtained from each investigation method. Table 2 shows basic descriptive values of the parameter used for the validation and further analyses. All TSP related parameters are calculated as well as the RMR. The accumulated deformations were measured.

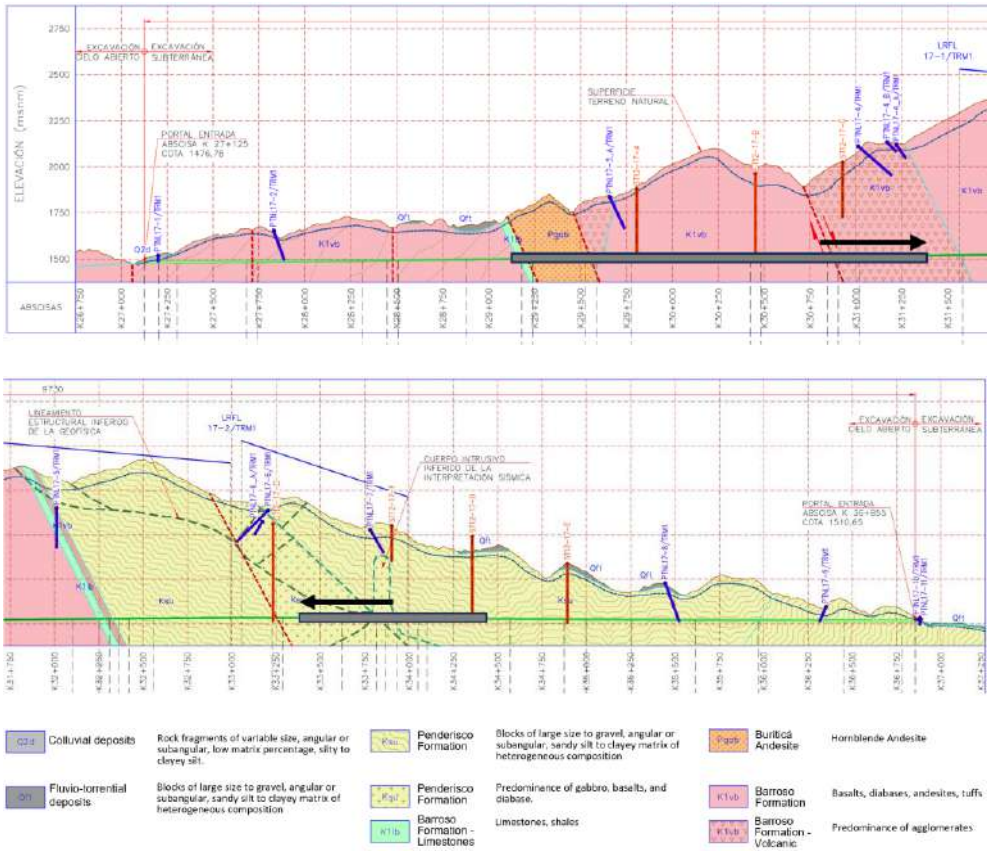

Fig. 3. Geological longitudinal section showing the main two type of rock formations: Barroso and Penderisco, pink and yellow, respectively. The tunnel sections covered by the seismic campaigns analysed in this study till 2021 are indicated by the grey box upon the tunnel alignment. Headings directions are also indicated, upper corresponding to the Entry Portal (EP) and bottom to the Exit Portal (OP).

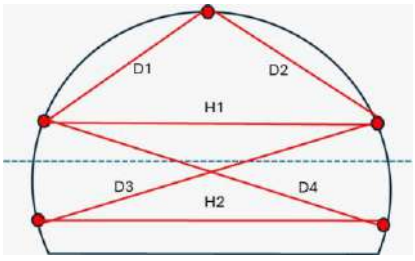

Fig. 4. Schema showing the strings measured for monitoring the tunnel convergences. In this study the strings H1 and H2 were used.

Table 1. List of parameters obtained by each investigation method.

Method	TSP	Face mapping	Extensometers
Parameter	TM: Tunnelmeter [m]	TM: Tunnelmeter [m]	TM: Tunnelmeter [m]
	V_p: P-wave velocity [m/s]	RQD: Rock Quality Design	D_{acc}: Accumulated deformation [cm]
	V_s: S-wave velocity [m/s]	RMR: Rock Mass Rating	
	v: Poisson coefficient [-]	RS: Rock Support	
	E_{stat}: Static Young's mod. [GPa]	Lit: Lithology	
	E_{dyn}: Dyn. Young's mod. [GPa]	FD: Fracturing degree	
	μ: Shear mod. [GPa]	WP: Water presence	
	K: Bulk mod. [GPa]	WA: Weathering/Alteration	

Table 2. Relevant parameter values as used for the analyses.

	Entry Portal				Exit Portal			
Parameter	Samples	Minimum	Maximum	Median	Samples	Minimum	Maximum	Median
V_p		3,170	5,675	4,605		3,440	5,500	4,225
V_s	161	1,900	3,160	2,660	119	1,840	2,770	2,420
E_{dyn}		20	70	45		21	50	32
RMR	341	18	74	45	299	16	56	37
D_{acc}	114	0.53	41.10	5.71	95	0.87	48.53	12.23

4.2. Data preparation

The spatial location of each parameter was referred to Tunnelmeter (chainage) of the project. Parameters laying within a range of 2 m from each other were used for each evaluation. Tunnel seismic results were carefully validated according to both the Rock Mass Rating (RMR) estimated at a given position and the geological description as presented in the face mappings for that location. In this qualitative evaluation, the closest values to a given position were compared considering the overall trends within a section.

In general, most of the seismic results were in good agreement with the RMR trends and the rock mass condition experienced along the prediction range. In only 2 cases, a reprocessing of seismic data was necessary, mostly due to campaigns performed at zones where the seismic layout was laying along weakness zones posing a challenge for estimating important reference parameters. After calibrating the processing parameters (mostly initial velocity for the seismic modeling), seismic results along zones of concern were in good to very good agreement with the geological parameters. Once the validation of the seismic results was finished, each individual parameter coming from the seismic was plotted against the maximum accumulated deformation. Again, the closest sample position was selected. Final results are presented as graphs unveiling important correlations between them.

5. Results

Fig. 5 shows *Edyn* calculated from seismic data versus RMR values for EP. The top graph shows the rock support as build, being 1: very light rock support to 5: very heavy rock support. *Edyn* curves from each individual TSP campaign can be easily identify since there was no overlap between campaigns. Some gaps were due to lack of seismic results. Special care must be taken when comparing *Edyn* and RMR values. Considering the nature of each data, a one-to-one comparison or analysis using simple statistics must be misleading. Instead, it is recommended to perform a qualitative analysis by observing overall trends and value changes within and between campaigns.

As can be seen, similar trends between *Edyn* and RMR are present in each campaign and throughout the investigated tunnel transept. Increasing *Edyn* values are in very good agreement with high RMR and vice versa with values ranging between 20 GPa and about 70 GPa (average 43 GPa). The estimated values indicated a moderate rock mass condition along most of the investigated area with high variability, showing good rock mass conditions at some areas, e.g. TSP#6, and poor rock mass at other locations, e.g. TSP#9 and TSP#10. For zones having low RMR (M 24+510 to 24+570, TM 29+990 to

30+060 and TM 30+330 to 30+470), the seismic results are either at the far end of the predictions or there isn't value since no seismic measurement was performed. Nevertheless, the *Edyn* towards the end of the prediction of campaigns TSP#3, TSP#7 and TSP#8, and those of the following campaigns (TSP#4, TSP#7, TSP#8, TSP#9 and TSP#10), resemble the low RMR or less competent rock mass conditions along these zones. In term of geological structures, the first zone with low *Edyn* and RMR corresponds to a highly fracture zone which actually represented the fault observed in the geological model, expected ahead of the actual location (See Fig. 3). The second zone with low values towards the end of the evaluated area, are due to the presence of a dioritic intrusion and the contacts with the diabase formation.

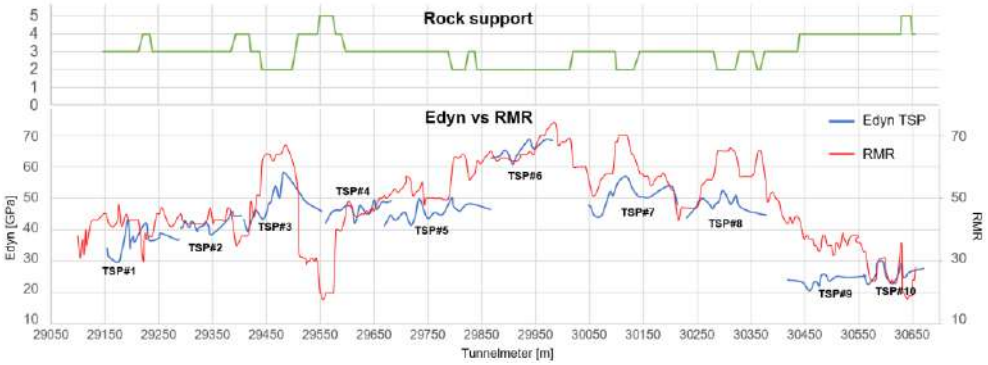

Fig. 5. *Edyn* vs RMR values for the Entry Portal (EP). The top figure shows the type of rock support employed (1: light rock support for favorable rock mass, 5: heavy rock support for very poor rock mass).

Selection and changes of the rock support while excavation was supported by the geological characterization (RMR values obtained) and also by the results of the convergence measurements near the face. Notice that at sections were low RMR values were estimated, rock support was changed to 4 and 5. It is important to mention that around TM 29+520 and TM 29+560, the highest accumulated deformations were measured, leading to an immediate change in the rock support (from 2 to 4, personal communication from site geologists). Similar situation occurred from TM 30+400 onwards. Regarding the elastic parameters, it can be observed that at sections where rock support 2 and 3 were used, the values for *Edyn* were > 50 GPa and *Edyn* > 40, respectively. At sections were rock support 4 and 5 was applied, decreasing *Edyn* values or lowest *Edyn* were estimated.

Fig. 6 shows *Edyn* calculated from seismic data versus RMR values for OP. The top graph shows the rock support as build. As in the opposite portal, *Edyn* curves from each individual TSP campaign can be easily identify since there was no overlap between campaigns.

As can be seen, similar trends between *Edyn* and RMR are present in each campaign and along the investigated transept. Increasing *Edyn* values are also in very good agreement with high RMR and vice versa with values ranging between 21 GPa and 50 GPa (average 34 GPa). In most campaigns, *Edyn* values follow to good precision local changes within short sections. Contrary to the result at PE, all parameters showed lower values at this heading as expected due to the predominant rock types of the Penderisco Formation. In addition, the rock mass condition itself was very poor to poor since the beginning of excavation at this portal.

At sections with RMR ranging between 40 and 60 (*Edyn* within 35 and 50), rock support 3 was applied (most of the section). Rock support 4 and 5 were employed at sections with lower RMR or high deformation, TM 33+580 to TM 33+660, TM 33+860 to TM 33+870, TM 33+900 to TM 33+915 and from TM 34+210 to TM 34+400. Along most of these weaker sections, *Edyn* values lower than 25 GPa were estimated. Only at TSP#4, those changes could not be identified by any reflector, likely due to a spatial resolution limitation.

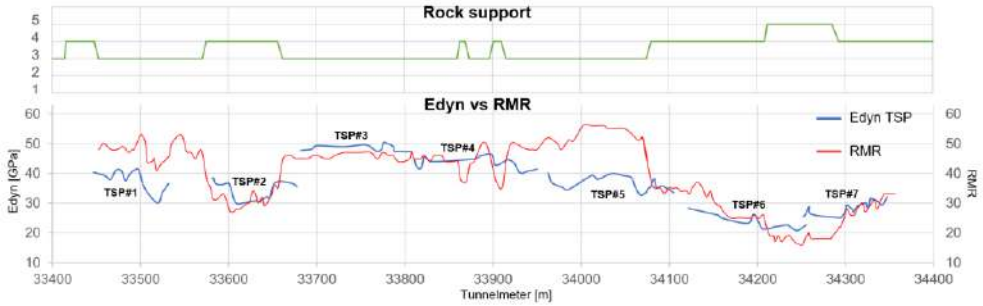

Fig. 6. *Edyn* vs RMR values for the Exit Portal (OP). The top figure shows the type of rock support employed (1: light rock support for favorable rock mass, 5: heavy rock support for very poor rock mass).

In addition to the above-mentioned validation and evaluation of seismic, *Edyn* values were plotted against maximum accumulated deformation as measured along the tunnel transept using tape extensometers (Fig. 7). Only the upper string (H1) was used since it showed the larger convergence values and variability compared to H2. The figures allow a simple verification of the *Edyn* areas for which a certain deformation is to be expected. By adding the type of support, additional conclusions can be drawn about the relationship between *Edyn*, the accumulated deformation and the selected support.

It is important to mention that prior to the elaboration of these figures, the relationship between overburden and deformation was scrutinized. For both headings, a positive correlation, i.e. larger convergence due to increasing overburden was not clearly identified. In EP, the largest convergences were measured at zones with lowest overburden or at sections where the overburden has a negative gradient. Similarly, in OP heading, even a negative correlation is observed, i.e. convergences were slightly higher as the overburden increased. Based on the correlations, the following main conclusions can be drawn per portal:

Entry Portal (EP)

- *Edyn* range: 20 – 30. Highest deformation possible, up to ca. 30 cm. RS 4 is used predominantly. RS 5 in punctual cases to control instantaneous deformations > 10 cm.
- *Edyn* range: 30 – 40. Low deformations, < 10 cm. RS 4 is used predominantly.
- *Edyn* range: 40 – 50. Low to high deformations, up to around 30 cm. RS 3 is used predominantly. RS 4 and 5 used in punctual cases to control instantaneous deformations > 10 cm.
- *Edyn* range: 50 – 70. Very low deformations, < 6 cm. Rock support 2 is used predominantly

Exit Portal (OP)

- *Edyn* range: 20 – 30. Highest deformation possible, up to around 50 cm.
- *Edyn* < 26, RS 5 is used predominantly, otherwise RS 4.
- *Edyn* range: 30 – 40. Still high deformation possible, up to around 40 cm.
- *Edyn* < 35, RS 4 is used predominantly, otherwise RS 3.
- *Edyn* range: 40 – 50. Moderate deformations, up to around 20 cm.
- RS 3 is used predominantly. RS 4 only in punctual cases to control instantaneous deformations > 10 cm.

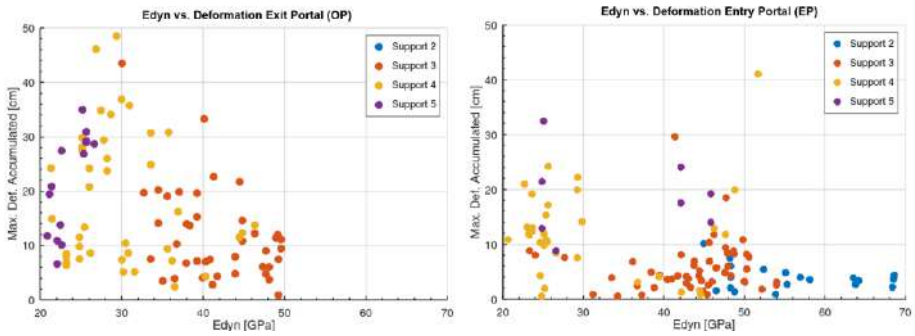

Fig. 7. Plots of *Edyn* versus maximum accumulated deformation including primary rock support as built. Left: Exit Portal, right: Entry Portal.

Table 3 and 4 present basic statistics for data shown in Figure 7. The data were classified in 4 different E_{dyn} ranges. Occurrences refers to the number of times a value lay within a given range. Additionally, they can also be interpreted as a probability, since the number of occurrences was divided by the total number of samples for each case. By looking at these results as a forecast tool, the probability of using a given type of rock support can be deviated from seismic results of future campaigns. For instance, if a campaign is done at the EP and along 50 m within the prediction range, Edyn values are between 30 and 40 GPa, the chance of applying rock support type 3 along this section is 83%. Moreover, inferences about the expected deformation can also be done, in this case, the minimum and maximum D_{acc} will be about 1.3 and 5.3 cm, respectively.

Table 3. Statistical analysis for the Entry Portal. Occurrence is expressed in percentage, Mean D_{acc} is in cm. Highest value for each group are highlighted in light blue and yellow, respectively.

			Rock Support (occurrence)			
E_{dyn}	Occurrence	Mean D_{acc}	2	3	4	5
20-30	27	12.96 ± 6.44	0	10	77	13
30-40	11	3.27 ± 1.99	0	83	17	0
40-50	45	6.90 ± 1.00	16	65	12	8
>50	20	4.54 ± 2.37*	60	35	5	0

*One sample (outlier) was not included in this calculation

Table 4. Statistical analysis of data shown in Figure 7 for the Exit Portal. Occurrence is expressed in percentage, Mean D_{acc} is in cm. Highest value for each group are highlighted in light blue and yellow, respectively.

			Rock Support (occurrence)			
E_{dyn}	Occurrence	Mean Dacc	2	3	4	5
20-30	39	21.45 ± 11.09	0	0	59	41
30-40	33	15.27 ± 10.74	0	52	48	0
40-50	28	9.41 ± 7.30	0	85	15	0
>50	0	0.00 ± 0.00	0	0	0	0

6. Conclusion

The TSP results and their comparison with the excavated geology and the estimated RMR values allowed for a detailed validation of the seismic results. In general, the seismic predictions matched very well the rock mass condition experienced while excavation. The seismic method proved its accuracy and benefit to the job site showing that it is an efficient and reliable tool to obtain geological information up to 150 m or more ahead of the face. Furthermore, by analysing data from different sources, such as geological information, rock classification and convergence measurements, additional useful information was obtained, which greatly supports the decision-making process for the appropriate support class during tunnelling.

A positive correlation between the parameters obtained from the in-situ seismic measurements and convergences was found, despite the transient nature of the tunnel deformation near the face. This important finding needs to be further studied and corroborated by performing similar evaluations in other job sites. Such reference works can be used as a tool for the interpretation of seismic data. They contribute to a more detailed prediction that includes information about the expected deformation and the rock support to be used. In addition, the reliability of the information obtained from the deformation-elastic modulus graphs is likely to increase considerably with the integration of further data to be collected. The results presented in this work were further employed for the following seismic measurements performed at the project. More than 60 seismic campaigns were performed. The tunnel excavation was completed in 2023.

Acknowledgements

The authors like to thank the Consorcio Antoquia al Mar (CAM) and the Gerencia del Toyo for their support on the publication of this work. Likewise, we express our special thanks to the project site geologists Edgar Morales and Carlos Castros for their valuable and steady support in providing information, clarifications and for their excellent work as TSP leaders at this impressive project.

References

Apoji, D., Sheil, B., Soga, K., 2023. Shaping the future of tunneling with data and emerging technologies. Data-Centric Engineering, 4 (e29). https://doi.org/10.1017/dce.2023.24

Dickmann, T., Krueger, D., 2014. How to turn geological uncertainty into manageable risk? Proceedings of the World Tunnel Congress 2014 – Tunnels for a better Life, Foz do Iguaçu, Brazil.

Kim, C.Y., Kim, K.Y., Baek, S.H., Hong, S.W., Bae, G.J., Lee, S.H., Schubert, W., Grossauer, K., Lee, Y.Z., 2005. Tunnel convergence analyses in heterogeneous/anisotropic rock masses. In Underground Space Use – Analysis of the Past and Lessons for the Future, Volume 2, pp. 1091–1097. Proceeding of the World Tunnel Congress 2005, Istanbul, Turkey.

Kontogianni, V., Stiros, S., 2003. Tunnel monitoring during the excavation phase: 3-D kinematic analysis based on geodetic data. Proceedings of the 11th FIG Symposium on Deformation Measurements, Santorini, Greece.

Southeastern Europe Tunnelling Conference (SETC-2025)
1-3 October 2025, Belgrade, Serbia

DOI: 10.5937/SETC25013L

Advanced Hydrogeological Modelling Tools for Metro - Groundwater Interaction Studies

Vladimir Lukić[a], Vesna Tripković[a] and Milenko Pušić[a]*

[a] Jaroslav Černi Water Institute, Belgrade, Serbia; vladimir.lukic@jcerni.rs, milenko.pusic@jcerni.rs, vesna.tripkovic@jcerni.rs

Abstract: Groundwater represents one of the most important resources for water supply, industrial production, and ecosystem preservation, which is why its sustainable use and protection from pollution are of paramount importance. Modern challenges such as rapid urbanization, climate change, and increasingly stringent legal regulations demand precise hydrodynamic analyses of groundwater flow regimes that often exceed the capabilities of traditional methodologies. In this context, the development and application of specialized software tools and platforms represent a key step forward in the modernization of the hydrogeological profession.

This paper presents experiences in the development and application of software systems designed for the preparation, analysis, and interpretation of hydrogeological data; execution of a large number of parallel numerical simulations, including simulation of the tunnel lining within the schematized layers of the mathematical model; automatic generation of results and reports; and data archiving. The importance of these tools is emphasized in the analysis of complex hydrogeological systems, particularly in the context of hydrodynamic modelling of spatially heterogeneous aquifers and the simulation of various exploitation or contamination scenarios.

The presented software tools enable high operational efficiency, reduce the risk of human error, and significantly shorten the time required for the preparation of technical studies, factors that are particularly important in decision-making and water resource management planning as it is illustrated on the example of the Belgrade Metro project. Process automation and the ability to conduct scenario-based analyses contribute to improved risk assessment, optimization, and timely response in emergency situations. In addition to technical advantages, the tools also offer centralized data management and support for collaborative work among multiple experts on the same project, thereby enhancing the quality and transparency of professional practice.

The application of modern software platforms in the field of hydrodynamic groundwater flow analysis represents an indispensable tool for achieving sustainable management of this valuable resource, as well as for further advancement of professional practice and scientific research in this domain.

Keywords: groundwater; hydrodynamic analysis; collaborative platform

1. Introduction

Groundwater is one of the most important natural resources, both in terms of providing drinking water and in the context of industrial, agricultural, and ecological sustainability. Managing this resource is becoming increasingly complex due to rising water consumption, climate change, urbanization, and industrial development - all of which affect the quantity and quality of groundwater (Foster et al., 2008; Howard, 2007). In this context, accurate hydrodynamic analysis of groundwater flow is essential for effective exploitation planning, aquifer protection from contamination, and the preparation of technical studies and environmental impact assessments (Bear, J., 1979; Domenico and Schwartz, 1998).

Traditional methods of hydrogeological analysis, while still valuable for certain aspects, are often insufficient to meet the demands of modern practice, which involve processing large volumes of data,

*Corresponding author: vladimir.lukic@jcerni.rs (V. Lukić).

modelling complex geological structures, and performing numerous computational variants for various exploitation or contamination scenarios (Anderson et al., 2015; Zheng and Bennett, 2021). Under such circumstances, the development of software tools and platforms for hydrodynamic modelling represents one of the most significant advances in the modernization of hydrogeological practice. These tools enable process automation, enhance the accuracy of analyses, and significantly reduce the time required to carry out complex calculations.

Software tools developed for this purpose encompass a wide range of functionalities, starting from the preparation, analysis, and interpretation of input data, through the execution of numerical simulations of groundwater flow, to the visualization of results, report generation, and data archiving. A key feature is the ability to perform a large number of calculations in parallel, which enables experts to quickly evaluate various scenario alternatives whether related to planning extraction activities, assessing the impact of infrastructure projects on groundwater regimes, or analysing remediation measures in cases of contamination.

The implementation of such tools significantly contributes to reducing the risk of human error, standardizing procedures, and increasing transparency, thereby enhancing the confidence of investors, regulatory authorities, and the broader professional community in the results of the analyses. In addition, modern software systems enable centralized data management, collaborative work among multiple experts on the same projects, as well as seamless integration with field monitoring or other databases.

The aim of this paper is to provide a concise overview of the development and application of software tools and platforms specialized in hydrodynamic analysis of groundwater flow, with a focus on the benefits they offer in terms of efficiency, accuracy, and reliability of calculations. By presenting the functionalities of these systems, the paper highlights their potential to enhance professional practice, accelerate decision-making, and improve management of this valuable natural resource, thereby creating the conditions necessary for sustainable use and protection of groundwater under contemporary challenges.

2. Challenges of Metro and Groundwater Interaction (Tunnels and Stations)

The construction of the Belgrade metro is based on the light metro concept (light rail transit), which prioritizes lower construction costs compared to a traditional heavy metro system.

Given the complex geomorphological and geological conditions of the Belgrade area, the construction methods for the metro are primarily limited to three approaches:

- **Deep excavation (Deep Tunnel)**, which utilizes specialized boring machines known as tunnel boring machines (TBMs) or "moles."
- **Shallow excavation (Cut and Cover)**, where the soil is first excavated, necessary infrastructure is installed, and then the area is backfilled, allowing for further construction of other structures on top.
- **At-grade construction**, where instead of backfilling, the excavation remains open. This approach, in addition to reducing construction costs, can offer other advantages.

The Belgrade metro study (JČWI, 2022) covers a network of three light metro lines, which can be upgraded to a high-capacity metro system:

- **Line 1** has a total length of 21.3 km, of which 11.3 km are in deep excavation (TBM tunneling), 7.7 km in shallow excavation (Cut & Cover), and 2.3 km at-grade. Along this route, 23 metro stations are planned (13 in deep excavation, 7 in shallow excavation, and 3 at-grade).
- **Line 2** spans 19.2 km, with 9.8 km in deep excavation (TBM) and 9.4 km in shallow excavation (Cut & Cover). This line includes 20 metro stations (9 in deep excavation and 11 in shallow excavation).
- **Line 3** covers the southeastern and southwestern parts of the city.

The constructed metro tunnel alignment and station structures are isolated from the surrounding environment by a waterproof concrete lining, thereby protecting them from direct contact with groundwater. The interaction between the metro system and groundwater can be considered from the perspective of potential resulting issues, depending on:

- whether the metro is in the construction or operational phase,
- whether the focus is on the tunnel route or the station site (zone),
- the excavation methods used,
- geological conditions,
- and the existing infrastructure along the route.

In general, it can be considered that an operational metro does not have direct contact points with groundwater. Such contact may occur only in cases of accidental infiltration, either as water ingress into the metro structures or as the leakage of fluids (often contaminated) into the surrounding groundwater.

Unlike the operational phase, the construction phase of the metro is subject to much more demanding conditions. Shallow excavation (Cut & Cover) is carried out under dry conditions. Station construction is particularly challenging, as it takes longer and often requires extensive dewatering measures. When using the deep excavation method (TBM), in addition to conventional dewatering techniques, new waterproofing technologies are also applied (e.g., special concrete).

A characteristic feature of the Belgrade metro is that its route passes through rock masses with diverse and complex hydrogeological conditions. The rocks are sedimentary, Quaternary, and pre-Quaternary in age (Tertiary and partially Mesozoic).

The issue of metro and groundwater interaction in Belgrade should also be viewed in the context of various existing interactions between groundwater and urban infrastructure, as well as land use. It is important to highlight the following:

- Dense urban zones, which often require (and implement) management of groundwater regimes through various drainage measures for structures.
- Peripheral, less densely populated urban zones, with or without established sewage systems.
- Green belts (forests and parks).
- Planned and developing settlements within urban areas, both with and without prior land filling (e.g., planned settlement construction in the Makiš field, and the initiated development of the EXPO settlement on the left bank of the Sava River). Land filling significantly alters the natural conditions for groundwater existence and its regime.
- Utility, transport, and industrial infrastructure (e.g., the marshalling yard in the Makiš field, located adjacent to Line 1, poses a potential risk of groundwater contamination).
- Groundwater sources - Belgrade's water supply is significantly dependent on wells with horizontal drains installed along the banks of the Sava River (99 wells in total, with over 60 located in the central urban core). The well capacity is determined by inflow (infiltration) from the river as well as from the alluvial aquifer (from the hinterland).
- Agriculture – agricultural production is developed on the outskirts of the city. In the alluvial zone of the flat terrain (Makiš field), there is a drainage system consisting of canals and a pumping station used to regulate the groundwater regime.

For the analysis of the interaction between the Belgrade metro and groundwater, it is necessary to understand the current natural and artificial (anthropogenic) conditions of the groundwater regime.

3. Methodological Approach to Hydrodynamic Analyses (Studies and Design Support)

The methodological approach to analysing the interaction between the Belgrade metro and groundwater stems from the established objectives and guiding criteria. The foundation for this approach included defining and elaborating primary and secondary goals of the hydrodynamic analysis, selecting and presenting output results, as well as addressing other requirements such as a unified data repository, maximum automation of certain processes, reliability, and efficiency in problem-solving.

The core component of the analysis lies in the application of mathematical modelling methods of groundwater flow regimes, the development of hydrodynamic models, and the flexibility of their use under different conditions.

The primary objectives of the hydrodynamic analysis were to determine the impact of metro construction on the existing groundwater regime both during and after the construction phase. In this context, it was necessary to identify and quantify changes in the existing groundwater regime caused by the construction and operation of the metro, specifically to define potential changes in groundwater levels, identify locations of possible groundwater infiltration into ongoing works and completed structures, quantify the inflow volume, and establish protective measures against groundwater intrusion. Additionally, based on the results of the conducted analysis, a monitoring project was planned as part of the system to protect groundwater from contamination originating from the metro as a potential source.

As secondary objectives of the analysis, assessments of the metro's impact on existing and future land users within the immediate and broader network zones were emphasized. Among these, the most significant are the impacts on dense urban areas (buildings), municipal, transport, and industrial infrastructure, and especially the city's groundwater source located along the banks of the Sava River.

The characteristics of hydrodynamic models are directly dependent on the properties of the porous media through which the metro construction is planned, with permeability being the most significant factor. The metro route passes through genetically, lithologically, and hydrogeologically diverse formations, predominantly composed of sedimentary rocks, which can be broadly categorized as:

- Alluvial (Quaternary) sediments of the Sava and Danube rivers, and
- Neogene and older sediments of the hinterland alluvium and the Belgrade uplands.

The alluvial sediments of the Sava and Danube rivers consist of **unconsolidated** rocks, characterized by typical intergranular porosity and pronounced continuous layering, predominantly extending horizontally. Sediments along parts of the metro route in the hinterland of the Sava and Danube rivers are primarily composed of limestones, marls, sandstones, and conglomerates. These rocks belong to the category of **consolidated** formations and are often tectonically disturbed, exhibiting fault and erosional discordant structures. The porosity of these rocks is fracture or fracture-cavernous (in the case of limestones), with hydraulic conductivity being very low or negligible, except for locally highly permeable zones.

As an example, the results of the analysis and categorization of the hydraulic conductivity of the rock masses (porous media) along the planned route of Line 1 of the Belgrade metro are presented, based on filtration coefficient values (Fig. 1). The majority of Line 1's route passes through practically impermeable ($Kf < 10^{-8}$ m/s) or poorly permeable ($1\times10^{-8} < Kf < 1\times10^{-6}$ m/s) rock masses. This primarily applies to the entire Section 5, nearly the entire Sections 3 and 6, as well as the marginal parts of Section 4.

Moderately permeable rocks ($1\times10^{-6} < Kf < 1\times10^{-4}$ m/s) dominate Section 4 and are also locally present within Section 3. Considering the structure of the rocks found here (both consolidated and unconsolidated), all the aforementioned types of porosity are encountered.

Highly permeable rocks ($1\times10^{-4} < Kf < 1\times10^{-2}$ m/s) are present along Sections 1 and 2 of the route (Makiš field), as shown in Fig. 1.

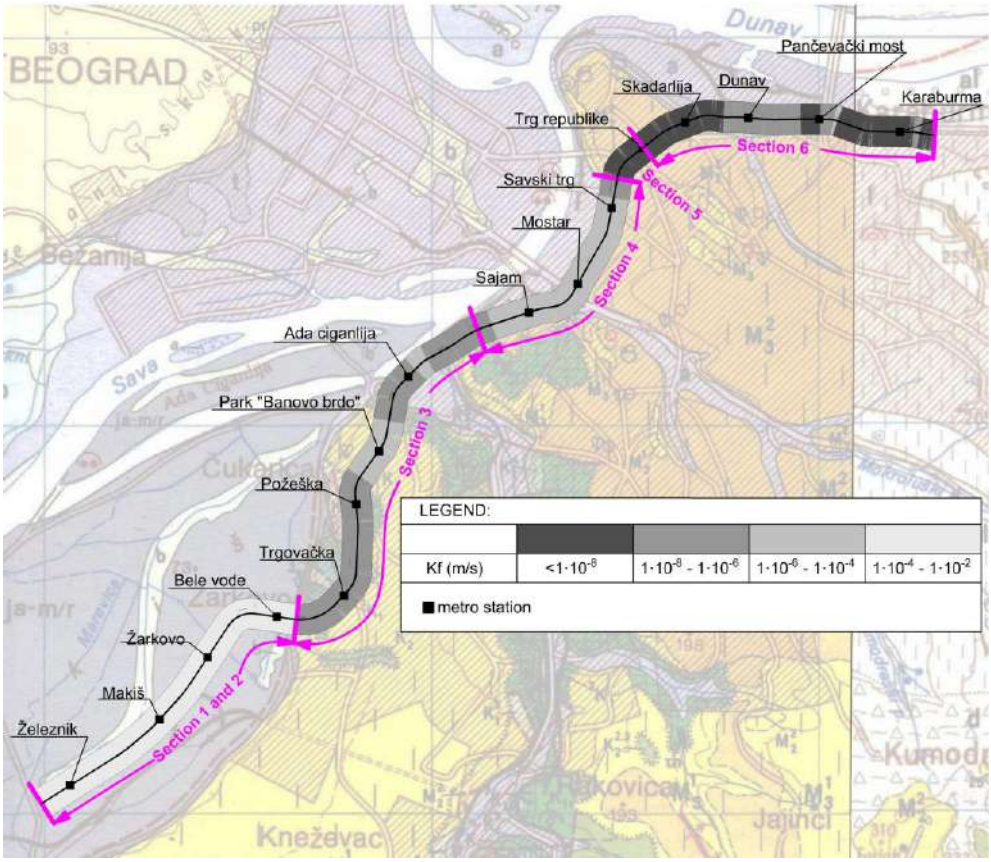

Fig. 1. Zoning of rock masses along Line 1 of the metro route by degree of permeability (based on filtration coefficient values), schematic representation.

Based on the analysis of the presented results, the selection of the number and characteristics of groundwater models was carried out. Groundwater regime analyses were performed using larger (regional) models both with and without the inclusion of the metro route, while on local (detailed) station models, the mutual impacts of their construction and surrounding groundwater were examined.

In the process of comparative analysis of the groundwater regime before and after metro construction, multiple variant calculations were performed. The calculations covered a long-term period (1/1/2005-12/31/2014), enabling a multi-parameter analysis of groundwater levels under varying hydrological conditions.

The calculation results are presented as differences in groundwater levels between the computed values before and after metro construction, shown for minimum and maximum piezometric levels within the historical hydrological record, as well as under extreme conditions (1% probability). Comparison of the results for both scenarios indicated whether mutual interaction exists and, if so, the extent to which it is manifested.

To efficiently and rationally address such a large and complex task, it was necessary to introduce innovation throughout the process. This involved thorough advance planning of all phases and steps, as well as the optimal use of available expert and personnel resources, which resulted in the creation of a dedicated project document. This document, allowing necessary adjustments and variations during the

work, formed the foundation for the entire project's execution. Maximum software utilization, automation, and centralized management of data and results were applied.

The major benefits of this approach included increased efficiency (speed, resource savings, cost reduction), versatility (variety of design alternatives), solution consistency (all derived from the same initial data source), and more.

4. Collaborative Platform (Process Workflow)

The hydrodynamic analysis involved the initial development of "macro" models (along the metro route) aimed at analysing groundwater interaction before and after metro construction. These macro models were created using the Modflow software package. Subsequently, "local" models for metro stations were developed to analyse their interaction with groundwater during construction. The local models were developed using the Plaxis3D software package.

The task required an integrated approach, logically connecting all phases of the solution and executing them efficiently. Several major steps in this process can be distinguished.

4.1. Step 1 - Task Analysis, Site Assessment, and Preparation of Materials

After analyzing the tasks to be performed, the process begins with identifying the main stakeholders affected by the changes in the groundwater regime (urban facilities, city infrastructure, municipal groundwater source, etc.). Their requirements regarding the maintenance of the groundwater regime under the new conditions (post-metro construction) are then defined.

Data are collected and entered into newly developed databases: HGIS (Hydrogeological Information System), HTO (HydroTechnical Database), HIS (Hydraulic Information System), and GIS (Geographic Information System). These systems (HGIS, HTO and HIS) are relatively new and have the specific purpose of storing and managing data necessary for the development of hydrodynamic, geomechanical, hydraulic, and hydrological models.

In the HGIS (Fig. 2) database, data on boreholes (drilling results and laboratory analyses of samples) are entered and subsequently transformed into a form and format suitable for direct import into numerical hydrodynamic and geomechanical models. This process provides initial information about the geological environment of the groundwater model and the boundary conditions required for calculations.

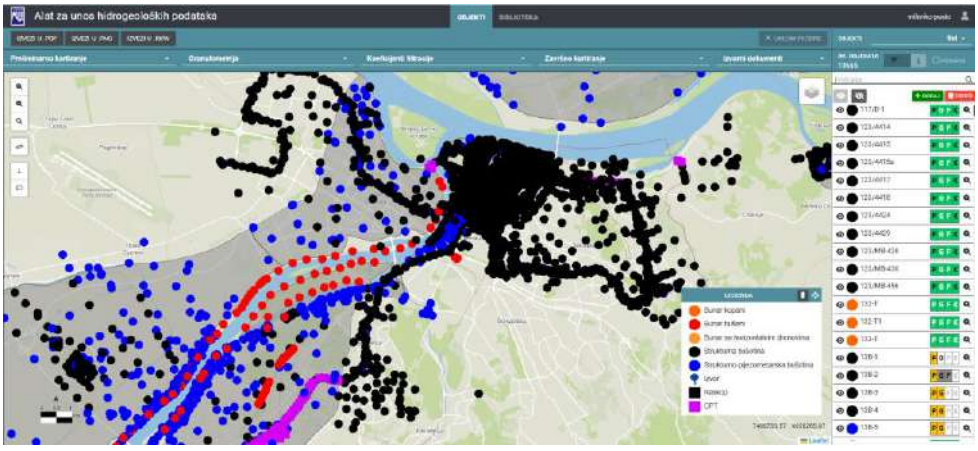

Fig. 2. Map from HGIS showing the objects.

Additionally, data and input layers for the altered-state models are prepared, including elements such as the metro route alignment, planned land filling, urbanization, changes in land use, and other relevant modifications.

4.2. Step 2 - Analysis of Requirements, Site Conditions, and Preparation of Input Data

To assist users in schematizing hydrogeological layers, which are later used for developing numerical groundwater models, a custom-built tool called the 'Hydrogeological Layer Schematization Tool' has been developed. This tool enables both automatic and semi-automatic extraction of typical hydrogeological layers. Based on the filtration coefficients of each lithological layer and the desired number of schematized layers, the algorithm assigns each lithological unit to one of the predefined schematized layers. This ensures horizontal continuity of the layers while maximizing the homogeneity of material properties within each individual layer.

Within the Clustering tab, a graphical representation is displayed to the user (Fig. 3). Each vertical line on the graph represents a single lithological unit of the object, with the values on the y-axis indicating the depth of the mapped interval, and the values on the x-axis representing the filtration coefficient defined for that interval. Lines of the same colour represent intervals that the algorithm has identified as belonging to the same layer.

Fig. 3. Application interface after data upload, selection of the number of schematized layers, and basic settings configuration.

The primary objective of groundwater model calibration is to obtain representative characteristics of the schematized layers. For comparison, the model results (groundwater levels and balance components) are evaluated against corresponding measured data in the form of time series. Unfortunately, under local conditions, measured data are often affected by errors of various origins. A *Time Series Correction Tool* is used for comparative validation and adjustment of these data. Only after thorough analysis and necessary corrections are the time series used in the calibration process (Fig. 4).

The boundary conditions of the model are derived based on the analysis of natural conditions and available data and are stored in the corresponding databases (HIS, HTO and GIS). The shapefile (shp) format contains data on the spatial, physical, and hydraulic characteristics of the boundary conditions, as well as the associated time series (Fig. 5), all in formats suitable for the development of numerical models.

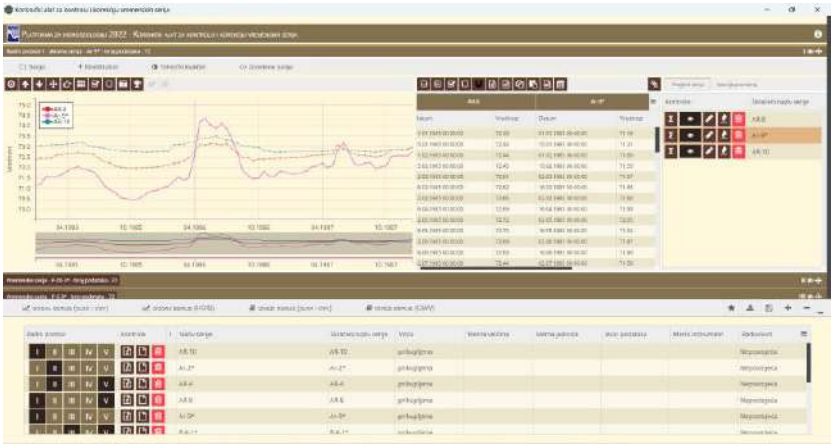

Fig. 4. Diagram from the Time Series Correction Tool, multi-diagram view

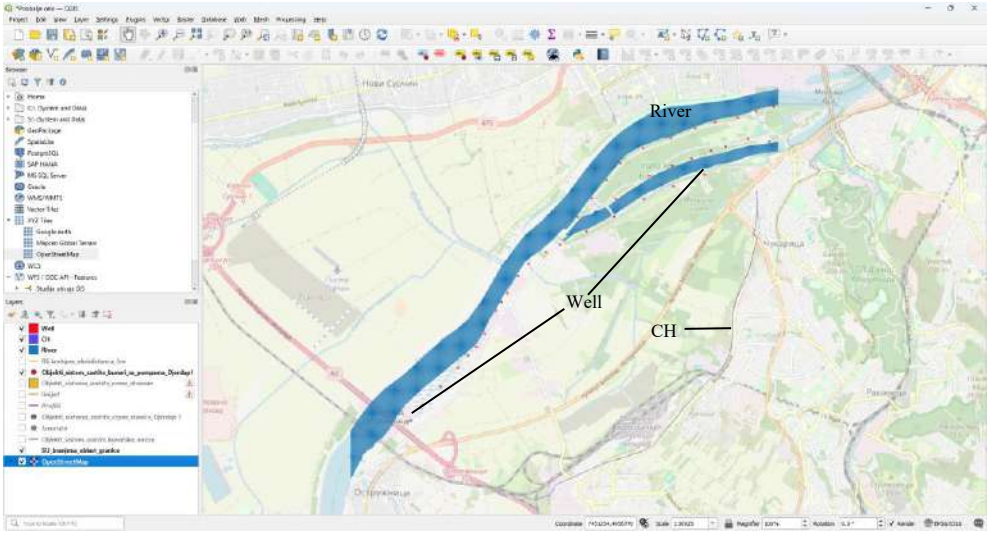

Fig. 5. Site image showing the model and boundary conditions (Source: QGIS).

Hydrodynamic calculations are performed using the MODFLOW platform under transient conditions, with grid generation based on the finite difference method. The initial version of the model is developed using a professional (commercial) user application, specifically GW Vistas (GWV) by importing shapefiles (shp) from the GIS platform.

Existing features of the GW Vistas (GWV) application, such as sensitivity analysis and PEST (Parameter ESTimation) are used for model calibration. The progress of model calibration is monitored using the proprietary application "PiezoFlow" developed by Jaroslav Černi Water Institute (JČWI). This software is designed to display the spatial distribution of calibration objects (piezometers, wells, etc.) on a map, along with measured and calculated parameter values presented as time series (piezometric levels, flows, etc.).

On the graphical display (diagram) it is possible to select one or multiple time series (objects) for simultaneous viewing (Fig. 6). The tool also allows importing and displaying multiple consecutive results from successive calibration calculations.

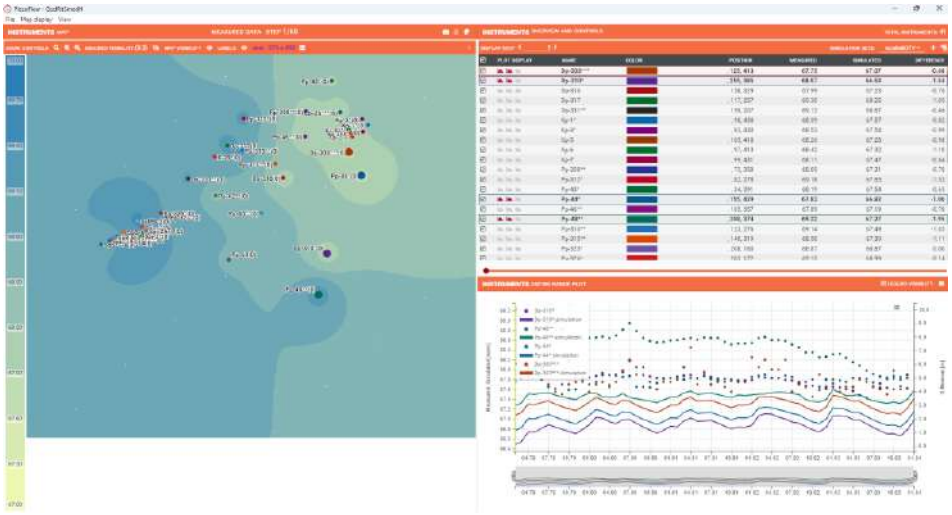

Fig. 6. PiezoFlow interface showing interaction between tabular, spatial (map), and temporal (diagram) views.

4.3. Step 3 - Hydrodynamic Analysis

Upon completion of groundwater model calibration, based on the simulation of groundwater flow under existing conditions, necessary updates and modifications are introduced into the model to support the analysis of the interaction between structures (tunnels, metro, underground and above-ground facilities) and groundwater.

As a concrete example of hydrodynamic analysis, the metro route will be presented. The metro route is simulated by adding an additional layer to the established model. The waterproof tunnel lining is represented by a "No Flow" boundary condition. By incorporating the metro route, the initial 5-layer model (Fig. 7a) is subdivided into 14 new layers; in other words, the model geometry is refined into smaller segments within the layers where the tunnel lining passes through (Fig.7b). This results in a reconfiguration of the model that enables simulation of groundwater flow under conditions specified by the project. The process is fully automated, according to the original algorithm of JČWI.

a) 5 layers – without metro

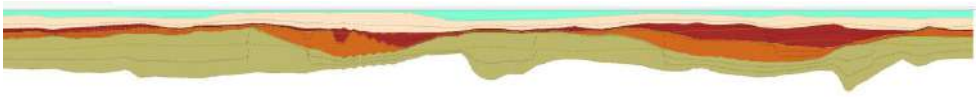

b) 14 layers – with the metro incorporated

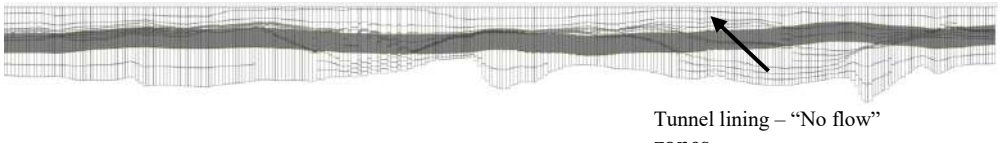

Fig. 7. Simulation of the tunnel lining within the schematized layers of the mathematical model.

For the analysis of groundwater flow in the metro station zones, detailed models with customized spatial schematization are used. Three-dimensional finite element (MKE) models for the considered stations were developed using the Plaxis 3D software package. This commercial software provides solutions for both stress-strain and flow (filtration) analyses by employing the finite element method.

For generating the model and performing groundwater regime calculations, a *Hydrogeological Analysis Support Platform* has been developed. Based on the previously established parameters of the calibrated model and the "reconfigured" model incorporating the metro route and current conditions from the GIS database, the Platform creates the groundwater model and executes the corresponding calculations.

The information necessary for creating groundwater models comes from various sources and can be grouped into three categories:

1. **Hydrodynamic inputs:** These include information about the model geometry, material properties of the soil and riverbeds (of the Sava and Danube Rivers), recharge from the hinterland, infiltration, and groundwater evaporation for the observed analysis period, among others. These data originate from the process of creating and calibrating groundwater models and may have multiple versions.
2. **Hydraulic inputs:** These consist of data on river profiles and water levels, which define the boundary conditions within the groundwater model. They are derived from the corresponding hydraulic calculations and may also exist in multiple versions.
3. **Hydrotechnical and other structures and their operating regimes:** This category includes the positions and geometric characteristics of hydrotechnical structures that must be considered for the given conditions, as well as their operating regimes. Positions and geometric data are obtained from the GIS database, while operating regimes are defined through the Platform.

For each completed calculation, it is possible within the *Platform* to generate appendices containing the calculation results in a predefined format according to the project requirements.

4.4. Step 4 - Final Processing and Storage of Results

For each calculation performed within the *Platform* for Supporting Hydrogeological Analyses, it is possible to generate appendices displaying the obtained results as specified by the project requirements. The *Appendix Generation Tool* was developed specifically to produce reports presenting the calculation outcomes.

Models, their inputs and components are stored in the so-called Project Repository (DAP), which is organized/divided into sections based on jobs (contracts or tasks being executed). The repository has two main purposes:

1. Storage of calibrated models, and
2. Storage of predictive calculation models defined by the Project assignment being addressed.

The difference between the mentioned types of models lies in the fact that calibrated models are based on real, measured data, whereas predictive models contain elements that are modified to a greater or lesser extent in accordance with the tasks being addressed. These modified elements essentially represent the assumptions or scenarios defined by the task setter.

5. Conclusion

The development of modern software tools and platforms for data preparation, analysis, and correction, as well as for simultaneous execution of numerous complex calculations, represents a significant contribution to the modernization and digitalization of processes across various engineering disciplines. This is especially evident in the field of hydrodynamic analyses of groundwater flow, where the complexity of natural systems and variability of hydrogeological parameters demand increasingly advanced computational methods and the processing of large volumes of data.

The implementation of the presented tools has enabled significantly more efficient handling of spatial and temporal data sets, their precise analysis and correction, as well as automation of processes that were previously highly demanding and prone to human error. The parallel execution of numerous

complex numerical simulations allows for the analysis of varying field conditions and their impacts on the groundwater regime, as well as the assessment of aquifer contamination risks. This substantially reduces the time required for the preparation of studies and expert evaluations, which is particularly important in the context of increasingly stringent regulatory requirements and the need for rapid response in crisis situations.

Generating results and reports through such platforms provides a high level of transparency and enables both experts and decision-makers easy access to key information for further planning and management of water resources. Particularly valuable is the capability for systematic archiving of all computational data, results, and analysis variants, which facilitates monitoring long-term changes in the groundwater regime, evaluating previous analyses, and simplifying the reuse of data in future projects.

The implementation of these solutions significantly contributes to improving the quality of hydrogeological studies and enables an interdisciplinary approach to addressing complex issues related to groundwater protection and exploitation as it is illustrated on the example of the Belgrade Metro project. Besides the technical advantages, such tools enhance collaboration among different professional profiles within teams, facilitating centralized work, faster information exchange, and synchronized decision-making.

Further development of software platforms in this field, particularly toward integration with real-time field data collection systems, the use of artificial intelligence for predictive modeling and advanced analyses, as well as improvements in result visualization, opens new possibilities for even more reliable and faster solutions. It is believed that such tools will play a key role in the future management and protection of groundwater, both in engineering practice and scientific research, where high-quality analysis and prediction of groundwater regimes are crucial for the sustainable use of this valuable resource.

Acknowledgements

UNESCO center II category Water for Sustainable Development and Adaptation to Climate change (WSDAC) – Belgrade, Serbia.

References

Anderson, M.P., Woessner, W.W., Hunt, R.J., 2015. Applied Groundwater Modeling: Simulation of Flow and Advective Transport (2nd ed.). *Academic Press*.

Bear, J., 1979. Hydraulics of groundwater, McGraw-Hill series in water resources and environmental engineering. *McGraw-Hill*, New York.

Domenico, P.A., Schwartz, F.W., 1998. Physical and Chemical Hydrogeology (2nd ed.). *John Wiley & Sons*, New York, Inc.

Foster, S., Lawrence, A., Morris, B., 2008. Groundwater in Urban Development: Assessing Management Needs & Formulating Policy Strategies. *Water P-Notes*, No. 18. http://hdl.handle.net/10986/11748

Howard, K.W.F. (Ed.)., 2007. Urban Groundwater, Meeting the Challenge: IAH Selected Papers on Hydrogeology 8 (1st ed.). CRC Press. https://doi.org/10.1201/9780203947050

Jaroslav Černi Water Institute (JČWI), 2022. Study of the Belgrade metro Line 1 and groundwater interaction, Book 4, geological structure and hydrogeological characteristics of the terrain. pp. 1-207

Zheng, C., Bennett, G.D., 2021. Applied Contaminant Transport Modeling (2nd ed.). *Wiley*.

Southeastern Europe Tunnelling Conference (SETC-2025)
1-3 October 2025, Belgrade, Serbia

DOI: 10.5937/SETC25014M

Advanced methods for assessment of the interaction dynamics of the hydrogeological environment and pressurized tunnel: A case study of HPP Pirot

Dušan Mikavica[a], Maja Todorović[b], Marina Ćuk Đurović[b] and Igor Jemcov[b]*

[a] Jaroslav Černi Water Institute Belgrade, Serbia; dusan.mikavica@jcerni.rs
[b] University of Belgrade, Faculty of Mining and Geology, Belgrade, Serbia; maja.todorovic@rgf.bg.ac.rs, marina.cuk@rgf.bg.ac.rs, igor.jemcov@rgf.bg.ac.rs

Abstract: This study presents a methodological framework for assessing the hydraulic behavior and hydrogeological sensitivity to pressure regimes induced by the operation of a pressurized tunnel at the Hydroelectric Power Plant Pirot. By integrating total-loss tests, structural assessments, and high-frequency monitoring of pore pressure, temperature, and electrical conductivity, along with hydrochemical analyses, a comprehensive understanding of flow mechanisms between the tunnel and surrounding rock mass, hydraulic connectivity, and water origins across different lithological zones has been provided. Total-loss tests quantified cumulative leakage, while sensors in the surge tank tracked key parameters, facilitating analysis of solute and thermal transport. Internal piezometers monitored transient pore pressures, revealing the hydraulic connections between the tunnel and its surrounding environment. Results show varying reactivity among hydrogeological units; highly fractured systems exhibited rapid pressure fluctuations in sync with tunnel operations, indicating direct connectivity, whereas others showed minimal response due to low permeability or isolation. Notably, significant lining cracks did not consistently correlate with leakage, suggesting that lining conditions alone are insufficient for evaluating hydraulic performance. Hydrochemical analyses confirmed interactions between the tunnel and groundwater, particularly in sensitive areas. Findings indicate that the hydraulic reactivity of the rock mass is primarily influenced by the geometry of pore spaces and proximity to the surge tank, with tunnel lining condition having a minor role in overall sensitivity. This methodological approach enhances understanding of the interplay between the performance of the concrete lining-grout-rock interface and the surrounding hydrogeological environment under different pressure loads, underscoring the importance of high-resolution hydrogeological monitoring in assessing the hydraulic response of the rock mass, detecting potential leakage, and identifying hydraulically critical zones along the tunnel and defining priorities for rehabilitation works.

Keywords: hydraulic tunnel; concrete lining; cracks; hydrogeological monitoring; hydrochemical indicators; tunnel-groundwater interaction

1. Introduction

Hydraulic tunnels are essential components of hydroelectric power plants (HPPs), enabling the conveyance of pressurized water across geologically diverse terrains. However, their construction and operational integrity are challenged by intersecting zones of heterogeneous lithology and structural complexity, resulting in spatially variable hydraulic behavior along the tunnel alignment. Different types of linings, such as cast-in-place concrete, precast segmental lining, or shotcrete, are often used to address ground conditions, but also introduce complexity in pressure transfer and inflow–leakage behavior. Concrete linings combined with grouting are designed to reduce permeability (Schleiss, 1997); however, operational pressure fluctuations often induce tensile stresses that can lead to cracking, particularly under transient flow conditions (Karami et al., 2019). In faulted or fractured rock, such cracks may create leakage paths that undermine the hydraulic isolation of the lining, making the achievement of complete watertightness challenging. The reduced water resistance of the tunnel,

*Corresponding author: dusan.mikavica@jcerni.rs (D. Mikavica).

combined with the initiation and propagation of cracks in the lining caused by operational pressure cycles, creates interconnected flow paths that alter the surrounding hydrogeological regime.

Considering the sustained influence of tunnel operation over time, the interaction between internal hydraulic loads and the surrounding rock environment becomes increasingly important. Water ingress and leakage through the lining–rock interface can alter local pore pressure regimes and cause mechanical-hydraulic coupling, which impacts the overall stability and function of the hydrogeological system (Liu and Li, 2022). These processes are strongly influenced by the type of tunnel lining. Segmentally lined tunnels tend to exhibit increased permeability through joints and connections, which elevates seepage velocities and affects stress distributions (Shin et al., 2012). In contrast, cast-in-place concrete linings are more prone to progressive crack development and connectivity, resulting in increased permeability over time (Yi et al., 2011; Gao et al., 2019).

Conventional monitoring methods, such as structural assessments and cumulative water loss measurements, provide valuable insights into performance and watertightness (Andjelković et al., 2013), but offer limited information on lining leakage points and transient behavior. In contrast, visual inspections can identify localized damage and quantify zones of water leakage but frequently fail to detect dynamic processes under actual conditions and are limited by low frequency and high costs. Recent studies have highlighted the benefits of high-frequency pore-pressure monitoring using internal piezometers in detecting transient hydraulic events and enhancing the characterization of aquifer response (Neupane, 2021; Jemcov et al., 2024). Additionally, hydrochemical indicators offer complementary insights into groundwater–tunnel interactions, particularly under variable pressure regimes (Ćuk et al., 2020).

This study presents advanced methods for investigating the pressurized headrace tunnel of the HPP Pirot in Serbia, situated in a complex hydrogeological environment with variable permeability. By integrating tunnel lining condition mapping data, high-frequency measurements of pore pressure, temperature, and electrical conductivity with hydrochemical analyses and total water loss testing, the study aims to identify zones prone to leakage and evaluate the hydraulic sensitivity of the rock mass. The primary objective is to develop a comprehensive methodological framework that elucidates flow mechanisms across different geological units, detects hydraulically weakened zones in tunnels, and evaluates the mutual interactions between the tunnel lining, the grout–rock contact zone, and the surrounding hydrogeological environment under variable pressure regimes.

1.1. Case study

The studied tunnel is part of a hydroelectric power plant (HPP) in southeastern Serbia. It conveys water from the Zavoj Reservoir (568–615 m a.s.l.) to a surge tank and penstock before discharging into the compensation basin. The pressurized tunnel is 8672 m long, circular in cross-section (4.5 m diameter), with a longitudinal slope of 3‰. Surge suppression is managed through a side surge tank, with measured transient levels reaching up to 630.4 m a.s.l. (Ilić et al., 2019). The tunnel lining is predominantly cast-in-place unreinforced concrete (CIP), except between stations 3+156 and 7+061, where precast segmental lining (PSL) was installed using a tunnel boring machine. The surrounding rock mass was treated with pressure and consolidation grouting to enhance structural stability and reduce permeability under internal pressure.

Geologically, the alignment crosses two major tectonic units of the Carpatho-Balkan system, the Getic and Danubian, separated by the east-vergent Vidlič thrust (Kräutner and Krstić, 2002). The Getic unit comprises Permo-Devonian clastics and Triassic–Jurassic carbonates, while the Danubian unit includes Triassic clastics and massive Jurassic–Cretaceous platform limestones (Fig. 1). Structurally, the tunnel alignment intersects a regional sub-vertical strike-slip fault and numerous secondary oblique faults (Krstekanić et al., 2022), which strongly control groundwater flow. Five hydrogeological systems were identified through earlier investigations, ranging from shallow karstic and fissured aquifers to deeper fault-controlled systems with thermal water discharge, reflecting the litho-structural heterogeneity of the terrain (Ćuk et al., 2020).

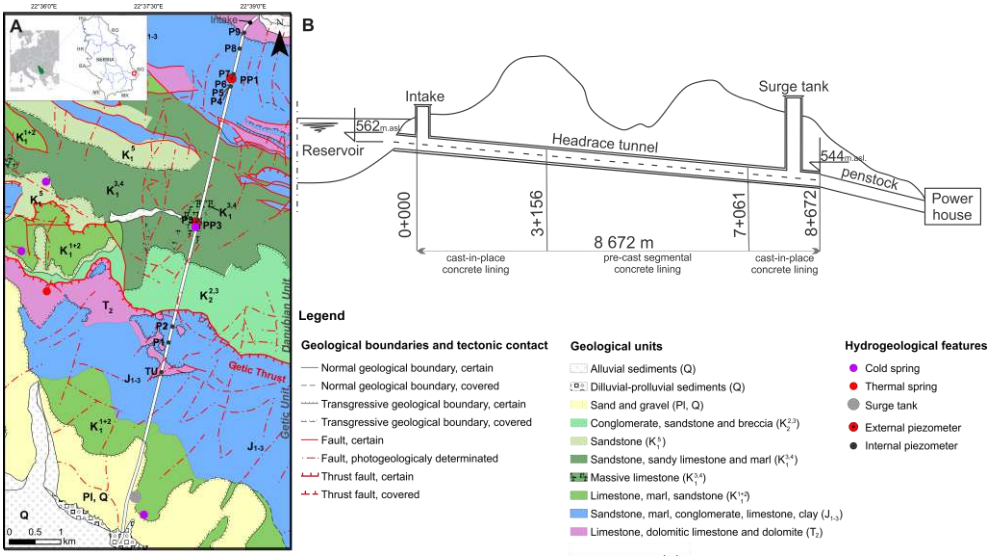

Fig. 1. (A) Geological sketch map of the study area (Anđelković et al., 1975); (B) Schematic representation of the Pirot HPP tunnel.

2. Applied methods

2.1. Measurements of the tunnel total water loss

To evaluate the watertightness of the concrete-lined tunnel and detect cumulative leakage, a multi-step total-loss measurement has been implemented as a standard procedure. The methodology was adapted from established hydraulic loss assessment protocols (Andjelković et al., 2013, Radovanović et al., 2022) and tailored to the site's geometry and operational conditions. Total-loss testing has been conducted by isolating the tunnel and monitoring water-level decline in the vertical inlet shaft (IN) with a five-step drawdown procedure. Each step consisted of a controlled discharge period followed by stabilization and an observation interval. The total leakage has been quantified by calculating volume loss over time. The test mentioned above provides a general evaluation of the hydraulic tightness of the tunnels. Therefore, the pressure lowering in the tunnel with each step results in a reduction in the total loss. A significant limitation of the implemented approach is the inability to detect water inflow from the surrounding geological environment, resulting from the induced reduction in water pressure within the tunnel. To overcome this problem, high-frequency multi-probes (measuring pressure, temperature, and electrical conductivity) have been installed in the water intake and surge tank to characterize water ingress when external groundwater pressure prevailed.

2.2. High-frequency pore pressure monitoring in the tunnel and internal piezometers

To examine the hydraulic interaction between the surrounding hydrogeological environment and tunnel pressure, an advanced monitoring system has been implemented. This system includes internal piezometers, which are situated within the tunnel and extend into the surrounding rock mass, ensuring they are completely isolated from the tunnel's water pressure. High-frequency probes have been installed in these internal piezometers to investigate the transient pressure propagation from the tunnel into the hydrogeological environment during HPP operations. While probes equipped with data loggers are effective for monitoring transient pressure, regardless of their distance from the tunnel access, they have a limited storage capacity for temporal data and require access to the tunnel for data retrieval.

Nine internal piezometers (up to 3 m deep into the rock mass) with probes, with minute logging intervals, were installed within the tunnel at points chosen based on seepage, lining damage, geological structures, and hydrochemical anomalies (Fig. 1). Additionally, internal hydraulic conditions in the tunnel and pressure fluctuations within the karst system connected directly to the tunnel were monitored by installing a pressure sensor (TU) at the open end of a karst conduit encased in a pipe within the tunnel. Furthermore, identical probes were installed in external piezometers, situated approximately 15 m from the tunnel line.

2.3. Evaluating tunnel lining damage and water leakage

To evaluate the structural condition and hydraulic performance of the tunnel lining, a combination of detailed tunnel mapping and flow assessment methods was applied to identify structural damage and spatially characterize water ingress in the depressurized tunnel. Detailed mapping of the tunnel lining is carried out on a base that incorporates the results of the previous phases. During mapping, the positions and characteristics of all fractures and water leakage events are recorded, which involves assessing or measuring their abundance. This method of collecting data on the condition of the tunnel lining provides a good database for analyzing the development of cracking over time, in relation to the geological and hydrogeological framework. A crack index (CI) was calculated and spatially correlated with inflow intensity and lithological features. Leakage was categorized into four classes (dry, wetting, dripping/seepage, leakage). To support the assessment of leakage through the lining, inflow measurements were taken at four measuring points within the tunnel: at the beginning (near the entrance structure), at two locations where the lining type changes, and finally at the tunnel exit (representing the cumulative inflow). To focus on sections of significant leakage through the tunnel, supplemental flow measurements are needed through a dense network of gauging sectors at zones where there is a considerable flow difference. Based on this approach, it is possible to detect hydraulically weakened zones, regardless of the tunnel lining. Starting from the need to perform measurements on a larger number of profiles, one possible rapid technique is the use of a flow meter that employs the tracer (salt) dilution method, which measures water flow based on the tracer concentration as a function of flow rate. The advantage of this technique lies in its simplicity and the ability to perform quick calculations, but a drawback is the potential variability in water conductivity within the measured section.

2.4. Hydrochemical analysis

A comprehensive hydrochemical monitoring campaign has been carried out, covering sampling sites within and surrounding the tunnel structure (key leakage points in the tunnel, internal and external piezometers, karst springs, and the reservoir) under different HPP operational statuses. Within an empty tunnel, successive in situ measurements of physicochemical parameters, pH, electrical conductivity (EC), redox potential (ORP), temperature, and dissolved oxygen (DO), were conducted at each leakage point to indicate possible changes in water chemistry and to select samples for chemical analyses. Water samples were analyzed for major cations (Ca^{2+}, Mg^{2+}, Na^{+}, K^{+}) and anions (HCO_3^{-}, SO_4^{2-}, Cl^{-}, NO_3^{-}). In addition to standard hydrochemical parameters, special attention was given to the determination of Sr, Li, and H_2S, to identify the presence of deep hydrogeological systems, and better understand their hydraulic interaction with the tunnel. Although carefully planned, sampling was limited to discrete points, preventing continuous tracking of hydrochemical changes during transient events. To address this, the sampling network needs to expand to under-monitored areas.

3. Results and Discussion

3.1. Total-loss measurements and pore pressure reactions

Total water loss measurements were conducted under pressurized conditions at a reservoir level, involving incremental reductions of the water level within the inlet shaft with stabilization periods

maintained between steps. Losses were quantified at five distinct water levels (Fig.2A). Initially, at the first step, losses reached 13.10 $L \cdot s^{-1}$, followed by 12.63 $L \cdot s^{-1}$at the next step, and a further reduction to 5.18 $L \cdot s^{-1}$. At the fourth step, the measured loss was 0.84 $L \cdot s^{-1}$, indicating minimal leakage. At the final measurement (the fifth step), a slight inflow of –0.40 $L \cdot s^{-1}$ was observed, indicating a reversal in the hydraulic gradient. Contrary to the detected inflow into the tunnel in only the fifth step, the changes in electrical conductivity indicated that water was inflowing from a specific part much earlier, thereby reducing the total losses from the tunnel (Fig. 2A). The measured total losses demonstrated that the tunnel's water retention capacity remained within long-term safe thresholds, with stepwise-measured losses maintained within controlled limits, indicating that no concerning hydraulic changes occurred within the system. The descending trend with decreasing water level confirms that the high pressure contributes most to leakage. Considering that highly mineralized waters have been identified in Zone 3 (Table 1), increased electrical conductivity suggests potential inflow in the zone of incomplete sealing of the segmental lining related to the anticline structure.

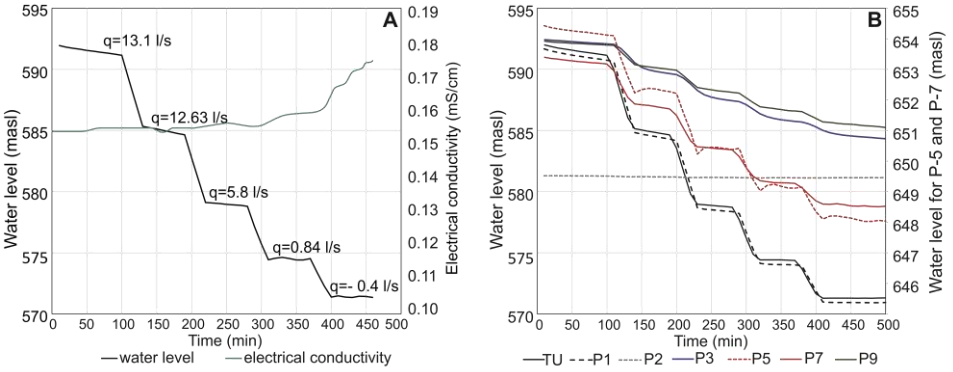

Fig. 2. (A) The results of total loss measurements (B), Pore pressures in the internal piezometers during total loss measurements.

Piezometric responses to controlled depressurization provided insights into the hydraulic conductivity of distinct hydrogeological sections along the tunnel, particularly in the vicinity of the surge tank, where important tunnel–rock mass interaction was observed (Fig. 2B). Pressure declines patterns reflected the influence of lithology, indicating zones of reduced impermeability and compromised sealing within the tunnel lining. A comparative analysis of internal pore pressure data and water level fluctuations in the inlet shaft during total loss measurements emphasized the heterogeneous connectivity and influence of natural groundwater conditions along the tunnel alignment.

High-frequency monitoring of tunnel pressure during HPP operation cycles revealed notable pore pressure responses to unsteady hydraulic phenomena (significant pressure variations caused by hydraulic transients during turbine operation changes). These fluctuations exhibited clear spatial patterns, with pronounced pressure oscillations observed due to the surge tanks' influence, which further attenuate toward the reservoir, indicating variations in pressure magnitude and transmission. Analysis of piezometric data identified four characteristic types of hydrogeological response shown on Fig. 3: (1) non-responsive zones, such as piezometeres P8 and P2, where stable pressures without oscillations indicated hydraulically isolated conditions; (2) attenuated responses, as seen in P5, P7, and P9, where small to moderate oscillations suggested limited but synchronous pressure transmission within the rock mass; (3) highly responsive zones, embodied by P1 and TU, which recorded large, rapid pressure fluctuations (15–20 m) that closely mirrored tunnel pressure variations, confirming direct hydraulic connectivity with the karst aquifer conduits and open fault zone; and (4) a unique response at P3, which displayed moderate pressure variations (~3 m), manifested by gradual pore pressure changes, without

a sharp drops caused turbine-start events, implying a well-structured karst aquifer acting over a broader scale as indicated with groundwater level response of external piezometer PP3.

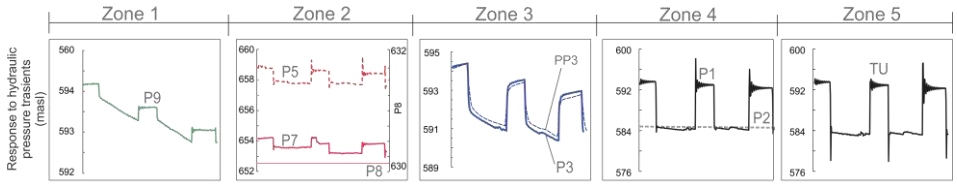

Fig. 3. Pore pressure transient during operational regimes of HPPP.

3.2. Qualitative evaluation of tunnel lining integrity and hydraulic behavior under depressurized conditions

The results of the structural and hydraulic integrity assessment of the tunnel lining under depressurized conditions identified five distinct zones (Jemcov et al. 2024.), which were further interpreted in relation to the geological and hydrogeological context (Table 1, Fig. 4).

Table 1. Summary of zonal classification based on field observations of structural and hydraulic integrity of tunnel lining across geological zones.

Zone Station (m)	Dominant lithology and structural features	Lining type	Groundwater inflow, crack pattern, and leakage	Piezometer
Zone 1 0+000 – 0+650	Triassic limestone, dolostone, and shale; thin-layered. Fault zone near 0+240–0+330. Low karstified – partially fissured	CIP	Relatively uniform moderate cracking lining (CI 0.13). Leakage has a diffuse distribution, with the highest rates near the fault intersection.	P9 0+370
Zone 2 0+650 – 2+775	Lower and Middle Jurassic conglomerate, shale, marl, and sandstone, tectonized with reverse faults (faulted interval 1+357–1+440). High-pressure aquifer system.	CIP	Cracking related to the fault zone (CI 0.19). Low-intensity, diffuse seepage from a high-pressure aquifer. Hydraulically low permeable.	P8 0+840 P7 1+360 PP1 1+400 P6 1+480 P5 1+500 P4 1+540
Zone 3 2+775 – 5+200	Cretaceous marl, marly limestone, and limestone, with a prominent anticline (4+230–4+280). Divided from the 2nd zone by reverse faults	CIP PSL	CIP-type of lining (CI 0.26) with diffuse seepage along the fractures. The PSL-type lining had a low crack index (mean CI = 0.01) and exhibited good hydraulic performance, only localized joint leakage connected to the karstified anticline core (4+230).	PP3 4+210 P3 4+230
Zone 4 5+200 – 7+031	Autochthon in the vicinity of the Getic thrust: marl, shale, silicified limestone, and sandstone intersected by multiple faults.	PSL	Segmental lining had a low crack index (mean CI 0.01). Leakage increased in several zones, particularly around station 6+100 and 6+700, where the expansion of preferential pathways within the faulted fracture zone facilitated drainage from a deep karst aquifer with subthermal waters, notably higher diffuse inflow.	P2 6+390 P1 6+715
Zone 5 7+031 – 8+900	Getic allochthonous limestone and sandstone, intensively folded.	CIP	Increased cracking (mean CI 0.19) and significant pressurized leakage occurred near the Getic thrust zone, especially around chainage 7+355. Karst conduit flow (5–10 L·s^{-1}) through the tube directly into the tunnel (7+355).	TU 7+350

The comprehensive leakage assessment identified that 353 m (4%) of the tunnel displays intense leakage, 2.7 km of diffuse seepage, 2.1 km of low-permeability sections with wetting, and 3.7 km of effectively impermeable sections. Cast-in-place lining is more prone to cracking and leakage, exhibits a higher crack index (mean CI 0.19), and diffuse seepage concentrated in faulted zones. Segmental precast lining exhibits very low cracking (mean CI 0.01) and improved watertightness, with elevated hydraulic sensitivity attributed to compromised gasket performance at segmental joints, resulting in localized zones of high inflow.

Inflow measurements in the dewatered tunnel were carried out in two phases: the first was conducted immediately after the tunnel was emptied, and the second measurement was carried out immediately before the tunnel was closed and placed into operational use. The temporal measurement design captures two distinct hydrogeological conditions of surrounding rock mass: one with residual pressurized tunnel water and another reflecting sustained leakage after drainage. The difference

between measurements is commonly observed, and when analyzed alongside groundwater level data and results from tunnel mapping allowed identification of leakage characteristics in sections of the tunnel that have different types of lining between the measurement profiles.

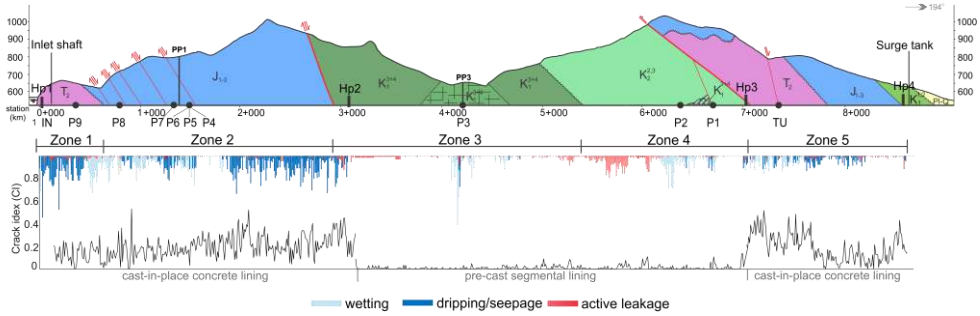

Fig. 4. Spatial distribution of quantified crack index and corresponding qualitative assessment of water leakage through the lining (legend as in Fig. 1). Hp1-4 hydraulic profiles for inflow measurements.

A more straightforward interpretation of the hydraulic responses in the hydrogeological environment and a deeper understanding of hydraulic sensitivity were achieved by correlating the results with the qualitative assessment of tunnel leakage. The structurally complex zones with significant cracking within Triassic and Jurassic limestones (Zones 4 and 5) acted as preferential pathways for the most persistent inflows of pressurized groundwater and subthermal karst water, with discharge rates reaching up to 10 $L \cdot s^{-1}$. In contrast, sections that traversed fine-grained marl and shale units, such as those of the Danubian formations, showed localized cracking but low leakage. This reveals an important insight: structural damage, as observed visually, is not a reliable indicator of hydraulic behavior. A quantitative assessment using the crack index highlighted these differences, with values ranging from 0.01 in segmental lining sections to 0.52 in cast-in-place concrete segments located in the fault zones. While segmental linings generally showed lower crack densities and surface damage, localized leakage was still observed at joints installed in transmissive formations, particularly in structurally significant areas like the anticline at station 4+230.

3.3. Hydrochemical analysis of groundwater–tunnel interaction

Spring and surface water samples remained hydrochemically stable over time, suggesting minimal impact from tunnel operations, likely due to their shallow occurrence and limited hydraulic connection with the deeper groundwater systems. In contrast, hydrochemical analysis confirms that the pressurized tunnel has a significant impact on the surrounding hydrogeological environment, as evidenced by notable changes in the tunnel's water chemistry. During the depressurization phase, significant hydrochemical variability occurred across different zones, indicating active interactions between the tunnel and the aquifer. Zone 3 (Station 4+230 m) exhibited the highest electrical conductivity (up to 10,200 µS/cm) with noticeable dilution due to the influence of the tunnel. External piezometer PP3 located near Zone 3, recorded increases in chloride and sulfate concentrations during depressurization, pointing to rapid hydraulic response and showing that the tunnel influence extends beyond its immediate vicinity. This zone also displayed elevated strontium and lithium levels, consistent with inflow from deep karst aquifers. Zone 2 showed increased pH and bicarbonate levels, alongside the presence of hydrogen sulfide, suggesting active sulfate reduction processes. In Zones 4 and 5, characterized by tectonic activity, hydrochemical fluctuations were more pronounced, with higher temperatures and complex compositions indicative of mixing between thermal and tunnel waters. Hydrochemical fingerprints provided validation of inferred flow paths and revealed permeability contrasts that were undetectable using hydraulic data alone.

4. Conclusion

An integrated methodological approach to pressurized tunnel hydrogeology in complex geological settings is crucial, as the interaction between the tunnel, lining, and rock mass is inherently geologically dependent and requires multi-parameter monitoring. Effective evaluation of tunnel-groundwater interaction were achieved through the integration of multiple complementary methods: (1) total-loss measurements quantified cumulative tunnel water losses; (2) pore pressure data captured pressure redistribution and revealed tunnel–rock mass hydraulic conductivity; (3) transient hydraulic analysis characterized connectivity; (4) structural surveys indicated lining damage and hydraulic behavior in depressurized conditions; and (5) hydrochemical data traced flow origins and mixing processes. Significant spatial variability in pore pressure responses was noted, influenced by geological conditions and lining types, with lining cracks producing varied leakage patterns. Monitoring demonstrated that hydroelectric power plant operations can rapidly redistribute pressure within the tunnel system, especially in zones under strong influence of the surge tank, with structurally complex or hydraulically sensitive conditions. Hydrochemical methods helped identify zones of interaction between groundwater and tunnel water, aligning observed changes with hydraulic signals, and highlighting the importance of a multidisciplinary approach to tunnel monitoring in geologically sensitive areas. Findings derived within this study indicate that pressure transmission to the hydrogeological environment and its behavior are primarily governed by the geological and structural features of the rock mass, rather than by the visible integrity of the concrete lining. A comprehensive approach is recommended for future tunnel surveillance and maintenance, especially in zones affected by faulting, karstification, or dynamic transient pressure changes, all of which necessitate continuous monitoring. This framework facilitates the early identification of hydrogeological risks and can help define priority zones for effective grouting interventions, thereby promoting the long-term safety and operational efficiency of tunnel infrastructure in complex geological and hydraulic settings.

Acknowledgements

This work was supported by the Ministry of Science, Technological Development and Innovation of the Republic of Serbia, contract on realization and financing of the scientific research work of the Faculty of Mining and Geology in 2025, contract number: 451-03-136/2025-03/200126.

References

Anđelković J., Krstić B., Ćirić D., Martinović D., Bogdanović P., 1975. National Geological Map of the former Yugoslavia, 1:100000, sheets K 34–34 Pirot and interpretations (in Serbian). Federal Geological Survey, Belgrade.

Andjelković, V., Lazarević, Ž., Nedović, V., Stojanović, Z., 2013. Application of the pressure grouting in the hydraulic tunnels. *Tunnelling and Underground Space Technology*, 37, 165–179.

Ćuk, M., Jemcov, I., Mladenović, A., and Čokorilo Ilić, M., 2020. Hydrochemical impact of the hydraulic tunnel on groundwater in the complex aquifer system in Pirot, Serbia. *Carbonates and Evaporites*, 35(2). https://doi.org/10.1007/s13146-020-00563-y

Gao, C.L., Zhou, Z.Q., Yang, W.M., Lin, C.J., Li, L.P., Wang, J., 2019. Model test and numerical simulation research of water leakage in operating tunnels passing through intersecting faults. *Tunnelling and Underground Space Technology*, 94 (4):103134, 10.1016/j.tust.2019.103134

Ilić, J., Petković, A., Božić, I., 2019. Numerical analysis of water hammer and water-mass oscillations in a hydropower plant for extreme operational regimes. *FME Transactions*, 47(1), 7–15. https://doi.org/10.5937/fmet1901007I

Jemcov, I., Todorović, M., Jemcov, A., Ćuk Đurović, M., 2024. Hydraulic impact of pressure transients from water conveyance tunnel on the complex hydrogeological system. *Journal of Hydrology,* 644:132068, https://doi.org/10.1016/j.jhydrol.2024.132068

Karami, M., Kabiri-Samani, A., Nazari Sharabian, M., Karakouzian, M, 2019. Effects of transient flow in concrete-lined pressure tunnels and developing a new analytical formula for pressure wave velocity. *Tunnelling and Underground Space Technology*, 91, 1–13. https://doi.org/10.1016/j.tust.2019.102992

Kräutner, H.G., Krstić, B., 2002. Alpine and Pre-Alpine structural units within the Southern Carpathians and the Eastern Balkanides. In: Proceedings of XVII Congress of Carpathian–Balkan Geological Association, Geologica Carpathica, 53 (Special Issue).

Krstekanić, N., Matenco, L., Stojadinovic, U., Willingshofer, E., Toljić, M., Tamminga, D., 2022. Strain partitioning in an extensive intracontinental strike-slip system accommodating backarc-convex orocline formation: The Circum-Moesian Fault System of the Carpatho-Balkanides, *Global, and Planetary Change*, Volume 208, 103714, ISSN 0921-8181, https://doi.org/10.1016/j.gloplacha.2021.103714.

Liu, S., Li, Z., 2022. Unloading behaviors of shale under the effects of water through experimental and numerical approaches. *International Journal of Geomechanics*, 22, 04022071. https://doi.org/10.1061/(ASCE)GM.1943-5622.000234

Neupane, B., 2021. Long-term impact on unlined tunnels of hydropower plants due to frequent start/stop sequences. PhD Thesis, *Norwegian University of Science and Technology*. ISSN 2703-8084.

Radovanović, S., Milivojević, M., Stojanović, B., Obradović, S., Divac, D., Milivojević, N., 2022. Modeling of water losses in hydraulic tunnels under pressure based on stepwise regression method. *Applied Sciences*, 12(18), 9019. https://doi.org/10.3390/app12189019

Schleiss, A., 1997. Design of reinforced concrete linings of pressure tunnels and shafts. *Hydropower&Dams* 4(3), 88–94: 53, 3073–3092.

Shin, J.H., Kim, S.H., Shin, Y.S., 2012. Long-term mechanical and hydraulic interaction and leakage evaluation of segmented tunnels. *Soils and Foundations*, 52, 38–48. 10.1016/j.sandf.2012.01.011

Yi, S.T., Hyun, T.Y., Kim, J.K., 2011. The effects of hydraulic pressure and crack width on water permeability of penetration crack-induced concrete. *Construction and Building Materials*, 25, 2576–2583. 10.1016/j.conbuildmat.2010.11.107

Southeastern Europe Tunnelling Conference (SETC-2025)
1-3 October 2025, Belgrade, Serbia

DOI: 10.5937/SETC25015K

Prediction and validation of stress-induced rock bursting in a deep Himalayan tunnel through empirical methods

Rahul Khanna[a], Rajeev Anuj Sharma[a] and Ranjit Singh[b]*

[a] NHPC Ltd., Parbati HE Project, Stage-II, Manikaran, Himachal Pradesh, India; rajeev@nhpc.nic.in
[b] NHPC Ltd., Parbati HE Project, Stage-II, Nagwain, Himachal Pradesh, India; ranjit@nhpc.nic.in

Abstract: The deep tunnels under construction in the tectonically active Himalayan terrain endure high magnitudes of field stresses, causing brittle failure. The instability caused by the tunneling media is manifested in the form of spalling and rock bursts. This paper focuses on determining the yielding capacity of the stressed rock strata through RMR-14 employing elastic behaviour index (ICE) and stress factor (Fs). The ratio of far-field maximum stress to compressive strength is used to evaluate tunnel stability. The rock-bursting potential is determined from the tangential stress components in the roof and side walls of the tunnel. The competency factor (C_g) for the brittle quartzite is also estimated. The results are validated for a 1.2 km stretch of the 31.56 km long head race tunnel of the Parbati 2 hydroelectric project. An innovative chart-based technique is developed for field recording of stress-induced incidents based on their severity, duration, periodicity, and impact on the tunnel profile. The back analysis indicates those reaches that witnessed frequent incidents of violent rock bursting and faced difficulty providing rock support have a ratio of maximum boundary stress (σ_1) and compressive strength (σ_c) greater than 0.5, C_g less than 1.0, and ICE ≤15. Results indicate that ICE is a handy tool for predicting the stress-deformation characteristics.

Keywords: rock burst; elastic behaviour index; competency factor; compressive strength

1. Introduction

The young and dynamic Himalayas present unusually challenging ground conditions during the construction of deep-seated transport and hydro tunnels. A prudent and thorough understanding of the expected geology, along with an unambiguous prediction of the stress-deformation characteristics of the rock mass, is crucial to the success of these tunneling projects. Failures in deep tunnels are a function of intact rock strength, joint distribution, and the magnitude and direction of in-situ stresses. Stress-induced fractures developed around the excavation boundary are termed as brittle failure (Hoek et al., 1995). When a deep-seated tunnel passing through hard and brittle rocks intercepts regions of high field stresses, localized brittle failures accompanied by the sudden release of elastic strain energy are observed (Palmström, 1995; Feng, 2017; Cai and Kaiser, 2018; Askaripour et al., 2022). Such failures are manifested as rock spalling, slabbing, and rock bursting (Ortlepp and Stacey, 1994). Several researchers have attempted to predict the phenomenon of rock bursting in deep mines and hydro tunnels through various techniques, such as empirical methods (Russenes, 1974; Barton et al., 1974; Palmström, 1995; Diederichs, 2007; Russo, 2014; Farhadian, 2021), machine learning and artificial neural network techniques (Zhang et al., 2020; Zhao et al., 2021), micro seismic monitoring (Jenkins et al., 1990; Kasier and Maloney, 1997; Urbancic et al., 2000; Shen et al., 2008; Ma et al., 2021) and numerical modelling techniques (Miranda, 1972; Hart, 1980; Zubelewicz and Mroz, 1983; Jing and Hudson, 2002; Cai et al., 2007; Wang and Cai, 2017; Gao, 2019). Numerical methods generally have limitations in considering factors and criteria. Micro seismic monitoring faces issues like elastic wave signal overlap, quantifying indicator sensitivity, and unreliable warning time. Machine learning methods exhibit good predictive ability but are limited by the quality of input indicators, the size of sample datasets, and data processing issues. On the other hand, accurate measurement of in situ field stresses is very cumbersome, as stress is a tensor quantity that varies in magnitude and direction in

*Corresponding author: rahul@nhpc.nic.in (R. Khanna).

three-dimensional space. Moreover, the complexity, discontinuity, and inhomogeneity of the rock mass also limit the possibility of its accurate measurement (Amadei et al., 1997). Experience with in-situ tests also suggests an inconsistency in results and variations within proximity (Dev, 2019). Moreover, in the ongoing construction projects, due to very hard-pressing schedules, it is not possible to carry out field tests as they are expensive and require dedicated, undisturbed space. Alternatively, understanding the instability of tunnels due to in-situ stress-deformation behavior and the reliable prediction of rock bursting through empirical relations offers a convenient and straightforward approach. This paper predicts stress-deformation behaviour for a 1.2 km reach of the 31.5 km long head race tunnel of the Parbati 2 hydroelectric project. Additionally, a chart-based technique devised for recording stress-induced conditions during tunneling is also presented.

2. About the project layout and geology

The Parbati 2 hydroelectric project, with an installed capacity of 800 MW, falls in the Kullu district of Himachal Pradesh, India. This project of national importance is owned by NHPC Ltd., a Government of India undertaking. It involves inter-basin transfer of water from Parbati to the Sainj River (Fig. 1). A gross head of 862.5m is utilized for the generation of 3124.6 GWH of annual energy in a 90% dependable year. Commercial operation commenced after the commissioning of all four 200 MW units each during March and April 2025. The head race tunnel is a pressurized tunnel with maximum and minimum static water heads of 1.07 bars and 7.9 bars at the downstream and upstream ends, respectively. The 31.56 km long and 6m diameter tunnel has a gradient of 1:461.6 carrying a design discharge of 116 m^3/sec with an average velocity of 4.10 m/sec. The maximum and minimum vertical cover above the tunnel are 1683 m and 123 m, respectively. About 5.7 km of the tunnel, which is excavated using an open shield Tunnel Boring Machine (TBM), is circular, while the remaining portion, excavated by the conventional drilling and blasting method, is horseshoe-shaped.

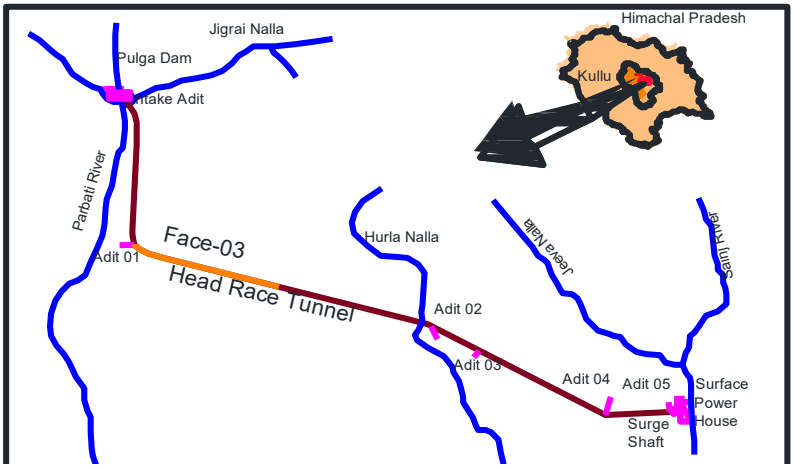

Fig. 1. Project layout showing head race tunnel alignment.

The project is located within the "Kullu Window" of the Lesser Himalayas, comprising crystalline and metasedimentary rocks of the Kullu and Rampur Groups, including granitic gneiss, mica gneiss, biotite and quartzite schist, quartzite, slate, phyllite, and dolomite. A major fault system structurally bounds the area, specifically the Main Central Thrust (MCT), and has undergone intense deformation, resulting in the formation of several faults, folds, shear zones, and intense jointing of the rock strata. The 5608 m tunnel section along the downstream face-03 discussed here was excavated from adit 01, starting from chainage 6364 m to 11385 m. The rock types encountered were biotite mica schist with quartzite, phyllite with carbonaceous phyllite, quartzite with bands of schists, and chlorite schists (Fig. 2). A faulted contact was intercepted around chainage 9684 m between carbonaceous phyllites and quartzites.

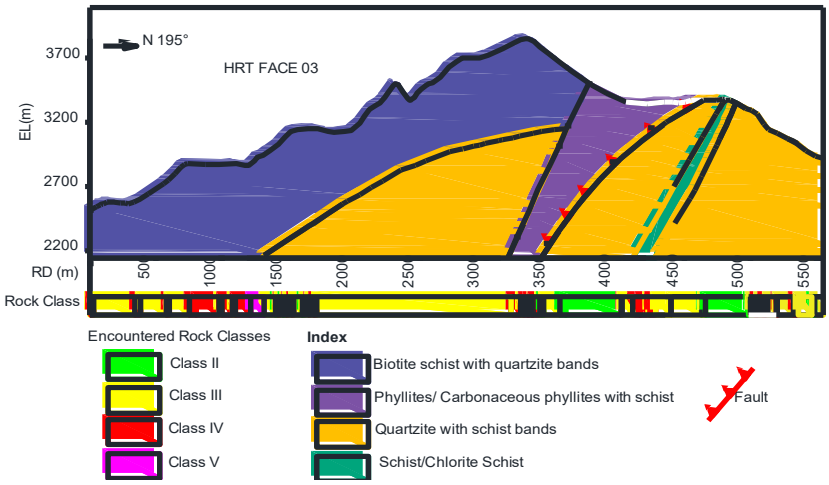

Fig. 2. Geological L-Section along head race tunnel (face 03) and encountered rock classes.

3. Prediction of stress-deformation characteristics through empirical methods

The deformation and rock burst potential in a deep tunnel can be predicted through a profound understanding of stress conditions and compressive strength of the rock mass using empirical correlations. Quantitative rock mass characterization systems such as RSR (Wickham et al., 1972), RMR (Bieniawski, 1973, 1989), Q-system (Barton et al., 1974), and RMi (Palmström, 1995) have been empirically developed utilizing rock mass data from various civil engineering projects with an attempt to incorporate most of the engineering geological parameters (Hoek, 2004). However, each system has its limitations in defining the holistic behavior of rock mass, considering that only limited input data sets have been utilized. RSR and RMR_{89} systems do not offer any means to evaluate the stress conditions of the rock mass.

3.1. Elastic Behavior Index (ICE)

Celada et al. (2014), based on 2,298 case histories, updated the most widely used RMR89 and came out with an improvised RMR14 system having five basic parameters and three adjustment factors, including stress factor (Fs) to consider stress-deformation behavior of the rock mass by employing "*Índice de Comportamiento Elástico*" referred to as ICE (Bieniawski et al., 2011) or Elastic Behavior Index, which is defined as:

$$Ko \leq 1: ICE = \frac{3704\sigma c * e^{\frac{RMR-100}{24}}}{(3-Ko)*H} * F \quad (1)$$

$$Ko \geq 1: ICE = \frac{3704\sigma c * e^{\frac{RMR-100}{24}}}{(3Ko-1)*H} * F \quad (2)$$

Where σ_c is the uniaxial compressive strength of the intact rock in MPa; Ko is the ratio of horizontal to vertical stresses; H is the tunnel depth in m, and F is the shape coefficient, considered as 1 for a 6 m diameter horseshoe-shaped tunnel. RMR above is corrected for discontinuity orientation. From ICE, the stress-deformation behavior of the tunnel is determined (Table 1). Excavation having an ICE < 70 exhibits stress-induced conditions. The stress factor (Fs) aims to account for the declining impact of yielding in the tunnel and is estimated from ICE (Mateus et al., 2023). Celada et al. (2014) showed that stress factor (Fs) ranged between 0 to 1.3. Fs is 1 for ICE>70 and 1.3 for ICE<15. The Fs values for the 1.2 km tunnel reach from Adit-1 plotted on the ICE-Fs curve (Fig. 3) indicate the stress-deformation condition, which has been predicted as mostly yielding to moderately yielding (ICE<50).

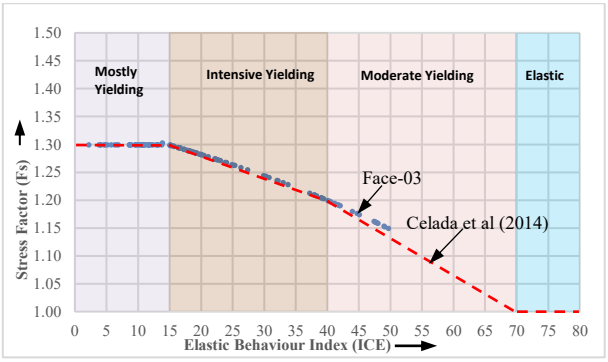

Fig. 3. Stress Factor (Fs) estimated for the 1.2km HRT reach plotted on the ICE-Fs of Celada et al. (2014).

Table 1. Stress-deformation behaviour as a function of ICE (Celada et al., 2014).

ICE	Stress-deformation behavior
>130	Completely elastic
70-130	Elastic with incipient yielding
40-69	Moderate yielding
15-39	Intensive yielding
<15	Mostly yielding

3.2. Hoek and Brown stability classes

Intact rock uniaxial compressive strength (σ_c) used in this study is measured in the field using an N-type Schmidt hammer. The rebound numbers (RN) are collected in the field according to the procedure outlined in the "ISRM Suggested Method" (Aydin, 2009). The UCS is estimated using the empirical equation (Bolla and Paronuzzi, 2021):

$$\sigma_c = 5.2251 * e^{(0.0449\ RN)} \tag{3}$$

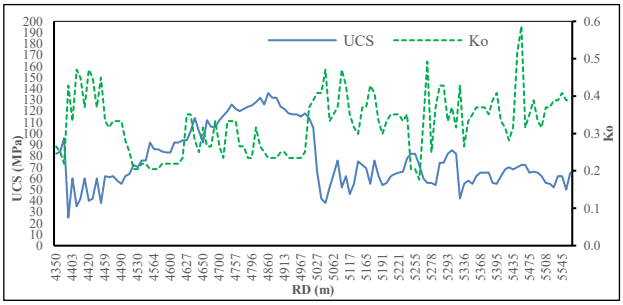

Fig. 4. RD-wise plot of compressive strength (σ_c) and stress ratio (Ko).

The vertical stress (σ_v) is calculated in MPa from the relation given by Hoek and Brown (1980)

$$\sigma v = 0.027 * z \tag{4}$$

Where z is the depth of the overburden. The horizontal-to-vertical stress ratio (K0) is considered as a function of the Poisson's ratio (μ) estimated from the tunnel seismic prediction using primary and shear wave velocities Vp and Vs using the expression Vp2-2Vs2/2(Vp2-Vs2). An RD-wise plot of K0for

Face 03 is shown in Fig. 4. The maximum and minimum horizontal field stresses (σ1 and σ3) are estimated using relations proposed by Stephansson (1993) for z<1000m.

$$\sigma_1 = \sigma_H = 2.8 + 1.48 * \sigma_v \quad (5)$$

$$\sigma_3 = \sigma_h = 2.2 + 0.89 * \sigma_v \quad (6)$$

The tangential stresses around the tunnel opening are estimated using the relation (Hoek and Brown,1980):

For the tunnel roof: $\sigma_{\theta r} = (A \times Ko - 1) * \sigma_v$ (7)

For side walls: $\sigma_{\theta w} = (B - Ko) * \sigma_v$ (8)

Where A and B are excavation geometry factors whose values are 3.2 and 2.3, respectively, for horseshoe-shaped tunnels. Hoek and Brown (1980) based on the observations made in South African mines suggested that for a stress environment where the ratio of maximum to minimum far-field stress (Ko) is equal to 0.5, the stability of underground excavations could be determined from the ratio of far-field maximum stress (σ1) and uniaxial compressive strength of intact rock (σc). The stability classes are shown in Table 2.

Table 2. Hoek and Brown (1980) stability classification.

σ_1/σ_c	Stress Condition	Support required
< 0.2	Stable	Unsupported
0.2-0.3	Minor spalling	Light support
0.3-0.4	Severe spalling	Moderate support
0.4-0.5	Rock bursting	Heavy support
> 0.5	Heavy/violent rock bursting	Difficult to support

Tunnel stability prediction (Hoek and Brown, 1980), as shown in Fig. 5, indicates that almost the entire tunnel reach beyond RD 4975m is prone to rock bursting.

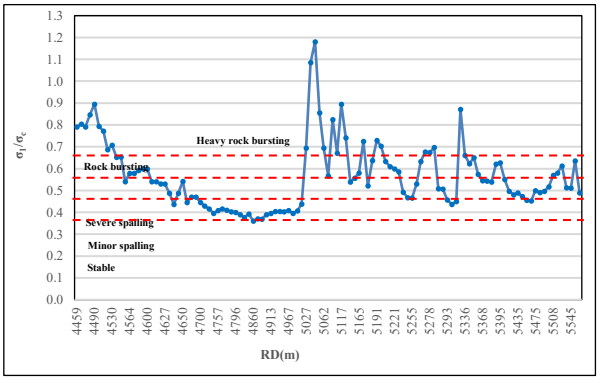

Fig. 5. RD-wise plot of (σ_1/σ_c) ratio along the tunnel.

3.3. Competency Factor (Cg)

RMi (Palmstrom, 1995) defines the "Competency Factor" (Cg) as the ratio of compressive strength and tangential stress to ascertain the rock-bursting potential:

$$Cg = RMi/\sigma_\theta = f_\theta \times \sigma_c/\sigma_\theta \approx 0.5 \times \sigma_c/\sigma_\theta \quad (9)$$

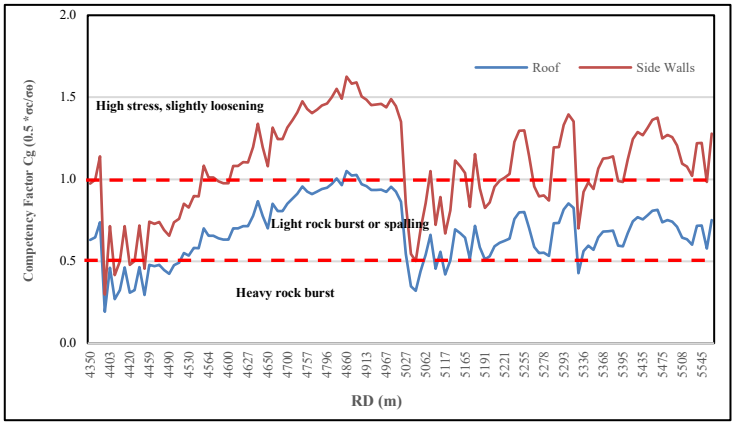

Fig. 6. The plot of the competency factor for tunnel roof and side walls.

For $C_g > 2.5$: No rock stress-induced instability; $C_g = 2.5\text{-}1.0$: High stress, slightly loosening; $C_g = 1.0\text{-}0.5$: Light rock burst or spalling, and $Cg < 0.5$: Heavy rock burst. The Competency factor (Cg) for the tunnel roof and side walls separately has been plotted for the head race tunnel under study (Fig. 6). The plot indicates that most of the tunnel reach beyond RD ±4975m has been predicted as prone to light to heavy rock bursting or rock spalling. The above prediction for stress-induced stability performed through various empirical methods has been validated with the actual incidents of rock bursting witnessed in the 1.2 km reach of HRT face 03.

4. Incidents of Rock-bursting at Parbati Hydroelectric Power Project, Stage-2

In this study, a 1.2 km horseshoe-shaped reach of HRT from the Adit-1 side, excavated through complexly jointed, hard, and brittle quartzite with bands of quartzite schist/mica-schist, is examined. The superincumbent cover varied from 1182m to 724m. A few rock bursts are discussed below, where significant time was consumed for providing stabilization measures. Two violent rock bursts occurred around RD ±5072m, followed by the ingress of a large quantity of muck (~800 m³) and groundwater (~300 l/min), resulting in the formation of a cavity. Ingressed muck/slush spread into the tunnel up to ±60m behind the face, burying the drill-jumbo (Fig. 7). The cavity was negotiated by carrying out extensive cement grouting, channelizing seepage through drainage holes, and by providing two sets of pipe roofing umbrellas beside forepoling, etc.

(a) (b) (c)

Fig. 7. (a) Formation of cavity due to rock bursts; (b) The flow of muck, slush, and groundwater ingress from the cavity; (c) Filling of the tunnel by muck and slush and burial of the drill jumbo.

Incessant rock spalling occurred between RD 5090m to 5106m during the mechanical removal of undercut when the muck suddenly erupted from the left wall and invert, followed by violent rock bursting from the face. Episodes of violent rock bursting continued after the blast taken at face, causing a sudden eruption of rock fragments from the crown and exposing all fore poles (Fig. 8a). Multiple violent rock bursts took place from the face and left crown at RD ±5240m just after completion of face drilling. The incident started with minor popping sounds followed by sudden rock bursts, resulting in spalling of rock fragments up to 6-8m. Later on, intermittent rock bursting continued about 15 to 18m behind the face from the left wall and invert, resulting in the eruption of rock fragments and detachment of rock anchors and shotcrete already applied (Fig. 8b).

On several occasions, already installed support has been disrupted due to severe rock bursts. As the tunnel got further excavated, two more major incidents of violent rock bursts happened around RD ±5284m and RD ±5297m towards the right wall and crown just after the face blast in the supported area. The incidents started with minor popping, followed by a heavy blast-like sound and spalling of rock fragments all over the area. The rock anchors got exposed while SFRS was detached from the tunnel surface due to rockfall (Fig. 9a). Recurring rock bursts around RD ±5352m resulted in rockfall and detachment of shotcrete and rock anchors. The rock bursts were so severe that fragments around 0.5 to >1.0m in size were thrown away from the face up to the operator's chamber of the drill jumbo. The above incidents resulted in the enlargement of the tunnel section (Fig. 9b).

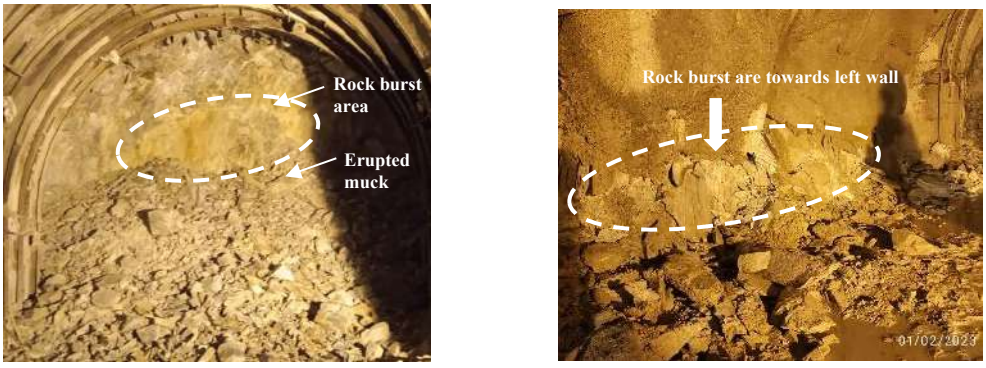

(**a**) (**b**)

Fig. 8. (a) Impact of intermittent and violent bursts at face around RD 5106m; (b) Multiple rock bursting from 18-15m behind the face around RD 5240m.

(**a**) (**b**)

Fig. 9. (a) Rock spalling resulted in detachment of shotcrete and rock anchors around RD ±5284m; (b) Fore poles detached and hanged after multiple episodes of rock bursts at the face and crown around RD ±5352m.

5. Stabilization and Support Measures

Normal rock support such as rock anchors, shotcrete with wire mesh, and steel rib sets with pre-cast concrete laggings, were provided depending on the rock class. In order to arrest the persistent rock bursting, support measures were required to be provided timely such that significant time is not lost. Therefore additional support measures were implemented for rock burst reaches. The layer-wise application of steel fiber reinforced shotcrete (SFRS) has been very useful. For stabilizing the face, SFRS, as well as normal shotcrete of thickness up to 100 mm, has been applied using a CIFA shotcrete spraying machine (Fig. 10a), besides keeping the face idle for redistribution of stresses.

Fig. 10. (a) Application of normal shotcrete and SFRS layer-wise on tunnel face, crown, and side walls; (b) Drilling of stress relief holes (SRH) at the face using a double boom drill jumbo.

When the rock fall has been arrested, rock anchors were installed. Stress relief holes (SRH) were drilled to destress the rock mass. Two to six SRH have been drilled, having 76 mm diameter and a length up to 6m on the face after every blast in the above tunnel reach (Fig. 10b). Cumulatively, about 4388m of drilling for SRH has been undertaken. To ensure the safety of men and machinery, it was felt prudent to provide steel ribs with steel lagging in rock-bursting reaches after spraying shotcrete. The drilling jumbo was retrofitted with a protective wire mesh screen to prevent the drilling crew from being hurt.

The influence of providing appropriate stabilization measures is evident through a comparative analysis of excavation cycle time (Fig. 11). The cycle time has significantly reduced from more than 72 hrs. to 15-20 hrs. in the tunnel reaches affected by incidents of violent rock bursting. Beyond RD 5250 m, the SRHs were provided on a progressive basis by making them part of the excavation cycle. The quantity of explosives during the face blasting was also controlled such that the pull is limited only up to 2-2.5m. These efforts have affected the intensity and frequency of the rock bursting to a greater extent.

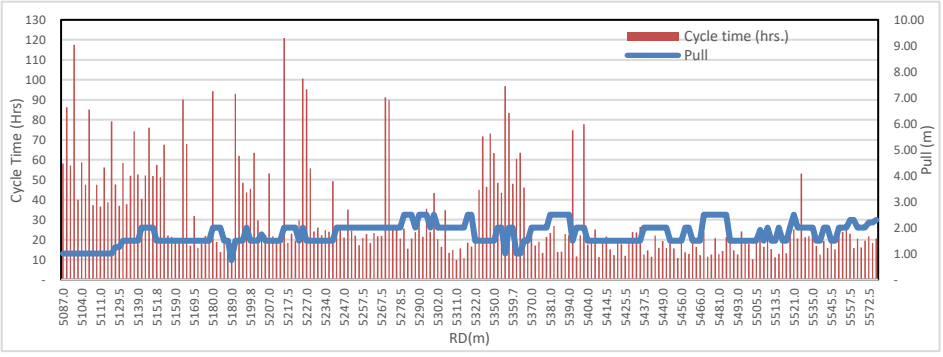

Fig. 11. RD-wise plot of cycle time and pull along head race tunnel face 03.

6. Validation and back analysis

Based on the Norwegian rule of thumb, a tunnel is likely to experience stress-induced rock bursts once the superincumbent cover exceeds 500m, and the severity of such incidents increases if the tunnel runs parallel to the valley side with a slope angle exceeding 25 degrees (Selmer-Olsen, 1965). Almost the entire head race tunnel reach considered in this study exceeds the above-mentioned threshold. Therefore, it is necessary to evaluate the stress-induced condition using more advanced empirical methods. For this purpose, the latest version of the rock mass rating system (RMR_{14}) developed by Celada et al. (2014) has been considered. It is an update of RMR_{89} (Bieniawski, 1989). An excellent correlation has been worked out between RMR_{89} and RMR_{14} for a 1226m stretch for the head race tunnel along the face 03, based on about 152 data points for $20 \leq RMR_{89} \leq 80$ (Fig. 12).

$$RMR_{14} = 1.22\ RMR_{89} + 2 \tag{10}$$

The above expression has a value of determination coefficient (R^2) as 0.97 and a correlation coefficient (R) equal to 0.985, thus indicating a strong correlation. The above relation shall be further implemented for the other portion of the head race tunnel as well in future studies.

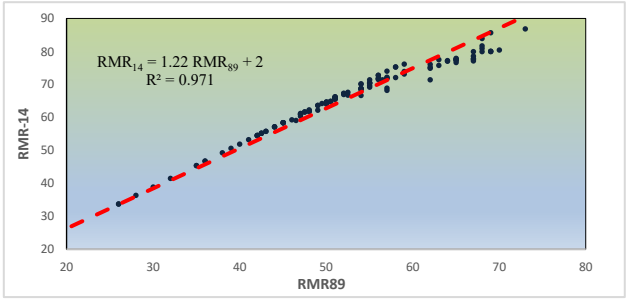

Fig. 12. The plot showing RMR_{89}-RMR_{14} correlation developed for the head race tunnel along face-03.

RMR 14 incorporates a stress factor (Fs) and Elastic Behavior Index (ICE) for the assessment of the stress-deformation behavior of rock mass. For ICE<70, substantial deformation in the rock mass is expected. For ICE< 15, the excavated rock mass is prone to brittle failures (Bieniawski and Celada, 2011). For the entire 1.2 km tunnel reach, RMR-14, Fs, and ICE values are estimated. The RD-wise plot of ICE along with rock cover (Fig. 13) shows that most of the rock bursting incidents fall in the intensive to mostly yielding zones with a higher possibility of rock bursting. From RD ±5025m onwards in the detoured part of HRT, the ICE value drops invariably below 15, thus indicating an increased possibility of stress-induced incidents.

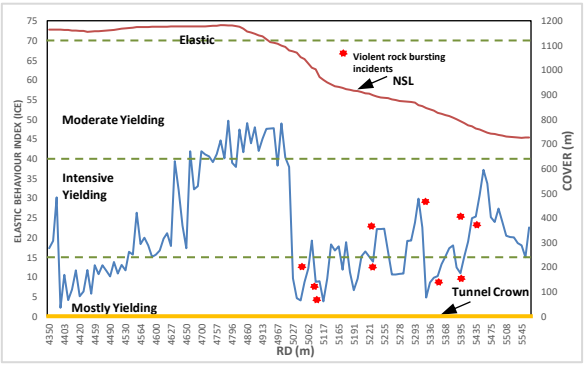

Fig. 13. The RD-wise plot of ICE and rock cover(h).

Further, all the major rock-bursting incidents discussed above are plotted (SC-4 to SC-5 category as per observational stress conditions) in the ICE curve coincides with lower ICE values (ICE<15), indicating high rock-bursting potential (Table 3).

Table 3. Assessment of rock-bursting potential (Celada et al., 2014).

RD (m)	Ko	ICE	RMR-14	Deformation Behavior	SC_{ob}
5069-5074	0.35	12.12	53.30	Mostly yielding	SC-4
5090-5106	0.43	08.92	41.60	Mostly yielding	SC-4
5225-5240	0.33	13.83	61.25	Mostly yielding	SC-5
5280-5284	0.37	10.85	58.50	Mostly yielding	SC-5
5297-5310	0.37	29.88	72.19	Intensely yielding	SC-4
5349-5352	0.33	09.76	52.00	Mostly yielding	SC-5
5394-5396	0.41	10.90	54.60	Mostly yielding	SC-5

Further, the conventional methodology proposed by Hoek and Brown (1980) for determining the stability of underground excavations using the ratio of far-field maximum stress (σ_1) and uniaxial compressive strength of intact rock (σ_c) is also applied for validating the tunnel reaches that witnessed heavy to violent rock burst tunnel (Fig. 14). It is evident that for all the major incidents of rock bursting, the σ_1/σ_c ratio is higher than 0.5 thus indicating severe to very severe rock bursting potential (Table 4).

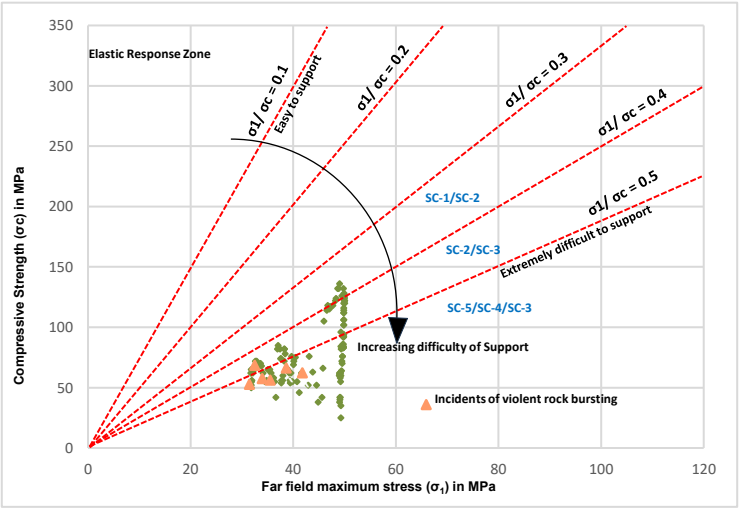

Fig. 14. The σ_1-σ_c plot shows the stability classes of Hoek and Brown (1980). The values for HRT are plotted. The triangles shown are violent rock-bursting reaches.

Table 4. Assessment of rock-bursting potential (Hoek and Brown, 1980).

RD (m)	σ_c	σ_1	σ_2	σ_3	σ_1/σ_c	Risk of violent rapture
5069-5074	63	43.7	27.6	26.8	0.69	Very severe
5090-5106	62	41.6	26.2	25.5	0.67	Very severe
5225-5240	66	38.4	24.2	23.7	0.59	Very severe
5280-5284	54	37.6	23.5	23.1	0.70	Very severe
5297-5310	85	37.0	23.1	22.8	0.44	Severe
5349-5352	55	34.4	21.2	21.2	0.63	Very severe
5394-5396	70	33.6	20.8	20.7	0.48	Severe

7. Observation-based recording of rock bursts

In tunneling projects, stress-induced deformations are monitored using geotechnical instrumentation. Besides, systematic recording of stress-induced incidents in deep tunnels that happen abruptly is also very useful. This information not only helps during back analysis and validation of the prediction but also assists in timely decision-making for undertaking appropriate stabilizing measures for safe excavation. With the above intent, an innovative chart-based technique is developed in this study for field recording, where the stress-induced conditions are categorized into five types: SC-1, SC-2, SC-3, SC-4, and SC-5. This categorization is based on the observed intensity, duration of occurrence, periodicity, sounds produced, and instability caused by the failure of the rock mass and its location (Table 1). Based on the above five stress-induced conditions, an assessment of their impact on the tunnel profile is also documented from the observational experience in tunnels (Table 5).

Table 5. Description of observation-based stress conditions in the head race tunnel.

Type	Intensity	Duration (Periodicity)	Sounds	Rock spalling/ Rockfall
SC-1	Very Mild	A few seconds (once or twice)	Popping	Nil
SC-2	Mild	From a few seconds up to one minute (continuous)	Popping /rapture	Nil
SC-3	Moderate	From a few seconds up to more than one minute (once, twice, intermittent)	Popping/ rapture/ mild blast	One, two or more incidents of minor rock spalling.
SC-4	Moderate to Violent	More than one minute (intermittent)	Rapture/ heavy blast	Multiple incidents of rock spalling/rockfall from several locations.
SC-5	Violent to intensely Violent	One minute to more than five minutes (continuous)	Rapture/ violent blast	Incessant rock burst/ rock fall/ shooting rock fragments from several locations.

Based on the above five stress-induced conditions, an assessment of their impact on the tunnel profile is also documented from the observational experience in tunnels (Table 6). SC-1 type incidents are very mild and have no impact on the tunnel profile. In contrast, SC-5 type incidents are characterized by heavy and violent rock bursting, resulting in rockfalls and enlargement of tunnel sections. The above technique has been extensively applied during the construction of the 1.2km stretch of the head race tunnel of the Parbati hydroelectric project, stage II excavated by the drilling-blasting method (DBM). Progressive recording of all stress-induced incidents, activity-wise, daily during each shift, has been made. More than 250 stress-induced incidents, ranging from mild popping to violent rock bursting, have been recorded during the excavation. An observation chart is prepared wherein each incident defined in Table 5 above has been recorded activity-wise (face drilling, loading, blasting, defuming, mucking, scaling, drilling of pressure relief holes, rock anchoring, shotcreting, and other support installation) throughout the cycle time in each shift. The rock mass rating (RMR) and location of the incident (left wall, crown, and right wall) are also indicated.

Table 6. Impact of stress condition on profile.

Type	Impact on the Tunnel profile
SC-1	None
SC-2	None to minor overbreak during scaling due to loosening/ opening of joints
SC-3	A few rock blocks may detach, causing a minor overbreak in the crown
SC-4	Detachment of blocks along joints, resulting in the enlargement of the tunnel section in the crown; minor to moderate overbreak towards the side walls
SC-5	Significant overbreak in crown and side walls. Rockfall/ spalling from the tunnel face may lead to face collapse.

Based on the above recording, all stress-induced incidents are plotted activity-wise (Fig. 15). The following inferences are drawn from the above plot:

1. Most incidents occurred when the face was disturbed, i.e., either during drilling of blast holes or pressure relief holes, or scaling and undercut removal.
2. Several mild to moderate incidents (SC-1 to SC-4) have occurred in Class-IV rock mass (RMR≤40). This is contrary to the belief that such failures occur only in good-quality rock.
3. The majority of stress-induced incidents have occurred towards the left wall and crown.
4. A significant number of incidents have occurred during the installation of rock supports. This has extended the cycle time of tunnel excavation.

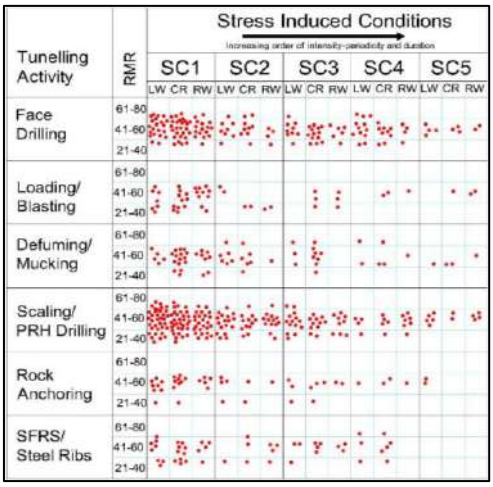

Fig. 15. Chart-based recording of stress-induced condition for a 1.25 km long stretch of HRT Face 03.

8. Conclusions

The prediction of stress-deformation behaviour for a selected portion of the HRT Face 03 from the Parbati 2 hydroelectric project suggests that a significant tunnel reach exhibits ICE≤40, indicating brittle failure. The back calculation of ICE for rock burst areas ranged between 9.76 to 13.83, indicating a very high potential. The (σ_1/σ_c) ratio ranges between 0.44 to 0.69, indicating severe to very severe risk of violent rock bursting and extremely difficult conditions for support installation. The competency factor (C_g) ranges between 0.49 to 0.85 for tunnel crown and 0.69 to 1.03 for side walls, predicting the possibility of moderate to heavy rock bursting. In deep tunnels, the scientific recording of rock bursts is significantly important. This study proposes an observation-based method that considers activity-wise recording of stress-induced conditions based on their intensity, duration, periodicity, sound, and nature of rockfall. Their impact on the tunnel profile is also discussed. The recorded data suggests that most rock-bursting incidents occurred when the face was disturbed during face drilling, scaling, undercut removal, etc. It is also inferred that some severe incidents occurred not only in hard and brittle quartzites but also in low-quality schistose quartzite/mica schist with RMR≤40. Keeping the face idle for some time, followed by drilling stress relief holes and the layer-wise application of SFRS, has helped control rock bursting. The application of the prediction and recording methodology suggested in this study shall help in keeping advanced provisions in contracts of future tunnelling projects for stabilization measures to arrest stress-induced spalling and rock bursts. Finite element and discrete numerical modelling techniques shall also be applied in future studies to validate the rock bursting potential of deep tunnels.

Acknowledgments

The authors thank NHPC management for granting permission to present and publish this work.

References

Amadei, B., Stephansson, O., 1997. Rock Stress and Its Measurement. Springer, Berlin.

Askaripour, M., Saeidi, A., Rouleau, A., Mercier-Langevin, P., 2022. Rock burst in underground excavations: A review of mechanism, classification, and prediction methods. *Underground Space*, 7 (4): 577-607.

Aydin, A., 2009. ISRM suggested Method for Determination of the Schmidt Hammer Rebound Hardness: Revised Version. *International Journal of Rock Mechanics and Mining Sciences*, 46: 627-634.

Barton, N.R., Lien, R., Lunde, J., 1974. Engineering Classification of Rock Masses for the Design of Tunnel Support. *Rock Mechanics*, 4:189-239.

Bieniawski, Z.T., 1973. Engineering Classification of Jointed Rock Masses. *Civil Engineering*, 12: 335-343.

Bieniawski, Z.T., 1989. Engineering Rock Mass Classification: A Complete Manual. New York, John Wiley and Sons: 251.

Bieniawski, Z.T., Celada, B., Aguado, D., Rodríguez, A., 2011. Forecasting tunnelling behaviour. *Tunnels & Tunnelling*. August 2011, 39-42.

Bolla, A., Paronuzzi, P., 2021. UCS field estimation of intact rock using the Schmidt hammer: A new empirical approach. IOP Conference Series: Earth and Environmental Science, 833(1): 012014

Cai, M., Kaiser, P. K., Morioka, H., Minami, M., Maejima, T., Tasaka, Y., Kurose, H., 2007. FLAC/PFC coupled numerical simulation of AE in large-scale underground excavations. *International Journal of Rock Mechanics and Mining Sciences*, 44(4): 550–564.

Cai, M., Kaiser, P.K., 2018. Rock burst phenomena and support characteristics. In: Rock burst Support Reference Book, I. Laurentian University, p. 191.

Celada, B., Tardaguila, I., Varona, P., Rodriguez, A., Bieniawski, Z.T., 2014. Innovating tunnel design by an improved experience-based RMR system. World Tunnel Congress, Iguassu Falls, Brazil.

Diederichs, M.S., 2007. The 2003 Canadian Geotechnical Colloquium: Mechanistic interpretation and practical application of damage and spalling prediction criteria for deep tunnelling. *Can. Geotech J.*, 44:1082–1116.

Farhadian, H., 2021. A new empirical chart for rock burst analysis in tunnelling: Tunnel rock burst classification (TRC), *International Journal of Mining Science and Technology*, 31 (4): 603-610.

Feng, X., Liu, J., Chen, B., Xiao, Y., Feng, G., Zhang, F., 2017. Monitoring, warning, and control of rock bursts in deep metal mines. *Engineering* 3:538-545.

Gao, F., 2019. Use of numerical modeling for analyzing rock mechanics problems in underground coal mine practices. *J. Min. Strata Contr. Eng.* 1 (1): 013004

Dev, H., 2019. Evaluation of in-situ stresses in Rock Mass: Challenges and Applications in Hydropower Development, *Journal of Rock Mechanics & Tunnelling Technology*, 25 (2): 103-112.

Hart, R.D., 1980. Geotechnical modelling of a cut and fill mining operation. In: Proceedings of the Conference on the Application of Rock Mechanics to Cut and Fill Mining. Lulea. Institute of Mining and Metallurgy, Sweden: 307-315.

Hoek, E., Brown, E. T., 1980. Underground Excavations in Rock. The Institution of Mining and Metallurgy, London.

Hoek, E., Kaiser, P. K., Bawden, W. F., 1995. Support of underground excavations in hard rock. Rotterdam, Netherlands: A. A. Balkema Publishers.

Hoek, E., 2004. Rock mass classification. Practical Rock Engineering, 2023 Ed., Rocscience.

Jenkins, F.M., Williams, T.J., Wideman, C.J., 1990. Rock burst mechanism studies at the Lucky Friday Mine. Proceedings of the 31st U.S. Symposium on Rock Mechanics. WV University, Rotterdam: Balkema: 955–962.

Jing, L., Hudson, J.A., 2002. Numerical methods in rock mechanics. *Int. J. Rock Mech. Min. Sci.* 39 (4): 409-427.

Kasier, P.K., Maloney, S.M., 1997. Ground motion parameters for design of support in burst-prone ground. In: Gibowicz and Lasocki, editors. Rock bursts and seismicity in mines. Rotterdam: Balkema. pp. 337–342.

Ma, T. H., Tang, C. A., Liu, F., Zhang, S. C., Feng, Z. Q., 2021. Micro seismic monitoring, analysis and early warning of rock burst. Geomatics. *Natural Hazards and Risk*, 12(1): 2956–2983.

Mateus, S., Afonso, M.J., Fernandes, I., Chaminé, H.I., 2023. RMR14 versus RMR89: A methodological approach for rock mass excavations (N Portugal). Advances in Geoengineering, Geotechnologies, and Geoenvironment for Earth Systems and Sustainable Georesources Management. Advances in Science, Technology & Innovation. Springer, Cham: 187–192.

Miranda, E.E., 1972. Deformation and Fracture of Concrete Under Uniaxial Impact Loading (Unpublished PhD Thesis). University of Missouri Rolla, Rolla, USA.

Ortlepp, W.D., Stacey, T.R., 1994. Rock burst Mechanisms in Tunnels and Shafts. *Tunnel and Underground Space Technology*, 91: 59–65.

Palmström, A., 1995. RMi-A Rock Mass Characterization System for Rock Engineering Purposes. PhD Thesis, The University of Oslo, Norway:400.

Russenes, B.F., 1974. Analysis of rock spalling for tunnels in steep valley sides [Unpublished Master's thesis]. Norwegian Institute of Technology.

Russo, G., 2014. An update of the "multiple graph" approach for the preliminary assessment of the excavation behaviour in rock tunnelling. *Tunnel and Underground Space Technology*, 41:74–81.

Selmer-Olsen, R., 1965. Stability of tunnels in valley sides. (In Norwegian), IVA-meddelande, Stockholm, 142: 77-83.

Shen, B., King, A., Guo, H., 2008. Displacement, stress, and seismicity in roadway roofs during mining-induced failure. *International Journal of Rock Mechanics and Mining Science*, 45(5):672–688.

Stephansson, O., 1993. Rock Stress in the Fennoscandian Shield. In Comprehensive Rock Engineering, Pergamon, 3 (17): 445-459.

Urbancic, T.I., Trifu, C.I., 2000. Recent advances in seismic monitoring technology at Canadian mines. *Journal of Applied Geophysics*, 45(4): 225–237.

Wang, X., Cai, M., 2017. Coupled numerical analysis of ground motion near excavation boundaries in underground mines. *Rock Soil Mech.* 38 (11):3347-3354.

Wickham, G.E., Tiedemann, H.R., and Skinner, E.H., 1972. Support determination based on geologic predictions. North American Rapid Excavation Tunnelling Conference, Chicago: 43-64.

Zhao, H., Chen, B., Zhu, C., 2021. Decision tree model for rock burst prediction based on micro seismic monitoring. *Advances in Civil Engineering*, 2021:1–14.

Zhang, L., Zhang, X., Wu, J., Zhao, D., Fu, H., 2020. Rock burst prediction model based on comprehensive weight and extension methods and its engineering application. *Bulletin of Engineering Geology and the Environment*, 79: 4891–4903.

Zubelewicz, A., Mroz, Z., 1983. Numerical simulation of rock burst processes treated as problems of dynamic instability. *Rock Mechanics and Rock Engineering*, 16(4):253–274.

Southeastern Europe Tunnelling Conference (SETC-2025)
1-3 October 2025, Belgrade, Serbia

DOI: 10.5937/SETC25016B

Experimental research of discontinuity parameters of soft rock mass

Miodrag Bujišić[a], Zvonko Tomanović[b]*

[a] University of Montenegro, Faculty of Civil Engineering, Podgorica, Montenegro; miodragb@ucg.ac.me
[b] GeoT doo Podgorica / University of Montenegro, Podgorica, Montenegro; zvonko@geot.me

Abstract: In everyday engineering practice, the ground surrounding tunnel structures consists of rock masses with discontinuitie. The falling and sliding of rock wedges during tunnel construction is common and mainly depends on the geometry and roughness of the discontinuities. Discontinuous surfaces with varying characteristics largely determine the quality of the rock mass, so knowledge of their behavior is extremely important. Due to various factors, local (and sometimes global) instabilities of rock blocks occur precisely on discontinuous surfaces. For this reason, analyzing and researching the strength parameters of discontinuities is crucial for developing rheological models of rock mass behavior. This paper presents research on discontinuity parameters in soft rock masses (marly limestone), conducted under laboratory conditions at the Faculty of Civil Engineering in Podgorica. The research was conducted as part of the authors' scientific work, with emphasis on time-dependent deformations of the rock mass. The uniqueness of the testing apparatus lies in the atypical dimensions of the samples used for this type of testing. Samples measuring 30 × 15 × 15 cm were cut from marly limestone taken from the coal mine basin in Pljevlja, Montenegro. A natural discontinuity was simulated by artificially creating one at half the height of each sample, after which the two halves were placed into a purpose-built steel apparatus. The samples were tested in the laboratory, using the existing equipment with necessary modifications and newly designed equipment to enable the proper execution of the experiment. The samples were placed in three frame constructions with three different constant values of normal loads. The horizontal load was applied using hydraulic cylinder simultaneously for all three frames, during which the increase in displacement and change in shear stresses were measured. Previously developed roughness models (in Agisoft software) serve as the basis for establishing the mathematical relationship between the roughness of discontinuous surfaces and their shear characteristics, used to generate roughness profiles for correlation analysis. Given the limited number of experimental studies on time-dependent deformations of soft rocks along discontinuities worldwide, this paper aims to contribute to the scientific literature by presenting initial results based on specific experimental data.

Keywords: soft rock; time-dependent deformations; experiment; discontinuity; roughness

1. Introduction

In engineering geology and geotechnics, rock mass fracturing is a key factor affecting the behaviour of rock material, especially in tunnel zones. Rock masses are rarely homogeneous and continuous; instead, they are typically intersected by discontinuities—joints, bedding planes, shear zones, and fractures—that determine their mechanical stability and deformation behavior.

Recent studies have increasingly emphasized the role of discontinuity roughness in determining the shear strength and overall stability of rock masses (e.g., Zhang et al., 2021; Wang et al., 2022; Dong et al., 2023). However, soft rocks—especially marly limestones—remain underrepresented in experimental datasets. While hard rock discontinuities have been extensively studied, the time-dependent deformation characteristics of soft rock discontinuities have received limited attention.

A significant research gap exists in understanding how discontinuity geometry, surface roughness, and time-dependent deformation interact in soft rocks under realistic loading conditions. This gap is particularly relevant in tunnelling projects, where insufficient experimental characterization of soft rock discontinuities has contributed to stability problems. For example, inadequate shear strength estimation

*Corresponding author: miodragb@ucg.ac.me (M. Bujišić).

in weak sedimentary formations has led to wedge failures during excavation and premature degradation of support systems in several case studies reported in Southeastern Europe and Asia.

The present study addresses this gap by experimentally quantifying the relationship between roughness profiles and shear strength parameters for soft rock discontinuities, with particular focus on time-dependent deformation.

Discontinuities, as natural planes of weakness, have a dominant effect on stress redistribution, load transfer, water flow, and deformation within the rock mass. Their properties—orientation, spacing, length, roughness, cohesion, friction, aperture, infill, and continuity—determine whether the rock mass behaves as a solid body or as a collection of interacting blocks.

In tunnel zones, the importance of discontinuities becomes pronounced due to stress redistribution from excavation, rock block instability potential (sliding, overturning, or falling), and increased water inflow along discontinuities.

Precise identification and characterization of discontinuities is essential for accurate geotechnical modelling and tunnel design. Without knowing their properties, any rock mass stability analysis remains unreliable. Without such analysis, rock mass models would be unrealistic and would not reflect actual resistance to destabilization caused by tunnel excavation.

The stability of rock blocks in tunnel zones largely depends on the mechanical properties of discontinuities, particularly their surface roughness and shear strength. Discontinuities are natural planes of weakness along which relative movement of rock blocks can occur, making their surface and mechanical characteristics crucial for stability analysis.

Discontinuity roughness determines the interlocking capacity of rock surfaces, while shear strength defines the resistance to sliding along these planes. The combination of these factors sets the limit of stability—if the driving forces acting on a block exceed the resistance provided by the contact surface, failure may occur in the form of sliding, toppling, or falling. Falling and sliding are most common in tunnels. Another important parameter is the time after excavation required for the rock block to fall out.

Accurate determination of roughness (e.g., via profilometry or 3D scanning) and shear strength (through laboratory and in-situ testing) enables realistic estimation of stability factors, selection of appropriate support systems, and prevention of instabilities during tunnel excavation and operation.

2. The necessity of experimental research

2.1. Importance of Experimental Investigation of Discontinuous Soft Rock Masses

Experimental investigation of discontinuous soft rock masses is crucial for developing reliable rheological models that accurately describe rock mass behavior under long-term loading. Due to the pronounced heterogeneity and complex behavior along discontinuities, theoretical models alone are often insufficient to capture all relevant mechanisms of deformation and shear. Through experimentation, it is possible to quantify time-dependent deformations, identify dominant displacement mechanisms, and determine the parameters required for mathematical modeling of rheological behaviour. Based on such results, realistic models of rock mass behavior can be formulated and applied in engineering practice, especially in the design of underground structures such as tunnels and shafts.

2.2. Complexity of Experimental Investigation of Soft Rock Masses and Its Importance

Experimental investigation of soft rock masses is challenging due to their sensitivity to changes in stress conditions, moisture, and time. Specific challenges arise in securing representative samples, preserving their structure and discontinuity geometry during preparation and testing. Furthermore, because of time-dependent deformations, experiments are often lengthy and require precise control of testing conditions.

Nevertheless, such investigations are of great importance as they enable a deeper understanding of rock mass behavior, particularly in zones dominated by plastic and viscous behavior. The results serve as a basis for developing numerical and analytical models, thereby improving the safety and efficiency of engineering solutions.

2.3. Validation and Comparison of Numerical and Experimental Results

The numerically estimated shear strengths derived from roughness profiles will be validated against direct shear test results for the same samples. The comparison allows assessment of the model's predictive capability while considering variations in surface roughness, humidity, and temperature. Differences are expected due to simplifications in the numerical model, but trends and relative variations among samples can be reliably captured. This approach provides a practical framework for integrating surface characterization with rheological modeling, ensuring that environmental factors such as moisture and temperature are incorporated into the analysis.

3. Experimental research on real samples

3.1. Sample's formating and equipment preparation

A block of approximately 3.5 tons was extracted from the open-pit mine at a depth of approximately 25 m, measured from the ground surface (Fig. 1). Immediately upon excavation, the material was loaded on transport equipment and transported from Pljevlja to Podgorica (approx. 180km). During unloading, precautions were taken to prevent any damage to the rock mass, ensuring that the block's natural orientation was maintained so that its geometry remained unchanged for processing.

Material used for testing has been sampled from the open pit "Potrlica" of the coal mine Pljevlja.

(**a**) (**b**)

Fig. 1. (a) Position of a bench from which the rock mass block was extracted; (b) loading of the rock mass block.

(**a**) (**b**)

Fig. 2. (a, b) Samples processed to target dimensions 30x15x15 cm.

A specialised plant for processing of stone was used to process material and form cuboid (prism) shaped samples with dimensions 30x15x15 cm (Fig. 2). During sample preparation, due to the highly demanding processing (with samples often splitting during cutting) of the irregularly shaped natural soft rock mass into the desired sample dimensions, the processing success rate was approximately 50%.

Simultaneously, a semi-quantitative analysis of samples was conducted the results of which confirmed the samples are marly limestone, dominantly composed (93.0%) of calcium carbonate (CaCO3), while the remaining 7% includes the following components: quartz 4.80% (SiO2), siderite 1.10% (FeCO2), muscovite 1.10% (KAl3Si3O10OH2).

3.2. Crack's formation

An artificial crack (Fig. 3) was created in the laboratory by splitting specimens into two halves. In order for the planes of discontinuity to have a regular shape, linear groove (Fig. 3(b)) was cut along the sample, after which a splitting force was applied at half its height (approximately 7.5 cm). At the cut grooves (Fig. 3c), using a cylinder to apply loading at a controlled rate, the samples were divided into two, approximately equal halves, followed by forming of discontinuity planes of different roughness. Upon defining discontinuity planes, all samples were wrapped in foil. Previously, after the geometry had been formed, all the samples were paraffin-coated to preserve their natural moisture content.

(**a**) (**b**)

Fig. 3. (a) Cutting a groove at the sample center; (b) forming of discontinuity.

3.3. Defining research equipment

When the samples have been prepared, the next step was to design new and modify the existing equipment to be used for uniaxial and triaxial creep testing of the intact rock samples. The trial series included testing three samples with different roughness levels. For this purpose, existing frames were specifically prepared at the laboratory of the Faculty of Civil Engineering. The frame operates on the principle of lever arm and deadweight.

The new equipment elements were designed by the authors with the aim of conducting an experiment that replicates natural rock mass conditions as closely as possible.

First, steel molds were formed, which serve to position the formed halves of the samples. Considering that the height of the half-sample is approximately 7.5 cm, the internal height of the mold was set to 5 cm to allow for undisturbed shear behavior along the discontinuity planes. Thickness of walls and bottom of the steel mold is 1cm. The samples are fixed using a factory produced mortar for casting and grouting, which takes several hours to set after have been poured to fill the voids between the sample and the mold, making the sample immovable in the mold. When securing both halves, efforts were made to fit them tightly to better simulate naturally closely spaced cracks.

In order to overcome friction that occurs in the apparatus, the experiment provided for adjustment of movable parts to fit over the cylinder-shaped steel elements. In addition to the samples, frames, benches and rollers, key components of the equipment are elements for measurement of change in stress and strain. For this purpose, steel rings (dynamometers) were developed with a base plate on which gauges for measurement of normal and shear displacements were mounted. The steel rings are of the same diameter but different thickness due to a different order of magnitude (forces) occurring in the normal and shear direction respectively, which are the subject of measurement by dynamometers (Fig. 4).

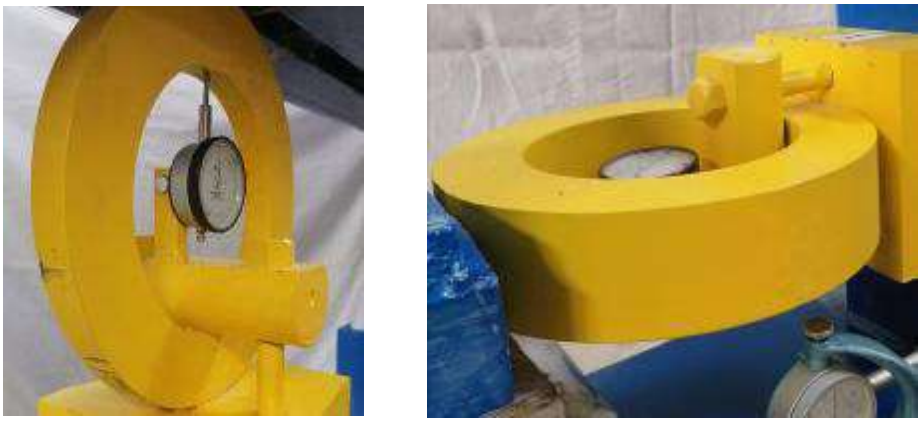

(**a**) (**b**)

Fig. 4. Rings with gauges for normal stress: (a) Rings no: 1, 2, 3, d = 2 cm; (b) Rings no: I, II, III, d = 6 cm.

3.4. Sample testing

After equipment was finalized, samples were ready for testing. During testing, numerical analysis of defining roughness model has been performed (detailed in part 3.5).

Experimental test was performed using frames such as shown in Fig. 5. First, trial test with 3 samples was performed. After that, in five series with three samples in each one was performed as a part of main experiment. The experiment included testing of samples of different roughness.

For all three foregoing discontinuity planes, the testing was performed under three different constant levels of normal stress. Normal stresses of 0.1 MPa, 0.2 MPa and 0.4 MPa were applied.

The horizontal load was applied to the sample via a hydraulic press horizontally positioned and connected to a large hydraulic cylinder positioned vertically in an additional frame with deadweight. The preferred hydraulic oil pressure was controlled by the weight of the deadweight on the frame's lever arm, which transferred a multiplied load onto the cylinder pivot. By means of the oil supply system from the large cylinder (principle of communicating vessels) and all smaller vessels on the shear apparatus (positioned horizontally), the shear force was applied to the lower half of the sample (lower fixed mould), as illustrated in Fig. 5.

Value of displacement of the lower mold, meaning differential displacement of the lower and upper half of the sample along discontinuity was recorded by the mechanical device for displacement measurement (Fig. 5).

As previously mentioned, the lower mold and the ring to which vertical loading is applied are placed on rollers to eliminate friction during the experiment duration. During the testing, it is required to maintain vertical loading constant, as it tends to change as the result of the vertical movement over the rough surfaces and changes in shear stress and strain.

(**a**) (**b**)

Fig. 5. (a) Equipment's elements for testing; (b) frame for testing with equipment.

The main characteristic of such an experiment is the creep phenomenon during discontinuity shearing. Time-dependent deformations were obtained under constant stress. The creep period of the samples varied from several days to several months, depending on the level of normal stress, sample roughness, temperature, and other factors. Bearing this in mind, we worked on numerical modeling and analysis of sample roughness while the laboratory tests were in progress.

4. Determination of sample's roughness by numerical methods

4.1. Creating of roughness model

For a long time, the very simple use of traditional methods with satisfactory accuracy had a justified primacy in relation to demanding and time-consuming mathematical calculations. Nowadays, with the development of modern computer aids, it is possible to develop models that are based on the mentioned mathematical formulations, but which solve the problem of the roughness of discontinuities in a much shorter time. In order to numerically describe the roughness of discontinuous surfaces, it is necessary to obtain a roughness model. Agisoft software was used for these purposes. The model creation process is based on importing photographs that capture the actual surface condition of the samples from multiple angles. The number of photographs depends on the need to capture the entire surface from several angles, based on which the software generates the model. The quality of the model depends on the quality of the photos. After creating the model, it is possible to export the non-continuous surface into a dwg file. This approach allows for deriving a mathematical formulation of the curvature for each generated profile, and, based on established theories of discontinuity roughness, determining the mathematical relationship between roughness and shear strength.

4.2. Production of photos for model

To create a quality model of the discontinuity plane with roughness, it is necessary to prepare high-quality photographs. For all 20 specimens analyzed in the experimental research, several photographs of each roughness plane were taken. A professional photographer took photos from different positions (Fig. 6), ensuring that the photographed surfaces overlapped.

(**a**) (**b**)

Fig. 6. (a) Making photos of discontinuity plane; (b) photo of sample plane.

4.3. Making roughness model

Photos of discontinuity surface for all samples were made in high quality resolution (300 dpi). This is a primary requirement for creating a high-quality model of the discontinuity plane with roughness. All photos have been used for importing in software and making sample's model.

Agisoft software package is used to create roughness models of the samples. The program works on the principle of importing photos on the basis of which the model is created. In order for the model to be used as an output data, it is necessary to ensure the matching of the size of the samples in the model and in the export file (cad file). In this regard, each sample was marked with red points along half its length and width before photography; these were later used in the model as reference points for adjusting the scale in the CAD file. The quality of the model also depends on the density of the points that form it. Through an iterative process, the number of points that produced a high-quality model without requiring excessive processing time was determined. The model shown in Fig. 7 is ready to be exported to a CAD file. After scaling to real dimensions, it could be analyzed in the next stage. In cad file, we could see surface with lines that define roughness surface (Fig. 8).

As mentioned above, the plan is to use five 2D profiles obtained from the 3D surface to develop numerical equations based on the shear strength of each small triangular segment along each line of discontinuity. Following mentioned, it's planning to use five 2D profiles obtained by 3D surface, that could be used for develop numerical equations based on shear strength of each small triangle entire each line of discontinuity.

After that, correlating the roughness and shear strength of each of the five profiles could provide insight into the surface behavior.

Fig. 7. Roughnes model made by photos.

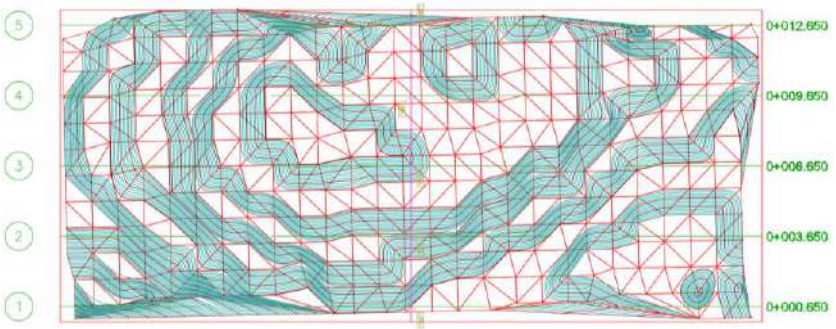

Fig. 8. Roughness surface of sample export from Agisoft.

5. Numerical Relationship Between Roughness and Shear Strength

The discontinuity surface profile is typically obtained as a series of X–Z coordinates exported from AutoCAD or similar software tools. These coordinates represent the actual uneven surface of the joint.

To quantify the roughness, several numerical descriptors are used. A common one is the root mean square (RMS) slope, Z_2:

$$Z_2 = \sqrt{(1/L \int_0^L (dz/dx)^2 \, dx)} \approx \sqrt{(1/n \sum (\Delta z_i/\Delta x_i)^2)} \quad (1)$$

Where:

- Δz_i = vertical difference between consecutive points,
- Δx_i = horizontal difference,
- L = total profile length,
- n = number of segments.

The Joint Roughness Coefficient (JRC) can be estimated empirically based on Z_2. One commonly cited relation is:

$$JRC = a \times (Z_2)^{\wedge} b \tag{2}$$

Barton and Choubey (1977) proposed an empirical model to estimate shear strength along rough joints:

$$\tau = \sigma_n \times \tan[JRC \times \log_{10}(JCS / \sigma_n) + \varphi_b] \tag{3}$$

Where:

- τ = shear strength,
- σ_n = normal stress,
- JCS = joint compressive strength,
- φb = basic friction angle.

Combining all the above steps, the final functional relationship is:

$$\tau = \sigma_n \times \tan[(a \times Z_2^{\wedge} b) \times \log_{10}(JCS / \sigma_n) + \varphi_b] \tag{4}$$

This allows the estimation of shear strength directly from surface geometry (Z_2), which is crucial for rock block stability analysis and classification of rock masses.

The application of Barton's empirical shear strength equation to numerically derived roughness profiles assumes that surface geometry fully captures the mechanical interlocking effects. However, scale effects, progressive surface degradation, and lithological variability may influence results, and laboratory-prepared discontinuities might not fully reproduce the complexity of natural joints.

Experimental constraints prevented repeated tests at multiple normal stress levels on the same sample, leading to separate specimens for each stress level. Sample moisture, varying from completely dry to fully saturated, significantly affects shear strength, and fluctuating laboratory temperature (14–35 °C) and relative humidity (40–100 %) during the long testing period may have influenced creep measurements. Variations in surface roughness further contribute to data variability.

Despite these limitations, the derived JRC values provide a useful quantitative measure of surface roughness for each specimen. These values can be applied to evaluate shear strength trends, compare samples, and support further modeling, while acknowledging the influence of moisture content, surface degradation, and environmental variability on the results

6. Conclusions

This paper presented the research of discontinuity parameters on examples of soft rock mass (marly limestone) carried out in experimental laboratory conditions at the Faculty of Civil Engineering in Podgorica.

The samples were tested in the laboratory, using the existing equipment with necessary modifications and newly designed equipment to provide for proper conducting of the experiment.

Previously developed roughness models (in Agisoft software) form the basis for establishing the mathematical relationship between the roughness of discontinuous surfaces and their shear characteristics, enabling the creation of roughness profiles for correlation analysis.

Finally, a closer determination of the discontinuity characteristics will enable a better understanding of the entire rock mass. Therefore, experimental research is invaluable for obtaining concrete, applicable data on which models of rock mass behavior can be based.

The formation of rheological models along discontinuities involves the assessment of time-dependent deformations (e.g., creep) under constant normal and shear stresses. These models are usually based on combinations of idealized rheological elements such as Hookean (elastic), Newtonian (viscous), and composite systems like Kelvin–Voigt or Burgers models.

In engineering practice, rheological models enable prediction of displacement along weak planes over time, which is essential for the design of tunnel structures, underground structures, slope stability assessment, and barrier performance in mining or hydropower systems.

Experimentally, long-duration shear tests under constant normal stress provide data for calibrating rheological models and determining parameters such as viscosity coefficient, relaxation time, and limiting strain. Also, data processing follows, which should introduce a time component into the rheological model of discontinuity sliding.

Bearing the above in mind, future research will define a rheological model for specific experimental testing, using the obtained data to more precisely determine the behavior of discontinuous soft rocks in practical engineering applications, including tunnel construction.

The correlations established between roughness profiles and shear strength parameters provide a practical tool for preliminary stability assessment in tunnelling designs involving soft rock masses. By integrating these correlations into rheological models, engineers can better predict time-dependent displacement along discontinuities and design more effective long-term support systems.

For tunnel design, this means improved estimation of stability factors under both short-term excavation loads and long-term operational stresses. In stability assessment, the method offers a means to evaluate potential wedge or block failures in cases where direct shear testing is impractical. In long-term support strategies, the time-dependent component of the model can inform the scheduling of maintenance and reconstractions.

References

Bujišić, M., Tomanović Z., 2024. "Experimental research of time-dependent deformation of soft rock along discontinuities", Laboratory of Faculty of Civil Engineering, University of Montenegro

Dong, L., Wang, D., Sun, X., Jiang, Y., Luan, H., Zhang, G., Zhou, G., Liang, B., 2023,. Experimental Study on the Mechanical Properties and Acoustic Emission Characteristics of Deep Soft Rocks under Low-Frequency Dynamic Disturbance. *Applied Sciences*, *13*(11), 6399. https://doi.org/10.3390/app13116399

Kozubal, J., Tomanović, Z., Zivaljević, S., 2016. The soft rock socketed monopile with creep effects – a reliability approach based on wavelet neural networks, *Arch. Min. Sci*., Vol. 61 (2016), No 3, p. 571–585,

Loiotine, L., Wolff, C., Wyser, E., Andriani, G. F., Derron, M.-H., Jaboyedoff, M., Parise, M., 2021. QDC-2D: A Semi-Automatic Tool for 2D Analysis of Discontinuities for Rock Mass Characterization. *Remote Sensing*, *13*(24), 5086. https://doi.org/10.3390/rs13245086

Pells, K. S., Skretting, K., Dershowitz, T., Herda, H. H., 2024. Rock Mass Structure Characterization Considering Finite and Folded Discontinuities: A Parametric Study. *Rock Mechanics and Rock Engineering*, DOI: 10.1007/s00603-024-03787-9.

Palmström, A., 2001. Measurement and characterization of rock mass jointing, Chapter 2 of the book: *In-Situ Characterization of Rocks*

Tomanović, Z., 2012. The stress and time dependent behaviour of soft rocks. *GRAĐEVINAR*, 64 (12), pp. 993-1007. https://doi.org/10.14256/JCE.815.2012.

Tomanovic, Z., 2006. Rheological model of soft rock creep based on the tests on marl. *Mech Time-Depend Mater* 10, 135–154. https://doi.org/10.1007/s11043-006-9005-2.

Wang, F., Wu, B., Wang, S., Meng, F., Xiu, Z., Wang, C., 2022. Shear Response of Rough Rock Discontinuities Subjected to Impact Loading: Experimental Study and Theoretical Modelling. *Lithosphere*, *GeoScienceWorld* Special Issue 11: Article 1192067. DOI: 10.2113/2022/1192067.

Zhang, Q., Luo, Z., Jang, B. A., Wang, Q., Zhong, Z., 2021. A Study of Instantaneous Shear Mechanical Properties on the Discontinuity of Rock Mass Based on 3D Morphological Properties. *Geofluids*, Volume 2021, Article 5549223. DOI: 10.1155/2021/5549223.

Zhang, G., Wu, S., Guo, P. et al., 2023. Mechanical Deformation, Acoustic Emission Characteristics, and Microcrack Development in Porous Sandstone During the Brittle–Ductile Transition. *Rock Mechanics and Rock Engineering*, 56: 9099–9120 (December 2023). https://doi.org/10.1007/s00603-023-03533-7.

Agisoft Metashape User Manual Professional Edition, Version 1.8: chrome-extension://efaidnbmnnnibpcajpcglclefindmkaj/https://www.agisoft.com/pdf/metashape-pro_1_8_en.pdf.

Southeastern Europe Tunnelling Conference (SETC-2025)
1-3 October 2025, Belgrade, Serbia

DOI: 10.5937/SETC25017D

Determination of ground deconfinement for Motorway A8 Targu Neamt-Iasi-Ungheni tunnels in soft ground conditions in Romania

Dragoș Dumitrăşcuță[a], Anton Ioanidi[a] and Silviu Dărăban[a]*

[a] Consitrans, Tunnelling Department, Bucharest, Romania; dragos.dumitrascuta@consitrans.ro, anton.ioanidi@consitrans.ro, silviu.daraban@consitrans.ro

Abstract: After decades of tunnelling scarcity, Romania has restarted its major infrastructure projects, resulting in a significant increase in tunnel design and construction. One of the challenges in designing the conventional tunnels for Motorway A8 Targu Neamt-Iasi-Ungheni is the determination of the deconfinement effect of in-situ stresses due to tunnel excavation and support sequencing. A 3-step approach is analysed, using the analytical Convergence-Confinement Method (Marc Panet), a 2D Axisymmetrical Finite Element Model, and a 3D Finite Element Model. The first two methods simulate the 3D effects generated by the construction sequence in a 2D model, whilst the third method models the tunnelling steps in 3D. This paper aims to compare the three methods, outline the difference in results, and calibrate the 3D effects in the 2D model, thus adding more clarity to the ground deconfinement determination process for conventional tunnels in soft ground conditions.

Keywords: Conventional Tunnelling; Finite Element Modelling; Ground Deconfinement; Romania

1. Project Background

1.1. Location

The proposed A8 Motorway Targu Neamț-Iasi-Ungheni crosses the Moldavian Hills per-pendicularly, in the East of Romania (see Fig. 1), generating a series of small to medium cover motorway tunnels. Based on a preliminary geotechnical study, the geology of the Moldavian Hills generally comprises of a combination of granular and cohesive deposits, predominantly with weak clays and thin sand layers. The groundwater table typically re-sides in the sand layers, varying in depth, and is recorded to be absent at locations where boreholes indicate the existance of clay only.

Fig. 1. Map of Romania illustrating the motorway system, including the A8 Motorway project.

*Corresponding author: dragos.dumitrascuta@consitrans.ro (D. Dumitrăşcuță).

1.2. Moimesti Tunnel overview

The Moimesti Tunnel is a proposed twin-tunnel located on Section 3 of the A8 Motorway, between km 72+960 – 73+480, and accommodating 2 lanes of traffic (see Fig. 2). The tunnel underpasses agricultural lands and has a total underground length of 470 m, a maximum cover of 36 m and an approximate 140 m^2 excavated tunnel cross-sectional area. The cross-section of the Moimesti Tunnel is presented in the figure below, illustrating one of the two tunnel tubes and the internal dimensions of the tunnel. The Moimesti Tunnel is currently in tender for construction.

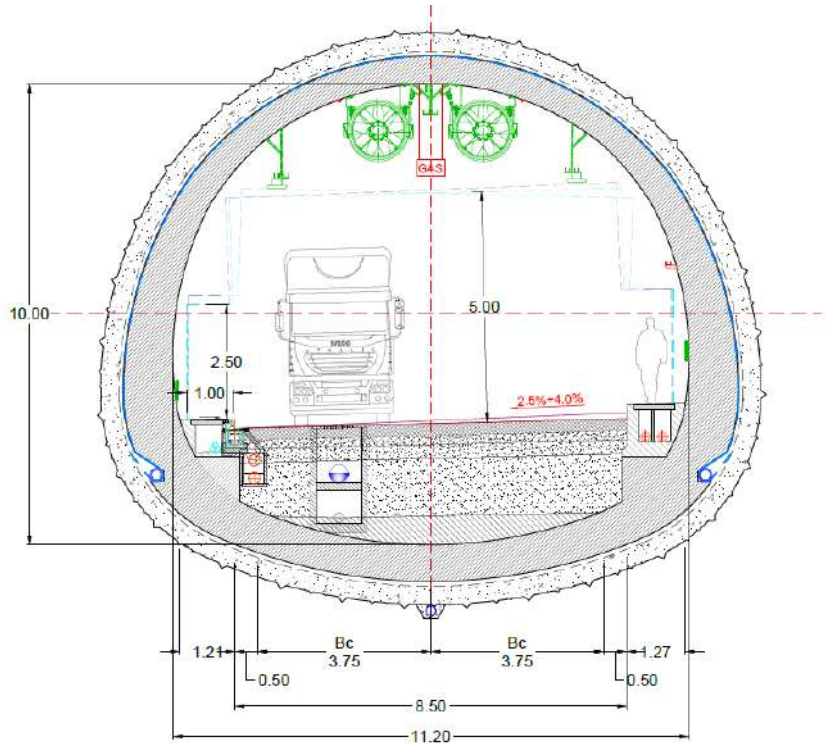

Fig. 2. Cross-section of the Moimesti Tunnel Tube 1 with internal dimensions in meters.

Due to its relatively short length, the tunnel is proposed to be excavated conventionally, using the Sequential Excavation Method (SEM), in a series of excavation steps (top heading, bench, invert) and supported by a 350 mm thick primary sprayed concrete lining (SCL). Additional ground support measures such as pipe umbrella for the low cover, forepoling and radial bolts are included in the design. A waterproofing membrane is installed prior to the construction of a cast in situ secondary reinforced concrete lining.

The geotechnical investigation conducted for the Moimesti Tunnel included 5 boreholes reaching below the tunnel invert, geophysics, in-situ and lab testing. The results of the investigations showed that the geology is generally homogenous and tunnel passes predominantly through a thick layer of clay, characterised as firm or stiff, with a fairly low Modulus of Elasticity (12-15MPa) and the groundwater table is reported to be below the tunnel invert. The geotechnical parameters are presented in Figure 3 of the following chapters. Unexpected, local variability of the geology (i.e. the presence of sand lenses) could result in local face instability, producing higher deformations and therefore increasing the ground relaxation; this paper however, focuses on the determination of the ground relaxation parameter for the predominant clay layer, following the results of the geotechnical study.

2. The ground relaxation parameter

One of the governing factors in the design of tunnel primary linings is the deconfinement of the ground, also known as the ground relaxation, which accounts for the stress redistribution in the ground after the excavation and before the installation of the tunnel support system. The deconfinement factor therefore plays a crucial role in the two-dimensional simulation of the three-dimensional effects generated by the excavation of the tunnel.

In order to determine the deconfinement factor for the Moimesti Tunnel, a number of analyses were undertaken, considering the 350 mm thick SCL primary lining, without taking into account the effects of any additional ground support measures. This methodology was chosen to ease the comparison between the different ground relaxation analysis methods.

The deconfinement factor obtained is introduced in finite element models using Plaxis 2D and the results are compared at the end of the paper.

3. Method 1: the convergence-confinement method (Marc Panet)

3.1. Methodology

The first method used to determine the deconfinement factor is the well-known Convergence-Confinement Method (CCM) developed by Marc Panet. The CCM is based on the analysis of a circular tunnel in homogeneous ground and on the assumptions that the tunnel is deep and the stresses in the ground are isotropic. A deconfinement factor (λ) be-tween 0 and 1 is determined using the unsupported advance length and the tunnel radius as presented in the empirical equation provided below (Panet, 2001):

$$\lambda_d = 1 - 0.75 \left[\frac{0.75R}{0.75R+d}\right]^2 \quad (1)$$

where d = Unsupported tunnel length from working face; R = Radius of circular tunnel;
λ_d = Deconfinement at distance d from working face.

Once the deconfinement of the ground is calculated, the stresses in the lining can be obtained by multiplying the deconfinement factor with the initial stresses in the ground, as shown in the equation below (Jones, 2022):

$$\sigma = (1-\lambda)\sigma_0 \quad (2)$$

σ = lining stress; λ = Ground deconfinement; σ_0 = initial ground stress.

3.2. Application to Moimesti Tunnel

The application of the CCM to the Moimesti Tunnel is considered to be partial, as the 3-diameter tunnel cover is not considered deep enough and the SEM tunnel shape isn't circular. However, the calculations can be performed using an equivalent tunnel radius to determine the ground deconfinement and then compare it against the other results to assess the suitability of the CCM for medium cover SEM tunnels. As the shape of the Top Heading-Bench-Invert is too different from a circular shape, the full face deconfinement factor will be used throughout the calculation.

A deconfinement factor of λ=0.48 is obtained using the CCM for a 1m advance and a 6.7 m equivalent tunnel radius for the 140 m2 excavated tunnel area. The deconfinement factor is introduced in the numerical analysis using Plaxis 2D as (1- λ) for the top heading, bench, and invert sequences. Because of the early ring closure, the deconfinement factor remains unchanged while progressing through the excavation phases.

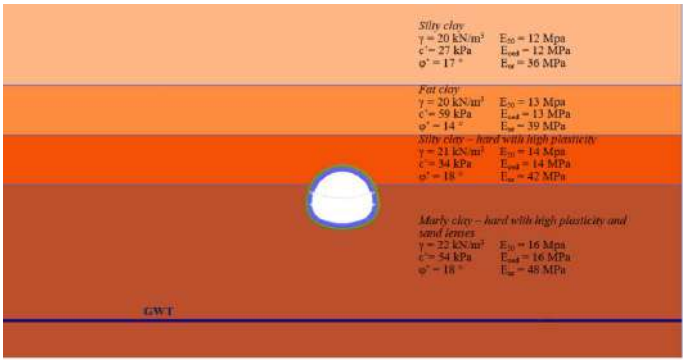

Fig. 3. Extract of Moimesti Tunnel in Plaxis 2D showing the geotechnical parameters.

3.3. Method 1 Results

The results of the numerical analysis using the deconfinement factor obtained through the CCM for the Moimesti Tunnel are listed in Table 1 below. The calculation results indicate high bending moments and deformations, which are primarily associated with the low stiffness of the ground.

Table 1. Method 1 CCM 2D Finite Element results for Moimesti Tunnel for 1m advance.

Method	Deconfinement factor (λ)	Horizontal Deformation u_x (cm)	Vertical Deformation u_y (cm)	Max. Axial Force (kN)	Max. Bending Moment (kNm)
2D SEM Tunnel Tunnel with deconfinment from CCM (panet-full face)	0.48	7.88	25.75	2236.00	313.70

4. Method 2: the axisymmetric finite element model method

4.1. Methodology

A second analysis is carried out using the method of axisymmetry with fixed field stress conditions. Two Plaxis models are created in 2D to calibrate the deconfinement factor. The first model is created using a circular tunnel, similarly to the CCM conditions, while the second model is created with axisymmetric conditions, vertical, similarly to a shaft, thus the model conditions, including the field stress, are effectively rotated, in order to allow for the simulation of the tunnel advance effects in 2D. The deconfinement is determined once the two models are calibrated, when the hoop force and the deformation is similar in both models. Finally, a third 2D model is created using the SEM tunnel shape and the excavation steps, using the deconfinement factor determined previously. Similarly to the CCM, the deconfinement factor is calculated only for the full cross-section of the tunnel.

4.2. Application to Moimesti Tunnel

The first Plaxis 2D model is created, assuming a circular tunnel with 6.7 m radius, homogenuous ground conditions and fully fixed boundaries in all directions. Then, a field stress is assigned to the ground, with a vertical stress $\sigma_{1(v)}=\gamma h=760$ kPa, and a $\sigma_{2(h)}=523$ kPa, corresponding to $k_0=0.7$.

A second, axisymmetric model is created in Plaxis 2D, with the same tunnel radius, the tunnel is modelled vertically, with 1m advances and simulating the strength gaining of the shotcrete at 1 days, 3

days, and 7 days (see Figure 4). The ground is assigned a field stress, inverse to the first 2D model, with σ_1=523 kPa and σ_2=760 kPa. Thus, the model conditions are effectively rotated in order to allow for the simulation of the tunnel advance effects in 2D. The sequential advances are modelled for the first 20 m, then a "wished-in-place" tunnel is created, independent of the sequential advances. This is done by creating a new Phase linked straight to the Initial Phase, where the primary lining is activated first, then a second Phase is created and the ground is deactivated, thus not allowing any confinement loss in the ground.

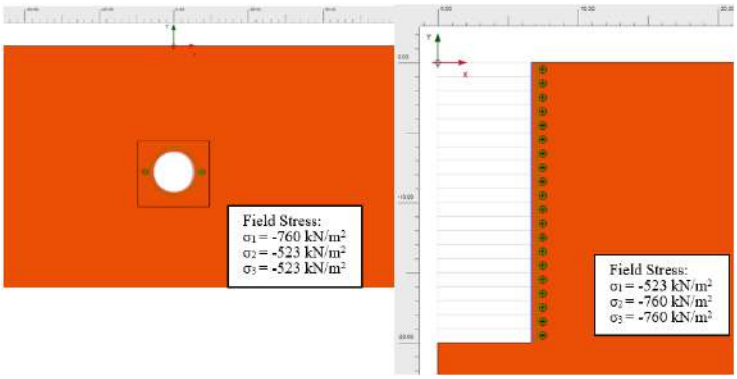

Fig. 4. Plaxis 2D FE of (a) circular and (b) axisymmetric models with field stress conditions.

Further on, the deconfinement factor is determined using two methods: A) the average hoop force of the 7 days strength SCL is divided by the hoop force of the "wished-in-place" SCL (also 7 days strength), then the deconfinement (λ) is equal to 1 minus the hoop force ratio (see Figures 5 and 6 below); B) the horizontal deformation in the axisymmetric model at the tunnel face is used as a reference for the 2D SEM model, then a deconfinement factor is determined in the 2D SEM model by trial and error, until the vertical crown deformation obtained in the 2D SEM model is similar to its correspondent in the axisymmetric model. The hoop force or deformation near the boundary are not considered.

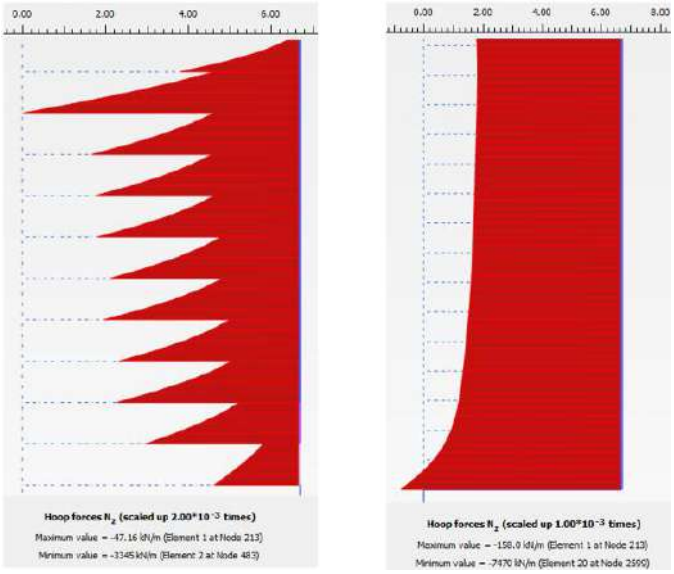

Fig 5. Method 2A showing the (a) sequential (left) and (b) "wished-in-place" (right) Hoop Force results.

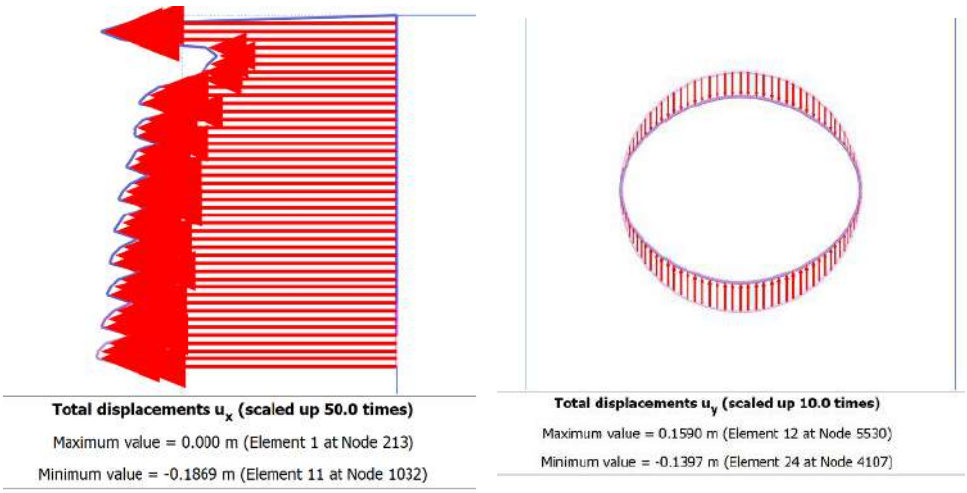

Fig 6. Vertical crown displacement at the front in the (a) 2D Axisymmetric and (b) circular models after calibration with λ=0.64.

4.3. Method 2 Results

A deconfinement factor of λ=0.64 is obtained using the Hoop Force ratio (method A), and a deconfinement factor of λ=0.49 is obtained using the Tunnel Crown Deformation (method B). The results are presented in Tables 2 and 3 below.

Table 2. Determination of Deconfinement using the Hoop Force ratio and the Vertical Crown Deformation.

Determination of Deconfinement factor using the Hoop Force ratio (method A)							
Analysis Method	Tunnel cross-section	Advance Length (m)	Face area (m^2)	Equivalent Radius (m)	Sequential Excavation Hoop Force (kN) average	Wished- in-place Hoop Force (kN)	Deconfinement (%)
Axisymmetric model	Full face	1.00	139.93	6.67	1752.5	4890	64.16
Determination of Deconfinement factor using the Vertical Crown Deformation at tunnel face (Method B)							
Analysis Method	Tunnel cross-section	Advance Length (m)	Face area (m^2)	Equivalent Radius (m)	Axisymmetric model Crown deformation at the face - u_x (cm)	SEM Tunnel model Crown deformation at the face - u_y (cm)	Deconfinement (%)
Axisymmetric model	Full face	1.00	139.93	6.67	17.80	17.50	49.00

The two deconfinement factors are used in two different 2D models of the SEM tunnel, obtaining the results presented in Table 3 below. The Hoop Force ratio (method A) results in higher deformations and lower bending moments than the Tunnel Crown Deformation (method B), because of the higher deconfinement factor. The high bending moments and deformations are also due to the relatively low cover of the tunnel and the reported low ground stiffness.

Table 3. Method 2 FE results for Moimesti Tunnel using the Axisymmetric method with 1m advance.

Method	Deconfinement factor (λ)	Horizontal Deformation u_x (cm)	Vertical Deformation u_y (cm)	Max. Axial Force (kN)	Max. Bending Moment (kNm)
2D SEM Tunnel Tunnel with deconfinement from Axisymmetric Model (Axial force derivation-Method 2A)	0.64	22.74	55.14	2033	259.60
2D SEM Tunnel Tunnel with deconfinement from Axisymmetric Model (Axial force derivation-Method 2B)	0.49	8.40	26.79	2220	309.10

5. **Method 3: THE full 3d finite element model method**

5.1. Methodology and application to Moimesti Tunnel

A full-scale 3D model is created in Plaxis 3D, modelling a 50 m long stretch of the SEM tunnel, with 1m sequential advances of top heading, bench, and invert, using the progressive 1 day, 3 days, and 7 days SCL strength gain (see Figure 7). The ground conditions are the same as for the 2D SEM models and the groundwater table is below the tunnel. After the sequential stages are modelled, an independent stage is created, modelling the "wished-in-place" tunnel conditions, as described previously.

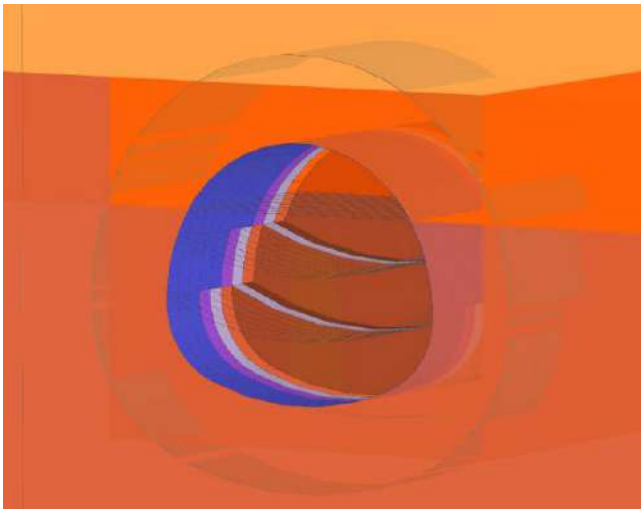

Fig 7. 3D model of Moimesti Tunnel showing the sequential excavation with top heading, bench, and invert.

The deconfinement factor is determined using the same methods as used in the axisymmetric analysis: A) the average axial force of the 7 days strength SCL is divided by the axial force of the "wished-in-place" lining (also 7 days strength), then the deconfinement (λ) is equal to 1 minus the axial force ratio. B) the vertical crown deformation at the front of the tunnel is used as a reference for the 2D SEM model, then a deconfinement factor is determined by trial and error, until the vertical crown deformation obtained in the 2D SEM model is similar to the one in the 3D model. The forces or deformations at the boundary are not considered.

5.2. Method 3 Results

The results of the 3D analysis are presented in the table and figures below. A deconfinement factor of λ=0.40 is obtained using the Axial Force ratio (method A), and a deconfinement factor of λ=0.50 is calculated using the Vertical Crown Deformation (method B) of the fresh (1day strength) SCL at the front of the tunnel. These two factors are used in two different 2D models of the SEM tunnel, and the results are included in the table below. The results are summarised in Table 4 and Figure 8 below.

Table 4. Finite Element results for the Moimesti Tunnel using the 3D model with 1m sequential advance.

Method	Deconfinement factor (λ)	Horizontal Deformation u_x (cm)	Vertical Deformation u_y (cm)	Max. Axial Force (kN)	Max. Bending Moment (kNm)
3D Model	N/A	7.60	23.30	2578	271.6
2D SEM Tunnel Tunnel with deconfinement from Axisymmetric Model (Axial force derivation-Method 3A)	0.40	4,61	19,16	2617	358.30
2D SEM Tunnel Tunnel with deconfinement from Axisymmetric Model (Axial force derivation-Method 3B)	0.50	9,55	27,89	2204	304.80

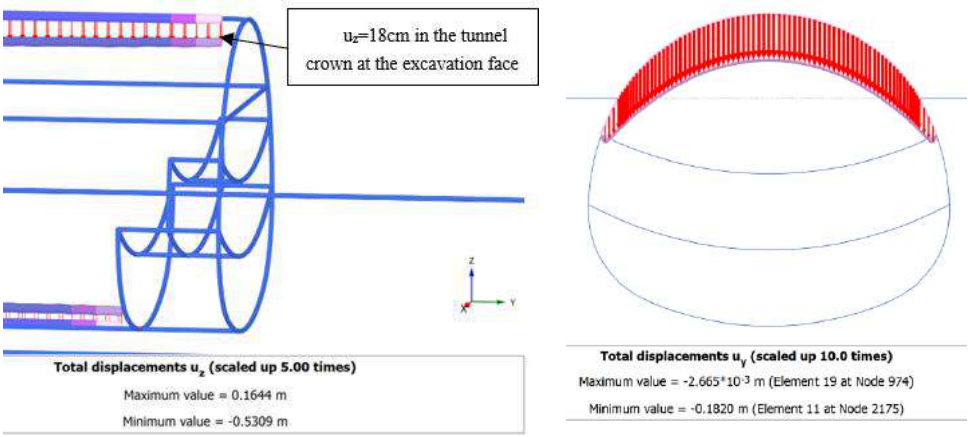

Fig. 8. Vertical crown displacement at the front in the 2D and 3Ds models after calibration with λ=0.50.

6. The three method deconfinement results comparison

The three methods utilised for the determination of the deconfinement factor (λ) have resulted in a range of results between 0.40 to 0.62, confirming that high deconfinement factors result in high deformations and lower support pressures. In the absence of real-life monitoring data, the 3D model created is considered to be the reference for the effects of the stresses in the ground acting on the primary lining, in the form of deformation, axial force, and bending moments. Table 5 below summarises the results obtained using the deconfinement factor (λ) resulted from each method (CCM, Axisymmetric, and 3D derivations).

Table 5. Summary table of the 2D and 3D Finite Element Analysis results for the Moimesti Tunnel.

Method	Deconfinement factor (λ)	Vertical Deformation u_y (cm)	Max. Axial Force (kN)	Max. Bending Moment (kNm)
2D SEM Tunnel with deconfinement from CCM (Panet-full face)	0.48	25.75	2236	313.70
2D SEM Tunnel with deconfinement from Axisymmetric Model (Axial Forces derivation-Method 2A)	0.64	55.14	2033	259.60
2D SEM Tunnel with deconfinement from Axisymmetric Model (Deformation derivation-Method 2B)	0.49	26.79	2220	309.10
2D SEM Tunnel with deconfinement from 3D Model (Axial Forces derivation-Method 3A)	0.40	19.16	2617	358.30
2D SEM Tunnel with deconfinement from 3D Model (Deformation derivation-Method 3B)	0.50	27.89	2204	304.80
3D Model	N/A	23.30	2578	271.60

It is observed that all three methods have generally obtained similar results, with the exception of the case when the deconfinement factor was determined using the Axial Forces ratio, referred to as method A, which resulted in higher deformations (55 cm) and bending moments (358 kNm) compared to the 3D model results. On the other hand, when the deconfinement factor was obtained using the CCM and the Axisymmetric and 3D models with the Vertical Crown Deformation (method B) as reference, the axial forces, bending moments, and deformations are consistently closer to the 3D model, corresponding to a deconfinement of approximately 50%.

7. Conclusion and further development

The aim of this paper was to present a three-step methodology for the determination of the deconfinement factor in soft ground, necessary for tunnel design. The methodology was applied to the proposed Moimesti Tunnel, part of the A8 Targu Neamt-Iasi-Ungheni Motorway project in Romania, which will be constructed using the sequencial excavation method. The three-step methodology comprised of using the Convergence-Confinement Method, a 2D Axisymmetric model, and a 3D model, each of them obtaining different deconfinement factors, that were in turn introduced in a 2D model, corresponding to each method.

The first two methods can be used successfully in early-stage or tender design, to reduce the duration of the evaluation and then confirmed by 3D numerical analysis and further one, compared and validated by convergence monitoring during construction. A back analysis should be conducted during construction to determine the real ground relaxation parameter.

The results, presented in the previous chapter, indicated that the CCM can be reliable for a 3 diameter cover SEM tunnel in soft ground conditions, and can be used at least as a tool for preliminary design stages. The axisymmetric method is also reliable, particularly when the deconfinement factor is determined by trial and error, using the fresh SCL vertical crown deformation near the tunnel front.

Finally, the analysis that used the deconfinement factor obtained from the 3D model, also using the fresh SCL vertical deformation near the tunnel front, has also provided results similar to those of the 3D model. This proved that the 2D and 3D models were calibrated successfully.

In conclusion, the results showed that the three-dimensional effects of the tunnel excavation can be successfully simulated in a two-dimensional analysis, using the Convergence-Confinement, 2D

Axisymmetric, and 3D numerical methods, and it is recommended to be done so, in order to check the accuracy and consistency of the deconfinement calibration.

It is acknowledged that although the analysis was successful, the results still indicate high deformations and bending moments, which is primarily due to the low stiffness of the ground. Therefore, additional geotechnical investigation is required to confirm the geotechnical parameters, particularly the Elastic Modulus. A further development step in the analysis is to determine the effects of the additional ground support in the form of bolts, spiles, lattice girders, in the determination of the ground deconfinement factor. Another further development step is to carry out the assessment in more competent ground, with longer advances and different deconfinement factors for the excavation sequences.

References

Bertuzzi, R., 2020. *Tunnel Design Handbook*, 87, 4th edition, Pells Sullivan Meynink.
John, M., Mattle B. 2003. *Factors of shotcrete lining design*, Tunnels & Tunnelling.
Jones, B. 2022. *Soft Ground Tunnel Design*, 195-198, Taylor & Francis Group, LLC.
Moller, S., 2006. *Tunnel induced settlements and structural forces in linings*, 74-81, Mitteilung 54, Instituts fur Geotechnik
Panet ,M. 2001. Recommendations on the Convergence-Confinement Method, 7-8, AFTES.
Thomas, A., 2008. *Sprayed concrete lined tunnels*, 84-86, 2nd edition, Taylor & Francis.

Southeastern Europe Tunnelling Conference (SETC-2025)
1-3 October 2025, Belgrade, Serbia

DOI: 10.5937/SETC25018P

Tunnel Portal Design in Landslide and Active Seismic Geotechnical Environment (T1 Tunnel, Türkiye)

Evren Poşluk[a], Servet Karahan[b], Candan Gökçeoğlu[c]*

[a] General Directorate of TCDD, Ankara, Türkiye; evrenposluk@outlook.com
[b] General Directorate of TCDD, Ankara, Türkiye; servetkarahan@gmail.com
[c] Cappadocia University, Nevşehir, Türkiye; candan.gokceoglu@kapadokya.edu.tr

Abstract: Portal design in extremely weak rock conditions is one of the most challenging tasks in tunnel construction. Because deformations experienced after the start of tunnel excavation, failures in the support system and surface subsidence are generally related to portal design. Therefore, the most suitable location is preferred for portal location. However, in structures such as High Speed Trains, which have various route design restrictions, sometimes the portal location cannot be chosen, a mandatory portal location is determined. In such cases, the most suitable portal design must be developed considering the adverse in-situ conditions. This study focuses on the T1 tunnel entrance portal located approximately 120 m away from the North Anatolian Fault (NAF), one of the most important active tectonic environments in the world. The T1 Tunnel Portal, located 1.5 km South East of Sapanca Station in the Ankara-Istanbul High Speed Train Project, had to be designed within the intercalation of loosely gravel, sandy gravel, sand and silt and the landslide formed in this unit. For the purpose of portal design, landslide geometry was determined with surface observations, drillings and in-situ experiments, and soil parameters were determined by back analysis in the 2D limit equilibrium method. In order to provide landslide rehabilitation and tunnel stability, an approach based on the combined use of bored piles in different patterns and cut-and-cover tunnel structures were designed. The design was controlled using 2D and 3D finite element methods and the most appropriate solution was obtained. As a result, T1 Tunnel Portal construction was completed without any problems in July 2023.

Keywords: Tunnel portal design; Landslide; North Anatolian fault; Bored pile; Numerical analysis; Back analysis

1. Introduction

Due to the design constraints of high-standard railways, tunnels are frequently used (Poşluk and Korkanç, 2018; Aygar and Gökçeoğlu, 2021; Poşluk, 2022; Poşluk et al., 2025). In tunnel construction, a tunnel portal structure is built for reasons such as optimizing the tunnel length, reducing aerodynamic effects at the tunnel entrance, and ensuring tunnel excavation. In regions where portal structures are located, the overburden thickness is generally low, weathering is high, highly jointed and weak rock masses exist (Fei et al., 2012). Construction of a portal in such environments can disrupt the balance and stability of the original slope and cause landslides or failures. In regions where seismic activity is high, tunnel portal stability under dynamic conditions is essential (Wang, 2023). Seismic damage studies of tunnels under multiple strong earthquakes show that tunnel portals are the most vulnerable areas to earthquake damage (Yu et al., 2013), and portal section supports are the weakest points (Dowding and Rozan, 1978). The Bolu Mountain highway tunnel portal was damaged in the Kaynaşlı, Turkey (7.2) earthquake on November 12, 1999. Similarly, in the study conducted in fifty-seven tunnels in the seismic region after the 1999 Chichi earthquake, it was stated that most of the tunnel portal damage was caused by lining damage and slope collapse (Wang et al., 2021). During the 2004 Niigata earthquake, a landslide occurred in the weak rock at the Kizawa tunnel portal, resulting in serious cracks in the tunnel portal (Asakura et al., 2000, Konagai et al., 2009). In the February 6, 2023 Kahramanmaras earthquakes, cracks occurred in the portal of the Erkenek highway tunnel (Apostolaki et al., 2024). A

*Corresponding author: candan.gokceoglu@kapadokya.edu.tr (C. Gökçeoğlu).

landslide occurred in the Aşık Mahsuni Şerif tunnel portal in Kahramanmaraş, but this landslide did not affect transportation. Following the same earthquake, the T3 and T7 conventional railway tunnel portals were damaged and a landslide occurred in the T3 tunnel portal (Karahan et al. 2025). Therefore, it is imperative that the factors affecting the portal be well studied and examined under dynamic loads during tunnel design. If this is not performed, the tunnel may be damaged and transportation networks may be closed. This is the last thing you want during a disaster. Consequently, the present study focuses on the T1 Tunnel Portal design, which is constructed within an active landslide and 150 m away from the Dokurcun active fault segment of the North Anatolian Fault Zone (NAF) (Fig. 1a), one of the most active tectonic environments throughout the world. The study is an interesting case study in terms of presenting new approaches in terms of portal design that includes both earthquake and landslide effects.

2. T1 Tunnel Setting

T1 Tunnel is located on the 530 km long Ankara-Istanbul High Speed Railway Project, 1.5 km east of Sapanca station (Fig. 1b). The T1 tunnel in the north-western part of Türkiye lies between km: 124 + 660–127 + 548 of the Ankara-Istanbul high-speed train project, with a total length of 2888 m (Aygar et al., 2023), and it is a 12.5 m wide and 8.1 m high double-track single-tube high-speed railway tunnel (Fig. 2). Approximately 60 m of the Entrance Portal area of the tunnel (km: 124+600 to 124+660) is within the active landslide (Fig. 1b).

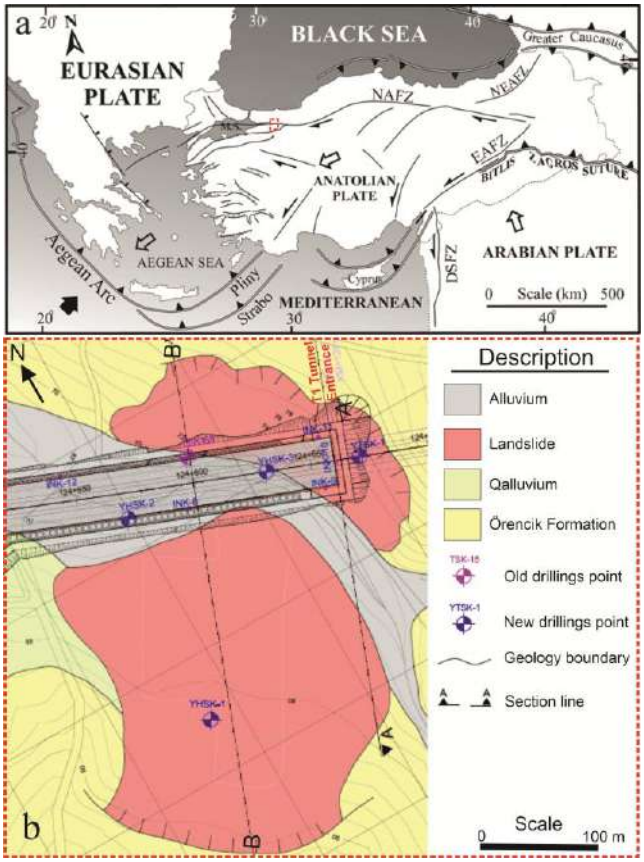

Fig. 1. (a) Tectonic outline of Turkey and eastern Mediterranean area. MS: Marmara Sea. NAFZ: North Anatolian Fault Zone. EAFZ: East Anatolian Fault Zone. DSFZ: Dead Sea Fault Zone. NEAFZ: North East Anatolian Fault Zone (Gürbüz and Güler, 2008) (b) Geological map of the study area (Fugro-Sial, 2020).

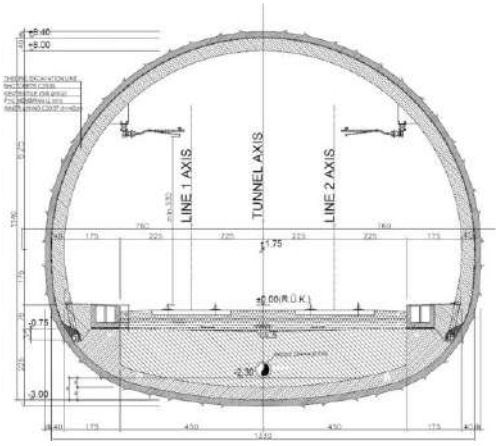

Fig. 2. Typical cross section of the T1 tunnel (units are in cm).

2.1. Geological setting

The Tunnel 1 entrance portal passes through terrestrial clastic sediment units. These units, called the Örencik Formation, are Pliocene-Quaternary in age (Aydın et al., 1987). In the tunnel portal, the units are beige, poorly consolidated, completely disintegrated and crushed claystone, sandstone units are observed to be intercalated due to atmospheric conditions and tectonic movements (Fig. 3a). Towards the T1 Tunnel route, where the overburden thickness increases, the gray-colored, medium-dense to very dense clayey sandstone, sandstone, fine conglomerate intercalation units are completely disintegrated and extremely weak (Fig. 3b).

There is an alluvial plain area starting from the region where the Tunnel 1 Entrance Portal is located and reaching up to Lake Sapanca (Koba, 2017). According to the MTA (2025) study, there is an active (> 2mm/year) landslide on this alluvial plain area, moved towards the NW with a width of 55 m and a length of around 230 m (MTA, 2025). The tunnel base is approximately 10 m below this alluvial plain. Therefore, the tunnel and this section remain within the landslide.

Fig. 3. (a) T1 Tunnel entrance general view, (b) gravel level general view.

2.2. Seismicity

The region where the T1 Tunnel Portal is located is within the North Anatolian Fault Zone (NAFZ). The NAFZ is one of the best known strike-slip faults in the world because of its remarkable seismic activity, extremely well-developed surface expression and importance from the tectonics of the eastern Mediterranean region (Ketin, 1968, 1969; Ambraseys, 1969; McKenzie, 1972; Bozkurt, 2001; Gürbüz and Gürer, 2008; Fig. 1a). This fault zone is a 1600 km-long, dextral strike-slip active transform fault running through northern Turkey in an E-W direction.

Ikeda et al. (1989a, 1989b) have presented some lines of evidence indicating that the NAFZ branches westward into two active fault zones from 30°E: the northern branch called the İzmit-Sapanca fault zone (Ikeda, 1988), and the southern branch called the Iznik-Mekece fault (Sipahioglu and Matsuda, 1986). These branch faults are synthetic faults, being developed at a low angle to the master fault, mainly in the contractional quadrant, but occasionally in the dilational quadrant (Kim and Sanderson, 2006; Fig 3a). These faults have produced devastating earthquakes in recent history. The largest of these earthquakes are the 17.08.1999 Marmara Earthquake (7.4), 12.11.1999 Düzce Earthquake (7.2) and 26.05.1957 Abant (7.1) Earthquake. As a result of these earthquakes, the region where the T1 Tunnel portal is located is in a region affected by very high earthquake accelerations, and according to the Turkish Earthquake Code (2018), the earthquake accelerations affecting the Portal are given in Table 1.

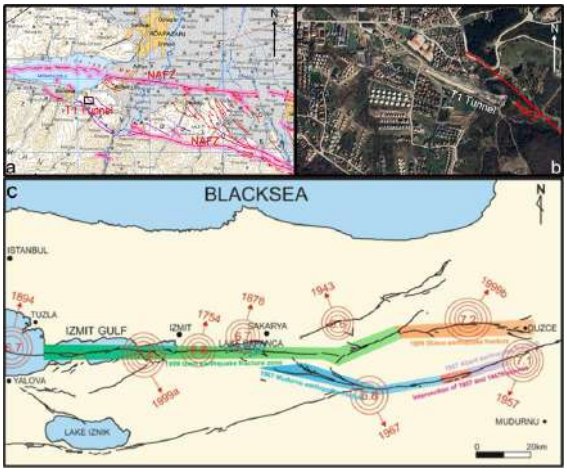

Fig. 4. Active faults around T1 Tunnel (a: Active fault map (Emre et al., 2011), b: Active fault satellite image of the tunnel portal area, (MTA, 2025), c: Fault map showing the location, magnitude and rupture zones of historical earthquakes around Sapanca Lake (Emre et al., 2013).

Table 1. Earthquake accelerations affecting the T1 Tunnel Portal (AFAD, 2025).

	PGA (g)	PGV (cm/s)	S_S	S_1
DD1	1,147	94,583	2,921	0,837
DD2	0,687	56,392	1,687	0,464
DD3	0,296	17,663	0,681	0,164
DD4	0,156	8,434	0,355	0,081

DD1: spectral magnitudes have a 2% probability of being exceeded in 50 years and the corresponding recurrence period is 2475 years; DD2: spectral magnitudes have a 10% probability of being exceeded in 50 years and the corresponding recurrence period is 475 years; DD3: spectral magnitudes have a 50% probability of being exceeded in 50 years and the corresponding recurrence period is 72 years; DD4: spectral magnitudes have a 68% probability of being exceeded in 50 years (50% probability of being exceeded in 30 years) and the corresponding recurrence period is 43 years; PGA: Peak ground acceleration; PGV: Peak ground velocity; SS: spectral acceleration coefficient for short period; S1: spectral acceleration coefficient for 1.0 s period.

3. Engineering Geology

A series of engineering geology studies were performed starting from field observations for design purposes in T1 Tunnel Portal and its close surroundings. In this context, borehole locations were determined on the general geology map prepared by field observations, and laboratory studies were

carried out after drilling and in-situ tests. In the last stage, material parameters were determined using the back analysis method for the landslide material employing the determined landslide geometry.

3.1. Borehole investigations

Nine drillings with a total length of 645 m were performed in the T1 Tunnel portal and its vicinity (Fig. 1b). The results obtained from the drillings showed that the groundwater level varied between 2.2 m and 8 m. Of these drillings, YTSK-1 and YHSK-3 were applied in order to determine the landslide failure surface depth. In the YTSK-1 drilling, landslide material is observed up to 14 m from the surface (Fig. 5a and Fig. 6). Then, Örencik Formation units (gravel clay, sand, silty clay) were cut. In the YHSK-3 drilling, on the surface, silty gravel-block sized alluvium with low clay content was passed up to 5 m, then silty clay (Tplö-2) up to 10 m, and landslide material was encountered 16.5 m (Fig. 5b). Starting from this depth, Örencik Formation (gravel clay, sand, silty clay) units were cut in the drilling.

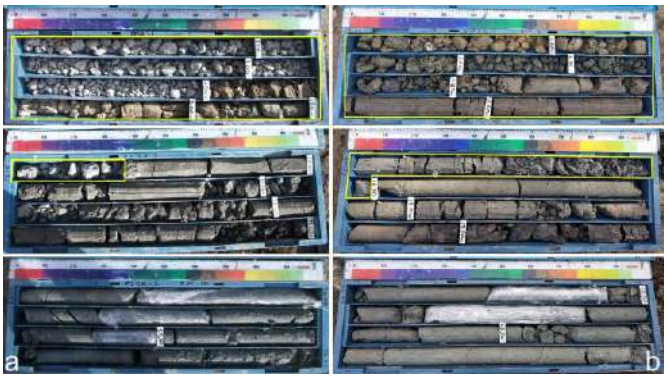

Fig. 5. Photographs of core boxes from the drillings at the T1 Tunnel Portal entrance (a: YTSK-1; b: YHSK-3 drillings, the area within the yellow lines shows the landslide material; Fugro-Sial, 2020).

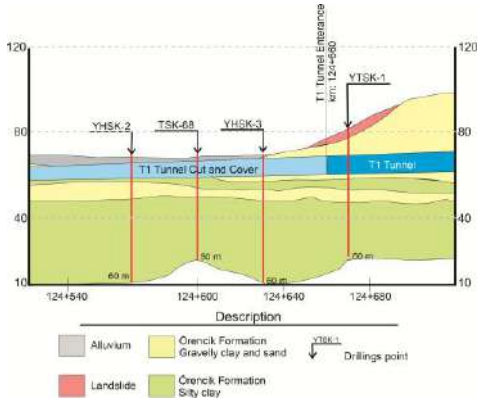

Fig. 6. Geological cross-section of the T1 Tunnel and T1 Tunnel Cut and Cover (modified after Fugro-Sial, 2020).

3.2. Laboratory tests

In the 9 drillings carried out in the T1 Entrance portal, in addition to landslide material, alluvium, gravelly clay and sand, clayey sand and silty clay units were observed. The results of the experiments carried out on the specimens taken from these units are summarized in Table 2. Accordingly, although the units were defined differently, the shear strength parameters were obtained quite close.

Table 2. Material parameters obtained from laboratory tests (Fugro-Sial, 2020).

Description	g (kN/m^3)	c' (kPa)*	♦ (°)
Alluvium	20.5	1	27
Gravelly clay and sand	21.1	1	30
Clayey sand	20	1	28
Silty clay	21.9	1	26

*The value c' is a mandatory value entered into the program.

3.3. Landslide model and back analyses

In order to determine the T1 Tunnel entrance portal landslide material parameters, first, Km: 124+600 (Fig. 1, B-B' section) was selected as the critical slope. Using the drillings performed in the region, 6 different unit boundaries were determined and the possible landslide model and slope geometry were determined (Fig. 7). In this slide model, the back analysis method was used for the parameter determination of the landslide material. The back analysis method covers the process of determining the conditions of a slope at the moment of movement (Ün and Yıldız, 2021, Poşluk et al., 2025). When a landslide occurs, it is assumed that the safety factor (FS) in the slope is equal to or below one. Therefore, the slope model at the moment of movement of a slope can be estimated in a way close to reality (Poşluk et al., 2025). The ground parameters obtained as a result of the calculations are the weighted average shear strength parameters on the sliding surface and the c: cohesion, ϕ: internal friction angle data pairs that provide the FS=1 condition are determined by trial and error (Ün and Yıldız, 2021).

T1 Tunnel portal were analyzed using the Plaxis V10 computer program using the Finite Element Method using the back analysis method. According to the analysis results, the shear strength parameters of the failure surface were determined as c'=1 kPa; ϕ =8.50° and as a result of this analysis, the factor of safety was calculated as 0.99 (Fig. 8).

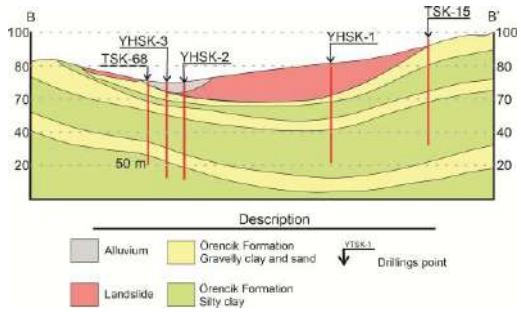

Fig. 7. Landslide model for the tunnel portal (section B-B', modified from Fugro-Sial, 2020).

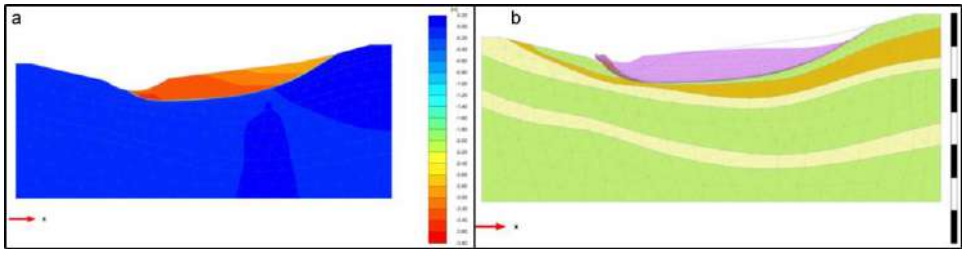

Fig. 8. Back analysis results for T1 Tunnel portal km: 124+600 (a: landslide model in the first case, b: analysis results in the last (current) sliding case; Fugro-Sial, 2020).

4. Slope Stability Analyses

The stability analyses of the T1 Tunnel were carried out in two stages. In the first stage, the required resistance force to ensure stability in the landslide model (Km: 124+600) was found, then the support model was created and the support model was searched using 2 and 3-dimensional finite analysis methods. The factor of safety for the stability of the slope should always be greater than "1" and should be at least "1.3" in short term and at least "1.5" in long-term stabilities (Poşluk et al., 2018). Therefore, in order to produce the optimum engineering solution, a support model was created that first included short-term conditions with bored piles and then long-term conditions with an cut-and-cover structure (Fig. 9). In order to create a temporary structure in a non-earthquake situation, the required resistance structure for a factor of safety of 1.3 was investigated. In this case, the required resultant resistance force was calculated as 1809 kN/m (Fig. 10).

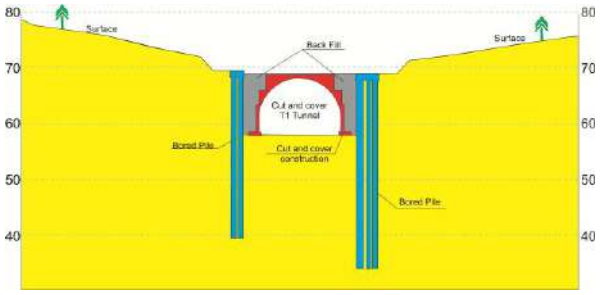

Fig. 9. Portal solution proposed for the T1 Tunnel portal (Fugro-Sial, 2020).

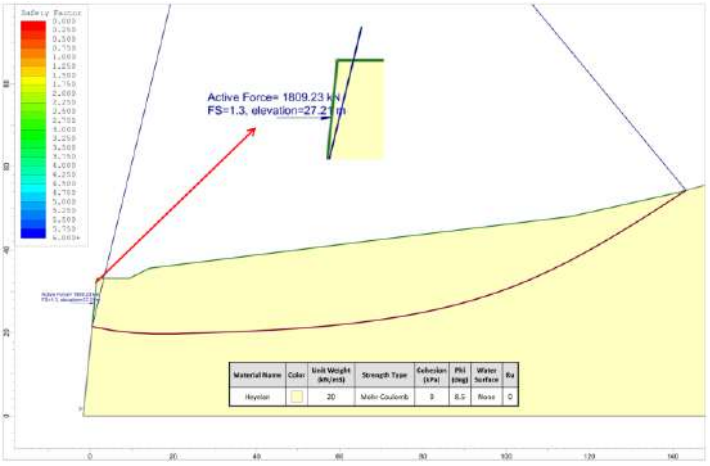

Fig. 10. Required bearing force determined by short-term slope analysis (Fugro-SIAL, 2020).

4.1. Pile retaining structure analysis

In the analyses performed for the safe construction of the cut and cover structure, the soil response was represented by spring coefficients. A vertical spring coefficient of k=200,000 kN/m3 was defined at the pile base. The lateral bearing coefficient was taken from the elasticity module as kn=19,000 kN/m3 for a 1.50 m pile spacing, and k»=29,000 kN/m3 for a 1.40 m pile spacing. The pile system was modeled in 3D in order not to overlook the effects that the geometric differences in plan and profile would create on the 3rd dimension. Plaxis 3D software, which allows analysis with the finite element method, was used in the analyses.

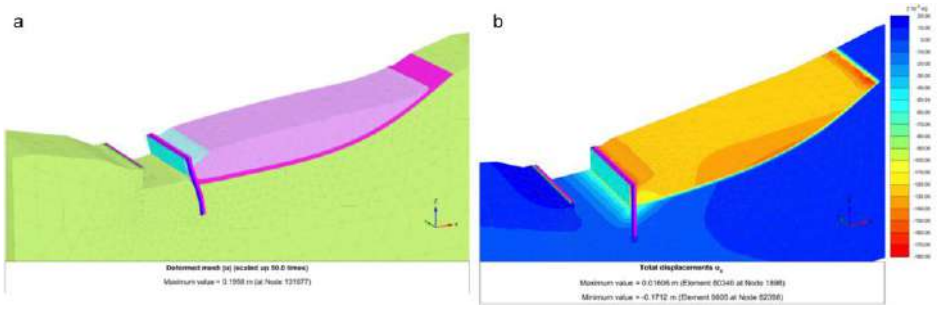

Fig. 11. 3D numerical analysis results for the T1 Tunnel portal landslide support model (a: model, b: analysis result, Fugro-Sial, 2020).

4.2. Analysis for Cut and cover structure

In the bored pile support system proposed in the T1 Tunnel entrance portal section, after the completion of the piles, cut-and-cover structure analyses were carried out in order to ensure seismic and long-term portal stability. Analyses were carried out using the previous material parameters in the critical sections of Km: 124+600 using 2D Plaxis V10 finite element software. For this purpose, excavation and support were divided into 8 stages, piles were placed in the first 3 stages, excavation was made for cut-and-cover in the 4th and 5th stages, cut-and-cover structure was constructed in the 6th stage, 2 m fill was performed on the cut-and-cover structure in the 7th stage and earthquake acceleration according to the DD2 condition (Table 1) was added to the analyses in the 8th stage. In the 7th stage, the factor of safety was determined as 1.56 and 8th stage 1.12 in the seismic (DD2) condition. Construction works started in 2021 and were completed in June 2023 (Fig. 12). To monitoring movement in the cut-and-cover structure during and after construction, seven inclonometer pipes were installed in the bored piles. Three convergence measurement points were determined at the midpoint of every 12 m of slab within the reinforced concrete cut-and-cover structure. Measurements were taken over 13 months, including the rainy season. According to the measurement results, the highest inclinometer readings were 0.7 mm and the highest convergence readings were 3 mm. These measurement results are negligible.

Fig. 12. T1 Tunnel portal construction stages (a: completion of bored pile construction, b: cut-and - cover construction and backfilling stage, c: T1 Tunnel portal completed status).

5. Conclusions

As a result of the technical standards and geometric restrictions required in high standard railways, tunnels sometimes that must be constructed in shallow and weak rocks/soils may inevitably need to be passed. In tunnels in such regions, the most challenging parts are the tunnel portal regions. Because the problems in these regions directly affect the tunnel excavation and cause cost and time loss. Therefore, the problems in the tunnel portal section should be solved before starting the tunnel excavation. The T1 Tunnel entrance portal in the Ankara-Istanbul High Speed Train Project, which is the subject of this study, is one of the best examples of portal structures constructed under difficult conditions. The T1 Tunnel portal is located in gravelly clay, sand, clayey sand, silty clay units and also passes through an active landslide. In addition to these, it is 150 m away from the Dokurcun active fault segment, which is one of the segments of the NAF. With these features, it requires quite challenging engineering solutions. In order to provide landslide rehabilitation and create a tunnel portal, the landslide geometry was tried to be understood with field observations and drillings, and then the material parameters were determined using in-situ tests, laboratory tests and back analysis method. The planned bearing and cut-and-cover structure was analyzed with 3D and 2D numerical analysis methods, considering the earthquake conditions, and the construction was completed in July 2023. It was concluded that the structure, which was evaluated with the measurements made in the structure, showed a successful performance. It was concluded that the research and application procedures proposed within the scope of the study are guiding for similar structures to be built in the future.

Acknowledgements

The authors thank the General Directorate of TCDD (Turkish State Railway) and Fugro-Sial Co. for their support.

References

AFAD, Disaster And Emergency Management Presidenc. Available online: https://www.afad.gov.tr (accessed on 3 May 2025.)..

Ambraseys, N. N., 1969. Some characteristic features of the North Anatolian Fault Zone. *Tectonophysics, 9*(1), 143–165.

Apostolaki, S., Karahan, S., Riga, E., Tsinidis, G., Gokceoglu, C., Pitilakis, K., 2025. Seismic performance of tunnels and verification of available seismic risk models for the 2023 Kahramanmaraş earthquakes. *Tunnelling and Underground Space Technology, 156*, 106185.

Asakura, T., Shiba, Y., Matsuoka, S., Oya, T., Yashiro, K., 2000. Damage to mountain tunnels by earthquake and its mechanism. *Doboku Gakkai Ronbunshu, 2000*(659), 27–38.

Aydın, M., Serdar, H. S., Şahintürk, Ö., Yazman, M., Çokuğraş, R., Demir, O., Özçelik, Y., 1987. Çamdağ (Sakarya) - Sünnicedağ (Bolu) yöresinin jeolojisi. *Türkiye Jeoloji Kurumu Bülteni, 30*(1), 1–14.

Aygar, E. B., Gokceoglu, C., 2021. A special support design for a large-span tunnel crossing an active fault (T9 Tunnel, Ankara–Sivas High-Speed Railway Project, Turkey). *Environmental Earth Sciences, 80*, 37.

Aygar, E.B., Karahan, S., Gullu, S., Gokceoglu, C., 2023. Analytical and Numerical Analyses of the Support System for a Large-span Tunnel in Challenging and Seismically Active Ground Conditions. *Transp. Infrastruct. Geotech.* 10, 988–1031. https://doi.org/10.1007/s40515-022-00251-5

Ün, B., Yıldız, A., 2021. Şev Stabilitesi Probleminin Geri Analizle Çözümü: Örnek Bir Vaka. *Journal of Engineering and Science*, vol. 9(1), pp. 174-181.

Bozkurt, E., 2001. Neotectonics of Turkey–a synthesis. *Geodinamica Acta,* 14*(*1), 3–30.

Dowding, C. H., Rozan, A., 1978. Damage to rock tunnels from earthquake shaking. *Journal of Geotechnical Engineering Division,* 104(2), 175–191.

Emre, Ö., Duman, T. Y., Özalp, S., Elmacı, H., Olgun, Ş., Şaroğlu, F., 2013. Türkiye Diri Fay Haritası. *Maden Tetkik ve Arama Genel Müdürlüğü, Özel Yayın Serisi-30*.

Gürbüz, A., Gürer, Ö. F., 2008. Tectonic geomorphology of the North Anatolian fault zone in the lake Sapanca Basin (eastern Marmara Region, Turkey). *Geosciences Journal*, 12, 215-225.

Ikeda, Y., Honkura, Y., Işıkara, A. M., 1989. Quaternary compressional deformation in the İzmit-Sapanca Trough, western Turkey, and its implications for the present tectonics near the western termination of the North Anatolian Fault Zone. In Honkura Işıkara (Eds.). *Multidisciplinary Research on Fault Activity in the Western Part of the North Anatolian Fault Zone (2)* (pp. 45–56). Tokyo Institute of Technology.

Ikeda, Y., Suzuki, Y., Herece, E., 1989. Late Holocene activity of the North Anatolian Fault Zone in the Orhangazi Plain, Northwestern Turkey. In Honkura Işıkara (Eds.). *Multidisciplinary Research on Fault Activity in the Western Part of the North Anatolian Fault Zone (2)* (pp. 16–30). Tokyo Institute of Technology.

Karahan, S., Poşluk, E., Büyükdemirci, B., Gökçeoğlu, C., 2025. Re-design of a railway tunnel intersected by surface rupture of the Erkenek fault segment during the 6 February 2023 Pazarcik (Mw 7.7) Earthquake (Türkiye). *Bulletin of Engineering Geology and the Environment*, 2025.:84:198.

Ketin, İ., 1968. Relations between general tectonic features and the main earthquake regions in Turkey. *Bulletin of the Mineral Research and Exploration Institute of Turkey,* 71*,* 63–67.

Ketin, İ. 1969. About the North Anatolian Fault. *Bulletin of the Mineral Research and Exploration Institute of Turkey,* 72*,* 1–25.

Kim, Y.-S., Sanderson, D. J., 2006. Structural similarity and variety at the tips in a wide range of strike-slip faults: A review. *Terra Nova,* 18*(*5), 330−344.

Konagai, K., Takatsu, S., Kanai, T., Fujita, T., Ikeda, T., Johansson, J., 2009. Kizawa tunnel cracked on 23 October 2004 Mid-Niigata earthquake: An example of earthquake-induced damage to tunnels in active-folding zones. *Soil Dynamics and Earthquake Engineering,* 29(2), 394–403.

McKenzie, D. P., 1972. Active tectonics of the Mediterranean region. *Geophysical Journal of the Royal Astronomical Society*, 30*,* 109–185.

MTA, The institute of Mineral Research and Exploration, GeoScience Map Viewer. Available online: https://www.yerbilimleri.mta.gov.tr (accessed on 3 May 2025.). www.yerbilimleri.mta.gov.tr

Poşluk, E., 2022. High-speed railway tunnel design in the framework of recent developments in the world and the situation in Turkey. *Railway Engineering,* 15*(*1), 13–29.

Poşluk, E., Dalgıç, S., Kuşku, İ., Apaydın Poşluk, E., 2018. Determining Support Force For Landslide Amendment Wıth Lımıt Equılıbrıum Method. *İstanbul Earth Science Review*, 27.2: 77-88.

Poşluk, E., Korkanç, M., 2018. Difficulty on performance prediction of excavation with machine in weak rocks. *Journal of Geological Engineering,* 42(2), 143–158.

Poşluk, E., Ogul, K., Bozkurt, H., 2025. Evaluation of landslide-tunnel relationship with numerical analysis (Ankara-Istanbul High-Speed Train Project T8 Tunnel). *Railway Engineering,* 21*,* 13–26.

Sipahioğlu, S., Matsuda, T., 1986. Geology and Quaternary faults in the İznik-Mekece area. In Işıkara Honkura (Eds.), *Electric and Magnetic Research on Active Faults in the North Anatolian Fault Zone* (pp. 25−41). Tokyo Institute of Technology.

Türkiye Bina Deprem Yönetmeliği. 2018. *Afet ve Acil Durum Yönetimi Başkanlığı, Ankara*.

Wang, Q., Geng, P., Chen, C., Chen, J., He, C., 2023. Determination of seismic response of reinforced tunnel portal slope using shaking table tests. *Tunnelling and Underground Space Technology,* 136, 105072.

Wang, T. T., Kwok, O. L. A., Jeng, F. S., 2021. Seismic response of tunnels revealed in two decades following the 1999 Chi-Chi earthquake (Mw 7.6) in Taiwan: A review. *Engineering Geology,* 287, 106090.

Ye, F., He, C., Wang, S. M., Zhang, J. L., 2012. Landscape design of mountain highway tunnel portals in China. *Tunnelling and Underground Space Technology*, 29, 52–68.

Southeastern Europe Tunnelling Conference (SETC-2025)
1-3 October 2025, Belgrade, Serbia

DOI: 10.5937/SETC25019E

Geological-geotechnical problems during the design stage of reservoir side portal of Babakaya water transmission tunnels

R. Emre Cakir[a], S. Mirac Karademir[a], Ilbuke Yalcinkaya[a], Orkun Er[a], Fevzi Tosun[a], I. Gorkem Tunay[a] and Candan Gökçeoğlu[b]**

[a] Yüksel Proje A.Ş. Birlik Mah. 450 Cad. No: 23 06610 Çankaya, Ankara, Türkiye; (rcakir, mkarademir, IUSLU, oer, ftosun, igtunay)@yukselproje.com.tr
[b] Cappadocia University, 50420 Mustafapasa, Urgup, Nevsehir, Türkiye; candan.gokceoglu@kapadokya.edu.tr

Abstract: Silvan Dam constructed by State Water Affairs of Türkiye (DSİ), the largest irrigation dam in the Southeastern Anatolia Project after the Atatürk Dam, was planned to have a reservoir volume of 7 billion cubic meters. The dam will provide agricultural water to an area of 235 thousand hectares. The height of the dam was 174.5 m while its crest length was 440 m. The irrigation water will be transmitted with Babakaya tunnels. The portal of the Babakaya tunnels is located on a slope with a height of 300 m, approximately 700 m northwest of the dam body in the reservoir. A water intake structure and two shafts will also be constructed in the portal area. The upper levels of the slope consist of high strength limestones, while the lower levels consist of weak and practically impermeable mudstone-claystone lithologies. Between these two lithologies, there is a transition unit with a thickness of approximately 15 m with weak strength. This lithological sequence has caused a very steep slope angle at the upper levels of the slope and lower slope angle at the lower levels. The project site is located in a region with high seismic activity. From this perspective, three basic engineering problems have emerged. These are: (a) rockfall problems, (b) slope stability and deterioration problems of the transition zone, and (c) stability problems and rapid dropdown problems of slopes that will remain under the dam water. In the present study, these problems are described clearly, and the necessary engineering measures are described and analyzed in detail. Consequently, an extremely complex engineering structure was defined in terms of both engineering geology and construction, and its possible measures are presented through analysis and interpreted with engineering principles.

Keywords: portal; rockfall; slope stability; clay-bearing rock mass; rapid dropdown condition

1. Introduction

According to Aygar and Gokceoglu (2021), portal excavation is one of the most crucial steps in tunnelling because a failure that may occur during portal excavation will completely interrupt the whole tunnel excavation. For this reason, tunnel portal designs were the subject of various scientific studies in addition to their special importance (Alija et al., 2014; Taromi et al., 2018; Khan et al., 2019; Ayoublou et al., 2019; Can et al., 2022). Sometimes, due to compelling reasons, tunnel portals are designed in locations with extreme difficult geological-geotechnical conditions. The purpose of the present study is to present the design of a complex portal of the Babakaya water transmission tunnels. The Babakaya transmission tunnels are the part of the Silvan Dam. The Silvan Dam, one of the largest irrigation investments in Türkiye, which is located in Diyarbakır (Fig. 1), is the second-largest dam after the Atatürk Dam in the Southeastern Anatolia Project, which aims to increase the productivity of agricultural lands in the southeastern region of the country. The project aims to increase agricultural activity in the region by 2 to 3 times (DSI, 2025).

*Corresponding author: candan.gokceoglu@kapadokya.edu.tr (C. Gokceoglu).

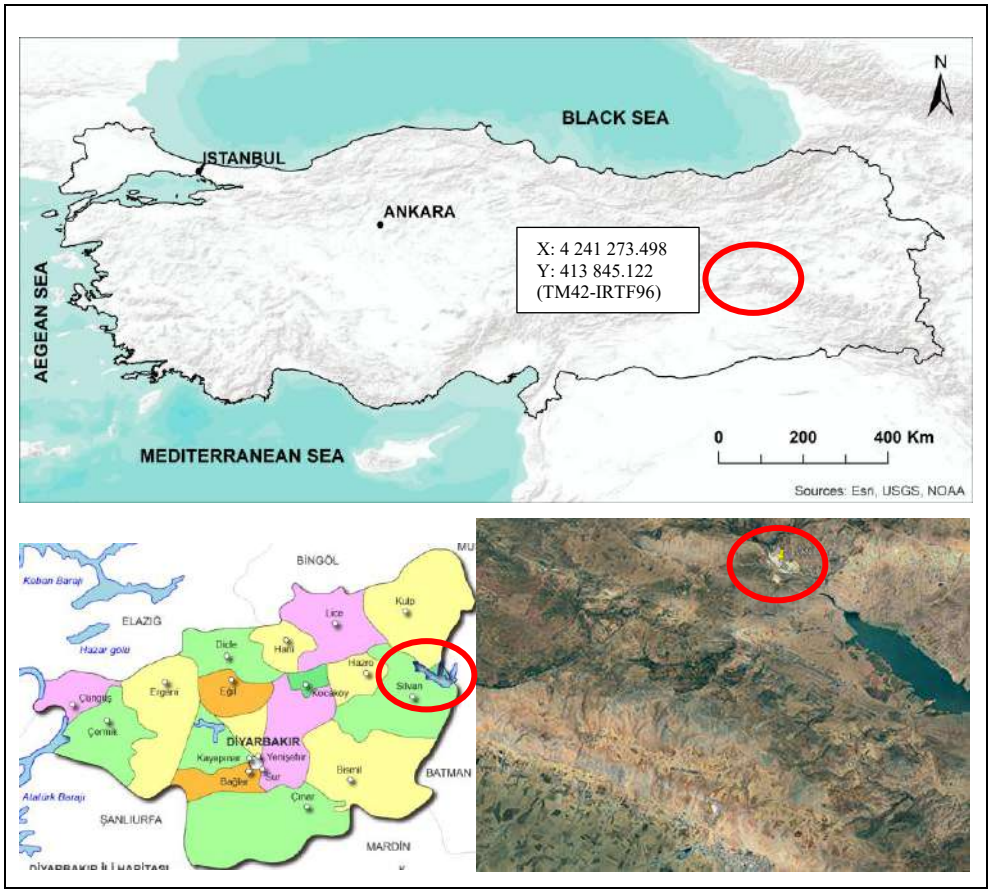

Fig. 1. Location Map of Project Site.

When the dam is completed, it will enable the irrigation of a total area of 235,000 hectares in the left-bank plains of the Tigris River. The project aims to provide employment for 308,000 people, and its annual contribution to the national economy is expected to be approximately 1 billion dollars (DSI, 2025). The dam has a reservoir capacity of 7 billion cubic meters, a dam height of 174.5 meters, and a crest length of 440 meters. In addition to the dam structure, the project includes two tunnels and one open canal.

Water will be transported from the right bank of the dam through the 5,280-meter-long Babakaya Tunnels to the open canal and then distributed to the irrigation areas via the 13,500-meter-long Silvan Tunnel. The Babakaya Tunnel is designed as a twin-tube TBM tunnel with an internal diameter of 7.0 meters, while the Silvan Tunnel is a single-tube TBM tunnel with an internal diameter of 10.0 meters. The upstream portal of the Babakaya Tunnel, located 700 meters northwest of the dam body, stands out as a critical area due to its complex structural and geological conditions (Fig. 2). The portal excavation will be carried out on a 300-meter-high slope, where twin-tube irrigation tunnels and one gate shaft per tube are planned. Moreover, for maintenance purposes there is an access tunnel at the shaft elevation (Fig. 3).

Consequently, the study presents a complex portal design of a transmission tunnel twin in the difficult geological and geotechnical conditions.

Fig. 2. General view of the portal area.

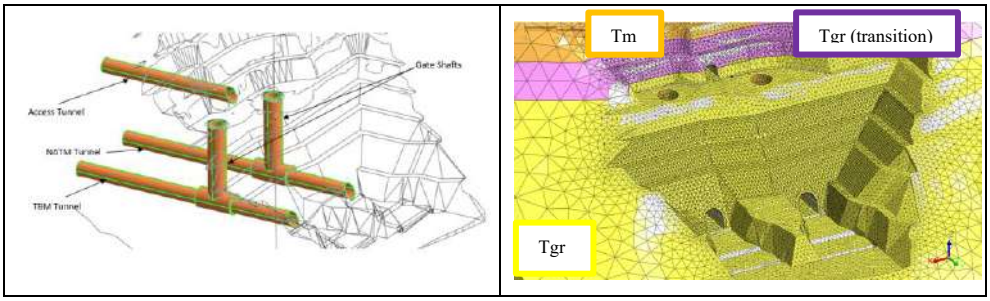

Fig. 3. 3D view of the general structures of the portal area.

2. Geological and Geotechnical Conditions

The portal considered in the study is located in the reservoir of the Silvan dam and toe of a high slope. General geological setting of the study area is represented by Paleocene Gercüş Formation overlain conformably by middle Eocene Midyat formation. Gercüş formation is mostly composed of reddish colored claystone, sandstone, mudstone and conglomerate alternation. Mudstone is red, brown color, generally composed of sandy mudstone and shows vertical and horizontal transitions with claystone levels. Midyat formation is represented by cream, gray and white colored limestone, clayey and chalky limestone unit. Between Gercüş and Midyat formations, there is a weak transition unit with a thickness of approximately 15 m (Fig. 4).

According to exploratory studies, Gercüş Formation generally comprises reddish brown - red colored, moderately - occasionally slightly weathered, competent mudstone, sandstone, conglomerate, claystone units. Discontinuities are inclined into the slope with ~ 5° - 15° and are clay infilled.

Geomechanical properties revealed after exploration studies regarding Gercüş Formation are summarized below.

Total Core Recovery : 70% $\leq$ TCR $\leq$ 100%
Rock Quality Designation : 40% $\leq$ RQD $\leq$ 84%

Uniaxial Compressive Strength : 9.85 MPa $\leq$ UCS $\leq$ 49.33 MPa
Unit Weight : 2.24 gr/cm^3 $\leq \gamma \leq$ 2.46 gr/cm^3

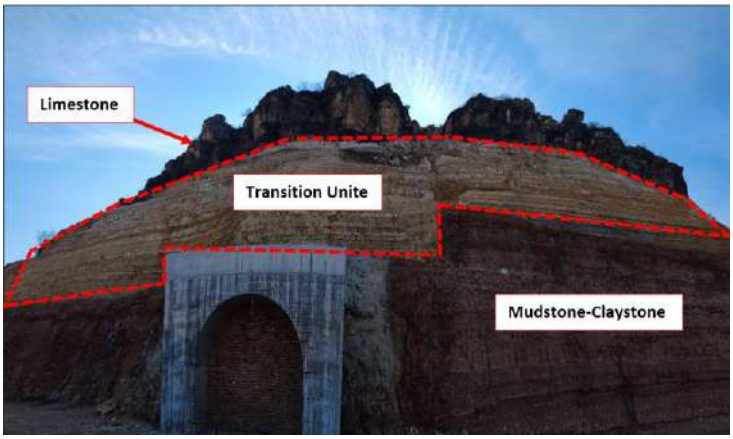

Fig. 4. Close view of the lithologies encountered in the Babakaya tunnel upstream portal area.

The transition zone between the two major formations is represented by claystone and clayey limestone levels. These units are generally yellowish brown - beige - yellow colored, highly weathered and weak. RQD values obtained in boreholes are generally below % 25.

The uppermost sequence belongs to Midyat formation which is basically composed of gray - white - beige colored, hard, moderately weathered and resistant limestone, clayey limestone levels, for which geomechanical properties are summarized below.

Total Core Recovery : 67% $\leq$ TCR $\leq$ 100%
Rock Quality Designation : 10% $\leq$ RQD $\leq$ 68%
Uniaxial Compressive Strength : 20.6 MPa $\leq$ UCS $\leq$ 71.5 MPa
Unit Weight : 2.18 gr/cm^3 $\leq \gamma \leq$ 2.47 gr/cm^3

In scope of subsurface investigation, groundwater level is measured 12.00m – 54.00m below the surface. Groundwater circulation is probable through discontinuity systems in the Midyat formation whereas, Gercüş formation is considered practically impermeable proven by lugeon tests having $L_u \leq 2$.

Apart from the geomechanical characteristics of lithologies, seismicity is another major component in the design. The portal area is located 12 km from the Kozluk Segment of the Southeastern Anatolia Thrust Fault Zone, posing additional geotechnical and structural challenges for design and construction. According to site specific seismic risk analysis, 475 year PGA = 0.27g is adopted in relevant engineering assessments. A horizontal seismic acceleration coefficient of k_h=0.162g was used for the pseudo-static analysis of slopes considering the data obtained from the site-specific seismic hazard assessment report.

The Midyat formation comprising limestone is more resistant to weathering compared to underlying the Gercüş formation where mudstone is the dominant lithology. Thus, upper levels are stable in natural slope whereas, lower levels are easily weathered causing instability problems in limestones. Although the Midyat limestone is stable in general, rock fall problem requires to be handled before construction stage. When morphology, lithological aspects of limestone unit, discontinuity character, seismicity etc. are considered, rock fall is an expected risk.

Engineering slopes will mostly be established in lower levels in the Gercüş formation which is mostly prone to degradation against groundwater. Although groundwater can be modelled in slope stability calculations, long-term deformability of clay bearing lithologies needs to be considered in design. Disintegration of the clay bearing lithologies in the Gercüş formation under cyclic wetting and drying

process shows that geomechanical strength will diminish when in contact with groundwater, a critical scenario for the engineering slopes under dam water.

3. Slope Stability Assessments

Slope stability analyses were performed considering the geomechanical properties of the formations and different scenarios that may occur during the service life of the structure. The design principals considered in the present study are summarized as follows.

The slopes were planned to be formed with a geometry of 1/2 (H/V) in the Gercüs formation. Limit-equilibrium based analyses were performed with the SLIDE2 (ver. 9.036) software and the GLE/Morgenstern–Price method. Circular failure modes were employed considering the highly jointed and weathered condition of the layers. During the analyses, the Hoek-Brown material model was used for rock masses. A disturbed zone of approximately 6.0 m is considered in the analyses taking into account the disturbance due to excavations and wetting/drying process during the design of the slopes. The target safety factors were selected as 1.30, 1.50 and 1.0 for temporary static, permanent static and extreme cases (such as seismic conditions, rapid drawdown etc.), respectively. A support pattern was selected which satisfies all the factor of safety presented above. As a general guideline for the internal stability of the support elements, such as pull out, tensile capacity etc., FHWA Soil Nail Walls Reference Manual (2003) was considered. In addition to geotechnical properties, four different groundwater configuration was considered in the design. These are (a) actual groundwater level; (b) the groundwater level is at the minimum water level of the dam; (c) the groundwater level is at the maximum water level of the dam; and (d) the rapid drawdown case (the water level is at the minimum level of the dam while the slope is under saturated condition due to the very low permeability of the rock mass. Self-drilling rock bolts were planned to use in order to maintain the stability of the drilled hole.

The stability analyses were performed considering all the design principles described above and the support properties are determined according to the most critical case which governs the design. It was found that the most critical case is the case with groundwater level configuration that represents the rapid drawdown and the design earthquake loading is applied simultaneously. In general, it is not a straightforward method to combine two different extreme events (such as rapid drawdown and seismic condition). On the other hand, it was found necessary to combine these effects since, these events may occur at the same time considering the operational scenarios. A sample analysis result is given in Fig. 5 which represents the most critical case which resulted in a factor of safety value just above unity. Material and support properties are given in Table 1 and 2.

Table 1. Material properties for the analysis

Material	Unit Weight (kN/m^3)	Strength Type	UCS (intact) (kPa)	GSI	mi	D
Tm	25	Generalized Hoek Brown B	40000	48	12	0
Tgr – df=0	23.5	Generalized Hoek Brown	30000	36	8	0
Tgr (wet) -df=0	24.5	Generalized Hoek Brown	18000	31	6	0
Tgr (transition) - df=0	21	Generalized Hoek Brown	10000	16	5	0.3
Tgr – df=0.3	23.5	Generalized Hoek Brown	30000	36	8	0.3
Tgr (wet) – df=0.3	24.5	Generalized Hoek Brown	18000	31	6	0.3

According to the analysis results, the following support pattern was designed:

- Self drilling rock bolt type - IBO R38 N
- Length of the rock bolts, L=15.0 m
- Horizontal and vertical spacing, s_h=s_v = 2.0 m
- Wall facing: Shotcrete t=20 cm + double layer of wire mesh (2x Q443/443)

Table 2. Support properties for the analysis

Support	Out of Plane Spacing (m)	Tensile Capacity (kN)	Plate Capacity (kN)	Bond Strength (kN/m)
IBO – R38N - fs_{ult}=400 kPa	2	277.8	277.8	47.73

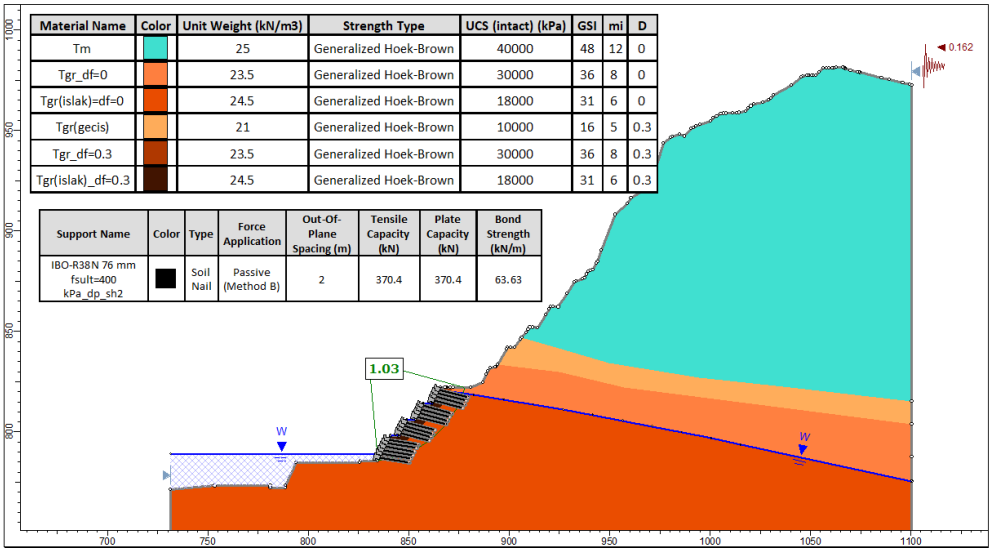

Fig. 5. Limit-equilibrium analysis result for the most critical case.

4. Rockfall Assessments

General geological – geotechnical conditions and accompanying engineering problems are introduced previously. As stated, one of the main problems in the portal area is rockfall on upper levels (Fig. 6). Limestone unit belonging to the Midyat formation is associated with rockfall problem evident by morphology, and weathered discontinuity conditions. Considering the stabilization or removal of blocks that have the potential to fall on the slope surface of the portal, analyses were conducted by modeling potentially falling blocks from the source area behind the slope crest. As a result of rock fall analysis, 2000 kJ barrier with a height of 6.00 m was confirmed to be sufficient to prevent rockfall hazard to jeopardize construction of shafts and relevant structures.

Initially, 2D rockfall analyses are conducted for the critical cross section adopting various size rock groups having potential rock fall risk (Fig. 8). The maximum total kinetic energy in the shaft location is determined as 1850 kJ (Fig.9a). Bounce height of free blocks in the same area is determined as 18m (Fig. 9b).

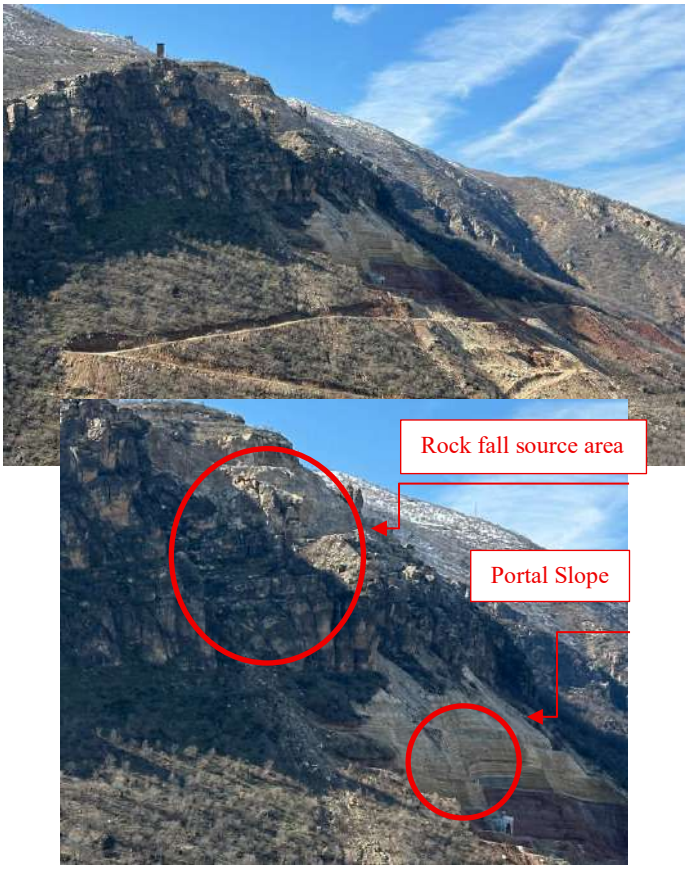

Fig. 6. General view of the portal area under rockfall hazard.

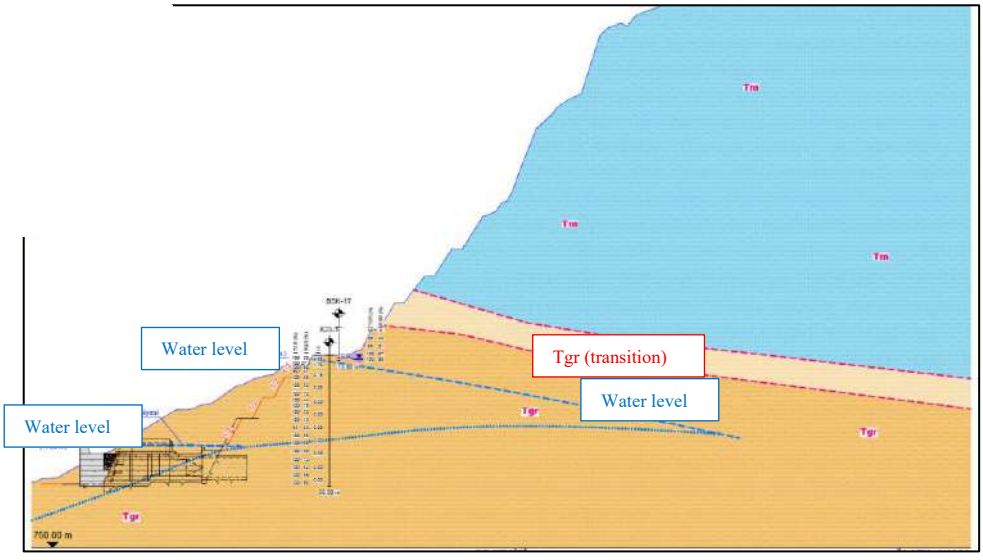

Fig. 7. Tunnel geological cross-section.

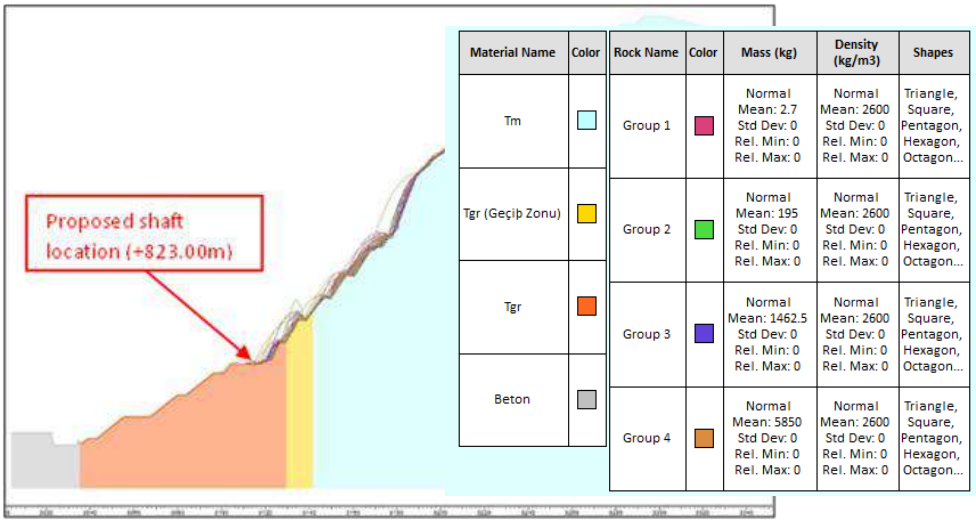

Fig. 8. Result of the rockfall analysis on the most critical section.

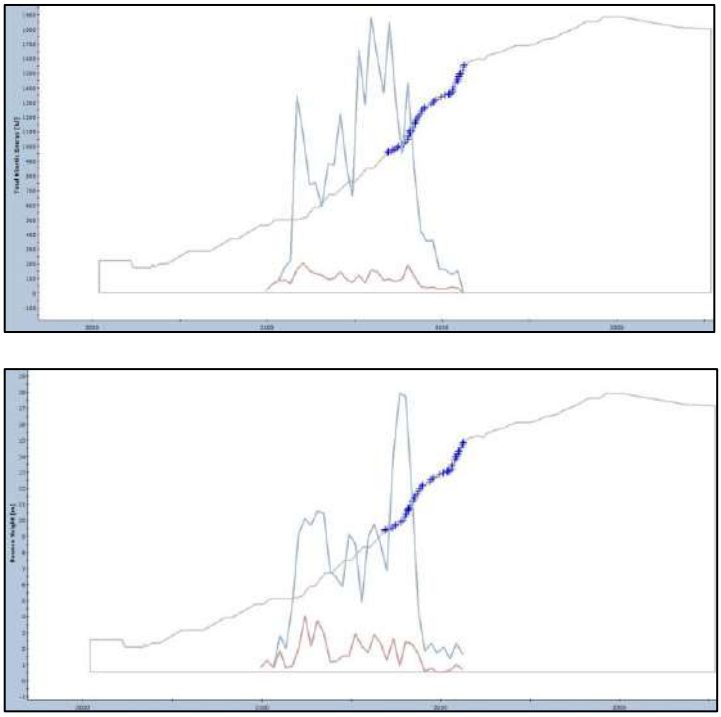

(a)

(b)

Fig. 9. Graphs showing the results of the rockfall analysis on the most critical section: (a) total kinetic energy and (b) bounce height.

Rockfall barriers are proposed to eliminate rockfall problems on the slope which is a practical and economical solution. Based on rockfall analyses, optimum dimension and setting of rockfall barriers are determined (Fig. 10).

As a result of rock fall analysis, 2000 kj barrier with a height of 6.00 m was confirmed to be sufficient to prevent rockfall hazard to jeopardize construction of shafts and relevant structures.

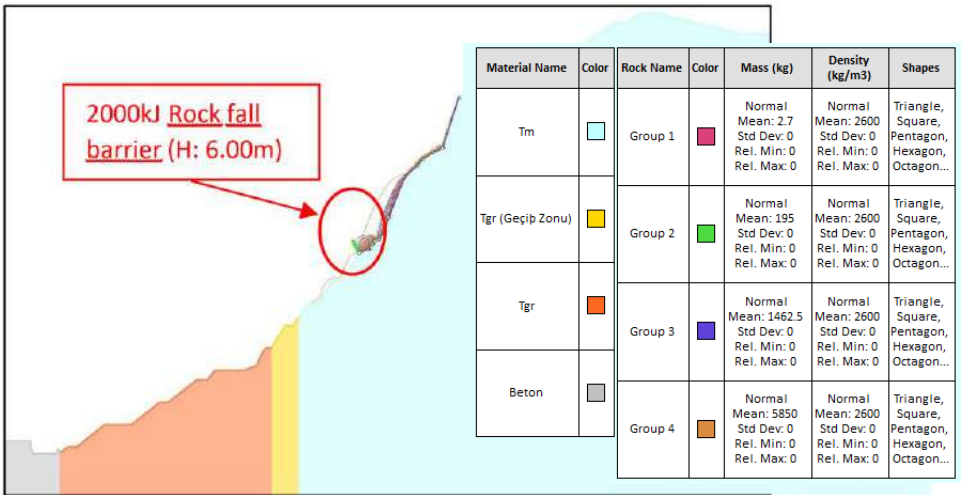

Fig. 10. Result of the rockfall analysis on the critical section with barrier.

5. Conclusion

Dams planned in mountainous regions with high seismic activity provide serious benefits, as well as challenging projects for engineers due to the serious geological and geotechnical problems they pose. In this study, it is aimed to discuss the geological-geotechnical problems of the reservoir portals of the Silvan Dam water transmission tunnels in the seismically active Southeastern Anatolian thrust zone and to present the engineering measures against to the possible problems described in the study.

The slopes will be constructed in weak-medium quality, clay-bearing rock masses. This situation may cause additional weakening in the rock mass during the service life of the dam. In addition, rapid dropdown conditions will cause additional water pressures and result in a serious decrease in the factor of safety. The design was performed by taking these issues into consideration. Since the planned slopes will remain under water after the dam is filled, the consequences of any failure will be very difficult to compensate. In addition, another important natural hazard is rockfall. Necessary analyses were applied for rockfall hazard and engineering measures were proposed.

Another important issue is that the portal area contains many engineering structures such as water intake structures, tunnels and shafts. It is very important to perform 3D numerical analyses to understand the interaction of all these structures with each other and with the natural environment. These analyses should be performed and their results should be assessed in future studies.

Acknowledgements

The authors would like to express the gratitude to officers of Irrigation Department Directorate of State Hydraulic Affairs of Türkiye and the site crew of Kalyon Construction J.S.C. for their supports.

References

Alija, S., Torrijo, F.J., Quinta-Ferreira, M., 2014. Study of the unexpected collapse of Ampurdan tunnel (Spain) using finite element model. *Bull Eng Geol Environ*, 73, 451–463. https://doi.org/10.1007/s10064-013-0534-z

Aygar, E.B., Gokceoglu, C., 2021. Effects of Portal Failure on Tunnel Support Systems in a Highway Tunnel. *Geotech Geol Eng,* 39, 5707–5726. https://doi.org/10.1007/s10706-021-01859-z

Ayoublou, F., Taromi, M., Eftekhari, A., 2019. Tunnel portal instability in landslide area and remedial solution: a case study. *Acta Polytech*, 59(5), 435–447.

Can, A., Baskose, Y., Gokceoglu, C., 2022. Stability assessments of a triple-tunnel portal with numerical analysis (south of Turkey). *Geotechnical Research,* 9 (2), 116-128. https://doi.org/10.1680/jgere.21.00028

DSI (State Hydraulic Affairs of Türkiye), 2025. Silvan Barajında Çalışmalar Aralıksız Devam Ediyor. https://www.dsi.gov.tr/Haber/Detay/8912 (accessed on April 5, 2025)

Geotechnical Engineering Circular No. 7 Soil Nail Walls, 2003, Federal Highway Administration

Khan, R.M.A., Mad, Z., Jo, B., 2019. Tunnel portal construction using sequential excavation method: a case study. *MATEC Conferences* 138, 04002.

Slide2 User Guide, https://www.rocscience.com/help/slide2/overview (accessed on April 5, 2025)

Taromi, M., Eftekhari, A., Hamidi, J.K., Aalianvari, A., 2017. A discrepancy between observed and predicted NATM tunnel behaviors and updating: a case study of the Sabzkuh tunnel. *Bull Eng Geol Environ*, 76(2),713–729.

Southeastern Europe Tunnelling Conference (SETC-2025)
1-3 October 2025, Belgrade, Serbia

DOI: 10.5937/SETC25020L

TBM Tunneling in geotechnically and structurally sensitive Metropolitan Areas

Lars Langmaack[a]*

[a] MC-Bauchemie, Bottrop, Germany; lars.langmaack@mc-bauchemie.de

Abstract: Frankfurt, one of the most densely populated capitals in Germany, needed an extension of its Metro Line U5 from the main railway station towards the newly created district 'Europaviertel' which is part of an urban rehabilitation plan affecting over 30.000 people.

For the first time in Frankfurt, TBMs were used for metro construction. Driving in full EPB mode at up to 3,2 bar in clay and sand/clay mixed face geology with sensitive surface construction as well as the connection to the existing tunnel system from the 1970s makes this project unique.

Apart from the 2k annulus grout – first time implemented in Germany for a city tunnel project, EPB startup with a prefilled working chamber has been used very successfully together with highly ecologic tail sealants and soil conditioning system with minimum impact on the excavated soil.

Keywords: TBM; Soil Conditioning; Foam; Polymer; Tail Sealant

1. Introduction

In the city center of Frankfurt, the Joint Venture U5 Europaviertel consisting of the companies Porr and Stump, builds a dual tube tunnel on behalf of Stadtbahn Europaviertel Projektbaugesellschaft (SBEV GmbH). The extension the of the existing metro line U5 will connect the new 'Europaviertel' district with the central railway station. The Europaviertel is an urban rehabilitation project for the area of the old railway freight terminal.

Fig. 1 illustrates well the inner-city center situation of the jobsite as well as the fact that the TBM is underpassing numerous buildings and other critical infrastructure. In addition, the project is in very close distance to the river Main.

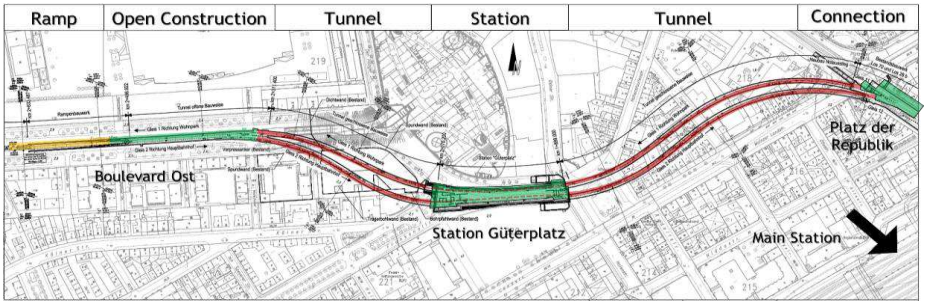

Fig. 1. Project overview, situation 2018.

*Corresponding author: lars.langmaack@mc-bauchemie.de (L. Langmaack).

The paper focuses on the identification of sensitive environments like inner city launching shafts and spans the spectrum from examination of soil samples in the laboratory, proposing suitable solutions for the jobsite, implementing these solutions at site and optimizing them – all for one goal: safe and secure tunneling through highly populated urban areas without disturbance and technical difficulties.

2. Project Description

2.1. Project location

The project includes the construction of the inner-city metro extension of the metro line U5 and the underground connection to the existing metro network at Platz der Republik. Fig. 2 shows the Platz der Republik close to the Center Railway Station from 1888 (mid right), the worldwide known Frankfurt Fair buildings (center) and the new Europaviertel on the left side.

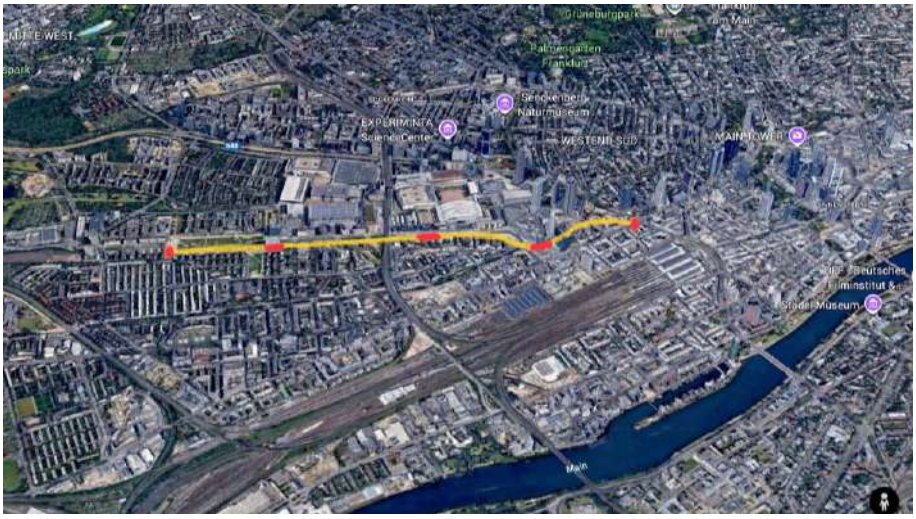

Fig. 2. Frankfurt City Center with river Main, the new Europaviertel district and the U5 extension line.

The metro extension will be build as a 186 m open construction section followed by a 2x830 m TBM section with two 7.10m outer diameter tunnels. For the connection to the existing metro tunnel, the TBMs will drive into a ground freezing area at Platz der Republik where they will be underground dismantled. The connection itself will be carried out conventionally by excavator under compressed air conditions supported by injections.

2.2. Geology

The geology in the metropolitan area of Frankfurt is generally characterized by cohesive soils with a high proportion of clay or silt and low permeability. Most of the project runs through “Frankfurter Clay” which is overlaid by 2 - 10m thick quaternary top layers of limestone and gravel, which is in the area of the excavation pit. Occasionally, sandstone formations up to 240 MPa can penetrate into the clay layer and also appear further along the planned TBM route, details are shown in Fig. 3.

Principally, the TBM drive can be divided into 3 main areas:

1. Start shaft to Station Güterplatz: mixed face conditions clay, sand, limestone
2. Station Güterplatz: 180m full face Frankfurt Clay, protected by sealing wall
3. Station Güterplatz to Frankfurt Main Station: full face Frankfurt Clay with Limestone layers

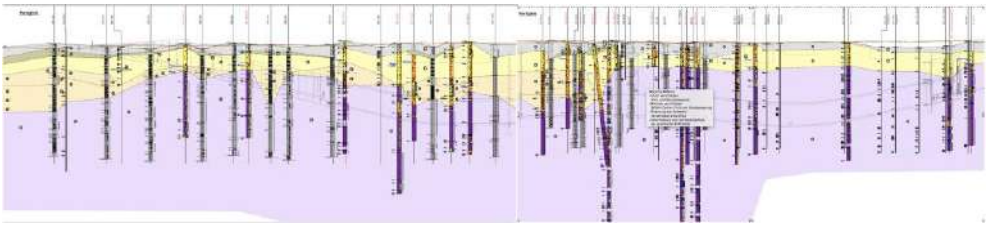

Fig. 3. U5 Extension geology: Frankfurt clay (purple) being dominant; sandstone, sand and gravel (yellow and grey).

2.3. TBM details

The U5 Extension project used a tunnel boring machine with earth pressure support (EPB TBM) which has been selected as ideal tunneling method for Frankfurt's Europaviertel. The TBM was baptized 'EVA' standing for "Europa-Viertel-Anbindung". The TBM has been already used in Doha (Qatar) for the Green Line Metro project and was refurbished and adjusted specifically for the U5 project in Frankfurt.

Due to the inner-city tunneling, very high demands were put into practice to minimize settlements. The support pressure of the shield machine had to be secured at any time according to the existing subsoil pressure as well as according to the existing loads to avoid settlement and the resulting damage of existing structures. Fig. 4 illustrates the used TBM cutterhead design and mentions further detailed TBM parameters.

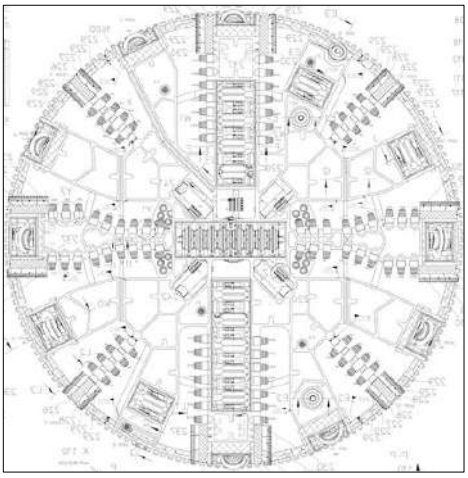

Manufacturer	Herrenknecht (S-1127)
TBM type	EPB
Nominal diameter	7.1 m
Installed power	960 kW
Cutterhead torque	4133 kNm
Max. push force	36'500 kN
TBM length total	84.0 m
Weight	580 tons

Fig. 4. TBM cutterhead schematics and TBM details.

3. Flying TBM start – EPB pressure on the run

3.1. Startup situation

To drive the TBM into the ground, it had to drill first through a 1.20m thick trench wall as well as tough a 1.10m thick sealing block. The EPB design pressure for the untreated ground was 1.4-1,6 bar at the

crown – mandatory to be reached already during blind ring No. 4 drilling through the sealing lamella. Fig. 5 describes the technical startup situation in the TBM launching shaft.

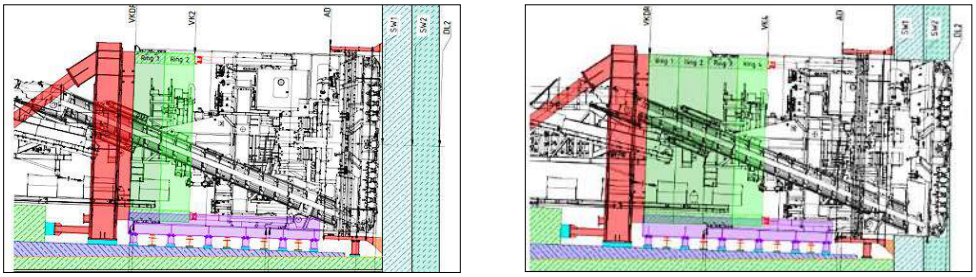

Fig. 5. (left) TBM start: cutterhead touching trench wall with blind ring No. 2; (right) TBM start: cutterhead touching untreated ground with blind ring No. 4.

3.2. Flying EPB start with ArtSoil™ technology

The aim of the Artificial Soil is to drive in a pressurized EPB mode through the remaining trench wall and sealing block into the ground. Just adding water and foam will not work and the addition of only Bentonite Slurry is not productive: The obtained rheology will be far to liquid to be handled on EPB machines, especially under pressure.

Therefore, MC proposed the use of an Artificial Soil based on HDSL Slurry together with the addition of a specialized MC Polymer (see Fig. 6):

HDSL Slurry + separate addition of **MC-Polymer**	**Hägermann Slump** Homogeneous paste with plastic behavior	**Hägermann Spread** 160mm

Fig. 6. Artificial Soil in different stages.

The HDSL was produced above ground with the existing grout plant and then pumped down to the TBM. Ideally, the Polymer will be mixed into the HDSL via Y-connector directly before running into the TBM working chamber.

3.3. Site use

The filling of the working chamber with artificial soil started with blind ring No. 3, reaching the top level and got pressurized on 2nd September 2019 early morning as shown in Fig. 7. During excavation of blind ring No. 4, the EPB pressure was rising to 1,5 bar crown pressure until end of the day. Pressure

drops are a result of releasing the air with was remaining in the working chamber as well as releasing water – until no air bubble was left and the muck showed a homogeneous consistency.

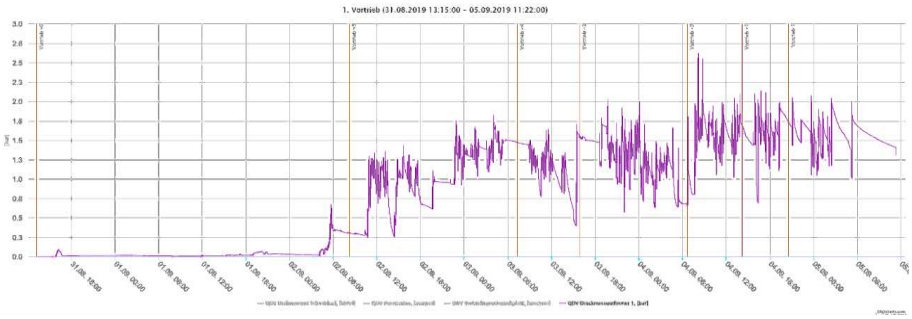

Fig. 7. Filling the TBM chamber and start of the 1st drive (pressure in bar over time / rings).

This procedure worked out very well and could guarantee a safe and secure full EPB start of the TBM out of the station into the challenging heterogeneous ground. This technology was used subsequently for all startup situations in Frankfurt as well as London City for example.

4. Soil conditioning – from laboratory to reality

As indicated already, the Frankfurt Clay is the predominant geology for the project. Especially the startup phase shows mixed face conditions of Frankfurt Clay, sand and gravel up to 25%.

Aims of the laboratory trials were

- Choice of the right foam type
- Determining the clogging risk
- Determining the amount of additional water if necessary
- Determining the best starting parameters concerning FER and FIR

4.1. Laboratory trials for full face Frankfurt Clay at Güterplatz

The Güterplatz area and the final drive towards the existing tunnel is characterized by full face Frankfurt Clay as shown in Fig. 8.

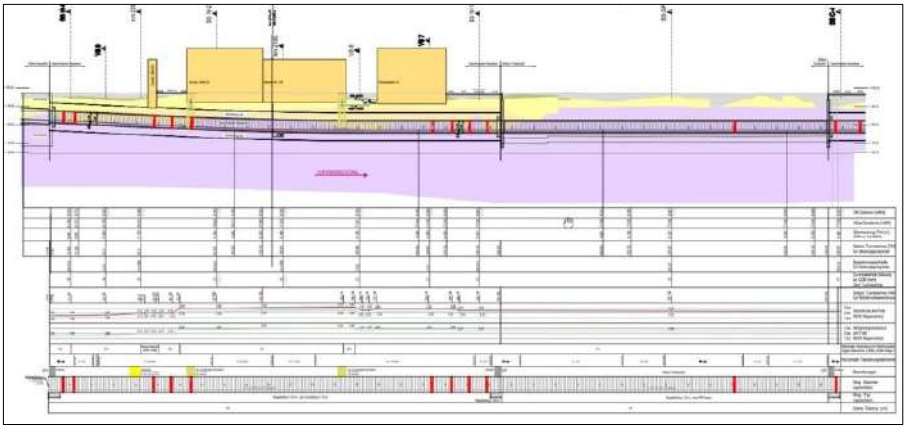

Fig. 8. Frankfurt Clay at Güterplatz, freshly hand-excavated.

Fig. 9. Frankfurt Clay at Güterplatz, freshly hand-excavated

Atterberg Limits of Frankfurt Clay (according to DIN 18122; samples taken from d-walls Bldv. Ost 2017 and Güterplatz 2020):

- Natural humidity Güterplatz : 34-45%, approx. weighted average 35-39%
- Plastic Limit (wP) : 25-56%, approx. weighted average 27-39%
- Liquid Limit (wL) : 74-108%, approx. weighted average 74-91%

The Atterberg Limits indicate a quite high clogging risk for this type of geology. In consequence, the aim of the soil conditioning is to reduce the clogging risk in general, particularly keeping the cutterhead openings free, allow the muck flow through the cutterhead into the working chamber and allow a consistent TBM advance speed.

To achieve these goals, the anti-clay soil conditioning foam MC-Montan Drive FL04 was used in a higher concentration and higher FIR than necessary for soil 4b, also the addition of water was found to be beneficial.

Again, the tasks of the laboratory tests are to find the correct starting parameters for the TBM. Once the clay clogging occurs on the cutterhead and in the working chamber, it can in most cases only be cleaned by intervention. Therefore, the TBM startup should be realized with an exceeding soil conditioning avoiding any kind of problem.

Proposal for TBM parameters after laboratory test results with MC-Montan Drive FL04:

- cF 2-4%
- FER 10
- FIR 80-120 → approx 150l/ring of foam concentration
- WIR 5-7% → approx 4.8-6.5m^3/ring additional water

4.2. Jobsite soil conditioning results

Since the Frankfurt Clay is the predominant geology, the following site examples are taken from the Güterbahnhof section, the TBM advancing full face in Frankfurt Clay.

Because the TBM is operating in semi-automatic mode, the laboratory soil conditioning results from chapter 4.1 need to be translated into flow rates for 2 different TBM target speeds.

Quantity range in l/min at 20 mm/min TBM speed

Foam	Water from the foam	Additional water	Foam FL 04
800-964	76-92	68	3,2-4,3

Quantity range in l/min at 25 mm/min TBM speed

Foam	Water from the foam	Additional water	Foam FL 04
1.005-1.205	96-115	85	4,0-5,4

The following Figures 10 and 11 illustrate the Foam and Water consumption of the TBM starting out of the Güterplatz Station over 100 rings and puts them in relation to the TBM speed.

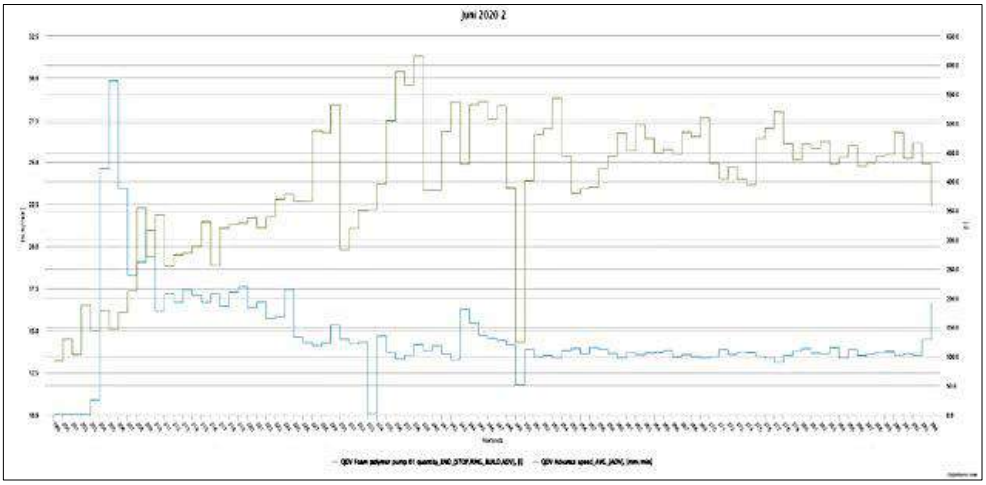

Fig. 10. TBM speed (green, mm/min) vs Foam consumption (blue, l/ring) Ring No. 199-294.

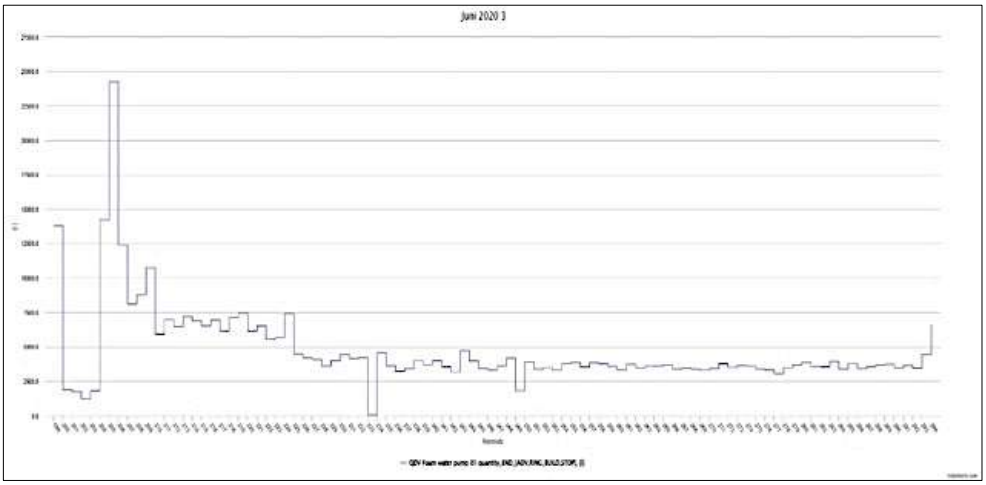

Fig. 11. Water addition (liters / ring), Ring No. 199-294.

On site optimization of the soil conditioning parameters result in speeding up the TBM to 20-22,5 mm/min and reducing the soil conditioner quantity by optimizing its efficiency. After some 20 rings, the TBM speed was subsequently increased to 25-30mm/min since the machine was running fine, reducing simultaneously the soil conditioner use from 200 l/Ring to 100-150 l/Ring.

The findings from the laboratory testing were confirmed and the TBM was driving steadily with excellent advance rates without any problem.

The TBM steady speed of 25-30 mm/min in Frankfurt Clay could be easily maintained even with TBM crown pressures of around 2 bar. Also the pressure level itself could be easily maintained, no air bubble in the crown level could be detected. The water injection was initially set to 6m^3 per Ring to start on the safe side. It could be further reduced due to the smooth TBM operation to around 4m^3 per Ring, the lower end of the laboratory findings (see Fig. 11).

Fig. 12. Conditioned Frankfurt Clay at station surface, June 2020.

The soil could be easily excavated and transported by muck cars, the muck car emptying process was without any difficulties. The further manipulation with excavators and truck loading, truck transport and transfer to barge carriers was smooth and without any problems (see Fig. 12).

4.3. Muck analysis

For environmental and disposal reasons, the excavated and conditioned muck underwent a environmental screening process. The test results given in Fig. 13 describe the effects of the soil conditioning, comparing values for the unconditioned soil with conditioned soil after 1 day as well as 4 days.

Soil conditioning parameters used for the following muck analysis:

MC-Montan Drive FL 04, cF=2.5%, FER=10, FIR=80, WIR=6.5%

Parameter	Einheit	Gehalt (bezogen auf die Trockensubstanz)					
		Null-1	Null-2	1d-1	1d-2	4d-1	4d-2
Arsen	mg/kg	33	31,2	23,7	21	29,7	26,3
Blei		20	21	18	17	21,0	21,0
Cadmium		< 0,2	< 0,2	< 0,2	< 0,2	< 0,2	< 0,2
Chrom (gesamt)		53	56	47	52	50	51
Kupfer		24	25	22	22	24	24
Nickel		49	50	45	43	46	47
Thallium		0,4	0,4	0,3	0,4	0,4	0,4
Quecksilber		< 0,07	0,08	0,07	< 0,07	< 0,07	0,07
Zink		77	76	68	67	73	75
TOC	M.-%	8,9	5,57	8,29	8,6	8,09	8,75
EOX	mg/kg	< 1	< 1	< 1	< 1	-	-
Kohlenwasserstoffe C_{10} - C_{22}		< 40	< 40	< 40	< 40	< 40	< 40
Kohlenwasserstoffe C_{10} - C_{40}		< 40	< 40	< 40	< 40	< 40	< 40

Parameter	Einheit	Gehalt (bezogen auf die Trockensubstanz)					
		Null-1	Null-2	1d-1	1d-2	4d-1	4d-2
pH-Wert [1]	-	7,99	7,79	8,2	7,66	7,55	7,54
Leitfähigkeit	µS/cm	443	592	510	583	842	795
Natrium	mg/L	36,0	23,0	83,0	84,0	117,0	95,0
Kalium		20,0	22,0	19,0	26,0	26,0	22,0
Calcium		15,4	21,4	19,4	20,4	43,0	25,9
Chlorid [2]		19,3	17,8	17,9	18,6	22,2	18,8
Sulfat [2]		102	146,7	120,8	128	311	200
Fluorid		0,4	0,3	0,5	0,4	0,4	< 0,1
Cyanide [3]		5	3	2	5	5	5
Arsen	µg/L	2	3	3	2	2	2
Blei		< 1	< 1	< 1	< 1	< 1	< 1
Cadmium		< 0,3	< 0,3	< 0,3	< 0,3	< 0,3	< 0,3
Chrom (gesamt)		< 1	< 1	< 1	< 1	< 1	< 1
Kupfer		< 5	< 5	< 5	< 5	< 5	< 5
Nickel		2	2	2	3	2	2
Thallium		< 0,2	< 0,2	< 0,2	< 0,2	< 0,2	< 0,2
Quecksilber		< 0,2	< 0,2	< 0,2	< 0,2	< 0,2	< 0,2
Zink		30	80	< 10	< 10	< 10	20

Fig. 13. (left) Solid content test results (excerpt) of conditioned Frankfurt Clay; (right) Eluate test results (excerpt).

None of the results show a significant change due to the soil conditioning, no metals were mobilized and even the TOC in the solid content test did not change really.

The Eluate results show only an increased Na content due to the soil conditioner used. The Sulfate values vary a lot even in the untreated soil, an indicator for geogenic soil contamination (see also chapter 5. annulus grout). The conductivity results are influenced accordingly.

5. 2-k Annulus Grout

For the first time in in a German inner city project, 2k annulus grout has been used.

5.1. Requirements & Formulation

The concerns on durability, lifetime and on ecologic aspects were high. Therefore, a sulfate resistant CEM III has been used for the annulus grout.

Formulation

Cement (CEM III/A 52,5N-HS/NA)	200 kg/m^3
Bentonite	40 kg/m^3
Water	883 kg/m^3
Plasticizer Grout 02	10 kg/m^3
Accelerator	103 kg/m^3
Gel time:	10-15 sec
Bleeding:	< 3% after 24h
Shear strength:	2h:98 kPa*s; 4h: 120 kPa*s; 6h: 185 kPa*s
Compr. strength:	24h: 1.5 N/mm^2; 7d: 1.8 N/mm^2; 28d: 3.1 N/mm^2

5.2. Ultrasonic fault detection

Various tests were carried out to check if the annular gap was completely filled with 2-component grout. Because of the high groundwater pressure and in order not to damage the segments, the use of control drillings was minimized.

An ultrasonic measuring device was used as an equivalent measuring method. This device was calibrated before each measurement on a sample segment (width 1.2m, thickness 0.45m). It was taken 3 measurements per ring and on over 150 rings per tube.

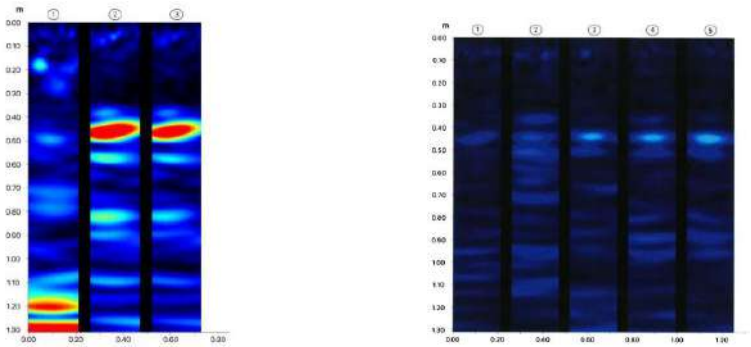

Fig. 14. (left) Ultrasonic reference measurement; (right) Ultrasonic site measurement of ring No. 80.

The reference measurement in Fig. 14 left shows well the segment concrete material (dark area from 0-0.45m), the gap (red area at around 0.45m) as well as the different material from 0.50m onwards. The site measurement of ring No. 80 (Fig. 14 right) indicates well again presence of the 3 different materials (segment, annulus grout, soil) without detection of any gap area which would be colored in red.

6. Tail Sealants

The U5 extension project used the highly ecologic MC-Montan Seal ST11 tail sealant, based on renewable oils and exempt of plastic fibers to protect the environment as best as possible.

Furthermore, HDT 200 T press plate pumps were plug and play installed on the gantry to ensure an almost revision free pumping (see Fig. 15). For the whole project, the sealing sets had to be replaced only once for the total of the 2 drives.

Fig. 15. HDT 200 T press plate pump installed on Herrenknecht gantry.

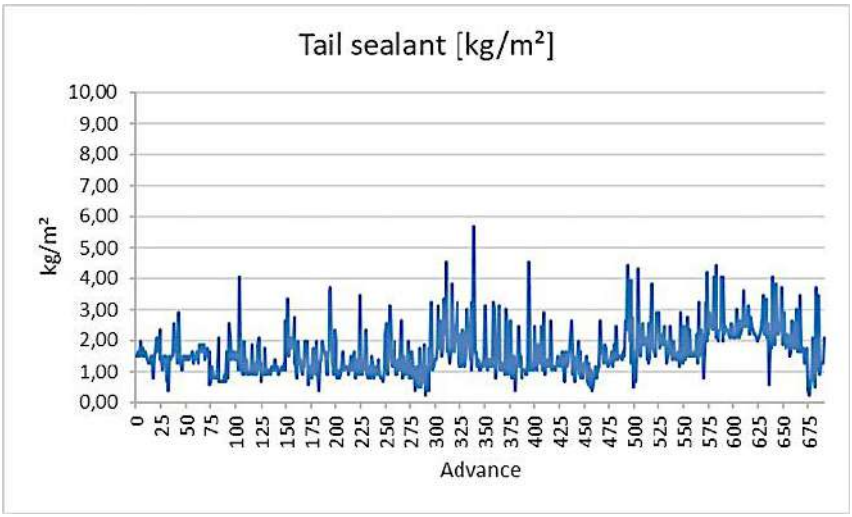

Fig. 16. Tail Sealant consumption in kg/m2 over the project rings.

The ST11 tail sealant worked very well with prefect consumptions rates (see Fig. 16) compared to the industry benchmark – despite relatively high EPB pressures and relatively liquid 2k annulus grout used. Over the whole project, the medium consumption reached 1.6 kg/m^2 segment surface.

7. Conclusion

The flying EPB start with artificial soil was as easy as efficient. It has been successfully repeated already at other jobsites.

The laboratory soil conditioning proposal with respect to the TBM parameters gave perfect and safe starting conditions for each main geology, avoiding clogging from the beginning. Only small scale-up adaption was realized on site – reducing the proposed foam and water consumption. The decision to drive the TBM with a steady speed especially within the clay section was definitely the right one, cutterhead and working chamber blockage was very successfully avoided even under high EPB pressures throughout the whole project by using adapted anti-clay foam. That illustrates quite well that detailed laboratory testing prior to the project execution saves time and money and also increases significantly the safety of tunneling.

The used 2k grout worked perfectly in inner-city conditions, the use of sulfate resistant cement – which has never been used before for such a project - did not lead to any difficulties.

The tail sealant pumps worked well under all conditions with just 1 service; and the highly ecologic tail sealant was as efficient as the industry standard, with bonus points for using renewable raw materials and easy acceptance from the authorities – similar than for the soil conditioning chemicals.

Acknowledgements

The author wants to express his thanks to the excellent cooperation, support and trust of Ronny Iffländer and Tillman Schade as well as Dirk Uhlmann for the great laboratory work.

References

Budach, C., Thewes, M., 2015. Application ranges of EPB shields in coarse ground based on laboratory research. *Tunn Undergr Sp Tech,* 50, 296–304. https://doi.org/10.1016/j.tust.2015.08.006

Bäppler, K., Burger, W., 2016. Innovation track of multi-mode machines for complex ground conditions. In Proceedings of the Swiss Tunnel Congress 2016; 2016 Jun 15-16; Luzern, Switzerland. p. 122–9.

EFNARC, 2005 Apr. *Specification and guidelines for the use of specialist products for mechanised tunnelling (TBM) in soft ground and hard rock.* Surry, UK: European Federation for Specialist Construction Chemicals and Concrete Systems; [M8]

Egli, H., Langmaack, L., 2008. Erddruckgestützter Schildvortrieb—Chancen und Risiken. *Felsbau Magazin*, 3:149–154. German.

Galli, M., Thewes, M., 2014. Investigations for the application of EPB shields in difficult grounds (Untersuchungen für den Einsatz von Erddruckschilden in schwierigem Baugrund). *Geomech Tunnelling*, 7(1):31-44. https://doi.org/10.1002/geot.201310030

Guglielmetti, V., Grasso, P., Mathab, A., Xu S., 2007. *Mechanized tunnelling in urban areas: Design methodology and construction control*. The Netherlands: Taylor and Francis/Balkema.

Häfliger, Ph., 2013. Choice of driving methods in soft ground. Biel East Bypass. In Proceedings of the Swiss Tunnel Congress, 2013, Luzern, pp. 178-201. [M2]

Herrenknecht, M., Thewes, M., Budach, C., 2011. Entwicklung der Erddruckschilde: Von den Anfängen bis zur Gegenwart. *Geomech Tunnelling*, 4(1):11–35. German.

Jancsecz, S., Steiner ,W., 1994. Face support for a large Mix-Shield in heterogeneous ground conditions. In Proceedings of Tunnelling '94, 1994 Jul 5-7, London, UK. Springer, Boston, MA, 1994. p. 531–50.

Jancsecz, S., Krause, R., Langmaack, L., 1999. Advantages of soil Conditioning in shield tunneling: Experiences of LRTS Izmir. ITA 1999 Oslo, p. 865 ff., Balkema. ISBN 90 5809 063 9

Jefferis, S.A., Merritt, A.S., 2013. Exploiting physic-chemical modification of soils in closed face tunneling. In *Coupled phenomena in environmental geotechnics*; Manassero M, Dominijanni A, Foti S, Musso G, editors. London: CRC Press/Balkema; 2013. [M4]

Krause, T., 1987. *Schildvortrieb mit flüssigkeits- und erddruckgestützter Ortsbrust*. Mitteilung des Instituts für Grundbau und Bodenmechanik, Heft 24, TU Braunschweig. [M3]

Langmaack, L., 2000. Advanced Technology of Soil Conditioning. North American Tunnelling Congress, Boston 2000, A.A. Balkema, Rotterdam, Brookfield, p. 525, ISBN 90 5809 162 7

Langmaack, L., 2001. Application of new TBM Additives. BAUMA 2001, 6th int. symposium for tunnel construction, Verlag Glückauf GmbH, Essen, p. 27, ISBN 3 7739 5964 8

Langmaack, L., 2004. EPB-Vortrieb in inhomogenen Böden: Möglichkeiten neuer Konditionierungsmittel. Tunnel- und Tiefbautagung, Györ, p. 121 ff

Langmaack, L., 2009. Chemische Additive für den maschinellen Tunnelvortrieb. Proceedings of the Swiss Tunnel Congress 2009; 2009 Jun 17-18; Luzern, Switzerland; p. 197–208.

Maidl, B., Herrenknecht, M., Maidl, U., Wehrmeyer, G., 2012. *Mechanised shield tunneling*. 2nd ed. Berlin: Ernst & Sohn.

Marchionni, et al., 2002. *Galleria Quattro Venti in Rome.* Tunnel No.8, p. 8 ff

Merritt, A.S., Mair, R.J., 2008. Mechanics of tunnelling machine screw conveyors: A theoretical model. *Géotechnique,* 58(2):79–94. https://doi.org/10.1680/geot.2008.58.2.79

Milligan, G.W.E., 2000. *Lubrication and soil conditioning in tunnelling, pipe jacking and microtunnelling: A state-of-the-art review*. London, UK: Geotechnical Consulting Group.

Peila, D., Oggeri, C., Borio, L., 2008. Influence of Granulometry, time and temperature on soil conditioning for EPBS applications. In Proceedings World Tunnel Congress 2008; 2008 Sep 22-24; Agra, India. New Dehli: Aravali Printers & Publishers; p. 881–91.

Rehm, 2004. Maschineller Tunnelvortrieb unter sehr schwierigen geologischen Verhältnissen. Tunnel- und Tiefbautagung, Györ, p. 99 ff

Thewes, M., Hollmann, F., 2016. Assessment of clay soils and clay-rich rock for clogging of TBMs. *Tunn Undergr Sp Tech*, 57:122–128. https://doi.org/10.1016/j.tust.2016.01.010

Vinai, R., Oggeri, C., Peila, D., 2008. Soil conditioning of sand for EPB applications: A laboratory research. *Tunn Undergr Sp Tech*, 23(3):308–17. https://doi.org/10.1016/j.tust.2007.04.010

Yu, H., Mooney, M.A., Bezuijen, A., 2017. A simplified chamber pressure model for EPB TBM tunneling in granular soil. In Proceedings of 9th International Symposium on Geotechnical Aspects of Underground Construction in Soft Ground; 2017 Apr 4-5; Sao Paulo, Brazil. [M5]

Zumsteg, R., Puzrin, A.M., Anangnostou, G., 2016. Effects of slurry on stickiness of excavated clays and clogging of equipment in fluid supported excavations. *Tunn Undergr Sp Tech,* 58:197–208. https://doi.org/10.1016/j.tust.2016.05.006

Zumsteg, R., Plötze, M., Puzrin, A.M., 2013. Reduction of clogging potential of clays: New chemical applications and novel quantification approaches. *Géotechnique*, 63(4):276–86. https://doi.org/10.1680/geot.SIP13.P.005

SETC-2025
BELGRADE

TOPIC 4

NUMERICAL MODELLING

Southeastern Europe Tunnelling Conference (SETC-2025)
1-3 October 2025, Belgrade, Serbia

DOI: 10.5937/SETC25021D

Modeling of ground support at Kokhav Hayarden Pumped Storage

Branko Damjanac[a], Ehsan Ghazvinian[a] and Zorica Radakovic-Guzina[a]*

[a] ITASCA, Minneapolis, USA; branko@oneitasca.com, eghazvinian@oneitasca.com, zorica@oneitasca.com

Abstract: The stability of the north walls of the Kokhav Hayarden Pumped Storage Plant powerhouse (PH) and transformer hall (TH) caverns was numerically analyzed. To achieve a calibrated model, this study includes a back-analysis of the displacements recorded by the extensometers in the north walls of the PH and TH caverns, as well as the recorded forces for the instrumented tendons and bar anchors in the same walls throughout the excavation of the caverns. The calibrated model is then used to assess the overall safety margin of the caverns' north wall. The factor of safety (FoS), determined by reducing strength parameters of different geological units, was selected as a simple and reasonable measure of the safety margin to failure. The analyses in these studies were conducted using three-dimensional models in the continuum code FLAC3D, a computationally efficient, state-of-the-art numerical code for modeling the deformation and damage of geo-materials. A few relevant discontinuities are explicitly represented in the model. The model was calibrated for the cavern designs in terms of wall geometry, ground support, and geological information by comparing with the monitoring data (extensometers, prisms, and stress cells) at different locations and throughout the entire excavation history, including the final state of the excavation. In addition to deformation and stability of the excavated caverns, the model predicts the loading (forces) in the ground support (tendons and bar anchors), which is explicitly represented as installed during excavation. The FoS of the north walls of the caverns after complete excavation is greater than 1.5. The forces in five of the tendons and bar anchors in the PH are predicted in the model to slightly exceed their allowable working limit in the final stage of excavation, which is not a concern because the current force measurements for all tendons and bar anchors are within the allowable working limits.

Keywords: pumped storage; powerhouse; excavation stability; tendons; bar anchors; numerical modeling

1. Introduction

Kokhav Hayarden (Fig. 1), Israel's largest pumped storage power project, officially began commercial operation on February 21, 2025. Located near the northern Israeli city of Beit She'an, the facility is the lowest-altitude power plant of its kind in the world. The station features an upper reservoir, a water conveyance system, an underground powerhouse (PH), a lower reservoir, and a central building/switchyard. At its core, the underground powerhouse houses two 172-MW reversible hydroelectric generating units, contributing to a total installed capacity of 344 MW. These units play a vital role in enhancing the security and stability of Israel's power grid. The reservoirs have a total capacity of 3.16 million m^3. During peak demand hours, the station will generate electricity by discharging water from the upper reservoir to the lower one and accumulating it by pumping water back into the upper reservoir. The capacity of the new pumped storage power plant will exceed that of the existing hydroelectric power plants in Israel, increasing from the current 306 MW to 650 MW. Solar panels are the primary source of "clean" energy in the country, with their capacity reaching 2.6 GW in 2021.

The PH was excavated in benches, starting with Bench I in the crown. An apparent non-convergent movement was observed for the north wall of the PH after excavation of Bench II exposed the pyroclastic layer on that wall. Installing four pre-tensioned tendons reduced the movement rate, and the wall stabilized further with the installation of an additional three pre-tensioned tendons. After the

*Corresponding author: branko@oneitasca.com (B. Damjanac).

excavation of Bench III was completed, all monitoring data indicated that the north wall had been stabilized.

Fig. 1. An aerial photo of the lower reservoir of Kokhav Hayarden pumped storage power plant.

As the excavations of the PH and adjacent Transformer Hall (TH) continued, the ground support and stability of the excavations were analyzed using a continuously calibrated numerical model. After the excavation of the PH and TH was completed, the monitoring data indicated that the north walls remained stable. The calibrated model was then used to assess the overall safety margin of the north walls of the PH and TH caverns. The factor of safety (FoS), determined by reducing strength parameters of different geological units, was selected as a simple and reasonable measure of the safety margin to failure of the north walls of the caverns. To achieve a calibrated model, this study includes a back-analysis of the displacements recorded by the extensometers in the north walls of the PH and TH caverns, as well as the recorded forces for the instrumented tendons and bar anchors in the same walls throughout the excavation of the PH and TH caverns. Thus, the model is calibrated using all available readings at the end of the excavation, including the tendon and bar anchor forces, as well as displacement information for the north walls. Expansion of the calibration database is crucial for increasing confidence in the calibrated model for FoS assessment.

Hoek (2013) discusses several examples of PH cavern stability and support analyses. The innovative methods for numerical modeling of cavern stability, including efficient and automatic model calibration and sensitivity analyses, are, for example, published by Behnia and Seifabad (2018), Ghorbani and Sharifzadeh (2009), Li et al. (2022), Li et al. (2025), and Zhu et al. (2010). The numerical code FLAC3D (ITASCA, 2019) was used in this study. The preliminary analyses have shown that potential failure mechanisms include failure through the rock mass and sliding on pre-existing structures. A few relevant discontinuities are explicitly represented in the model.

This paper describes the model construction and calibration, as well as input properties used for the numerical analysis, and it provides a summary of the modeling results.

2. Methodology and Model Description

2.1. Model Geometry and Initial Conditions

The three-dimensional model includes the PH and TH caverns as well as the connecting Busbar tunnel between them. The model geometry is shown in Fig. 2. The PH cavern is 82.2 m long, 43 m high, and has a span of 18 m. The cavern axes (y-axis) have orientation N30˚W. Fig. 2 also depicts the lithologies that are explicitly represented in the model. Fault F16, the influence zone of Fault F16—including basalt

(bs)-weak Class V (very degraded) material and bs-weak material (above the pyroclastic layer)—as well as the weak pyroclastic layer (Pyr9), are explicitly simulated as zones of finite thickness. Compared to Fault F16, Faults F18 and F22 have a smaller thickness and are not part of the failure mechanism observed in the north wall. Therefore, they are modeled as explicit, discrete features using interfaces (i.e., elements with zero thickness). The preliminary analyses indicate that including a finite thickness for Fault F16 in the model improves the match of the failure mechanism. Ubiquitous joints (i.e., closely spaced fractures) are assumed in the vicinity of the north walls of the PH and TH, where plastic deformation was expected.

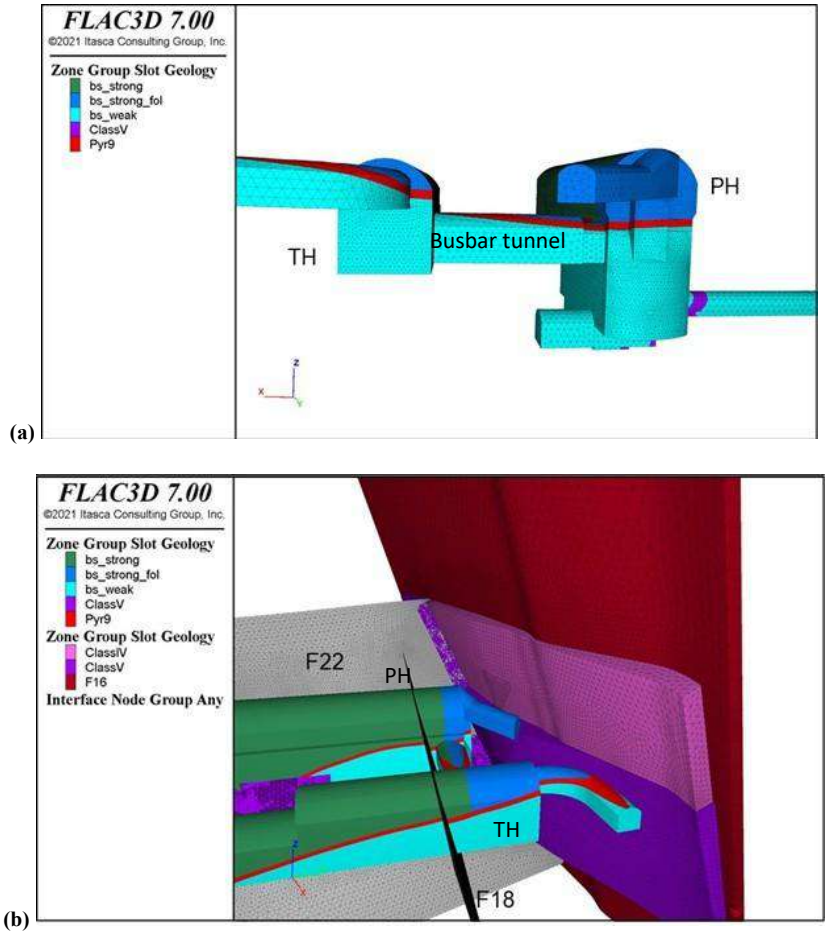

Fig. 2. (a) Lithologies intersecting the north wall of the PH and TH. (b) Model representation of fault F16, bs-weak Class V material and bs-weak Class IV material (above the pyroclastic layer) in the vicinity of the north wall of the PH and TH.

The in-situ stresses were initialized in the model based on the field measurements. The vertical stress at the PH depth was initialized to 10 MPa (for an approximate depth of 400 m). K_H and K_h of 1.5 and 0.7 were assumed, respectively, with σ_H oriented at N11°W.

The excavation stages are shown in Fig. 3. Note that the excavation of the Busbar tunnel is completed concurrently with the excavation of Bench II and the completion of the excavation of the TH.

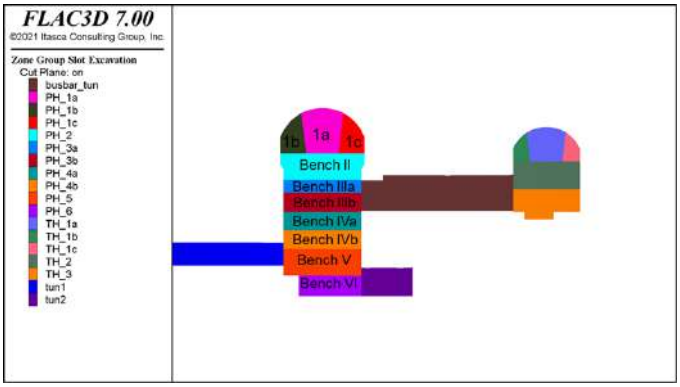

Fig. 3. Excavation stages of the PH.

2.2. Calibrated Rock Mass Properties

The joint set with dip/dip direction of 83°/335°, believed to be the most critical joint set contributing to the wall movement, is represented as ubiquitous joints in the model. The other two joint sets are implicitly represented in the rock mass model, contributing to the calibrated rock mass properties. The volume of the rock mass encompassing the northern section of the caverns (shown in dark blue in Fig. 2) is represented with the SUBI constitutive model, which combines the ubiquitous joints and strain-softening behavior for the rock mass.

The calibrated properties using the observations and monitoring data from the north walls of the caverns are listed in Table 1. The interface properties for F18 and F22 are summarized in Table 2.

Table 1. Rock Mass Properties

Lithology	Constitutive model	E [GPa]	v	UCS [MPa]	Cohesion (residual) [MPa]	Friction angle (residual) [°]	Tensile strength (residual) [MPa]	Critical strain	Dilation angle (residual) [°]
Basalt strong	Strain softening	11.25	0.25	13.7	2.7 (0.1)	47 (47)	0.06 (0.06)	0.03 *[0.014]*	5 (5)
Basalt strong with UB	Subi	11.25	0.25	-	2.7 (0.1) UB: 0.45 (0.05)	47 (47) UB: 31 (31)	0.06 (0.06) UB: 0.0 (0.0)	0.03 *[0.014]* UB: 0.03 *[0.014]*	5 (5) UB: 5 (5)
Basalt weak	Strain softening	7.1	0.25	9.0	2.05 (0.1)	41 (41)	0.03 (0.03)	0.03 *[0.014]*	5 (5)
Faults	Mohr-Coulomb	1.8	0.25	0.3	0.1 (0.1)	23 (23)	0 (0)	-	5 (5)
Pyroclas.	Mohr-Coulomb	1.2	0.25	2.0	0.7 (0.7)	20 (20)	0 (0)	-	5 (5)
Basalt Class V	Mohr-Coulomb	0.97	0.25	2.3	0.76 (0.76)	23 (23)	0 (0)	-	5 (5)

Table 2. Properties Used for F18 and F22 Faults

Contact	Constitutive model	Kn [GPa/m]	Ks [GPa/m]	Cohesion (residual) [MPa]	Friction angle (residual) [°]	Tensile strength (residual) [MPa]
F18 and F22	Coulomb slip	15.0	7.5	0.1 (0)	23 (23)	0 (0)

The strain-softening response is assumed only for the cohesive component of rock mass strengths. The friction angle is assumed to remain constant irrespective of plastic deformation. This is an assumption frequently used in modeling and seems logical from a mechanistic perspective. The damage and plastic deformation create fractures, degrading the cohesive strength of the rock. At the same time, friction is a property of surface contacts and their roughness, and it would not typically decrease with deformation. The discussion of rock mass post-peak behavior and strength softening, including justification of the non-softening frictional behavior, is provided in several publications, such as Kaiser (2019) and Lorig et al. (2020). In any case, the assumption of non-softening friction does not mean that the model is non-conservative, because the model (with constant friction angle, independent of the shear strain and plastic deformation) is calibrated with actual field data and observations.

The calibrated model was able to match the following field observations:

- PH north wall extensometer data.
- Measured forces in the tendons and bar anchors in the north wall throughout the excavation of the PH (this inherently also means matching the wall displacement magnitude).
- The overall deformation of the north wall of the TH.

These comparisons, performed as part of the calibration effort, are discussed in Section 3.

2.3. Ground Support

The typical ground support in the cross-section is shown in Fig. 5(a). The ground support (tendons and bar anchors) designed for the north walls of the PH and TH, in addition to the shotcrete and rock bolts, was installed in the model following the excavation and installation sequences of the caverns.

The additional ground support includes the following:

1. Seven initial tendons (or strand anchors) installed to stop the non-convergent movement that was observed for the north wall after excavation of Bench II. The collar locations of the tendons on the north wall, as represented in the model, are shown in Fig. 4. The tendons are pre-tensioned.
2. Bar anchors that were installed before excavation of Bench III-1, most of which were pretensioned and instrumented with load cells.
3. Additional ground support designed to provide the necessary stability of the north wall and to prevent excessive loads in the previously installed tendons and bar anchors.

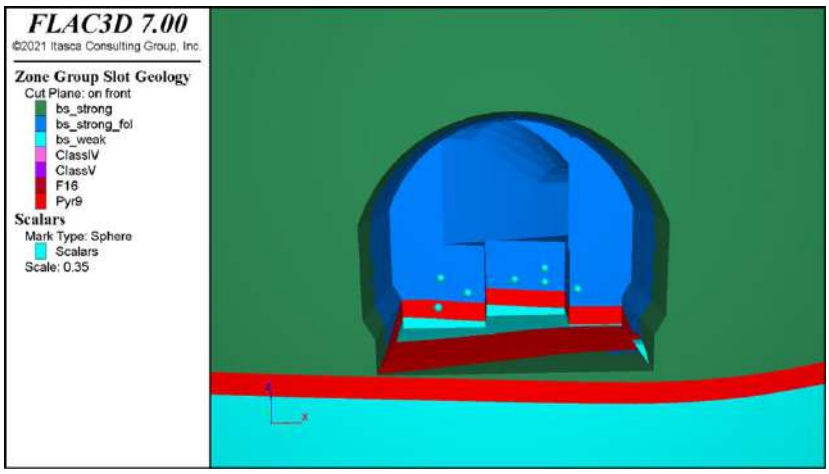

Fig. 4. Collar location of the seven initial tendons in the north wall of the PH.

Fig. 5(b) shows a layout of all the tendons and bar anchors in the north wall of the PH, sidewall, and floor of the adit tunnel in the crown of the PH, installed in addition to the shotcrete and rock bolts at various stages of excavation.

The analysis of the north walls of the PH and the TH includes tendons and bar anchors as the only ground support. Other types of ground support, such as bolts and shotcrete, which do not significantly affect global stability, are not explicitly represented in the model. This approximation is also conservative.

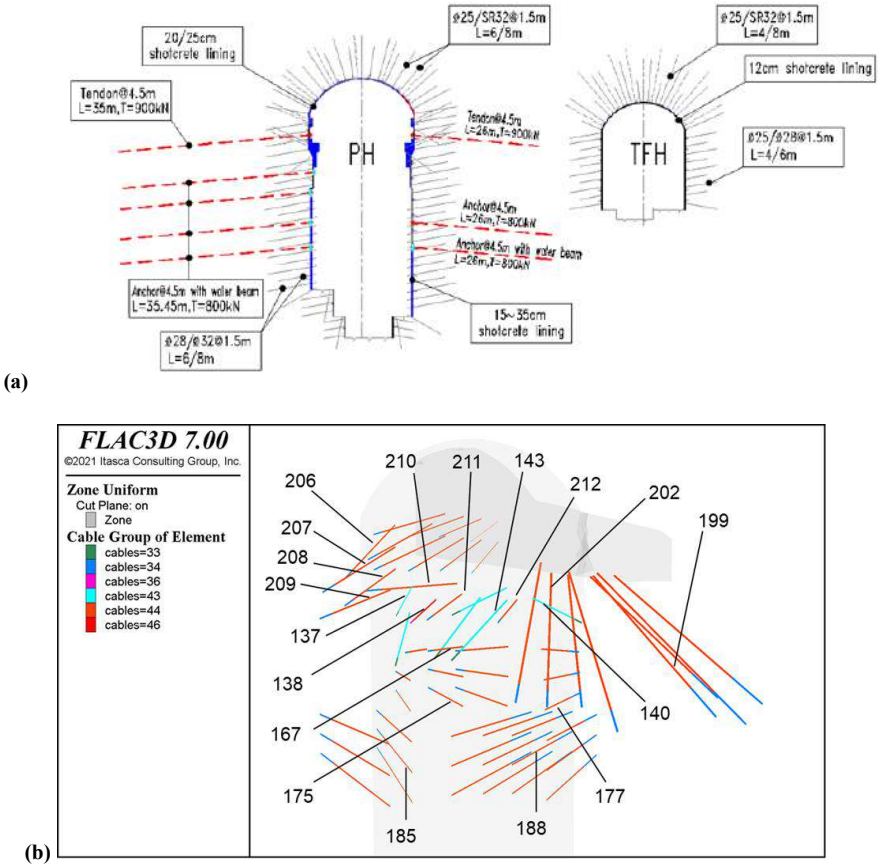

Fig. 5. (a) Typical ground support of PH and TH caverns. (b) Layout of the tendons and bar anchors in the north wall of the PH, sidewall, and floor of adit PT1. (The cable element is used to represent both tendons and anchor bars in the model. Colors indicate cable material number, and numbers indicate cable ID for instrumented cables).

In the current model, the tendons and bar anchors behave elastically at forces below their ultimate force capacity, with a subsequent drop to their residual force capacity upon further straining. After softening to residual force, the cables behave as perfectly plastic until reaching the ultimate deformation limit. In the absence of any information regarding the post-failure softening rate for the cables, a brittle response is conservatively considered for the transition from ultimate force capacity to residual force.

Based on the pull-out test in the field, the ultimate force capacity of the tendons was set as 1800 kN in the models, similar to the axial force capacity of the bar anchors. The residual force capacity of the

tendons and bar anchors is set to 750 kN. The allowable working force is 900 kN in the tendons and 800 kN in the bar anchors.

3. Model Calibration

Estimation of some rock mass properties (i.e., model input data), including dilation angle, residual friction angle, and critical strain, with limited laboratory and field data and field observations is challenging. Experience and engineering judgment are part of the model calibration procedure. It should be noted that the solution to the calibration process is usually not unique. Multiple sets of properties can potentially satisfy the calibration criteria.

3.1. Extensometer Data from the North Wall of the PH

The displacements measured by the three extensometers installed on the north wall of the PH are shown in Fig. 6. The most important observation from these plots is that the north wall is equilibrated after installation of seven tendons. The depths of the moving ground inferred from the extensometer data are similar to what the model predicts for the same locations (see Fig. 7), which increases confidence in the calibrated model. Note that the goal of the calibration effort was not to exactly match the displacements in the model with those measured by the field extensometers but rather to capture the correct displacement trend and depth of movement in the model.

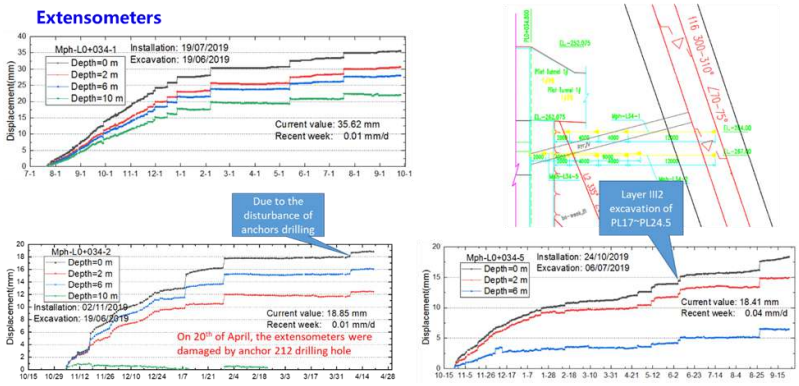

Fig. 6. Displacement data from the extensometers in the north wall of the PH.

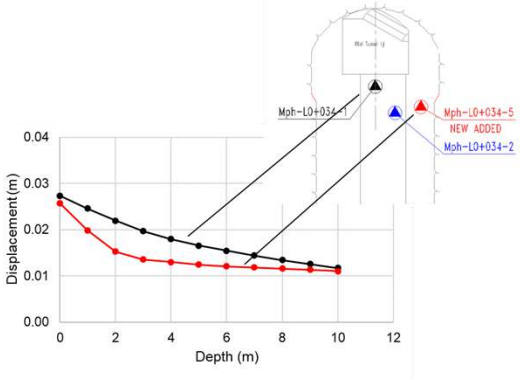

Fig. 7. Displacement data from the numerical model at approximate locations of extensometers in the north wall of the PH after excavation of Bench II.

The exact magnitude of displacements measured in the field can differ from those estimated by the model for a multitude of reasons, such as:

- Inability to replicate the exact installation time of the extensometers in the model. The displacements in the model were zeroed after excavation of Bench I; therefore, the displacements reported in Fig. 7 are the model response to excavation of Bench II.
- The extensometers are measuring the displacement of different sections along the hole relative to their anchor points. In contrast, in the model, the absolute values of deformation at different depths in the north wall are reported.

3.2. Load Cell Data

The calculated forces for all tendons and bar anchors in the north wall after complete excavation of the PH are listed in Table 3 and compared to the measured forces at the site (for instrumented tendons and bar anchors). In general, it is observed that the forces calculated by the numerical model are in good agreement with the load cell data. The forces in five (137, 140, 142, 143, and 210) of the tendons and bar anchors in the PH are predicted in the model to slightly exceed their allowable working limit in the final stage of excavation.

Table 3. Comparison of Forces (t) Measured in the Field and Calculated by the Calibrated Model for Tendons and Bar Anchors after Complete Excavation of the PH.

ID #	Measured	Simulated	ID #	Measured	Simulated
137	83	103	197	21	16
138	28	75	199	31	31
140	75	92	202	36	39
142	58	89	206	30	14
143	62	84	207	21	18
167	21	54	208	39	34
175	19	36	209	34	53
177	28	30	210	78	91
185	24	20	211	31	56
188	26	18	212	24	50
190	24	17			

4. Factor of Safety Analyses

Once the model was calibrated to the monitoring data and other field observations, it was used to demonstrate that the north walls of the PH and TH have sufficient overall FoS with respect to a major failure. For permanent excavations, the FoS should be equal to or greater than 1.5.

The FoS analysis was performed by applying the Strength Reduction Factor (SRF) method to both the rock mass and the strength properties of the faults. It was found that reducing the friction angle of the faults, Class V, and the pyroclastic layer below their nominal values as listed in Table 1 caused them to yield under in-situ stress conditions (far from the excavation), which suggests that either the estimated in-situ stress or the properties of those materials as represented in the model are too conservative. It is most likely that the friction angles of 20–23° for those units are underestimated. Therefore, in the FoS analysis, the SRF is not applied to the friction angle of the materials mentioned

above because it is physically inconsistent that rock mass yields under in-situ equilibrium stress conditions.

In the FoS calculations, the response of ground support, including tendons and bar anchors, is represented by a realistic force-displacement curve, including the ultimate force and rupture strain or pull-out displacement (when the support can be assumed to carry no load). During FoS calculations, limiting the response of the ground support to a linearly elastic range would be too conservative because that would result in application of FoS twice, i.e., to the response of the ground support and to the overall response of the supported excavation.

A maximum axial displacement criterion of 0.4 m was used to eliminate the cables from the model based on in-situ pull-out tests. The 0.4 m axial displacement threshold accounts for a minimum of 0.1 m elastic deformation in the unbonded portion of the support at its ultimate force capacity and 0.3 m plastic deformation combined in the unbonded steel and grouted portion of the cable (elastic deformation in the grouted length of the cable is conservatively disregarded). This value is a conservative approximation of the overall cable displacement limit before its load-bearing capacity is drastically reduced based on full-scale pull-out tests performed on anchors ranging between 14 m to 29 m in length with 4 m bonded length (Liu et al., 2017). The bonded sections of the anchors studied by Liu et al. (2017) sustained 0.3–0.4 m of movement, while in this study, and conservatively, the elongation of the cables at their head/collar is limited to 0.4 m (which means smaller movements at their bonded portions). A schematic representation of tendon/bar anchor behavior in the model is shown in Fig. 8. (The representation was selected as a good approximation of the field data and as recommended by Liu et al. (2017).) During the pull-out test, tendon #138 was pulled 10 cm at a constant peak force of 1900 kN without rupture.

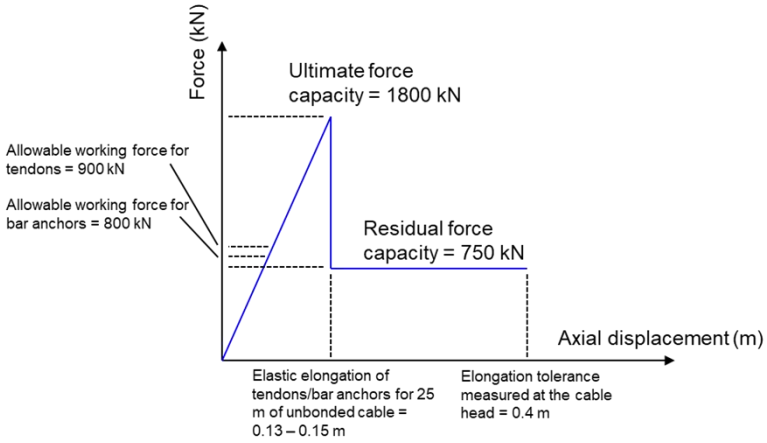

Fig. 8. A schematic representation of tendon/bar anchor behavior in the model.

For FoS analysis, a strength reduction factor (SRF) of 1.5 was applied to the model after complete excavation of the PH and TH. The model reaches equilibrium without signs of instability or non-convergent movement for the north walls of both caverns. The calculated axial forces for the support elements are shown in Fig. 9. Only Tendon 141 (with its collar installed in the pyroclastic layer) reaches 1800 kN, the ultimate force capacity for the tendons, which results in reducing its load capacity to a residual level of 750 kN. The results also indicate that the demand for a FoS of 1.5 in terms of axial displacement of the tendons and bar anchors is well within their 0.4 m displacement tolerance (i.e., the elongation tolerance measured at the head/collar).

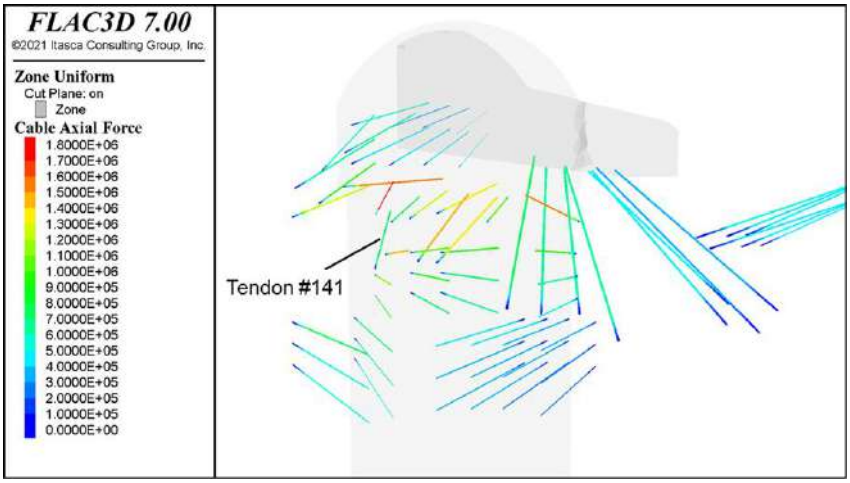

Fig. 9. Contours of axial forces (N) calculated for the support elements after complete excavation of the PH and TH (SRF applied for FoS = 1.5).

5. Conclusion

The detailed model of deformation and stability of the north wall of the PH and TH was developed because of observations of apparent non-convergent deformation in that wall after excavation of Bench II. The seven tendons installed in the north wall of the PH have stabilized it before the excavation of Bench III. The monitoring data indicate that the north wall of the PH remained stable after subsequent excavations, including the final cavern geometry. The additional bar anchors installed on the north wall, as well as the floor and sidewall of the adit tunnel, ensured the required FoS for the final configuration. The calibrated model, in addition to deformation and stability of the excavated cavern, predicts the loading (forces) in the ground support (tendons and bar anchors), which is explicitly represented as installed during excavation. It was also used to evaluate the stability margin expressed by FoS for the north walls of the caverns.

The analysis has shown that the FoS of the north walls of both the PH and TH after complete excavation is greater than 1.5. The forces in five of the tendons and bar anchors in the PH are predicted in the model to slightly exceed their allowable working limit in the final stage of excavation, which is not a concern because the current force measurements for all tendons and bar anchors are within the allowable working limits.

Only one tendon in the PH is predicted to exceed the ultimate force capacity during the FoS calculation. The model reaches equilibrium, and the tendon elongation remains smaller than the pullout tolerance after the force in that tendon is decreased to the residual value.

The conclusions are based on the numerical results. Although a significant effort has been made to calibrate the model to the available field observations, there will always be uncertainties associated with numerical predictions. Monitoring the field response, such as displacements of critical points, and the performance of the installed support, including forces or stresses in the tendons and bar anchors, throughout the operation of the cavern was recommended to ensure that stability conditions do not change.

References

Behnia, M., Seifabad, M.C., 2018. Stability analysis and optimization of the support system of an underground powerhouse cavern considering rock mass variability. *Environ. Earth. Sci.*, 77, pp. 645. https://doi.org/10.1007/s12665-018-7835-2.

Ghorbani, M., Sharifzadeh, M., 2009. Long term stability assessment of Siah Bisheh powerhouse cavern based on displacement back analysis method. *Tunnelling and Underground Space Technology*, 24 (5), pp. 574-583, ISSN 0886-7798, https://doi.org/10.1016/j.tust.2009.02.007.

Hoek, E., 2013. Practical Rock Engineering, Hoek Notes by Evert Hoek. http://www.rocscience.com

Itasca Consulting Group, Inc. (2019) FLAC3D — Fast Lagrangian Analysis of Continua in Three Dimensions (Version 7.0). Minneapolis: Itasca.

Kaiser, P. K., 2019. From common to best practices in underground rock engineering. 8th Mueller lecture presented at the 14th ISRM Congress, Brazil, CRC Press, pp. 141-182.

Li, H., Chen, W., Tan, X., Chen, E., 2022. Digital design and stability simulation for large underground powerhouse caverns with parametric model based on BIM-based framework. *Tunnelling and Underground Space Technology*, 123, pp. 104375, ISSN 0886-7798, https://doi.org/10.1016/j.tust.2022.104375.

Li, H., Chen, W., Tan, X., Wang, X., 2025. Spatial and temporal stability analysis and assessment of underground powerhouse caverns: A case study. *Environ. Earth Sci*., 84, pp. 146. https://doi.org/10.1007/s12665-025-12157-9.

Liu, X., Wang, J., Huang, J., Jiang, H., 2017. Full-scale pullout tests and analyses of ground anchors in rocks under ultimate load conditions. *Engineering Geology*, 228, pp. 1-10.

Lorig, L., Potyondy, D., Varun, 2020. Quantifying Excavation-Induced Rock Mass Damage in Large Open Pits. in Proceedings, 2020 International Symposium on Slope Stability in Open Pit Mining and Civil Engineering (Virtual Conference, May 2020), pp. 969–982. Perth: Australian Centre for Geomechanics.

Zhu, W.S., Li, X.J., Zhang, Q.B., Zheng, W.H., Xin, X.L., Sun, A.H., Li,S.C., 2010. A study on sidewall displacement prediction and stability evaluations for large underground power station caverns. *International Journal of Rock Mechanics and Mining Sciences*, *47*(7), pp 1055-1062, ISSN 1365-1609, https://doi.org/10.1016/j.ijrmms.2010.07.008.

Southeastern Europe Tunnelling Conference (SETC-2025)
1-3 October 2025, Belgrade, Serbia

DOI: 10.5937/SETC25022S

Parameter determination of the hardening soil model with small strain stiffness: an optimization approach coupling finite element simulations and genetic algorithms

Jovan Šaponjić[a], Nikola Divac[a], Boban Stojanović[b,c], Vladimir Bačanin[c], Slobodan Radovanović[a], Dejan Divac[a]*

[a] Jaroslav Černi Water Institute, Department for Civil Structures, Belgrade, Serbia; office@jcerni.rs
[b] University of Kragujevac, Faculty of Science, Kragujevac, Serbia; boban.stojanovic@pmf.kg.ac.rs
[c] Vodéna, Kragujevac, Serbia; office@vodena.rs

Abstract: In the scope of Phase I of Line 1 of the Belgrade Metro project, a large laboratory and in-situ testing database of the soils and rock masses of Belgrade was used for determining the parameters of the hardening soil model with small strain stiffness (HSS). Due to the complexity of parameter determination of the HSS model based on conventional laboratory testing results, an optimization approach coupling finite element analyses and genetic algorithms was taken in the parameter determination process with the goal of defining a framework for full, reliable, and unified implementation of the HSS model in all necessary numerical analyses. For the selected geotechnical soil layer, each of the available laboratory tests (direct shear test and CD triaxial test) and in-situ tests (pressuremeter) were numerically simulated and the HSS parameters were calibrated so that each individual simulated test, consisting of multiple test specimens, could achieve its respective experimental recordings as best as possible by minimizing the value of the applied criterion function. The resulting parameters from the calibration process, alongside the analytically derived parameters for laboratory results, were compared and analyzed, and it is realized that while analytically derived parameters provide a reasonable first estimate, numerical calibration is essential for accurately capturing soil stiffness behavior and stress dependency and therefore creating reliable design solutions based on realistic soil properties.

Keywords: hardening soil model; optimization; genetic algorithms; direct shear; triaxial; pressuremeter

1. Introduction

1.1. Context and focus of the research

Within the upcoming infrastructural development of the City of Belgrade, a large number of underground construction projects of varying purposes have been planned. Among these, in terms of scale, complexity, importance, and current relevance, the most prominent are the Tunnel Connection Project from Karađorđeva Street to the Danube Slope and Phase I of Line 1 of the Belgrade Metro project. In the near future, additional underground infrastructure projects are also planned, such as the Interceptor Project, the Topčider Tunnel, and others.

The planned tunnel projects traverse geologically complex environments along their alignments, characterized by varying lithological compositions, mechanical properties, the presence of groundwater, and other influencing factors. For the purpose of defining the geotechnical properties of the soils and rock masses in which the subject infrastructure will be constructed and considering the high degree of urbanization of the project area, extensive geological investigations have already been carried out, with additional investigations planned for the forthcoming period. Accordingly, there arises a need to systematize the large volume of results from experimental geotechnical tests and to enable their application in the development of reliable and robust technical solutions.

* Corresponding author: jovan.saponjic@jcerni.rs (J. Šaponjić).

The specific requirements of designing and constructing underground facilities – which are in complex interaction with both the surrounding ground and the groundwater regime – necessitate the use of numerical models based on the finite element method (FEM). In the development of such models, a key role is played by the selected constitutive material model used to describe the behavior of the geological medium in which construction is carried out. Consequently, the reliability of determining the parameters of the chosen material model is of critical importance for adequately simulating construction conditions and thereby ensuring the validity of reached conclusions and proposed designs.

Ever since the formulation of the Hardening Soil (HS) material model (Schanz et al., 1999) and its modification to take into consideration the small-strain stiffness of soils (Benz, 2007), the Hardening Soil with Small-Strain stiffness (HSS) material model has been widely used for numerical modelling and design of geotechnical structures. The approach to parameter calibration of the HSS model based on laboratory and/or in-situ test results has been covered by only a few authors. Surarak et al. (2012) calibrated the stiffness and strength parameters of the HSS model of Bangkok clays based on oedometer tests and standard undrained and drained triaxial tests (without an unload-reload loop) while Govindasamy et al. (2019) used discrete FEM models of standard triaxial and pressuremeter tests to calibrate some of the HSS parameters of the Kenny Hill formation by applying regression analysis. Tazakka and Tirta (2024) used a direct field curve fitting method to develop a correlation between SPT tests and stiffness parameters of the HS model, while analytically deriving the strength parameters from triaxial tests. The implementation of genetic algorithms was used by Mendez et al. (2021) for calibrating a hypoplastic sand model based on oedometer and drained triaxial tests, and related work was also done by Mahaček et al. (2022) that implemented Differential Evolution and Particle Swarm Optimization methods.

The planned underground infrastructure development in Belgrade emphasizes the need for dependable numerical analyses supported by accurate constitutive modeling. Although the HSS model is widely applied in geotechnical engineering, existing studies on its parameter calibration during the design phase of a project are relatively limited and often focused on singular test specimens or simplified procedures. Advanced optimization techniques show encouraging potential opportunities, however, comprehensive approaches that integrate multiple laboratory and in-situ tests remain insufficiently explored, indicating opportunities for further development in this area.

1.2. Overview of the Hardening Soil with Small-Strain Stiffness material model

In contrast to ideally elastoplastic models, the Hardening Soil (HS) model accounts for the increase in shear strength (hardening) under dominant deviatoric stresses, as well as the increase in compressive strength under uniaxial and isotropic stress states during plastic behavior of the material. The main characteristics of the HS constitutive model are:

- The failure surface corresponds to the Mohr–Coulomb failure criterion (parameters c, φ, ψ);
- Plastic deformations develop due to primary compression (parameter E_{oed}^{ref}) and primary deviatoric loading (parameter E_{50}^{ref});
- An increase in stiffness occurs during elastic unloading and reloading (parameter E_{ur}^{ref}).

Beyond the advantages provided by the HS constitutive model, the Hardening Soil with Small-Strain Stiffness (HSS) model introduces a nonlinear variation of stiffness at very small strains. Consequently, this model provides an improved description of characteristic shear deformations in the vicinity of geotechnical structures, as well as a more accurate representation of deformations in laboratory tests.

In addition to the parameters required for defining the HS model, the HSS model requires two additional parameters that describe small-strain behavior: the initial small-strain shear modulus G_0^{ref} and the shear strain threshold $\gamma_{0.7}$. Below, all parameters necessary for defining the HSS model are presented, under the assumption that the tensile strength of the soil is $\sigma_{t=}0$, that no increase in soil cohesion with depth is considered ($c_{inc} = 0$), and that parameters are defined for the reference stress $p_{ref} = 100$ kPa.

Table 1. Relevant parameters for defining the HSS model.

Parameter	Description	Parameter	Description
c (kN/m^2)	Soil cohesion	m (-)	Exponent governing stress dependency of stiffness
s_u (kN/m^2)	Undrained shear strength (relevant only for undrained tests)	ν_{ur} (-)	Poisson's ratio corresponding to the unloading–reloading branch of the stress–strain curve (default ν_{ur} = 0.2)
φ (°)	Angle of internal friction	K_0^{nc} (-)	Coefficient of earth pressure at rest (for normally consolidated soils, default K_0^{nc} = 1 -sin φ)
ψ (°)	Dilatancy angle	R_f (-)	Failure ratio q_f/q_a (default R_f = 0.9)
E_{oed}^{ref} (kN/m^2)	Tangent stiffness for primary oedometer loading	G_0^{ref} (kN/m^2)	Initial shear modulus at very small strains ($\varepsilon<10^{-6}$)
E_{50}^{ref} (kN/m^2)	Secant stiffness corresponding to a deviatoric stress equal to 50% of the failure deviatoric stress in a drained triaxial compression test	$\gamma_{0.7}$ (-)	Shear strain threshold at which shear stiffness is redefined as G_s= 0.722 G_0^{ref}
E_{ur}^{ref} (kN/m^2)	Unloading/reloading stiffness		

2. **Methodology**

2.1. General approach to parameter determination

For practical design purposes, the tunnel alignment must be subdivided into a number of geotechnical macro-zones, each characterized by the general behavior of the soil, the physical and mechanical properties of the soil and rock layers, hydrogeological conditions, the thickness of the overburden relative to the structure, and the potential occurrence of faults or other geotechnical hazards. Individual underground structures along the tunnel alignment should then be classified within the corresponding macro-zones according to their location. Subsequently, all relevant stress-strain analyses must be performed for each of the defined macro-zones in order to establish safe and robust engineering solutions for the tunnel and associated underground structures.

Within each geotechnical macro-zone, it is necessary to determine a consistent set of design parameters for every geotechnical layer present in that zone. The parameters thus established are then applied in all required stress-strain analyses of the structures (or structural segments) located within the given macro-zone. The procedure for defining these parameters is illustrated schematically in the following figure and is described in detail in the subsequent text.

For the considered macro-zone, the number of characteristic geotechnical layers is first established. For each geotechnical layer within the macro-zone, the available soil samples belonging to that layer are identified, i.e., the laboratory and field tests that best describe the behavior of each geotechnical layer are determined.

Since the tests are performed on individual test specimens (TS), these specimens are grouped according to the type of test conducted. For each test type within a given geotechnical layer, a test specific calibration procedure is performed. This results in determining a single – unified set of parameters of the HSS model for which the numerical simulation of the entire test (encompassing simultaneously all the test specimens that make up the test) provides the best overall correlation with the corresponding laboratory results.

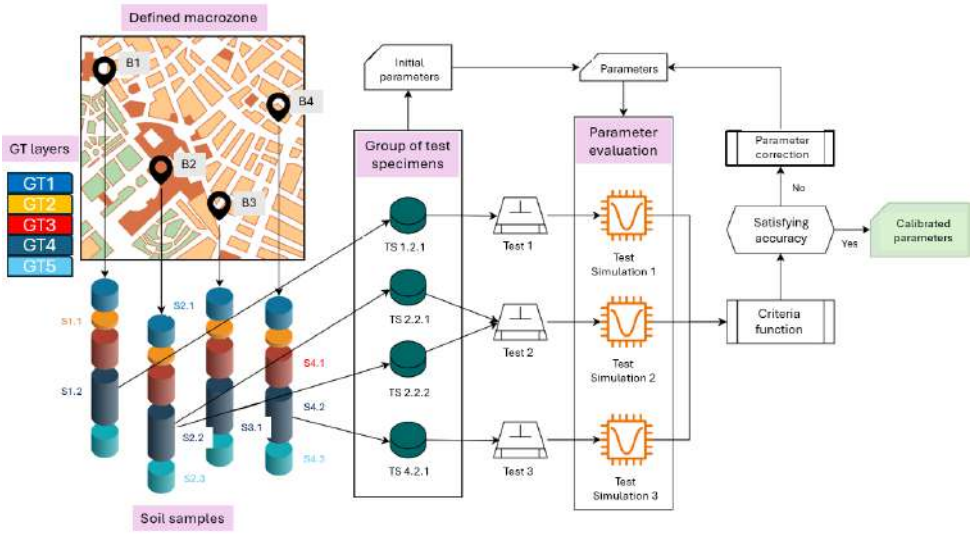

Fig. 1. Workflow for parameter calibration of a specific geotechnical layer in a defined macro-zone.

The correlation between the numerical simulation and the laboratory records is evaluated on the basis of the criterion function defined in Section 2.5, by optimizing it to its minimum value. The parameter sets obtained from the test specific calibration of each test type are then compared with each other and with the analytically derived parameters from the laboratory records.

2.2. Assessed laboratory and in-situ tests

For the purposes of the analysis presented in this study, the macro-zone in the vicinity of the Bele Vode metro station is considered, located on the margin of the Makiš Field area between chainages km 4+070 and km 4+250 of Phase I of Line 1 of the Belgrade Metro project. This macro-zone is of particular significance as it represents the launching zone for the TBM excavation of the tunnel section extending from the Bele Vode station to the Sajam station, with a total excavation length of 5760 m.

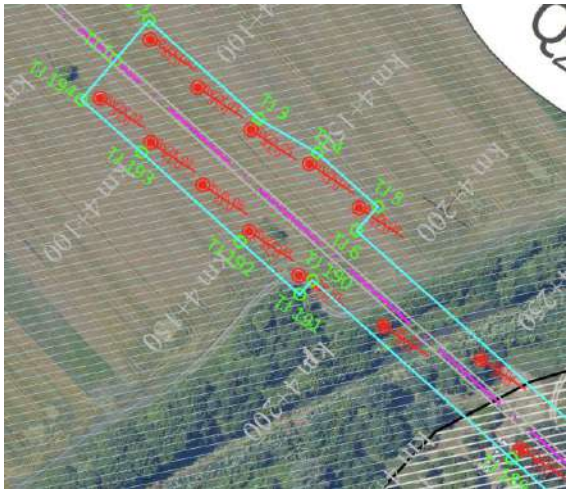

Fig. 2. Analyzed macrozone in the vicinity of metro station Bele Vode with indicated position of boreholes (BVZK and BK).

Within the considered macro-zone, the geotechnical layer of overlapping Neogene limestone–marl sediments, denoted as $M^1{}_3KL$, is analyzed. This layer consists of silty to clayey marlstones/limestones with a heterogeneous carbonate content and exhibits layered textures with irregular thicknesses. This geotechnical layer is of particular importance as its depth extends through the zone of the tunnel, exerting the greatest influence on the stress-strain behavior of the tunnel lining, as well as on the stress-strain response of the diaphragm walls of the Bele Vode metro station during TBM breakthrough.

The following laboratory and in-situ tests are available, which can be reliably attributed to the same analyzed geotechnical layer within the considered macro-zone:

- Drained direct shear test
  - Borehole BVZK-05, sample depth 28.10–28.40 m; Specimen TS 1 (σ_c = 100 kPa)
  - Borehole BVZK-05, sample depth 28.10–28.40 m; Specimen TS 2 (σ_c = 200 kPa)
  - Borehole BVZK-05, sample depth 28.10–28.40 m; Specimen TS 3 (σ_c = 400 kPa)

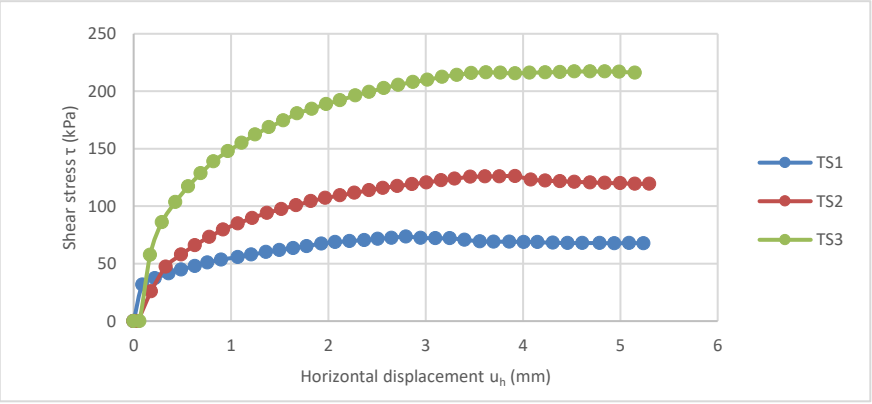

Fig. 3. Test results of the drained direct shear test on test specimens from borehole BVZK-05 (28.10 – 28.40 m).

- Consolidated drained (CD) triaxial compression test
  - Borehole BK-02, sample depth 29.10 – 29.45 m; Specimen TS 1 (σ_c = 100 kPa)
  - Borehole BK-02, sample depth 29.10 – 29.45 m; Specimen TS 2 (σ_c = 200 kPa)
  - Borehole BK-02, sample depth 29.10 – 29.45 m; Specimen TS 3 (σ_c = 400 kPa)

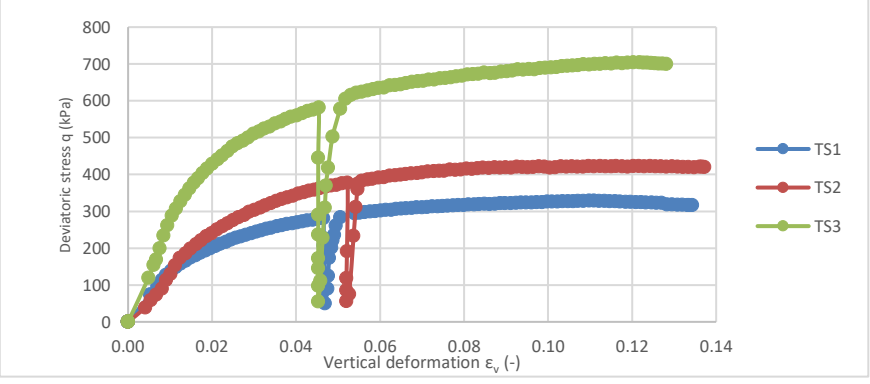

Fig. 4. Test results of the CD triaxial test on test specimens from borehole BK-02 (29.10 – 29.45 m).

- Pressuremeter test
  - Borehole BK-02, sample depth 29.12 – 29.58 m

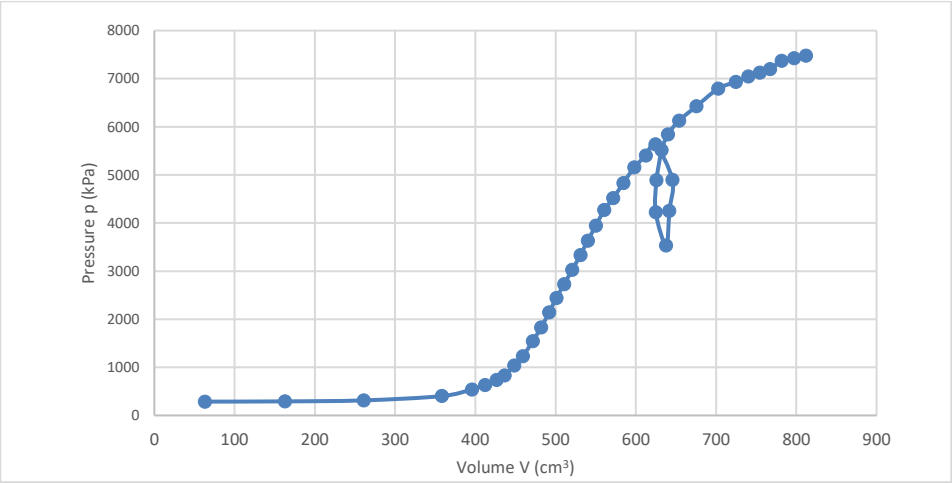

Fig. 5. Test results of the pressuremeter test conducted on test specimen from borehole BK-02 (29.12 – 29.58 m).

It should be noted that the analyzed triaxial compression tests and the pressuremeter test were conducted to include a cycle of unloading and reloading up to failure, and as such, do not represent the "standard" testing procedures for these tests. These tests were intentionally performed in this manner to increase their practical value for defining the parameters of the HSS model, particularly with regard to the unloading–reloading stiffness, which is characterized by the parameter E_{ur}^{ref}.

2.3. Analytical determination of HSS parameters

Certain parameters of the HSS model can be determined analytically from the available laboratory and in-situ tests, while others cannot be determined analytically but can be somewhat reliably estimated for preliminary assessments and the development of basic engineering solutions according to the literature and recommendations of numerical software (e.g., Plaxis). Among these parameters are, for example, the Poisson's ratio, which for elastic states can be assumed as $\nu_{ur} = 0.2$, the coefficient of earth pressure at rest for normally consolidated soils $K_0^n = 1\text{-}\sin\varphi$, the failure ratio $R_f = 0.9$ and others.

For the purposes of this study, the calibrated parameter sets are compared with each other and with analytically derived parameters based on laboratory test results. The analytical determination of parameters from laboratory records follows standard practice, with only certain parameters being reliably derived from specific laboratory and in-situ tests.

From the drained direct shear test, the parameters c, φ, E_{50}^{ref} and m can be somewhat reliably determined analytically. From the CD triaxial test, conducted with an unloading–reloading cycle, the parameters c, φ, E_{50}^{ref}, E_{ur}^{ref}, m, R_f, and G_0^{ref} can be determined analytically with relative reliability. From the pressuremeter test, no parameter can be analytically determined, but the pressuremeter modulus and unload-reload modulus can be used for an approximate estimation of the material stiffness parameters.

2.4. Finite element numerical simulations

All numerical simulations of the laboratory tests will be conducted using Plaxis' SoilTest tool. This tool functions as a virtual laboratory, allowing numerical simulation of laboratory tests on single test specimens without the need to create a complete finite element model.

Within the SoilTest tool, the predefined module for the drained direct shear test is used. In this module, the HSS model parameters are calibrated to achieve the best possible correlation between the $\gamma_{xy} - \tau_{xy}$

curve (shear strain – shear stress) from the numerical simulation and the corresponding curve obtained from laboratory records.

Due to the specific nature of the CD triaxial compression test, which includes an unloading–reloading cycle, the predefined module for this laboratory test cannot be used for numerical simulation. Instead, the test is simulated using the General module. In this case, the curve analyzed to assess the quality of HSS parameter calibration is the ε_1 – q curve (axial strain – deviatoric stress).

Unlike laboratory tests, the in-situ pressuremeter test cannot be numerically simulated using Plaxis' SoilTest tool. For this test, a two-dimensional axisymmetric finite element model must be developed, taking into account all specific conditions of the given test – depth, geotechnical layers, groundwater level, drainage etc. In this approach, the model domain is approximated as a single material layer corresponding to the material in which the test was performed, while the overlying layers above the test location are approximated by adjusting the intensity of the vertical load applied to the top of the model. Both drained and undrained conditions are analyzed. The model simulates all phases of the test in sequence: initial phase, excavation and lining of the investigative borehole, borehole excavation for the pressuremeter, and staged application of pressure steps (test execution).

The curve analyzed for the pressuremeter test in the assessment of parameter calibration quality is the p – V curve (pressure – volume), taking into account the membrane stiffness compensation, probe deformability, and water column between the probe and the instrument pump. Additionally, since a certain amount of pressure must be applied to the probe before it achieves contact with the borehole walls, the calibration of parameters is performed only for the portion of the p – V curve from the step of the test when the probe membrane achieves full contact with the borehole wall to the final step of the test.

2.5. Quality assessment of the calibrated parameter set – application of genetic algorithms

The soil material model parameters were estimated using the JARE optimization service (Ivanovic et al., 2015), which applies a Genetic Algorithm (GA) to fit simulation results to experimental curves. The optimization process relied on evolutionary operators to explore the parameter space efficiently, while the Fréchet distance method (Alt and Godau, 1995) was employed as the goal function to evaluate the similarity between simulated and experimental responses. By minimizing this metric, the service successfully identified parameter sets that ensured close agreement between the model predictions and the experimental data.

The criterion for overall quality assessment is defined as a function of the difference (error) between the numerical and experimental results for all tests incorporated in the calibration process, with the objective of minimizing the value of this criterion function. In general form, taking into consideration all possible test types, the criterion function is defined as follows:

$$
\begin{aligned}
K = \Bigg(&\sum_{i=1}^{N_{oed}} w_{oed,i} + \sum_{i=1}^{N_{dsd}} w_{dsd,i} + \sum_{i=1}^{N_{dsu}} w_{dsu,i} + \sum_{i=1}^{N_{CD}} w_{CD,i} + \sum_{i=1}^{N_{CU}} w_{CU,i} \\
&+ \sum_{i=1}^{N_{UU}} w_{UU,i} + \sum_{i=1}^{N_{pres}} w_{pres,i}\Bigg)^{-1} \\
&\cdot \Bigg(\sum_{i=1}^{N_{oed}} w_{oed,i}K_{oed,i} + \sum_{i=1}^{N_{dsd}} w_{dsd,i}K_{dsd,i} + \sum_{i=1}^{N_{dsu}} w_{dsu,i}K_{dsu,i} \\
&+ \sum_{i=1}^{N_{CD}} w_{CD,i}K_{CD,i} + \sum_{i=1}^{N_{CU}} w_{CU,i}K_{CU,i} + \sum_{i=1}^{N_{UU}} w_{UU,i}K_{UU,i} \\
&+ \sum_{i=1}^{N_{pres}} w_{pres,i}K_{pres,i}\Bigg)
\end{aligned}
\tag{1}
$$

In the above formula, the suffixes of the notations used refer to the type of laboratory or in-situ tests, as specified in the following table.

Table 2. Criterion function suffix definitions.

Notation	Test type	Notation	Test type
oed	Oedometer test	CD	Consolidated drained triaxial test
dsd	Drained direct shear test	CU	Consolidated undrained triaxial test
dsu	Undrained direct shear test	UU	Unconsolidated undrained triaxial test
pres	Pressuremeter test		

The notations in the criterion function refer to:

- K – partial criterion function for a specific test type,
- N – number of tests of a specific test type,
- w – weighting factor representing the reliability of the results of tests of a specific test type (for the purposes of this study, w = 1 for all test types)

3. Results and discussion

3.1. Drained direct shear test

For the drained direct shear test, based on a previously conducted sensitivity analyses it was determined that the parameters of greatest significance on the resulting numerical simulation curve are the cohesion c, internal friction angle φ, and secant stiffness E_{50}^{ref}. A relatively good correlation between curves of the laboratory recordings and numerical simulations of all consolidation pressure levels is achieved for the calibrated parameter set (as can be seen in Fig. 6). This is indicated by the low criterion function value of K = 0.041, and by visual verification of the resulting curves. The resulting calibrated parameters are given in Table 4, alongside the values of parameters that can be analytically derived from this type of test.

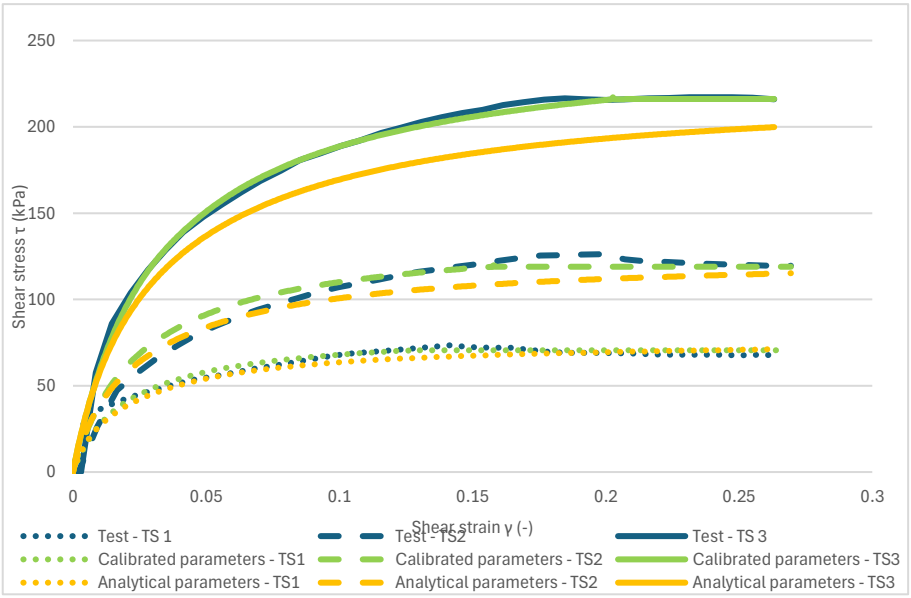

Fig. 6. Comparison of test curves (blue), numerical simulations with calibrated parameter values (green) and numerical simulations with analytical + default parameter values (yellow) for the drained direct shear test.

For comparison, a numerical simulation was also run with a parameter set consisting of the analytically derived parameters, and the default or recommended values of the remaining parameters according to the literature and software recommendations (yellow curves in Fig. 6). This simulation resulted in a lower level of correlation with the laboratory results, indicated by a higher criterion value K = 0.074, but with an increasing discrepancy with increasing consolidation stresses.

The small-strain behavior is well captured with the calibrated numerical simulations, and the peak values of the effective strength parameters – soil cohesion c and angle of internal friction φ is in good accordance with the analytically derived values from the laboratory results. The secant stiffness parameter E_{50}^{ref} and exponent m are slightly underestimated via analytical derivation although it should be kept in mind that these parameters are primarily determined based on drained triaxial compression tests, and their analytical derivation based on direct shear tests is for preliminary estimation purposes only.

Table 3. Comparison of calibrated parameters and analytically derived parameters for the drained direct shear test.

Parameter	Analytical derivation (K=0.074)	Test specific calibration (K = 0.041)
c (kN/m^2)*	28.0	23.1
φ (°)*	27.3	27.0
ψ (°)	-	9.89
E_{oed}^{ref} (kN/m^2)	-	16521
E_{50}^{ref} (kN/m^2)*	3223	6666
m (-)	0.405	0.576
ν_{ur} (-)	-	0.358
K_0^{nc} (-)	0.542	0.544
R_f (-)	-	0.803
G_0^{ref} (kN/m^2)	-	54040
$\gamma_{0.7}$ (-)	-	0.0008

* Parameters with greatest influence on resulting numerical curve

3.2. Consolidated drained triaxial test

According to previously conducted sensitivity analyses it was determined that for CD triaxial tests conducted with this testing procedure the parameters of cohesion c, internal friction angle φ, secant stiffness E_{50}^{ref}, unload-reload stiffness E_{ur}^{ref} and failure ratio R_f are of the greatest significance on the resulting numerical simulation curve. For the CD triaxial test, the resulting criterion function value K = 0.050 is obtained for the calibrated parameter set (Table 5) – indicating a relatively good correlation between curves of the laboratory recordings and numerical simulations, although with a visible greater discrepancy for the higher consolidation stresses (Fig. 7). In order to attain a relevant K value, it should be noted that the criterion function was calculated only up to the final point of the numerical simulation or laboratory test (whichever came first), which is justified since the failure deviatoric stress was reached in each simulation.

A numerical simulation was also run with a parameter set consisting of the analytically derived parameters, and the default or recommended values of the remaining parameters according to the literature and software recommendations (yellow curves in Fig. 7). This simulation resulted in a comparable level of correlation with the laboratory results, indicated by the criterion value K = 0.124, with the majority of the "error" originating from the lowest consolidation stress, i.e. test specimen TS1. The similarity between the analytically derived parameters and calibrated parameters is to be somewhat expected considering that the HSS material models parameter derivation is based on this type of triaxial test specifically. Samples with even more test specimens could show an even greater similarity between these parameter sets.

Like in the case of the direct shear test, the peak values of the effective strength parameters are in good accordance with the analytically derived values from the laboratory results while the stiffness parameters are slightly less correlated, especially the initial shear modulus G_0^{ref}. The differences

between the calibrated parameter sets of the direct shear test and the CD triaxial test, especially the cohesion c and initial shear modulus G_0^{ref}, indicate that the analyzed geotechnical layer exhibits a certain level of heterogeneity depending on the relation of marl and limestone in the engineering-geological complex.

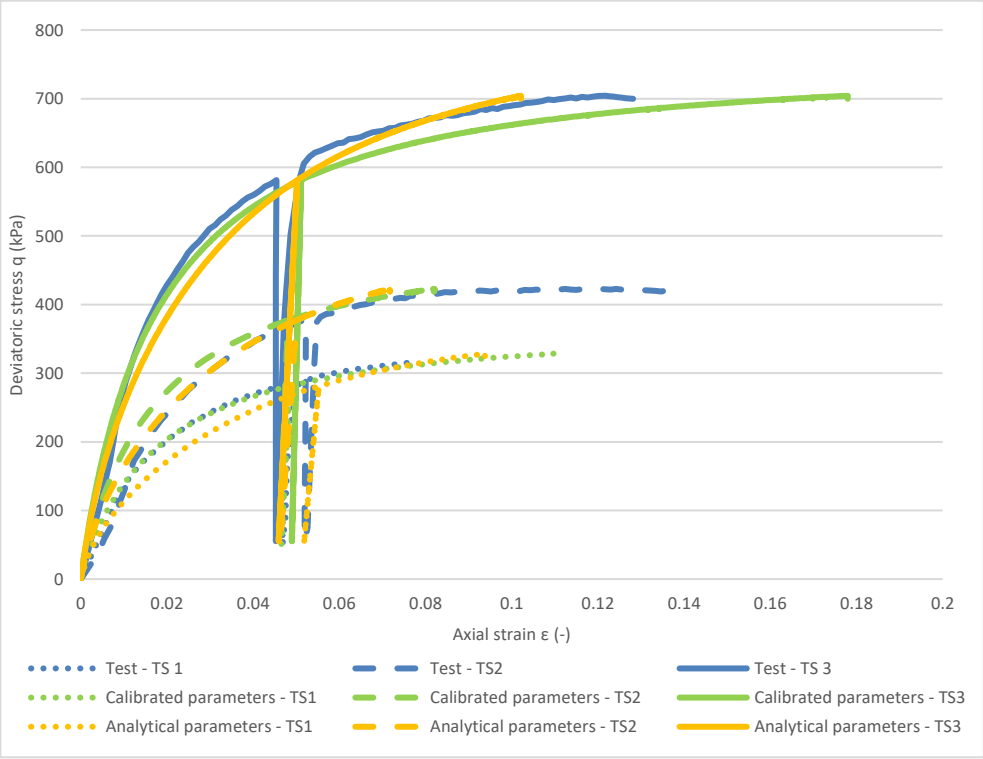

Fig. 7. Comparison of test curves (blue), numerical simulations with calibrated parameter values (green) and numerical simulations with analytical + default parameter values (yellow) for the CD triaxial test.

Table 4. Comparison of calibrated parameters and analytically derived parameters for CD triaxial tests.

Parameter	**Analytical derivation (K=0.124)**	**Test specific calibration (K = 0.050)**
c (kN/m²)*	72.0	80.2
φ (°)*	22.9	23.0
ψ (°)	-	9.43
E_{oed}^{ref} (kN/m²)	-	28945
E_{50}^{ref} (kN/m²)*	12307	11618
E_{ur}^{ref} (kN/m²)*	66716	121869
m (-)	0.813	0.968
ν_{ur} (-)	-	0.222
K_0^{nc} (-)	0.611	0.477
R_f (-)*	0.865	0.987
G_0^{ref} (kN/m²)	8788	122733
$\gamma_{0.7}$ (-)	-	0.00001

* Parameters with greatest influence on resulting numerical curve

3.3. Pressuremeter test

Due to the fact that the pressuremeter test represents an in-situ test, the specificities of each testing procedure and the conditions it is executed in have a great influence on the setup of the numerical model with which it is simulated, and in turn, a great influence on the resulting test curves. One of the major effects to consider when calibrating HSS parameters based on the pressuremeter test is the drainage conditions. Depending on the soil medium in which the test is executed, specifically its permeability, but also depending on the time component of the testing procedure, a case-by-case assessment is to be made if the test subjected to numerical simulation is conducted under drained or undrained conditions.

A calibration procedure was carried out on the analyzed pressuremeter test with two approaches – as a drained analysis and as an undrained analysis. The undrained analysis corresponds to the Plaxis' "Undrained B" analysis in which the stiffness parameters are defined with their effective values, and the strength is defined as the undrained shear strength. The corresponding resulting curves are shown in Fig. 8, and the values of the calibrated parameter set for both conditions are summarized in Table 6. As can be seen based on the values of the criterion function K, a fairly similar estimate is obtained for the two numerically simulated curves. However, the resulting parameters are quite diverse.

The drained analysis results in a calibrated parameter set consisting of significantly larger values of the internal friction angle φ and the stiffness parameters E_{50}^{ref}, E_{oed}^{ref} and E_{ur}^{ref} in comparison with the values obtained in the calibration process of the CD triaxial test sample from the same borehole and sample depth (Table 5). The undrained analysis results in a numerical curve with a slightly lower criterion function value K, but with significantly lower stiffness parameters E_{50}^{ref} and E_{oed}^{ref}. These attained parameters better correspond to the analytically derived pressuremeter moduli, but it should be kept in mind that the pressuremeter moduli do not represent the actual HSS material model parameters and their physical meaning.

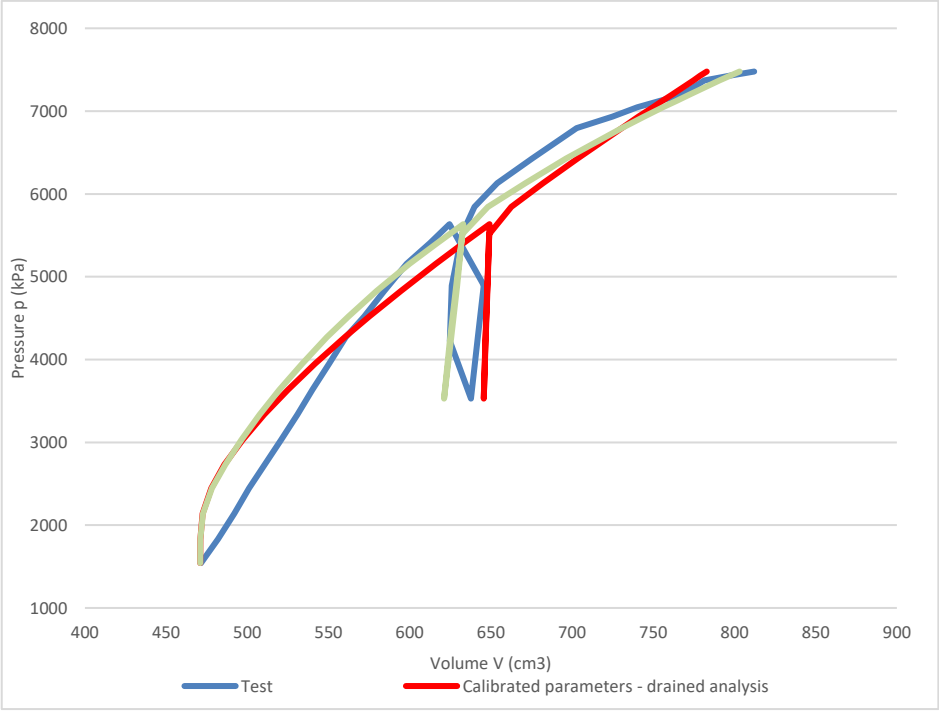

Fig. 8. Comparison of test curve and numerical simulation of pressuremeter tests with calibrated parameter values.

Table 5. Comparison of calibrated parameters and analytically derived parameters for the pressuremeter test.

Parameter	Analytical derivation	Test specific calibration Drained analysis (K = 0.067)	Test specific calibration Undrained analysis (K = 0.063)
c (kN/m^2)	-	76.6	/
φ (°)	-	43.6	/
ψ (°)	-	6.1	/
s_u (kN/m^2)	-	/	2616
E_{oed}^{ref} (kN/m^2)	183667*	334775	100622
E_{50}^{ref} (kN/m^2)		291386	85424
E_{ur}^{ref} (kN/m^2)	774951*	1098971	700560
m (-)	-	0.635	0.401
ν_{ur} (-)	-	0.190	0.327
K_0^{nc} (-)	-	0.383	0.435
R_f (-)	-	0.892	0.760
G_0^{ref} (kN/m^2)	-	671723	564532
$\gamma_{0.7}$ (-)	-	0.00032	0.00067

* Values refer to the pressuremeter moduli, not the specific HSS parameter

4. Conclusions

The conducted calibration of the HSS material model parameters based on drained direct shear, consolidated drained triaxial, and pressuremeter tests has shown that reliable parameter identification requires an approach encompassing a combination of multiple laboratory and in-situ tests. Besides that, careful consideration of the numerical modeling procedure including boundary conditions and drainage assumptions is instrumental in achieving realistic simulations that adequately capture soil behavior under varying stress conditions.

For both the direct shear and triaxial tests, the peak strength parameters – cohesion c and internal friction angle φ – were consistently well reproduced by the calibrated numerical simulations showing good agreement with the analytically derived values from laboratory results. The stiffness-related parameters (E_{50}^{ref}, E_{ur}^{ref}, m, G_0^{ref}) were less consistently matched, with some discrepancy between analytically derived and calibrated values. Besides underlining the importance of correct grouping of soil samples according to their originating soil layer, this highlights the inherent limitation of deriving stiffness parameters solely from singular laboratory test specimens.

The pressuremeter calibration further emphasized the complexity of parameter derivation, especially regarding drainage conditions. Both drained and undrained analyses yielded similarly acceptable levels of correlation with the experimental curve, but the resulting calibrated parameter sets were markedly different. The drained calibration led to unrealistically high stiffness and strength values compared to triaxial test results on specimens of the same borehole and depth, while the undrained calibration produced lower stiffness moduli more consistent with derived values from pressuremeter results – though these do not directly correspond to HSS input parameters. In general, this calls attention to the careful consideration of the drainage conditions of each specific pressuremeter test sample when calibrating parameter values for further design.

The discrepancies of calibration results observed between test types also suggest a degree of material heterogeneity in the analyzed geotechnical layer. This necessitates future research which should focus on calibration strategies that encompass even more specimens and different test types simultaneously.

Overall, the research demonstrates that while analytically derived parameters provide a useful starting point for preliminary design, calibration against numerical simulations is essential for capturing the realistic stress-dependent stiffness behavior of soils and weak rocks, especially for use cases like urban tunnel design where soil deformations play a critical role in the development of technical design solutions. Together with the successful application of genetic algorithms, this research demonstrates the potential of optimization-based calibration methods to enhance the reliability and efficiency of geotechnical numerical modeling.

5. References

Alt, H., Godau, M., 1995. Computing the Frechet Distance Between Two Polygonal Curves, *International Journal of Computational Geometry & Applications,* 5(1), 75-91. https://doi.org/10.1142/S0218195995000064.

Bentley, 2023a. *PLAXIS Material Models Manual 2D.* Bentley Systems Incorporated, Pennsylvania, USA.

Bentley, 2023b. *PLAXIS Reference Manual 2D.* Bentley Systems Incorporated, Pennsylvania, USA.

Benz, T., 2007. Small-strain stiffness of soils and its numerical consequences. PhD thesis, University of Stuttgart, Germany.

Briuad, J.L., 2005. *The Pressuremeter*, 2nd ed; Taylor & Francis Group plc, London, UK.

Govindasamy, D., Mohamad Ismail, M.A., Zaki, F., Zainal Abidin, M.H., 2019. Calibration of stiffness parameters for Hardening Soil Model in residual soil from Kenny Hill Formation. *Bulletin of the Geological Society of Malaysia*, 67, 119-125. https://doi.org/10.7186/bgsm67201915.

Huynh, Q.T., Lai, V.Q., Boonyatee, T., Keawsawasvong, S., 2022. Verification of soil parameters of hardening soil model with small-strain stiffness for deep excavations in medium dense sand in Ho Chi Minh City, Vietnam. *Innovative Infrastructure Solutions*, 7(1). https://doi.org/10.1007/s41062-021-00621-x.

Ivanovic, M., Simic, V., Stojanovic, B., Kaplarevic-Malisic, A., Marovic, B., 2015. Elastic grid resource provisioning with WoBinGO: A parallel framework for genetic algorithm based optimization. *Future Generation Computer Systems*, 42, 44-54. https://doi.org/10.1016/j.future.2014.09.004.

Lade, P.V., 2016. *Triaxial Testing of Soils*, 1st ed.; John Wiley & Sons, Ltd, West Sussex, UK.

Mahacek, J., Staubach, P., Grandas Tavera, C.E., Wichtmann, T., Zachert, H., 2022. On the automatic parameter calibration of a hypoplastic soil model. *Acta Geotechnica*, 17, 5253-5273. https://doi.org/10.1007/s11440-022-01669-4.

Marzouk, I., Tschuchnigg, F., Schweiger, H.F., Hodlmoser, N., 2024. Parameter identification for constitutive models based on pressuremeter test. Proceedings of the XVIII European Conference on Soil Mechanics and Geotechnical Engineering, Lisbon, Portugal, 26-08-2024 – 30-08-2024

Méndez, F. J., Pasculli, A., Méndez, M. A., Sciarra, N., 2020. Calibration of the von Wolffersdorff model using Genetic Algorithms. https://doi.org/10.48550/arXiv.2006.08433

Obrzud, R.F., Truty, A., 2018. *The Hardening Soil Model – A Practical Guidebook*, 1st ed.; Zace Services Limited, Preverenges, Switzerland

Roctest, 2020. *TEXAM^e PRESSUREMETER Instruction Manual*. Roctest Limited: Saint-Lambert, Canada

Schanz, T., Vermeer, P., Bonnier, P., 2019. The Hardening Soil Model: Formulation and verification. *Beyond 2000 in Computational Geotechnics,* 1st ed.; CRC Press: Florida, USA, pp. 276-291

Surarak, C., Likitlersuang, S., Wanatowski, D., Balasubramaniam, A., Oh, E., Guan, H., 2012. Stiffness and strength parameters for hardening soil model of soft and stiff Bangkok clays. *Soils and Foundations*, 52(4), 682–697. https://doi:10.1016/j. sandf.2012.07.009

Southeastern Europe Tunnelling Conference (SETC-2025)
1-3 October 2025, Belgrade, Serbia

DOI: 10.5937/SETC25023B

On the use of numerical methods to assess underground excavation stability: continuum versus discontinuum and hybrid approaches

Neil Bar[a]*

[a] Gecko Geotechnics, Kingstown, Saint Vincent and the Grenadines; neil@geckogeotech.com

Abstract: Empirical methods for characterizing rock exposures, drill core, and tunnels under construction, such as RMR and Q, have developed from 50+ years of experience and case records. Both methods continue to be routinely used for the selection of ground support for tunnels, caverns and in underground mines around the world. Through progressive improvements in computing capability and availability of software over the last two decades, numerical modelling techniques such as finite element analysis have increased in popularity in recent years. Initially, numerical methods were applied by experts with significant experience in computing, geomechanics, and the design and construction of underground excavation; however, in recent years with generational change, a higher demand for numerical modelling and reducing number of geotechnical experts, numerical modelling in many cases is being more frequently undertaken by engineers with very limited field and operational experience. When used thoughtfully and appropriately in terms of representing engineering geological and geotechnical conditions, numerical models are powerful tools for predicting ground behaviour and the effectiveness of support measures. However, when applied thoughtlessly or misused, numerical model outputs often present incorrect and inappropriate results with 'perceived confidence' to project managers and directors. This paper uses case studies to demonstrate appropriate and inappropriate numerical methods for different rock masses using continuum, discontinuum and hybrid approaches to assist engineers to improve the reliability and usefulness of their models.

Keywords: underground excavations; numerical methods; continuum; discontinuum; hybrid

1. Introduction

Fifty years ago and beyond, rules-of-thumb and empirical methods formed the basis of underground excavation and ground support design.

Empirically-derived rock mass classification systems such as Rock Mass Rating, RMR (Bieniawski, 1973; 1989) and the Q-system (Barton et al. 1974; 2024), were developed to assess rock mass quality from drill core and face mapping for predicting or updating support requirements for underground excavations.

Erharter et al (2024) undertook a global study on the use of 37 rock mass classification systems and identified that the most used systems for tunnels, caverns and underground mines were the Q-system, RMR and Geological Strength Index, GSI (Hoek and Brown, 1997; Marinos, 2019).

GSI is a key component of the Hoek-Brown Failure Criterion (Hoek and Brown, 1980; 2019), which is used for estimating rock mass strength and stiffness characterization in various numerical models. The Hoek-Brown failure criterion for intact rock is based on a strong set of empirical data. GSI offers an intuitive classification of rock mass quality that uses nomographs and can also be derived from RMR and Q. Limitations of GSI and the Hoek-Brown Failure Criterion include, but are not limited to:

- The Hoek-Brown failure criterion requires that the rock mass behave isotropically and that failure does not follow a preferred direction imposed by the orientation of a specific discontinuity or a

*Corresponding author: neil@geckogeotech.com (N. Bar).

combination of two or three discontinuities. In these cases, the use of GSI is *meaningless* as the failure is governed by the shear strength of these discontinuities and not of the rock mass (Marinos et al. 2005).
- The GSI system should not be applied to those rock masses in which there is a clearly defined dominant structural orientation (Marinos et al. 2005).
- It is inappropriate to assign GSI values to excavated faces in strong hard rock with a few discontinuities spaced at distances of similar magnitude to the dimensions of the tunnel (Marinos et al. 2005).
- The GSI system assumes that, because the rock mass is made up of a sufficiently large number of joint sets and randomly oriented discontinuities, it can be treated as a homogeneous and isotropic mass of interlocking blocks (Hoek and Brown, 2019).

Numerical simulations or models can be used to overcome limitations of kinematic and limit equilibrium analyses. Numerical simulations can be completed in 2D or 3D and have the capability to calculate stresses, deformation (strain) and pore pressure using a variety of constitutive relationships. In many cases, linear-elastic analysis is adequate; however, non-linear constitutive relationships should be applied if the focus of the analysis is deformation, not stress distribution (Duncan, 1996).

As conceptualized in Figure 1, numerical models can divide the rock mass into finite or discrete elements. Each element is assigned an idealized stress-strain relation and properties that describe how each material behaves. These elements are connected in a continuum model (e.g. boundary element, BEM; finite element or finite difference elements, FDM/FLAC), separated by discontinuities in a discontinuum model (discrete elements or discrete fracture networks), or hybrid models (e.g. combined finite-discrete elements, DEM/UDEC). Jing (2003) and Stead and Coggan (2012) provide detailed descriptions of continuum and discontinuum methods and Mahabadi et al. (2012) discusses a type of hybrid finite-discrete element (FDEM) approach.

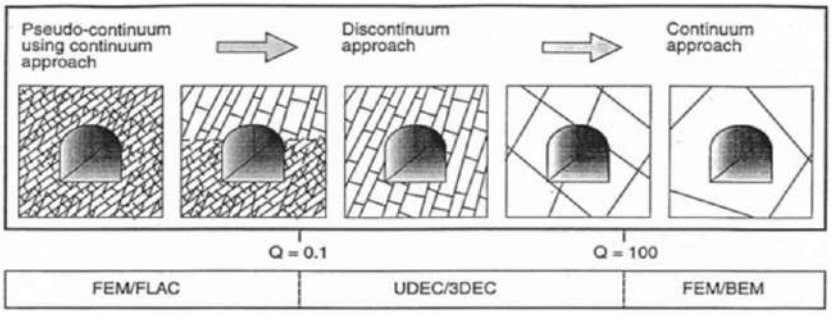

Fig. 1. Conceptual Rock Masses separated by broadly appropriate modelling techniques, approximately 90% of which are likely to require discontinuum treatment (Barton, 2025).

Continuum models assume materials behave isotropically as a continuous body. Large discontinuities such as faults are explicitly modelled as interfaces; however, persistent joints, bedding or foliation and other smaller scale discontinuities are implicitly modelled by user defined ubiquitous joint models or directional shear strengths. In continuum models, no actual failure surface is formed; however, an estimation of slip surface location and shape can be inferred from the concentration of shear strains (or sometimes, stresses) in the model. Deformation (strain) in a continuum model is represented as a continuous displacement field, which may not be realistic for large slope deformations (Sjöberg, 1999).

Discontinuum models represent the rock mass as an assemblage of discrete blocks, and discontinuities are treated as boundary conditions between blocks (Gigli et al. 2012). The discrete blocks can be rigid or deformable. A termination criterion is required to stipulate whether a discontinuity terminates in the rock mass or against other discontinuities and is fundamental for providing the rock mass with strength derived from intact rock bridges. However, it is practically impossible to represent every discontinuity within a rock mass, so simplifications are required. Holistically, in a practical problem, site

investigations and geological uncertainty are a key limitation in precisely representing the geometry and geomechanical characteristics of individual intact rock blocks and discontinuities.

Irrespective of the modelling method applied, several simplifications are necessary (Sjöberg, 1999) and include but are not limited to the mechanics of the predicted failure mechanism, slope geometry, loads acting on the slope, geology and complexity of geological structure. Model calibration is required to ensure that numerical simulations, including many or all of the aforementioned simplifications, produce results that represent actual ground behaviour.

Numerical models in 3D require significantly more computational time and computing power compared to 2D. In this paper, only 2D numerical models are examined. It should be noted from the outset that simplifying to two-dimensional cross-sections inherently creates significant limitations, particularly when anisotropic or faulted rock masses are under consideration.

2. Predicting the Behaviour of Underground Excavations

As part of an underground excavation design procedure (Figure 2), three key steps are usually followed (Schubert et al., 2003):

1. Determining rock mass types (i.e. assessing engineering geological conditions and geotechnically relevant key parameters for each ground type).
2. Determining actual rock mass behaviour types (i.e. observing excavations for signs of excessive stress, deformation patterns and failure mechanisms).
3. Determining excavation and ground support criteria and verifying system behaviour.

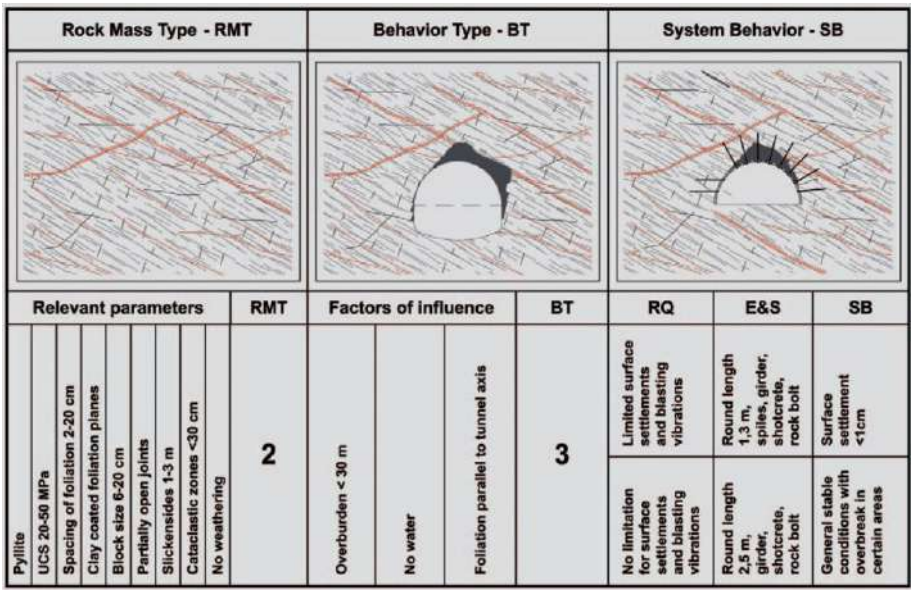

Fig. 2. Example of the underground excavation design procedure (Schubert et al. 2003).

When determining behaviour types for each rock mass, consideration must be given to local influencing factors including the relative orientation of discontinuities to the excavation, groundwater conditions, stress situation, etc.

The behaviour of underground excavations should be evaluated for the full excavation without considering any excavation method or sequence and support or other auxiliary stabilization measures. Table 1 summarizes eleven general categories that most-commonly occur. Such can be conceptualized

using sketches as shown in Figure 2, and later evaluated using numerical methods, which can then form the basis for determining excavation requirements and ground support systems.

Table 1. General Underground Excavation Behaviours and Potential Failure Mechanisms (after Schubert et al. 2003; Oke et al. 2013).

Behaviour Types (BT)			Description of Potential Failure Mechanisms during Excavation of the Unsupported Ground
Stable	1		Stable ground with the potential of small, local, gravity-induced falling or sliding of blocks.
Discontinuity-controlled block fall	2		Voluminous discontinuity-controlled, gravity-induced fall and sliding of blocks (or wedge failures) with the occasional local shear failure on discontinuities. Stability is controlled by the geometrical and mechanical characteristics of the discontinuities.
Shallow failure	3		Shallow stress-induced failure in combination with discontinuity- and gravity-controlled failure.
Voluminous stress induced failure	4		Stress-induced failure involving large ground volumes and large deformation (i.e. squeezing ground).
Rock burst	5		Sudden and violent failure of the rock mass, caused by highly stressed, brittle rocks, and the sudden release of accumulated strain energy. Brittle failure and rock bursting typically occurs at depth.
Buckling	6		Buckling and anisotropic strain of rocks with a narrowly-spaced discontinuity set, frequently associated with shear failure.
Crown failure	7		Voluminous overbreak in the crown with progressive shear failure (also termed chimney type failure).
Ravelling ground	8		Ravelling of dry or moist, intensely fractured, poorly interlocked rocks or soil with low cohesion.
Flowing ground	9		Flow of intensely fractured, poorly interlocked rocks or soil with high water content.
Swelling ground	10		Time dependent volume increase of the ground caused by physical-chemical reaction of the ground and water in combination with stress relief.
Frequently changing behaviour	11	N/A	Combination of several behaviours with strong local variations of stresses and deformations over long sections due to heterogeneous ground (e.g. in heterogeneous fault zones; block-in-matrix rock, tectonic melanges, etc).

Hoek and Brown (1980) presented concepts, which have been developed over 40+ years to relate intact rock strength (UCS or σ_c) and the maximum principal stress ($\sigma 1$) using the stress versus strength ratio and GSI (formerly RMR_{76}) to indicate potential failure modes of underground excavations (Figure 3). Barton et al. (1974; 2024) provide similar stress versus strength ratios (Stress Reduction Factor B, SRF_b) to provide insights into potential stress-related rock mass damage.

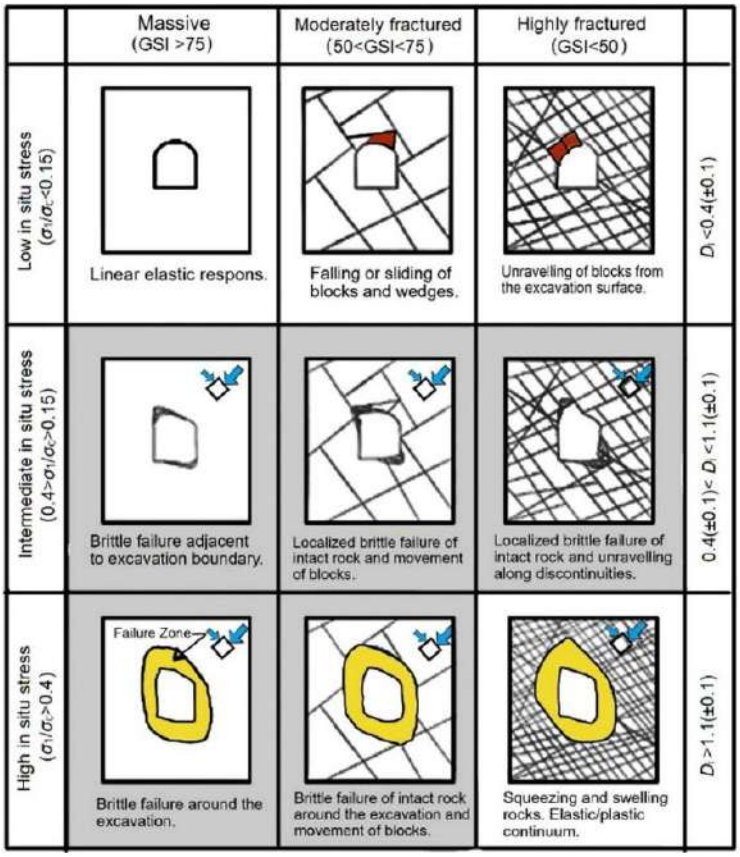

Fig. 3. Potential Failure Modes based on the Ratio of In-Situ Stress and Intact Rock Strength and GSI (after Askaripour et al. 2002; Castro et al. 2012; Hoek and Brown, 1980; Martin et al. 1998).

The continued use of rock mass classifications, such as RMR or the Q-system, for assessing excavation stability and ground support requirements remains invaluable, particularly for validating the appropriateness of numerical modelling outputs prior to the commencement of excavations (i.e. when validation will be possible).

3. Numerical Methods for Assessing Underground Excavation Stability

Case studies are presented to demonstrate the effects of different numerical methods including:

- Continuum assuming homogeneous and isotropic conditions using GSI and the Hoek-Brown Failure Criterion with 2D Finite Element Method (FEM) software, RS2 by Rocscience Inc.
- Hybrid-continuum using the Hoek-Brown Failure Criterion for intact rock and a network of discontinuities to enable heterogeneity and anisotropy with 2D FEM software, RS2.
- Hybrid-discontinuum using 2D Finite-Distinct Element Method (FDEM) software, PROROCK by Scientia.
- Discontinuum using 2D Distinct Element Method (DEM) software, UDEC, by Itasca Inc.

Over the last 20 years, the use of 2D continuum models assuming homogenous and isotropic rock mass conditions by adopting the Hoek-Brown failure criterion and GSI has become very common for tunnel and underground excavation design studies. Barton (2023) indicated that a generational change, persuaded by the ease of software use, has promoted the use of such 2D continuum modelling.

3.1. Case Study I: Drainage Tunnel in Papua New Guinea

Case study I involves the development of a 5m x 5m drainage tunnel in Papua New Guinea (Bar and Baczynski, 2018). As shown in Figure 4, the siltstone rock mass is blocky to very blocky, and has sub-horizontal bedding with two to three sets of sub-perpendicular joints. Bedding and joint conditions are generally *fair* with smooth and slightly altered joint walls. Q values range from 1 to 4, and GSI typically ranges from 40 to 55.

In-situ stresses are low with the tunnel depth not exceeding 300 m ($\sigma_1/\sigma_c<0.12$), and intact rock strength, σ_c, is in the order of 70 MPa.

Potential failure modes are generally expected to involve discontinuity-controlled block falls (considering Fig. 3), which have also been observed in an existing exploration tunnel.

Fig. 4. Very blocky siltstone. Left: fresh siltstone in existing exploration tunnel (3 m wide x 3.5 m high). Right: Slightly weathered siltstone outcrop (approx. 2m high).

Numerical methods were used to assess drainage tunnel behaviour using two approaches using 2D FEM software, RS2, with a summary of material properties shown in Table 2:

- Continuum assuming homogeneous and isotropic conditions (CHI) using the estimated GSI and the Hoek-Brown Failure Criterion. Young's Modulus (E_m) for the rock mass was estimated to be 9 GPa based on the approach by Hoek and Diederichs (2006). Hoek-Brown Damage Factor, D, was set to zero (note: this significantly improves strength and stiffness, i.e. reduces modelled displacements).
- Hybrid-continuum (HC) using the Hoek-Brown Failure Criterion for intact rock (GSI set to 100) and a network of discontinuities to enable heterogeneity and anisotropy with 2D FEM software, RS2. E_m was estimated using Hoek and Diederichs (2006) to be 40 GPa (i.e. equal to the intact rock modulus, E_i).

Table 2. Material Properties for Drainage Tunnel Numerical Models.

Numerical Method	UCS (MPa)	m_i	GSI	D	E_i (GPa)	E_m (GPa)	ν	Joint Stiffness (MPa/m)	
								k_n	k_s
CHI	70	10	45	0	40	9	0.26	N/A	N/A
HC	70	10	100	0	40	40	0.26	100,000	10,000

Elastic numerical modelling outputs are shown in Figure 5 and indicated vastly different results between the CHI and HC numerical methods:

- Behaviour type predicted by CHI was a potential for voluminous stress induced failure (BT 4, Sq.) whilst HC predicted discontinuity-controlled block falls (BT 2, Wg.).
- CHI predicts a modelled 'plastic zone' (σ_1 negative to zero) that is approximately five times deeper around the tunnel perimeter compared to the HC model.

- CHI models displacements up to ten times greater on the tunnel perimeter compared to the HC model. Similarly, at a depth of approximately 1 m behind the side walls and below the floor, CHI models at least five times higher displacements compared wo the HC model.

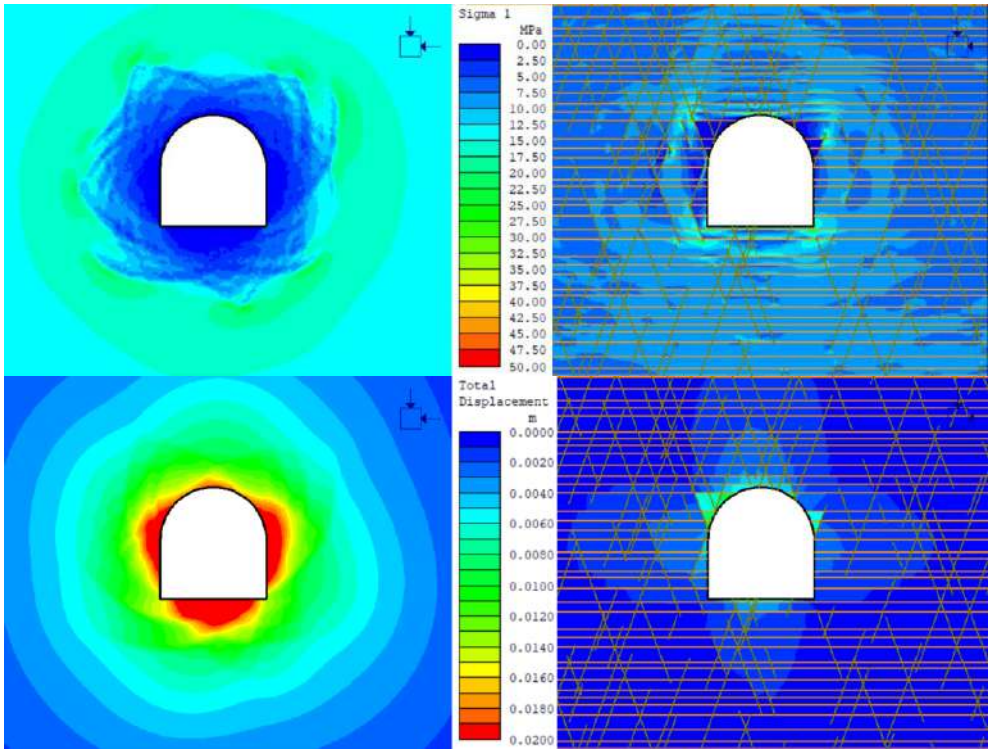

Fig. 5. Drainage Tunnel (5 m wide x 5.5 m high) 2D FEM Model Results. Top Row: Maximum Principal Stress (σ_1). Bottom Row: Total Displacement. Left: CHI (continuum, homogeneous and isotropic) model outputs showing yielded zone with depth of 2-3 m around the tunnel perimeter. Modelled behaviour type: potential for voluminous stress induced failure (BT 4, Sq.) with over 20 mm displacements up to a depth of approx. 1 m behind side walls and below floor. Right: HC (hybrid-continuum) model outputs showing minimal yielded zone of less than 0.5 m on side walls and locally unstable blocks at the tunnel shoulder. Modelled behaviour type: discontinuity-controlled block fall (BT 2, Wg.) with less than 3 mm displacements at a depth of approx. 1 m behind side walls and roof.

Ground support requirements based on the CHI model (combination of shotcrete, mesh and bolting) would be significantly higher than predicted by the HC model, which indicates only a need for spot bolting. Based on the observed excavation performance in the existing exploration tunnel (Fig. 4), the HC model outputs are significantly more realistic than the CHI model.

3.2. Case Study II: Mine Stope in Australia

Case study II involves an unsupported mine stope in an Australian gold mine. As shown in Figure 6, the stope has experienced local block falls from the metasandstone within the hanging wall. The rock mass is generally blocky with the foliation dipping at approximately 45 degrees (i.e., shallower than the ore body and stope dip), typically with two orthogonal joint sets. GSI is normally in the range of 60 to 70. Ground support and stope sizes are typically designed using Q', which range from 10 to 40.

The stope is located 500 m below surface with regional horizontal stresses approximately twice the vertical stress ($\sigma_1/\sigma_c \approx 0.26$), and σ_c is in the order of 100 MPa. The development drives are 5.5 m wide x 5 m high, and the distance between the top and bottom (extraction) drives is 40 m (stope height).

Potential failure modes are generally expected to involve localized brittle failure of intact rock and movement of blocks (discontinuity-controlled block falls), which have been observed.

Fig. 6. Blocky metasandstone on extraction level. Block falls observed from hanging wall of unsupported stope.

In a similar manner to Case Study I, CHI and HC models were used; however, plastic numerical modelling was undertaken with shear strength reduction (SSR) to estimate Factor of Safety ($SRF_{critical}$). The plastic modelling outputs in Figure 7 have vastly different results:

- CHI model predicts crown failure, i.e. Factor of Safety less than one for large span on the hanging wall of the stope.
- HC model predicts a marginally stable hanging wall with a Factor of Safety of 1.1. The potential for discontinuity-controlled block fall for kinematically unstable blocks exists.

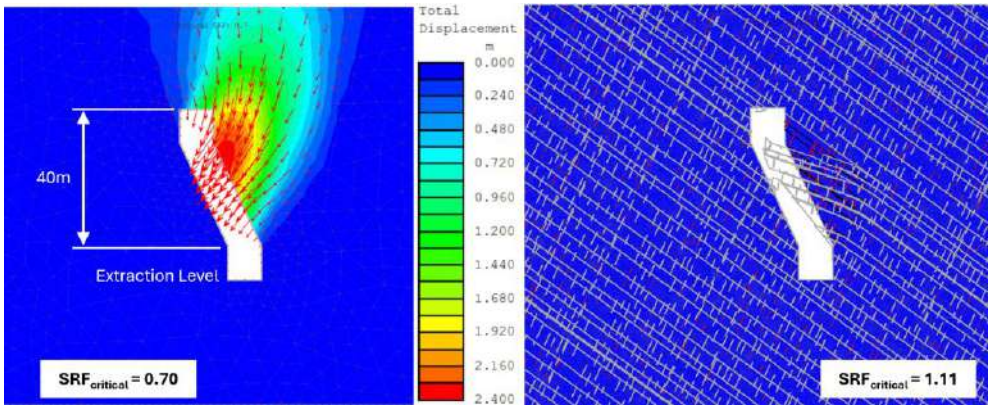

Fig. 7. Unsupported Mine Stope 2D FEM Model Results showing Total Displacement. Left: CHI (continuum, homogeneous and isotropic) model outputs show a large volume overbreak in the crown, i.e. crown failure (BT 7, Ch.), which may be a result of chimneying or progressive shear failure with a Factor of Safety of 0.7 (i.e. unstable). Right: HC (hybrid-continuum) model outputs show an exaggerated mesh distortion to illustrate discontinuity-controlled block fall (BT 2, Wg.) potential in the hanging wall; however, with the exception of kinematically unstable blocks, the hanging wall appears to be marginally stable with a Factor of Safety of 1.1.

If the stope were designed with CHI, the stope span, and therefore, height between development drives, would need to be significantly reduced to achieve stable conditions. Reduced distance between

development drives incurs significant additional costs and may result in an uneconomical mine design. The HC model appeared to be more realistic and was validated with actual stope performance (Fig. 6).

3.3. Case Study III: Cavern in Norway

Case study III reviews a 62 m span cavern excavated at Gjøvik in Norway that was initially analysed with a discontinuum approach using UDEC and model outputs were later validated with monitored displacements from extensometers (MPBX) which were installed from surface into the roof of the cavern (Barton et al. 1994). This modelling included sequenced excavation and support installation.

The cavern was constructed near surface within a gneiss rock mass that is typically blocky with Q values ranging from 1 to 30, with a weighted mean of about 9, i.e. *fair* quality rock. Based on available data, GSI is likely be in the range of 70 to 80. Stresses are very low and intact rock strength is high. Based on Figure 3, expected ground behaviour is discontinuity-controlled block falls.

Figure 8 shows modelled displacements replicating the UDEC models of Barton et al (1994) using elastic continuum and hybrid-continuum approaches using RS2 and FDEM or hybrid-discontinuum using PROROCK software.

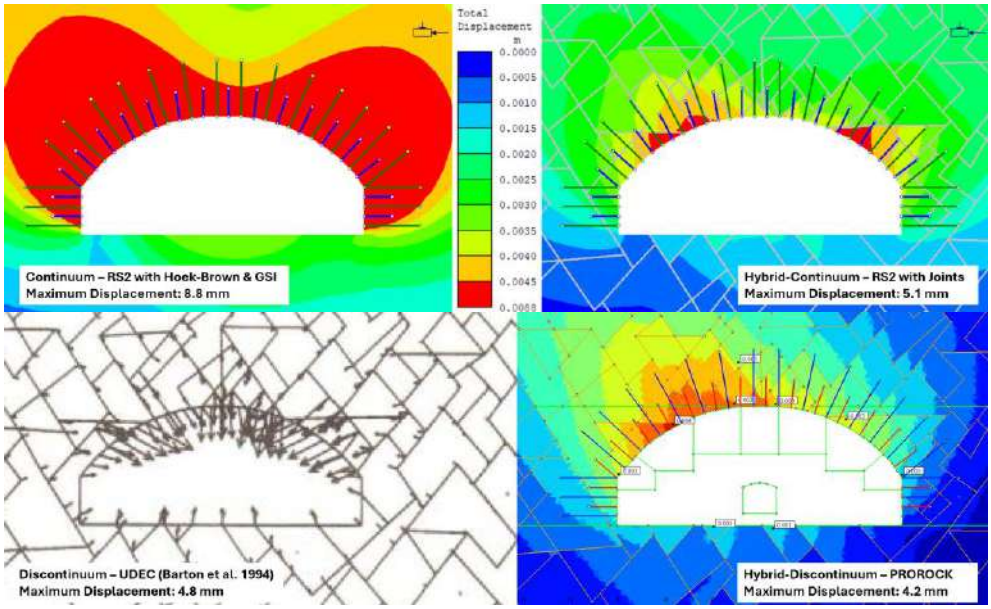

Fig. 8. Gjøvik Cavern (62m Span) 2D FEM, FDEM and DEM Elastic Model Results showing Total Displacement or Displacement Vectors. CHI (continuum, homogeneous and isotropic) model outputs show a significantly larger zone of displacement than the HC, FDEM and DEM models.

In a similar manner to Case Studies I and II, the CHI (continuum, homogenous and isotropic) model outputs show a significantly larger zone of displacement than the HC, FDEM and DEM models. The HC (hybrid-continuum) also shows a slightly larger zone of displacements compared to the FDEM and DEM models. In terms of absolute, modelled displacements, CHI predicted approximately twice the displacements of HC, FDEM and DEM models, which all had quite similar results.

4. Discussion and Key Findings

The number of experienced rock engineers appears to be decreasing over the last decade with a significant drop in university graduates from the discipline. The demand for rock engineering projects requiring numerical methods is increasing, which means less experienced engineers with more projects around the world. At the same time, access to easy-to-use numerical modelling software has become ever more abundant, i.e. more engineers are applying numerical methods, and often they have less experience than their predecessors.

Continuum modelling approaches offer a simple and fast means of predicting ground behaviour. By way of example, in three case studies presented, the homogeneous, isotropic, continuum models using the Hoek-Brown failure criterion presented in this paper each took less than one hour to develop and a few seconds to compute results. The hybrid continuum and FDEM models to several hours to develop, and perhaps a few minutes to compute.

When applying continuum approaches and the Hoek-Brown Failure Criterion, an engineer or practitioner should be considerate of:

- Limitations of GSI and the Hoek-Brown Failure Criterion as described by Marinos et al (2005) and Hoek and Brown (2019).
- The simplification of engineering geological characteristics of the rock mass such as the complex assemblage of bedding, foliation, joints and other discontinuities is simplified into a single number (GSI), which assumes homogeneous and isotropic strength and stiffness. As demonstrated in the three case studies, this simplification often results in:
  - Model predicting an incorrect behaviour type or inappropriate failure mechanism.
  - Over-estimating the depth of yielding and over-estimating total displacements (potential requirement for additional support, and therefore, additional cost).
  - Under-estimating Factor of Safety (potential requirement for additional support and reduced excavation spans, and therefore, additional cost).
- GSI and Damage Factor, D, have a profound effect on the estimated rock mass modulus, E_m, when applying the approach by Hoek and Diederichs (2006). Estimation of E_m using different empirical methods yields vastly different and variable results (Bar and Schubert, 2023).
- Limitations in continuum approaches for modelling absolute displacements since it is represented as a continuous displacement field (Sjöberg, 1999) in which 'detachment' cannot occur. As such, continuum models often predict 'larger zones of displacement'.
- The above limitations are also applicable to Mohr-Coulomb and other failure criteria.

Discontinuum approaches including hybrid continuum, FDEM and DEM, offer a more comprehensive representation of engineering geological conditions and generally provide more realistic outputs in terms of modelling ground behaviour, failure mechanisms and predicting displacements. However, each model provides results for only a single assemblage of discontinuities, i.e. several iterations of possible assemblages should be modelled to ensure ground behaviour is adequately assessed.

With limitations in site investigations and inherent uncertainty in ground conditions, practitioners should always remember that *all models are ultimately wrong, but some are useful*, and that wherever possible, calibration or validation with actual ground behaviour should be a key point of focus.

Acknowledgements

The writer sincerely thanks Dr Nick Barton of Nick Barton and Associates for familiarization with the Gjøvik cavern project and Mr Bulat Iliasov of Scientia for his assistance with 2D FDEM modelling using PROROCK.

References

Askaripour, M., Saeidi, A., Rouleau, A., Mercier-Langevin, P., 2002. Rockburst in underground excavations: A review of mechanism, classification, and prediction methods. *Underground Space*, 7, 577-607.

Bar, N., Baczynski, N.R.P., 2018. Ground Characterization and Design of a Drainage Gallery Tunnel Network for a Large Open Pit Mine in a High Rainfall Environment. Proceedings of ARMS10: 10th Asian Rock Mechanics Symposium, Singapore, 29 October to 3 November 2018, 12p.

Bar, N., Schubert, W., 2023. Evaluation of different methods for determining rock masses stiffness. Proceedings of 15th ISRM Congress & 72nd Geomechanics Colloquium, Salzburg, 9-14 October 2023, 2290-2295.

Barton, N., 2023. GSI or JRC -continuum or discontinuum modelling -some suggestions and some critique. Proceedings of 15th ISRM Congress & 72nd Geomechanics Colloquium, Salzburg, 9-14 October 2023 7p.

Barton, N., 2025. Twenty Strange Years in the World of Rock Mechanics and Engineering Geology. *Current Trends in Civil & Structural Engineering*, 11(4), 13p.

Barton, N., By, T.L., Chryssanthakis, P., Tunbridge, L., Kristiansen, J., Løset, F., Bhasin, R.K., Westerdahl, H., Vik, G., 1994. Predicted and Measured Performance of the 62m Span Norwegian Olympic Ice Hockey Cavern at Gjøvik. International Journal of Rock Mechanics, Mining Science & Geomechanics Abstracts, 31(6), 617-641.

Barton, N., Grimstad, E., Abrahão, R., Bar, N., 2024. Q-based developments during the last 50 years. Fjellsprengningskonferansen 2024, 24.1-24.34.

Barton, N., Lien, R., Lunde, J., 1974. Engineering classification of rock masses for the design of tunnel support. *Rock Mechanics*, 6(4), 189-236.

Bieniawski, Z.T., 1973. Engineering Classification of Jointed Rock Masses. *Transactions of the South African Institution of Civil Engineering*, 15(12), 335-344.

Bieniawski, Z.T., 1989. Engineering rock mass classifications. John Wiley & Sons, United States, 251p.

Castro, L.A.M., Bewick, R.P., Carter, T., 2012. An overview of numerical modelling applied to deep mining. In Innovative Numerical Modelling in Geomechanics, CRC Press, 22p.

Duncan, J.M., 1996. State of the Art: Limit Equilibrium and Finite-Element Analysis of Slopes. *Journal of Geotechnical Engineering*, 122(7), 577-596.

Erharter, G.H., Bar, N., Hansen, T.F., Jain, S., Marcher, T., 2024. International Distribution and Development of Rock Mass Classification: A Review. Rock Mechanics and Rock Engineering.

Gigli, G., Frodella, W., Mugnai, F., Tapete, D., Cigna, F., Fanti, R., Intrieri, E., Lombardi, L., 2012. Instability mechanisms affecting the cultural heritage sites in the Maltese Archipelago. *Natural Hazards and Earth System Sciences*, 12(6), 1883-1903.

Hoek, E., Brown, E.T., 1980. Empirical Strength Criterion for Rock Masses. *Journal of the Geotechnical Engineering Division*, ASCE 106 (GT9), 1013-1035.

Hoek, E., Brown, E.T., 1997. Practical estimates of rock mass strength. *International Journal of Rock Mechanics and Mining Sciences*, 34, 1165-1186.

Hoek, E., Brown, E.T., 2019. The Hoek-Brown failure criterion and GSI - 2018 edition. *Journal of Rock Mechanics and Geotechnical Engineering*, 11, 445-463.

Hoek, E., Diederichs, M.S., 2006. Empirical estimation of rock mass modulus. International Journal of Rock Mechanics and Mining Sciences, 43, 203–215.

Jing, L., 2003. A review of techniques, advances and outstanding issues in numerical modelling for rock mechanics and rock engineering. *International Journal of Rock Mechanics & Mining Sciences*, 40, 283-353.

Mahabadi, O.K., Lisjak, A., Munjiza, A., Grasselli, G., 2012. Y-Geo: New Combined Finite-Discrete Element Numerical Code for Geomechanical Applications. *International Journal of Geomechanics*, 2012, 12, 676-688.

Marinos, V., 2019. A revised, geotechnical classification GSI system for tectonically disturbed heterogeneous rock masses, such as flysch. Bulletin of Engineering Geology and the Environment, 78, 899-912.

Marinos, V., Marinos, P., Hoek, E., 2005. The geological strength index: applications and limitations. *Bulletin of Engineering Geology and the Environment*, 64, 55-65.

Martin, C.D., Kaiser, P.K., McCreath, D.R., 1998. Empirical estimation of rock mass modulus. *International Journal of Rock Mechanics & Mining Sciences*, 43, 203-215.

Oke, J., Vlachopoulos, N., Marinos, V., 2013. Umbrella Arch Nomenclature and Selection Methodology for Temporary Support Systems for the Design and Construction of Tunnels. *Geotechnical and Geological Engineering*, 32(1), 97-130.

Schubert, W., Goricki, A., Riedmüller, G., 2003. The Guideline for the Geomechanical Design of Underground Structures with Conventional Excavation. Felsbau, 21(4), 13-18.

Sjöberg, J., 1999. Analysis of Large Scale Rock Slopes. PhD Thesis. Luleå University of Technology, Sweden.

Stead, D. and Coggan, J. 2012. Numerical modeling of rock-slope instability. In Landslides: Types, Mechanisms and Modeling. Cambridge University Press, United Kingdom.

Southeastern Europe Tunnelling Conference (SETC-2025)
1-3 October 2025, Belgrade, Serbia

DOI: 10.5937/SETC25024M

Optimal Shield TBM Face Pressure for Surface Settlement Control: Belgrade Metro Case Study

Uroš Mirković[a], Nikola Mirković[a], Slobodan Radovanović[a], Nikola Divac[a], Jovan Šaponjić[a], Nikola Milivojević[a] and Dejan Divac[a]*

[a] Jaroslav Černi Water Institute, Belgrade, Serbia; uros.mirkovic@jcerni.rs, nikola.mirkovic@jcerni.rs, slobodan.radovanovic@jcerni.rs, nikola.divac@jcerni.rs, jovan.saponjic@jcerni.rs, nikola.milivojevic@jcerni.rs, dejan.divac@jcerni.rs.

Abstract: Precise control of face pressure is essential in shield TBM tunneling to limit surface settlements and ensure the stability of surrounding structures, particularly in densely built-up urban environments. This study focuses on determining the optimal shield TBM face pressure for the specific geotechnical conditions of Phase 1, Line 1 of the Belgrade Metro, along the section from Bele Vode Station to Trgovačka Station. Three-dimensional numerical models, developed using a staged construction approach, realistically simulate sequential excavation, shield advancement, and segment installation, while incorporating representative ground properties and structural characteristics. A sensitivity analysis is conducted by systematically varying face pressure values to assess their influence on the magnitude and distribution of surface settlements. The results identify an optimal face pressure range that minimizes surface settlements while maintaining excavation stability. These findings provide practical guidance for shield TBM operation in urban tunneling, contributing to more effective settlement control and improved risk mitigation in shallow urban tunnel construction.

Keywords: shield TBM; face pressure; surface settlement; numerical modelling; sensitivity analysis; urban tunneling

1. Introduction

The rapid growth of urban areas has increased the demand for infrastructure solutions that are both sustainable and space-efficient, leading to a greater reliance on underground construction. With surface space becoming increasingly limited, metro and other subsurface transit systems offer an effective way to reduce congestion and meet rising transportation needs. Mechanized tunneling, and in particular the use of shield tunnel boring machines (shield TBMs), enables excavation with minimal disruption to surface activities while maintaining high safety standards in densely populated environments.

In shield TBM tunneling, face pressure is one of the most critical parameters influencing ground stability. Inadequate control of this parameter can cause excessive surface settlements, posing serious risks to buildings, utilities, and other surface infrastructure. Establishing the optimal face pressure is therefore a key requirement for ensuring excavation stability and controlling ground movements, especially in shallow tunnels and geologically variable conditions. In addition, maintaining appropriate confinement pressure around the shield, ensuring face stability, and controlling the annular overcut while continuously backfilling the tail void are recognized as critical factors for effective ground control. Real-time monitoring of these operational parameters is essential for minimizing volume losses and surface settlements, further highlighting their significance in shield TBM tunneling (, 2018). Previous research has investigated settlement mechanisms, employed numerical modeling techniques, and evaluated shield TBM operational parameters to manage ground deformation. Building on this foundation, the present study concentrates on determining the optimal face pressure for shield TBMs under the specific geotechnical and urban conditions of the Belgrade Metro. This is achieved through detailed three-dimensional numerical simulations and sensitivity analysis, applied to the site-specific

*Corresponding author: nikola.mirkovic@jcerni.rs (N. Mirković).

conditions of Phase 1, Line 1, along the section from Bele Vode Station to Trgovačka Station.

Extensive studies have examined how key operational and geotechnical factors influence ground behavior during shield tunneling. Fargnoli et al. (2013) investigated how face pressure, grouting pressure, and machine thrust affect settlement patterns in earth pressure balance (EPB) tunneling through coarse-grained soils, and introduced a translated Gaussian cumulative curve to more accurately describe subsidence trough development. Do et al. (2021) demonstrated that face pressure, grouting pressure, and shield geometry significantly influence settlements, and identified critical parameter values for the Hanoi Metro case. Similarly, Ter-Martirosyan et al. (2022) found a strong correlation between TBM face pressure and increased surface settlement during EPB tunneling in the Moscow Metro. Beghoul and Demagh (2019) used 3D numerical modeling to show that moderate face pressure, shield conicity, and tail grouting pressure can effectively control settlement and prevent face instability in soft ground. Similarly, Kavvadas et al. (2017) confirmed through 3D finite element analysis that while moderate face pressure reduces ground loss, cutterhead overcut and shield geometry significantly affect surface settlement, which can be further minimized with optimized tail grouting.

Advanced numerical models are widely used to simulate TBM-ground interaction and optimize excavation parameters. Ring and Comulada (2018) employed a 3D iterative model to simulate TBM face and grouting pressures, achieving results that closely matched field data from Rio de Janeiro's Line 4 tunneling project. Luo et al. (2023) studied surface settlement from shield tunneling using grey relational analysis and numerical simulations, identifying thrust force, grouting pressure, earth pressure, and soil elastic modulus as the key factors influencing ground deformation during metro tunnel construction. Numerous studies have used numerical modeling to examine factors influencing ground and structural responses during TBM tunneling. Comodromos et al. (2014) employed a 3D numerical model to evaluate ground and building movements during TBM-EPB tunneling, demonstrating the effects of face pressure, gap grouting, and slurry on settlement, with findings validated on the Thessaloniki metro. Alsirawan et al. (2023) created a numerical model to evaluate TBM-induced settlements, highlighting tunnel diameter, eccentricity, and overburden depth as key factors, and proposed a validated equation to predict maximum structural settlement.

Accurate prediction of ground settlement has been a central focus of previous research, aiming to enhance tunnel design and tailor excavation parameters to site and geometric conditions. Kim et al. (2020) found modest statistical correlations between surface settlement and various geotechnical, geometrical, and operational factors, concluding that settlements result from the combined effect of multiple parameters. Zhu and Li (2017) improved settlement prediction by incorporating six operational and soil parameters into a modified gap parameter model, validated on the Xi'an Metro project. Bogusz et al. (2021) investigated the empirical variability of settlement trough parameters in EPB tunneling, highlighting the importance of deriving these values from data under similar ground and operational conditions.

Numerous studies have also examined the influence of soil types and time-dependent behaviors on settlement during mechanized tunneling. Ayasrah et al. (2020) found that slurry shield tunneling in granular soils usually produces maximum transverse settlements within a zone about 2.6 times the tunnel diameter. For sandy soils, Chen et al. (2022) developed a new analytical method that accounts for soil arching to predict subsurface settlement along the tunnel centerline. In clayey soils, Hashimoto et al. (1999) proposed a two-phase deformation model for shield tunneling, separating immediate deformations during shield passage from later, delayed deformations. Building on this, Meng et al. (2022) applied 3D finite element analysis to examine soil disturbance in various clays, identifying characteristic disturbance zones influenced by soil properties and cover-to-depth ratios.

Effective control of shield TBM tunneling-induced settlements requires an integrated approach combining realistic operational parameters, advanced soil models, and numerical methods. When supported by analytical assessment, these tools enable accurate simulation of soil behavior, TBM mechanics, and tunnel lining response, which is essential for safe urban tunneling. The most important factor, however, is ensuring proper control of machine performance through an experienced team supported by a comprehensive monitoring program. Equally important is the selection of an experienced contractor and an appropriate machine type. In this context, the primary goal of this study

is to develop and validate a methodology based on staged 3D numerical simulations and sensitivity analysis of face pressure for controlling surface settlements. The proposed framework provides practical guidance for managing shield TBM operations, enhancing ground stability, and minimizing risks to adjacent and overlying structures, streets and underground utilities.

In addition to the introductory Chapter 1, the paper includes four further chapters. Chapter 2 provides a technical overview of Belgrade Metro - Phase 1, Line 1. Chapter 3 presents the proposed methodology, including the development of numerical models and the calculation procedures. Chapter 4 details the results of the numerical simulations and provides a discussion of them. Chapter 5 summarizes the main findings and presents the conclusions.

2. Technical Overview of Belgrade Metro - Phase 1, Line 1

Belgrade, the capital of Serbia, is experiencing rapid urbanization and population growth, which is placing significant strain on its public transportation network. This has underscored the need for a high-capacity and sustainable mass transit system. To address this, the city has initiated the construction of a modern metro as part of its long-term urban mobility plan, starting with Phase 1 of Line 1.

This chapter presents a comprehensive overview of the route alignment, subsurface and geotechnical conditions, tunnel design characteristics, shield TBM specifications, constructability and risk management considerations for Phase 1 of Line 1 of the Belgrade Metro. These aspects form the basis for the numerical modeling and optimization methodology described in the subsequent section.

2.1. Route alignment

Route of Phase 1, Line 1 of the Belgrade Metro covers about 15.4 km, extending from Železnik Station in the south to Pančevački Most Station in the north (Fig. 1). Along the route, there are 15 metro stations and 10 ventilation and evacuation shafts.

Fig. 1. Route of Phase 1, Line 1 of the Belgrade Metro, showing sections and stations.

Approximately 11.3 km of Phase 1 of Line 1 (from km. 4+174.98 to km. 15+441.15) will be constructed using shield TBMs, divided into southern (Bele Vode Station to Sajam Station) and northern

(Karaburma Launching Shaft to Sajam Station) sections. The remaining sections will use cut and cover (from km. 2+066.45 to km. 4+174.98) and at grade construction (from km. 0+000 to km. 2+066.45).

The geometric parameters of the route alignment are carefully defined to optimize construction and operational performance. A minimum horizontal curve radius of 350 m is adopted on mainline tracks to ensure consistent shield TBM performance during tunnel excavation. The vertical alignment includes a minimum curve radius of 2500 m, while the maximum longitudinal gradient is set at 4.5% (Figure 2).

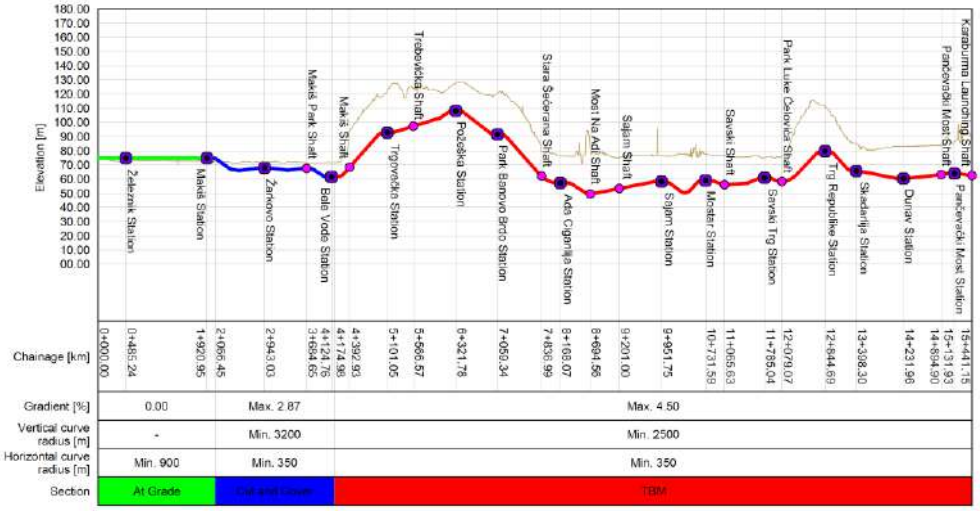

Fig. 2. Vertical alignment of Phase 1, Line 1 of the Belgrade Metro.

2.2. Subsurface and geotechnical conditions

The TBM tunnel alignment traverses a geologically complex urban corridor characterized by alternating soil and rock units, tectonic discontinuities, and variable groundwater conditions, all of which significantly influence tunneling performance.

The shield TBM excavating the southern section begins at Bele Vode Station and advances toward Sajam Station. From Bele Vode to Trgovačka, the alignment includes 150 m of shallow, water-saturated fluvial deposits, then passes through compact interbedded marls, limestones, sandstones, and claystones with weathered rock and cavernous fractures. From Trgovačka to Požeška, it crosses tectonically deformed, highly permeable Cretaceous rocks with karstification and multiple discontinuities. From Požeška to Park Banovo Brdo, geology consists of coarse conglomerates, breccias, and fractured porous karstified limestones. From Park Banovo Brdo to Ada Ciganlija, the tunnel passes layered conglomerates, breccias, fractured reef limestones, and tectonized clays and marls. From Ada Ciganlija to Sajam, it crosses clay deposits, gravelly sands, marls, friable clays, and karstified limestones.

The northern section excavated by the shield TBM starts at Karaburma Launching Shaft and progresses toward Sajam Station. Initial excavation passes through porous, karstified limestones and firm to semi-firm marls. From Pančevački most to Dunav Station, the alignment includes marl-limestone sediments, compressible clays, and silty sands, with fossil landslide deposits near Dunav Station. Between Skadarlija and Savski Trg, the TBM advances through gravelly sands, silty and marly clays, and laminated limestones. From Savski Trg to Mostar and Sajam, it passes fractured karstified limestones, coarse sandstones, gravelly sands, local marls and clays, with faults and stabilized landslide zones.

Based on the geological assessment conducted through investigative works along the metro alignment, distinct macro-zones were identified within the TBM excavation (Figure 3). The analysis focuses on

macro-zones B1 and B2, along the section from Bele Vode to Trgovačka Station, which will be constructed first, with the experience used to adapt excavation for the remaining sections.

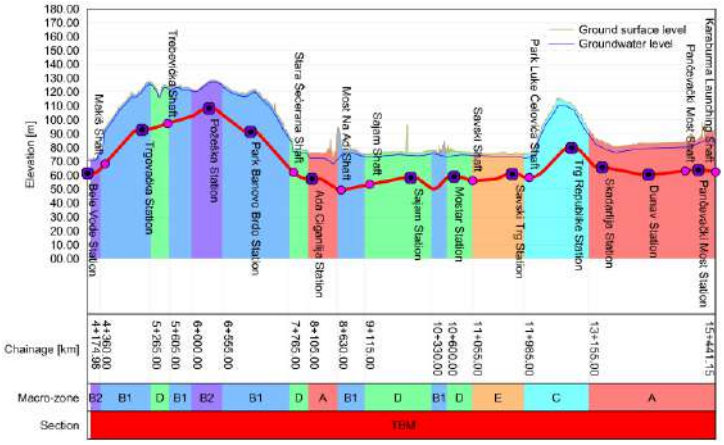

Fig. 3. Macro-zone distribution along the TBM section of Phase 1, Line 1 of the Belgrade Metro.

The stratigraphic distribution and corresponding geotechnical parameters for macro-zone B1 and B2 are presented in Table 1, providing essential data for tunnel design and construction planning.

Table 1. Stratigraphic distribution of ground layers by macro-zones B1 and B2 of Phase 1, Line 1 of the Belgrade Metro, along the section from Bele Vode Station to Trgovačka Station.

Macro-zone	Geotechnical parameters
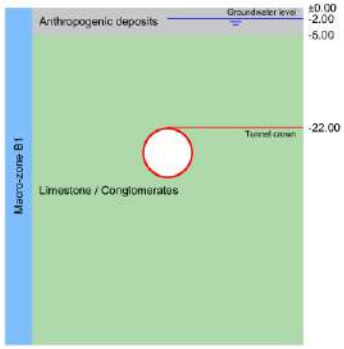	Ground layer | γ [kN/m³] | c [kPa] | ϕ [°] | E [GPa] 1 | 19 | 5 | 21 | 0.003 2 | 26 | 100 | 40 | 0.300
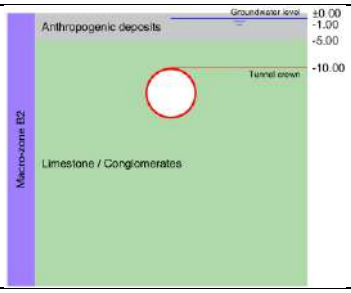	Ground layer | γ [kN/m³] | c [kPa] | ϕ [°] | E [GPa] 1 | 19 | 5 | 21 | 0.003 2 | 26 | 90 | 45 | 0.600

2.3. Tunnel design characteristics

The TBM tunnel has a nominal internal diameter of 8.55 m and a minimum functional diameter of 8.35 m. The segmental lining is 40 cm thick, with each tunnel ring consisting of seven segments and having a ring width of 1.6 m. Figure 4 illustrates a typical cross-section of the TBM tunnel, showing the tracks, the structure gauge based on rolling stock clearance requirements, and the arrangement of tunnel equipment.

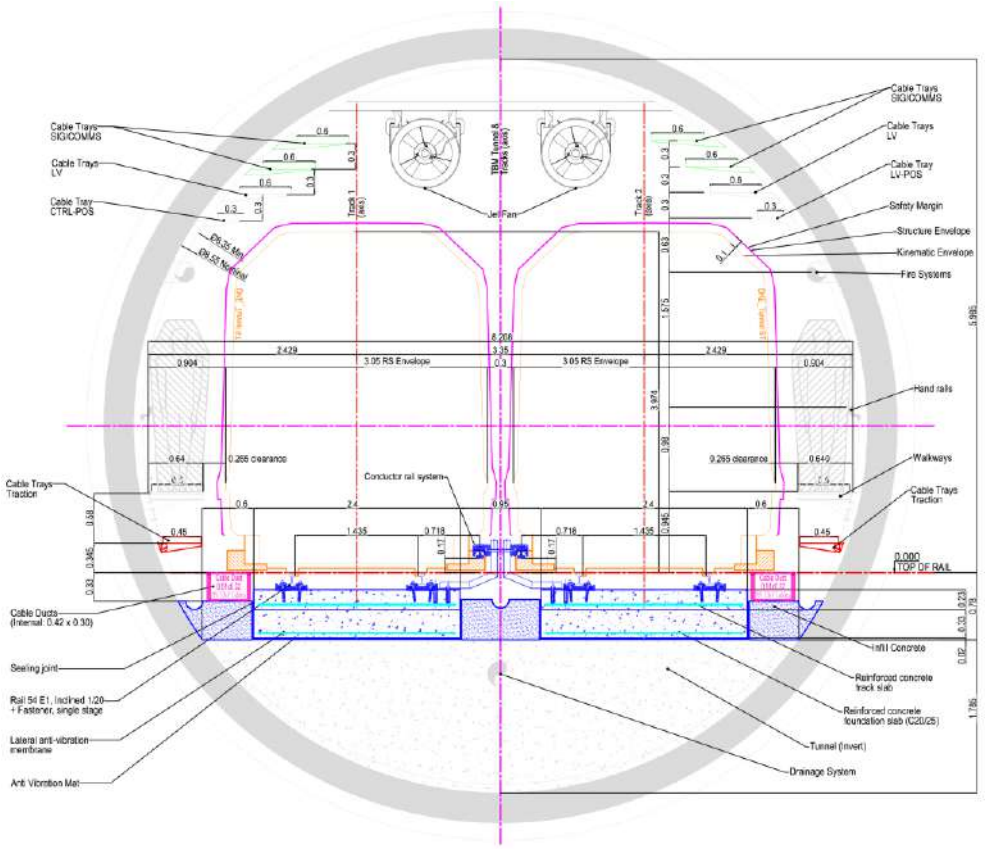

Fig. 4. Typical cross-section of the TBM tunnel on the main line (Alstom, 2025).

2.4. Shield TBM specifications

The TBM used for this project is an EPB machine with a total system length of approximately 100 m, while the main body, which includes the cutterhead and screw conveyor, measures around 12.3 m (Fig. 5). It is engineered to navigate horizontal curves with a minimum turning radius of 300 m and to manage vertical gradients of up to 5.0%, ensuring adaptability to complex tunnel alignments.

The cutterhead features a robust structure designed for balanced load distribution and efficient excavation. With a diameter of 9.6 m, an overall opening rate of 38%, and a center opening rate of 32%, it facilitates effective soil removal and stable face pressure. Its main components are fabricated from high-strength Q355 steel, providing the necessary durability for challenging urban tunneling environments.

The shield structure is optimized for excavation in mixed ground conditions, with the front shield featuring an outer diameter of 9550 mm and a plate thickness of 70 mm, while the tail shield measures 9520 mm in diameter with 60 mm thick plating. The average shield diameter is 9535 mm, and the entire structure is fabricated from high-strength Q355 steel to ensure durability and rigidity. The TBM features a synchronous bi-component grouting system with 8+8 tail shield pipes for precise annular gap filling, alongside a probe drilling and injection unit for targeted pre-excavation grouting, enhancing ground stability in challenging geology.

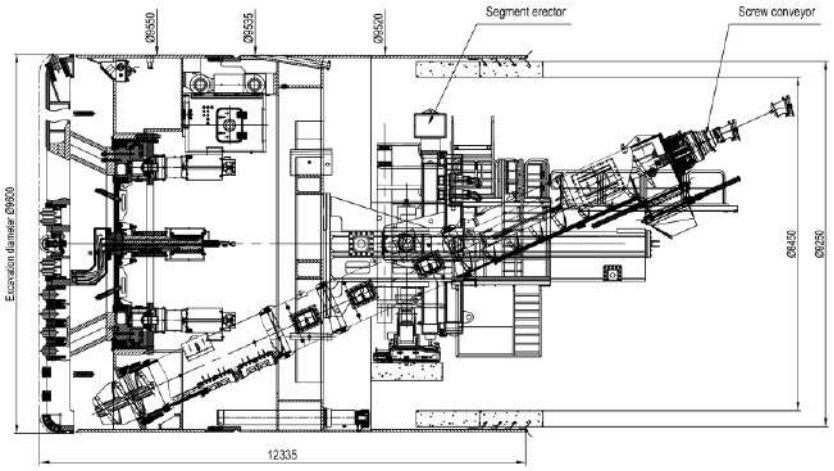

Fig. 5. Longitudinal section of the EPB TBM (main machine only) (CRCHI, 2025).

The propulsion system comprises 38 thrust cylinders (Φ300/260-2600 mm), delivering a maximum thrust force of 94,012 kN at 350 bar and a propulsion speed of up to 80 mm/min. This configuration ensures reliable advance through varying geological formations.

Material removal is handled by a screw conveyor with a 1120 mm internal cylinder diameter and a maximum discharge capacity of 900 m³/h. The excavated material is then transferred to a belt conveyor system featuring a 1000 mm wide belt and an approximate length of 70 m, enabling spoil transport at rates of up to 1000 m³/h.

2.5. Constructability and risk management considerations

The construction of Phase 1 of Line 1 of the Belgrade Metro presents a complex engineering challenge due to its integration into an urban environment characterized by diverse subsurface and geological conditions, dense infrastructure, and a high population density. To ensure the project's success, a comprehensive approach to constructability and risk management is essential.

The alignment crosses karstified limestones, fractured rocks, and water-saturated deposits, necessitating thorough geotechnical investigations to inform tunnel design and TBM selection. The southern section of route is relatively favorable for TBM excavation, while the northern section presents greater challenges due to complex geology. Macro-zones B1 and B2 are suitable, whereas other zones are less optimal. In some segments, the overburden is only around 10 m, complicating surface settlement control, while the high groundwater level presents a significant engineering challenge.

For the approximately 11.3 km TBM tunnel section, feasibility is challenged by a minimum horizontal curve radius of 350 m and a maximum longitudinal gradient of 4.5 %. Although the TBM can navigate curves as tight as 300 m and gradients up to 5.0 %, these conditions approach its design limits and may require careful management in demanding sections.

Furthermore, while the conceptual design for the TBM-driven tunnel follows standard practices for double-track metro tunnels, issues related to emergency evacuation, fire safety, and smoke management in a single-bore bi-directional tunnel remain crucial importance. These aspects will need to be carefully addressed through detailed analysis by specialized teams and integrated into the overall tunnel safety and emergency planning framework.

Advanced technologies are key to managing constructability and risks in Phase 1 of Line 1. Digital tools such as Building Information Modeling (BIM) and Geographic Information Systems (GIS) support detailed planning and help identify potential conflicts before construction. Real-time monitoring systems track ground movements, structural integrity, and environmental conditions to enable proactive management of anomalies.

Managing risks during tunnel excavation with a shield TBM requires both qualitative and quantitative assessments. Identifying potential hazards, such as ground instability, water ingress, or equipment failure, allows for prioritizing mitigation measures. The following risk assessment scale (Table 2) provides a framework to evaluate risk severity and guide appropriate actions before excavation begins.

Table 2. Risk assessment level with corresponding scores and descriptions.

Score	Level	Description
1	Insignificant	No immediate action needed; risks should still be monitored, and procedures for the construction phase must be in place.
2	Moderate (acceptable)	Work may proceed; risks should be monitored, and construction phase procedures must be maintained.
3	Important (to monitor)	Work cannot begin until risks are mitigated; resolution may require minor adjustments to the project.
4	Unacceptable	Work cannot begin until risks are mitigated; resolution requires significant project changes.

From a quantitative analysis perspective, the preliminary design of Phase 1 of Line 1 of the Belgrade Metro evaluates the sensitivity of existing structures, classifying them into six categories, with Category F covering infrastructure. Example thresholds (e.g., 10 mm settlement) are provided, but actual allowable limits must be set by the asset owner. Applying a single settlement value to all structures is oversimplified and ignores risk analysis, which is essential in modern tunnelling design. Strict adherence to low thresholds would slow TBM progress and increase costs, whereas risk-based assessments indicate that higher settlements (up to 20 mm) may be acceptable for some buildings.

Lake et al. (1996) associated slope values and maximum absolute settlement in structures with defined categories of damage, thereby providing a framework for assessing the potential impact of ground movements on the structural integrity of buildings. This classification, summarized in Table 3, serves as a practical guideline for engineers to evaluate the severity of tunnelling-induced deformations in urban environments.

Table 3. Damage classifications with typical values of maximum building slope and settlement for risk assessment (Lake et al., 1996).

Risk category	Maximum building slope	Maximum building settlement [mm]	Risk description
I	< 1/500	< 10	Negligible: Superficial damage is unlikely.
II	1/500 - 1/200	10 - 50	Slight: Superficial damage is possible but unlikely to have structural significance.
III	1/200 - 1/50	50 - 75	Moderate: Superficial damage is expected, with possible structural damage to buildings and potential damage to relatively rigid pipelines.
IV	> 1/50	> 75	High: Structural damage to buildings and rigid pipelines is expected, with possible damage to other types of pipelines.

3. Methodology

This chapter presents the methodology for simulating sequential excavation, shield advancement, and segment installation of the Belgrade Metro Phase 1, Line 1. The approach enables systematic evaluation of face pressure variations and their effects on the surrounding ground, providing a basis for defining optimal operational parameters to ensure safe tunnel construction and effective control of surface settlements.

3.1. Numerical modeling of shield TBM excavation

Three-dimensional Finite Element Models (FEMs) were developed using Midas GTS NX (2025), including the shield TBM, tunnel segmental lining, and surrounding soil and rock mass (Figure 6). The rock and soil mass were represented by solid elements defined according to the macro-zones described in the previous chapter, enabling realistic simulation of ground settlements and stress-strain behavior during tunnel excavation. The constitutive behavior of the rock mass was modeled using the Mohr-Coulomb model, which has been adopted as the initial framework for this study. In subsequent design phases, and as required by the results of additional geological investigations, the model may be adjusted or replaced with other suitable models, depending on the geological conditions along the tunnel alignment.

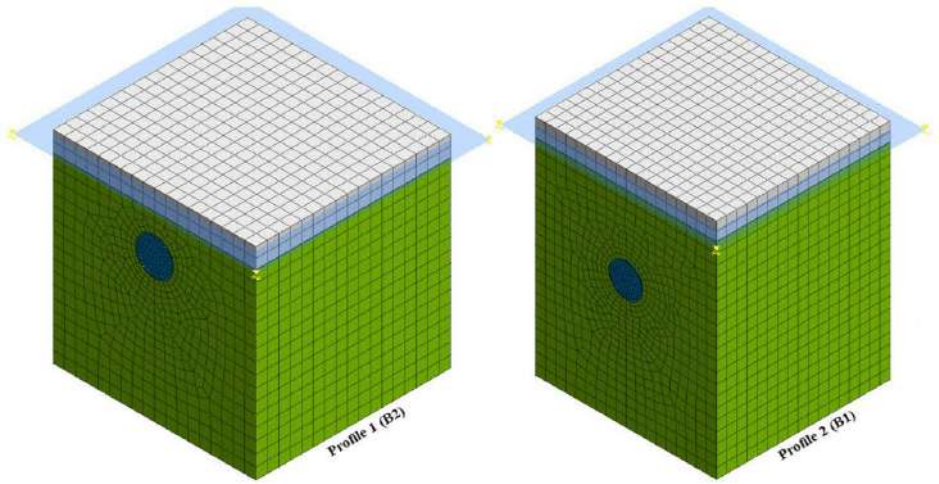

(**a**) (**b**)

Fig. 6. Three-dimensional FEMs with macro-zones B2 (a) and B1 (b) for Phase 1, Line 1 of the Belgrade Metro, along the section from Bele Vode Station to Trgovačka Station.

The finite element mesh was generated from the model geometry in accordance with the TBM construction method. Excavation was simulated in phases, with each step representing a separate stage of tunnel advancement. A hybrid mesh was employed, resulting in models with approximately 25,000 elements and 155,000 nodes for Profile 1 (B2), and about 26,000 elements and 165,000 nodes for Profile 2 (B1). Figure 7 shows the basic elements of the models, including the overburden layer, which ranges in thickness from 10 m at Profile 1 (B2) to 22 m at Profile 2 (B1).

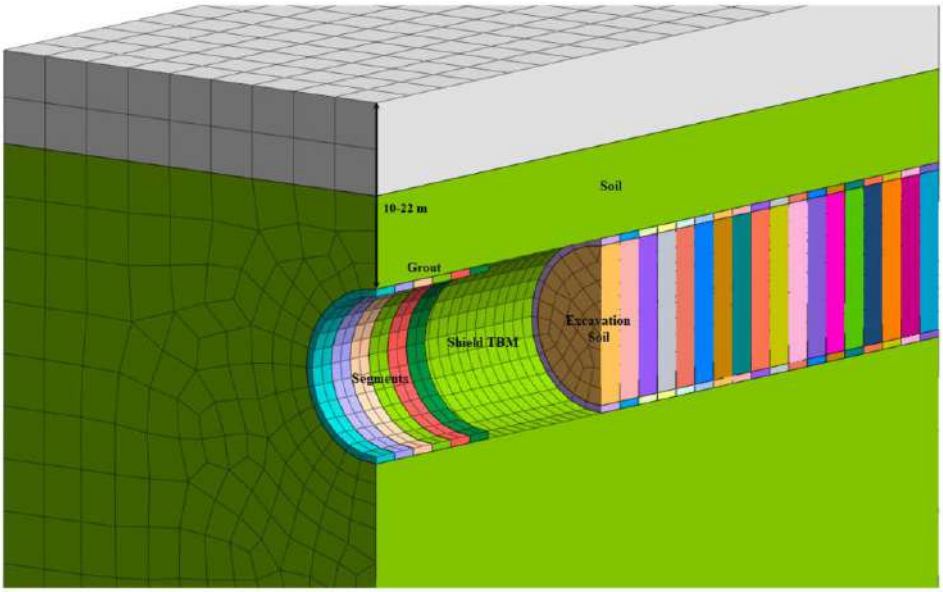

Fig. 7. Vertical cross-section of the model elements.

The steel shield of the TBM, 6.5 cm thick, together with the injection grout of equal thickness, is modeled as a surface element, while the segmental concrete lining, 40 cm thick and 1.60 m wide, is modeled as a volumetric element. All components are represented using linear elastic material models (Figure 8).

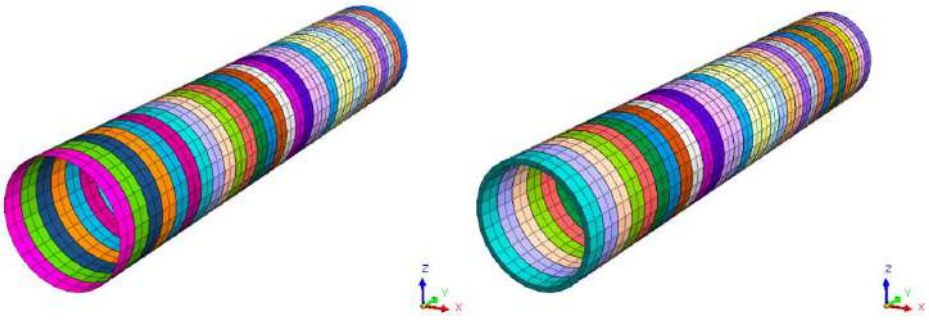

(**a**) (**b**)

Fig. 8. Shield / injection grout (a) and segmental lining (b) in the model.

Displacement boundary conditions are defined such that displacements are fully restrained at the bottom boundary of the rock mass, while at the lateral boundaries, displacement is restricted in the direction perpendicular to the model plane (Figure 9). This setup ensures a realistic representation of rock mass behavior and its deformation under self-weight. The groundwater level is 1.0 m below the ground surface at Profile 1 (B2) and 2.0 m below the ground surface at Profile 2 (B1).

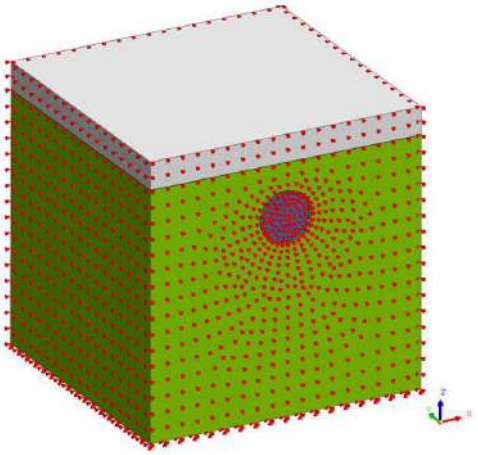

Fig. 9. Applied boundary conditions of the model.

The shield of the TBM in the model has a length of 12.8 m and a diameter of 9.35 m. The machine advances through the model in increments of 1.6 m, corresponding to the length of one concrete ring. Shield movement is simulated by sequentially activating elements at the front and deactivating elements behind the shield. During the analysis, the load due to self-weight is automatically generated in the FEM model based on the adopted geometry of the structure and surrounding soil. Self-weight is considered the initial load, establishing the initial stress state of the model.

A key feature of excavation with an EPB TBM is the continuous application of pressure on the tunnel face (Figure 10(a)). The pressure is controlled within the cutterhead chamber and depends on the design profile, including the mechanical properties of the ground, pore pressure, and overburden height. Face pressures were varied within a range of 75.0 - 350.0 kPa for Profile 1 (B2) and 200.0 - 750.0 kPa for Profile 2 (B1) to evaluate their influence on ground surface settlements.

In addition to face pressure, the model included the following loads: thrust pressure from the thrust cylinders acting on the surface of each concrete ring (4500.0 kPa, see Figure 10(b)), and the combined effect of grouting pressure at the interface between the ground and the concrete lining together with ground pressure acting directly on the lining (1000.0 kPa). A volume loss of 0.35% was also included in the numerical model to account for ground deformation associated with tunnel excavation, ensuring a more realistic representation of soil-structure interaction.

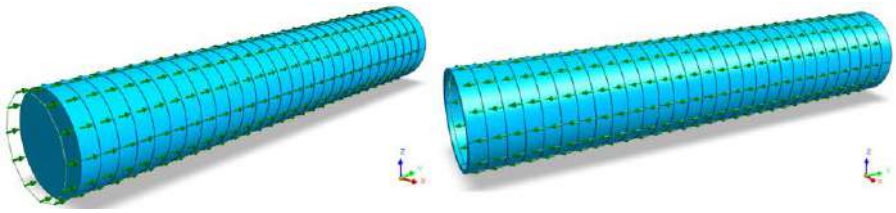

(**a**) (**b**)

Fig. 10. Shield TBM loads: excavation face pressure (a) and thrust pressure (b).

Stress-strain analyses were performed for the design scenario corresponding to the tunnel construction phase. The analysis is steady-state and encompasses all excavation and concreting stages occurring during the construction process. The first calculation phase represents the initial state. After computing stresses and deformations, displacements are reset. From the second phase onward, tunnel lining

excavation is carried out in 45 steps over a total length of 48.0 m. The excavation sequence is simulated through the sequential activation and deactivation of model elements, representing the TBM advancing through defined quasi-homogeneous zones. Tables 4 and 5 present the construction stages of the tunnel using the shield TBM, showing the activation/deactivation of model elements as well as the applied loads and boundary conditions.

Table 4. Activation and deactivation of model elements during construction stages.

Construction	Excavation / Element removal			Element installation		
stage	Internal circle	External ring	Shield	Shield	Segment	Grout
0	-	-	-	Ground, Internal circle 1-30, External ring 1-30		
1	1	1	-	1	-	-
2	2	2	-	2	-	-
3	3	3	-	3	-	-
4	4	4	-	4	-	-
5	5	5	-	5	-	-
6	6	6	-	6	-	-
7	7	7	-	7	-	-
8	8	8	-	8	1	-
9	9	9	1	9	2	-
10	10	10	2	10	3	-
11	11	11	3	11	4	-
12	12	12	4	12	5	-
13	13	13	5	13	6	-
14	14	14	6	14	7	-
15	15	15	7	15	8	-
16	16	16	8	16	9	1
17	17	17	9	17	10	2
18	18	18	10	18	11	3
19	19	19	11	19	12	4
20	20	20	12	20	13	5
21	21	21	13	21	14	6
22	22	22	14	22	15	7
23	23	23	15	23	16	8
24	24	24	16	24	17	9
25	25	25	17	25	18	10
26	26	26	18	26	19	11
27	27	27	19	27	20	12
28	28	28	20	28	21	13
29	29	29	21	29	22	14
30	30	30	22	30	23	15
31	-	-	23	-	24	16
32	-	-	24	-	25	17
33	-	-	25	-	26	18
34	-	-	26	-	27	19
35	-	-	27	-	28	20
36	-	-	28	-	29	21
37	-	-	29	-	30	22
38	-	-	30	-	-	23
39	-	-	-	-	-	24
40	-	-	-	-	-	25
41	-	-	-	-	-	26
42	-	-	-	-	-	27
43	-	-	-	-	-	28
44	-	-	-	-	-	29
45	-	-	-	-	-	30

Table 5. Application and removal of loads and boundary conditions during construction stages.

Construction stage	Load application				Load removal		Boundary condition			
	Face pressure	Shield pressure	Segment pressure	Thrust pressure	Shield pressure	Thrust pressure	Displacement	Shield contraction	Change segment property	Change grout property
0	-	-	-	-	-	-	Foundation displacement constraint	-	-	-
1	HP 1	S 1	-	-	-	-	-	C 1	-	-
2	HP 2	S 2	-	-	-	-	-	C 2	-	-
3	HP 3	S 3	-	-	-	-	-	C 3	-	-
4	HP 4	S 4	-	-	-	-	-	C 4	-	-
5	HP 5	S 5	-	-	-	-	-	C 5	-	-
6	HP 6	S 6	-	-	-	-	-	C 6	-	-
7	HP 7	S 7	-	-	-	-	-	C 7	-	-
8	HP 8	S 8	E 1	J 1	-	-	-	C 8	1	-
9	HP 9	S 9	E 2	J 2	S 1	J 1	-	C 9	2	-
10	HP 10	S 10	E 3	J 3	S 2	J 2	-	C 10	3	-
11	HP 11	S 11	E 4	J 4	S 3	J 3	-	C 11	4	-
12	HP 12	S 12	E 5	J 5	S 4	J 4	-	C 12	5	-
13	HP 13	S 13	E 6	J 6	S 5	J 5	-	C 13	6	-
14	HP 14	S 14	E 7	J 7	S 6	J 6	-	C 14	7	-
15	HP 15	S 15	E 8	J 8	S 7	J 7	-	C 15	8	-
16	HP 16	S 16	E 9	J 9	S 8	J 8	-	C 16	9	1
17	HP 17	S 17	E 10	J 10	S 9	J 9	-	C 17	10	2
18	HP 18	S 18	E 11	J 11	S 10	J 10	-	C 18	11	3
19	HP 19	S 19	E 12	J 12	S 11	J 11	-	C 19	12	4
20	HP 20	S 20	E 13	J 13	S 12	J 12	-	C 20	13	5
21	HP 21	S 21	E 14	J 14	S 13	J 13	-	C 21	14	6
22	HP 22	S 22	E 15	J 15	S 14	J 14	-	C 22	15	7
23	HP 23	S 23	E 16	J 16	S 15	J 15	-	C 23	16	8
24	HP 24	S 24	E 17	J 17	S 16	J 16	-	C 24	17	9
25	HP 25	S 25	E 18	J 18	S 17	J 17	-	C 25	18	10
26	HP 26	S 26	E 19	J 19	S 18	J 18	-	C 26	19	11
27	HP 27	S 27	E 20	J 20	S 19	J 19	-	C 27	20	12
28	HP 28	S 28	E 21	J 21	S 20	J 20	-	C 28	21	13
29	HP 29	S 29	E 22	J 22	S 21	J 21	-	C 29	22	14
30	-	S 30	E 23	J 23	S 22	J 22	-	C 30	23	15
31	-	-	E 24	J 24	S 23	J 23	-	-	24	16
32	-	-	E 25	J 25	S 24	J 24	-	-	25	17
33	-	-	E 26	J 26	S 25	J 25	-	-	26	18
34	-	-	E 27	J 27	S 26	J 26	-	-	27	19
35	-	-	E 28	J 28	S 27	J 27	-	-	28	20
36	-	-	E 29	J 29	S 28	J 28	-	-	29	21
37	-	-	E 30	-	S 29	J 29	-	-	30	22
38	-	-	-	-	S 30	-	-	-	-	23
39	-	-	-	-	-	-	-	-	-	24
40	-	-	-	-	-	-	-	-	-	25
41	-	-	-	-	-	-	-	-	-	26
42	-	-	-	-	-	-	-	-	-	27
43	-	-	-	-	-	-	-	-	-	28
44	-	-	-	-	-	-	-	-	-	29
45	-	-	-	-	-	-	-	-	-	30

3.2. Analytical assessment of optimal shield TBM face pressure

Analytical approaches for determining the optimal shield TBM face pressure are mainly based on limit equilibrium and limit state methods, both aimed at evaluating the critical conditions for tunnel face stability.

Limit equilibrium methods assume a predefined kinematic failure mechanism at the tunnel face, commonly represented as a sliding wedge subjected to the weight of the overlying soil and surcharge,

which acts as destabilizing forces. These forces are counteracted by stabilizing contributions from the applied face pressure and the shear resistance along the boundaries of the wedge. The classical concept, introduced by Horn (1961), was later extended to mechanized tunneling by Anagnostou and Kovári (1994) and Jancsecz and Steiner (1994).

Limit state methods, derived from plasticity theory, define two reference values for tunnel face stability: an upper bound (kinematic) and a lower bound (static). The upper bound represents an optimistic, theoretically unsafe estimate, as it predicts a lower face pressure than what is actually required to prevent collapse. In contrast, the lower bound provides a conservative, safe estimate, yielding a higher value of the necessary support pressure. In practice, the tunnel face is stable if the applied pressure exceeds the lower bound, will collapse if it falls below the upper bound, and may be conditionally stable if the applied pressure lies between these two limits. This framework allows engineers to assess face stability under varying geotechnical conditions while providing a clear understanding of the safe and unsafe operating ranges.

In summary, analytical methods therefore provide a theoretical basis for estimating optimal face pressures, offering insight into safe and unsafe conditions, and can be further refined and validated through detailed numerical simulations under site-specific geotechnical conditions.

Table 6 presents the values calculated using selected analytical approaches, illustrating the range of face pressures estimated through different methodologies. These results provide a reference for comparison with numerical simulations and help evaluate the reliability and applicability of the analytical methods under varying geotechnical conditions.

Table 6. Face pressures for shield TBM calculated using selected analytical approaches.

Analytical approach	Profile 1 (B2)	Profile 2 (B1)
	Face pressure [kPa]	
Cone of bearing	183	230
Jancsecz and Steiner	139	210
DIN 4085 (2017)	62	235
Blow out limit pressure	410	1150

4. Results and Discussion

Figures 11 and 12 present the vertical displacement results obtained from the developed numerical models at Phase 28. Two representative cases are illustrated: Profile 1 (B2), simulated with a face pressure of 250.0 kPa, and Profile 2 (B1), simulated with a face pressure of 450.0 kPa. For Profile 1 (B2), face pressures were varied within the range of 75.0 - 350.0 kPa, while for Profile 2 (B1) they were varied within 200.0 - 750.0 kPa, in order to evaluate their influence on ground surface settlements. The comparison between profiles highlights the sensitivity of surface and subsurface displacements to the applied face pressure, emphasizing the importance of careful pressure control in shield TBM tunneling. In the presented results, negative displacement values indicate ground settlement, whereas positive values correspond to ground heave.

From the presented diagrams, it can be seen that along the ground surface cross-section following the shield TBM excavation axis, ground heave occurs at the tunnel face and along the shield, partially counteracting the settlement induced by volume loss. For Profile 1 (B2), the maximum heave reaches 0.17 mm, whereas for Profile 2 (B1), the settlement is reduced to -1.64 mm. In contrast, ground settlement occurs in the zone of the installed concrete lining, with a minimum settlement of -4.86 mm for Profile 1 (B2) and -3.38 mm for Profile 2 (B1).

In the ground surface cross-section perpendicular to the shield TBM excavation axis, settlement occurs above the tunnel crown zone, with minimum values of -1.08 mm for Profile 1 (B2) and -2.78 mm for Profile 2 (B1). Meanwhile, ground heave is observed outside the tunnel crown zone, reaching a maximum of 0.47 mm for Profile 1 (B2) and without heave for Profile 2 (B1).

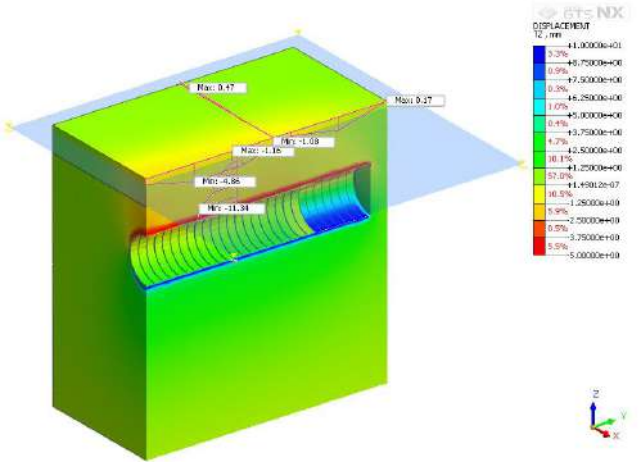

Fig. 11. Vertical displacement (Tz, mm) of Profile 1 (B2) at Phase 28.

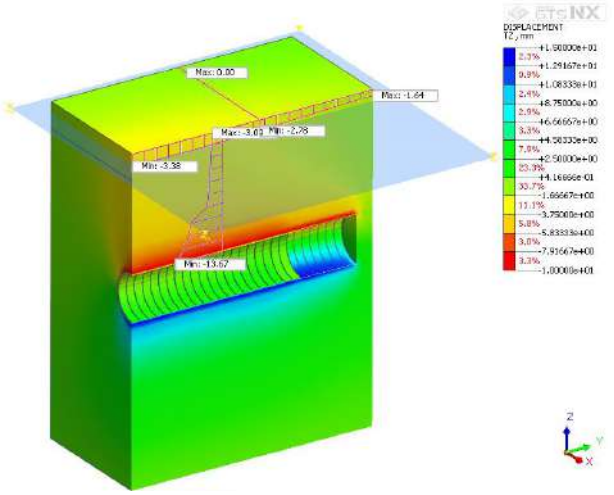

Fig. 12. Vertical displacement (Tz, mm) of Profile 2 (B1) at Phase 28.

It is also evident that settlement at the tunnel crown is significantly greater than surface settlement. For Profile 1 (B2), the crown settlement reaches -11.34 mm, compared to a surface settlement of -1.16 mm. For Profile 2 (B1), crown settlement reaches -13.67 mm, whereas the surface settlement is only -3.09 mm. This difference clearly indicates that the maximum ground deformations are concentrated in the immediate vicinity of the tunnel, while the effects transmitted to the surface are considerably smaller. Such behavior is consistent with the stress redistribution around the excavation and highlights the importance of accurate modeling of tunnel-soil interaction when predicting surface impacts in urban environments.

Figures 13-16 show the vertical displacements at the ground surface for each phase of the calculation models, considering all analyzed face pressure scenarios. These diagrams allow a detailed comparison of settlement and heave along the tunnel alignment, highlighting how variations in face pressure influence both the magnitude and spatial distribution of ground movements. Systematic examination of the results helps identify deformation trends and evaluate the effectiveness of different shield TBM face pressures in controlling settlements.

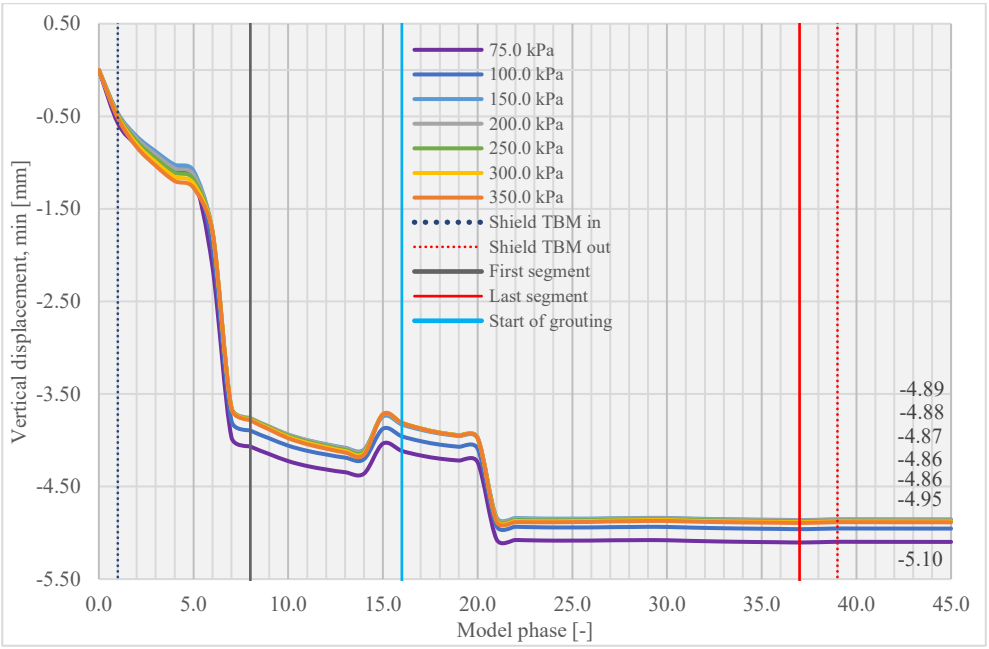

Fig. 13. Minimum ground surface vertical displacements for each calculation model phase of Profile 1 (B2).

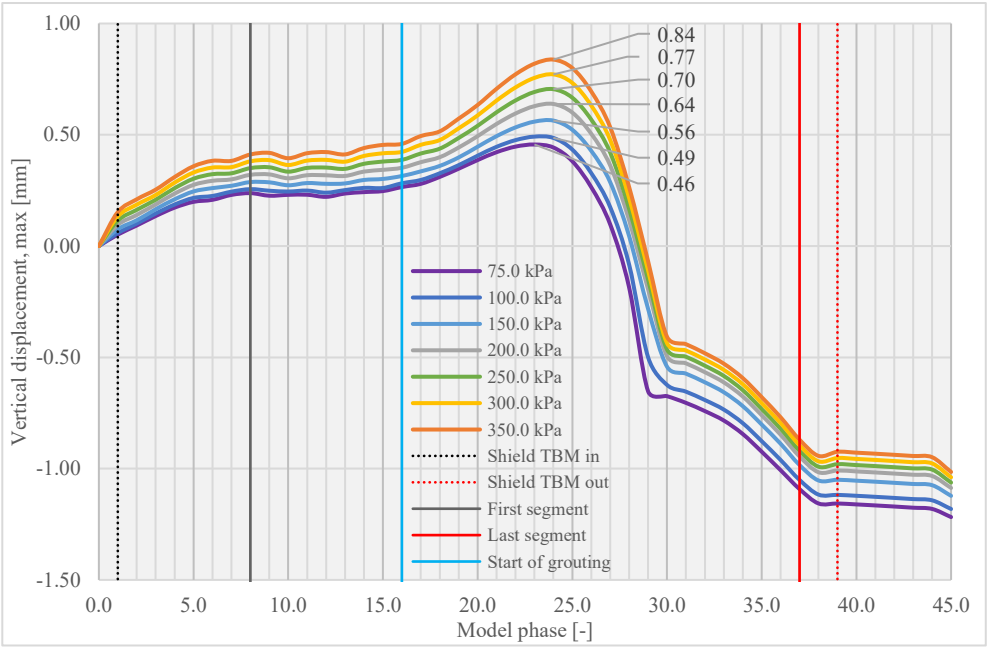

Fig. 14. Maximum ground surface vertical displacements for each calculation model phase of Profile 1 (B2).

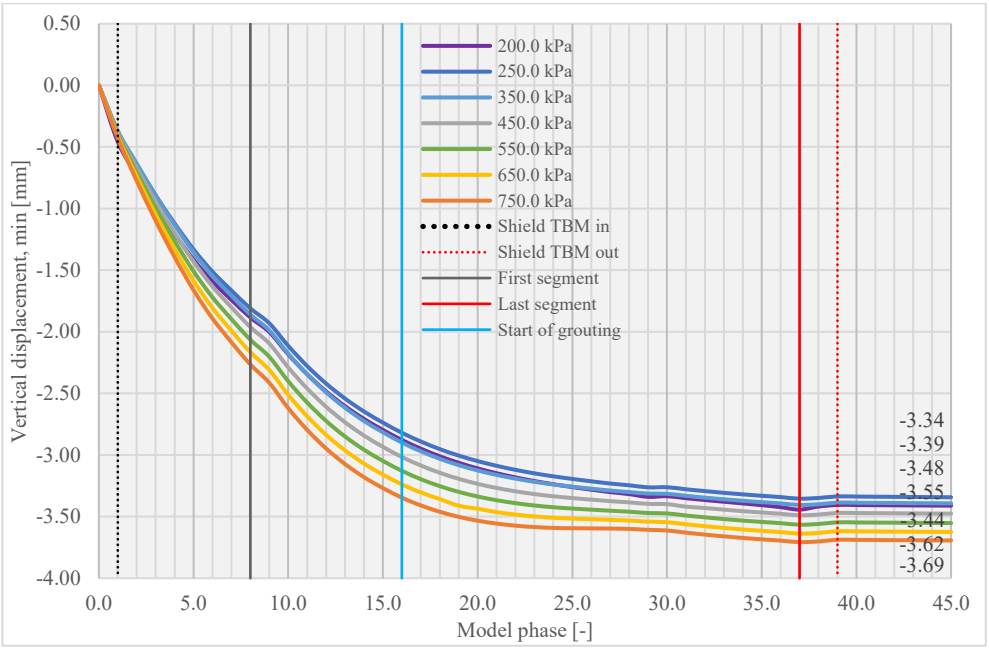

Fig. 15. Minimum ground surface vertical displacements for each calculation model phase of Profile 2 (B1).

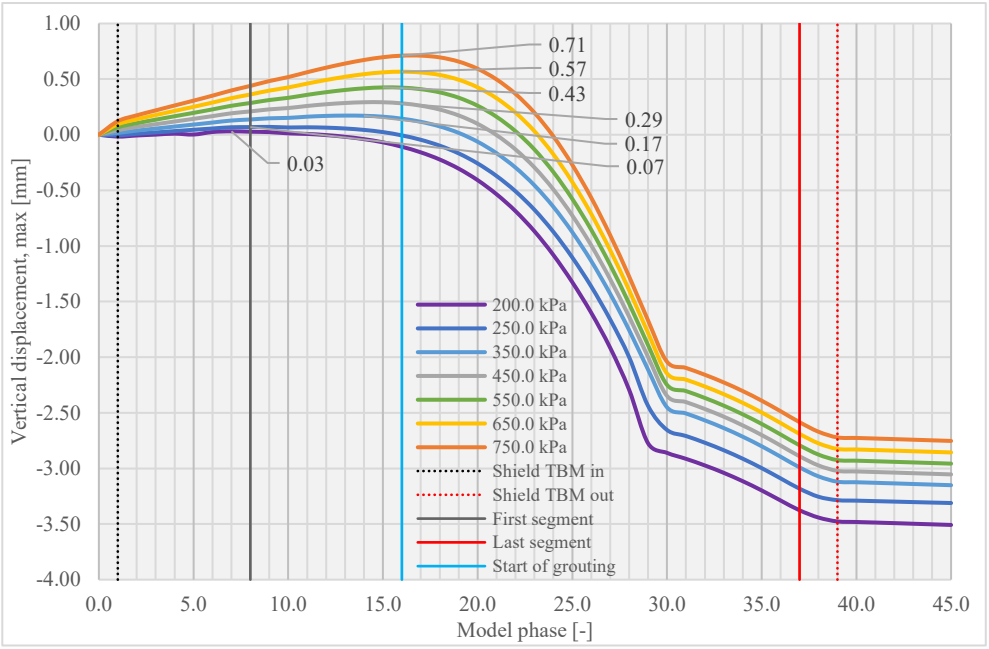

Fig. 16. Maximum ground surface vertical displacements for each calculation model phase of Profile 2 (B1).

Tables 7 and 8 present the ground surface vertical displacement values corresponding to the different face pressure scenarios analyzed in the study. These results provide a quantitative basis for evaluating

the influence of face pressure on settlement and heave behavior, offering insights into the optimal operational range for minimizing ground displacements during shield TBM tunneling.

Table 7. Ground surface vertical displacements for Profile 1 (B2).

Face pressure [kPa]		75.0	100.0	150.0	200.0	250.0	300.0	350.0
Surface vertical	Minimum	-5.10	-4.95	-4.86	-4.86	-4.87	-4.88	-4.89
displacement [mm]	Maximum	0.46	0.49	0.56	0.64	0.70	0.77	0.84

Table 8. Ground surface vertical displacements for Profile 2 (B1).

Face pressure [kPa]		200.0	250.0	350.0	450.0	550.0	650.0	750.0
Surface vertical	Minumum	-3.44	-3.34	-3.39	-3.48	-3.55	-3.62	-3.69
displacement [mm]	Maximum	0.03	0.07	0.17	0.29	0.43	0.57	0.71

Tables 9 and 10 present the vertical displacements at the tunnel crown obtained from the numerical models for the full range of considered face pressures, providing a direct measure of the deformation around the tunnel excavation, where the crown represents the most critical point in terms of settlement and structural response. These results highlight the sensitivity of crown displacements to variations in face pressure and can be used to guide TBM operational strategies for minimizing excessive ground movements and ensuring tunnel stability.

Table 9. Vertical displacements at the tunnel crown for Profile 1 (B2).

Face pressure [kPa]		75.0	100.0	150.0	200.0	250.0	300.0	350.0
Crown vertical	Minimum	-12.23	-11.76	-11.45	-11.52	-11.53	-11.53	-11.50
displacement [mm]	Maximum	0.47	0.51	0.60	0.68	0.76	0.84	0.93

Table 10. Vertical displacements at the tunnel crown for Profile 2 (B1).

Face pressure [kPa]		200.0	250.0	350.0	450.0	550.0	650.0	750.0
Crown vertical	Minimum	-17.19	-15.56	-14.30	-14.08	-14.02	-14.00	-13.99
displacement [mm]	Maximum	0.04	0.08	0.18	0.30	0.46	0.67	0.91

5. Conclusion

The present study focused on assessing the optimal face pressure for shield TBM tunneling along Phase 1, Line 1 of the Belgrade Metro using staged three-dimensional numerical simulations. The results indicate that both surface and subsurface vertical displacements show limited sensitivity to the applied face pressure. For Profiles 1 (B2) and 2 (B1), maximum vertical displacements were observed in the immediate vicinity of the tunnel crown, while surface vertical displacements remained significantly smaller. The analysis also showed that surface ground heave develops at the tunnel face and along the shield, whereas settlements are primarily concentrated in areas with installed concrete lining. Furthermore, the observed differences between Profiles 1 (B2) and 2 (B1) reflect the influence of varying geotechnical conditions and overburden thickness along the alignment, underlining the importance of site-specific analysis for reliable shield TBM operation.

The numerical results indicate optimal face pressure ranges that minimize both crown and surface vertical displacements, providing practical guidance for shield TBM operation (Tables 7-10). Compared to analytical methods proposed by various authors, the numerical approach offers several advantages: it accounts for complex ground-structure interaction, simulates sequential excavation stages, and allows detailed sensitivity analyses under varying operational parameters. Unlike analytical methods, which provide single-value estimations, numerical modeling can capture the spatial and temporal distribution of deformations, offering a more reliable and risk-informed basis for operational decisions. The obtained results indicate that the analyzed calculation profiles (macro-zones) are located

within relatively competent limestone and conglomerate formations, which exhibit limited sensitivity to variations in applied face pressure, suggesting favorable conditions for shield TBM tunneling.

Future research will cover all calculation profiles (macro-zones) along the entire alignment of Phase 1, Line 1 of the Belgrade Metro, with particular focus on zones characterized by less favorable ground conditions. A more comprehensive sensitivity analysis will be conducted using Midas GTS NX in conjunction with PEST++ (2025), incorporating not only face pressure but also other key shield TBM operational parameters. While contact elements between the tunnel lining and the surrounding ground were not included in the current numerical models, they could be implemented in future, more detailed studies to account for soil-structure interaction. In Midas GTS NX, interface elements with defined frictional behavior can be used to model the interaction between lining segments and the surrounding soil or rock. Incorporating such elements would allow for more accurate predictions of lining stresses, deformation patterns, and load transfer mechanisms during tunnel excavation. This methodology will enable a detailed evaluation of the combined effects of multiple operational variables on both surface and subsurface settlements, thereby supporting the development of robust risk mitigation strategies and providing enhanced operational guidance for shield TBM tunneling in complex urban environments.

References

Alsirawan, R., Sheble, A., Alnmr, A., 2023. Two-dimensional numerical analysis for TBM tunneling-induced structure settlement: A proposed modeling method and parametric study. *Infrastructures*, 8(5), 88. https://doi.org/10.3390/infrastructures8050088

Alstom. 2025. Belgrade Metro, Main Line - Typical Cross-Sections.

Anagnostou, G., Kovári, K., 1994. The face stability of slurry-shield-driven tunnels. *Tunnelling and underground space technology*, 9(2), 165-174. https://doi.org/10.1016/0886-7798(94)90028-0

Ayasrah, M., Qiu, H., Zhang, X., Daddow, M., 2020. Prediction of ground settlement induced by slurry shield tunnelling in granular soils. *Civil Engineering Journal*, 6(12), 2273-2289. https://doi.org/10.28991/cej-2020-03091617

Beghoul, M., Demagh, R., 2019. Slurry shield tunneling in soft ground. Comparison between field data and 3D numerical simulation. *Studia Geotechnica et Mechanica*, 41(3), 115-125. https://doi.org/10.2478/sgem-2019-0003

Bogusz, W., Godlewski, T., Siemińska-Lewandowska, A., 2021. Parameters used for prediction of settlement trough due to TBM tunnelling. *Archives of Civil Engineering*, 351-367. https://doi.org/10.24425/ace.2021.138504

Chen, R.P., Song, X., Meng, F.Y., Wu, H.N., Lin, X.T., 2022. Analytical approach to predict tunneling-induced subsurface settlement in sand considering soil arching effect. *Computers and Geotechnics*, 141, 104492. https://doi.org/10.1016/j.compgeo.2021.104492

China Railway Construction Heavy Industry (CRCHI). 2025. Belgrade Metro, TBM Technical Specification.

Comodromos, E.M., Papadopoulou, M.C., Konstantinidis, G.K., 2014. Numerical assessment of subsidence and adjacent building movements induced by TBM-EPB tunneling. *Journal of Geotechnical and Geoenvironmental Engineering*, 140(11), 04014061. https://doi.org/10.1061/(ASCE)GT.1943-5606.0001166

Cording, E J., 2018. Muir Wood lecture 2018 - Monitoring and controlling ground behavior at the source recent applications to pressurized tunnelling., ITA-AITES.

DIN 4085. 2017. Baugrund – Berechnung des Erddruckes.

Do, N.A., Dias, D., Vu, T.T., Dang, V.K., 2021. Impact of the shield machine's performance parameters on the tunnel lining behaviour and settlements. *Environmental Earth Sciences*, 80(16), 507. https://doi.org/10.1007/s12665-021-09820-2

Fargnoli, V., Boldini, D., Amorosi, A., 2013. TBM tunnelling-induced settlements in coarse-grained soils: The case of the new Milan underground line 5. *Tunnelling and Underground Space Technology*, 38, 336-347. https://doi.org/10.1016/j.tust.2013.07.015

Hashimoto, T., Nagaya, J., Konda, T., 1999. Prediction of ground deformation due to shield excavation in clayey soils. *Soils and foundations*, 39(3), 53-61. https://doi.org/10.3208/sandf.39.3_53

Horn, N., 1961. Horizontaler erddruck auf senkrechte abschlussflächen von tunnelröhren. *Landeskonferenz der ungarischen tiefbauindustrie*, 7-16.

Jancsecz, S., Steiner, W., 1994. Face support for a large mix-shield in heterogeneous ground conditions. In *Tunnelling'94: Papers presented at the seventh international symposium,'Tunnelling'94'*, 531-550. https://doi.org/10.1007/978-1-4615-2646-9_32

Kavvadas, M., Litsas, D., Vazaios, I., Fortsakis, P., 2017. Development of a 3D finite element model for shield EPB tunnelling. *Tunnelling and Underground Space Technology*, 65, 22-34. https://doi.org/10.1016/j.tust.2017.02.001

Kim, D., Pham, K., Park, S., Oh, J.Y., Choi, H., 2020. Determination of effective parameters on surface settlement during shield TBM. *Geomechanics and Engineering*, 21(2), 153-164. https://doi.org/10.12989/gae.2020.21.2.153

Lake, L. M., Rankin, W.J., Hawley, J., 1996. Prediction and effects of ground movements caused by tunnelling in soft ground beneath urban areas. CIRIA.

Luo, M., Wang, D., Wang, X., Lu, Z., 2023. Analysis of surface settlement induced by shield tunnelling: Grey relational analysis and numerical simulation study on critical construction parameters. *Sustainability*, 15(19), 14315. https://doi.org/10.3390/su151914315

Meng, F., Chen, R., Mooney, M.A., Wu, H., Jia, Q., 2022. Evaluation of shield tunneling-induced soil disturbance in typical structured clays. *Bulletin of Engineering Geology and the Environment*, 81(4), 133. https://doi.org/10.1007/s10064-022-02625-y

Midas GTS NX. https://www.midasuser.com/en/product/gts-nx (accessed 01.07.2025.)

PEST++. https://pesthomepage.org/pest (accessed 01.07.2025.)

Ring, B., Comulada, M., 2018. Practical numerical simulation of the effect of TBM process pressures on soil displacements through 3D shift iteration. *Underground Space*, 3(4), 297-309. https://doi.org/10.1016/j.undsp.2018.09.003

Ter-Martirosyan, A. Z., Cherkesov, R. H., Isaev, I. O., Shishkina, V.V., 2022. Surface settlement during tunneling: Field observation analysis. *Applied Sciences*, 12(19), 9963. https://doi.org/10.3390/app12199963

Zhu, C., Li, N., 2017. Prediction and analysis of surface settlement due to shield tunneling for Xi'an Metro. *Canadian Geotechnical Journal*, 54(4), 529-546. https://doi.org/10.1139/cgj-2016-0166

Southeastern Europe Tunnelling Conference (SETC-2025)
1-3 October 2025, Belgrade, Serbia

DOI: 10.5937/SETC25025S

A 3D Numerical Modelling Case Study in a Complex Granitic Rock Mass

Gábor Somodi[a,b], János Kocsis[c], Gyula Bögöly[a,b]*

[a] Department of Engineering Geology & Geotechnics, Faculty of Civil Engineering, Budapest University of Technology and Economics, Hungary; somodi.gabor@edu.bme.hu, bogoly.gyula@emk.bme.hu
[b] Gecko Geotechnics Hungary Ltd., Hungary
[c] Speciálterv Kft., Hungary

Abstract: The study analyses the excavation of a repository chamber in a radioactive waste storage facility in Hungary, using three-dimensional numerical modelling to assess tunnel deformations. The project's comprehensive field mapping and monitoring system made it possible to compare the results of numerical calculations based on field and laboratory measurements with the real behaviour of the tunnel. During excavation, tunnel displacements were continuously recorded using extensometers and two types of convergence measurements, which allowed a comparison of the deformations of the real and modelled environment. The displacements between the measuring points defined in the model during the convergence measurement were investigated. A mechanically realistic but simple 3D model was developed, based on extensive field and laboratory data, which reproduced tunnel displacements of the same order of magnitude as observed in monitoring measurements.

Keywords: tunnel deformation; granite; extensometers; convergence measurements; 3D numerical modelling

1. Introduction

Tunnelling in fractured rock masses presents a complex geomechanical challenge due to the heterogeneous and anisotropic nature of the subsurface environment. Accurate prediction of rock deformation during tunnel excavation is essential for ensuring construction safety, optimising support design, and decreasing project costs. 3D numerical models provide a comprehensive framework for simulating the interaction between tunnel structures and the surrounding geological media, especially if appropriate field observations and monitoring data are available.

The construction phases of a tunnel are particularly critical, as the excavation process alters the in-situ stress field and initiates time-dependent deformations. Capturing these transient effects requires advanced numerical techniques and an accurate representation of fracture mechanics and rock mass behaviour at various scales. These models facilitate predictive analysis of deformation zones, potential failure mechanisms, and support system performance under realistic geological conditions.

At the Hungarian National Radioactive Waste Repository (NRWR), repository chambers are excavated within the Mórágy Metagranite Complex, where dense fracture networks and aplite veins complicate prediction. The present study develops a mechanically realistic yet deliberately simple homogeneous 3-D model of chamber I-K3 and compares calculated displacements with in-situ measurements from extensometers and convergence sections acquired during construction. The objective is to assess how far a homogeneous model can reproduce the order of magnitude and trends of monitored deformations at the chamber scale, and to identify the principal sources of mismatch that should guide model refinement.

*Corresponding author: somodigabor@gmail.com (G. Somodi).

2. Geology

The models tend to characterise the mechanical behaviour of a repository chamber construction in the Hungarian National Radioactive Waste Repository (Fig. 1), approximately 280 m below the surface. The host rock of the repository is the Carboniferous Mórágy Metagranite Complex.

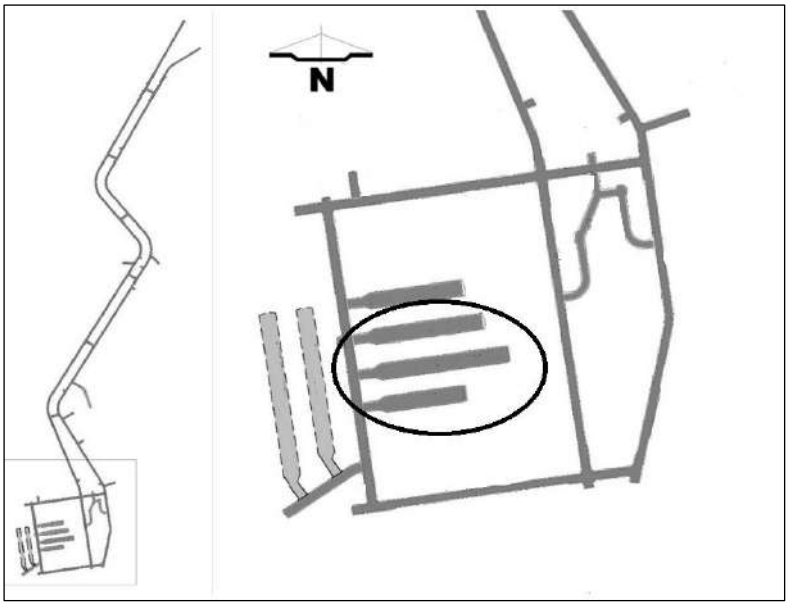

Fig. 1. Location map of the studied repository chambers.

Based on extensive empirical observations, the evolution of rock quality - and, consequently, the anticipated geotechnical conditions - within the Mórágy Granite is predominantly governed by fractures and fracture networks that developed during its tectonic evolution.

Surface and underground geological investigations have delineated six principal paleo-stress fields, within which a wide array of fracture orientations and generations have been identified. Under these distinct stress regimes, the pre-existing fracture systems exhibit varying degrees and modes of deformation, reactivation, and subsequent evolution. (Maros et al., 2003, 2009)

As a result, a complex and dense network of fracture zones and cracks has developed, characterised by significant heterogeneity in dimensions, orientations, and infilling materials. The spatial trajectories of individual fractures are generally irregular, and their terminations are frequently unpredictable due to the overprinting effects of multiple tectonic events.

The investigations further revealed that fracture infill materials cannot be uniquely associated with specific deformation phases delineated by the orientation of paleo-stress fields. In addition to discrete fractures, particular attention is warranted - from geotechnical and hydrogeological perspectives - for the more extensive fractured zones, which locally attain thicknesses of 10 meters. These zones are typically infilled with clay minerals. (Maros et al., 2009)

Findings from the early stages of the research already indicated that the geological and tectonic history of the Mórágy Formation has resulted in pronounced inhomogeneity in rock mechanical and geotechnical parameters. Consequently, the spatial extrapolation of these parameters across the site is subject to considerable limitations. (Kovács et al., 2016)

The surroundings of the survey section were overlain by monzogranite and ridge-bedded with several aplite dykes.

3. Methodology

The methodology of this study integrates field data collection and advanced three-dimensional numerical modelling to evaluate the influence of construction stages on tunnel deformation in a granitic rock mass. During excavation, deformation was continuously monitored through a network of extensometers and convergence gauges. (Krupa et al., 2015; Zierkelbach et al., 2016) Measurement sections were established along the I-K3 tunnel alignment, with specific anchor locations identified within the model domain (Fig. 2). These observational datasets were used to calibrate and validate the numerical models.

Fig. 2. A typical rock mass condition in the top heading of the repository chambers.

Numerical modelling was carried out using the RS3 software suite developed by Rocscience, which supports 3D finite element analysis. A simple homogeneous rock mass model was constructed due to the dense fracture network, representing the continuum approach without explicit fractures.

Tunnel heading advancement, excavation stages, and support installation were simulated in the RS3 environment. Displacement predictions were extracted at locations corresponding to monitoring instruments, allowing direct comparison between modelled and observed deformation patterns.

3.1. Input parameters

The numerical model adopted several simplifications that were validated and checked later in the workflow. A single chamber was modelled because the pillars between the chambers are sufficiently thick relative to the tunnel dimensions. The tunnel has a curved horseshoe profile with a crown radius of 6.4 m, overall height of 10.6 m, sidewall radius of 11.4 m, invert width of 11.08 m, and an invert dish depth of 0.91 m. To ensure that the analysed ±20 m section was not affected by end effects, a 60 m long tunnel segment was modelled. Excavation advances were 2 m for the top heading, while the bench was excavated in 4 m advances with a 20 m lag.

The rock mass was represented using the Generalized Hoek–Brown failure criterion with plastic behaviour. Table 1 summarises the adopted median properties of the monzogranite rock mass, which is the result of the statistical evaluation of approximately 600 laboratory tests. The support system consisted of 200 mm of reinforced shotcrete and 4 m-long rock bolts. The heading was additionally supported with steel lattice girders at 2 m spacing. The in-situ stress field was assumed to be constant: 8,725 kPa perpendicular to the tunnel axis, 7,261 kPa parallel to the axis, and 6,870 kPa vertically, derived from theoretical calculations and confirmed by in situ stress measurements. (Kovács et al., 2016).

Table 1. Median values of the monzogranite rock mass parameters.

GSI [-]	mi [-]	γ [kN/m^3]	UCS [MPa]	Ei [GPa]	μ [-]
42	14.4	27.06	133.1	68.07	0.235

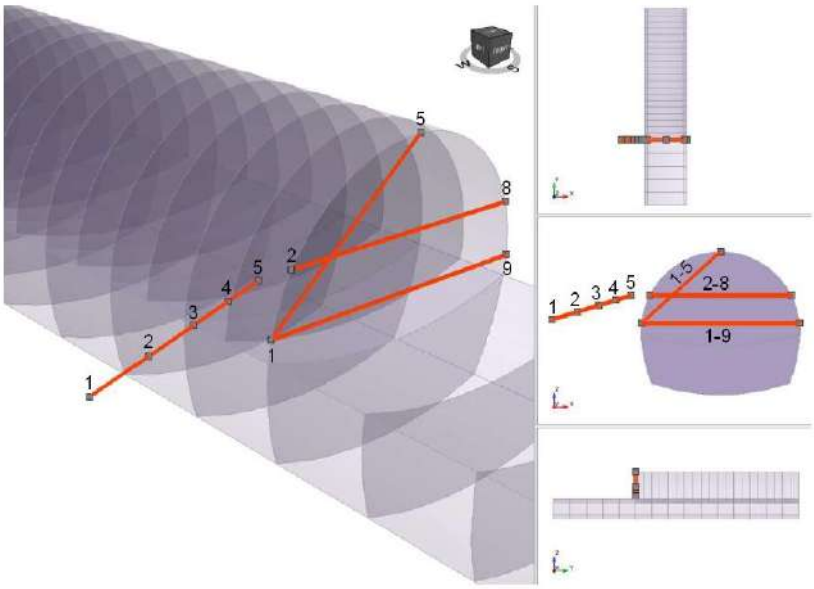

Fig. 3. Measuring sections in the RS3 model. The convergence section is inside the tunnel (1-5,2-8, 1-9), while the extensometer (1, 2, 3, 4, 5) is located outside the tunnel.

4. Results

4.1. Comparison of the displacements of the extensometer and the numerical model

Figure 4 illustrates how the calculated displacements of the modelled anchors of the extensometer varied as a function of the distance between the measurement section and the current top heading excavation face of the chamber. It can be observed that displacements remain relatively small over the first 20 m while the top heading face has not yet reached the measurement section. Once the top heading face reaches the measurement section, larger displacements are recorded at anchors 3–5, closest to the tunnel excavation. The excavation process has less effect on the displacements of anchors 1–2. The maximum displacement is shown by anchor 5, the one closest to the tunnel cross-section; its peak value, when the measurement section and the current top heading face are 20 m apart, is 0.38 mm.

The magnitude of the model's displacements is of the same order as those from on-site measurements (Fig. 5); however, their progression is slightly different. The differences can be explained by the model interpreting the surrounding rock mass as a homogeneous body, disregarding possible tectonic variations, faults, or veins.

The geology of the area surrounding the I-K3 chamber shows that cracks and aplite veins are present in the rock mass, along with displacements that could have occurred due to the excavation. In addition, the model's excavation stages are uniform, whereas the blasting depths vary slightly on-site. Due to the

excavation technology, inequalities in the cross-section can easily develop, while in the model, this remains constant.

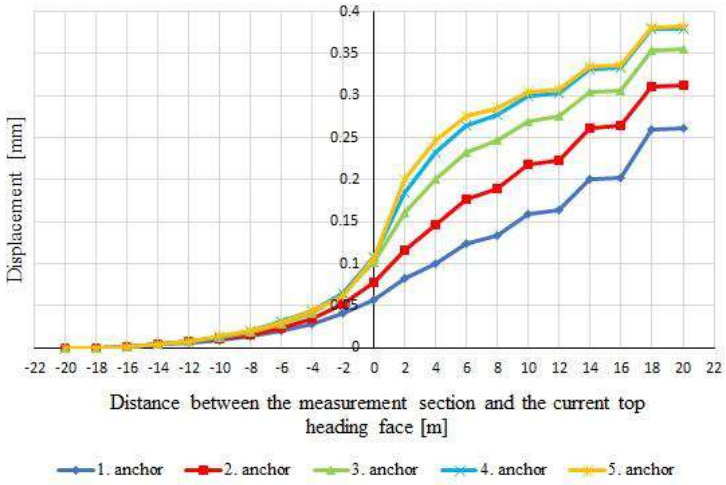

Fig. 4. Development of calculated displacements of extensometer anchors in the model as a function of the distance between the measurement section and the current top heading excavation face of I-K3.

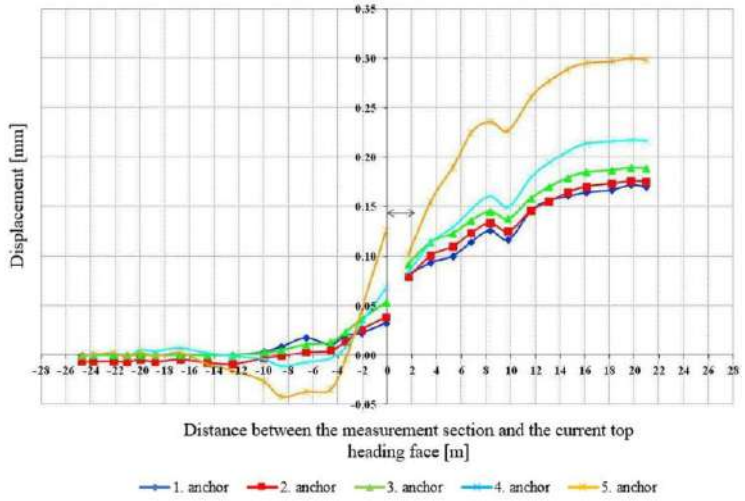

Fig. 5. Development of measured displacements of extensometer anchors as a function of the distance between the measurement section and the current top heading excavation face of I-K3.

4.2. Comparison of the measured and calculated convergence

During the mechanical convergence monitoring, the time history of tunnel lining deformation—resulting from excavation-induced changes in the stress state—was determined, tracking the successive excavation stages. Using the model's monitoring points, horizontal convergence was computed along the 1–9 and 2–8 lines, while an inclined (oblique) convergence was calculated along the 1–5 line. Figure 6 shows how the deformation between the measured points evolves regarding the convergence value as a function of the distance between the measurement section and the current top heading excavation face

of I-K3. In the case of the five repeated measurements, the displacements increase uniformly in all cases. The maximum measured displacement is in the 2–8 direction (1.45 mm), while the 1–9 direction is slightly lower (1.36 mm). The smallest displacement is seen in the 1–5 direction, with a maximum value of 0.51 mm.

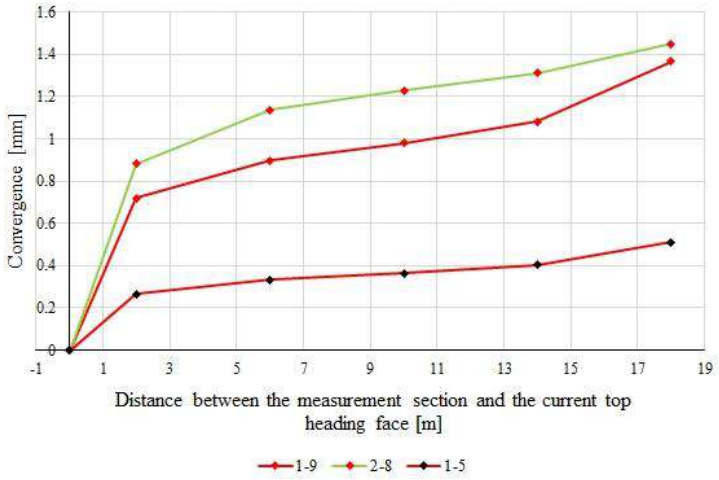

Fig. 6. Development of convergence values calculated between model-defined measurement points as a function of the distance between the measurement section and the current top heading excavation face of I-K3.

The measured values consistently show similar magnitudes and trends across repeated tests. The maximum measured displacement in the 1-9 direction is approximately 1.45 mm, in the 1-5 direction, 1.9 mm, but their order has changed. In the 2–8 direction, the measured convergence is -0.2 mm, which does not match the calculated result either in magnitude or direction. The trend also breaks down in the case of repeated measurements. During the evaluation of the convergence section's measurement results, it was noted that measuring point 8 is moving away from the tunnel axis. (Zierkelbach-Kovács, Kovács and Kiss, 2016.)

Overall, it can be said that the model did not consistently reproduce the convergence values from on-site measurements, which can be explained by the fact that the rock environment in the model is homogeneous and does not consider tectonic irregularities (presence of faults and veins). Therefore, the model results (Fig. 7) show only symmetric displacements along the tunnel lining.

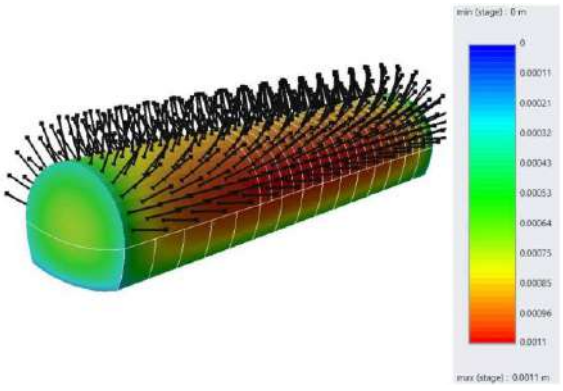

Fig. 7. Total displacements in the RS3 model.

5. Conclusion

The presented 3D numerical case study of chamber I-K3 shows that a homogeneous Generalized Hoek–Brown model, calibrated from field and laboratory data and analysed with staged excavation and support, reproduces the same order of magnitude of displacements observed on site, both for extensometer anchors and convergence measurements. Extensometer results also captured the increase in displacement as the top-heading face approached the measurement section, with the anchor closest to the tunnel cross-section showing the most significant response.

The model-predicted peak convergences of approximately 1.145 mm (2–8), 1.366 mm (1–9), and 0.511 mm (1–5) were comparable in magnitude to the measured maxima of 1.45 mm (1–9) and 1.9 mm (1–5). However, the model failed to consistently reproduce the directional trends and observed asymmetries. While the numerical simulation predicted a uniform and nearly symmetrical increase in displacement around the lining, the field data exhibited a clear direction-dependent behaviour, including negative convergence in the 2–8 direction and localised deformation peaks.

The most plausible explanations for these discrepancies are the homogeneous rock-mass assumption, which overlooks key tectonic heterogeneities such as faults, fracture corridors, and aplite veins, and the associated stiffness and strength anisotropy. Additionally, the model's simplification of construction realities, such as variations in blast rounds and minor deviations in the excavation profile, likely contributed to the differences between the predicted and observed behaviour.

Implications for design and analysis. A homogeneous equivalent-continuum can be adequate for first-order magnitude checks and preliminary support sizing for fractured granites, provided it is confronted with monitoring data. Still, it is insufficient to reliably capture directionality and localisation of deformations. This aligns with wider experience that monitoring (convergence and extensometers) is essential to validate and update predictions during construction.

Recommendations for future modelling:

- Introduce heterogeneity (mapped fracture corridors/aplite veins as reduced-stiffness/strength volumes) or adopt a DFN-informed equivalent to better capture anisotropy and asymmetric convergence. (Li and Elmo, 2024)
- Reflect construction nuances by varying the lengths of the advances and face shapes in the staging, and by including realistic support-installation lags.

The study demonstrates that a simple, homogeneous 3-D model is a useful baseline and decision aid. Still, it should be augmented—guided by monitoring—to incorporate site-specific heterogeneity if directional behaviour and localisation are critical to support verification at the chamber scale.

Acknowledgements

All the data and figures belong to PURAM, and this paper has been published with the permission of the Public Limited Company for Radioactive Waste Management (PURAM). We would like to thank all current and former employees of RockStudy Ltd. for their joint field work.

References

Li, Y., Elmo, D., 2024. A Critical Discussion on the Use of Discrete Fracture Network Models in Rock Engineering Practice: Why Rock Mass Characterisation Methods can Benefit from Considering Fracture Connectivity. *Rock Mechanics and Rock Engineering* (2024). https://doi.org/10.1007/s00603-024-04049-4

Király, E., 2009. A Magyar Állami Földtani Intézet Évi jelentése: A Mórágyi ránit magmás fejlődéstörténete pp. 58-59.

Kovács L., Kádár B., Krupa Á., Mészáros E., Pöszmet T., Rátkai O., Vásárheyi B., 2016. A Geotechnikai Értelmező Jelentés (GÉJ) aktualizálása. 2016. július. Kézirat - Kőmérő Kft., RHK Kft. Adattára, RHK-K-028/16

Krupa, Á., Rátkai, O., Zierkelbach-Kovács, B., Kovács, L., 2015. Értékelő jelentés az EXT-11-12 és az EXT-13 jelű extenzométeres szelvények mérési eredményeiről pp. 7-9., 14-16., 20. *Radioaktív Hulladékokat kezelő Kft*.

Maros, Gy., Koroknai, B., Palotás, K., Fodor, L., Dudko, A., Forián-Szabó, M., Zilahi-Sebess, L., Bán-Győry, E. Tectonic Analysis and Structural Evolution of the north-eastern Mórágy Block. *Annual Report of the Geological Institute of Hungary*. 2003. pp. 370–386.

Maros, Gy., Koroknai, B., Palotás, K., Musitz, B., Füri, J., Borsody, J., Kovács-Pálfy, P., Kónya, P., Viczián, I., Balogh, K., Pécskay, Z. Brittle Fault Zones in the Mórágy Granite (South Transdanubia): New Structural and K-ar Data. *Annual Report of the Geological Institute of Hungary* 2009. pp. 91–112.

OUnitef'83 Műszaki Tervező és Fejlesztő Zrt. (2013). Bátaapáti Nemzeti Radioaktívhulladék-tároló, Kiviteli terv III. ütem 2. szakasz, I-K3 és I-K4 tárolókamra, AJKUN00001R009

Zierkelbach-Kovács, B., Kovács, L., Kiss, M., 2016. Jelentés a HKON-1 és HKON-2 jelű húzott szalagos konvergenciamérő szelvények telepítéséről és méréseiről. pp. 6. *Radioaktív Hulladékokat Kezelő Kft*

Southeastern Europe Tunnelling Conference (SETC-2025)
1-3 October 2025, Belgrade, Serbia

DOI: 10.5937/SETC25026M

Computer-aided ground modelling incorporating soil variability for geotechnical applications

Ksenija Micić[a,b], Hoang-Giang Bui[c] and Jelena Ninić[c]*

[a] University of Belgrade, Faculty of Mining and Geology, Department for Geotechnics, Belgrade, Serbia
[b] University of Belgrade, Faculty of Civil Engineering, Department of Geotechnical Engineering, Belgrade, Serbia; kmicic@grf.bg.ac.rs
[c] University of Birmingham, School of Engineering, Department of Civil Engineering, Birmingham, United Kingdom; b.hoanggiang@bham.ac.uk, j.ninic@bham.ac.uk

Abstract: This paper presents an end-to-end workflow for generating three-dimensional, voxel-based ground information model that seamlessly integrates geological complexity and soil-property variability into finite-element analyses. First, lithology is interpolated on a structured grid via Empirical Bayesian Kriging in ArcGIS Pro, producing a voxelized subsurface architecture. Next, spatial variability of key geotechnical parameters is characterized with conditional random fields using GSTools, utilizing borehole observations to ensure realistic site-specific conditions. All modelling components are stored and linked in NetCDF file, preserving dimensions and metadata, while allowing for the efficient data exchange. Finally, voxel-based ground information model is imported into a CutFEM solver for adaptive finite element simulations. We demonstrate the workflow on a synthetic excavation scenario, highlighting its computational efficiency and improved accuracy in predicting deformation compared to deterministic models. By automating the entire process and leveraging open data standards, this approach addresses interoperability challenges and enables engineers to incorporate uncertainty directly into numerical designs.

Keywords: GIM; soil variability; CutFEM; AMR

1. Introduction

In the past decades, as digital tools and technologies introduced an immersive need for digital transformation in engineering, the geotechnical community has witnessed a shift from traditional ways of ground modelling, such as 2D or block-based subsurface representations, toward 3D data-rich ground models that can capture geological and geotechnical complexity and directly be integrated with numerical solvers. Although many significant advancements have been made in this field (Erharter et al., 2023; Tian and Wang, 2024), there still appears to be a persistent gap between fully developed ground models and their practical application in geotechnical engineering, primarily due to poor interoperability among diverse data formats, software packages, and digital platforms.

While numerous high-quality research works on ground modelling (Erharter et al., 2023; Huang et al., 2022; Khan et al, 2023; Shi and Wang, 2022; Tian and Wang, 2023; Xie et al., 2023) mostly focus on just one aspect of the workflow (e.g. stratigraphy modelling, sparse data inference, BIM integration, FEM analysis), not many offer a simple, computationally efficient, and fully integrated 3D system that carries the ground model directly into FEM. Moreover, majority of the studies stop short of including the spatial variability of soil properties, which arises from complex geological processes (Phoon and Kulhawy, 1999a) and represents an inevitable part of ground characterization. It can effectively be assessed employing the Random Field Theory (Chen et al., 2024; He et al., 2022; Huang et al., 2020; Pan and Dias, 2017; Vanmarcke, 1977). To fully pair all the unknowns with the 'known' ground information, it is of great importance to constrain the stochastic predictions with the actual field

*Corresponding author: kmicic@grf.bg.ac.rs (K. Micić).

observation data, which is achievable by conditioning the random simulations for the known values at specific locations (Gong et al., 2018; Huang et al., 2020; Hu et al., 2025; Wang et al., 2024; Xie et al., 2023; Zhao et al., 2023).

Numerical analysis plays an important role in initial assessment of settlement-induced construction process. For tunnelling application, CutFEM is a method of choice for design of tunnel track (Bui et al., 2023). This approach allows for independent modelling of analysis components. In particular, the ground can be modelled using regular geometry without initial generation of boundary fitted excavation domain. This fits naturally with ground data defined on a structured grid and enables seamless integration of ground information model (GIM) during the simulation.

In this work we present an end-to-end workflow that: (1) uses borehole data to produce a 3D lithology model in ArcGIS using Empirical Bayesian Kriging, (2) enriches the lithology voxel model with conditional random fields of key soil properties to reach a holistic voxel-based GIM, and (3) seamlessly incorporates GIM into Kratos-based CutFEM solver. The main objective of the study is to establish a reproducible, interoperable and automated pipeline for adaptive FEM analysis using 3D spatially variable ground models.

2. Voxel-based ground model

2.1. Field investigation data

Geotechnical datasets from individual projects are typically limited in size and often irregularly distributed, due to constraints of budget, schedule, or access (Phoon et al. 2023, Wang and Tian, 2023). Even though geotechnical standards prescribe a wide range of investigation methods, each offering its own benefits for characterizing ground conditions, the borehole drilling remains the cornerstone technique. It provides multiple streams of information directly from subsurface materials, including lithology, groundwater conditions, and sampling for laboratory testing.

In this study, boreholes form the foundational data layer from which all the other ground modelling components are derived. Whilst the entire framework is built on synthetic data, great attention has been put into configuring the inputs as realistically as possible, ensuring that every subsequent analysis and simulation retains physical and geotechnical validity.

To that end, Fig. 1 shows 50 random synthetic boreholes distributed over the domain of interest measuring 400 × 300 × 60 m in X, Y and Z, respectively. Each digital borehole is organized into distinct elements, with each element carrying its own characteristic set of data (Fig. 1). To be able to achieve full connectivity between the distinct elements, parent-child mappers are established.

2.2. Lithology modelling in GIS

2.2.1. Empirical Bayesian Kriging

Lithology modelling is conducted using the ArcGIS Pro's Geostatistical Analyst toolbox that contains a suite of tools for data analysis, interpolation and validation, among which Empirical Bayesian Kriging (EBK) stands out as an advanced and well-equipped algorithm for lithology spatial delineation (Esri, 2025).

Empirical Bayesian Kriging (EBK) is a geostatistical interpolation approach that embeds the iterative semivariogram fitting within a Bayesian framework and combines two underlying models within a unified computational procedure - an intrinsic random function kriging (IRFK) component and a linear mixed model (LMM) component. In the computational model, observations z_i at locations s_i are expressed as:

$$z_i = y(s_i) + \varepsilon_i, \qquad i = 1, \dots, K \tag{1}$$

where $y(S)$ is the underlying Gaussian spatial process, ε_i denotes measurement error and K is the number of observations (Gribov and Krivoruchko, 2020; Krivoruchko and Gribov, 2019).

The core EBK workflow first estimates semivariogram parameters using the restricted maximum likelihood method (REML), then produces multiple unconditional simulations to build an empirical prior of parameter sets. Each set is weighted by its likelihood of producing the observed data, and final predictions at unsampled locations are obtained by averaging the individual predictions generated by each parameter set, using the weights. For large datasets, the input is divided into overlapping subsets, each processed independently. In full 3D mode in ArcGIS Pro, the EBK logic is preserved while adapting distance metrics and search neighbourhood definitions to three dimensions (Esri, 2025).

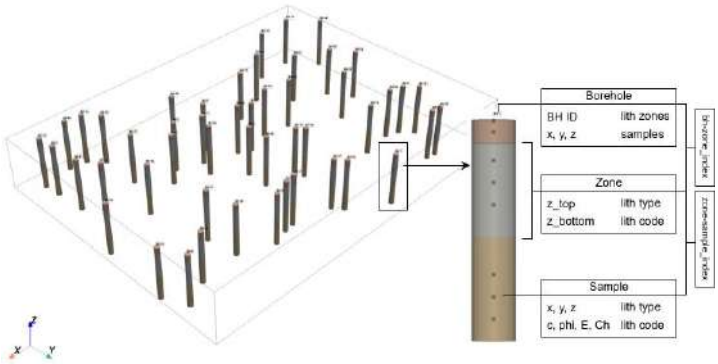

Fig. 1. Borehole distribution in 3D domain of interest. Digital borehole contents presented on the right.

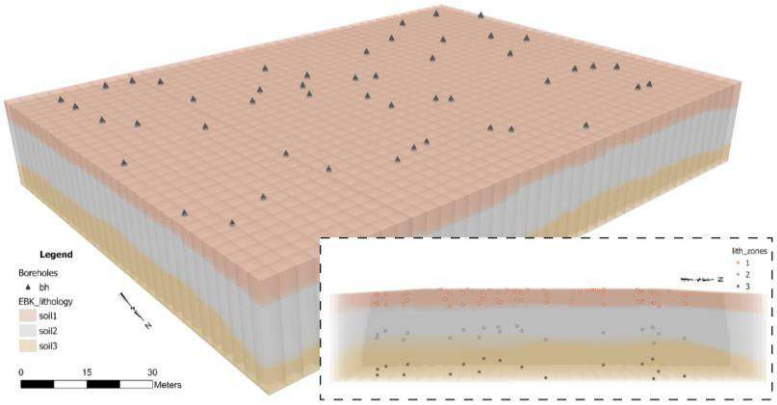

Fig. 2. 3D lithology model generated using ArcGIS Pro's EBK, with an excerpt of a vertical view showing the zone points used for modelling.

2.2.2. Voxel-based lithology model

We produce the 3D lithology model using the ArcGIS Pro's EBK tool in several steps. First, we prepare the input lithology data as point feature layer containing 3D spatial coordinates, as well as lithology index (Fig. 2). Then, we configure the EBK model: semivariogram type, subset size, number of simulations. This part also allows for data transformation, if needed. After defining the vertical anisotropy with trend removal and elevation inflation factor, we set the search neighbourhood parameters: radius, sectorization scheme and number of neighbours. Next, the tool is being run and the performance is evaluated through error diagnostics. Final step includes reclassifying EBK continuous prediction into discrete lithology units.

Upon execution, the output is stored as a geostatistical layer that shows a horizontal transect at a given location. It encapsulates the source dataset path, all EBK parameters used for the interpolation, and metadata for subsequent mapping or re-evaluation. Geostatistical layer is further used to generate a multidimensional voxel-based raster that stores volumetric data in NetCDF format (see Section 2.4.). In this study, we employ voxels for building and representing the digital ground model, which seamlessly integrate with subsequent modelling components. The entire workflow is fully automated with ArcPy, Esri's comprehensive Python library for spatial analysis, data management, and conversion (Esri, 2025). The lithology model derived from synthetic digital borehole data (Section 2.1.) is presented in Fig. 2.

2.3. Soil spatial variability

2.3.1. Conditional random field (CRF) generation in GSTools

The conditional simulation process can reliably be executed in GSTools (Müller et al., 2022), which is an open-source Python library designed for efficient geostatistical modelling and spatial random field simulation. A CRF is generated following a three-step procedure that includes: 1) computing kriging weights and generating a kriged field, 2) generating an unconditional realization of a random field, and 3) conditioning the unconditional random field with the kriging correction for the observed measurements, as detailed below.

Regardless of the generation technique, an unconditional simulation greatly depends on a covariance model whose definition typically involves specifying variance (σ^2), nugget (n), correlation length (ℓ), and a chosen form of correlation function *cor(h)*. Once a variogram model is in place, a common way to simulate a Gaussian random field is by utilizing the Randomization method (Heße et al., 2014; Kraichnan, 1970) that employs the variogram model's spectral density to simulate a Wiener process in the Fourier domain. In this approach, the field $U_u(x)$ is estimated with:

$$U_u(x) = \sqrt{\frac{\sigma^2}{N}} \sum_{i=1}^{N} \left(a_i cos(k_i \cdot x) + b_i sin(k_i \cdot x) \right) \tag{2}$$

where N is the number of Fourier modes used in the simulation, a_i and b_i are independent standard normal random variables ($\mathcal{N}(0,1)$), and k_i represent independent random wave vectors sampled from the spectral density corresponding to the variogram model.

Then, with kriging, the unknown values of a field U_k at a spatial point x_0 are estimated by applying the weighting factor λ_i to the observed values Z_1, Z_2, ..., Z_n at spatial points x_1, x_2, ..., x_n:

$$U_k(x_0) = \sum_{i=1}^{N} \lambda_i Z_i = \sum_{i=1}^{N} \lambda_i(x_0) Z(x_i) \tag{3}$$

for which N is the number of observations, and the weights are determined by minimizing the kriging error variance σ_e^2.

Thus, a conditional random field can generally be observed as a set of three components, which make up the CRF generation process:

$$U_c(x) = U_u(x) + \left(U_k(x) - U_{ks}(x) \right) \tag{4}$$

where x represents a spatial location, $U_u(x)$ refers to the unconditional random field, $U_k(x)$ denotes the kriging estimate based on measured data at their locations x_i for $i = 1, 2, ..., N$, and $U_{ks}(x)$ is the kriging estimate based on the simulated values from the unconditional field at the same locations.

2.3.2. Conditional realizations of soil properties

Here, we generate conditional realizations of four soil properties considered most relevant for conducting numerical analysis – cohesion, internal friction angle, Young's modulus and plastic hardening modulus, for each soil type. For assessing the domain of interest's spatial variability, we fully utilize the previously presented workflow by conditioning the stochastic simulation for the measurement data obtained from soil samples. Table 1 shows a set of statistical parameters used for CRF simulation in soil 1, 2 and 3, which are adopted based on author's previous work (Bui and Meschke, 2020).

Table 1. Set of adopted soil properties from soil samples

	Soil 1			Soil 2			Soil 3		
	min	max	μ	min	max	μ	min	max	μ
c (kPa)	24.09	32.88	28.42	26.00	34.93	30.48	82.23	91.76	86.81
φ (°)	26.05	30.95	28.29	28.02	32.95	30.59	30.01	34.99	32.82
E (MPa)	25.03	31.98	28.17	42.09	49.95	45.99	60.07	69.96	65.38
Ch (kPa)	27.05	32.98	30.14	40.00	47.97	44.13	57.06	64.95	61.02

Soil properties' distribution is modelled using the exponential covariance model paired with ordinary kriging routine, conditioning the simulation at 400 measurement points in total. The simulation is performed on a structured voxel grid inherited from the lithology model. Generated CRFs of soil properties preserve the domain's original spatial structure, realistically evaluating their variability, as shown in Fig. 3. Generally, soil properties' values perform greater variability in horizontal, than in vertical direction, clustering over the lengths defined by the correlation structure, while simultaneously respecting the known values from the borehole samples. Higher fluctuations and sharper transitions in cohesion and Young's modulus values at the interface of soil 2 and soil 3 are expected to form stress concentration zones along the contact.

2.4. Ground Information Model

2.4.1. Voxelization and Network Common Data Format

Voxel-based ground models greatly benefit the ground modelling procedure with their ability to refine the resolution at multiple scales, represent heterogeneous geological information across the domain and incorporate semantic data (Khan et al., 2023). Voxel represents a 3D cell or a cube that can carry volumetric and semantic information. Depending on the model complexity and further integration schemes, voxels can either be of uniform or differing size in three dimensions. Usually, a set of information that a voxel carries is assigned to its centre point, offering simplicity in voxel grid and data reconstruction across different modelling tools and software.

Since ArcGIS Pro produces voxel-based EBK models in NetCDF format (see section 2.2.), it is recognized as convenient, efficient and promising way of constructing GIM. NetCDF (Network Common Data Form) is a standardized, array-oriented file format designed for storing and exchanging diverse scientific datasets (NSF Unidata, 2025; Rew and Davis, 1990). It is self-describing, portable across platforms, and scalable, enabling efficient access to subsets of large datasets without requiring the entire file loading.

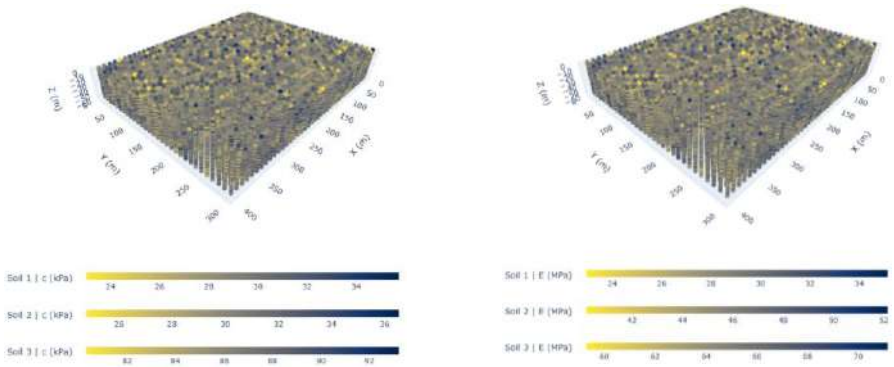

Fig. 3. 3D conditional realization of cohesion on the left and Young's modulus on the right (the other two CRFs are left out from visualization for the space sake).

2.4.2. GIM structure

GIM is structurally and hierarchically derived using the bottom-up approach (Fig. 4), such that each modelling component (group, subgroup) is generated in a staged workflow by consuming the data output of the previous stage, before writing its own results back into NetCDF. The starting layer is represented by the field observation data and its correlated metadata, stored as a root group. This non-gridded dataset is organized within three primary dimensions each corresponding to the borehole investigation elements and storing their specific variables (Fig. 1). Next, the GIS lithology voxel model is created loading the root-level variables (borehole coordinates, zone elevations, lithology types) and following the procedure described in Section 2.2. Besides the GIS projection data, this gridded model stores a number of voxels used for its construction, represented by the length of each dimension (based on voxel size), voxel centre coordinate arrays and the domain of interest bounding box. Within this group, the primary variable is a three-dimensional integer array *lithology[z,y,x]*, consisting of the interpolated lithology codes at each voxel centre. Built on top of the GIS voxel model, the CRF subgroup represents spatially varying soil parameters and their gradients, essentially using sample data for simulating the parameters on the voxel grid inherited from the lithology model. Soil parameter CRFs are generated as described in Section 2.3., resulting in a suite of 3D float arrays, each augmented with its own metadata (such as units and descriptions).

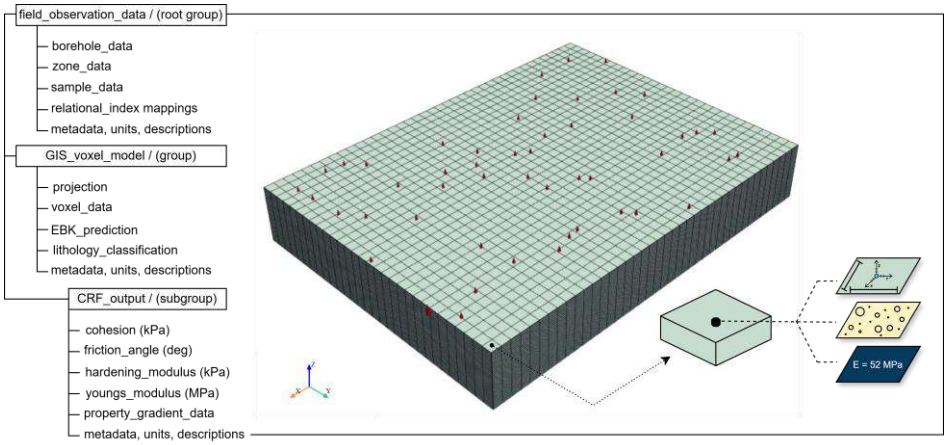

Fig. 4. GIM structure and voxel contents.

GIM constructed in this manner offers: a) full traceability – starting from the investigation data, and deriving multiple models in stages, b) modularity – modelling components are organized into groups of different characteristics, and c) reusability – groups can be accessed and used separately. Owing to its geometrical and structural features, voxel-based GIM provides all the necessary input for numerical modelling, allowing for seamless interoperability with FEM solvers, as presented in the following sections.

3. Finite element modelling with ground model input

3.1. Computational model for soils

Soil is a typical porous media, characterized by the void ratio between the solid skeleton and the matrix water. This ratio is often denoted as porosity. Depending on the working condition, soil can include air, especially when compressed air is flushed into the tunnel chamber during maintenance. Nevertheless, in the normal condition, soil below the groundwater table is considered to be fully saturated and fully dried above the groundwater level, i.e., drain condition. In terms of energy, the equilibrium state of the soil mixture is characterized by the balance of momentum and the mass balance equation. The whole set of equation is time dependent, and the discretised weak form can be integrated in time using Generalized Newmark-α method (Chung and Hulbert, 1993). For the details of the saturated soils formulation, the reader is referred to Nagel and Meschke (2010) and Bui et al. (2022).

3.2. CutFEM for excavation analysis

Robust treatment of material removal procedure is crucial for the success of excavation analysis. In the traditional FEM analysis, material removal is characterised by element deactivation. Although simple, this approach does not allow to fine grain control the removal domain, which is governed by the element size. To do that, one must either refine the mesh or using a load reduction technique, e.g., CCM (Pham et al., 2025). In contrast, CutFEM treats the material removal at the integration point by applying suitable penalisation factor. By using adaptive quadrature, the material point can be penalised as prescribed by the cut boundary. An exemplary demonstration of this concept is illustrated in Fig. 5 (Left) for material point penalisation and in Fig. 5 (Right) for adaptive quadrature.

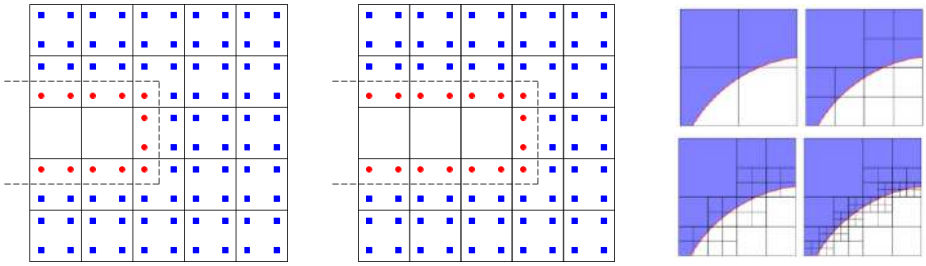

Fig. 5. (Left) Illustration of material point penalisation in excavation analysis with CutFEM. Red (•) dots are the inactive points and blue (■) dots are the active points; (Right) Illustration of CutFEM adaptive quadrature.

3.3. Adaptive mesh refinement

The stark change in the gradient of the stress field typically signifies a reduction of local accuracy (Szabó and Babuška, 2011), hence it is necessary to refine the mesh locally in this area. The spatially variable ground model often contains abrupted changes in the material properties, as presented in

Section 2.3. In this work, the Young's modulus E is selected to drive the mesh refinement due to its direct influence on the stress level. Following that, the gradient of E is used to decide if a refinement is needed for an element if $\|grad\ E\| > \epsilon_E$.

The mesh refinement procedure based on subdivision approach (Burstedde et al., 2011) is used due to its simplicity and readily available of high-performance package, i.e., p4est. This technique is based on binary subdivision in space. For 3D problem, a number of eight sub-cells will be created for a box grid cell of the structured grid. This division introduces hanging nodes. The displacement at the hanging nodes must be constrained to maintain the continuity of the displacement field (Bui et al., 2022).

The refinement criterion requires the calculation of grad E by the ground information model. In case it is not available, grad E can be approximated as

$(grad\ E)_{i,j,k} = \frac{1}{2}\left[\frac{E_{i+1,j,k} - E_{i-1,j,k}}{dx}, \frac{E_{i,j+1,k} - E_{i,j-1,k}}{dy}, \frac{E_{i,j,k+1} - E_{i,j,k-1}}{dz}\right]$, in which i, j, k is the index of the grid cell and dx, dy, dz are the size of a cell in the Cartesian directions respectively. It is noted that this scheme possesses second-order accuracy.

3.4. GIM integration

Integration of the GIM into geotechnical analysis is straightforward, providing that it can provide the parameter evaluation spatially. Having said that, a material parameter χ can be considered as mapping χ: R3 → R. In the voxel-based GIM described in Section 2.4.3., the material field value is stored in the discrete form at the grid vertices. Hence, the level set approach, i.e., using finite element shape function, can be employed to interpolate the value in space. The parameter setting problem reduces to global search of a grid cell which contains the spatial point, then determining its local coordinates. The final step is to interpolate the grid value based on shape functions evaluated at the local point.

4. Numerical example

To demonstrate the computational approach in this work, we set up a tunnel analysis with the background mesh of size 400 × 300 m. As for the ground model, it is constructed in full accordance with the procedure presented earlier (see Section 2.), such that it covers the domain of interest shown in Section 2.1. It consists of 39 401 voxels total, all equally dimensioned in x, y and z with 10, 10, 2 m, respectively. Each voxel stores the specific geological-geotechnical dataset assigned to its centre point, making the data exchange simple and straightforward. There are three different soil types delineated within the ground model (soil1, soil2 and soil3, see Fig. 2), and each one of them is characterized with spatially variable soil properties derived using conditional realizations of random field (Section 2.3).

For simplicity, only drained analysis is performed, and simple deactivation of the tunnel is used to simulate the excavation sequence. In this approach, the soil is deactivated along the tunnel track by setting the quadrature weight of the integration point within the excavation region to 10^{-12}. Subsequently, the tunnel lining is activated and tied with the background mesh. The analysis step is done by letting the soil consolidates freely. The constitutive law is selected as linear elastic for both the lining segment and the soil, in which the modulus of the lining is 3×10^{10}. As a result, the analysis will converge in at most one iteration.

It is well known in literature that Young's modulus (E) is one of the most sensitive parameters in predicting settlement in the tunnel analysis problem, e.g., (Nguyen et al., 2024; Ninić et al., 2015). In Ninić et al. (2015), the global sensitivity analysis employing FEM is analysed for E in each soil layer. In Nguyen et al. (2024), the feature importance analysis is performed on the lining-soil interaction model. The results show that E is the most important feature to affect the lining displacement. Hence, we select E as the primary parameter to study the effect of soil variability in numerical analysis.

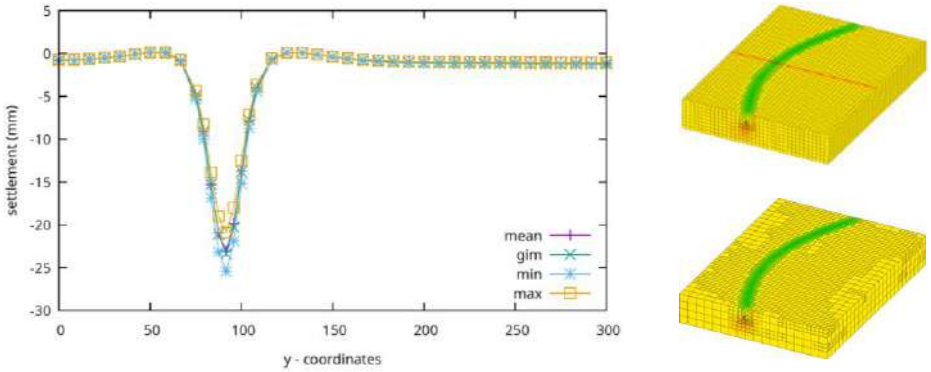

Fig. 6. (Left) Obtained settlements for deterministic and GIM analyses and (Right) Settlement field of the analysis with mean E in each soil layer (Top left) and with soil variability (Bottom left).

Fig. 6 (Right) presents the settlement field of both analyses using mean values and with soil variability respectively. It also shows the meshes used for the analysis with deterministic soil parameters and with soil variability. Due to the change in Young's modulus fields, the mesh is refined for the analysis with GIM. In Fig. 6 (Left), the settlement is sampled in the middle section (red line) and compared with the deterministic analyses using the minimum and maximum values of the Young's modulus field. As expected, the results using mean values and GIM are bounded by the curves with minimum and maximum values. The difference in the largest settlement of "mean" and "GIM" results is ~ 1.3%. We anticipate that the fluctuation in the variability model compensates each other, thus giving very closed results to the "mean" analysis. Nevertheless, the "GIM" analysis is able to capture local changes in the stress field, as visualised in Fig. 7 for σ_{zz} and Fig. 10 for vertical stress sampling at points along the tunnel. This observation verifies an important theoretical aspect, that the displacement field is the integral of the strain and is generally smoother than the stress field, see Fig. 6 (Right).

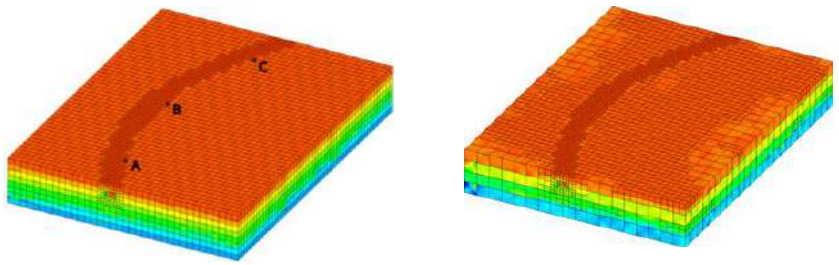

Fig. 7. σ_{zz} field of the analysis with mean E in each soil layer (left) and with soil variability (right)

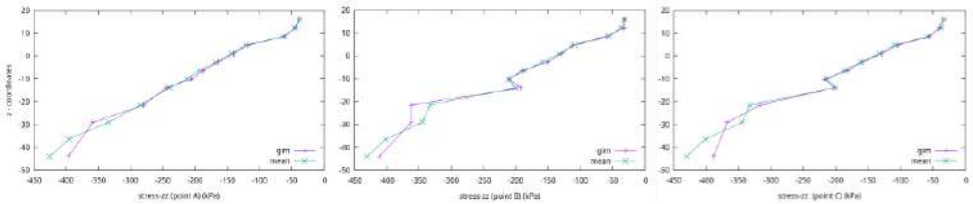

Fig. 8. Vertical stress field sampling at point A, B and C, see Fig. 7.

5. Conclusions

This study presents the incorporation of soil variability into geotechnical analysis via ground information model. It underpins the effort to account for uncertainty in geotechnical design, opening a new paradigm for expanding the applicability and improving the reliability of numerical analysis in engineering. The proposed approach is conducted by establishing an efficient data exchange interface between voxel-based ground model and finite element analysis. By providing the procedure to import spatial data from NetCDF of GIM and approximate the field gradient, the method enables mesh refinement technique that enhances the computational accuracy.

To demonstrate the methodology, the tunnel excavation analysis is carried out employing the CutFEM concept for material removal. This approach is shown to be effective, since structured grid is used consistently for both data representation and simulation mesh. The results reveal that the GIM analysis can capture localised changes in the stress field, offering more detailed look into soil-structure interaction. Future work includes studying the effect of soil parameters in nonlinear analyses, incorporating realistic constitutive models for soil behaviour, as well as enriching and updating GIM with a bigger scope of relevant geological and geotechnical data. In terms of applicability, the computational approach can then be relevant for other types of analysis, such as foundation excavation and incorporation of buildings and structures.

Acknowledgements

The first author acknowledges the support of the Science Fund of the Republic of Serbia through project #345 - Digital and Numerical Model Integration for Optimization in Geotechnics – DiNum-GEO. The second author is supported by Marie Sklodowska-Curie project TwinSSI (UKRI – EP/Z001072/1).

References

Bui, H-G. and Meschke, G. 2020. A parallelization strategy for hydro-mechanically coupled mechanized tunneling simulations. *Computer and Geotechnics*, 120, 103378. https://doi.org/10.1016/j.compgeo.2019.103378

Bui, H.-G., Schillinger, D., Zendaki, Y., Meschke, G., 2022. A CutFEM based framework for numerical simulations of machine driven tunnels with arbitrary alignments. *Computers and Geotechnics*, 144, 104637. https://doi.org/10.1016/j.compgeo.2022.104637

Bui, H.-G., Cao, B.-T., Freitag, S., Hackl, K., Meschke, G., 2023. Surrogate modeling for interactive tunnel track design using the cut finite element method. *Engineering with Computers*, 39, 4025–4043. https://doi.org/10.1007/s00366-023-01867-y

Burstedde, C., Wilcox, L., and Ghattas, O., 2011. P4est: Scalable algorithms for parallel adaptive mesh refinement on forests of octrees. *SIAM Journal on Scientific Computing*, 33(3), 1103–1133. https://doi.org/10.1137/100791634

Chen, X. J., Fang, P. P., Chen, Q. N., Hu, J., Yao, K., Liu, Y. 2024. Influence of cutterhead opening ratio on soil arching effect and face stability during tunnelling through non-uniform soils. *Underground Space*, 17, 45–59. https://doi.org/10.1016/j.undsp.2023.11.003

Chung, J., Hulbert, G. M., 1993. A time integration algorithm for structural dynamics with improved numerical dissipation: The generalized-α method. *Journal of Applied Mechanics*, 60(2), 371–375. https://doi.org/10.1115/1.2900803

Esri. What is empirical Bayesian kriging? ArcGIS Pro documentation. Available online: https://pro.arcgis.com/en/pro-app/latest/help/analysis/geostatistical-analyst/what-is-empirical-bayesian-kriging-.htm (accessed on 1 June 2025)

Esri. What is ArcPy? ArcGIS Pro documentation. Available online: https://pro.arcgis.com/en/pro-app/3.4/arcpy/get-started/what-is-arcpy-.htm (accessed on 1 June 2025)

Gong, W., Juang, C.H., Martin, J. R., Tang, H., Wang, Q., Huang, H. 2018. Probabilistic analysis of tunnel longitudinal performance based upon conditional random field simulation of soil properties. *Tunnelling and Underground Space Technology*, 73, 1–14. https://doi.org/10.1016/j.tust.2017.11.026

Gribov, A., and Krivoruchko, K. 2020. Empirical Bayesian kriging implementation and usage. *Science of the Total Environment*, 722, 137290. https://doi.org/10.1016/j.scitotenv.2020.137290

Heße, F., Prykhodko, V., Schlüter, S., Attinger, S. 2014. Generating random fields with a truncated power-law variogram: A comparison of several numerical methods. *Environmental Modelling & Software*, 55, 32–48. https://doi.org/10.1016/j.envsoft.2014.01.013

He, Z., Xu, H., Gardoni, P., Zhou, Y., Wang, Y., Zhao, Z. 2022. Seismic demand and capacity models and fragility estimates for underground structures considering spatially varying soil properties. *Tunnelling and Underground Space Technology*, 119, 104231. https://doi.org/10.1016/j.tust.2021.104231

Huang, L., Zhang, Y., Lo, M., Cheng, Y. 2020. Comparative study of conditional methods in slope reliability evaluation. *Computers and Geotechnics*, 127, 103762. https://doi.org/10.1016/j.compgeo.2020.103762

Hu, L., Kasama, K., Wang, G., Takahashi, A. 2025. Assessing the influence of geotechnical uncertainty on existing tunnel settlement caused by new tunnelling underneath. *Tunnelling and Underground Space Technology*, 155(Pt 1), 106189. https://doi.org/10.1016/j.tust.2024.106189

Khan, M. S., Kim, I. S., Seo, J. W. 2023. A boundary and voxel-based 3D geological data management system leveraging BIM and GIS. *International Journal of Applied Earth Observation and Geoinformation*, 118, 103277. https://doi.org/10.1016/j.jag.2023.103277

Kraichnan, R. 1970. Diffusion by a random velocity field. *Physics of Fluids*, 13, 22–31. https://doi.org/10.1063/1.1692799

Krivoruchko, K., Gribov, A. 2019. Evaluation of empirical Bayesian kriging. *Spatial Statistics*, 32, 100368. https://doi.org/10.1016/j.spasta.2019.100368

Müller, S., Schüler, L., Zech, A., Heße, F. 2022. GSTools v1.3: A toolbox for geostatistical modelling in Python. *Geoscientific Model Development, 15*, 3161–3182. https://doi.org/10.5194/gmd-15-3161-2022

Nagel, F., Meschke, G., 2010. An elasto-plastic three phase model for partially saturated soil for the finite element simulation of compressed air support in tunnelling. *International Journal for Numerical and Analytical Methods in Geomechanics*, 34(6), 605–625. https://doi.org/10.1002/nag.828

Nguyen, T.T, Cao, B.T, Pham, V.V, Bui, H.G., Do, N.A, 2024, Design optimization of quasi-rectangular tunnels based on hyperstatic reaction method and ensemble learning. *Journal of Rock Mechanics and Geotechnical Engineering*. https://doi.org/10.1016/j.jrmge.2024.10.020

Ninić, J., Meschke G. 2015. Model update and real-time steering of tunnel boring machines using simulation-based meta models. *Tunnelling and Underground Space Technology*, 45, 138–152. https://doi.org/10.1016/j.tust.2014.09.013

NSF Unidata. Network Common Data Form (NetCDF). Available online: https://www.unidata.ucar.edu/software/netcdf/ (accessed on 1 June 2025)

Pan, Q. J., Dias, D. 2017. Probabilistic evaluation of tunnel face stability in spatially random soils using sparse polynomial chaos expansion with global sensitivity analysis. *Acta Geotechnica*, 12, 1415–1429. https://doi.org/10.1007/s11440-017-0560-9

Pham, V.-V., Do, N.-A., Osinski, P., Do, N.-T., Bui, H.-G., Cao, B.-T., Nguyen, T.-T., Dias, D., 2025. Effect of the pile foundation and soil constitutive models on the behavior of twin circular tunnels considering the deconfinement process. *Environmental Earth Sciences*. https://doi.org/10.1007/s12665-025-12365-3

Rew, R. K., Davis, G. P. 1990. NetCDF: An interface for scientific data access. *IEEE Computer Graphics and Applications*, 10(4), 76–82. https://doi.org/10.1109/38.56302

Shooib Khan, M., Kim, I. S., Seo, J. W. 2023. A boundary and voxel-based 3D geological data management system leveraging BIM and GIS. *International Journal of Applied Earth Observation and Geoinformation*, 118, 103277. https://doi.org/10.1016/j.jag.2023.103277

Shi, C., Wang, Y. 2022. Data-driven construction of three-dimensional subsurface geological models from limited site-specific boreholes and prior geological knowledge for underground digital twin. *Tunnelling and Underground Space Technology*, 126, 104493. https://doi.org/10.1016/j.tust.2022.104493

Szabó, B., Babuška, I., 2011. Introduction to finite element analysis: Formulation, verification and validation. *Wiley*.

Tian, H., Wang, Y. 2023. Data-driven and physics-informed Bayesian learning of spatiotemporally varying consolidation settlement from sparse site investigation and settlement monitoring data. *Computers and Geotechnics*, 157, 105328. https://doi.org/10.1016/j.compgeo.2023.105328

Vanmarcke, E. H. 1977. Probabilistic modeling of soil profiles. *Journal of the Geotechnical Engineering Division, ASCE*, 103(11), 1227–1246. https://doi.org/10.1061/AJGEB6.0000517

Wang, L., Pan, Q., Wang, S. 2024. Data-driven predictions of shield attitudes using Bayesian machine learning. *Computers and Geotechnics*, 166, 106002. https://doi.org/10.1016/j.compgeo.2023.106002

Wang, Y., Tian, H.-M. 2024. Digital geotechnics: From data-driven site characterisation towards digital transformation and intelligence in geotechnical engineering. *Georisk: Assessment and Management of Risk for Engineered Systems and Geohazards*, 18(1), 8–32. https://doi.org/10.1080/17499518.2023.2278136

Xie, P., Chen, K., Skibniewski, M., Wang, J., Luo, H. 2023. Parametric geological model update and probabilistic analysis of shield tunnel excavation: A borehole-based conditional random fields approach. *Computers and Geotechnics*, 157, 105349. https://doi.org/10.1016/j.compgeo.2023.105349

Zhao, C., Gong, W., Juang, C.-H., Tang, H., Hu, X., Wang, L. 2023. Optimization of site exploration program based on coupled characterization of stratigraphic and geo-properties uncertainties. *Engineering Geology*, 317, 107081. https://doi.org/10.1016/j.enggeo.2023.107081

Southeastern Europe Tunnelling Conference (SETC-2025)
1-3 October 2025, Belgrade, Serbia

DOI: 10.5937/SETC25027V

Tunnel boring works with the use of information modelling technology in Moscow metro design

V. Viazovoi[a], A. Khidisheli[b], D. Koniukhov[a,c], V. Korobkova[a], S. Popova[a], A. Moskalev[a], I. Agapov[a]*

[a] JSC Mosinzhproekt, 125252, Khodynsky boulevard 10, Moscow, Russia, gidrotehnik@inbox.ru
[b] JSC «INGEOKOM», 119019, Bolshoj Afanasievkij per. 8, s. 3, Moscow, Russia,
[c] Russian Technological University MIREA, 119454, Vernadsky Avenue 78, RTU MIREA, Moscow, Russia

Abstract: Designing and construction of new transport infrastructure objects in large megacities is caused by dense urban development, dense network of engineering communications and operating underground facilities. The location of stations and tunnelling of underground tunnels in such conditions is associated with an increase in the cost of construction and installation works. Special methods as well as the use of information modelling technology serve as tools to optimize the costs arising in the course of project implementation within a tight schedule. This is illustrated in the example of the construction of distancing tunnels from the station 'Klenovy Boulevard' to the station 'Kuryanovo' of the projected Biryulevskaya line of the Moscow Metro crossing the station 'Klenovy Boulevard' of the existing Big Circle Line. As part of the design, two options for the crossing were analysed: under the Klenovy Boulevard station of the Big Circle Line and, respectively, above the existing tunnel of the station complex. Thanks to the application of information modelling technology, the second option was chosen, where the route was modelled with coordinated information models reflecting the already implemented design solutions for Klenovy Boulevard on Big Circle Line station, as well as a fragment of the projected crossing between Klenovy Boulevard and Kuryanovo stations, passing over the technical inspection station. At the same time, the distance between the existing and under construction structures in the cross-section according to the adopted structural solutions will be no more than 1,7 m. It is therefore necessary to increase the bearing capacity of the soils and prevent possible deformations. To preserve the strength and stability of the soil massif, a part of the excavation is to be filled with expanded clay concrete in the tunnelling zone of the tunnel boring mechanized complex. The described experience reflects the practical significance of information modelling technology implementation in the construction of structures within the framework of dense urban development and creates an economic effect.

Keywords: construction; information modelling technology; metro; tunnel; tunnelling

1. Introduction

The design and construction of new transport infrastructure facilities in large metropolitan areas is due to dense urban development, a dense network of utilities and existing metro facilities (Agafonov et al., 2024). The placement of stations and the passage of subway tunnels within the specified conditions leads to an increase in the cost of construction and installation work. Considering major construction projects in the city of Moscow, it is impossible not to mention the construction of the Big Circle line (BCL) of the Moscow metro (Fig. 1). This is the largest metro construction project in Russia and one of the largest in the world – the length of the line is 70 km, 31 stations and 2 electric depots. And 20% of the stations were already built with the support of the information model (Viazovoi et al., 2024; Kivlyuk at al., 2024).

In recent years, information modelling technologies have become the basis for improving the efficiency and reducing the risks inherent in underground construction projects (Arayici, at al., 2011; Azhar, 2011; Liu, at al., 2017). The use of special methods, as well as the use of information modelling technology (BIM), are tools for optimizing costs incurred during the implementation of a project in a short time frame. This technology promotes closer collaboration, accuracy, and efficiency in the design process,

*Corresponding author: gidrotehnik@inbox.ru (Viazovoi V.).

shifting the industry paradigm towards an approach focused on timely and operational data exchange between participants in the construction process (Charehzehi, and Ahankoob, 2012; Paskaleva, Beronneau, and Bednar, 2024; Zhaofeng, 2024).The article (Nadot, at al., 2024) notes that the creation of information models within the framework of the BCL project of the Moscow Metro allowed:

- to detect and prevent conflict situations in the design process in advance;
- identify priorities in a timely manner and focus resources on the most important areas of work;
- use the BIM database when conducting copyright supervision;
- to implement 4D planning, which integrates a 3D model with the construction schedule, which allowed for a dynamic analysis of the planned and actual progress of work;
- to implement spatial coordination of the premises used in the cramped conditions of underground construction.

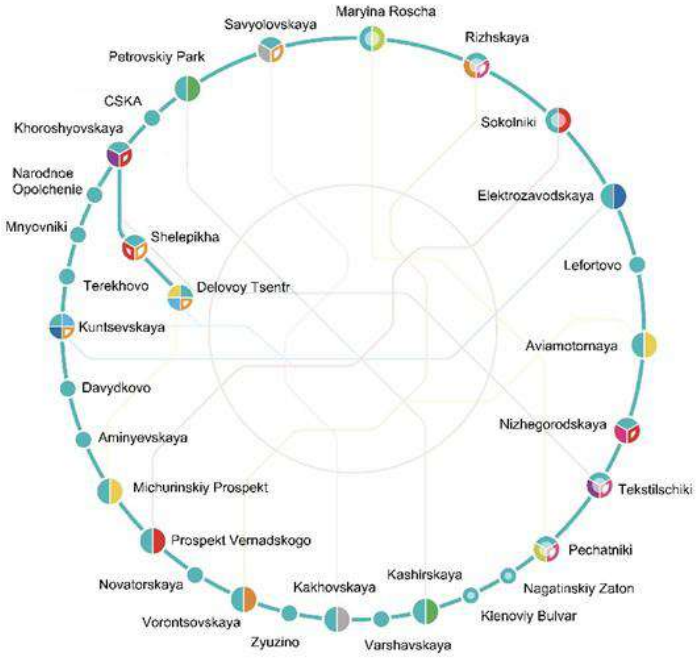

Fig. 1. Diagram of the Moscow Metro's Big Circle line.

Additionally, it should be noted that Guinness World Records has recorded a world record on the Big Circle line for the number of tunnel-boring mechanized complexes (TBM) used in the construction of the subway: 23 billboards did not work simultaneously on one project in any megacity in the world.

This article discusses the construction of transfer tunnels from Klenovy Bulvar station to Kuryanovo station of the projected Biryulevskaya line of the Moscow Metro with the intersection of the existing BCL, which is a complex of underground and aboveground structures providing not only transportation of people, but also the functioning of the BCL as a whole.

2. Methodology

As part of the design, two intersection options were analysed: under the Klenovy Bulvar BCL station (option 1) and, accordingly, between the current tunnel of the station complex and the above-ground metro lobby (option 2, shown in Fig. 2).

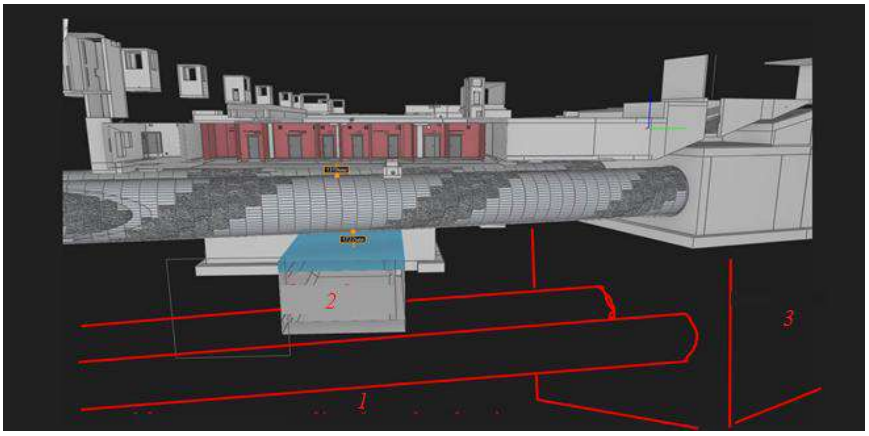

Fig. 2. Options for the route of the Biryulevskaya metro line tunnels: 1 – option 1 for the tunnel route (under the existing line); 2 – double-track tunnel for the Biryulevskaya metro line; 3 – additional wall volume in the ground.

Option 1 required significant deepening of the foundation pit of the future Klenovy Boulevard station, which would lead to a multiple increase in the cost and duration of construction and installation work, as well as additional costs for appropriate measures for buildings and structures that were in the increased zone of influence of construction.

Thanks to the use of BIM, option 2 was chosen, where the route was modelled taking into account coordinated information models reflecting already implemented design solutions for the Klenovy Bulvar BCL station, as well as a fragment of the projected stretch between Klenovy Bulvar station and Kuryanovo station, passing over the technical inspection point. This solution leads to optimization of the construction process and reduction of the project budget (Fig. 3).

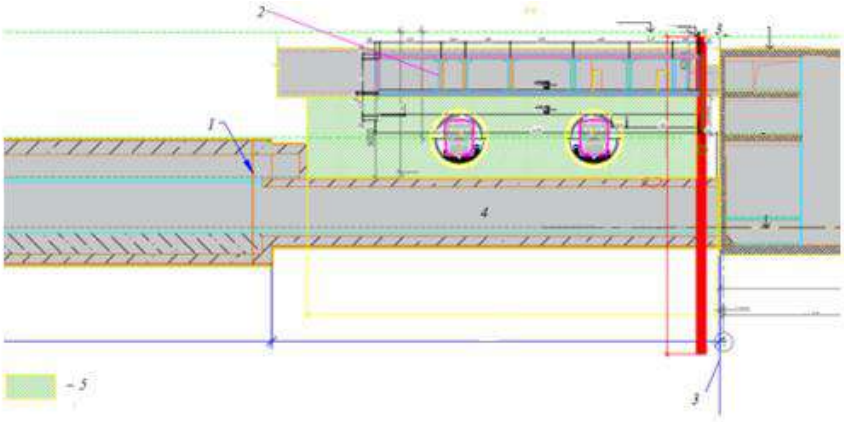

Fig. 3. Longitudinal section for option 2 at the intersection of the Biryulevskaya metro line tunnels with the existing Klenovy Boulevard station: 1 – expansion joint; 2 – pedestrian crossing; 3 – beginning of the station complex; 4 – railhead level; 5 – backfill work area at the intersection of lines.

At the same time, the distance between existing and under construction structures in cross-section according to the adopted design solutions will be no more than 1.7 m. Therefore, it is necessary to increase the bearing capacity of soils to prevent possible deformations (Konyukhov, 2021; Kulikova et al., 2023). To preserve the strength and stability of the soil mass during the construction of the BKL, a part of the excavation was filled with expanded clay concrete in the TPMK sinking area.

The expanded clay concrete installation is provided in two stages:

1. laying expanded clay concrete up to the 109.45 mark (1 m below the axis of the 3rd tier of fastening). After gaining strength with expanded clay concrete of at least 75 %, the 3rd tier of fastening is dismantled;
2. laying expanded clay concrete and backfilling to the bottom of the preparation for permanent structures of the pedestrian crossing (Fig. 4).

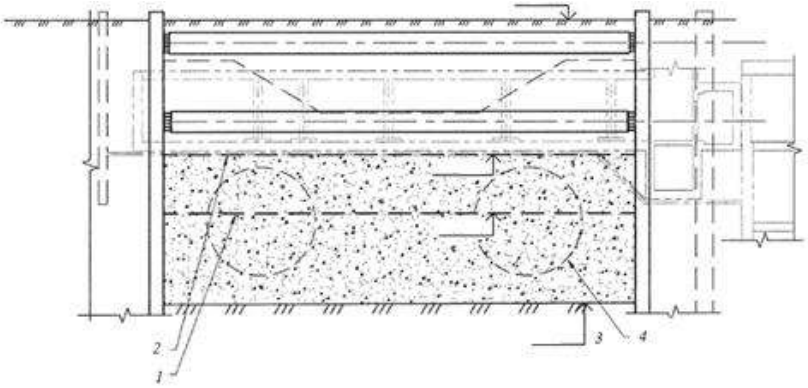

Fig. 4. Diagram of expanded clay concrete laying and backfilling: 1 – first stage of expanded clay concrete laying; 2 – second stage of expanded clay concrete laying; 3 – excavation depth mark; 4 – TBM rotor dimensions.

The TPMK 'Herrenknecht' tunnelling complex with a 6.25 m diameter hydraulic face loader has been selected for the passage of the Biryulevskaya line of the metro, which has successfully completed the passage of 13 tunnels in the city of Moscow, which is more than 16 thousand running meters.

A tunnelling complex with a bottom-hole hydraulic loader, compared with a shield with a ground loader, allows for more accurate control of the physical properties of the slurry and pulp, as well as maintaining a set pressure in the bottom-hole chamber (Jarast et al., 2023; Konyukhov, 2023; Mahdi et L., 2019).

The chisel head performs the function of a means of penetration, while the fastening of the bottom hole space is carried out by counterpressure of a special solution, in particular, bentonite or clay-water (mud) suspension (Mazein et al., 2019).

The slurry is pumped into the hydraulic loading chamber, from where it enters the bottom hole space, and then seeps into the ground, forming a filtration crust, either a waterproof partition (fine-grained soil), or a fully impregnated zone (coarse-grained) to provide back pressure in the head of the shield.

The clastic material developed by the working tools of the rotary chisel head consists partly of soil, and partly of bentonite or a clay (mud) mixture. This mixture is pumped (hydraulic excavation) from the hydraulic loading chamber into a separation unit on the surface, which processes it for subsequent use..

3. Results

These measures were taken into account when assessing the impact of tunnelling on the operating station, taking into account the recommendations (Lebedev, 2018); the calculation model was performed in the PLAXIS software package. The calculations were performed in a 3D formulation using the Hardening Soil model. The physical and mechanical characteristics of the soils were determined based on the results of laboratory studies and optimized using mathematical modelling in the PLAXIS SOIL TEST virtual laboratory. The results of model studies of the effect of the passage of distillation tunnels on the operating station are shown in Tables 1 and 2 and in Fig. 5.

Table 1. Predicted maximum additional vertical total displacements of tracks falling within the calculated zone of influence of construction.

Track number at 'Klenovy Boulevard' station of BCL	Total vertical displacement of tracks (taking into account previous stages) [mm]		Settlement [mm]	Deviation in level [mm]	Skew [mm]	Track widening (narrowing) [mm]
	Calculation stage					
	Tunnelling of the first tunnel	Drilling of the second tunnel				
1st	0,18	0,67	Less than 1			
2nd	0,15	0,74	Less than 1			

Table 2. Predicted maximum additional vertical and horizontal displacements of metro structures falling within the calculated zone of influence from TBM tunnelling ('Klenovy Boulevard' station on the BCL).

Structure	Tunnelling stage	Maximum additional displacements, mm		Technical condition category	Maximum permissible additional settlement, mm, according to SP 474.1325900.2019
		vertical	horizontal		
Underground vestibule and staircase	First	12,1	1,4	II	30
	Second	16,2	2,8		

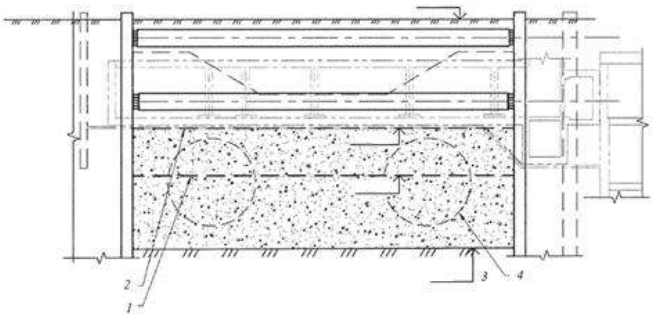

Fig. 5. Additional vertical movements of the Klenovy Bulvar BCL station at the stage of tunnelling the 2nd tunnel.

According to the results of mathematical modelling, the maximum additional total vertical movements and the relative difference in precipitation of buildings, structures, and utilities do not exceed the maximum permissible values established by regulatory documents of the Russian Federation. The integrity and operability of the building structures of the BCL, structures, and engineering communications are ensured, additional safety measures are not required.

The use of numerical modelling of the impact of the passage of the Biryulevskaya Line tunnels on the operating Klenovy Bulvar station of the BCL made it possible to clarify the relative location of structures in the BIM model of the line under construction. However, monitoring of existing metro facilities and the surrounding buildings is provided for the entire period of tunnel driving.

4. Conclusion

The methods used in the design of the considered section of the Biryulevskaya metro line will make it possible to implement complex capital construction projects. The described experience reflects the

practical significance of the introduction of BIM in the construction of structures in dense urban areas and shows the economic effect (Table 3).

In the near future, information modelling technology may become the main tool for implementing complex capital construction projects, which undoubtedly include the metro. The introduction of information modelling technologies creates an opportunity to improve the detection of collisions, prioritize work, optimize planning accuracy and cost control, which will increase the efficiency and profitability of the construction process.

Table 3. Predicted maximum additional vertical and horizontal displacements of metro structures falling within

№	Parameters under consideration	Option 1	Option 2
1	Volume of excavated soil, m^3	203.970,0	97.278,0
2	Volume of trench 'wall in the ground', m^3	24.613,9	12.252,2
3	Volume of excavation pit support, t	5.275,2	2.515,9
4	Construction period of the pit, months	17,9	12,0
5	Cost of construction and installation works, thousand rubles	5.084.442,7	2.489.097,7

References

Agafonov, V., Konyukhov, D., Kulikova, E., 2024. A conceptual framework for the creation of an integrated planning system for the strategy of implementing technologies for underground urban construction. Tunnelling for a Better Life – Proceedings of the ITA-AITES World Tunnel Congress (WTC 2024). Jinxiu Yan, Tarcisio Celestino, Markus Thewes, Erik Eberhardt (Eds.), 3157-3159.

Guinness World Records: 23 TPMK stroyat metro Moskvy. 2020. https://stroi.mos.ru/infographics/guinness-world-records-23-tpmk-stroiat-mietro-moskvy?from=cl 11.06.2025. (In Rus.).

Jarast, P., Bakhshi, M., Nasri, V., 2023. Carbon footprint emissions of different tunneling construction methods // Expanding Underground – Knowledge and Passion to Make a Positive Impact on the World. Edited by G. Anagnostou, A. Benardos, V. P. Marinos, Proceedings of the ITA-AITES World Tunnel Congress 2023. (WTC 2023), 65-73.

Kivlyuk, V.P., Paschenko, A.I., Konyukhov, D.S., Xue Liqiang, Zhou Jimin, Vinogradov, S.N., Orlov, K.V., Song Yangchun, Huo Jiuyuan, Lyu Yongfang, Gu Zhiqiang, Wang Ting, 2024. Experience of Russian-Chinese industrial cooperation on the construction of the Moscow metro. BRICS transport, 3(1), 1-8.

Konyuhov, D.S., 2023. Prognoz tekhnologicheskih deformacij pri stroitel'stve zdanij i sooruzhenij na podrabatyvaemyh territoriyah. Ugol', 4,61-64. (In Russ).

Konyukhov, D.S., 2021. Criteria analysis of modern technologies of underground construction. *Geotekhnika*, 1, 40-55. (In Russ).

Kulikova, E.Yu., Balovtsev, S.V., Skopintseva, O.V., 2023. Complex estimation of geotechnical risks in mine and underground construction. *Sustainable Development of Mountain Territories*, 15(1), 7-16. (In Russ).

Lebedev, M.O., 2018. Choosing a calculation method for stress-strain of supports and lining of transport tunnels. 16thWorld Conference of the Associated Research Centers for the Urban Underground Space (ACUUS 2018), 5-7 November 2018. Hong Kong, 678-687.

Mahdi, S., Gastebled, O., Khodr, S., 2019. Back analysis of ground settlements induced by TBM excavation for the north extension of Paris metro, line 12. Tunnels and Underground Cities: Engineering and Innovation meet Archaeology, Architecture and Art – Peila, Viggiani&Celestino (Eds), 2606-2615.

Mazein, S.V., Pankratenko, A.N., Polyankin, A.G., Sharshova, E.A., 2019. Soil improvement in tunnel face using foam reagents in EPB TBM. Tunnels and underground cities: engineering and innovation meet archaeology, architecture and art. Proceedings of the World tunnel Congress and the 45th General Assembly of the International tunnelling and underground space association, 2663-2670.

Viazovoi, V.V., Evtushenko, R.A., Koniukhov, D.S., Petunina, D.S., 2024. Research and development support for the construction of the big circle line on the example of the line's intersection with the existing facilities of the Moscow metro. Tunnelling for a Better Life - Proceedings of the ITA-AITES World Tunnel Congress (WTC 2024). Jinxiu Yan, Tarcisio Celestino, Markus Thewes, Erik Eberhardt (Eds.), 1602-1609.

SETC-2025
BELGRADE

TOPIC 5

INSTRUMENTATION AND MONITORING/TESTING AND INSPECTION

Southeastern Europe Tunnelling Conference (SETC-2025)
1-3 October 2025, Belgrade, Serbia

DOI: 10.5937/SETC25028T

Muon Tomography and its Application to Non-Invasive Tunnelling Investigations

Lee F. Thompson[a]*, *Chris A. Steer*[a]

[a] Geoptic Infrastructure Investigations, South Warnborough, RG29 1SD, UK; lee.thompson@geoptic.co.uk, chris.steer@geoptic.co.uk

Abstract: Muon tomography is a novel technique that utilises highly-penetrating but free and abundantly-available natural radiation to image large-scale objects in a totally non-invasive and non- destructive way. This paper reports on the successful application of muon tomography to the imaging of railway tunnels on the UK rail network and outline a number of other applications that are relevant to the tunnelling industry. Specifically, the technique employed to image critical infrastructure using muon tomography technique is described. To place this work into context a brief summary of the recent and past applications the muon imaging method is also presented. Subsequently, there follows a more detailed description of a case study for the technique, specifically that of using muon tomography to image an Victorian era railway tunnel in the United Kingdom. This case study exemplifies the power of the muon tomography technique in that suspected hidden shafts are both identified and characterised in a totally non-invasive manner. There then follows a discussion of the methods involved in extracting visualisations of the tunnel overburden which includes examples of results from a UK railway tunnel. In conclusion, an outlook of potential future applications of muon tomography to the worldwide tunnelling sector is discussed.

Keywords: muon; imaging; non-invasive; tunnel; infrastructure

1. Introduction

Muon tomography exploits muons which are naturally-occurring and fundamental particles (which means that that cannot be broken down into smaller particles). Muons are created, in abundance, in the Earth's upper atmosphere as the result of high-energy particles from the Sun and other sources such as supernovae interacting with gas molecules - such as Nitrogen and Oxygen - in the atmosphere. Muons have properties similar to that of a heavy electron (they have approximately 200 times the mass of the electron) which results in them being highly-penetrating particles, capable, for example, of passing through tens to hundreds of metres of rock with ease.

The combination of muons being highly penetrating and the fact that muons have a high relative abundance (for example, at sea level there are 10,000 muons per square metre per minute), results in them being an ideal candidate to be used for the tomographic imaging of objects that would otherwise be difficult access.

The muon tomography method is completely analogous to that of a medical X-ray. In the case of an X-ray, the density information in an object of interest (for example, a bone in a patient's leg) is imaged when a beam of X-rays passes through the object and subsequently observed by a suitable "detector" (usually an X-ray film) on the other side of the object. Muon tomography works in exactly the same way except that, in order to detect the muons, a muon-sensitive detection system is needed. It should be stressed that muon tomography is a non-invasive and non-destructive method - capable of returning vital information on the structural integrity of objects at a distance and without the need to interact with

*Corresponding author: lee.thompson@geoptic.co.uk (L.F. Thompson).

the object. Furthermore, just as an X-ray can diagnose issues that are otherwise hidden, muon tomography can identify features in, e.g. a tunnel overburden that would otherwise be invisible.

The parallels between muon tomographic imaging and X-ray imaging are useful to introduce the technique however there are a couple of important differences to note. First, in the case of muon tomography, the particles performing the imaging are free, unlike X-rays which have to be artificially produced. However since muon tomographic imaging relies on a flux of particles that comes from the sky then it is not possible to look down with this technique, muon detectors must be placed (ideally) underneath or to the side of the object(s) to be imaged.

The application of muon tomography to tunnelling is introduced below via a case study that took place on a disused railway tunnel in the UK which demonstrated, for the first time, the value of muon tomography in terms of providing essential and unique information to tunnel asset managers on live rail networks, as a consequence of this work, the technique has been successfully applied to the imaging of more than 20 historic Victorian rail tunnels within the UK. Within the context of tunnelling infrastructure other potential applications are documented in the conclusions section.

At this point it is worthwhile providing a short history of the technique's applications. The first documented use of muons in such applications took place in Australia in 1955 - just over 70 years ago - where the overburden in a tunnel system around a hydro-electric power station was measured. (George 1955). More recently muon tomography has been famously used to identify hidden chambers in the Great Pyramid (also known as "Khufu's pyramid") of Giza (Morishima et al. 2017). The presence of these voids was confirmed with the use of endoscopes in 2023. A summary of the broad range of applications of muon tomography has recently been published by the International Atomic Energy Authority (IAEA 2022). As an indication of the broad scope of the potential of muon tomography other recent applications of the technique within the tunnelling sector (Khaw et al, 2025), (Gebhart et al., 2023) and (Mao et al., 2023) are included in the references.

2. Methodology

2.1. Case study - Background

The muon tomography technique and its application to tunnels - which is of most interest to the SETC audience - is best introduced via a case study. The background to this case study is as follows. Much of the UK's railway infrastructure dates back to the Victorian era with an enormous increase in the UK rail network taking place between the 1850s and early 1900s. During this time significant numbers of bridges, tunnels and viaducts were built. In Victorian times the construction of railway tunnels commonly involved a number of additional vertical shafts being created along the length of the tunnel. These vertical shafts enabled the overall construction process to progress more rapidly. However, after the tunnel was completed what happened to these shafts varied greatly. In some cases the shafts were left open, in others they were bricked over in both the tunnel and on the surface, whereas some shafts have a combination of these approaches. In many cases any documentation regarding the location of hidden shafts is either incomplete or lost completely. In the present day, hidden shafts in particular are a concern to tunnel asset managers within the rail sector since they have potential for dramatic and unfortunate consequences, for example, in the early 1950s several houses near Manchester collapsed into an unknown hidden void, an incident that resulted in the loss of life.

Muon tomography is capable of locating areas of under-density (or, over-density) in an overburden and is thus well-suited to the identification of hidden shafts within rail tunnels. Furthermore, a more detailed tunnel survey with muon sensors is able to characterise any hidden shaft by locating its exact position and extent and also by returning valuable information on the opacity (effectively the integrated density along the column height above the tunnel) of any observed density deficit. Current methods used in the identification of voiding in ageing rail tunnels include invasive investigations, clearly a non-invasive method such as muon imaging is preferred over such techniques. Muon imaging is able to provide

valuable information on the tunnel's condition, in certain cases this is used in parallel with other methods such as GPR, ERT and seismic to provide complementary information for the asset manager.

The technique is exemplified in the following case study which details a programme of work which took place on a disused Victorian-era rail tunnel in the UK and is particularly relevant to the tunnelling community as it clearly demonstrates that muon tomography is capable of accurately identifying hidden density changes in tunnel structures.

If required, long-term monitoring of railway tunnel infrastructure is also possible whereby density variations can be monitored to see if there are temporal changes in the density which could be correlated to, e.g. extreme rainfall events. In such cases, this would be evidence of water ingress being observed. Clearly such information is vital to tunnel asset managers.

2.2. Case study - Instrumentation

Figure 1 depicts a typical muon detection system that can be deployed directly onto a "Permaquip" link trolley (a manual propelled, stand- alone load-bearing rolling platform for use on-track) and rolled into a rail tunnel.

Fig. 1. Image of two planar muon systems deployed on railway tracks.

The detectors used in this measurement campaign are somewhat different to those used in some of the earlier studies discussed above and are designed specifically to be robust and to operate outside of the laboratory in what can be challenging environments. The system comprises a total of 5 Explorer 154116 cases for the detectors and a Explorer 5122 case for the control box. Inside each of the black, IP68-rated detector cases is an array of sheets or bars of a material called plastic scintillator. This results in an overall "field-of-view" for the instrument of typically 45 to 60 degrees along the direction of travel however this field-of-view is further subdivided into 12 sub-fields of view - a feature that is subsequently used in the analysis of the data (see Section 2.4 below). The control box carries a battery and all of the associated electronics to record the detected muon signals. When assembled the system measures 1629 mm x 1629 mm x 1300 mm and is able to operate for 40 off a single battery charge.

Plastic scintillator comprises a suitably transparent base material, usually polystyrene, which is impregnated, at the polymerisation stage, with small quantities of compounds called "fluors" which comprise benzene rings. When a muon passes through the scintillator the energy deposited by them causes the fluors to excite and de-excite, leading to a short-duration light flash which can be detected and recorded using devices called photosensors The time of the light flash is also recorded which can be used to further pin-point the trajectory information of the passing muon.

In the case of muon tomography, large area detectors work best as this maximises the statistics acquired in what is typically short duration data acquisition periods (access to rail tunnels on live lines is usually restricted to a few hours overnight). The instruments shown in Figure 1 above demonstrate the best compromise between surface area and robustness. However, for other tunnelling applications it is possible to configure bars of plastic scintillator into cylindrical detectors that can, for example, be deployed in a borehole. Other, smaller format planar detectors are suitable for longer duration data acquisition times such as those required to correlate overburden changes with rainfall events as discussed earlier.

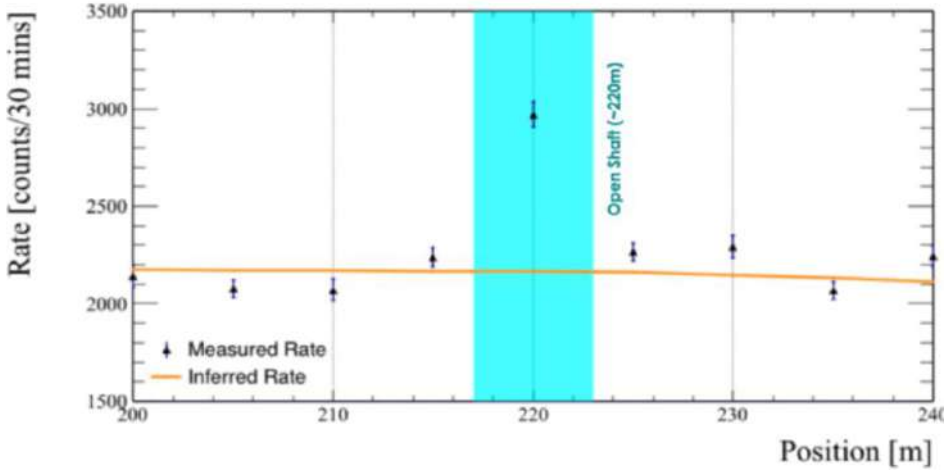

Fig. 2. Results of muon tomography scan of the Alfreton Old tunnel, observed data from muon instruments (points) and predicted data from digital twin assuming no hidden shafts (orange line).

2.3. Case study - Alfreton Old Tunnel

The world's first use of muon tomography in identifying and characterising hidden voids in railway tunnels was demonstrated at a disused railway tunnel located at Alfreton in Nottinghamshire, UK. This tunnel, known as "Alfreton Old Tunnel" has 3 shafts which are fully open to the surface and so this tunnel served as an ideal demonstrator for this particular application of muon tomography.

Muon sensors, as discussed in section 2.2 above, were deployed in the Alfreton Old Tunnel and a series of readings of the observed muon rate taken at regular 5 metre intervals along the tunnel. The observed muon rate was compared against that expected from prior desk studies using a digital twin of the tunnel. (A full report of the tunnel survey is published in (Thompson et al. 2020).

Figure 2 above shows the results of scanning the entire length of the tunnel at regular 5 metre intervals with 30 minutes of data-taking at each point. The "inferred rate" is that predicted, by the digital twin, to be seen in the muon instrumentation (via computer simulations) assuming the known geology (overburden depth and rock type) for the tunnel. The 3 open shafts (indicated by blue vertical lines) are clearly visible in the data as a highly significant excess of muons compared to that predicted by the digital twin in assuming no shaft (and hence more density and so fewer muons).

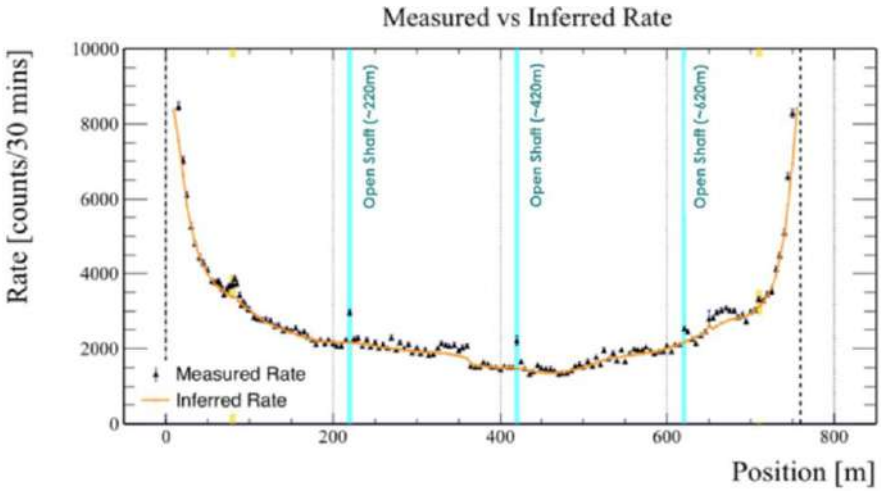

Fig. 3. Observed (points) and predicted (orange line) muon sensor system data observed around known open shaft

Fig. 3 shows a zoom-in of the data around 220 metres from the access portal. In this case the statistical significance of the open shaft observation is extremely high - 11 standard deviations. Figure 2 shows other features visible in the data: the discontinuity at approximately 350 metres was due to a system replacement and is understood, there is also some indication of an elevated muon rate around650-700 metres which may be the result of incorrect modelling of the overburden close to the tunnel portal. A further feature in the data of particular interest however is the deviation in the data around 80 metres, which is magnified in Fig. 4.

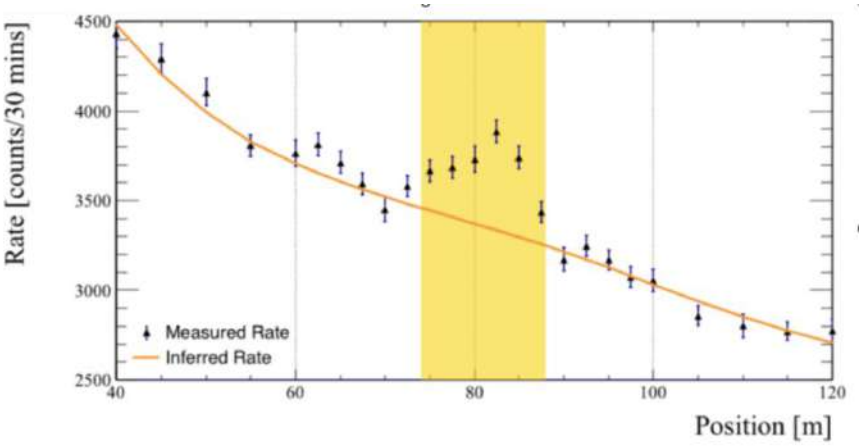

Fig. 4. Data from the suspected hidden shaft region.

The observed muon rate in this region demonstrates features that are indicative of a hidden shaft. Further discussions with the rail operator confirmed that there is a suspected hidden shaft in the area - information that wasn't available prior to the muon tomography survey.

A second stage of the Alfreton Old Tunnel field trial was subsequently carried out which demonstrates a further benefit of the use of muon tomography for this type of interrogation of civil infrastructures such as tunnels, namely that the technique is able to swiftly identify density anomalies of interest and,

if required, can subsequently, with a more detailed survey, return additional characterisation data on the object of interest.

In the case of the Alfreton Old tunnel, the results from this second characterisation phase are included in Figure 5 which indicates that the hidden shaft is centred at the tunnel crown with a diameter of approximately 3.5 metres, the data also indicates that the overburden of the shaft is equivalent to 1 metre of standard density rock (5 metres of rock at 1 standard deviation), which suggests that the feature is highly likely to be a hidden shaft with minimal backfill material.

In addition to the identification and characterisation of features discussed above, muon tomography is also capable of performing longer-term monitoring of a region of interest. This could, for example, identify density changes in a region of interest and correlate them with, e.g. extreme rainfall events, in which case water ingress could be taking place.

2.4. Case study - Data Interpretation Techniques

Prior to any muon survey it is important to develop a complete-as-possible understanding of the geology and overburden that the muons will pass through. In general, such information may be a combination of, e.g., satellite, Lidar and additional topographic data. Where available, surface features such as houses, etc. are included in the "digital twin".

With the digital twin completed it is then necessary to estimate the expected muon flux through a specific sensor deployed at a point under the tunnel overburden. Here standard muon tracking software from the particle physics community is used such as GEANT (Agostinelli et al. 2003, Allison et al. 2006, Allison et al. 2016). Importantly this software samples the expected muon surface flux, as a function of energy. This process is important since high-energy muons are less plentiful but more penetrating.

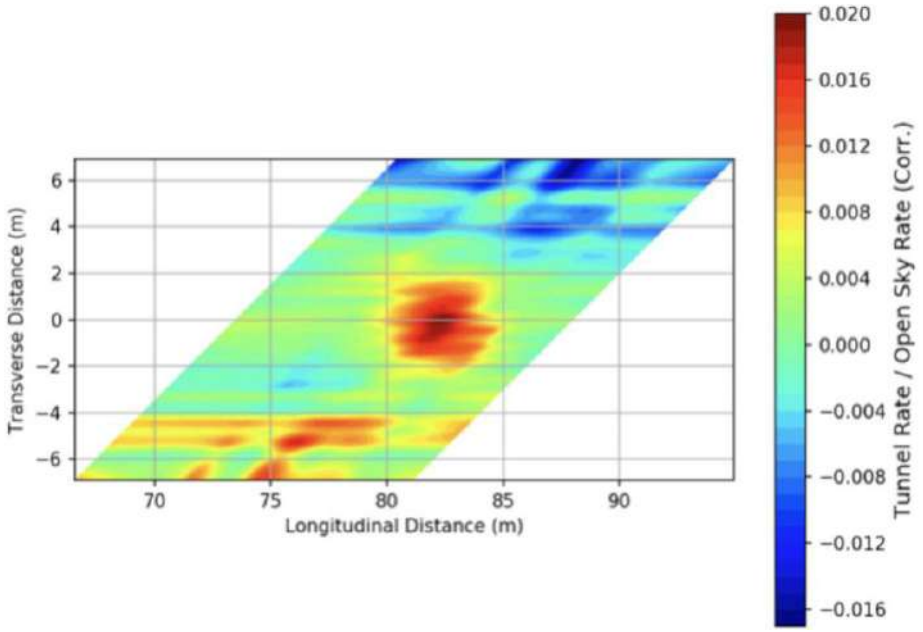

Fig. 5. Visualisation of the hidden void in the Alfreton tunnel.

With the digital twin complete it is then possible to compare the expected muon flux with the empirical data from a muon survey. As mentioned above, at each measurement the muon sensor has a particular

field-of-view (depicted by the red V shapes in Figure 6 below). However, this field-of- view is subdivided enabling computer tomographic techniques to be applied which result in a 2D or 3D visualisation of the density changes, with respect to expectation, in the data.

An example of the 2D tomographic image that can be achieved through this technique is included in Figure 6 (note this is a 2D image of a different tunnel, not the Alfreton tunnel) where orange(red) colouration indicates medium(high) levels of under-density from the muon measurement compared with that expected assuming a solid overburden. In this particular case, evidence for several full-height hidden shafts can be seen.

In general, measurement times are largely dictated by the overburden of the tunnel. In the programme of work carried out in the UK following this initial study, data-taking campaigns have taken place in tunnels varying in depth typically between 30 metres and 80 metres. Given the large area instrumentation used for these surveys measurement times of typically between 10 and 60 minutes per point along the survey are required. The muon-sensitive instrumentation used in particular application is chosen to be compatible with the size of feature to be imaged in the rail tunnel surveys which is typically one the metre-scale. Other instrumentation exists which is capable of imaging down the centimetre scale.

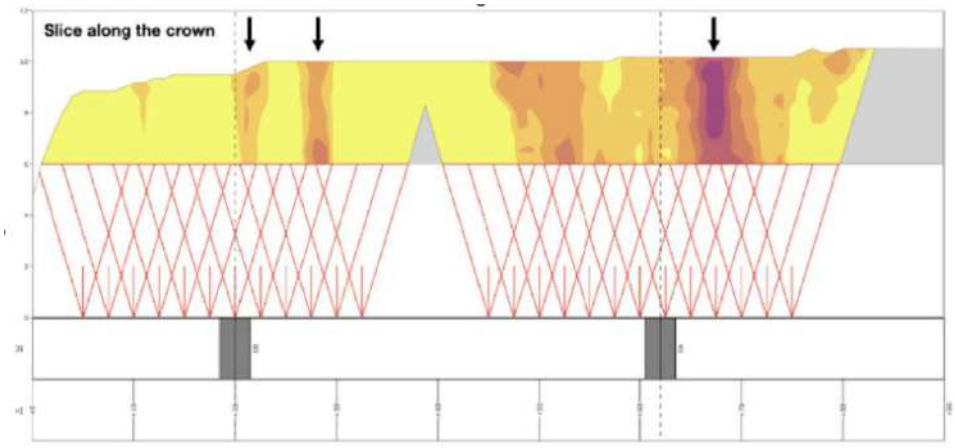

Fig. 6. 2D slice through a 3D tunnel overburden density reconstruction.

Other non-invasive techniques exist however, in the context of tunnel imaging Geoptic has not been party to any direct comparisons with the results delivered by, e.g. Electrical Resistivity Tomography (ERT), seismic or ground penetrating radar (GPR). Of note however is that in 2023 Geoptic completed a programme of work in Norway that measured the density change in the sub-surface as a result of an injection of CO2, in that case both muon instrumented and seismic techniques were co-deployed and both techniques returned the same result (Thompson et al., 2024).

3. Conclusion

This paper outlines the muon tomography technique and details its application to the identification and characterisation of hidden voiding in legacy rail infrastructure, specifically rail tunnels. A scan at 5 metre intervals through the area of interest with typically 30-60 minutes of data-taking per point (depends exactly on the depth of overburden of the tunnel) is sufficient to enable features such as hidden construction shafts and other areas of under-density (e.g. “cut and cover”) to be successfully identified. The programme of work as described above has led to muon tomography being embraced as a standard asset management tool for understanding the condition of Victorian era rail tunnels within the UK (to date around 20 tunnels have undergone scans using muon imaging). As highlighted above,

an important aspect of this technique is the fact that this imaging takes place without any need for contact with the tunnel itself. However, clearly, this technique is not limited to hidden shaft identification and characterisation. Other tunnelling-related applications that are under consideration for muon imaging, for example, include possible geology "look ahead" for tunnel-boring machines, water ingress monitoring (since water ingress changes the density of the object of interest - something that muon imaging is directly sensitive to) and potential sinkhole avoidance by identifying undocumented lower density regions in urban environments. Density changes in other objects such as bridges and viaducts can also be identified - these applications, using smaller format, high resolution muon sensor systems, are currently being trialled.

In conclusion, muon tomography is a powerful non-invasive imaging technique capable of returning detail on density changes in an overburden without the need to make contact with the object of interest. As demonstrated in the case study, the technique is capable of both identifying and characterising otherwise invisible features behind the tunnel lining such as hidden shafts and voids in railway tunnels on the UK's rail network. Of particular note is that this technique has been adopted as a standard tool by tunnel asset managers on the UK's Network Rail infrastructure.

References

Agostinelli, S. et al., 2003. Geant4 - A Simulation Toolkit. *Nucl. Instrum. Meth. A* 506: 250-303

Allison, J. et al., 2016. Recent Developments in Geant4. *Nucl. Instrum. Meth. A* 835: 186-225

Allison, J. et al., 2006. Geant4 Developments and Applications. *IEEE Trans. Nucl. Sci.* 53: 270-278

Gebhart, L, et al., 2023. Muon tomography for detection of dynamic border tunnels. *Nucl. Instrum. Meth. A* 1053, 168383.

George, E.P., 1955. Cosmic Rays Measure Overburden of Tunnel. *Commonwealth Engineer* 42: 455-457

Khaw, K.S. et al., 2025. Non-Invasive Assessment of Sediment Accumulation Using Muography: A Pilot Run at the Shanghai Outer Ring Tunnel., 10.48550/arXiv.2504.00582.

Mao, X, et al., Muon radiography experiments on the subway overburden structure detection, https://arxiv.org/abs/2303.09819

Morishima, K. et al., 2017. Discovery of a big void in Khufu's Pyramid by observation of cosmic-ray muons, *Nature* 552: 386–390

INTERNATIONAL ATOMIC ENERGY AGENCY, 2022. Muon Imaging: Present Status and Emerging Applications. IAEA TECDOC 2012

Thompson, L.F. et al., 2020. Muon tomography for railway tunnel imaging. *Phys. Rev. Research* 2: 023017

Thompson, L. et al., 2024. Muon Tomography - a Novel Imaging Technique for Monitoring the Carbon Capture and Storage Process. *European Association of Geoscientists and Engineers*, 2214-4609, 1-5.

Southeastern Europe Tunnelling Conference (SETC-2025)
1-3 October 2025, Belgrade, Serbia

DOI: 10.5937/SETC25029K

Laser Scanning for Underground Monitoring: Insights from the Copenhagen Metro

Filip Kasapovski[a], Martin Boskovski[b] and Zlatko Zafirovski[c]*

[a] Ss. Cyril and Methodius University in Skopje, Faculty of Civil Engineering, Department of Higher Geodesy, Skopje, North Macedonia; kasapovski@gf.ukim.edu.mk
[b] Master of science in geodesy, Moniterra Group; m.boskovski@live.com
[c] Ss. Cyril and Methodius University in Skopje, Faculty of Civil Engineering, Department of Railways, Skopje, North Macedonia; zafirovski@gf.ukim.edu.mk

Abstract: Ensuring the sustainability and long-term durability of infrastructure depends heavily on how well we can monitor structures over time. Accurate, consistent data on how buildings and underground structures behave is essential for making informed decisions about their maintenance and safety. One of the most effective tools for this purpose is laser scanning. It's a fast, contact-free method that creates detailed 3D models of surfaces by capturing dense point clouds in just minutes. While laser scanning offers clear benefits such as speed, precision, and complete surface coverage it hasn't been widely used in the past. Laser scanning adoption has been limited by high equipment costs, accuracy concerns, and complex data handling. Recent improvements in technology and integration with tools like BIM are beginning to overcome these challenges, making the method more practical for structural monitoring. This paper explores the application of laser scanning and other digital technologies for underground monitoring, focusing on the Copenhagen Metro's M4 extension to Sydhavn and Valby. Monitoring with this methodology involves processing point clouds using a consistent template and grid. Significant changes are identified by variations in the projection cells, making these differences easy to detect. By combining advanced monitoring with sustainable design practices, we can build infrastructure that's not only safer and more durable, but also more in tune with the needs of our environment and future generations.

Keywords: Metro infrastructure; laser scanning; point cloud; underground monitoring

1. Introduction

Underground infrastructure development presents complex engineering challenges, where safety, durability, and environmental responsibility must be carefully balanced. As urban areas continue to grow and demand for public transport increases, expanding metro networks becomes a priority. In such settings, continuous and reliable monitoring of underground structures is essential, not only to identify structural changes and validate design assumptions but also to mitigate potential risks before they escalate into costly or dangerous issues. Among the tools now shaping the future of underground monitoring, Terrestrial Laser Scanning (TLS) has emerged as a leading solution. This technology offers rapid, non-contact data acquisition with high spatial resolution and dense 3D point clouds, changing the monitoring paradigm from sparse, point-based to holistic surface-level observation (Teng et al., 2022). TLS allows engineers to detect and assess subtle deformations and movements in tunnels, station walls, and excavation faces over time, providing the insight needed to make informed, proactive decisions during construction. TLS's effectiveness for geometry validation, excavation profile control and construction management, outperforming traditional surveying in speed and detail (Gikas V., 2012).

A notable example of TLS application is the M4 metro line extension in Copenhagen, which connects the city center to the evolving districts of Sydhavn and Valby. Designed and delivered by TUNN3L JV

*Corresponding author: kasapovski@gf.ukim.edu.mk (F. Kasapovski).

with Arup as a multidisciplinary design partner, the project placed strong emphasis on sustainability, digital innovation, and structural performance. TLS was implemented extensively throughout the project to monitor tunnels and station boxes, generating a continuous flow of spatial data to support design validation and construction management. To interpret and visualize these large point cloud datasets, the project team used the OPSIS software platform for deformation analysis. OPSIS enabled the projection of 3D point clouds onto fitted surface templates and their subdivision into statistical grids. This allowed small deformations to be tracked over multiple time intervals with a high degree of precision. The software generated 2D projection maps, animated surface changes, and time-series graphs helping engineers detect anomalies early and respond effectively.

The Copenhagen Metro case illustrates how combining TLS with powerful data analysis platforms can transform structural monitoring from a passive task into a proactive strategy. This integration not only improved safety and quality during construction, but also supported the long-term sustainability goals of the metro network ensuring that modern infrastructure evolves in step with both urban growth and environmental responsibility.

This paper is structured as follows: Section 2 presents the methodology from data acquisition to software processing; Section 3 presents scanning results for tunnel portals, atrium walls, and V-beams; Section 4 concludes with the effectiveness of TLS-OPSIS integration for structural deformation monitoring.

2. Methodology

The deformation monitoring approach employed during the Copenhagen Metro M4 line extension integrates Terrestrial Laser Scanning (TLS) with advanced point cloud analysis using the OPSIS software platform. This combined methodology enables accurate, non-invasive, and consistent tracking of surface deformations throughout all stages of underground construction. By capturing dense, high-resolution 3D data and systematically assessing changes over time, it allows for early detection of structural shifts and potential issues. This proactive monitoring enhances overall project reliability, reduces risks associated with unexpected deformations, and supports data-driven decision-making. Ultimately, the approach contributes significantly to the sustainable management and long-term durability of underground infrastructure, ensuring safety and resilience in a complex urban environment.

2.1. Data acquisition using TLS (Topcon GLS-2000)

The Topcon GLS-2000 terrestrial laser scanner was used as the primary scanning instrument. (Fig. 1b) Known for its high accuracy and reliability in construction and infrastructure environments, the GLS-2000 captures dense 3D point clouds with millimeter accuracy. Scans were conducted at various stages during construction, capturing the geometry of tunnel portals, station walls, and other structural elements.

All TLS scans were georeferenced using existing polygonal points from the previously developed geodetic control network of the construction site. These control points served as a stable spatial reference base, ensuring that all point cloud datasets from different epochs were precisely aligned and comparable. This approach eliminated the need for artificial markers and significantly improved repeatability across measurements.

2.1.1. Development of the geodetic control network

Before starting the TLS scans, a reliable geodetic control network was established to provide a solid reference framework. High-precision total station Leica TS16 (Fig. 1a) was used to create a polygonal network of control points around and within the construction area. These points were carefully positioned and measured with millimeter-level accuracy to ensure stability throughout the project. This

network enabled precise alignment and comparison of all subsequent scans, which was essential for effective deformation monitoring.

(a) (b)

Fig. 1. Measuring technologies used in the project: (a) Leica TS16 total station for geodetic control network establishment, (b) Topcon GLS-2000 terrestrial laser scanner for detailed 3D data acquisition.

2.1.2. Measurement Error Analysis

To ensure the reliability of TLS data, potential measurement errors were carefully assessed, including instrument limitations, as well as systematic and random errors. The geodetic control network, established with a high-precision Total station, provided accurate orientation and georeferencing for all scans. During scanning, the TLS instrument was oriented using these control points, with each individual scan defined as a "station" with precise coordinates and orientation. This procedure ensured accurate registration of scans and the generation of correctly georeferenced point clouds.

Table 1. Orientation and registration errors of TLS scan stations.

X	Y	Z	Occ.	Inst. Height	BS	Backsight Error X	Backsight Error Y	Backsight Error Z
1000.000	1000.000	2.535	A2	1.535	A3	0.003	0.000	-0.001
981.890	998.652	2.531	A1	1.526	A2	0.000	0.001	0.000
1032.630	999.708	2.543	A4	1.548	A3	0.003	0.000	0.000
1033.229	1012.283	2.584	b4	1.565	A5	0.002	0.001	-0.001

Additional control points, which were not used for registration, were also measured to validate the accuracy of the registered datasets. Comparisons between these points and the registered point clouds confirmed an overall accuracy of approximately ±3 mm.

Table 2. Validation of TLS measurements using Total Station data

Point	X	Y	Z	Error X	Error Y	Error Z
A5	1050.545	1000.000	2.580	0.003	0.000	0.002
B3	1015.432	1011.798	2.632	0.000	0.001	0.003
B2	998.733	1011.628	2.633	0.000	0.002	0.002
B5	1044.344	1016.825	2.550	0.002	0.001	0.002

This methodology allowed true structural displacements to be distinguished from measurement errors, ensuring that deformation monitoring results could be confidently applied to design evaluation and construction decision-making.

2.2. Software processing of point clouds

After data acquisition, the dense 3D point clouds captured by the Topcon GLS-2000 were imported into the OPSIS software platform for detailed analysis. This platform is designed to handle large volumes of spatial data efficiently, allowing for comprehensive processing and interpretation. The monitoring workflow efficiently processes point cloud data by projecting it onto a mathematically defined reference surface, conducting detailed statistical analyses within grid cells, filtering out noise, and producing precise deformation maps and comprehensive reports to support accurate structural evaluation.

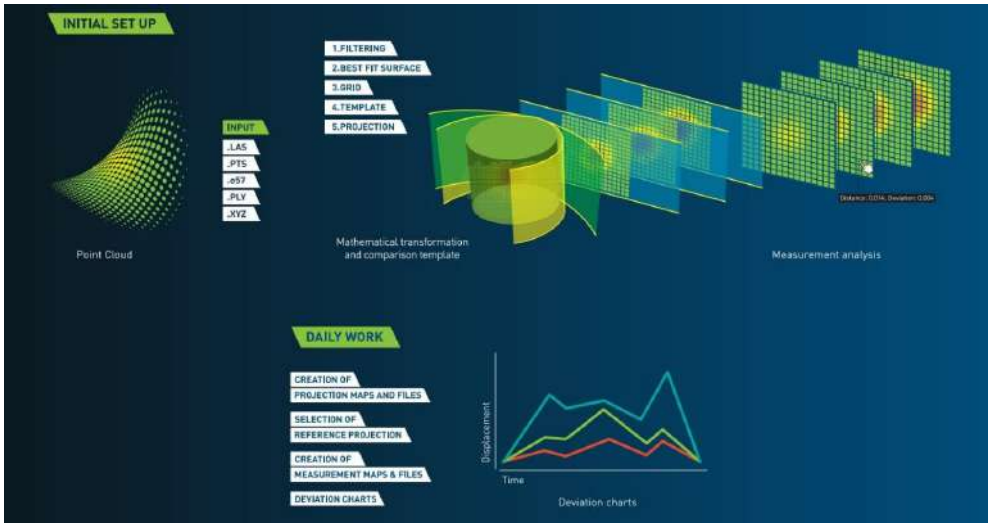

Fig. 2. Workflow and deliverables in OPSIS monitoring procedures.

2.2.1. Projection of point cloud onto reference surface

Once captured, the point clouds were imported into the OPSIS software platform, where a mathematically defined 3D reference surface, called a template was fitted to the geometry of the structure. Depending on the shape of the monitored surface, the template could be a plane, cylinder, or conical surface, similar to those used in standard mathematical projections.

The template was then subdivided into a uniform square grid of user-defined cell size. Within each grid cell, all point distances to the template surface were evaluated statistically. Cells were only accepted if the standard deviation of point distances met quality criteria, ensuring data reliability.

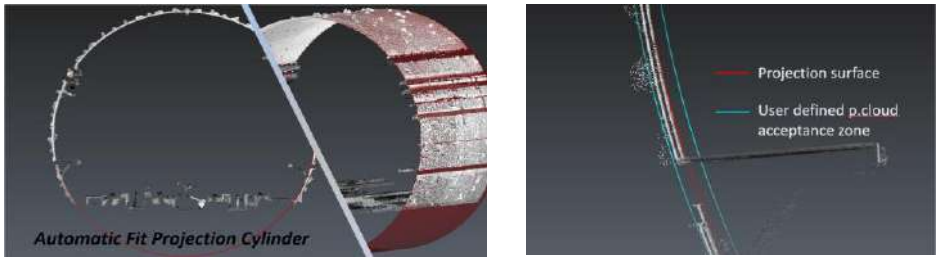

(**a**) (**b**)

Fig. 3. Processing of point clouds: (a) Automatic projection processing, (b) Cleaning unnecessary "Phantoms" during point cloud projection onto a mathematical surface.

2.2.2. Noise filtering and tolerance Control

In OPSIS, noise filtering works by checking how far each scan point is from the fitted template surface. We define a tolerance zone around that surface in our case set to ±5 mm, so that only points inside the zone are kept, while anything outside is treated as an outlier (phantom). The size of the zone is chosen in relation to the scanner's accuracy, usually about 3–5 times the instrument's natural measurement noise. Setting it this way gives a good balance: it removes spurious points without discarding real surface changes. The result is cleaner, more consistent data between scans, which in turn improves the reliability of the deformation measurements.

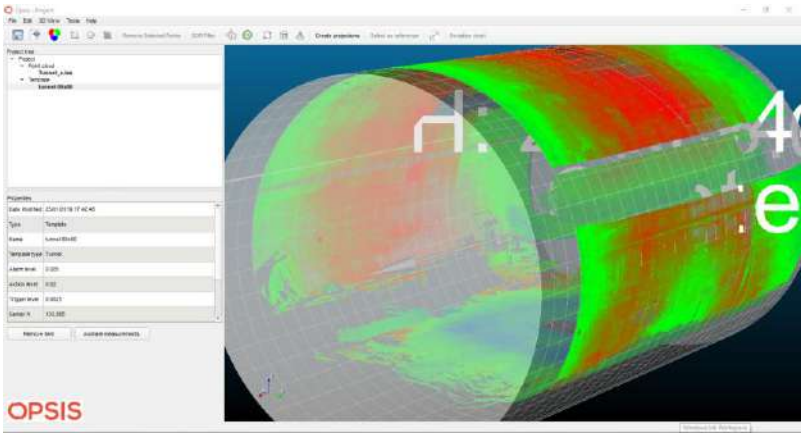

Fig. 4. 3D visualization of tunnel template creation using OPSIS software.

2.2.3. Temporal monitoring and surface deformation visualization

Each new TLS scan, aligned using the same geodetic reference and surface template, was compared with previous datasets to track changes over time. By observing variations in the values of individual grid cells, localized surface deformations could be clearly identified. These changes were visualized through 2D projection maps, animated sequences, and time-series deformation graphs. This intuitive visual output made it easier for engineers to spot early signs of structural movement and respond proactively, improving decision-making and helping to prevent potential issues before they became critical. Additionally, the measured deformations were compared not only with previous scans but also directly against the original design situation, allowing for a clear assessment of how the structure's actual behavior aligned with design expectations and safety thresholds. This comparison ensured that any deviations were identified early and evaluated in the context of acceptable limits, supporting effective risk management throughout the project.

3. Results and Discussion

The implementation of TLS and OPSIS analysis across various segments of the Copenhagen Metro M4 extension provided valuable insights into both the structural performance of underground elements and the broader utility of point cloud data within construction workflows. Beyond its role in deformation monitoring, the high-resolution data proved essential for a range of practical application most notably in generating precise as-built models used for the design and fabrication of prefabricated components. In the constrained and geometrically complex environments typical of underground construction, this level of detail helped ensure dimensional accuracy, minimized on-site adjustments, and improved the overall efficiency and coordination between design, manufacturing, and installation processes.

3.1. Scanning of the tunnel portal

An important application of TLS was the scanning of the tunnel portal, where high-resolution point cloud data served both monitoring and design purposes. Beyond tracking potential deformations, the data enabled precise vectorization of the as-built geometry, forming the basis for accurate digital models. These models were crucial for the design and fabrication of prefabricated components, ensuring that each element matched the real-world conditions of the site. By relying on this detailed and reliable reference, the installation process became more efficient, with fewer adjustments needed on-site. This case underscores the broader utility of TLS technology not only as a tool for structural monitoring but also as a bridge between digital design and efficient, high-quality construction.

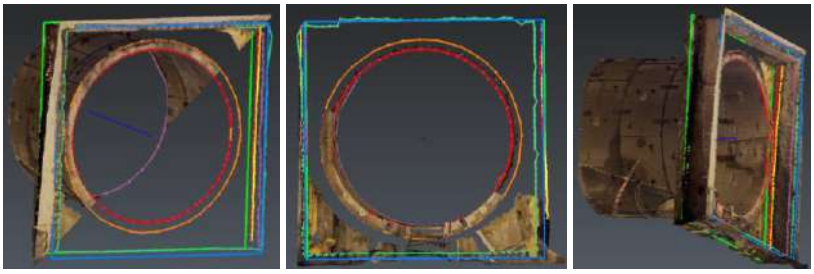

Fig. 5. Point cloud-based vectorization of tunnel opening.

3.2. Scanning of stations atrium walls

The additional scanning of the atrium walls at the metro stations provided highly detailed 3D models that formed the basis for a thorough assessment of their current condition. By comparing the latest laser scan data with the original design models, even the smallest deformations or deviations from the planned geometry could be identified.

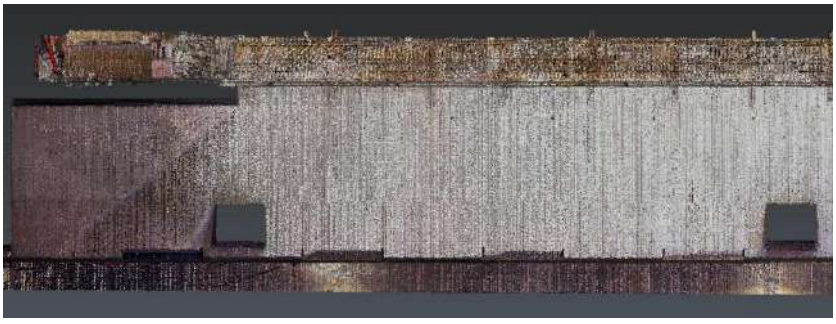

Fig. 6. Detailed point cloud data of a portion of the atrium wall.

This methodical approach not only enhances the accuracy of maintenance planning but also supports predictive modeling to prevent future deterioration, ensuring the long-term safety and functionality of the metro infrastructure.

Fig. 7. Comparison of actual vs. reference geometry of atrium walls, visualized through OPSIS.

For the atrium walls, quantitative deformation metrics were closely integrated into the project's risk management protocols. A 15 mm deformation threshold was established to trigger alarms and guide adjustments in the prefabrication of components. Real-time TLS data were continuously compared with the original design, and any deviations exceeding this limit prompted immediate corrective actions or design modifications. This proactive, data-driven approach ensured that potential structural issues were addressed early, safeguarding both construction quality and overall project safety.

3.3. Scanning of V-beams

As part of the broader structural documentation and quality control process, terrestrial laser scanning (TLS) was applied to capture the geometry of prefabricated V-beams used in the station construction. The high-resolution point cloud data enabled accurate verification of the beams' as-built dimensions against the design models. This was particularly important for ensuring proper alignment and fit during installation, minimizing the need for adjustments on site.

Working with TLS and OPSIS came with its own set of challenges. One significant limitation was access to complex and constrained spaces, such as areas with scaffolding, high walls, or narrow corridors. Scanning difficult or tall areas, such as the 12 m-high atrium walls, required multiple setups and repeated scans to capture everything accurately. Reflective surfaces, aligning scans, and managing large amounts of data added further complexity. These challenges were overcome through careful planning, repeated measurements, and detailed post-processing.

4. Conclusion

The application of Terrestrial Laser Scanning (TLS) combined with the OPSIS software platform demonstrated a highly effective approach for monitoring structural deformations throughout the Copenhagen Metro M4 extension project. This method enabled precise, non-invasive tracking of changes in critical infrastructure elements, allowing early detection of localized movements and supporting timely, informed decisions during construction. Beyond monitoring, the rich point cloud data served multiple purposes supporting the accurate fabrication and installation of components like

tunnel portals, atrium walls, and prefabricated V-beams. By reducing the need for on-site adjustments and rework, the workflow enhanced construction efficiency and accuracy. The experience highlights how integrating advanced scanning technologies with intelligent software tools can strengthen structural reliability and sustainability in complex underground projects, setting a strong example for future infrastructure development.

References

Afrazi, M., Jahed Armaghani, D., Afrazi, H., Fattahi, H., Samui, P., 2025. Real-time monitoring of tunnel structures using digital twin and artificial intelligence: a short overview. *Deep Undergr Sci Eng.*,1-16. https://doi.org/10.1002/dug2.70029

Arup – Copenhagen M4 Metro Line to Sydhavn and Valby. Available online: https://www.arup.com/projects/copenhagen-m4-metro-line-to-sydhavn-and-valby/ (accessed in 2025).

Boskovski, M., 2023. Application of laser scanners in the reconstruction of cultural heritage objects, Master thesis. University of Ss. Cyril and Methodius in Skopje, Faculty of Civil Engineering, Skopje, North Macedonia.

Gikas, V., 2012. Three-dimensional laser scanning for geometry documentation and construction management of highway tunnels during excavation. *Sensors*, 12(8), 11249–11270. https://doi.org/10.3390/s120811249

Jia, D., Zhang, W., Liu, Y., 2021. Systematic Approach for Tunnel Deformation Monitoring with Terrestrial Laser Scanning. *Remote Sensing*, 13(17), 3519. https://doi.org/10.3390/rs13173519

OPSIS – Every Point Matters. Available online: https://www.opsis-scan.com/ (accessed in 2025).

Teng, J., Shi, Y., Wang, H., Wu, J., 2022. Review on the Research and Applications of TLS in Ground Surface and Constructions Deformation Monitoring. *Sensors*, 22(23), 9179. https://doi.org/10.3390/s22239179

Topcon GLS-2000. Available online: https://mytopcon.topconpositioning.com/support/products/gls-2000 (accessed in 2025).

Southeastern Europe Tunnelling Conference (SETC-2025)
1-3 October 2025, Belgrade, Serbia

DOI: 10.5937/SETC25030D

Assessment of vibrations induced by the blast during mining operations in the tunnel "Iriški Venac"

Dejan Dragojević[a], Željko Zugić[b], Milan Uljarević[c]*

[a] SK Engineering, Serbia; dragojevic.dejan@yahoo.com
[b] Power Construction Corporation of China Limited, Ogranak Beograd; zeljko.zugic@powerchina-intl.eu
[c] CRBC Serbia, Novi Sad, Serbia; umilan89@gmail.com

Abstract: This paper presents results of the vibration measurements on the surface of the terrain above the tunnel "Iriški Venac" induced by the blast during mining operations in the tunnel. The vibrations were measured on the terrain surface approximately 180m above the tunnel blast spots in the immediate vicinity of the small settlement. The main goal of the study was to estimate possible impact of vibrations on the structures of existing buildings and to provide material evidence of true levels of amplitudes of vibrations in case of possible legal dispute. Maximum measured peak particle velocities were 1mm/s and 1.25mm/s. The estimation of vibration on structures was performed according to standard DIN 4150-3, by the comparison of measured velocities with threshold values in the standard. The key findings are that the measured velocities were well below the threshold values that could cause any harm to existing buildings.

Keywords: vibration measurement; tunnel; blasting impact; ground vibration; vibration standards

1. Introduction

Vibrations that cause harm to buildings are mechanical oscillations of solid bodies that have the potential to cause discomfort to persons or damage to structures. The purpose of vibration measurements during the mining operations that include explosions in the process of breaking of solid rock can be, among others, to estimate possible impact of induced vibrations on existing buildings, or that could cause discomfort to occupants.

The effects of ground vibrations include damage to buildings structure, such as fatigue damage like cracking and breakage, damage to buildings contents, disturbance to human comfort, and audible effects such as structure-borne noise and secondary rattling of building elements or contents.

Several studies have addressed this problem, for instance (K.M. Norén-Cosgriff et al., 2020) focuses on effects of test blast on new buildings that were constructed and monitored for the purpose of study. Test blasts were designed to produce increasing vibration values, starting with peak particle velocities (PPVs) around 20 mm/s and ending with PPVs above 250 mm/s. No visible cracks were found on any of the two buildings. However, the last blast, which produced PPVs above 260 mm/s, resulted in a residual displacement of 0.05 mm across the 110 mm strain gage length above the door of the concrete building. The results of the test indicate that the limit values of most national standards include a large safety margin for buildings founded on rock.

P.K. Singh et al., 2010 addressed the effect of blast produced ground vibration on damage potential to residential structures to determine safe levels of ground vibration for the residential structures and other buildings in mining areas. For that purpose, impacts of 341 blasts detonated at two mines were monitored at the test structures and 1871 blast vibrations signatures were recorded on or near the test

*Corresponding author: dragojevic.dejan@yahoo.com

structures. The study found that at peak particle velocities of ~51.6 – 56.3 mm/s cosmetic cracks appeared.

In the study Zhang et al. 2022, focused on the effect of a blasting vibration from an excavating tunnel on an adjacent excavated tunnel. The important conclusion from this study is that the attenuation of the vibration waves caused by blast varied in different regions, and particle velocities in the region along the excavating direction were 1.12 to 1.79 times larger than in the region opposite to the excavating direction.

In the paper Zhou et al., 2024 authors dealt with comparison of overbreak and underbreak value with the traditional method to determine the degree of overbreak and underbreak. It also provided useful insights into the instrumentation for the monitoring of the blasts .

In this study, the impact of the measured vibrations on the structures was estimated according to the DIN 4150-3 standard (DIN 4150-3).

For the purpose of estimating the aforementioned effects of vibrations on buildings and occupants, the vibration measurements took place during the mining operations in the tunnel “Iriški Venac”. The aim of the measurements was to estimate possible impact of induced vibrations on the existing buildings above the tunnel. The existing buildings are located somewhat 180 m directly above the tunnel and the place of blast during mining operations and consist of small settlement of one to two storey buildings. The vibrations were measured on the terrain surface i.e. - “free field” measurements took place in the immediate vicinity of existing buildings. In total two measurements were recorded when the mining operations took place approximately directly below the settlements, that were estimated to be the events that could cause largest amplitudes of vibrations on the buildings.

The significance of such measurements besides estimating the potential damage to structures and excess of certain threshold of vibrations on occupants is to acquire material evidence of vibrations in case of potential court proceedings. Thus, such measurements present cost - effective way either to prevent such cases or to obtain material evidence of true levels of amplitudes of vibrations in case of possible dispute. The results of this study showed that no negative effects on buildings should be expected.

2. Methodology

Measurements took place in the late February and early March of 2025. In total two measurements were taken on the soil surface in the immediate vicinity of buildings (Fig. 1). The surface soil layer covered with vegetation was excavated, and the instrument was placed on the natural ground below the surface vegetation layer. Both measurement locations are very close to each other so that the results of the different recordings could be comparable. The measurements took place during the favourable weather conditions without wind, rain or other meteorological impact that could increase ambient noise. Also, during the recording there were no traffic inside the settlement, and the nearest public road with low traffic is located 70m from the recording location.

Fig. 1 shows the locations of the measurement with excavated surface layer of soil. In the background of the measurement locations, the typical building types of the small settlement can be seen. It is noticeable that the buildings are predominantly consistent of ground floor buildings.

The sensor were placed on ground surface in the middle of the small settlement in order to possibly cover the most relevant ground surface vibration quantities for the whole settlement. In this particular case, the possibility of placing instrument inside the buildings was excluded due to property limitations. However, that would possibly limit the measured quantities for the particular building, since the measured signal could be affected by the building foundation system, floor coverage etc. In that case the recorded signal could even be possibly attenuated compared to the free field measurement.

Since the majority of the buildings in the settlement were ground floor buildings, no significant amplification of the recorded signal is expected due to modal response of building.

(**a**) (**b**)

Fig. 1. (a) Location of the instrument during the first measurement (b) Location of the instrument during the second measurement.

Longitudinal section of the tunnel with the measurement location marked with arrow is presented on the Fig. 2. The blast position is approximately directly below the measurement location. There is approximately 180m meters between the blast location and the measurement location.

The material surrounding the tunnel on the spot of the blast located below the measurement location consist of mechanically less damaged serpentinite, with silicified and carbonated serpentinite - listwanite. As it can be seen from the Fig. 2, this part of the material where the blast took place is the new section of the tunnel material that extends on the previous larger sections consisted of cretaceous flysch consist of claystones with interlayers of siltstones. Claystones are laminated to thin plated, with noticeable shearing marks on laminas, and easily splits. Siltstones are thin bedded, hard and compact, grey to light grey in colour. Bedded sandstones are brittle, and they are subordinately represented in rock mass with about 10% share. Flysch sediments are folded, with frequent fractures.

As it can be noticed from the Fig. 2, the material of the tunnel is non-homogenous along the length of the tunnel.

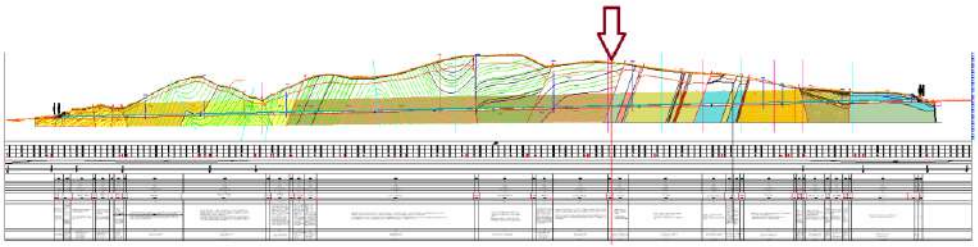

Fig. 2. Longitudinal section of the tunnel with the measurement location marked with arrow. The blast position is approximately directly below the measurement location.

Layout of the tunnel on the background satellite map is presented on the Fig. 3, together with the marked measurement location with arrow. The public road is located north and west from the measurement location.

Fig. 3. Layout of the tunnel on the background satellite map. Measurement location is marked with arrow.

The measurement included two three-component sensors for direct measurement of velocity and accelerations. The components are oriented in three orthogonal directions (NS-EW and Z) and the NS component is placed according to the magnetic north.

The measurement was performed by a new and factory calibrated sensor with low self-noise. The lowest recordable quantities are 0.00003051804 mm/s for velocity and 0.06866560000 mm/s^2 for acceleration. The maximum acceleration measurement range is ±2g. The sampling rate was set to 512 Hz.

For the measurement of velocity, two separate modes were used – both high-gain and low-gain range was used, which included the record of the lowest and highest possible measurement values, and in addition, acceleration was measured. Therefore, a record of velocity was made on six channels (three channels each for high and low gain), and three channels for measuring acceleration, which makes a total of nine channels of measured quantities.

The first measurement was performed over a duration of 32 minutes and 24 seconds in order to record the ambient noise besides the event itself. The second measurement lasted 5 minutes and 48 seconds and was focused solely on the effects of the blast.

For the purpose of evaluating the effects of measured vibration on structures, the provisions of standard DIN 4150-3 were used. The DIN 4150-3 standard sets different guidelines for vibration velocities depending on the three building types and frequency ranges which are divided into three groups. The frequency ranges are divided into groups ranging from 1 Hz to 10 Hz, from 10 Hz to 50 Hz, and from 50 Hz to 100 Hz. Building are categorized into three types: type 1 - commercial and industrial, type 2 - residential and type 3 – sensitive buildings. For commercial and industrial buildings, the limits range from 20 mm/s up to 50 mm/s depending on the frequency range, while for residential buildings, the limits range from 5 mm/s up to 20 mm/s. For buildings sensitive to vibration that have great intrinsic value, the limits range from 3 mm/s up to 10 mm/s depending on the frequency range.

The standard also divides vibrations into short-term and long-term vibrations, where short-term vibrations do not occur frequently enough to cause fatigue and do not cause resonance in the assessed structures, while long-term vibrations are all vibration types that cannot be classified as short-term vibrations. Above mentioned values and thresholds correspond to the criteria in the standard that are corresponding to the short-term vibrations.

3. Results

The traces of all recorded signals are shown in the Fig 4. At the beginning and at the end of the record, noise caused by the distancing from the sensor and approaching to the sensor was observed. From the signal trace itself it can noticed that the amplitudes of motions caused by the blast are approximately on the level of the noise of human steps of approaching the instrument and distancing from the instrument. Distancing from the instrument during the recording of the blast event is estimated to be

minimum 30 meters to minimize any possible impact of human noise on the recordings. The blast recording itself can be seen on the signal trace, as well as the fact that at the moment of the explosion there were no artificially induced vibrations nearby the instrument that could compromise the recording.

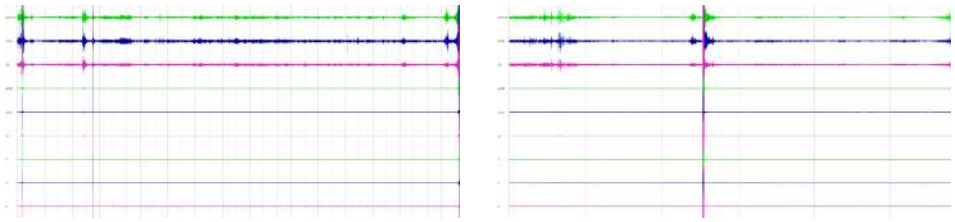

(a) **(b)**

Fig. 4. (a) Signal trace of the first measurement (b) Signal trace of the second measurement.

Maximum observed measured quantities are presented in the Table 1.

Table 1. Maximum observed measured quantities.

Measurement No	Component	Max. velocity [mm/s]	Max. acceleration [mg]
1	NS	1.03	-45.66
	EW	1.25	-71.82
	Z	0.74	40.71
2	NS	-1.01	26.99
	EW	-1.03	39.21
	Z	0.78	28.98

In both measurements maximum values of recorded velocity is approximately 1 mm/s with 1.25 mm/s in first measurement as the largest value on the EW component. On this component the maximum acceleration of 71.8 mg is recorded which is the largest value among all recorded accelerations.

For the first measurement, the part of the signal traces with the blast are shown on the Fig. 5 (a) together with the accompanying spectral diagrams (b).

The frequency content of the signal on horizontal components is majority in the range of frequencies between 20 Hz and 90 Hz. Z component has some spectral accelerations above 100 Hz, while on the horizontal components these spectral accelerations are negligible.

EW and Z component have distinguished one peak around 60 Hz, while the NS component has broader zone of spectral amplifications ranging from 20 Hz to 90 Hz.

For the purpose of evaluating the velocity values according to the DIN 4150-3 standard, the threshold of 1mm /s is set having in mind the largest recorded values, in order to separate epochs in which these vibration levels exist, together with the accompanying frequency content. The results are presented on the Fig. 6 for the NS component (a), and EW component (b).

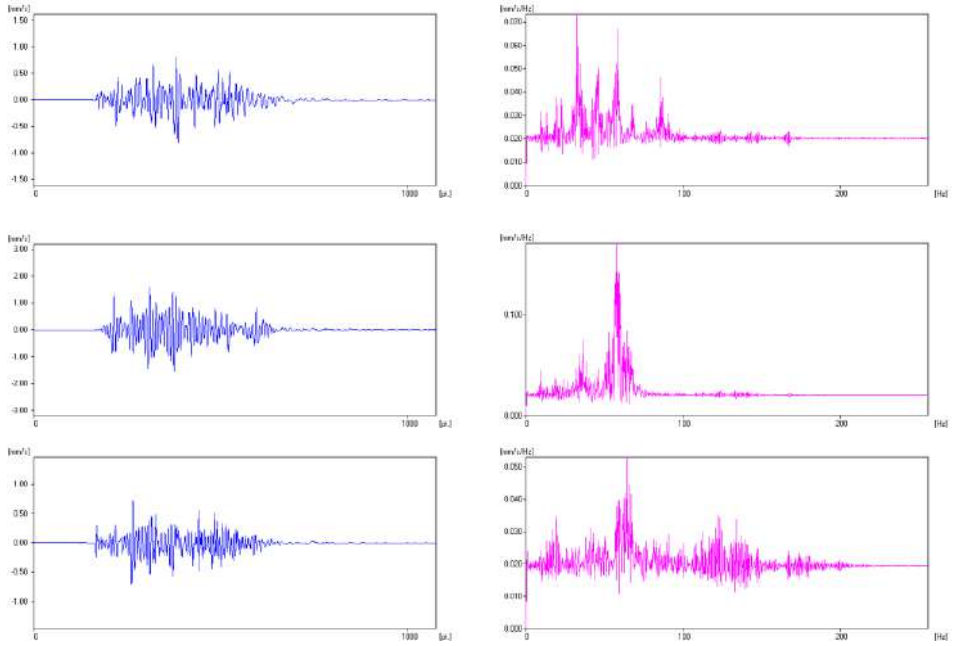

(a) (b)

Fig. 5. (a) Traces of the part of the signal with the blast of the first measurement with NS, EW and Z component going from top to the bottom of the figure (b) Corresponding spectral diagrams of the NS, EW and Z component going from top to the bottom of the figure.

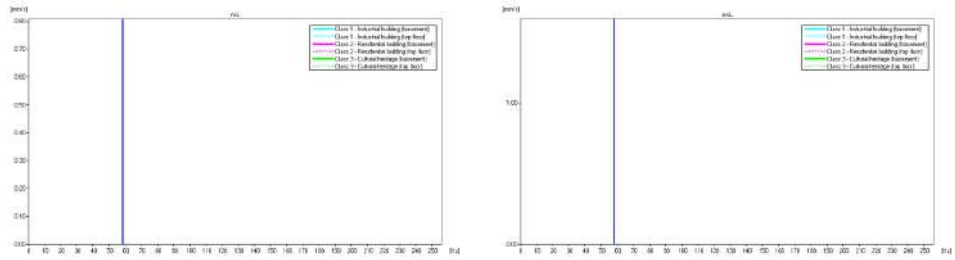

(a) (b)

Fig. 6. (a) separated epoch above the threshold of 1 mm/s on the NS component for the first measurement (b) separated epoch above the threshold of 1 mm/s on the EW component for the first measurement.

The frequency content of the threshold is approximately 60 Hz which makes use for the comparison of the threshold values with the values defined by the standard DIN 4150-3.

For the second measurement the same procedure is applied and the results of the measurements according to the same principle are presented on the Fig. 7 and Fig. 8.

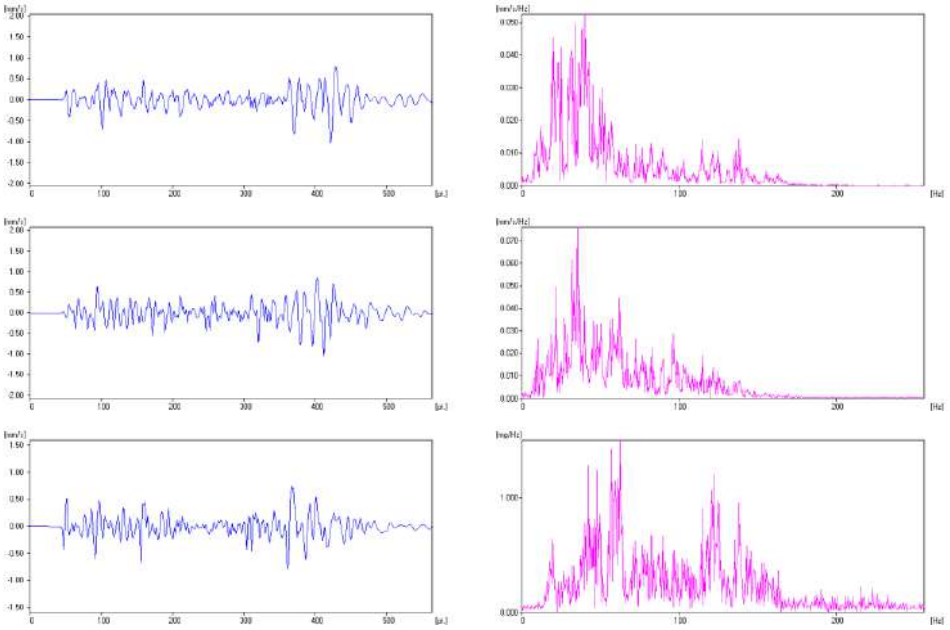

(a) (b)

Fig. 7. (a) Traces of the part of the signal with the blast of the second measurement with NS, EW and Z component going from top to the bottom of the figure (b) Corresponding spectral diagrams of the NS, EW and Z component going from top to the bottom of the figure.

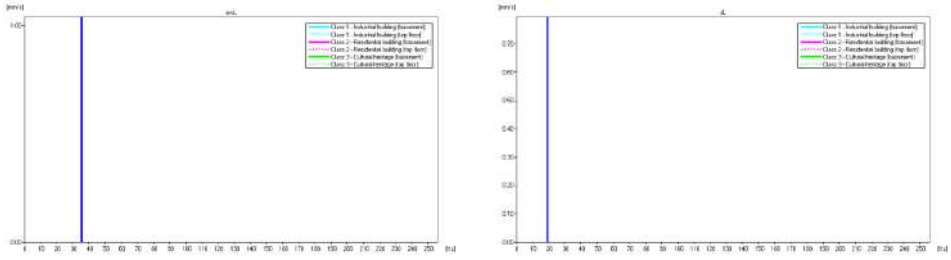

(a) (b)

Fig. 8. (a) separated epoch above the threshold of 1 mm/s on the NS component for the second measurement (b) separated epoch above the threshold of 1 mm/s on the EW component for the second measurement.

On the Fig. 7 the part of the signal traces with the blast are shown (a), together with the accompanying spectral diagrams (b) for the second measurement. The spectral characteristics of this blast is somewhat different that the first measurement. On the horizontal components, the frequency content is lower that the first measurement and the most spectral energy is concentrated in the zone up to 50 Hz. For Z component there is again higher frequency content above 100 Hz, up to 150 Hz, while on the horizontal components this spectral content is not significant.

For the purpose of evaluating the velocity values according to the DIN 4150-3 standard, the threshold of 1mm /s is set having in mind the largest recorded values, in order to separate epochs in which these

vibration levels exist, together with the accompanying frequency content. The results are presented on the Fig. 8 for the NS component (a), and EW component (b). The frequency content of the threshold is approximately 35 Hz for NS component, and 19 Hz for EW component, which makes use for the comparison of the threshold values with the values defined by the standard DIN 4150-3.

For both measurements, the maximum-recorded values are well below the threshold values even for lowest frequency range of 1 Hz to 10 Hz. For the first measurement, the recorded maximum values in corresponding frequency ranges according to Fig. 6 are 12 times lower than the threshold value for residential buildings and 6 times lower for sensitive buildings. For the second measurement, the recorded maximum values in corresponding frequency ranges according to Fig. 8 are 5 times lower than the threshold value for residential buildings and 3 times lower for sensitive buildings.

The measurement results indicate that the recorded values of vibrations caused by the blasts are well below the threshold values defined by the standard DIN 4150-3 and according to the standard's criteria could not pose any damage to structures on the location of interest.

4. Conclusion

Vibrations caused by explosions during the construction of the tunnel "Iriški venac" were measured in order to estimate possible impact of induced vibrations on the existing structures located above the tunnel. In total two measurements of ground surface vibrations above the tunnel were performed. Measurements of velocity and acceleration were carried out in two independent blasts (February and March 2025).

The measured maximum velocity values were compared with the velocity values according to the standard DIN 4150-3 Vibrations in buildings – Effects on structures, which relates to the effects of vibrations on structures. It was determined that all measured values are less than the values specified in the standard, and that the vibrations caused by the mining operations could not cause any structural damage, not could pose detrimental effect on people in the buildings.

The limitations of the study is that the effects of blast was measured only in two occasions. Although these measurements were performed when the blast location was closest to the site, a more extensive study would be advisable in order to include directivity effects of the blast (Zhang et al. 2022), as well as to address the attenuation of waves in different directions and distances. For this purpose, long-term measurements would be most suitable with sensor settings on more locations. Furthermore, the sensors could be placed in buildings as well.

Since in the particular case the measured values of velocities were well below the damage threshold specified by DIN 4150-3, the recorded vibrations can be considered acceptable. Based on the performed analysis, the velocity values induced by the blast during mining operations were below the permissible levels by the order of several magnitudes.

References

DIN 4150-3:2016-12 Vibrations in buildings - Part 3: Effects on structures, https://dx.doi.org/10.31030/2579353

Norén-Cosgriff, K.M., Ramstad, N., Neby, A., Madshus, C., 2020. Building damage due to vibration from rock blasting. *Soil Dynamics and Earthquake Engineering*, Volume 138, 106331, ISSN 0267-7261. https://doi.org/10.1016/j.soildyn.2020.106331.

Singh, P.K., Roy, M.P., 2010. Damage to surface structures due to blast vibration. *International Journal of Rock Mechanics and Mining Sciences*, Volume 47, Issue 6, Pages 949-961, ISSN 1365-1609. https://doi.org/10.1016/j.ijrmms.2010.06.010.

Zhang, Q., Zhang, Z., Wu, C., Yang, J., Wang, Z., 2022. Characteristics of Vibration Waves Measured in Concrete Lining of Excavated Tunnel during Blasting in Adjacent Tunnel. *Coatings*, 12(7), 954. https://doi.org/10.3390/coatings12070954.

Zhou, J., Gao, S., Luo, P., Fan, J., & Zhao, C. (2024). Optimization of Blasting Parameters Considering Both Vibration Reduction and Profile Control: A Case Study in a Mountain Hard Rock Tunnel. *Buildings*, 14(5), 1421. https://doi.org/10.3390/buildings14051421.

Southeastern Europe Tunnelling Conference (SETC-2025)
1-3 October 2025, Belgrade, Serbia

DOI: 10.5937/SETC25031S

Rehabilitation of the Pressurized Hydraulic Tunnel: A Case Study of the Pumped-Storage Hydropower Plant "Bajina Bašta"

Dušan Stevanović[a], Miloš Dumić[a], Uroš Mirković[a], Slobodan Radovanović[a], Vladimir Danilović[b]*

[a] Jaroslav Černi Water Institute, Civil Engineering Department, Belgrade, Serbia; dusan.stevanovic@jcerni.rs, milos.dumic@jcerni.rs, uros.mirkovic@jcerni.rs, slobodan.radovanovic@jcerni.rs
[b] Joint stock company Elektroprivreda Srbije, Branch Drinsko - Limske HPPs, Serbia; vladimir.r.danilovic@eps.rs

Abstract: The "Bajina Bašta" pumped-storage hydropower plant was commissioned in September 1982. The facility is located in the Drina River valley, immediately downstream from the existing Bajina Bašta hydropower plant dam, whose reservoir serves as the lower basin. The "Beli Rzav" pumped reservoir, located in the valley of the river of the same name in the Zaovine region, functions as the upper basin.

In addition to the upper and lower reservoirs, the power plant complex comprises a powerhouse and a headrace–tailrace system, which consists of several interconnected components: upper and lower intake/outlet structures, the headrace–tailrace tunnel, the tunnel bifurcation, a surge shaft, an inclined penstock, and a horizontal penstock with a bifurcation.

Based on the monitoring and maintenance performed during the operational period of the tunnel, as well as on the condition of the structure observed in 2005, the scope of rehabilitation works was defined.

This paper initially presents a description of the facility and its condition immediately prior to the rehabilitation, with particular emphasis on the hydraulic tunnel. The core focus is on the presentation of the rehabilitation technology and execution, which involved pressure grouting, the installation of prestressed rock anchors and chemical grouting. The paper discusses the results and challenges encountered during the rehabilitation process, offering a critical analysis aimed at emphasizing the significance of rehabilitation works and encouraging the exchange of experience in the restoration of capital infrastructure with extended service life.

Keywords: hydraulic tunnel; concrete lining rehabilitation; grouting; "Bajina Bašta" hydropower plant; pumped-storage hydropower plan; case study

1. Introduction

The Bajina Bašta pumped-storage hydropower plant was commissioned in September 1982. The facility is located between the "Perućac" reservoir, created by damming the Drina River, and the upper pumping reservoir "Beli Rzav," situated in the valley of the river bearing the same name, in the Zaovine region. In addition to these reservoirs, the PSHPP Bajina Bašta includes the powerhouse and a complex water conveyance system. This system consists of several key structures: the upper and lower intake/outlet structures, a bifurcation with associated components, a surge shaft, an inclined penstock, and a headrace/tailrace tunnel. Under operational conditions, the PSHPP Bajina Bašta enables efficient utilization of hydraulic energy for electricity generation (Radovanović et al., 2022).

According to the literature Savić (2009) and Zabuski (2019) hydrotechnical tunnels are generally categorized as either pressurized tunnels or free-surface (non-pressurized) tunnels. Pressurized tunnels, which enable water intake regardless of the reservoir water level, are the most common solution for hydropower intake systems (Savić, 2009). These tunnels may be a part of complex hydroelectric systems – as is the case in this facility – but can also be integral components of large industrial plants

*Corresponding author: milos.dumic@jcerni.rs

or irrigation networks. Regardless of their operational context, after decades of use, such tunnels require well-defined and properly implemented rehabilitation projects, based on detailed investigations and inspections (Krukovskyi et al., 2024).

(a)

(b) **(c)**

Fig.1. (a) Map of Serbia showing the River Drina and the position of the PSHPP Bajina Bašta (Radovanović et al., 2022), (b), (c) Hydrotechnical Tunnel of the Reversible Hydroelectric Power Plant "Bajina Bašta".

The importance of inspection planning as a key aspect of tunnel maintenance has been emphasized in the study by Ai et al. (2020), which also outlines the influence of inspection frequency on both total maintenance costs and the risk of structural failure over the service life of the tunnel. The paper highlights the limitations of traditional periodic inspection regimes and proposes degradation modes (accelerated, decelerated, and stationary). These modes are intended to both describe structural deterioration trends and serve as reference models for the planning of tunnel inspection strategies on real-world projects. In the study by Strauss et al. (2020), an overview is provided of various inspection methods and the classification of monitoring strategies and tools, with a focus on both international

technical literature and contemporary engineering practice in Austria. Current research trends emphasize a shift toward automation and 3D reconstruction, as opposed to manual tunnel inspections and conventional data management approaches (Sanfilippo et al., 2025). Technologies such as point cloud data (PCD) and advanced modeling techniques have significantly improved tunnel inspection and model generation processes (Machado et al., 2025).

In discussing recent innovations in visual inspection methods, it is essential to highlight the trend described by Montero et al., (2015) regarding the application of robotic technologies in tunnel inspection. Hazards encountered during tunnel lining mapping and construction work – including dust, poor lighting, and, in some cases, exposure to toxic substances – underscore the necessity for automation in tunnel inspection processes (Montero et al., 2015). Further contributions from the literature (Attard et al., 2018) focus on capturing the tunnel environment conditions using photogrammetry, computer vision, and image processing techniques.

A detailed description of pressure grouting applied in pressurized hydrotechnical tunnels is provided in Anđelković et al. (2013). The same study presents an experimental method for measuring water leakage along the entire length of the tunnel. This leakage measurement was also conducted during the most recent tunnel rehabilitation campaign. In this paper, we present only the results recorded following tunnel dewatering – i.e., at the beginning of the rehabilitation works – and after the completion of the remedial interventions.

The tunnel in question has a circular cross-section with a diameter of 6.30 meters. Its total length is 8030 meters, with a longitudinal slope of 4.5‰. This tunnel belongs to the category of pressurized hydrotechnical tunnels, in which, under operational conditions, a maximum hydrostatic pressure of 1.3 MPa occurs (Ai et al., 2020).

(a) **(b)**

Fig. 2. (a) Longitudinal tunnel profile with a schematic view of the upper lake, pipeline, PSHPP and HPP "Bajina Bašta", (b) Cross-section of tunnel (Radovanović et al., 2022).

2. Tunnel Rehabilitation – Technologies and Construction Techniques

The repair works on the hydrotechnical tunnel were executed in accordance with the rehabilitation project, developed based on observations, previous maintenance activities on the headrace–tailrace tunnel (HTT), and experience gained during the last rehabilitation conducted in 2005, as well as from monitoring of the HTT throughout the subsequent years of operation. Selection of intervention zones was based on visual inspections and testing of the HTT, aiming to identify sections with moderately to severely cracked concrete lining. Under operational conditions, such locations represent a potential risk of significant water seepage, which could in turn affect the structural stability of the tunnel lining.

Due to the scale and complexity of the planned activities, the rehabilitation works were carried out across four designated work zones:

1. Work Zone 1 included the access tunnel leading to the bifurcation, and the HTT section from chainage 0+010 to 0+600.
2. Work Zone 2 covered the lower surge chamber areas, including parts of the shaft body and the tunnel crown (kalotte).
3. Work Zone 3 encompassed the main HTT section from chainage 0+600 to 7+000.
4. Work Zone 4 involved the final kilometer of the tunnel, located directly adjacent to the "Beli Rzav" pumping reservoir (HTT section from chainage 7+000 to 8+000).

2.1. Scope of Rehabilitation Works Defined in the Project Documentation

2.1.1 Inspection of the Headrace–Tailrace System of the PSHPP "Bajina Bašta" During the Reconstruction Phase

During the reconstruction of the headrace–tailrace system (HTT), the following investigations were carried out: Visual inspection of the hydrotechnical tunnel, surge shaft, and inclined penstock, Chemical and physico-chemical testing of water and sediment in the tunnel, Terrestrial laser scanning (TLS) of the concrete lining in both the tunnel and the surge shaft, Geophysical surveys using ground-penetrating radar (GPR) and electrical resistivity imaging (ERI). In accordance with the Updated Technical Monitoring Project, the existing monitoring system was revitalized by replacing damaged and malfunctioning instruments, expanding the system with new, primarily electronic, instruments, and automating the data acquisition process through their integration into an automatic data logging and archiving system.

The updated system includes the following types of monitoring: Mechanical displacement measurements along neotectonic faults, Telemetric temperature monitoring of water and concrete in the surge shaft, Telemetric monitoring of hydrostatic pressure exerted on the tunnel lining, Telemetric monitoring of displacements along cracks and joints in the tunnel, Telemetric piezometric readings in the access tunnel and gate shaft.

Following dewatering of the tunnel, the initial activity conducted in the hydrotechnical tunnel was a visual inspection, which, as similarly described in Krukovskyi et al., (2024), included the prepartion of graphical documentation for mapping cracks in the concrete lining. The main objective of the visual inspection was to either confirm or adjust the proposed rehabilitation design, in case certain areas – originally not included in the project – were found to be in a critical condition. As part of project implementation, two visual inspections were performed: the first prior to the commencement of reconstruction works, the second upon completion of all works, to assess the effectiveness of the interventions with respect to the project specifications.

Fig. 3. Visual Inspection – Mapping of Changes in Concrete Lining.

The visual inspection of the surge shaft, unlike the tunnel inspection, required the application of speleological industrial alpinist techniques. The process was carried out in several phases, beginning with a trial descent, which involved the inspection and technical outfitting of the structure. In the subsequent phases of the visual inspection of this system section, markers were installed for laser scanning, marking the start of the phases for scanning the concrete lining and mapping cracks and damages.

The geophysical investigations of the concrete lining of the HTT were performed using ground penetrating radar (GPR) and electrical resistivity imaging (ERI) methods. The objective of these investigations was to assess the condition of the tunnel lining and the surrounding rock mass in direct contact with the concrete lining, focusing on crack patterns, water flow paths in both vertical and horizontal planes, and the presence of cavities and voids behind the concrete lining.

(a) **(b)** **(c)** **(d)**

Fig. 4. Geoelectric Testing: (a) Ground Penetrating Radar (GPR); (b), (c) Preparation for Geoelectric Measurements – Placement of Metal Electrodes; (d) Geoelectric Measurement System – VS-1 Resistivity Meter, Electrode Selector, External Power Module and Cables with Metal Electrodes.

Following the completion of the rehabilitation works, the application of this type of investigation enabled verification and quality control of the implemented remedial measures. In the case of this specific project, a total of 7,000 m' of ground penetrating radar (GPR) surveys and 175 m' of electrical resistivity imaging (ERI) surveys were performed.

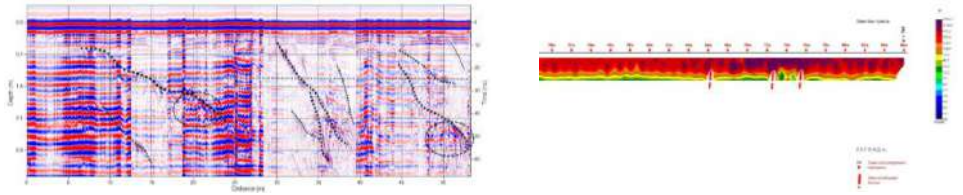

(a) **(b)**

Fig.5. Geoelectric Testing: (a) Results of Ground Penetrating Radar (GPR) Surveys; (b) Results of Geoelectric Measurements.

2.1.2. Stress Grouting Technique

Stress grouting is a specific type of pressure grouting applied in engineering practice when it is necessary to induce pre-stressing of the tunnel lining, i.e., to increase tangential stresses within the lining. This grouting method is most commonly used in pressurized hydrotechnical tunnels, where the effect of prestressing is intended to counteract the internal water pressure acting on the tunnel lining during the operational phase.

The works were carried out at predefined locations along nearly the entire alignment of the tunnel, starting with machine drilling using rotary-percussive drilling with water cooling. The equipment used included the Hydra Joy 2P drill rig, equipped with a hydraulic hammer.

The drilling procedure differed only in two areas: within the surge shaft and at the very beginning of the tunnel, in the bifurcation zone. In the surge shaft, drilling was performed manually using pneumatic hand drills, while in the bifurcation zone and the initial tunnel stations, a Hydra SL200 hydraulic hammer mounted on a JCB 3CX skip loader was used to ensure better mobility and maneuverability.

(a) **(b)** **(c)**

Fig. 6. (a) Hydra Joy 2P equipped with a hydraulic hammer; (b), (c) Hydraulic hammer Hydra SL200 mounted on the JCB 3CX skip carrier.

Drilling was executed in a radial pattern, as specified by the design, with 5-meter spacing between boreholes, a drilling depth of 4 meters, and a borehole diameter of Ø56 mm. The design also included a provision for modifying the technical solution in the event of increased grout consumption – specifically, by reducing the radial spacing between boreholes to 2.5 meters.

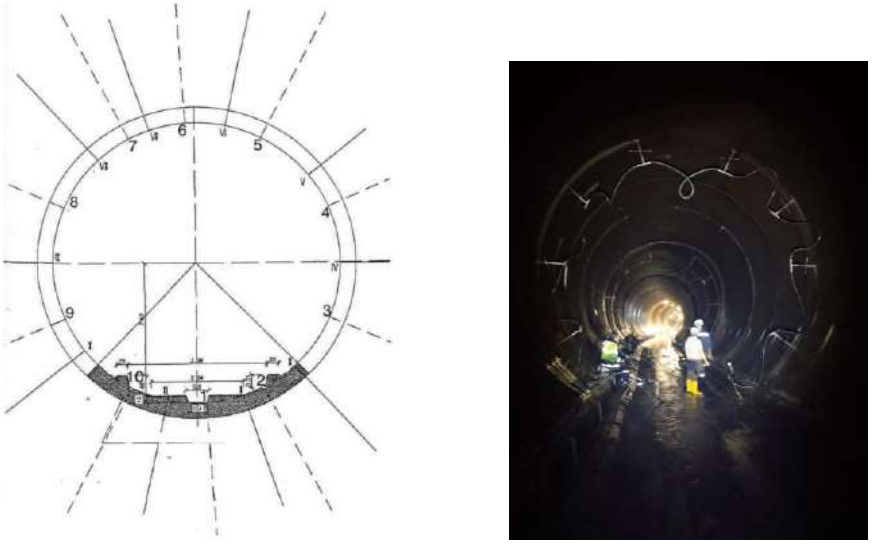

(a) **(b)**

Fig. 7. (a) Detail of stress grouting according to the rehabilitation project; (b) Drilling execution inside the tunnel.

2.1.3. Installation of Self-Drilling Anchors (SDAs)

The rehabilitation project specified the installation of self-drilling anchors (SDAs). The maximum designed anchor length was L = 6 m (Type 3), while in certain locations, shorter anchors were prescribed: L = 3 m (Type 1) and L = 4 m (Type 2).

The installation procedure was the same for all SDA types. Prior to installation, Ø56 mm boreholes were drilled to the required depth, using the same equipment as for the stress grouting works.

(a) **(b)** **(c)**

Fig. 8. (a) Drilling of tunnel lining, (b) Appearance of tunnel lining after installation of anchors, (c) Anchor type "SDA".

The grouting process begins after the anchor and the grouting tubes are inserted into the borehole. One tube is used to deliver the grout, while the other serves to release excess air during injection. The completion of the injection process is marked by the moment when grout begins to exit through the air-release tube, indicating that the borehole is fully filled. After grouting and removal of the excess tubing, anchor bearing plates and nuts are installed. Once the grout has fully cured, the plate is tightened against the rock surface by tensioning the nut.

2.1.4. Chemical grouting

Chemical grouting was performed using polyurethane-based injection materials. To prevent leakage of the injection grout, the cracks were prepared by cutting triangular grooves along their length. These grooves measured 3 cm × 3 cm and were filled with fast-setting mortar prior to injection.

Drill holes were made at an angle of 45°, diagonally across the crack, with spacing between 25 and 35 cm, resulting in borehole lengths ranging from 45 to 55 cm, placed alternately on both sides of the crack (left and right). Drilling was performed mechanically, using electric drills with a borehole diameter of Ø10 mm. Upon completion of the chemical grouting process – i.e., after the polyurethane material had cured – the packer was removed and the borehole was sealed with mortar.

(a) **(b)** **(c)** **(d)**

Fig. 9. (a) Placement of packer; (b) Overview of complete chemical injection; (c) Saw-cutting of crack; (d) Completed chemical injection

2.2. Adapting the Technical Solution to Actual Tunnel Conditions

2.2.1. Adapting the Technical Solution to Actual Tunnel Conditions during Works at Work Site 1

Based on the results of the visual inspection of the headrace–tailrace tunnel (HTT), mapping of the concrete tunnel lining, and preliminary analyses, certain adaptations of the designed solution were made to the actual tunnel conditions in the section between chainage km 0+010 and 0+100. These adaptations primarily concerned the locations for carrying out rehabilitation works – drilling and grouting, as well as anchor installation.

The condition of the lining with the positions of the newly designed works is illustratively shown in Figure 10. For better understanding of the illustrated executed works, square symbols indicate the positions of the self-drilling anchors (SDAs), with color differentiation depending on their length (SDAs of L = 6 m or L = 4 m). Injection boreholes are represented by circular symbols, varying according to the diameter and length of the borehole. Green lines in Figure 10 denote locations of chemical grouting, while brown rectangles with green borders indicate positions of segregation remediation.

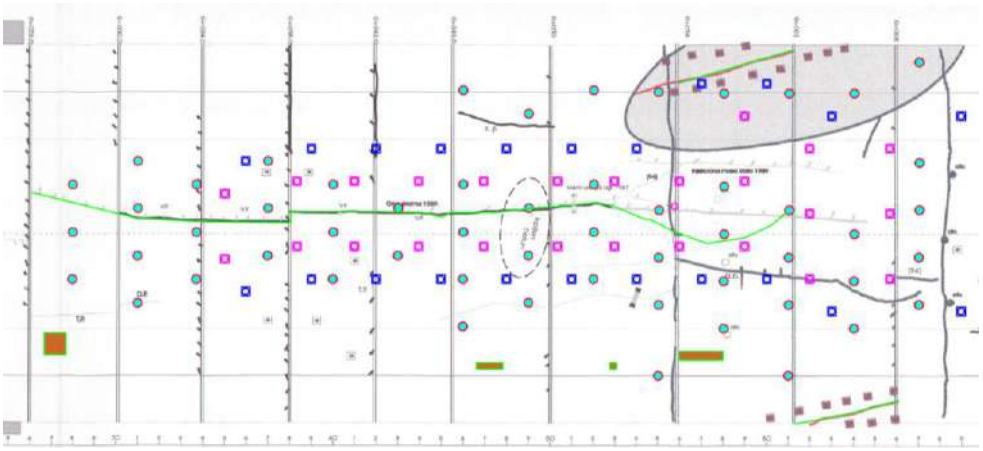

Fig. 10. Condition of the concrete lining with locations of newly designed works on the section between st. km 0+026 and 0+070 (illustrative representation).

After the initial assessment of the condition, it was decided to adapt the execution of the rehabilitation works at work site 1 by correcting the locations of the injection boreholes and their grouting. The borehole layout was revised based on the damage mapping analysis, taking into account the history of works on this section. The arrangement of injection boreholes was defined so that grouting could be performed for all newly detected damages as well as for several existing defects assessed as potential water leakage points in the tunnel. In addition to the layout, the drilling depth was also adjusted according to the revised borehole arrangement, with the most common drilling depth being 3 m. These changes during the rehabilitation works also necessitated adjustments in injection pressures, which were generally applied at 12 bar. It is important to note that on this section, the total planned drilling length of 352 m exceeds that of the original Rehabilitation Project, but based on the conducted investigations this proved to be necessary.

On the section between chainage km 0+502 and 0+580, the condition of the concrete lining has not significantly changed compared to the mapping performed during the 2005 reconstruction. A short crack with minor opening and leakage was identified at chainage 0+541, another short crack with minor opening and leakage at chainage 0+575, several short dry fissures, and several wet spots related to old

injection boreholes. Accordingly, no significant changes in the positions were made during the works on this section.

To improve the tunnel's operational conditions, the previously planned pre-stressing grouting at Work Site 1, originally designated for the section from chainage 0+500 to 0+580, was shifted to the section between chainage km 0+100 and 0+180. This created a unified rehabilitation zone from chainage 0+010 to 0+180 to reduce tensile stresses in the concrete caused by water pressure, which will also decrease water losses in the downstream slope area, thus enhancing its stability (Figure 11).

Considering the pressure values during grouting in the empty tunnel, the pressure-induced stresses in the concrete lining depend on the pressure intensity, tunnel diameter, and lining thickness. The project assessment concluded that the maximum grouting pressure should not exceed 20 bar to keep the concrete stresses within allowable limits.

On the left side of Figure 11, the odd-numbered profiles (cross-sections 1 to 15) are shown, while the right side displays the even-numbered profiles (cross-sections 2 to 16). The rehabilitation works were carried out so that the borehole layout within all even profiles is identical, as well as within all odd profiles. However, the borehole arrangements in even profiles differ from those in odd profiles, with boreholes in consecutive profiles offset by an angle of 18°. The spacing between injection profiles is 5 meters.

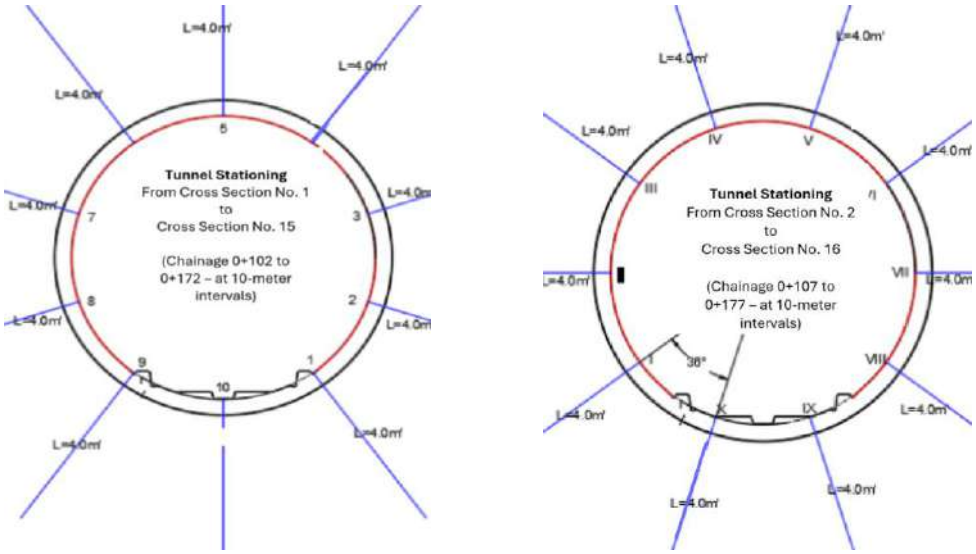

Fig. 11. Layout of tension grouting injection boreholes (profiles at Work Site 1).

2.2.2. Adapting the Technical Solution to Actual Tunnel Conditions during Works at Work Site 2

The investment maintenance project for the headrace-tailrace system of the PSHPP "Bajina Bašta" defined rehabilitation works for work site 2, which includes the hydropower surge chamber structure. The planned works on the lower vault of the surge chamber included the installation of SN anchors, tension grouting, and chemical grouting.

The maximum pressure defined by the project is 25.0 bar. According to the concluding considerations of the project "Tension-Deformation Analysis of the Surge Chamber and Steel Pipelines," conducted by the Institute for Water Management "Jaroslav Černi" in 2024, it was stated that, given the cracking of the concrete lining combined with the high pressures of tension grouting, which could lead to damage of the concrete lining, it is necessary to reduce the maximum tension grouting pressures to 15 bar.

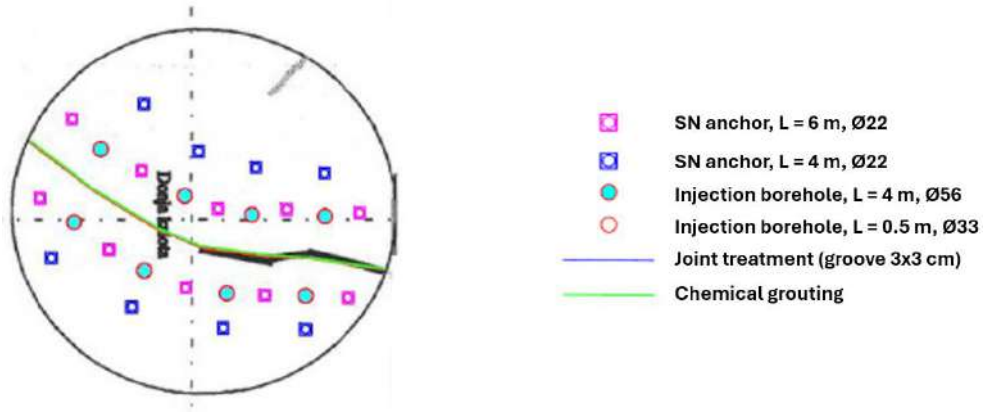

Fig. 12. Repair works on the lower crown of the water reservoir.

During the execution of the works, monitoring of cracks in the surrounding concrete lining of the lower vault of the surge chamber was conducted, and no changes indicating deficiencies in the execution of the rehabilitation works were observed.

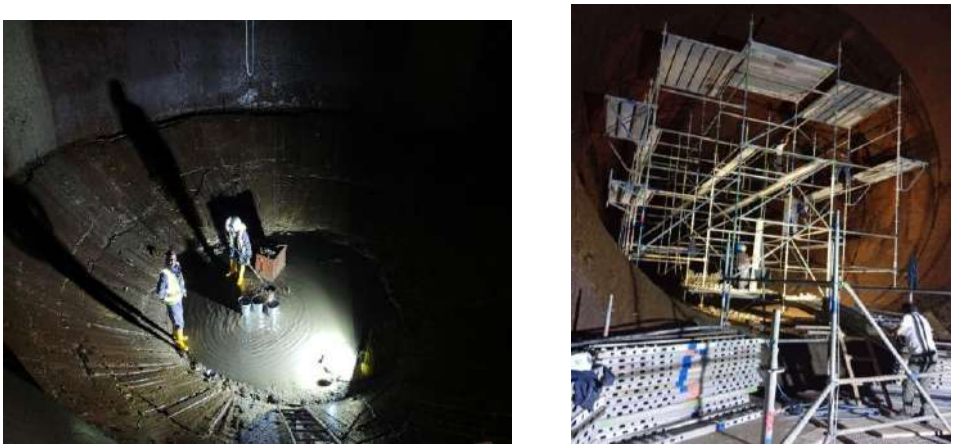

(a) **(b)**

Fig. 13. (a) Mapping of cracks in the concrete lining of the lower crown of the water reservoir, (b) Assembly of scaffolding in the water reservoir chamber

2.2.3. Adapting the Technical Solution to Actual Tunnel Conditions during Works at Work Site 4

Rehabilitation works at Work Site 4 represented the greatest challenge in the implementation of this project. Work Site 4 is located in the zone of significant influence of the "Beli Rzav" reservoir, which was at operating level during the project execution. There were risks of excessive water leakage through the boreholes, so the work had to be carried out carefully and sequentially.

The rehabilitation works began according to the project design by drilling holes and installing SDA anchors shown in Figure 14, marked as B4 and An2. During the drilling for the installation of anchor A2 at a depth of 4 m, water inflow was registered in the borehole with slight leakage. The anchor was installed, but injection grouting could not be performed.

During the drilling for the installation of the anchor marked B4 at a depth of 4.2 m, significant water leakage was registered from the borehole, which, unlike the previous situation, prevented the installation of the anchor. At this position, a packer was installed with a valve at its end, and on the other side, a pressure gauge was mounted, which recorded a pressure of 7.5 bar.

In accordance with the condition of the lining at the location, the project design, and the observed phenomena, an additional 5 injection boreholes were drilled at the site to reliably locate water-filled cracks behind the concrete lining, determine pressures, and collect data for the successful execution of further rehabilitation works.

Drilling started at the location marked B0, but after drilling through the concrete lining at a depth of 0.65 m, metal (from reinforcement or straps) was encountered, so further drilling was abandoned and drilling continued below the initial borehole B4. In the zone of borehole B4 at chainage 7+942 on the vertical profile, 5 boreholes of various depths were drilled, as shown in Figure 14. They were drilled at mutual distances of about 1.1 m. Drilling was carried out sequentially, starting with drilling to a depth of 0.6 m. At this depth, the drill string was withdrawn to check for water inflows from the surrounding rock. This procedure was then repeated every 0.3 – 0.5 m until the final depths were reached. The relevant criterion for completion was to drill until water appeared indicating the presence of a discontinuity that needed to be injected. The decision was made not to drill deeper than 2.2 m to avoid entering the zone of reduced effectiveness of previous injections, where larger water inflows under a pressure of 7.5 bar were observed in the cracks.

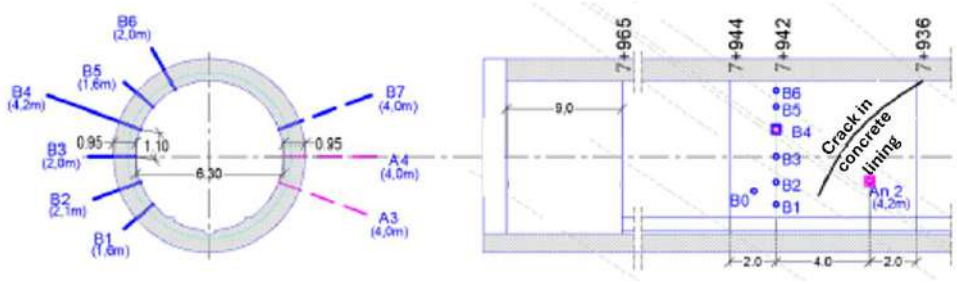

Fig. 14. Overview of initial anchor installation and grouting works in the section from chainage km 7+944 to 7+936.

From boreholes B1-B5, after the first meter of drilling, water carried out finely ground samples of grey marl, unlike in anchor borehole A2 where the water expelled many pieces of limestone. After drilling, water from B1 and B2 flowed gently, from B3 and B5 more significantly in a jet, while B6 only slightly moistened. After drilling and a brief analysis of the observed phenomena and results, injection of the boreholes commenced.

Due to site conditions, which involved significant risks of water leakage under full pressure from the "Beli Rzav" reservoir, on-site decisions were made that required corrections to the project. The holes for installing 6 m long anchors, as originally planned for this section, were replaced with the installation of 4 m long anchors. At positions where installation of 4 m anchors was not possible due to large water inflows from the borehole, borehole grouting was performed. The proximity of the reservoir and the objective conditions during the work execution meant that, out of the total 177 planned SDA anchors, only 8 were installed at the specified work site (Work Site 4).

The Jaroslav Černi Water Institute pointed out to the other project participants the importance of future repair works in the zone of Work Site 4, which is located upstream of the closure structure. This zone needs to be approached under conditions of reduced water pressure on the lining, which can be achieved by lowering the water level in the "Beli Rzav" reservoir, so that the planned works can be carried out in full scope in order to have a significant impact on the safety and security of the headrace–tailrace tunnel system and the operation of the hydroelectric power plant itself.

Fig. 15. Installed packers in the right side of the tunnel cross-section at chainage km 7+942.

3. Discussion on the Effects of Rehabilitation and Guidelines for Further Work

The rehabilitation works described in the previous chapter significantly improved the condition of the concrete lining at the work sites in the access tunnel to the bifurcation, as well as in the initial chainages of the hydrotechnical tunnel, in the lower chamber of the surge tank, and parts of the cylinder and vault. The most demanding location for the rehabilitation works was at the final chainages of Work Site 4 near the fixed wheel gate, i.e., the upper reservoir. Considering the overall picture during the project execution, the section of the tunnel adjacent to the upper reservoir represents an area that will receive great attention in the next rehabilitation project, while in the meantime its behavior will be monitored through the proposed tunnel monitoring measures.

Because of all the above, one of the most important guidelines for the upcoming operational period is continued monitoring with the existing and newly installed monitoring equipment, as well as planning for future maintenance of the fixed wheel gate, which will require carrying out works differently, given that such maintenance requires draining the upper reservoir. When the upper reservoir is drained, it will also be possible to undertake maintenance of the maintenance gate and other elements that could not be performed under current conditions. Furthermore, draining the reservoir can have a highly positive effect on the rehabilitation outcomes on the last section, about 1500 m long, through the application of prestressed grouting and anchor installation. If the investor decides that it is unacceptable to drain the upper reservoir during the works, lowering the reservoir level by 15-20 m can significantly improve the quality and speed of the works, thus avoiding potential problems during concrete lining drilling in the indicated zone.

Regardless of the tunnel's purpose, regular inspections are necessary throughout the operational life to prevent potential incidents caused by structural failure and to contribute to extending the service life of the structure. Carrying out rehabilitation works on such types of structures involves working in a potentially hazardous environment. Inspections of this kind rely heavily on the subjectivity of the project team, especially during concrete lining mapping. Considering all challenges, various systems have been developed to automate certain procedures for tunnel inspection and monitoring (Attard et al., 2018).

To ensure quality control after the completed works, the use of modern technologies such as artificial intelligence (AI), photogrammetry, BIM, and GIS in tunnel construction and monitoring is becoming increasingly common. The application of these technologies in infrastructure management brings numerous benefits, with automated data collection, structural condition assessment, and digital data management being particularly emphasized (Sanfilippo et al., 2025). The use of technologies like laser

scanning and photogrammetry allows for faster data acquisition about the tunnel structure's geometry and condition. Utilizing such technologies and improving automation in data collection ensures a higher degree of objectivity, repeatability, and data quality compared to manual data collection methods. The management and use of collected data in modern trends aim toward BIM technology, which allows BIM models of such hydrotechnical structures to be integrated with GIS, which remains the primary tool for managing large sets of geospatial databases (Sanfilippo et al., 2025).

One of the challenges in modern tunnel monitoring trends focuses on digital twin technology (Ai et al., 2020). This technology, applied in monitoring hydrotechnical structures, provides the possibility of continuous and efficient object condition monitoring. Continuous monitoring and early-stage change detection contribute to effective maintenance during the operational phase, timely planning of rehabilitation projects, and elimination of potential undesirable scenarios regarding structural failure. Developing advanced information models improves the understanding of tunnel behavior throughout its operational life and enables faster damage detection (Machado et al., 2025). The main challenges highlighted by the authors concern the development of digital twins, particularly in integrating heterogeneous data sources. Implementing such modern approaches requires anticipating challenges and potential limitations at the project's outset, as digital twin models demand highly detailed models based on realistic data from the actual structure to minimize approximations (Machado et al., 2025). After overcoming initial challenges, it should be noted that applying such technologies can greatly enhance the monitoring process of demanding tunnels, where digital inspection is supported by an integrated tunnel model database. This type of result enables an automated model linked to the actual structure, facilitating management, identification of specific damages, and optimization of maintenance plans (Machado et al., 2025).

4. Conclusion

The rehabilitation works on the hydrotechnical tunnel project presented in this paper were carried out with quality, expertise, and within the planned budget. Accurately forecasting the budget for rehabilitation works on complex structures, such as the headrace–tailrace system of the reversible hydroelectric power plant "Bajina Bašta," is an exceptionally challenging endeavor. The fact that most of the rehabilitation works foreseen in the project were completed, with modifications necessitated by site conditions and still fitting within the budget limits, speaks to the good practice and professionalism of all team members involved in the project's implementation.

The execution of such projects highlights the necessity of adjusting project designs during works to adapt to field conditions. System investigations immediately prior to the commencement of works are of utmost importance. Thoroughness in this phase of project execution largely focuses the project team on current problems that cannot be ignored and that, due to objective circumstances, may not always be fully covered by the project design.

Attention was also drawn to the section that posed the greatest challenge during the execution of works. Work site 4, located just before the gate near the "Beli Rzav" reservoir, is in a zone heavily influenced by the reservoir, which was at operating level during the works. Since the high water presence prevented the installation of the full length of anchors specified in the design and significantly reduced the number of installed anchors in this section, a discussion arises regarding the necessity of reservoir draining during similar rehabilitation projects.

The importance of modern methods for monitoring structural behavior was emphasized. The development of advanced monitoring systems allows for real-time assessment of structural condition and timely interventions that can greatly affect the operational life of the tunnel. The methods presented in this paper, which reflect the research focus of various authors in this field, clearly highlight the importance of quality systems for monitoring the condition and safety of such structures, which are components of complex hydrotechnical systems.

Based on all the above, the authors emphasize the importance of automation systems that reduce subjective assessments of tunnel structural conditions and thus enhance the safety of project

participants. Developing systems for continuous condition monitoring would enable active surveillance and assessment of the optimal timing for rehabilitation projects, as well as detection of sensitive tunnel sections. Draining the reservoir and potential modifications in future project designs at specific locations would yield better results during execution, thereby contributing to a certain extent to reducing losses during the operation of the headrace–tailrace system of the "Bajina Bašta" hydroelectric plant.

References

Ai, Q., Yuan Y., Shen, S.-L., Wang, H., Huang, X., 2020. Investigation on inspection scheduling for the maintenance of tunnel with different degradation modes. *Tunnelling and Underground Space Technology*, Vol. 106, https://doi.org/10.1016/j.tust.2020.103589

Anđelković, V., Lazarević, Ž., Nedović, V., Stojanović, Z., 2013. Application of the pressure grouting in the hydraulic tunnels. *Tunnelling and Underground Space Technology*, Vol. 37, 165-179. https://doi.org/10.1016/j.tust.2012.08.012

Attard, L., Debono, C.J., Valentino, G., Castro, M.D., 2018. Tunnel inspection using photogrammetric techniques and image processing: A review. *ISPRS Journal of Photogrammetry and Remote Sensing*, Vol. 144, 180-188. https://doi.org/10.1016/j.isprsjprs.2018.07.010

Krukovskyi, O., Skipochka, S., Serhiienko, V., 2024. From the experience of the technical examination of hydro-technical tunnels. V International Conference "Essays of Mining Science and Practice", Proceedings of the IOP Conference Series: Earth and Environment Science, Dnipro, Ukraine, 08–10. November 2023.

Machado, L.B., Poncetti, B.L., Silva de Assis, L., Futai, M.M., 2025. Automated procedural modeling for tunnel inspection and digital twin development. *Tunnelling and Underground Space Technology*, Vol. 165, https://doi.org/10.1016/j.tust.2025.106929

Montero, R., Victores, J. G., Martínez, S., Jardón, A., Balaguer, C. 2015. Past, present and future of robotic tunnel inspection. *Automation in Construction*, Vol. 59, 99-112. https://doi.org/10.1016/j.autcon.2015.02.003

Radovanović, S., Milivojević, M., Stojanović, B., Obradović, S., Divac, D., Milivojević, N., 2022. Modeling of Water Losses in Hydraulic Tunnels under Pressure Based on Stepwise Regression Method, *Applied Sciences*, Vol. 12 (Issue 18), https://doi.org/10.3390/app12189019

Sanfilippo, R., Esfandiari, M., Foria, F., Garbutt, D., Glab, K., Karlovšek, J., Menozzi, A., Paskaleva, G., Robert, F., 2025. ITA – AITES tunnelling information modelling – A BIM approach for a sustainable life cycle management. *Tunnelling and Underground Space Technology*, Vol. 165, https://doi.org/10.1016/j.tust.2025.106711

Savić, Lj., 2009. Uvod u hidrotehničke građevine [Introduction to Hydraulic Structures]. Faculty of Civil Engineering University of Belgrade. Belgrade, Serbia, pp. 421-427

Strauss, A., Bien, J., Neuner, H., Hrmening, C., Seywald, C., Österreicher, M., Voit, K., Pistone, E., Spyridis, P., Bergmeister K., 2020. Sensing and monitoring in tunnels testing and monitoring methods for the assessment of tunnels. *Structural Concrete*, Vol. 21 (Issue 4), 1356-1376. https://doi.org/10.1002/suco.201900444

Zabuski, L., 2019. Construction of Pressure Tunnels. *Archives of Hydro-Engineering and Environmental Mechanics, Sciendo*, Vol. 66, 77-100. https://doi.org/10.1515/heem-2019-0006

SETC-2025
BELGRADE

TOPIC 6

DIGITAL AND INFORMATION TECHNOLOGY IN DESIGN AND CONSTRUCTION

Southeastern Europe Tunnelling Conference (SETC-2025)
1-3 October 2025, Belgrade, Serbia

DOI: 10.5937/SETC25032S

EcoScan: Empowering Carbon-Optimised Design in the Digital Era

Vira Alice Stupina[a], Filippo Cuccagna[a]*

[a] TRACTEBEL ENGINEERING S.A. Business Area Infrastructures Europe- Direction Urban France et Monaco - Unité Urban - No 7, rue Emmy Noether, 93400 Saint Ouen – France; vira.stupina@tractebel.engie.com, filippo.cuccagna@tractebel.engie.com

Abstract: Poised for recognition at the ITA Awards for Digital and Information Technology, EcoScan is redefining sustainability in tunnel and underground infrastructure. With Scandinavian countries set to enforce strict carbon footprint limits on new-builds from 2025, the need for efficient, transparent, and adaptable carbon assessment tools has never been greater. This user-friendly web application answers the call—delivering rapid, precise, and visually engaging carbon calculations tailored for complex projects.
Seamless integration with the Autodesk ecosystem enables element-level optimisation using locally sourced materials, crucial for minimising embedded carbon in tunnel and metro station construction. Exportable 3D visualisations replace static regulatory tables, streamlining communication with stakeholders and authorities. Customisable material databases and real-time scenario comparisons empower teams to make environmentally responsible decisions at every phase.
Unlike conventional BIM tools, EcoScan's open-source approach fosters flexibility and user-driven innovation across the project lifecycle. Ongoing development—including construction site emissions analysis—positions this platform as a transformative solution for sustainable, high-impact infrastructure worldwide.
Engineered for the digital age, EcoScan doesn't just keep pace with the future of tunnelling—it helps shape it. Experience a new era of efficiency, transparency, and measurable impact in underground projects.

Keywords: Digital technology; Life Cycle Assessment; EcoScan; BIM, AI; Eco-design

1. Introduction

Digital and information technology are revolutionising the way we conceive and construct our cities. Nowhere is this transformation more profound—or more vital—than in the delivery of mega-projects such as the Grand Paris Express (GPE). Spanning over 200 kilometres of new metro lines and 68 stations, the GPE embodies the extraordinary scale, complexity, and ambition shaping contemporary infrastructure. These ventures are not merely engineering marvels; they are pivotal arenas for addressing some of the planet's most urgent environmental challenges. While their construction inevitably generates vast quantities of material and emissions, their enduring legacy lies in enabling a shift towards sustainable, high-capacity public transport—offering genuine and lasting environmental gains.

As the built environment sector is increasingly challenged to achieve more with fewer resources, digital innovation has become central to enabling smarter and more sustainable outcomes throughout the project lifecycle.

Against a backdrop of tightening global climate targets, the construction industry must now consider the entire lifespan of infrastructure—from material sourcing through to end-of-life disposal—instead of focusing solely on operational efficiency. Life Cycle Assessment (LCA) has therefore become indispensable, providing a holistic understanding of a project's environmental impact and revealing opportunities to meaningfully reduce carbon, energy consumption, and waste.

*Corresponding author: vira.stupina@tractebel.engie.com (V.A. Stupina).

As regulations evolve and carbon limits are tightened—especially in progressive regions such as Scandinavia—traditional methods of eco-design, often manual, slow, and reliant on rough estimates, are no longer fit for purpose. Enter innovative digital tools like EcoScan. Seamlessly integrated within established design platforms, the tool enables rapid, detailed LCA at the element level, harnessing local material data and delivering results in a fraction of the time required by conventional processes. Its open-source, visual interface turns compliance into a collaborative, transparent, and efficient endeavour, setting a new benchmark for environmental responsibility in construction.

2. Digital Transformation in Underground Structures: Integrating Sustainability with EcoScan

The construction and operation of underground structures, such as tunnels and underground railways, have long posed unique challenges for engineers and project managers. Traditionally reliant on manual calculations and fragmented data sources, infrastructure projects are increasingly adopting digital-first approaches. Building Information Modelling (BIM), artificial intelligence (AI), and data analytics are enabling engineers to design, simulate, and optimise projects before construction begins (Smith et al., 2021; ISO 19650, 2018).

At the same time, the demand for sustainable construction has intensified. Lifecycle Assessment (LCA) provides a framework for evaluating environmental impacts, as defined in ISO 14040/44 (ISO, 2006). Applying these methodologies within BIM environments allows project teams to integrate carbon and environmental performance directly into early-stage decision-making (Jones & Meyer, 2020).

At the forefront of this shift is EcoScan, an innovative tool developed by TRACTEBEL team to redefine sustainability management in underground infrastructure. EcoScan integrates seamlessly with Autodesk's API and viewer, empowering users to calculate carbon emissions and assess vital environmental parameters directly from Building Information Modelling (BIM) data. This integration enables project teams to evaluate environmental impacts at the earliest design stages and to continually monitor them throughout the project lifecycle. The objective is clear: to support sustainable decision-making throughout the lifecycle of a project.

Successfully integrating tunnel projects into this digital and sustainable process requires a strategic approach. It starts with a clear understanding of digital workflows and a willingness to embrace innovative technologies. Project teams must know how to manage data-rich BIM environments and coordinate effectively between engineering disciplines. The ability to adapt and incorporate EcoScan's insights into day-to-day decision-making is essential for achieving truly sustainable underground structures.

Rather than obscuring analysis within spreadsheets, EcoScan generates compelling 3D visualisations of environmental, energy, and waste impacts—outputs that are ready for direct regulatory submission. Its open-source nature sets it apart from the closed systems of traditional BIM providers, empowering users to customise and apply the tool across the entire infrastructure lifecycle: design, construction, operation, and maintenance.

In essence, EcoScan reimagines LCA as a swift, visual, and collaborative process, empowering infrastructure projects not merely to meet, but to define, the next frontier of environmental performance.

3. Building Information Modelling (BIM)

At the heart of this transformation is Building Information Modelling (BIM). Far surpassing simple 3D geometry, BIM acts as the digital DNA of a project, capturing every tunnel element—from concrete linings and reinforcement steel to ventilation shafts, cabling, and drainage systems. However, a static model alone is not sufficient; it must be interactive, intelligent, and communicative. To achieve this, we extended Autodesk's API and viewer, developing bespoke Java and HTML functions that convert

passive models into dynamic, navigable, and measurable environments. As a result, the tunnel evolves from a basic drawing into a fully realised digital twin.

Expanding upon this foundation, the proposed Life Cycle Assessment (LCA) tool—presented at the ITA Awards & SETC-2025—takes integration further by embedding LCA methodologies directly within BIM-enabled design workflows. Engineers can upload BIM models into the Autodesk Viewer, assign materials from a standardised database, and instantly calculate life cycle indicators and carbon footprint metrics. The tool supports the comparison of alternative material scenarios, with results visualised within the model using a green-to-red colour scale for immediate spatial feedback on environmental performance.

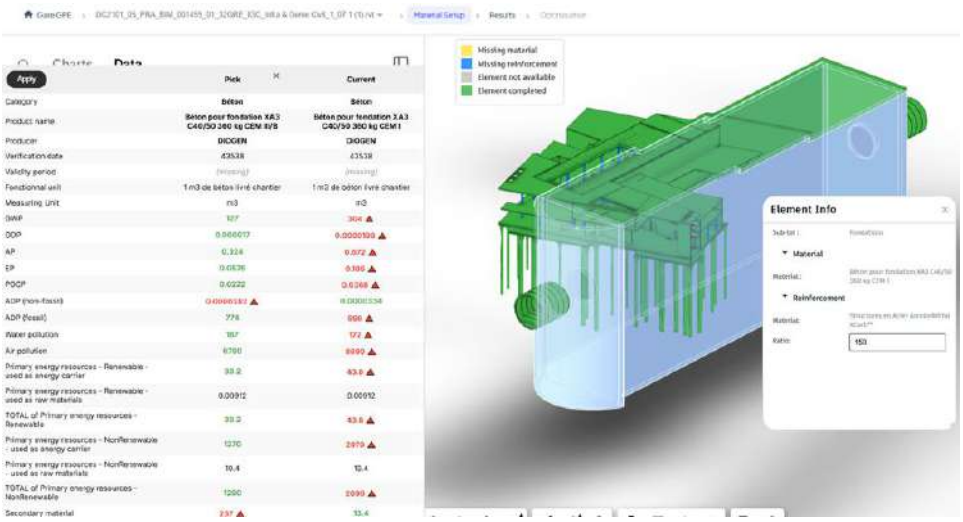

Fig. 1. Iterative Testing—Measuring Incremental Improvement at Each Stage.

Simultaneously, structured data on elements, materials, and impacts is exported via EcoScan-generated Excel files. A Python-based interoperability layer then feeds optimised material choices back into authoring tools such as Revit or Tekla, ensuring that assessment outcomes remain embedded within the BIM environment. This workflow yields three key research contributions: (i) it enhances the accuracy and usability of LCA in the early design stages; (ii) it ensures seamless interoperability across platforms and data formats; and (iii) it eliminates rework by directly linking assessment results to the BIM model. Ultimately, the convergence of BIM, LCA, and digital twin principles demonstrates how performance-driven material optimisation can be operationalised, empowering more sustainable and data-driven decision-making in underground infrastructure design.

4. Lifecycle Assessment (LCA)

The construction and operation of underground structures, such as tunnels and underground railways, have long posed unique challenges for engineers and project managers. Traditionally reliant on manual calculations and fragmented data sources, infrastructure projects are increasingly adopting digital-first approaches. Building Information Modelling (BIM), artificial intelligence (AI), and data analytics are enabling engineers to design, simulate, and optimise projects before construction begins (Smith et al., 2021; ISO 19650, 2018).

Infrastructure projects have traditionally carried substantial environmental footprints. Lifecycle Assessment (LCA) provides a rigorous, systematic method for measuring and reducing these impacts throughout every stage of a project.

EcoScan elevates Building Information Modeling (BIM) by automatically calculating carbon emissions and other environmental indicators directly from model data. This seamless integration offers:

- Clear visual outputs, enabling teams to identify precisely where environmental impacts occur within the tunnel design.
- Comprehensive, Excel-based reports that deliver detailed numerical results for in-depth analysis and optimisation.

Tasks that once required weeks of manual data extraction and computation can now be completed in minutes. More crucially, EcoScan empowers project teams to consider sustainability at the earliest design stages, when interventions are most effective and cost-efficient.

EcoScan incorporates a wide set of environmental parameters, ensuring that the assessment extends beyond carbon emissions alone. The tool follows internationally recognised LCA categories (ISO 14040/44; CML, 2001).

Table 1. LCA Indicators.

Environmental indicator	Unit
Climate Change Total	kg CO_2e
Climate Change Fossil	kg CO_2e
Climate Change Biogenic Removals and Emissions	kg CO_2e
Climate Change Land Use and Land Use Change	kg CO_2e
Ozone Depletion	kg CFC11e
Acidification	mol H+e
Eutrophication Aquatic Freshwater	kg PO_4e
Eutrophication Fresh Marine	kg Ne
Eutrophication Terrestrial	mol Ne
Photochemical Ozone Formation	Kg NMVOCe
Abiotic Depletion- Minerals and Metals	kg Sbe
Fossil Fuels	MJ
Water Use	m^3e depr.

Resource use indicators	Unit
Use of renewable primary energy excluding renewable primary energy resources used as raw materials	MJ
Use of renewable primary energy resources used as raw materials	MJ
Total use of renewable primary energy resources (primary energy and primary energy resources used as raw materials)	MJ
Use of non-renewable primary energy excluding non-renewable primary energy resources used as raw materials	MJ
Use of non-renewable primary energy resources used as raw materials	MJ
Total use of non-renewable primary energy resources (primary energy and primary energy resources used as raw materials)	MJ
Use of secondary material	kg
Use of renewable secondary fuels	MJ
Use of non-renewable secondary fuels	MJ
Net use of fresh water	m3
Biogenic carbon indicators	**Unit**
Biogenic carbon content in the product	kg CO_2
Biogenic carbon content in packaging	kg CO_2

Table 2. Waste & output indicators.

Waste & output indicators	Unit
Hazardous waste disposed	kg
Non-hazardous waste disposed	kg
Radioactive waste disposed	kg
Components for re-use	kg
Materials for recycling	kg
Materials for energy recovery	kg
Exported energy	MJ

By automating these calculations, our tool enables a multi-dimensional sustainability assessment. Instead of focusing solely on carbon, decision-makers gain a holistic view of environmental performance. This allows trade-offs to be evaluated (e.g. lower Climate Change Total vs. higher water use), supporting more balanced and sustainable design choices.

Fig. 2. Indicators by Category.

5. Eco-Design Integration

In today's infrastructure landscape, environmental performance is no longer a secondary consideration—it is a core design requirement. Yet, the greatest opportunities to reduce a project's carbon footprint are often missed at the very earliest stages, well before construction begins. Traditionally, material selection within BIM (Building Information Modelling) platforms has been guided by cost or technical criteria, with sustainability assessed only at the project's conclusion—when change is most difficult and costly.

EcoScan overturns this outdated approach. Purpose-built for modern design and construction, the tool empowers project teams to make environmentally conscious choices from the outset, turning every material selection into an opportunity to minimise impact.

At its core lies a dynamic, adaptable material database—far more than a static catalogue. This resource encompasses a wide spectrum of materials, including concrete mixes, steel grades, and insulation types, each one accompanied by comprehensive life cycle data: CO_2eq, embodied energy, recyclability, waste generation, and other vital sustainability indicators. What distinguishes EcoScan is its flexibility: users can customise the database, add new materials from local suppliers, and integrate low-carbon innovations to suit specific project needs. Continuous updates ensure that assessments reflect the latest developments in sustainable design.

EcoScan's intuitive workflow keeps environmental impact central to every decision. If a model element lacks material data, the tool prompts designers to select from the database. As alternatives are considered, EcoScan instantly analyses each option's effect on the project's carbon footprint—enabling rapid, informed comparisons before any material is locked in. This immediate feedback loop drives smarter, greener choices from the very beginning.

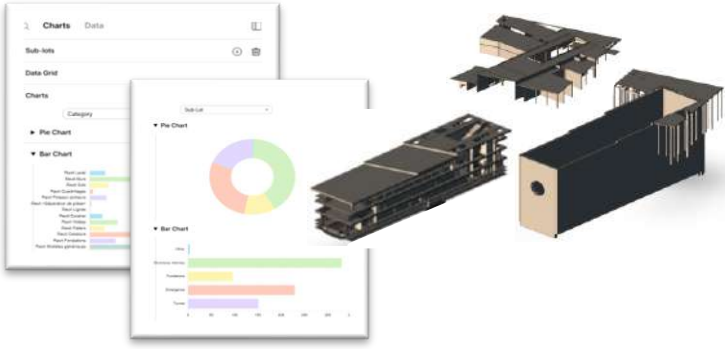

Fig. 3. Work environment.

Once a model is accurately populated with material data, EcoScan elevates optimisation to a new level. Teams can generate and compare multiple design scenarios in minutes, with environmental indicators—such as CO_2eq and energy use—recalculated at every iteration. Whether refining a single element or undertaking a comprehensive redesign, the tool delivers detailed impact assessments at both the component and project levels. Life cycle analyses that once took days now take less than an hour, empowering agile, iterative design.

Fig. 4. Ensuring Results and Data Transparency for Project Stakeholders

But EcoScan is more than a number-crunching tool. It translates sophisticated sustainability metrics into compelling, actionable visuals: bar charts that highlight the results of each optimisation, and dynamic 3D colour-coded BIM models that pinpoint areas of greatest environmental impact. These outputs can be exported as PDFs or images, making it easy to engage stakeholders and communicate the value of sustainable design.

By transforming complex technical data into practical, accessible insights, EcoScan enables project teams to integrate eco-design seamlessly into every BIM workflow. For the tunnelling and infrastructure community, EcoScan is not just a digital tool—it is an engine for a more innovative and sustainable future.

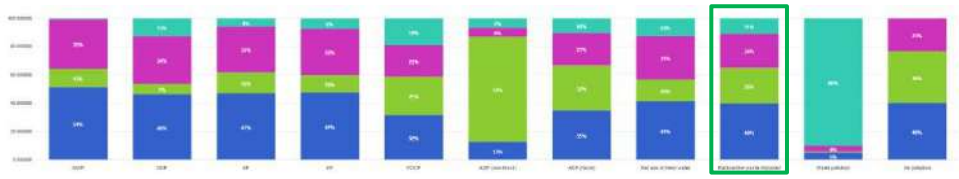

Fig. 5. Optimising Digital Data Through Targeted Approaches.

6. Challenges and Future Outlook

While EcoScan represents a significant leap forward in environmental assessment for tunnel and underground infrastructure projects, the journey is ongoing. Integrating diverse data sources, maintaining consistent data quality, and keeping pace with evolving regulatory standards require sustained collaboration and development across the sector. Moreover, as digital tools become ever more advanced, continuous training and upskilling are essential to ensure project teams can fully harness their potential.

Looking to the future, EcoScan is set to evolve alongside breakthroughs in BIM, machine learning, and real-time analytics. Forthcoming enhancements may include increased automation, expanded environmental metrics, and even deeper integration with project management platforms. With AI-powered capabilities, the tool will soon enable early-stage estimations for major infrastructure projects—even before detailed models are completed.

By embracing these digital innovations, the industry is moving towards truly sustainable infrastructure, where environmental stewardship is embedded at every phase of the project lifecycle. EcoScan stands at the forefront of this transformation, empowering engineers and decision-makers to deliver projects that are not only efficient and cost-effective, but also responsible stewards of our shared environment.

7. Conclusion

In the spirit of bold innovation and quiet resolve, EcoScan brings together a suite of digital tools and stands as more than a technological leap—it is a call to reimagine what responsible engineering can achieve. By weaving environmental stewardship directly into the fabric of infrastructure design, this tool offers not just efficiency but a principled path forward. It equips engineers and designers with the clarity and conviction to shape a built environment that honours both progress and the planet. As we face the pressing challenges of our age, EcoScan reminds us that true leadership is found not in following trends, but in setting the standard. The future of sustainable engineering, quietly and confidently, starts here.

References

ISO 14044, 2006.

ITA-AITES, 2016. Environmental assessment must be integrated into the design process—not treated as an afterthought.

Kunz, A., Smith, B., & Lee, C., 2019. Digital technologies such as BIM and data analytics are essential enablers of efficiency and accuracy in tunnel design.

Maherzi, W., Safhi, A.e.M., Soliman, A., Abriak, NE., 2024. Potential Recycling of Excavated Tunnel Materials from Grand Paris Express Disposal as a Construction Material. In In: Desjardins, S., Poitras, G.J., Alam, M.S., Sanchez-Castillo, X. (eds) Proceedings of the Canadian Society for Civil Engineering Annual Conference 2023, Volume 7. CSCE 2023. Lecture Notes in Civil Engineering, vol 501. Springer. https://doi.org/10.1007/978-3-031-61511-5_13

NF EN 15804+A2, 2019.

Paris, S.d.G., Protecting the environment during the build. Available online: https://www.grandparisexpress.fr/worksites/environment (12.08.2025).

Southeastern Europe Tunnelling Conference (SETC-2025)
1-3 October 2025, Belgrade, Serbia

DOI: 10.5937/SETC25033G

Risk Assessment of railway tunnel segments using machine learning models

Vasko Gacevski[a], Marijana Lazarevska[a] and Zlatko Zafirovski[a]*

[a] Ss. Cyril and Methodius University in Skopje, Faculty of Civil Engineering, Skopje, Republic of North Macedonia; gacevski@gf.ukim.edu.mk, marijana@gf.ukim.edu.mk, zafirovski@gf.ukim.edu.mk

Abstract: Tunnels, as unique structures, have a wide range of applications for different purposes; however, their specificity is accompanied by numerous uncertainties that can generate risks. In Republic of North Macedonia, a significant number of tunnels are planned along the railway of Corridor 8. Across three sections of this railway corridor, 49 tunnels have been designed with varying characteristics influenced by multiple factors. The detailed processing and classification of data for these tunnels provide a substantial database that can be utilized for risk assessment. This research aims to conduct a comprehensive analysis using machine learning models for assessing risks of tunnel segments application, taking into account various project data without predefined risk categories.

Keywords: Tunnel construction, assessment of uncertainties, risk analysis, machine learning

1. Introduction

In the lifecycle of infrastructure projects, risk and uncertainty are inevitable, particularly in complex underground construction. Tunnel projects are highly sensitive to varying geological conditions and unforeseen events, making implementation of effective risk management crucial. This paper addresses risk identification in tunnel construction through a combined methodological approach, integrating traditional techniques with modern data-driven machine learning models.

Tunnel construction along Corridor 8 in North Macedonia, a major pan-European transportation axis, serves as a case study. A total of 49 railway tunnels spanning approximately 25,5 km had been planned across three sections, providing a solid dataset for risk modelling. For all three railway sections, complete project documentation has been prepared at the level of main design, which also include the tunnels. The first two sections are in similar area (2 continuous sections with total length of 57,4 km) in the north-east part of the country, while the third section (with length of 63,2 km) is in different area in the south-west part. Also, one section is under construction, while the other two have not yet started.

2. Data overview

The dataset used comprises detailed information for total of 341 tunnel segments designed, according to the New Austrian Tunneling Method (NATM). The main parameters (numerical values) are grouped into four main categories:

- General-geometric characteristics (segment length, maximum overburden, excavation area);
- Geological-geotechnical characteristics (coefficient for investigative boreholes, deformation module, global strength, RMR, RQD, GSI, UCS, probability of appearance of faults);
- Support characteristics (quantities per one meter for anchors, shotcrete, reinforcement mesh, steel ribs/girders, tunnel face support (shotcrete), pipe roof umbrella, final concrete lining);
- Construction technology characteristics (excavation step length, blasting disturbance, groundwater conditions-coefficient).

*Corresponding author: gacevski@gf.ukim.edu.mk (V. Gacevski).

After creating the first models some parameters (tunnel slope and curve radius, volume weight, cohesion and angle of friction) were removed due to their apparent lower importance level, illogical correlation with other parameters and/or overall anomaly exhibited through modeling.

3. Methodology

The general idea for this research was to use machine learning (ML) models to assess the risk level of each segment using the available design data, without previously defining the risk in quantitative or qualitative form as a target variable.

At first, basic statistical and corelation analysis were performed in order to identify the most significant factors and to make distribution of values for each parameter (Fig. 1). Segment length and the maximum overburden have a wide distribution, i.e. there are quite different geometric conditions in these tunnels, which is expected. The geotechnical characteristics have different distribution shapes (normal and asymmetric). Support elements have a variation that can be associated with different geological condition. The construction technology data have specific values that can be grouped.

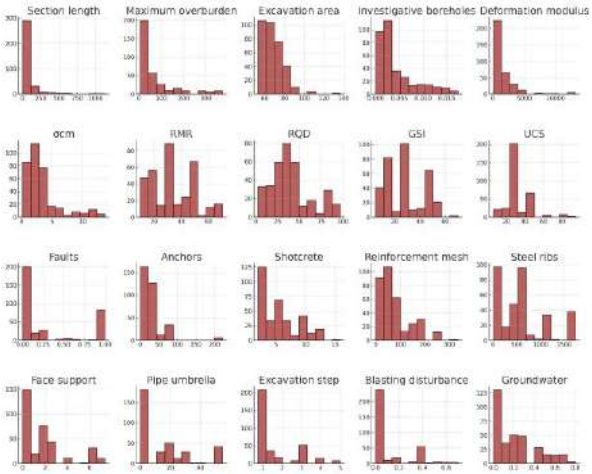

Fig. 1. Histograms of distribution for each parameter.

After a correlation analysis, the correlations between the parameters show similar conditions as for real tunnel states. Here are some of the more important correlations:

- RMR, RQD and GSI are highly correlated, which is expected as they all reflect rock mass quality;
- Deformation modulus has a moderate correlation with RMR and RQD, suggesting that weaker rocks have lower stiffness;
- Fault probability has a negative correlation with RMR and RQD, suggesting that fault zones often have weaker rock mass;
- Anchors, shotcrete and reinforcement mesh have a positive correlation with lower RMR and RQD values, suggesting that more of reinforced support is applied to weaker rocks;
- Steel ribs and pipe umbrella show a strong relationship with critical geological conditions;
- Excavation sequencing is negatively correlated with weak rocks, suggesting that in weaker conditions a shorter excavation advances are applied for increased stability;
- Groundwater has a negative impact on RMR and is associated with increased use of support.

Because this research approach is implemented without predefined target value, the next step was arriving at cluster analysis for determination of groups of tunnel segments with similar characteristics (Fig. 2).

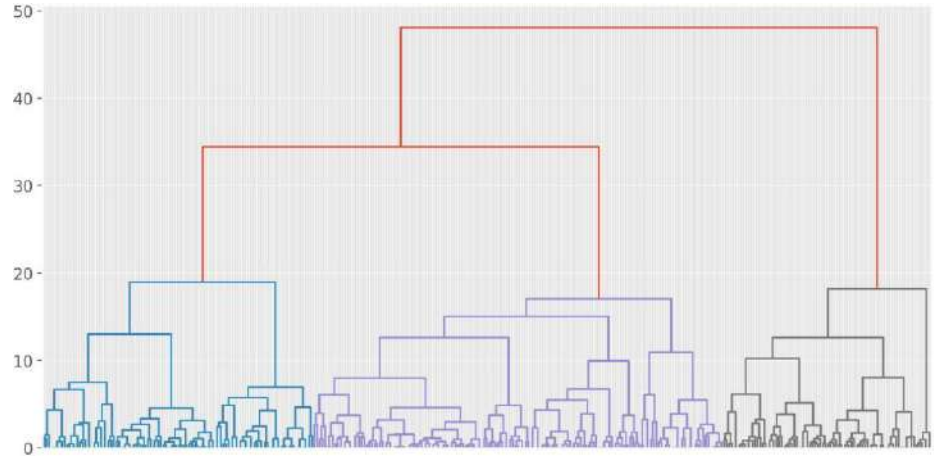

Fig. 2. Dendrogram of tunnel segments with similar characteristics (the horizontal axis represents the segments and the vertical axis is the Euclidean distance)

According to the cluster analysis, three clusters or risk categories are assessed. Some of the main characteristics with their average values for the clusters are:

- Category (cluster) 1 – High risk
  - Low values for RMR (17,1), RQD (29,3) and GSI (12,6) – very weak rock mass.
  - High probability of faults (0,99).
  - High use of anchors (54,4 m/m), shotcrete (9,99 m³/m), reinforced mash (123,9 m²/m) and steel ribs (1269,8 kg/m).
  - Highest use of pipe roof umbrella (32,2 m/m) for protection.
  - Very short excavation step (0,81 m).
  - Significant presence of groundwater (0,42).

- Category (cluster) 2 – Medium risk
  - Medium values for RMR (31,0), RQD (32,7) and GSI (25,1).
  - Low probability of faults (0,09).
  - Moderate use of anchors (26,3 m/m), shotcrete (5,08 m³/m), reinforced mash (60,2 m²/m) and steel ribs (593,3 kg/m).
  - Occasional use of pipe roof umbrella (13,7 m/m).
  - Longer excavation step (1,09 m) compared to category 1.
  - Moderate presence of groundwater (0,17).

- Category (cluster) 3 – Low risk
  - RMR (52,6), RQD (56,8) and GSI (44,8) – better rock mass compared to previous categories.
  - Very low probability of faults (0,03).
  - Low or no usage of anchors (15,0 m/m), shotcrete (3,16 m³/m), reinforced mash (56,4 m²/m) and steel ribs (42,3 kg/m).
  - Longer excavation step (2,95 m).
  - Small presence of groundwater (0,09).

With such defined clusters, 3 models were developed using machine learning technique which based on the input data (numerical values of the characteristics) can predict the target variable in this case risk category.

3.1. ML models for prediction of risk categories

The first ML model is based on the so-called Random Forest Classifier, which is perhaps one of the most popular machine learning algorithms used for classification tasks. It consists of multiple decision trees that are similar to fault and event trees with different subsets of the data. Each of the trees gives its own prediction, and most often the predicted class becomes the final result. To build the model, a set of training and prediction data (80-20%) was first created, and then with the resulting model, a prediction was made for all sections. The dependences of the influence factors are most balanced in this model (Fig. 3).

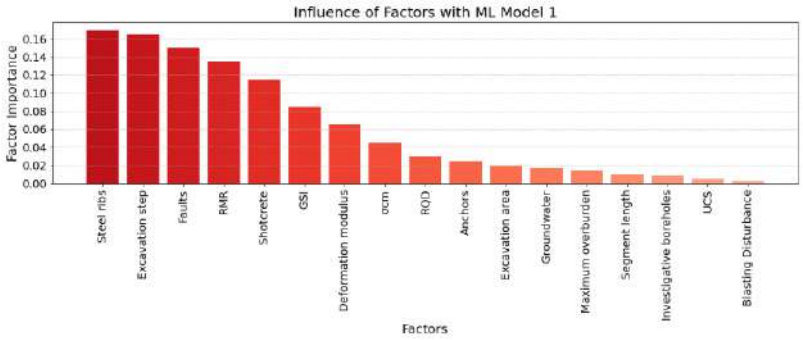

Fig. 3. Dependences of the influence factors with the first ML model.

The results in this model indicate that geological conditions are the most influential factor group in determining the risk category of tunnel segments, contributing over 50% of the total importance (Fig 4). These conditions drive subsequent decisions, such as support measures and excavation advances. This supports the observation that weak or faulted rock masses typically require heavier support and more controlled excavation (excavation in phases with smaller areas).

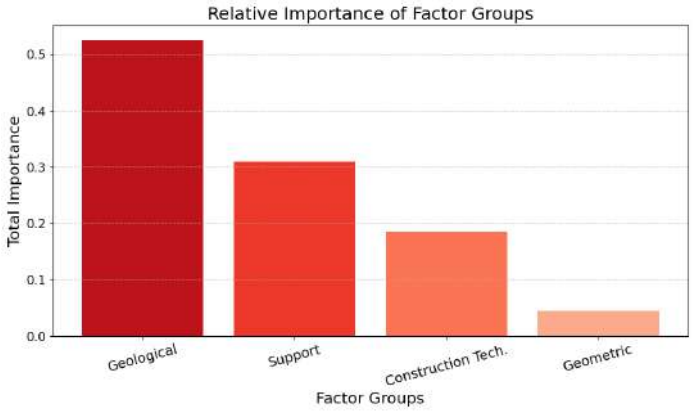

Fig. 4. Feature importance analysis by factor groups with the first ML model.

The second ML model is also a very popular and powerful machine learning algorithm, which is an improved version of Gradient Boosting and is called XGBoost. It is known for its speed, efficiency and high accuracy, and is similar to the first model because it also uses learning trees. The difference is that this model builds the trees one by one, where each new tree improves the previous one, i.e. corrects the error. This model has the most logical dependences for the influence of the factors, but they are not so balanced as the first model.

The last ML model is logistic regression. This is a basic and, in some cases, efficient classification model in machine learning. This model provides more illogical dependencies for the influence of the factors compared to the first two models. A combination with linear regression, i.e. a hybrid model, was also made, but still the model does not improve with respect to the influence of the factors.

Table 1. Prediction of the models according to number of predicted segments.

Model	Category 1 High Risk	Category 2 Medium Risk	Category 3 Low Risk
Cluster analysis	80 (23%)	157 (46%)	104 (31%)
ML model 1	81 (24%)	156 (45%)	104 (31%)
ML model 2	74 (22%)	127 (38%)	140 (40%)
ML model 3	78 (22%)	158 (46%)	105 (31%)

All three ML models have the ability to make prediction of the risk category (Table 1), but with different influences of the factors (data). The first two models have generally good logic for the dependences, where the main dominant factors are: faults, RMR, steel ribs, excavation step, shotcrete, anchors, GSI and global strength. They can be used for different kinds of tunnels segments even with reduced amount of data. The third model although it gives solid prediction, makes dependences that are not very much applicable in real scenarios so its use is limited. ML models can be also compared according to their accuracy MAE (Mean Absolute Error), RMSE (Root Mean Squared Error) and R^2 (Coefficient of determination) as shown in Table 2, where the first model has the best results.

Table 2. Assessment of the accuracy of the models.

Model	MAE	RMSE	R^2
ML model 1	0,0145	0,1204	0,9697
ML model 2	0,0435	0,2085	0,9420
ML model 3	0,0435	0,2085	0,9091

4. Discussion

ML models can outperform classical approaches in terms of scalability, predictive accuracy, and ability to capture complex interactions. Clustering reveals that segments can be assessed in 3 main risk categories according to their parameters. The number of categories can be expanded using the same or different available data and also manual (expert opinion) modifications can be done for assessing the risk categories. The presented models can make predictions of the main risk categories, but the all have different dependences of the influence of factors. Correction of the influence of factors can be made with elimination of some parameters, including more data (if available), making changes in the model (optimising) or changing the model itself. The third model for example even with modification did not improve, giving him usability in more basic or preliminary analysis.

5. Conclusion

This research demonstrates the practical value of applying machine learning techniques for risk assessment in tunnel construction, particularly in the context of the railway tunnels planned along Corridor 8 in North Macedonia. The study focused on evaluating 341 tunnel segments without predefined risk categories, utilizing detailed project design data encompassing geometric, geotechnical, support, and construction technology characteristics.

By applying clustering and supervised ML models such as Random Forest, XGBoost, and Logistic Regression, three distinct risk categories were successfully identified and predicted. Among the tested models, the first one showed the best performance in terms of accuracy and logical correlation between input parameters and risk classification. Key influencing factors such as fault probability, rock mass

quality indicators (RMR, RQD, GSI), groundwater conditions, and support measures (anchors, shotcrete, steel ribs) were consistently identified as dominant risk contributors.

The results confirm that ML models can outperform traditional methods by offering scalable, data-driven solutions for automated risk classification and prediction. Furthermore, they provide insights that can assist engineers, planners, and decision-makers in designing more resilient and cost-effective tunnel support systems, while reducing uncertainties during construction.

Future work should focus on expanding the models to include cost and time dimensions, integrating expert judgment, and adapting them to other tunneling environments and construction techniques to enhance generalizability and robustness. Models can be modified to predict a certain numeric value (such as probability of occurrence) to one or multiple risks related to different hazards. The numerical approach can also be used as a backward analysis where risks have already occurred, to determinate the influence of the input parameters and their dependences.

References

Bergmeister, K., 2022. *Models for financing, cost, and risk assessment - Major railway tunnel projects in Europe*, Ernst & Sohn – Wiley.

Binu, D., Rajakumar, R.B., 2021. *Artificial Intelligence in Data Mining – Theories and Applications*, Academic Press, Elsevier.

Eskesen, D.S., Tengborg P., Kampmann J., Veicherts H.T., 2004. Guidelines for tunnelling risk management: International Tunnelling Association, Working Group No. 2. *Tunnelling and Underground Space Technology* 19, pp. 217-237. https://doi.org/10.1016/j.tust.2004.01.001

Ettouney, M.M., Alampalli S., 2017. *Risk Management in Civil Infrastructure*, CRC Press.

Fang, M., Zhang Y., Zhu, M., Chen, S., 2022. Cause Mechanism of Metro Collapse Accident Based on Risk Coupling. *Int J Environ Res Public Health*, 19(4):2102. https://doi.org/10.3390/ijerph19042102.

Hoek, E., 2006. *Practical Rock Engineering*.

Kantardzic, M., 2020. *Data Mining – Concepts, Models, Methods, and Algorithms,* 3rd Edition, IEEE Press, John Wiley & Sons.

Mahmoodzadeh, A., Mohammadi M., Daraei, A., Faraj, R.H., Omer, R.M.D., Sherwani, A.F.H., 2020. Decision-making in tunneling using artificial intelligence tools. *Tunnelling and Underground Space Technology*, 103, 103514. https://doi.org/10.1016/j.tust.2020.103514.

Moss, S.E.R., 2020. *Applied Civil Engineering Risk Ana*lysis, 2nd Edition, Springer Nature Switzerland.

Pamukcu, C., 2015. Analysis and management of risks experienced in tunnel construction. *Acta Montanistica Slovaca*, Volume 20, number 4, pp. 271-281.

Olson, L.D., Wu, D., 2020. *Predictive Data Mining Models*, 2nd Edition, Computational Risk Management, Springer.

Sousa, L.R., 2010. Risk Analysis for Tunneling Projects. PhD Thesis, Massachusetts Institute of Technology, Department of Civil and Environmental Engineering.

Stille, H.E., 2017. *Geological Uncertainties in Tunnelling – Risk Assessment and Quality Assurance*, International Tunnelling and Underground Space Association (ITA), Sir Muir Wood Lecture 2017.

Witten, H.I., Frank, E., Hall, A.M., Pal, J.C., 2017. *Data Mining – Practical Machine Learning Tools and Techniques*, 4th Edition, Morgan Kaufmann, Elsevier.

Yoe, C., 2019. *Principles of Risk Analysis – Decision Making Under Uncertainty*, 2nd Edition, CRC Press.

Zhou H., 2020. *Learning Data Mining Through Excel – A Step-by-Step Approach for Understanding Machine Learning Methods*, Apress Berkeley, CA.

Špačková, O., 2012. Risk management in tunnel construction projects. PhD Thesis, Czech Technical University in Prague, Faculty of Civil Engineering.

SETC-2025
BELGRADE

TOPIC 7

STRATEGIC PLANING

Southeastern Europe Tunnelling Conference (SETC-2025)
1-3 October 2025, Belgrade, Serbia

DOI: 10.5937/SETC25034B

Revealing the latent potential and social value of underground infrastructure development

Andreas Benardos[a]* *and Doris Skenderas*[a]

[a] National Technical University of Athens, School of Mining and Metallurgical Engineering, Athens, Greece; abenardos@metal.ntua.gr, skenderasdoris@metal.ntua.gr

Abstract: In an era of accelerating urbanization and spatial constraints, the strategic use of underground infrastructure is gaining increasing importance as a sustainable, long-term solution. Despite their recognized advantages—such as improved mobility, reduced travel time and emissions, enhanced safety, and preservation of surface land—underground projects often face reluctance due to high capital costs, technical complexity, and extended return-on-investment periods. This paper aims to reassess the value proposition of underground infrastructure by highlighting its broader socio-economic benefits and demonstrating a holistic evaluation framework that supports more informed decision-making. A real-world tunnel case between Melissourgoi and Theodoriana in Greece is analyzed, showcasing how a relatively small infrastructure investment can yield disproportionately large benefits in terms of accessibility, regional development, and environmental performance. Quantified indicators such as vehicle operating cost, travel time savings, and accident cost reduction reveal annual savings for the users of the infrastructure, allowing cost recovery within just 4–5 years, depending on traffic volume. To further support comparative evaluations, the study also presents the Tunnel-to-Road Equivalent Length (TREL) ratio—a decision-support tool that considers traffic volumes (AADT), geotechnical conditions (GSI), and life-cycle cost–benefit parameters. Results indicate that while geotechnical conditions impact construction costs, traffic volume is the dominant factor in determining long-term economic viability. Finally, the paper advocates for integrating social and economic impact assessments into early-stage project planning, enabling a fairer evaluation of underground alternatives, as the latent social benefits presented by underground infrastructure solutions can shift the decision towards the "going underground" option.

Keywords: underground infrastructure; decision support; life cycle cost-benefit analysis; socio-economic evaluation

1. Introduction

The rapid pace of urbanization and population growth has led to intensified pressure on existing urban infrastructure. With land being a finite and increasingly contested resource, the strategic development and utilization of underground space have become increasingly important in modern societies, offering an effective and sustainable alternative solution. Across the world, governments are turning to underground solutions, from metro transit systems to highway tunnels, to address urban congestion and geographic barriers. Underground transportation projects, such as road tunnels and metro systems, have emerged as pivotal components of modern infrastructure, facilitated mobility while preserving valuable surface land (Kaliampakos and Benardos, 2008).

However, the development of underground infrastructure is often marred by perceptions of high initial investment costs, long construction durations, and technical risks, which frequently result in cost overruns and schedule delays (Flyvbjerg et al., 2002; Paraskevopoulou et al., 2022). This can dissuade stakeholders and policymakers from pursuing such projects, even when their long-term benefits significantly outweigh the costs. Despite these challenges, underground infrastructure provides numerous advantages. These include reduced travel times, lower CO_2 emissions, decreased accident rates, less traffic congestion, and uninterrupted 24/7 operation (Benardos and Skenderas, 2025).

*Corresponding author: abenardos@metal.ntua.gr (A. Benardos).

Moreover, these systems can reclaim surface space for green areas or urban development and stimulate regional economic growth (Kaliampakos et al., 2024).

Based on the above, the provision of a clear understanding of the net costs and net benefits offered by underground projects is the key issue for reaching a well-balanced and rational decision. Of course, this is something that requires not only the surficial data that can be easily assembled, but also needs to take into account the whole life cycle costing of the project (Daub, 2023). Finally, emphasis is required in depicting the social value of the project, that is, gathering and monetizing its impact on its users or the communities that it serves (Soleymani and Ismail, 2022).

This paper aims to reveal the latent value of underground transportation solutions by examining both their socio-economic benefits and their broader strategic relevance. It begins with an in-depth assessment of a real-world example, a small mountainous tunnel project in Greece, demonstrating how underground infrastructure can deliver transformative impacts in terms of accessibility, safety, and regional development. Building on the insights from this case, the paper introduces a generalized, holistic evaluation framework designed to support comparative analyses between tunnel and surface road alignments. This framework integrates life-cycle cost-benefit analysis (LCCBA) and introduces the Tunnel-to-Road Equivalent Length (TREL) ratio as a decision-support tool. Together, these cases illustrate a continuum, highlighting how underground infrastructure can be systematically assessed, justified, and prioritized within long-term development strategies.

2. Costs and benefits from the development of underground projects

2.1. Main issues to consider

The development of an infrastructure project is often associated with a vast amount to be spent that will eventually develop a new set of prevailing conditions that can either solve problems or improve the performance of a system. Thus, the decision to proceed with a certain project requires a comprehensive assessment of the costs as well as the impacts that will be brought and that can be quantified properly so as to have the required indicators for assessing the most prominent and most beneficial alternative.

The initial costs that can be measured under a simple financial framework are associated with the capital expenditures and the operation and maintenance required throughout the lifespan of the project. On the other side, the development of the new infrastructure brings either new benefits to its users and society in general or decreased cost conditions by employing the new infrastructure over the previous one. These socio-economic costs (or benefits) are related to the costs affecting the impacts and indirect economic costs generated by the project's development (e.g., travel time costs, CO_2 emissions cost, accident, noise or traffic disruption costs, fuel cost, etc. (OECD, 2017).

Despite these compelling benefits, underground projects have historically struggled to attract investment due to their high initial costs and risk profiles (Godard and Hugonnard, 1989). Large tunneling and metro projects are capital-intensive; for example, expanding a subway network costs on the order of $200 million per kilometer to recent estimates, while annual operating and maintenance expenses, approx. 2% of the initial investments add further to lifecycle costs (Blankespoor et al., 2024). Such heavy upfront expenditures, combined with typically long payback periods, make financiers and officials cautious (Godard and Hugonnard, 1989). Moreover, many high-profile underground projects have incurred substantial budget overruns and schedule delays pattern documented by Flyvbjerg et al. (2002) in a study of global infrastructure projects. This track record feeds a perception that "underground space development is an expensive venture" fraught with uncertainty, prompting some stakeholders to favor cheaper surface solutions or to postpone needed investments.

However, focusing only on immediate costs can be misleading. A growing body of research and project experience shows that the latent social and economic benefits of underground infrastructure often far outweigh the initial expense when examined over the long term. These benefits, improved connectivity, time savings, safety gains, environmental protection, and induced economic development tend to

accumulate for decades after construction. If properly quantified and monetized, they can counterbalance the costs and make a strong case for tunneling solutions (Benardos and Skenderas, 2025).

To assess and reveal to the full extent this latent potential of underground space projects, the following 2 cases are presented. The first utilizes a singular small-scale project having a clearly defined scope, cost, and impacts generated, while the second utilizes a more generic approach that entails a greater set of features to be considered, and more particular geotechnical conditions encountered, and the time discounting principle that can be a significant parameter for the financial valuation of major infrastructure projects.

2.1.1. Monetizing the Socio-Economic Benefits for the Melissourgoi – Theodoriana Tunnel Project

The proposed development project is a mountainous road tunnel between the villages of Theodoriana and Melissourgoi, which are located in the area of Central Tzoumerka, Epirus, Greece. These two settlements are located approx. 10 km apart, but, due to topographical constraints, their connection is now rather difficult as they are connected through an existing circular road network, almost 75 km in length, resulting in a travel time of approximately 2.5 hours and raising concerns about safety and accessibility. For the evaluation of the Melissourgoi–Theodoriana tunnel project, the analysis captures not only the development cost but also the tangible and intangible benefits accruing from its operation, comparing them with the current, less efficient road alternative.

The construction cost of the tunnel has been estimated using two parallel methodologies: (i) an empirical model based on as-built tunnel cost data from Greek projects and (ii) a detailed cost breakdown based on a bill of quantities derived from the design phase. Both approaches comply with official Greek guidelines and state contracting principles. The estimated development cost for the tunnel ranges between €16.7 million and €23.6 million (excluding VAT).

The benefits arising from the proposed infrastructure are multifaceted, impacting several domains (Kaliampakos et al., 2024):

- Travel Time Reduction: The tunnel enables a direct connection between Melissourgoi and Theodoriana, reducing the travel time from approximately 2.5 hours to just 20 minutes. The existing 75 km circuitous route will be replaced by a 16 km tunnel alignment. This dramatic reduction in travel time enhances regional connectivity and reduces isolation, especially for mountainous communities facing aging populations and demographic decline.
- Improved Accessibility: The tunnel significantly improves local accessibility across the broader Tzoumerka region. Travel time reductions of up to 70% between key settlements (e.g., Pramanta to Theodoriana) and 26% for regional links (e.g., Pramanta to Trikala) result in up to 15% increase in the ARI (gr) accessibility index, according to prior studies.
- Tourism and Regional Development: Enhanced connectivity will promote regional tourism by consolidating the Tzoumerka area into a more coherent travel destination. Reduced distances and shorter travel times are expected to increase the inflow and retention of visitors, contributing to the economic revitalization of the region.
- Environmental Impact: The tunnel solution introduces significant environmental advantages. Unlike surface road alternatives, it minimizes visual and ecological disruption to the sensitive mountainous landscape. CO_2 emissions are also reduced due to shorter travel distances and times. Furthermore, construction-phase impacts are reversible and of low to moderate intensity.

To quantify the benefits in monetary terms, the analysis focused on three main factors: (i) vehicle operating costs, (ii) travel-time value, and (iii) accident costs. Thus, CO_2 emissions reduction and regional development benefits haven't been included. Having the afore-mentioned impacts the values used to conclude the assessment, using value data from Greek conditions, vehicle operating cost at €0.20/km, time value at €10.7/h per passenger, and normalized accident cost at €256,000 per event, the annual use/service cost was calculated under different AADT (Average Annual Daily Traffic) scenarios, for the usage of light vehicles only (Kaliampakos et al., 2024).

In Fig. 1, the overall service cost/user cost of the new project and the currently used ring road (do-nothing alternative) is given, over several Average Annual Daily Traffic (AADT) scenarios. For an AADT of 300, the tunnel scenario yields an annual service cost of approx. €1 million, compared to million €6 for the road alternative. This results in annual savings for the users of the infrastructure of €5 million. When the AADT rises to 500 or even 1000, this difference escalates to 7.5 million and 17.4 million, respectively. The difference between the service cost of the infrastructure represents direct economic gains to its users in the form of monetized time savings, reduced fuel and maintenance costs, and improved road safety features. This represents the basis on why to pursue new infrastructure, to create new, improved conditions that will finally redistribute and diffuse the benefits to society (Kaliampakos et al., 2024).

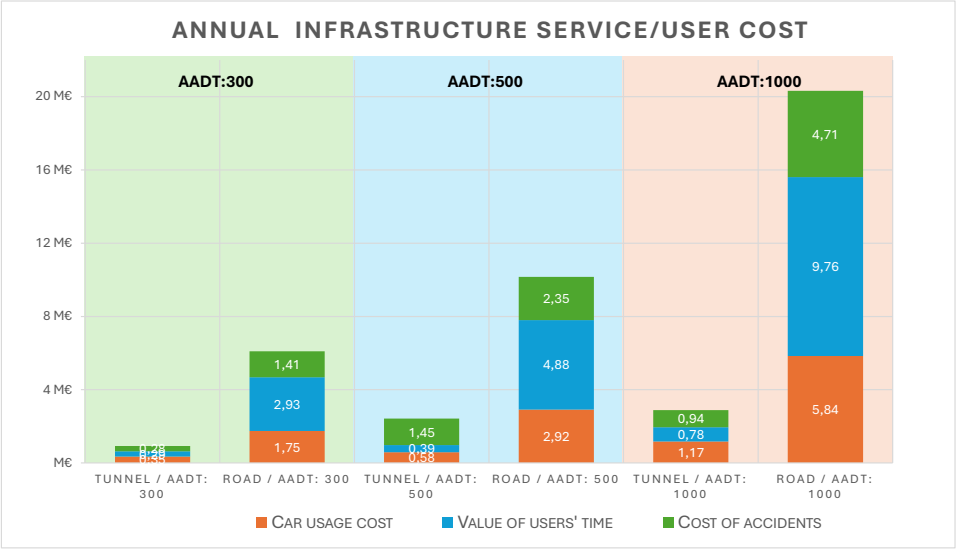

Fig. 1. Comparison of the annual infrastructure service/user cost (veh.oper.cost, travel-time cost, accident cost) between the proposed tunnel project and the current surface road option, concerning AADT values.

2.1.2. Tunnel to Road Equivalent Length (TREL) Ratio

Benardos and Skenderas (2025) presented a more thorough and well-structured approach. The analysis is focused on a life cycle perspective to evaluate the alternatives in the long term, and thus, the proposed methodology deployed entails implementing a gate-to-gate LCC analysis combined with a conventional CBA, to evaluate a project's market and non-market costs and benefits in a long-term perspective, resulting in a Life Cycle Cost-Benefit Analysis (LCCBA) (Benardos and Skenderas, 2025).

As in the previous case presented, the benefits deriving from the infrastructure are travel time savings, reduction in vehicle operating costs and fuel consumption, accident costs, etc. These are compared against capital requirements covering the construction, electrical, and mechanical installations, as well as operation and maintenance costs. Nevertheless, in establishing a more generic framework of analysis, the construction cost data also takes into account the differentiation of geotechnical conditions that are crucial for capital expenditure. The data is coming from a Greek tunnel construction dataset (Paraskevopoulou and Benardos, 2013) that has recorded the as-built construction cost, while all cost values have been adjusted to 2020 prices, setting them all to a common reference period.

In addition to the above feature, all financial/economic data is used in a discounted cash flow approach, in an attempt to minimize the impact of time in the valuation of the project. For the latter, the economic valuation from a societal perspective is selected, focusing on deriving the Economic Net Present Value

(ENPV) of the project over a 30-year evaluation period ($ENPV_{30}$), minimizing long-term forecasting errors and being aligned with the European Commission's suggestions (European Commission, 2015).

The adopted methodological framework enables a comprehensive and comparative evaluation of infrastructure development alternatives, particularly between surface road and tunnel solutions. The cost analysis is structured around key influencing parameters: the total length of each infrastructure option, the Annual Average Daily Traffic (AADT), and the site-specific geotechnical conditions that significantly impact construction complexity and associated expenditures. By incorporating these variables, the approach allows for realistic scenario modelling and the assessment of cost variations under changing traffic demands and ground conditions.

To provide a consistent basis for comparison, the Tunnel-to-Road Equivalent Length (TREL) ratio is introduced. This metric expresses the length of a tunnel that would be economically equivalent to a given length of surface road, taking into account not only direct construction costs, but also operational, environmental, and socio-economic factors. The TREL ratio thus functions as a decision-support tool, facilitating the evaluation of cost-effectiveness between alternatives. It allows stakeholders to account for the higher unit costs typically associated with tunnel construction while recognizing the long-term benefits tunnels may offer, such as shorter travel distances, reduced environmental impact, improved safety, and lower ongoing user/service costs (Benardos and Skenderas, 2025).

The results of the analysis are given in the following Table 1 and Figs 2 (a) and (b) (Benardos and Skenderas, 2025). For example, from Table 1, it can be seen that for GSI in the range of 15-35, 1 km of tunnel construction has the equivalent cost of 11.3 km of surface road (or 1 km of tunnel can replace 11.3 km of surface road). This ratio is either shortened in case of having better geotechnical conditions as the construction tunnel cost drops and cost equivalency can be reached with reduced road length - meaning that a tunnel can be more promising alternative to replace shorter road distances - or elongated when more adverse conditions are encountered and construction cost increases, having more adverse final performance over a surface road alternative. Likewise, when considering also the operation phase of the infrastructure, an increase of AADT value results to a significant drop in the length of surface road that can be replaced, meaning that the tunnel alternative can be utilized in decreased road lengths. Hence, for the same GSI category (12-35) for an ADDT of 1,000 cars, the TREL ratio drops to 3.3, or even further to 1.7 when an AADT of 5,000 is foreseen (Benardos and Skenderas, 2025).

Table 1. Tunnel to Road Equivalent Length ratio (TREL ratio) (adapted from Benardos and Skenderas, 2025).

		Geotechnical Conditions - Rock mass category (GSI)				
		55-100	35-55	15-35	<15	<<15 (soil behavior)
Construction only		4.4:1	6.2:1	11.3:1	15.5:1	16.6:1
Annual Average Daily Traffic (AADT)	500	2.4:1	3.0:1	4.2:1	5.3:1	6.0:1
	1,000	2.0:1	2.4:1	3.3:1	3.9:1	4.4:1
	2,500	1.5:1	1.7:1	2.2:1	2.5:1	2.8:1
	5,000	1.3:1	1.4:1	1.7:1	1.9:1	2.0:1
	7,500	1.2:1	1.3:1	1.5:1	1.6:1	1.7:1

In Figs 2 (a) and (b), this is presented graphically; the first graph is how the geotechnical conditions influence the TREL ratio concerning the geotechnical conditions, while the second is just the opposite, exploring the influence of the AADT's values in the TREL ratio, while also counting the geotechnical conditions in the form of GSI values.

Ultimately, the integration of the TREL ratio into the decision-making process enhances transparency and consistency, enabling planners and decision-makers to identify the most sustainable and value-generating solution in line with technical feasibility and regional development objectives.

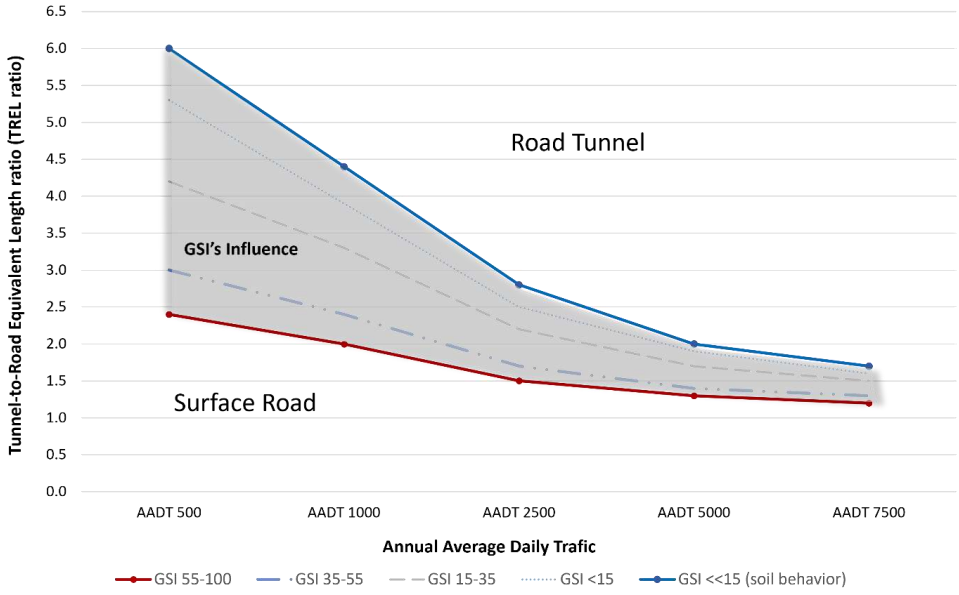

(**a**)

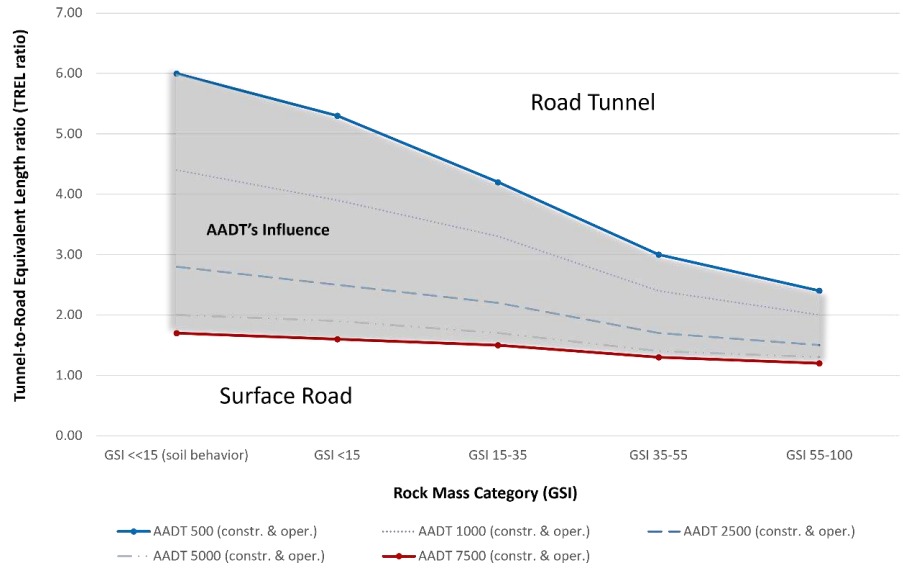

(**b**)

Fig. 2. (a) Impact of geotechnical conditions on the Tunnel-to-Road Equivalent Length (TREL) with respect to AADT. (b) Influence of AADT Tunnel-to-Road Equivalent Length (TREL) with respect to the rock mass categories (GSI) encountered during construction (Benardos and Skenderas, 2025).

3. Discussion - Conclusions

The selection between a tunnel and a surface road alignment is not always the clearest and most straightforward decision, as many parameters tend to fog the view of the stakeholders. The paper attempts to provide a clear statement on the value given by underground solutions.

This is evidenced by the analysis of the Mellisourgoi–Theodoriona tunnel alternative which demonstrates that the proposed tunnel alignment presents a robust investment with substantial socio-economic returns. The quantified benefits are significant, with annual savings enabling the full recovery of construction costs in just 4 to 5 years, depending on traffic volume. Beyond financial returns, the tunnel offers strategic value by improving mobility, stimulating regional development, and fostering environmental stewardship.

The addition of the comprehensive methodological framework and the introduction of the TREL ratio is particularly useful to accurately take into account biases in the form of geotechnical conditions and time valuation issues in a single index. The generalized tunnel vs. road analysis reinforces the idea that underground solutions often shine when evaluated in a holistic, long-term context. It provides evidence that, under a wide range of realistic conditions, a tunnel can deliver more net value than a surface road, especially as traffic grows. Some key takeaways from the study include:

- Traffic volume is the primary driver of cost-efficiency. Higher AADT means more users reap the travel time and cost benefits, thus justifying the tunnel's high initial cost more quickly. In high-traffic corridors, tunnels are highly advantageous if they shorten the route at all significantly.
- Geotechnical difficulty, while impacting construction cost, is a secondary factor in economic viability. Difficult ground raises a tunnel's cost, but in scenarios with substantial traffic, the incremental user benefits still outweigh these extra costs. However, in low-traffic cases, bad ground can indeed tip the balance against a tunnel by requiring an impractically large distance saving to justify it. Thus, both factors should be weighed, but one should not automatically dismiss tunnels due to geology without considering traffic and benefits.
- Underground alternatives generally have higher socio-economic value than surface roads for equivalent service, when one accounts for all external benefits. This stems from the fact that tunnels often enable superior service (shorter travel, less environmental impact) that is not captured in a simple construction cost comparison. The holistic analysis confirms the "generally stated opinion" that, beyond pure finances, tunnels provide broad societal advantages over roads in many cases.

It gives decision-makers a concrete threshold to consider when debating a tunnel investment. By establishing "how much longer can a road be before a tunnel is worth it," the TREL approach injects clarity into early project debates that are often clouded by uncertainty or bias. It encourages a direct comparison of alternatives on the basis of comprehensive cost-benefit outcomes, rather than merely comparing construction bids or initial budgets. In doing so, it helps reveal the latent value of tunnels that might be overlooked if one looked only at construction cost per kilometer (where tunnels fare poorly against open roads).

Hence, efforts like the ones presented in the paper strengthen the arsenal of those advocating for underground space development, while at the same time providing a structured threshold for decision-makers to seriously consider this option. Beyond the technical and financial metrics, what truly enhances the credibility of such projects is the systematic recognition of the broader societal value they generate, benefits that are often overlooked in conventional evaluations. These social benefits and the value offered to the community are key to "uncovering and monetizing the latent social benefits" of going underground, thereby shifting the cost–benefit calculus in favor of underground space development.

References

Benardos, A., Skenderas, D., 2025. Exploring the true cost of infrastructure transit projects: Road vs Tunnel alternatives. *Tunnelling and Underground Space Technology*, 162, 106624. https://doi.org/10.1016/j.tust.2025.106624

Blankespoor, B., Dasgupta, S., Wheeler, D., 2024, February 14. Riding into a greener future: How widespread use of subways could slash CO_2 emissions. World Bank Blogs.

Daub, 2023. Recommendations for the Determination of Lifecycle Costs for Tunnels. www.daub-ita.de

European Commission, 2015. Guide to cost-benefit analysis of investment projects: economic appraisal tool for Cohesion Policy 2014-2020. Publications Office. https://ec.europa.eu/regional_policy/sources/studies/cba_guide.pdf

Flyvbjerg, B., Holm, M. S., Buhl, S., 2002. Underestimating Costs in Public Works Projects: Error or Lie? *Journal of the American Planning Association*, 68(3), 279–295. https://doi.org/10.1080/01944360208976273

Godard, J. P., Hugonnard, J. C., 1989. Appraisal of underground urban public transportation projects. *Tunnelling and Underground Space Technology*, 4(1), 31–41. https://doi.org/10.1016/0886-7798(89)90030-8

Kaliampakos, D., Benardos, A., 2008. Underground space development: Setting modern strategies. WIT Transactions on the Built Environment, 102, 1–10. https://doi.org/10.2495/US080011

Kaliampakos, D., Benardos, A., Nomikos, P., Marinos, V., Zevgolis, I., 2024. Developing Mountainous Tunnels in Greece—The Case of the Melissourgoi Tunnel. In Proceedings of the 18th Conference of the Associated Research Centers for the Urban Underground Space, ACUUS 2023, 1–4 November; Singapore, Editors:Wei Wu, Chun Fai Leung, Yingxin Zhou, Xiaozhao Li. pp. 195–200. https://doi.org/10.1007/978-981-97-1257-1_26

Paraskevopoulou, C., Benardos, A., 2013. Assessing the construction cost of Greek transportation tunnel projects. *Tunnelling and Underground Space Technology*, 38, 497–505. https://doi.org/10.1016/j.tust.2013.08.005

Paraskevopoulou, C., Dallavalle, M., Konstantis, S., Spyridis, P., Benardos, A., 2022. Assessing the failure potential of tunnels and the impacts on cost overruns and project delays. *Tunnelling and Underground Space Technology*, 123, 104443. https://doi.org/10.1016/j.tust.2022.104443

OECD (2017). Quantifying the Socio-economic Benefits of Transport. https://doi.org/10.1787/9789282108093-en

Soleymani, H. R., Ismail, M., 2022. Challenges and new trends in infrastructure life cycle cost analysis. *International Journal of Sustainable Building Technology and Urban Development*, 13(2), 221–230. https://doi.org/10.22712/susb.20220018

Southeastern Europe Tunnelling Conference (SETC-2025)
1-3 October 2025, Belgrade, Serbia

DOI: 10.5937/SETC25035S

Strategic Planning for the start and completion of the longest sub-sea tunnel in the Middle East

Khalid Saif Al-Khayareen[a], Gary Peach[b] and Hernan Vigil Fernandez[c]*

[a] Public Works Authority, Doha, Qatar; kkhayareen@ashghal.gov.qa
[b] Mott MacDonald, Doha, Qatar; gary.peach@mottmac.com
[c] HBK-PORR JV, Doha, Qatar; hernan.vigil@auccqatar.com

Abstract: The outfall tunnel, which forms part of the Musaimeer Pump Station and Outfall Project (MPSO), is a 10.2 km long subsea tunnel that extends from the south coast of Doha, starting onshore, and continuing under the Arabian Gulf to end in a connection with a diffuser field via riser shaft. Whilst the tunnel presented many challenges on its own, this paper will concentrate on the extensive project management undertaken on the Tunnel Boring Machine (TBM) launching and supply arrangements, located only 50 m from the seashore and the equally complex arrangements for the outfall tunnel to connect 10.2 km offshore with the riser shaft and diffuser bed structure. The excavation of the outfall tunnel using a TBM with a 4.42 m diameter and 180 m long gantries, started from a 40 m deep shaft and has an inclination of 0.05% upward to the riser shaft. The enabling works which were substantial within themselves commenced 16 months before the TBM arrived on site.

The diffuser structure was a 6-arm structure, measuring 294 m by 40 m connected to a central manifold in turn connected to the TBM constructed tunnel via a riser shaft drilled from an offshore platform and barges. These works took 28 months to complete to ensure the outfall tunnel which was the most critical portion of the whole project was completed on time.

This technical paper will discuss the planning, methodology and construction practices employed to the onshore and offshore structures to ensure the outfall tunnel was a project success

Keywords: TBM; Sub-Sea tunnel; enabling works; logistics tunnel; riser shaft

1. Introduction

The complex enabling work starts on the surface where all the required facilities to run the TBM must be strategically deployed. In general terms those facilities are related to the logistics to receipt of the container where the TBM is delivered in major or minor parts and areas to store TBM parts and preassemble them. Other facilities are related to the store of temporary materials, e.g. high and low voltage cables, water pipes in the tunnel, ventilation ducts, rails and rails preassembly facilities, power plant generation, silos for cement, bentonite and additives, precast segments. In addition, the road layout and traffic management must be perfectly designed to allocate the heavy traffic while transporting all the consumables required including the precast rings and muck disposal from the TBM.

There is another type of enabling works with less visual impact, but one of the most critical from the TBM operatives' point of view. This is access to the tunnel portal via shaft not only for the lowering and assembly of the TBM but also to provide the bay via tunnel to park and operate the rolling stocks which provide the logistics to the TBM, i.e. transportation of personnel in and out of the tunnel, removal of excavated soil, transportation of the precast rings, grout and general consumables needed to operate the TBM in regular basis.

*Corresponding author: kkhayareen@ashghal.gov.qa (Khalid Saif Al-Khayareen).

The project requirements were set in 3 trains making necessary to excavate a logistic tunnel to have space enough to park the trains and facilitated the operation of loading and unloading at the bottom of the shafts.

Last but not least, the location and quality of the welfare to serve the site team also need to be established with the project boundaries along with the workshop area which provide services to the TBM.

2. Underground enabling works

2.1. Main elements

The connection between the outfall tunnel and the pumping station is through a drop shaft. Water is pumped out from the wet well into an outfall chamber before being discharged via the drop shaft into the outfall tunnel. The drop shaft will be used not only as the TBM launching shaft during the construction phase but also to provide logistics and access to the TBM and outfall tunnel itself.

The drop shaft is a 10 m internal diameter circular shaft, which is approx. 11.4 m above ground level (i.e. at the level of +14.0 m QNHD, Qatar National Height Data) and extends to about 43 m below ground (i.e. at level of -41.23 m QNHD) with total of height of approx. 55.23 m.

The diameter size of the drop shaft is not big enough to be used as TBM logistics shaft and for that the initial plan was to enlarge it to allow the assembly of the TBM, its regular operation including logistic operations and access during the construction of the outfall tunnel.

2.2. Initial concepts

Once the Qatari Public Works Authority (Ashghal) awarded the MPSO project to joint venture HBK-PORR at the end of 2017, the initial option 1 was to use a launching shaft with rectangular pit shape and size of (31 x 20 on the surface and 25 x 14 at the bottom) and 43 m deep. The bottom of the launching shaft provides access to the logistics tunnel and TBM launcher chamber that were planned to be excavated to allocate the 3 tracks and switches required to operate the rolling stocks which serves the logistics to operate the TBM and the required chamber to launch the TBM. Fig. 1 below, shows the top and longitudinal profiles of the logistics tunnel, drop shaft and TBM launching chamber.

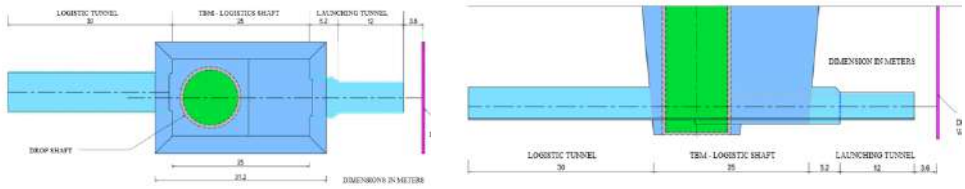

(a) **(b)**

Fig. 1. Initial proposal Top view (a) longitudinal view; (b) Logistics tunnel, drop shaft and launching chamber.

Option 2 evaluated at the early stage of the project was an oval shape launching shaft, as indicated in Fig. 2. Instead of a rectangular pit, the aim would be to reduce the excavation and support quantities while simultaneously improving the stability of the shaft due to the oval shape.

The options of a launching shaft allocating internally the drop shaft once the TBM finishes the excavation of the outfall tunnel seemed to be the optimum solution. However, considering the constraints and particularities of the outfall tunnel i.e. only one TBM to excavate the outfall tunnel, a long subsea tunnel with more than 10 km and only one access and egress, all together represented a risk increment of unexpected delays and if any delay happens during construction of the outfall tunnel,

it directly affects the construction of the drop shaft and the connection of the outfall chamber and subsequent installation of utilities and land scape activities on the surface, jeopardizing the overall completion date of the project.

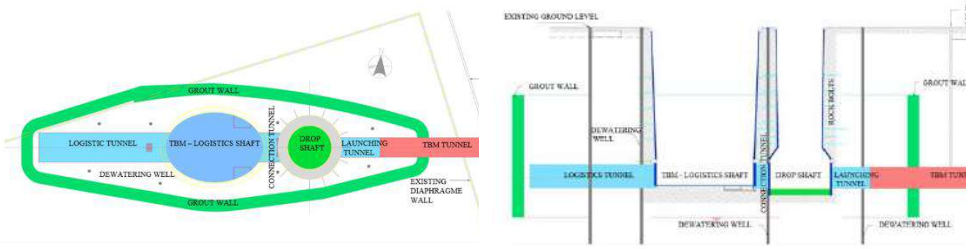

(a) **(b)**

Fig. 2. Option 2 Top view (a) Longitudinal view; (b) of Logistics tunnel, drop shaft and launching chamber.

2.3. Logistics Shaft and Drop Shaft (concept)

The decision to excavate independent shafts simultaneously aimed to reduce the pressure on the project completion date. Delays during the construction of the outfall tunnel would still allow the construction of the permanent works of the drop shaft, its connection with the outfall chamber and the surrounding land scape and rock armour among others to go ahead. This method also foreseen the possibility of back filling with low strength mass concrete in the case of time constraints.

Fig. 2 show the location of the drop shaft and logistics shaft connected in between by a short connection tunnel.

The mechanical excavation method was the method selected to excavate both shafts and Sprayed Concrete Lining (SCL) with wet shotcrete, wire mesh and rock bolts was the primary lining support. The logistics shaft construction due to the oval shape resulted in the construction of concrete reinforced stiffening rings to improve the stability of the shaft. The drop shaft had the provision of the key at the bottom, not only to allocate the base slab and to control the buoyancy, but also to allow the simultaneous construction of the final concrete lining support and provide the required openings to move the TBM logistics trains.

2.4. Logistics Shaft and Drop Shaft (Grouting and dewatering works)

The project area is enveloped within a cut off wall of an average depth of -34 m QNHD. This cut off wall was constructed on a pretender project phase to approximately 18m below ground level. No water or very small water ingress was expected. However, the excavation depth reaches at maximum -40 m QHND and therefore dewatering was required to lower and maintain the water table below formation level. Dewatering was performed through 8 deep wells, installed with submersible pumps which discharged ground water to the sea through sedimentation tanks.

In addition to dewatering, to mitigate the risk of water ingress, extensive rock grouting was carried out around the shaft, the future logistics tunnel and TBM launching chamber. Fig. 3 shows the location of the boreholes used to create another cut of wall (with primary and secondary boreholes for water tightness) all the way around the shafts and tunnels with a tertiary borehole within the excavation area of the shaft and tunnel. This acted as a grout plug preventing the ingress of water from the invert and reduced any settlement, see Fig. 3. In total 76 primary, 75 secondary and 62 tertiary grouting boreholes were drilled resulting in 10,468 meters of boreholes and 1,421,754 litres of grout. The grout mix design was based on OPC cement, bentonite, and stabilizer with W/C ratio from 1.2 to 1.8 depending on the site conditions.

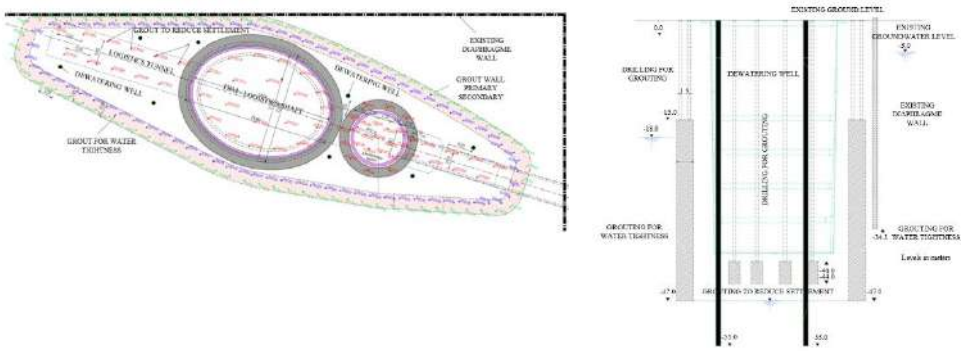

(a) **(b)**

Fig. 3. Rock grouting primary, secondary and tertiary plan (a) and section (b).

2.5. Logistics Shaft and Drop Shaft (excavation works)

The excavation works and application of the primary support consisting of Sprayed Concrete lining (SCL) in logistics and drop shaft was designed to be installed simultaneously. The excavation was done by using conventional excavators (with more than one excavator working in the shaft at the time as shown in Fig. 4 with drum cutter and hydraulic hammer while the primary support was based on sprayed wet shotcrete reinforced with wire mesh (double layer) with rock bolts.

The adjustment of every cycle length (between 2 and 3 m) along with the type of support to be applied was determined on site by the Geotechnical Engineer based on actual face mapping.

Excavation was executed in 3 different phases, each phase having its own method of works. Fig. 4 illustrates the 3 separate phases of excavation for the logistics and drop shaft works.

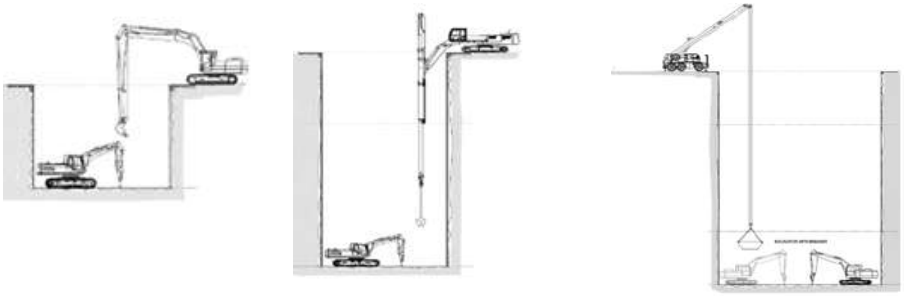

(a) **(b)** **(c)**

Fig. 4. Logistics and Drop Shaft Excavation Plan. (a) Phase 1: GL to -8 m; (b) Phase 1: GL to -8 m to -30m; (c) Phase 3: -30 m to -43 m.

As a preventive measure, where some water could penetrate inside the shaft because of the rock porosity and where rock grouting method could not seal all the gaps in hard rocks, weep holes were installed to drain the water and to reduce the water pressure on the shotcrete lining.

The water was collected at a dedicated water sump at the bottom of the excavation (one sump at each step of excavation), from the sump the water was pumped to the surface sedimentation tank.

Fig. 5. Photo of the logistics and drop shaft during TBM operations.

2.6. Logistics and Connection Tunnel. Launching Chamber Tunnel (excavation works)

The configuration of logistic and drop shafts required an internal connection tunnel, the TBM rolling stock required space to operate, load, offload and park the trains underground according to the logistics cycle. The launching technique of the TBM required a launching chamber, see Fig 5. The New Austrian Tunnelling Method (NATM) was the method selected to excavate the required tunnels namely:

- The NATM connection tunnel section between the 2 shafts of 4.30 m length.
- The NATM logistics tunnel extending to the land side of 30 m length.
- The NATM launching tunnel extending to the seaside (launching tunnel) of 10 m length.

The NATM sections commenced with the connection tunnel between drop and logistic shaft allowing full access for equipment and manpower at the formation level. Then NATM logistics and launching tunnel excavation commenced. The breakthrough of the connection tunnel was performed when both shafts had reached final NATM invert formation level (-38.23m QNHD).

NATM tunnel construction sequence included repeating the same sequence until full completion of each excavation cycle. Once the excavation step was fully supported according to the design drawings, then the following step could commence following the exact same sequence.

The sequence was as follows: survey works, excavation, soil disposal, scaling, survey check of the excavation line and correction if and where required, geological mapping and classification of the rock mass, recommendation of the supporting class for the rock mass classification and design criteria.

Fig. 6 summarized the NATM tunnel sections required for each tunnel.

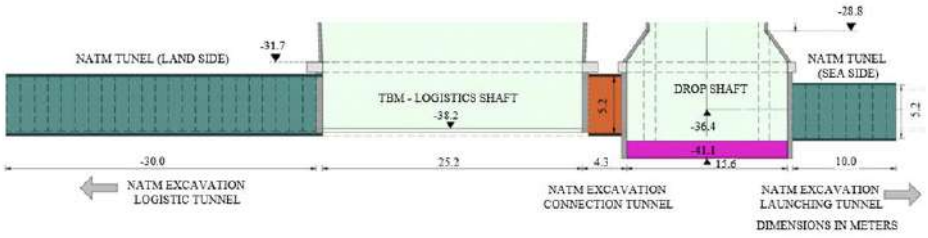

Fig. 6. NATM tunnel sections logistics, connection and launching tunnels. (a) Longitudinal profile Logistics Tunnel, Logistics Shaft, Connection Tunnel, Drop Shaft, TBM Launching Tunnel.

3. Geotechnical risk, other risks and mitigation measures during Outfall tunnel Construction

3.1. Karstification

Karst features are widespread in Qatar, with more than 9,700 depressions, sinkholes, and caves, mainly within the Eocene Rus and Dammam Formations. Gypsum, far more soluble than limestone, accelerates the formation of voids and collapses, especially in central and southern Qatar. These features often align NE-SW and NW-SE, following fracture systems, and were formed through dissolution of carbonate and sulfate deposits during Middle Pleistocene wet periods.

Large subterranean voids (>2 m) cause localized weakness that may collapse into sinkholes, simple, or compound depressions. Larger features are prevalent in central and southern Qatar, linked to dissolution of the sulphate facies in the Rus Formation. In the north, smaller features formed downward through fractures in the Simsima Limestone and Rus Formations during tectonic uplift, with upper layers more affected than deeper strata.

3.2. Hydraulic connection to the seabed

Potential hydraulic connectivity between the seabed and the TBM tunnel would impose full hydrostatic pressure on the cutterhead. Although 55% of the alignment passed through competent, low-permeability rock (confirmed by RQD and Lugeon tests), 25% consisted of weaker, more permeable zones. To mitigate, the TBM was designed to withstand up to 4.5 bar.

3.3. Mitigation of geotechnical risks

The contract required 24 offshore boreholes, but these were deemed of limited benefit for understanding hydrogeology and karst. Instead, the contractor proposed detailed marine geophysical surveys to identify cavities, seawater zones, weak rock, and discontinuities between existing boreholes. This approach, approved by the Client, provided a broader and more continuous geological model. Two advanced offshore methods were implemented: Electrical Resistivity Tomography (ERT) and Seismic Reflection Geophysical Tomography, delivering critical insights to reduce tunnelling risks.

3.4. Other risks mitigations

Plan for Advance Tunnel (PAT) was developed and implemented. This tool combining geotechnical and geophysical data improved understanding of rock mass, identified critical tunnelling areas, optimized TBM intervention points, and reduced risks. Cutterhead inspections, maintenance, and repairs are safest under atmospheric conditions; in poor ground, hyperbaric support may be required. Ground conditions are classified per meter: favourable (atmospheric only), moderate (atmospheric preferred, hyperbaric possible), and unfavourable (interventions avoided unless essential).

The TBM, designed per 2010 tunnelling specs and manufactured by CREG/Wirth, is an EPB type capable of 4.5 bar pressure. Key components include cutterhead, chamber, main bearing, screw conveyor, shields, personnel locks, thrust and erector systems, and tail brushes. With 18 gantries (160 m long), it houses electromechanical parts, tanks, and rescue chambers. The TBM installs six-segment concrete rings, 1.35 m long, with a 3.7 m internal diameter.

Real-Time Non-Destructive Monitoring. The TBM features BEAM (Electrical Ahead Monitoring), a non-intrusive polarization system predicting ground conditions up to three diameters ahead. It detects resistivity variations and displays predictions in a matrix combining resistivity and Percentage Frequency Effect (PFE).

4. Outfall tunnel construction

The outfall tunnel was constructed using an Earth Pressure Balance EPB TBM, which was designed to withstand the full hydrostatic pressure of 4.5 bar. The outfall tunnel alignment encountered and successfully managed three main geological strata, namely: Rus formulation, Midra shale and Simsima limestone. Several technical challenges arose and were managed, and the outfall tunnel was completed 56 days ahead of programme. For omitted details please refer to Peach et al 2022 and Stypulkowski et al 2023.

4.1. TBM utilization

The design and selection of tunnel logistics directly impact excavation, and performance is measured through TBM utilization. This allocates time to designated activities, eliminating overlaps, and is calculated from daily shift reports consolidated into spreadsheets. Utilization analysis helps assess efficiency, workmanship, and issues, while identifying areas for optimization such as locomotive transport idling.

Production activities are:

1. Excavation,
2. Ring building,
3. Maintenance, and
4. Extending temporary services.

All other activities are delays, classified into three groups: Mechanical & Electrical, Operational, and Geological. Operational delays also include data to evaluate transport efficiency and the need for a second California crossing.

Excavation was required to achieve 40% of the available time; logistics exceeded this benchmark. Fig. 7 illustrates a typical of TBM utilization summary recorded during tunnel construction.

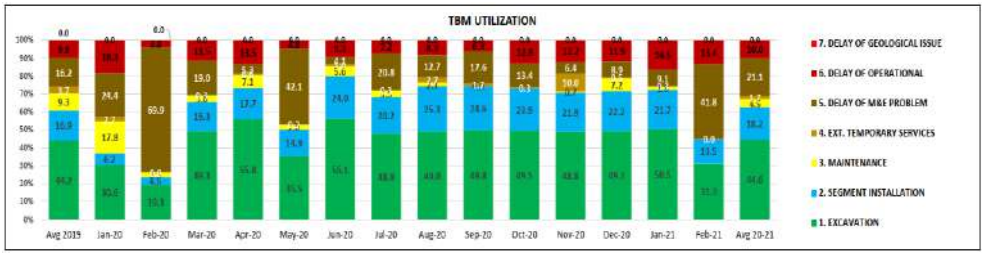

Fig 7. TBM utilization graph 2019 – 2021.

4.2. TBM progress: Baseline vs actual

The baseline programme planned a 300 m learning curve (May–June 2019) followed by 27 sections up to April 2021, assuming 24 h/day and 6 d/week.

Due to early TBM procurement and logistics, excavation began 90 days early. Despite delays causing a 14.1-day deficit by May 2020, operations recovered, and the tunnel was ultimately completed 58 days ahead of schedule. This achievement was more notable as only one California crossing was used. Refer to Fig.8.

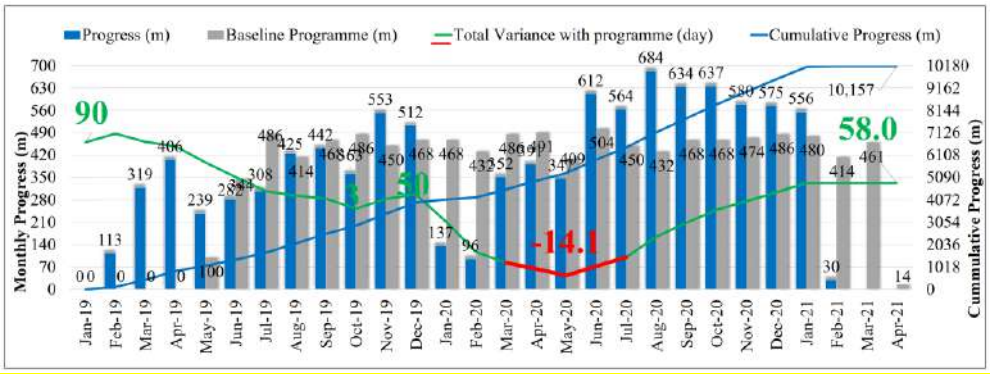

Fig 8. TBM tunnel progress summary V baseline programme up to 03 February 2021.

5. Diffuser field structure

5.1. Riser Shaft and diffuser filed arrangements

The marine diffuser field structure is shown in Fig. 9. The central manifold was located directly on top of the riser shaft and a concrete structure measuring 4 m x 4 m x 4 m and weighing 120 tons. Connected to the main manifold were 6 radial arm structures which either directly connected to the manifold or were connected by short secondary manifolds. Each arm is 140 m long and is separated from the adjacent arm by 35 m. This makes the entire structure outline 294 m x 70 m. The secondary manifolds and 6 arms were manufactured out of High-Density Polyethylene (HDPE) pipe and are of various diameters i.e. 2000,1400, 1200 and 710 mm to ensure an even flow throughout the various arms at varying flow rates from the pump station. The discharge from the structure to the sea is via 84 duck bill valves located equal spacing along the 6-arm structure.

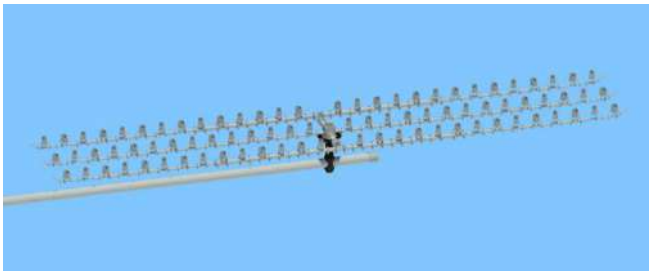

Fig. 9. Marine diffuser field structure, riser shaft and TBM outfall tunnel.

5.2. Riser Shaft Construction

The riser shaft is the structure which connects the TBM outfall tunnel to the marine diffuser bed. The invert of the outfall tunnel is 14.5 m below the seabed and the depth of the sea at this location is 15.5 m. The first stage in the construction was carried out by a dredger which on average removed 2.5 m of loose sediments located on the seabed. Near the riser shaft a further 2 m is excavated to ensure competent strata is exposed which will improve the drilling operation required to construct the riser shaft.

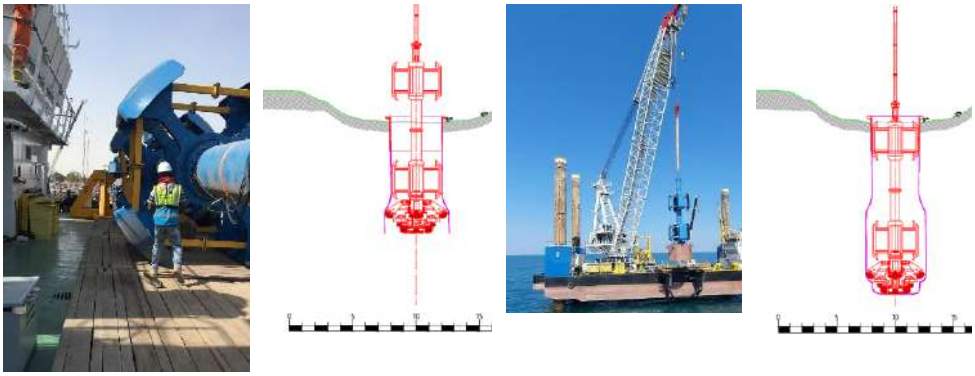

(a) (b) (c) (d)

Fig. 10. With the dredging complete the next stage of the construction was carried out from a jack-up rig which was located directly adjacent to the centre line of the riser shaft. A cantilever frame was then installed to the side of the jack-up rig, this was the location the drilling equipment was installed. (a) The drilling rig or Bottom Hole Assembly (BHA); (b) and (c) the BHA was lowered down to the correct location and commenced to drill the rise shaft; (d) the BHA can drill various diameter holes from 4 to 5.3 m by use of extending hydraulically activated arms to suit the desired diameter of the shaft. In this case the first section was drilled at 4 m diameter and the arms or extended out, to the 5.3 m settings. The 5.3 m section was the location through which the TBM excavated, giving a clearance of 500 mm each side of the TBM, which has an outer diameter of 4. 3 m.

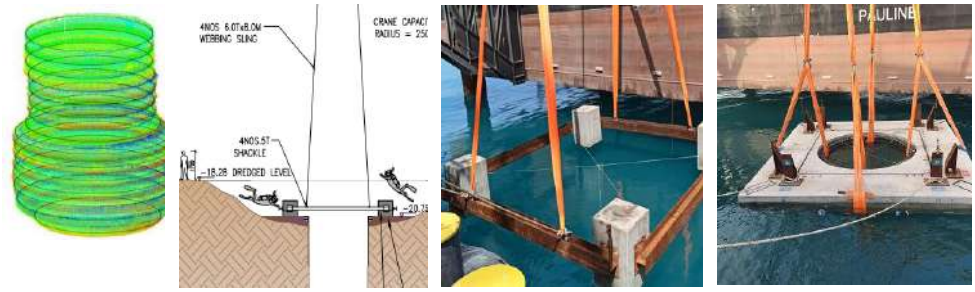

(a) (b) (c) (d)

Fig. 11. (a) on completion of the riser shaft drilling the BHA was then removed, and a three-dimensional survey carried out to determine the exact dimensions and position of the riser shaft; (b) the next stage was to install a steel casing into the top 3 m of the riser shaft, to provide stability and prevent collapsing of the shaft inwards; (c) Four Concrete manifold foundation blocks were then positioned and levelled into the correct requirements and connected to the steel casing; (d) a manifold concrete base slab was then positioned on top manifold foundation blocks.

The void between the GRP cylinder and the whole of the lower portion was then filled with a grout mixture which filled the void in a controlled manner, slowly displacing the seawater.

When the grout had cured the kentledge was removed and then the internal steel frame was removed, and the upper flanged secured and sealed to the top of the GRP cylinder. Both top and bottom ends of the GRP cylinder had a series of valves installed to allow venting of water. The upper valves were then used in connection with compressed air to remove all the seawater within the GRP cylinder and leave only air inside.

The central manifold which collects the combined ground and storm water from the outfall tunnel and then distributes evenly to the diffuser structure, was constructed onshore, and weighed 120 tons. The

concrete manifold is shown in Fig. 13 (b) and is then lowered and positioned on top of the riser shaft and connected to the manifold base slab as shown in Fig. 13 (c).

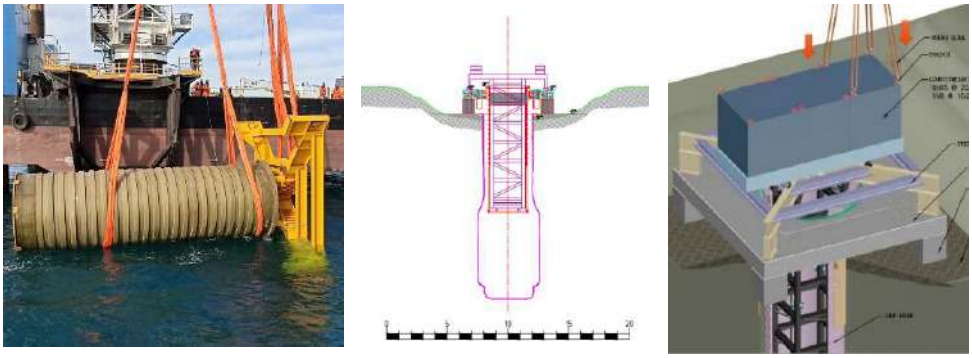

(a) (b) (c)

Fig. 12. (a) the riser shaft internal lining protects downwards from the base of the concrete manifold to 500 mm above the TBM outfall tunnel and is made from Glass Reinforced Plastic (GRP). This is a cylindrical shape with a fixed end at the lowest end and a removable flange at the other end. The upper flanged end is removed, and a temporary steel support frame is installed within the GRP cylinder; (b) The GRP cylinder and steel frame were then installed into the riser shaft and positioned centrally within the riser shaft and connected to the four manifold foundation blocks and base slab. At this point the riser shaft was still full of sea water; (c) shows the temporary kentledge which was then placed on top of the whole structure to prevent uplift during the grout placement.

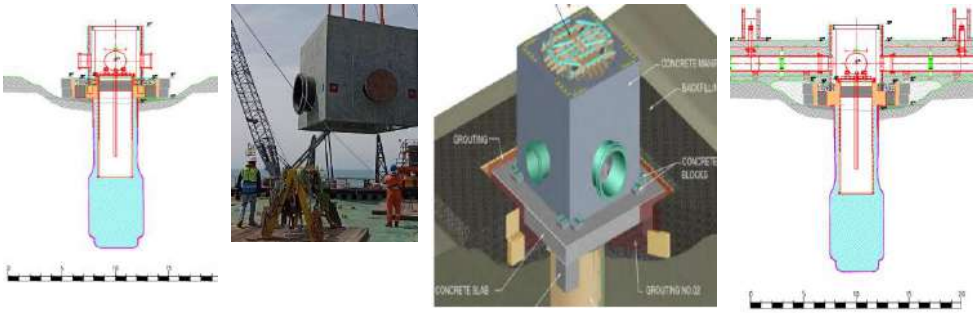

(a) (b) (c) (d)

Fig. 13. (a) the grouting operation; (b) concrete manifold; (c) manifold base slab; (d) diffuser field connection.

In due course all the diffuser field structure is connected piece by piece to the central manifold until the full diffuser bed structure is installed and covered with back fill material. Then a final layer of scour protection was installed covering the entire diffuser bed structure. At this point the riser shaft structure is ready to receive the TBM constructing the outfall tunnel.

5.3. Onshore fabrication

All the major components of the offshore diffuser bed structure were manufactured at two onshore locations in the Doha area. The major components include pipe work in a) HDPE Pipe and Connections b) Concrete Manifold c) Concrete Protection box d) Concrete collars

The main fabrication site was located at Milaha port south of Wakra, Doha. In this site all the above except the concrete collars were fabricated and assembled. These are shown in Fig. 14. To ensure an equal flow through the entire length of each of the six arms each start at 2.0 m diameter and then reduce to 1.4 m and then finally to 1.2 m.

(a) **(b)** **(c)**

Fig. 14. Onshore fabrication works. (a) Milaha Port site; (b) HDPE pipework being assembled; (c) HDPE pipework transition.

5.4. Component transportation

When each section of the diffuser field pipe structure was complete it was then assembled on shore, end was then capped with a blank flange to ensure water does not get the inside of the pipe. The pipe was then launched onto the sea, the structure was then towed out to the diffuser bed location. Fig. 13 (c) shows a pipe structure in process of being towed out to the diffuser bed location. The Concrete manifold was transported separately by barge.

5.5. Installation of Diffuser Field Structure

After the various elements of the diffuser structure had been transported to the final location, they were anchored and stored ready for installation. The main barge was positioned in line with the final seabed location. The individual sections were then manoeuvred into correct position and then the central manifold sections lowered into position first using a barge mounted crane. Final under water positioning was carried out by specialist divers. The sections of pipework and then the next section of the structure were installed. The first sections installed were the ones which connect to the central manifold, then followed by sections moving out from the central manifold. The pipe section was manoeuvred into position and buoyancy aids attached to the full length of the pipe. Water acting as ballast was slowly allowed to enter the pipe section resulting in the structure submerging in a controlled manner to the seabed, refer to Fig. 15. The final positioning was carried out by specialist divers simultaneously attaching to the already installed elements. The whole structure was then assembled section by section in this manner until the full diffuser arrangement was complete.

(a) **(b)** **(c)**

Fig. 15. Launching of pipe elements from onshore to the sea. (a) Central manifold; (b) Pipe section with buoyancy aids; (c) Submerging the pipe.

5.6. Backfilling and Scour protection

On completion of the diffuser bed structure the sequence of work was to backfill the structure for stability. The scour protection installation made of specially designed concrete followed. For the protection boxes for each of the 84 duck bill valves

5.7. Connection to Outfall Tunnel

The programme for the overall project required the diffuser bed structure to be completed prior to the arrival of the TBM, which was achieved, refer to Fig. 16.

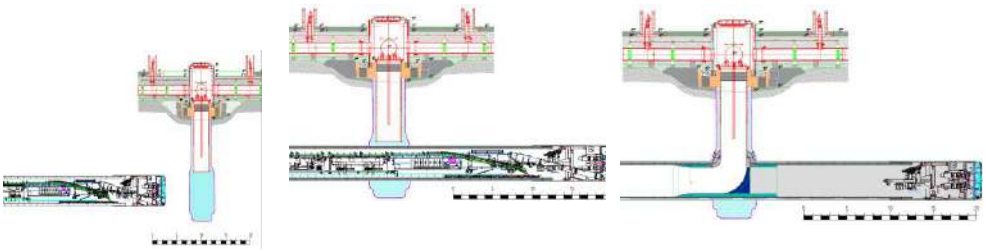

(a) **(b)** **(c)**

Fig. 16. (a) The TBM reached to within 5 m of the riser shaft and depressurized the cutterhead and monitored the situation for any water inflow over 8 hours; (b) Since there was no water inflow the TBM excavated through the lower portion of the riser shaft and stopped 25 m beyond the riser shaft; (c) Embedding the unsalvageable part of TBM.

The TBM and associated plant and equipment was then dismantled and removed back through the outfall tunnel and at the pump station location removed to the surface. The 25 m section of tunnel beyond the riser shaft was filled with concrete. What followed was very intricate and complex series of construction activities requiring precise logistical planning and execution to complete the connection of the outfall tunnel to the riser shaft and installation of the permanent works all of which was carried out 10.2 km offshore.

6. Lessons learnt

6.1. TBM in very dry conditions

During the learning curve, excavation in the Rus Formation met expectations. After ring 450, mixed Rus–Midra Shale with higher clay slowed progress. Between rings 550–1150, fully in dry Midra Shale, large amounts of foam and water were required to control torque and thrust. Conditioner use rose from 2.4 to 25.5 m³/ring, doubling excavated volume from 4 to 8–9 skips per ring. This required 2–3 trains instead of one. To mitigate, the California crossing was advanced to ring 550.

6.2. TBM in very high-water pressure

Two high-pressure zones occurred in weathered Simsima Limestone connected to the seabed: rings 2,000–2,130 and 2,830–4,100, where face pressure reached 3.5 bar. The TBM was adjusted to closed mode, operators briefed, and polymers tested to stabilize inflow. Two strategies were compared: slow advance with polymers (4–6 mm/min) or faster advance without polymers, conditioned only with foam (12–15 mm/min). The second option was adopted to balance safety and progress. Logistics adapted to

5 skips per ring, with all three trains modified. Only one California crossing was installed, relocated weekly to minimize idle time.

6.3. Covid pandemic

Considering the tunnel construction period incorporated the entire COVID-19 pandemic period, 2020/21 Effectiveness of COVID-19 Mitigation Measures: The absence of recorded COVID-19 cases among tunnel operatives highlights the efficacy of the safety measures. Strategies such as social distancing protocols, enhanced disinfection routines, and isolated accommodations minimized transmission risks and ensured personnel safety.

7. Conclusions

The construction of the drop shaft and its connection to the outfall chamber was accomplished before the TBM achieved the tunnel completion, and there was no TBM idle time due to logistics issues neither on the surface or underground.

The construction of other permanent structures in the pump station were not impacted due clashes with the TBM enabling works which confirms the importance of a good plan and clash analysis at the early stage of the project. Starting the required enabling works with 16 months ahead of the TBM arrival mitigated the risk associated with the underground enabling works.

This was the first of three possible outfall projects planned by Ashghal for the long-term management of rising ground water level and storm events, which will bring significant benefits to the population of Doha and surround areas.

Acknowledgements

The project was a significant success, and appreciation is extended to all parties for the successful completion of this project.

References

Aradas, R., Tsingas, D., & Martini, M. 2020. The design of a segmentally lined tunnel for a large sewer outfall – Lot 3, Riachuelo Outfall, Argentina. In Tunnels and Underground Cities: Engineering and Innovation Meet Archaeology, Architecture and Art

Construction Management Plan C2017_109-PLN-CO-0003

Design criteria report for Drop Shaft C2017_109-RPT-PD-ST-DS-0001

Stypulkowski J.B., Najder Olliver A.M., Khalid Saif F S Al-Khayareen, 2023. Risk Management in Outfall Tunnelling, the MPSO Tunnel, Doha, Qatar. in "*Expanding Underground. Knowledge and Passion to Make a Positive Impact on the World*" Anagnostou, Benardos & Marinos (Eds) © 2023. The Editor(s), ISBN 978-1-003-34803-0, Open Access: www.taylorfrancis.com, CC BY-NC-ND 4.0 license, ITA-AITES WTC 2023, Athens, Greece

Peach, G., Vigil, H. & Sucipto, H. 2022. TBM Sub-Sea Tunnelling in the Arabian Gulf. WTC 2022. Copenhagen, Denmark.

Public Works Authority 201). Contract Documents for Design, Build, Operate and Maintain of Musaimeer Pumping Station and Outfall, Project ID: IA 14/15 C 015 G, Contract Number: C2017/109.www.ashghal.gov.qa

Peach, G. & Vigil, H. 2022. TBM Tunnel logistics management on the longest outfall tunnel in the Middle East. NAT 2022. Philadelphia, USA.

Qatar Construction Specifications 2014. (QCS-2014)

Specification for tunnelling, Third edition, The British Tunnelling Society, and Institution of Civil Engineers, 2010

The British Standards Institution 2011. BS 6164:2011 Code of practice for health and safety in tunnelling in the construction industry, BSI Standards Publication, London. www.bsigroup.com

Valiante, N., Martini, M., & Gaggioli, L. 2019. Riachuelo Lot 3 – Innovative method for the construction of the sea outfall. Proceedings of the World Tunnel Congress 2019 (WTC 2019), Naples, Italy.

Southeastern Europe Tunnelling Conference (SETC-2025)
1-3 October 2025, Belgrade, Serbia

DOI: 10.5937/SETC25036L

Tunnelling Under Great Lakes

Boro Lukajic[a]* *and Milica Milojevic*[b]

[a] Chairman Emeritus TAC, 2593 Vineland Rd. Mississauga, Ontario, Canada; tac@interlog. com
[b] Independent research consultant, 19 Misdale Road, Brampton, Ontario, Canada; milicamilojevic05@gmail.com

Abstract: Ontario has constructed five large diameters under the Great Lakes (Lake Erie, Lake Huron and Lake Ontario). Tunnels were driven by a drill-blast method through a variety of rock conditions, ranging from high water inflow conditions to highly stressed ground. This combined with the design and operational requirements had a major influence on construction approach, which ranged from continuous grouting to control water seepage to a special excavation and tunnel lining sequence to accommodate time-dependent deformations. The emphasis in this paper will be on the construction approach in completion of cooling water tunnels driven under Lake Erie, Lake Huron and Lake Ontario. Tunnels serve Ontario nuclear generating station.

Keywords: maximum 6 keywords; paper format; instructions; use of template

1. Introduction

The locations of three generating stations (Nanticoke, Bruce and Darlington), subject of this paper, were chosen on the basis of their proximity to the residential and industrial markets of Ontario as well as an abundant supply of cooling water from the adjacent lakes. Tunnels, described in this paper, are needed to convey cooling water from lakes into the generating stations. Currently, Ontario operates three nuclear stations, using CANDU type technology in a partnership with Atomic Energy of Canada Limited (AECL), the Hydro-Electric Power Commission of Ontario, Canadian General Electric, and other companies.

2. Ontario Electricity by Fuel Source

Ontario's electricity system is designed to support the needs of approximately 5.25 million residential and small business customers, 53,000 commercial consumers and 400 industrial consumers. The Province has over 30,000 km of transmission lines and over 260,000 km of distribution lines.

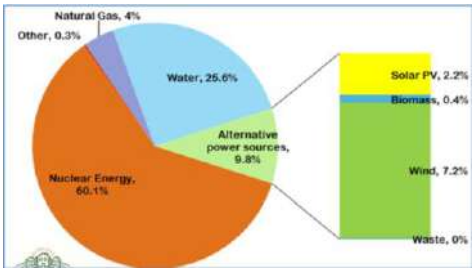

Fig. 1. Ontario electricity by fuel type.

*Corresponding author: tac@interlog.com (B. Lukajić).

3. Canadian Reactor (CANDU)

The CANDU (Canada Deuterium Uranium) is a Canadian pressurized heavy-water reactor design used to generate electric power. The acronym refers to its deuterium oxide (heavy water) moderator and its use of (originally, natural) uranium fuel. CANDU reactors were first developed in the late 1950s and 1960s. Fig. 2 is a schematic view of the reactor.

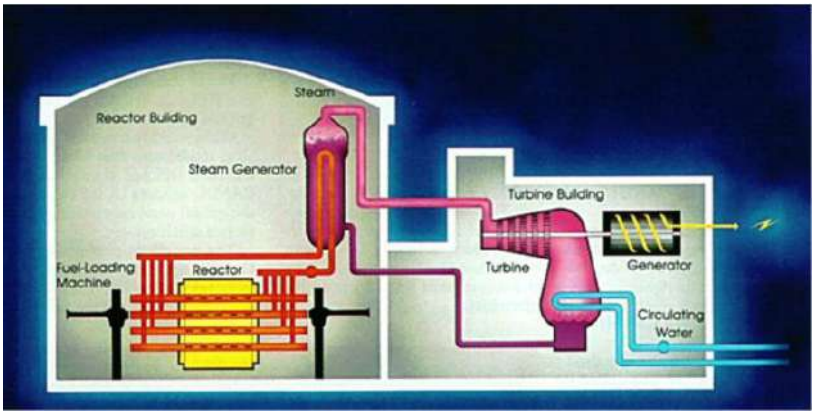

Fig. 2. Schematic view of the CANDU reactor.

4. Waters of the Great Lakes

Fig. 3. Great Lakes geographic layout.

For many years Ontario has used the waters of the Great Lakes for the generation of electricity for the Province; first for the hydro-electric developments on the Niagara River leading from Lake Erie to Lake Ontario and more recently as cooling water in nuclear generating stations. Domestic use for drinking water from Great Lakes has been practiced for many years. The Great Lakes began to form at the end of the Last Glacial Period around 14,000 years ago, as retreating ice sheets exposed the basins they had carved into the land, which then filled with melt-water. The Great Lakes consist of five

freshwater interconnected lakes being Lake Superior, Michigan, Huron, Erie and Ontario. They are a critical component of the regional economy on both sides of the border. Great Lakes vary in depth, Lake Superior being the deepest (over 400m) and largest in size (over 82,000 km²).

5. Tunnelling Under Lake Erie

Lake Erie is the fourth-largest lake by surface area of the five Great Lakes in North America and the eleventh largest globally. It is the southernmost, shallowest, and smallest by volume of the Great Lakes. It is situated on the international boundary between Canada and the United States. As per Figure 4, the Nanticoke Generating Station is located on the Northern shore of Lake Erie. It was constructed as a coal-fired power station, in operation from 1972 to 2013. At the time, it was the largest coal-fired station in North America and it provided 3,964 MW of power into the southern Ontario power grid. A few years back, it has been transformed into a 44-megawatt clean energy facility that hosts 192,431 solar panels across 260 acres.

Fig. 4. Lake Erie location

As illustrated in Figure 5, an intake, cooling water tunnel, was constructed under the lake. The geology of the area consists of sedimentary rocks, limestone and shale. His was the first cooling water tunnel constructed for thermal generating station. Since the tunnel was driven through water-tight sedimentary formations there were no challenging risks facing the contractor's works. Conventional drilling, blasting, scaling, rock bolting and concreting were used to construct/excavate the tunnel. Tunnel was excavated with Atlas-Copco ladder drills. A crew of 12 men worked on the drill Jumbo assembly. Total time to drill an 11 feet advance was 3.5 hours. Shotcreting was used to temporarily support the tunnel arch. Concrete lining was installed in a final phase of the construction.

Fig. 5. Tunnel profile and concrete liner sequence.

6. Tunnelling Under Lake Ontario

Figure 6 shows Lake Ontario configuration. The lake is one of the five Great Lakes of North America. It is bounded on the north, west, and southwest by the Canadian province of Ontario and on the south and east by the U.S.

The Canada–United States border spans the centre of the lake. The Canadian cities of Hamilton, Kingston, Mississauga, and Toronto are located on the lake's northern shorelines. Lake Ontario serves

as the outlet to the Atlantic Ocean via the Saint Lawrence River, comprising the western end of the Saint Lawrence Seaway.

Fig. 6. Lake Ontario Location.

A 3,512 MW Darlington Generating Station is located on the north shore of Lake Ontario approximately 60 km east of Toronto, Ontario, (see Figure 6 above). The construction cost was $14.4 billion, 1980s CAD ($23.8 billion in 2021approximately). A required cooling water flow is conveyed into the station via a 1,000 meters long intake tunnel and discharged into the lake through a series of vertical diffusers extending 1800 m offshore, see Figure 8, below.

Fig. 7. Layout of the Darlington generating station.

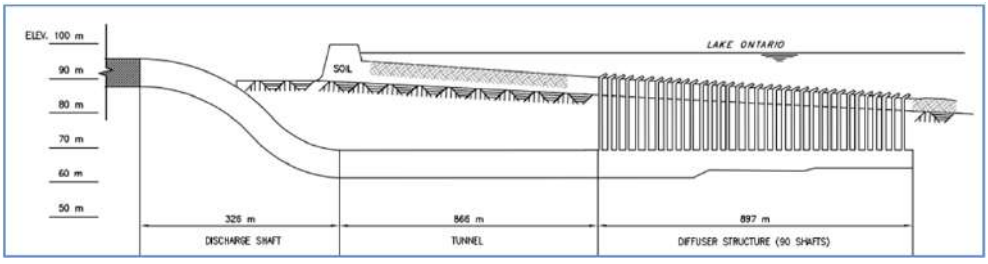

Fig. 8. A profile of the diffuser tunnel at Darlington generating station.

The intake and discharge tunnels were excavated through massive limestone. Due to the presence of high horizontal stress in rock, the rock joints remained closed and as a result, tunnels were dry, not yielding any water inflows. This resulted in high excavation daily rates. A comprehensive rock mechanics program was carried out in both tunnels to address in-situ stress issue and to ermine the time delay required between excavation and installation of concrete lining. A waiting period of 90 days was built into the construction schedule to allow for time-dependent deformation stress relief.

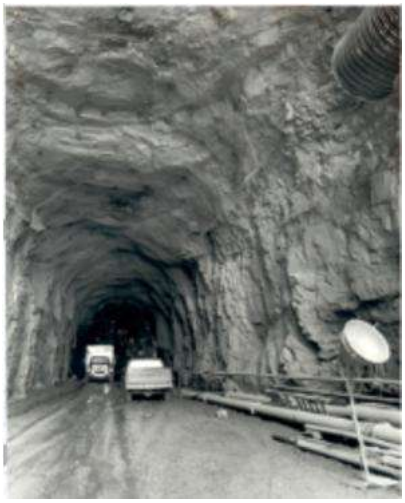

Fig. 9. View of discharge tunnel.

7. Tunnelling Under Lake Huron

Lake Huron is one of the five Great Lakes of North America. It is shared on the north and east by the Canadian province of Ontario and on the south and west by the U.S. state of Michigan, see Figure 10. Lake Huron comprises the eastern portion of Lake Michigan–Huron, having the same surface elevation as Lake Michigan, to which it is connected by the 8.0 km Straits of Mackinac. Combined, Lake Michigan–Huron is the largest freshwater lake by area in the world.

Fig. 10. Location of Lake Huron.

The Bruce nuclear generating station is located on the east shore of Lake Huron, 300 km northwest of the City of Toronto, see Figure 11. Ontario. With eight CANDU pressurized heavy-water reactors and the capacity close to 6000 MW, it is one of the largest energy complexes in the world. An 8:7 m diameter, 900 m long tunnel was excavated beneath the lake. The main portion of the tunnel was positioned within the bedded limestone of the Detroit River Formation. The results of water pressure testing indicated that open wet rock conditions would be encountered at various locations

Fig. 11. Layout of the Bruce generating station.

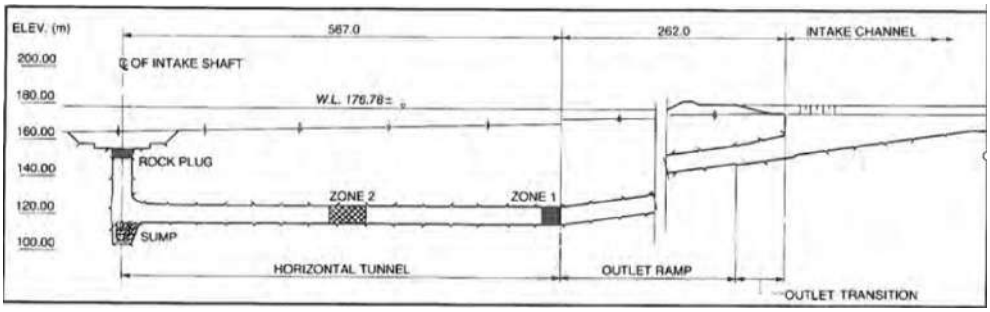

Fig. 12. Bruce intake tunnel profile.

During design phase, it was estimated that one-third of the excavation time would be spent on water control. An 11 m^3/min inflow was estimated for bidding purposes. The tunnel was excavated by full face blasting rounds combined with grouting. Normally the excavation cycle consisted of grouting a minimum of 30 m beyond the tunnel face, to control seepage followed by excavating for 24 m. A total of 49 grout cycles were required to grout the entire tunnel length.

Each grouting cycle consisted of 15 to 46 grout holes, depending on local conditions. This operation resulted in a total of 40,000 m of probe and grout hole drilling and injection of 5,300 m^3 of cement grout. Water seepage was minimized by grouting, while excess water was pumped from the tunnel via a weir box to the ground surface. Progressive estimates of the potential water seepage indicated a cumulative total of 112 cubic metres per minute for the full tunnel length.

Fig. 13. Illustrates large flow under pressure.

8. Conclusion

Tunnelling under Great Lakes poses a challenge of tidal resonance, sometimes preventing conducting any operation from the lake side. The cooling water intake tunnel constructed under Lake Huron exhibited high water pressure acting upon the tunnel floor. Large water inflows have caused stoppage of work and loss of tunnel temporarily. Tunnelling under Lake Ontario mandated special design and construction approach to deal with high in situ rock stresses.

9. Authors

Boro Lukajic is Professional Canadian engineer, since 1968. Fellow Engineering Institute of Canada – inducted in 2000, lifetime achievement award, TAC 2017. Experience covers projects worldwide in hydro power and nuclear energy. In Canada: Labrador, Yukon Territory, Ontario, British Columbia and Manitoba. Internationally: US, Brazil, Hong Kong, Costa Rica, Colombia and United Arab Emirates.

Milica Milojevic is an independent research consultant, Niagara River and Great Lakes.

Acknowledgement

We dedicate this publication to a great individual, father-mentor, Milisav Milojevic, 1924 – 2012.

11. References

Lo, K.Y., and Lukajic, B., 1984. Predicted and measured stresses and displacement around Darlington intake tunnel, *Canadian Geotechnical Journal*, 21 (1), 147-165. https://doi.org/10.1139/t84-012

Lukajic B., 1982. Geotechnical Experience with Tunnel Portal Construction. 14th, Canadian Rock Mechanics Symposium - Vancouver, B.C. 1982.

Lukajic, B., and Azis I., 1983. Brief Review of Rock Support in Two Cooling Water Intake Tunnels. CNCRM Symposium on Underground Support Systems, September 19-21, 1983, Sudbury, Ontario.

Lukajic Boro, 2017. Great Lakes Journey. *Tunnels and Tunnelling*, North American Edition, April-May 2017, 32-34.

Southeastern Europe Tunnelling Conference (SETC-2025)
1-3 October 2025, Belgrade, Serbia

DOI: 10.5937/SETC25037Z

Toronto Metro - Sheppard Line Twin Tunnels

Mike Zegarac[a]*

[a] Hatch tunneling construction supervisor emeritus, Toronto, Ontario, Canada; mikzeg@hotmail.com

Abstract: The City of Toronto operates a rapid transit system totaling 70 km in length. The system is used for local transport within the greater metropolitan area to transport large numbers of people (1,105,700-weekdays), often over short distances at high frequency. The Transit Commission's Sheppard Subway twin tunnels run east from the existing station on the Yonge line along Sheppard Avenue east to Don Mills Road. The tunnels were excavated using a Lovat-type earth pressure balance machine (EPB). This was the first use of earth pressure balance tunnel boring machines in the Toronto area.

Keywords: TBM; tunnel; tunnel lining; machine

1. Introduction

Due to the lower cost and its reduced impact on the community, the design mandated that the tunnel boring machine (TBM) be used to construct the tunnels. The cut and cover method was used locally, where the alignment was off the populated area and where the tunnel horizon was close to the surface. The excavated tunnel diameter was 5.9-m, while the internal diameter was 5.2-m. Tunnel alignment and project layout are shown in Figure 1

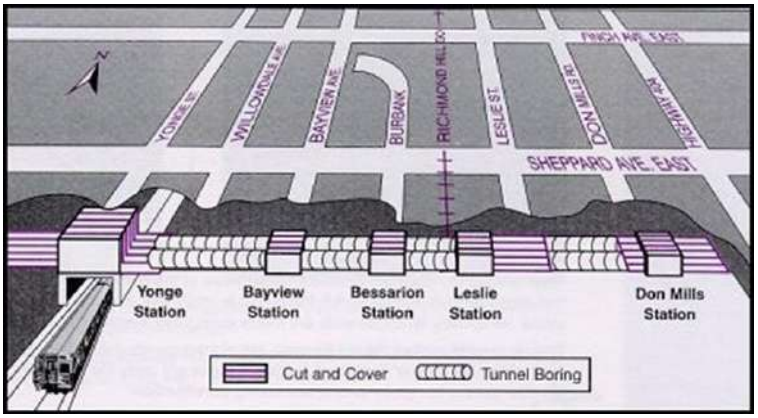

Fig. 1. Tunnel Alignment and Project layout

2. Tunnelling Conditions

Tunnels were driven through soil formations. In the greater Toronto area, the overburden deposits are generally clay/silt till. They are expected to exhibit numerous boulders. Most of the alignment was below the groundwater table.

*Corresponding author: mikzeg@hotmail.com (M. Zegarac).

3. Contractual Arrangement

Tunneling work was done by a Canadian consortium of three local area contractors. The owner, Toronto Transit Commission (TTC), provided the machine and precast segmental lining. The TTC had procured the machines from Lovat, a manufacturer located in Toronto. Hatch Mott MacDonald was the prime consultant responsible for the detailed design and design support during construction.

4. TBM System

The key to tunneling in soil is to minimize surface settlement by maintaining the natural earth pressure at the tunnel face. As noted, Earth-pressure Balance (EPB) boring machine was used at the project. The machine was designed to allow the operator to switch from open mode in self-supporting ground to pressurized mode when positive support of the excavated face was needed. The development of earth pressure balance tunnel boring machine had solved the problem of having to pressurize tunnel face during excavation to prevent their collapse and the ingress of water.

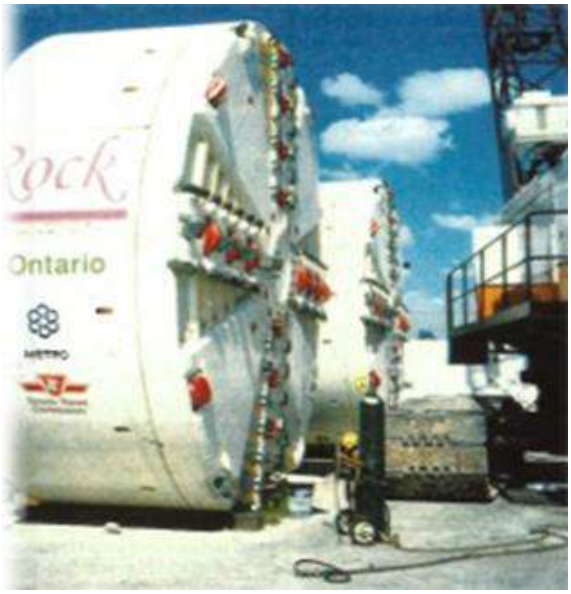

Fig. 2. View of Lovat TBM used for the project.

5. TBM Operational Aspects

The system operated with good measurement and control of the excavated materials at all times. The actual volume of excavated materials was continuously compared with the theoretical excavated volume, and any deviation would alert the operator to potential ground loss problems.

Initially, it was estimated that the machine might be required to operate in a pressurized mode for about 80 percent of the total tunnel length. The balance of the tunnel (approximately 20 percent) was assumed to be excavated with the TBM in open-face mode when the tunnel alignment was located in a denser soil formation.

When significantly more boulders were encountered in the ground (more than forecasted), Hatch Mott MacDonald recommended replacing the machine's cutting heads with new heads designed for both cutting rock and excavating in soft ground. They also recommended adding protection devices to prevent large boulders entering the machine.

Fig. 3. View of tunnel portal

6. Tunnel Lining

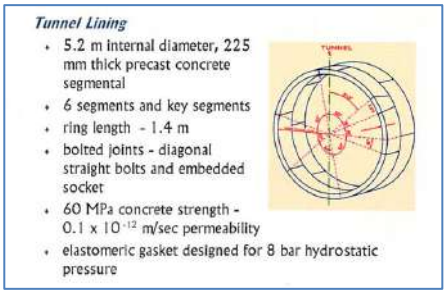

The designers had to develop a tunnel lining that addressed the range of ground loading conditions. In addition, the lining had to be suitable for easy installation, the same time being economical. The system selected was a precast concrete lining made up of segmented rings that are bolted from ring to ring. The connections between the rings were designed to yield at a certain load level, allowing the rings to act as more flexible, independent units. The linings are made of high-performance 60 MPa concrete with very low permeability and diffusivity. The lining segments were equipped with standard EPDM gaskets designed for 8 bar of hydrostatic pressure, and were bolted radially and longitudinally with straight diagonal bolts. All the rings were tapered to provide tunnel direction control.

7. Conclusions

Tunnels were completed on the initially estimated 35-month schedule. The construction contract was well within budget and included less than 3% for contract changes. Critical elements of the project included dealing with difficult launch sites for the boring machine and operating the TBM in proximity to the existing storm sewer and water mains.

Acknowledgement

Award-winning firm was Hatch Mott MacDonald, Toronto (prime consultant). Hatch's design leaders were Brian Garrod, P.Eng. and Tomas Gregor, P.Eng.

8. Author

Mike Zegarec recently retired as a HATCH employee. His 46 years of experience have been in major heavy construction projects in North & South America, Europe and Africa. In 2023 Mike received an award from Tunnelling Association of Canada, titled: Canadian Tunneller of the Year. This award is awarded for leadership and the profound impact the recipient has had in the tunneling industry.

Southeastern Europe Tunnelling Conference (SETC-2025)
1-3 October 2025, Belgrade, Serbia

DOI: 10.5937/SETC25038G

Tunnel Construction: Time Scenarios by Risk Level

Stefani Gjorgjevska[a], Zlatko Zafirovski[b] and Vasko Gacevski[b]*

[a] Civil Engineering Institute Macedonia, Skopje, Republic of North Macedonia; stefani.gjorgjevska@gim.com.mk
[b] Ss. Cyril and Methodius University in Skopje, Faculty of Civil Engineering, Skopje, Republic of North Macedonia; zafirovski@gf.ukim.edu.mk, gacevski@gf.ukim.edu.mk

Abstract: This study investigates the construction duration of 124 tunnel segments along the Pan-European Railway Corridor VIII in the Republic of North Macedonia, focusing on the impact of rock types according to the S classification. Employing a quantitative research approach, the study develops three risk scenarios (low, medium, and high) based on geological characteristics, including rock strength, fracture presence, and hydrogeological conditions. The S classification, adapted to local geological conditions, aligns with international systems such as the Q system and RMR (Rock Mass Rating). The analysis involves calculations of construction duration per meter and total duration for each scenario, using data from field surveys, geotechnical reports, and project documentation. Results indicate that in Scenario 1 (low risk), the average construction duration is 1.9 days/m, in Scenario 2 (medium risk) 4.3 days/m, and in Scenario 3 (high risk) 7.9 days/m, resulting in total durations of 359, 753, and 1359 days, respectively. The comparison shows a 109.75% increase in Scenario 2 and a 278.55% increase in Scenario 3 compared to Scenario 1. These findings facilitate improved planning, resource optimization, and enhanced safety in tunnel engineering, particularly in regions with complex geology. The study also discusses the limitations of assuming a single rock type and the potential influence of factors such as excavation methods and crew experience.

Keywords: tunnel; tunnel construction; construction time duration; risk;

1. Introduction

Tunnels are underground structures designed to overcome terrain obstacles and to ensure the technical elements of the road on which they are planned and constructed. A tunnel is an underground passage created by humans without removing the upper layers of soil and rock. A key characteristic of a tunnel is that it is a structure built beneath the surface of the terrain.

In a broader sense, the term "tunnel" also refers to larger underground spaces intended for energy or other facilities, garages, commercial spaces, warehouses, shelters, sports facilities, permanent underground mining rooms, and underground landfills for hazardous waste.

This study examines the impact of rock classification on the construction duration of 124 tunnel segments along the Pan-European Railway Corridor VIII in the Republic of North Macedonia. Its unique contribution lies in developing three risk scenarios (low, medium, and high) based on the S classification, enabling precise prediction of construction duration and resource optimization. This approach contributes to enhanced planning and safety in tunnel engineering in regions with complex geology, which is particularly relevant for projects like the Pan-European Corridor VIII.

Risk is a calculated forecast of potential damage, or in a negative case, loss or danger. The level of risk is a function of the probability and severity of the damage. Most risks in tunnels arise from the fact that hazardous events occur in a space that is almost completely enclosed and usually connected to the open space only through the two tunnel portals. The effects of the "enclosed space" are particularly pronounced in long tunnels when the accident site is far from the portal.

*Corresponding author: stefani.gjorgjevska@gim.com.mk (S. Gjorgjevska).

General risks:

- Risk before tunnel construction;
- Risk during tunnel construction;
- Risk during tunnel operation.

Types of risks can be categorized into three basic types:

- Completion risk, where there is a danger that the project will not be finished within the planned timeframe;
- Cost risk, where there is a possibility that the project costs will exceed the planned budget;
- Performance risk, which refers to the possibility that the project outcome will contain technical flaws that may lead to problems and project losses.

This paper presents an analysis of the construction time of 124 tunnel segments that are part of the Pan-European Railway Corridor VIII in Republic of North Macedonia.

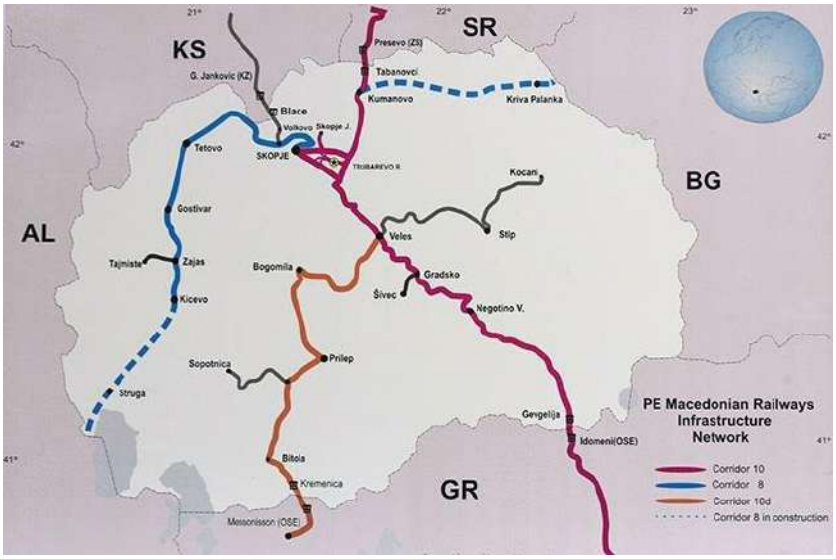

Fig. 1. Pan-European Corridors on the territory of Republic of North Macedonia.

The analysis aims to examine the impact of different rock types according to the S classification and the corresponding variation in tunnel construction time. The purpose of this analysis is to support efficient planning and execution, ensure safety during construction, and optimize the use of resources and budget.

The rock class has a significant influence on the excavation of tunnel segments and, consequently, on the total construction time of the tunnels, as it allows for the creation of a realistic construction schedule.

The S classification of rocks includes several categories, where SI represents the strongest and most stable rock, while category SVII or higher represents the weakest and most unstable rock. The rock classification is based on: rock strength, cracks, hydrogeological conditions, and overall rock mass condition.

The scenarios developed in this analysis are:

- Scenario 1 – Low risk;
- Scenario 2 – Medium risk;
- Scenario 3 – High risk.

The first scenario, or low-risk scenario, involves the most favorable rock conditions. The tunnels that are part of the first scenario have the most optimal working conditions, with minimal construction risks, which in turn results in the shortest construction time. By analyzing the segments and comparing the construction time of the tunnel by individual segments versus when the segments are classified under the first, low-risk scenario, a reduction of approximately 35% in total construction time is achieved.

The second scenario, or medium-risk scenario, includes moderate challenges. The tunnels that are part of the second scenario are the most common in real-world projects. They are positioned somewhere between Scenario 1 and Scenario 3, that is, between ideal and unfavorable conditions. By analyzing the segments and comparing the construction time of the tunnel by individual segments versus when the segments are classified under the second, medium-risk scenario, an increase of approximately 35% in total construction time is observed.

The third scenario represents high risk, with the least favorable conditions for the construction of the tunnel segments. The third scenario includes tunnels with unfavorable construction conditions and represents significant challenges for engineers. These tunnels are characterized by unstable geology, which leads to an increase in construction time compared to initial estimates. By analyzing the segments and comparing the tunnel construction time by individual segments versus when the segments are classified under the third, high-risk scenario, an increase of approximately 130% in total construction time is observed.

2. Overview of Available Data

Data for the 124 tunnel segments were collected from field surveys, geotechnical reports, and design documentation for the Pan-European Railway Corridor VIII. Each segment is characterized by: (1) segment length, (2) excavation method (e.g., mechanical excavation or blasting), (3) construction duration, and (4) rock type according to the S classification. Risk scenarios were assigned based on geological characteristics, including rock strength, fracture presence, and hydrogeological conditions. In cases of incomplete data, estimates were based on average values from similar segments or expert judgments from project reports. Data on excavation methods were derived from project documentation, with mechanical excavation predominant in stable rocks (SI-SIII) and blasting more common in unstable rocks (SVII).

2.1. Definition of S Classification and Risk Scenarios

The S classification is a rock categorization system based on rock strength, degree of fracturing, hydrogeological conditions, and overall rock mass condition. Category SI denotes strong, stable rocks with minimal fractures and favorable hydrogeological conditions, while SVII represents weak, unstable rocks with significant fractures and adverse conditions, requiring enhanced support and slower excavation methods. This classification aligns with international systems, such as the Q system and RMR (Rock Mass Rating), but is adapted to local geological conditions in North Macedonia.

Risk scenarios were defined based on the following criteria:

- Low Risk (Scenario 1): Rocks from SI to SIII, with high strength, minimal fractures, and no significant hydrogeological challenges, allowing rapid excavation with minimal support;
- Medium Risk (Scenario 2): Rocks from SIV to SVI, with moderate strength, moderate fractures, and occasional hydrogeological issues, requiring additional stabilization measures;
- High Risk (Scenario 3): Rocks from SVII or weaker, with low strength, intense fracturing, and complex hydrogeological conditions, increasing construction time due to enhanced support needs and collapse risks.

3. Methodology

In the book "Research Design: Qualitative, Quantitative, and Mixed Methods Approaches" (2014) by John W. Creswell, the three main research approaches—qualitative, quantitative, and mixed methods—are thoroughly explained. These approaches are discussed in the context of their application, philosophical foundations, and practical implementation.

- The qualitative method focuses on understanding individual experiences, meanings, and social processes;
- The quantitative method emphasizes the measurement and analysis of numerical data to test hypotheses or determine statistical relationships;
- The mixed method combines both qualitative and quantitative approaches to provide a more comprehensive understanding of the research question.

The research in this paper is focused on data analysis and graphical representation of results for different tunnel segments, utilizing the quantitative research method.

According to Creswell, quantitative research is defined as “the collection, analysis, and interpretation of numerical data to explain phenomena.”

In this analysis, based on the available data, each tunnel segment includes three different types of rock according to the S classification. The analysis includes a prediction of how many days it would take to construct the tunnel if it were entirely composed of a single type of rock. Therefore, three scenarios were developed, each calculating the total construction time of the tunnel assuming it is entirely in rock material from segment 1, segment 2, or segment 3.

Based on the obtained data, the following calculations were made:

- Total tunnel length:

$$\textit{Total tunnel length} = \textit{Sum of the lengths of all segments [m]} \quad (1)$$

- Construction duration per meter:

$$\textit{Duration per meter} = \textit{Construction time} / \textit{Length of segment [days/m]} \quad (2)$$

- Construction time:

$$\textit{Construction time} = \textit{Total length} \times \textit{Duration per meter [days]} \quad (3)$$

Tunnel construction duration is influenced not only by rock type but also by excavation methods, the experience of construction crews, and the use of specialized mechanical equipment. For example, mechanical excavation using tunnel boring machines (TBM) is faster and more efficient in stable rocks (SI-SIII), while blasting is more common in unstable rocks (SVII), increasing construction time due to the need for additional stabilization measures. Crew experience affects work efficiency, particularly in complex geological conditions, where skilled teams can reduce construction time. Equipment efficiency and availability also play a critical role, with modern equipment potentially accelerating the process compared to outdated technology. These factors were not fully analyzed in this study due to data limitations but were considered in interpreting the results to ensure practical applicability. To enhance the analysis’s accuracy, excavation method data were categorized based on project documentation, with the percentage of mechanical excavation and blasting specified for each segment.

The following tables present a portion of the tunnel segments along with the calculations made for them by scenario:

Table 1. Scenario 1 – Low risk.

Tunnel No.	Section No.	Length [m]	Construction time of segments [day]	Tunnel construction time [day]	Total tunnel length [m]	Percentage type of substructure	Duration per meter [m/day]	Constuction time [day]
	1	119.50	155					
1	2	42.68	160	375	170.71	SI 70%	1.3	222
	3	8.54	60					
	4	35.06	46					
2	5	26.30	98	303	87.66	SI 40%	1.3	114
	6	26.30	159					
	7	36.91	45					
3	8	88.59	300	489	147.65	SI 25%	1.2	181
	9	22.15	143					
	10	35.79	47					
4	11	20.88	78	143	59.65	SI 60%	1.3	78
	12	2.98	18					

Table 2. Scenario 2 – Medium risk.

Tunnel No.	Section No.	Length [m]	Construction time of segments [day]	Tunnel construction time [day]	Total tunnel length [m]	Percentage type of substructure	Duration per meter [m/day]	Constuction time [day]
	1	119.50	155					
1	2	42.68	160	375	170.71	SVI 25%	3.7	639
	3	8.54	60					
	4	35.06	46					
2	5	26.30	98	303	87.66	SVI 30%	3.7	328
	6	26.30	159					
	7	36.91	45					
3	8	88.59	300	489	147.65	SVI 60%	3.4	500
	9	22.15	143					
	10	35.79	47					
4	11	20.88	78	143	59.65	SVI 35%	3.7	223
	12	2.98	18					

Table 3. Scenario 3 – High risk

Tunnel No.	Section No.	Length [m]	Construction time of segments [day]	Tunnel construction time [day]	Total tunnel length [m]	Percentage type of substructure	Duration per meter [m/day]	Constuction time [day]
	1	119.50	155					
1	2	42.68	160	375	170.71	SVII 5%	7.1	1205
	3	8.54	60					
	4	35.06	46					
2	5	26.30	98	303	87.66	SVII 30%	6.0	529
	6	26.30	159					
	7	36.91	45					
3	8	88.59	300	489	147.65	SVII 15%	6.5	955
	9	22.15	143					
	10	35.79	47					
4	11	20.88	78	143	59.65	SVII 5%	6.0	360
	12	2.98	18					

At the end of this calculation, the average construction duration per meter was calculated for each scenario across all 124 tunnel segments.

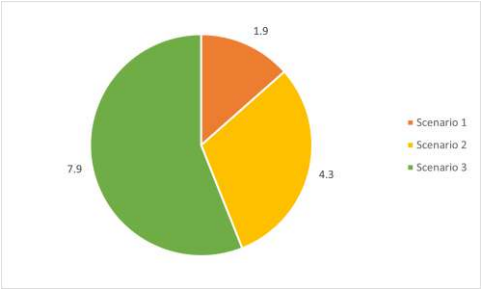

Fig. 2. Average construction duration per meter.

Additionally, the average total construction time of all tunnel segments was calculated for each scenario.

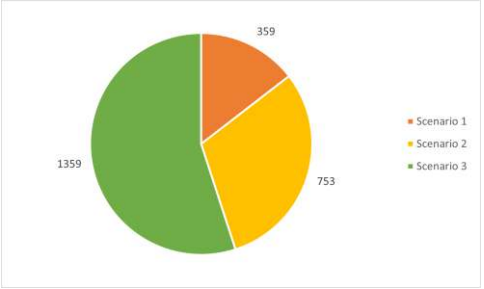

Fig. 3. Average total construction time.

4. Results

The analysis of 124 tunnel segments from the Pan-European Railway Corridor VIII reveals significant variations in construction duration based on risk scenarios, driven by the geological characteristics of rocks according to the S classification. In Scenario 1 (low risk), involving rocks from SI to SIII with high strength and minimal fractures, the average construction duration per meter is 1.9 days/m, resulting in a total duration of 359 days for all tunnels. In Scenario 2 (medium risk), which includes rocks from SIV to SVI with moderate strength and occasional hydrogeological challenges, the duration per meter increases to 4.3 days/m, with a total duration of 753 days. In Scenario 3 (high risk), involving rocks from SVII or weaker with intense fracturing and complex hydrogeological conditions, the duration per meter is 7.9 days/m, leading to a total duration of 1359 days. These results are illustrated in Figure 2 (average construction duration per meter) and Figure 3 (total construction duration).

The comparison shows that Scenario 2 takes 109.75% longer than Scenario 1, while Scenario 3 takes 278.55% longer than Scenario 1. These differences are attributed to increased geological instability and the need for additional support measures, such as reinforced concrete structures or slower excavation methods in unstable rocks. Statistical analysis of the duration per meter indicates that the standard deviation in Scenario 1 is relatively low (0.3 days/m), suggesting consistency in predictions for stable rocks. In Scenario 2 and Scenario 3, standard deviations are higher (0.7 days/m and 1.2 days/m, respectively), reflecting greater variability due to the heterogeneity of geological conditions.

Furthermore, a comparison with initial estimates from the project documentation for the Pan-European Corridor VIII shows that the duration in Scenario 1 aligns closely with planned values, while in

Scenario 2 and Scenario 3, the actual duration significantly exceeds estimates due to unforeseen geological challenges, such as local collapses or the need for additional stabilization. These findings highlight the importance of detailed geotechnical analysis prior to construction to minimize deviations from the plan. The results provide a foundation for future tunnel project planning, particularly in regions with similar geological conditions.

5. Conclusion

This paper presents an analysis of the construction time of 124 tunnel segments that are part of the Pan-European Railway Corridor VIII in the Republic of North Macedonia.

Based on the conducted analysis, it can be concluded that the type of material in which the tunnel is to be constructed has a significant impact on its total construction time. The presented results show that tunnels to be built in stable rock formations have the shortest construction time compared to the other two scenarios. This is also illustrated in the graphical representations in Fig. 2 and Fig. 3.

Fig. 2 presents the average construction duration per meter, where the value for Scenario 1 is 1.9 days/meter, for Scenario 2 it is 4.3 days/meter, and for Scenario 3 the value is 7.9 days/meter.

Fig. 3 shows the total construction duration of the tunnels for all three scenarios. The average value for Scenario 1 is 359 days, for Scenario 2 it is 753 days, while for Scenario 3, the total construction duration of the tunnels is 1359 days.

If a percentage comparison is made based on these results, Scenario 2 lasts 109.75% longer than Scenario 1, and Scenario 3 is approximately 278.55% longer than Scenario 1.

Through the scenarios presented in this paper, the analysis enables accurate planning, precise scheduling, and effective resource management.

If 21st-century technologies (such as software and modeling tools) are integrated into this analysis, the complexity of tunnel engineering challenges could be significantly reduced.

Furthermore, this analysis can also be useful in the planning of tunnels where delays in deadlines could have negative consequences on the overall tunnel construction process.

5.1. Limitations of the Analysis

This analysis assumes that an entire tunnel consists of a single rock type in each scenario, simplifying real-world conditions where tunnels typically traverse varied rock types. This assumption may affect the accuracy of predictions, particularly for tunnels with heterogeneous geology. Additionally, construction duration is influenced by factors such as the experience of construction crews, availability of mechanical equipment, and specific excavation methods (e.g., blasting versus mechanical excavation), which were not fully considered due to data limitations. Future research should incorporate detailed data on these variables to enhance result applicability.

References

Creswell, J., Creswell D., 2014. Research Design: Qualitative, Quantitative and Mixed Method Approaches, SAGE Publications, Inc.

Bilotta, E., Casale E., di Prisco C., 2022. Handbook on tunnels and underground works – Volume 1: Concept – Basic principles of design, CRC Press/Balkema.

Tatiya, R., 2017. Civil excavations and tunneling, Published by ICE Publishing, One Great George Street, Westminster, London SW1P 3AA.

Carvajal, M.A.A., 2014. Cost estimation for underwater tunnel projects based on uncertainty and risk analysis. Master thesis , Norwegian University of Science and Technology.

Tomanović, Z., 2015. Tuneli i podzemne konstrukcije. Univerzitet Crne Gore, Građevinski fakultet.

SETC-2025
BELGRADE

TOPIC 8

OPERATIONAL SAFETY

Southeastern Europe Tunnelling Conference (SETC-2025)
1-3 October 2025, Belgrade, Serbia

DOI: 10.5937/SETC25039K

Methodology for Geoecological Risks Assessing during the Operation of Metro Facilities

Elena Kulikova[a], Sergey Zhukov[b]*

[a] Russian Technological University MIREA, National University of Science and Technology "MISIS", Department of Environmental and Industrial Safety, Moscow, Russia; fragrante@mail.ru
[b] JSC "Mosmetrostroy"; reception-3@metrostroy.ru

Abstract: When assessing the geo-ecological risk of operating underground facilities, it is necessary to take into account dangerous hydrogeological (the nature of groundwater migration, its temperature regime, composition and mineralization, hydrostatic and piezometric pressure, etc.) and geological (karst, suffusion-erosion, landslide processes, rock collapse, etc.) processes. The most visible type of geological risk assessment is the compilation of geological risk maps and the development of a system of indicators of the level of geological danger for a specific mining area, which is implemented through a matrix of the level of geological risks for various territorial objects. The geo-ecological risk has been calculated for each technological process for shallow and deep tunnels. An expert method was used to rank geo-ecological risks and determine their quantitative characteristics at the stage of operation of metro facilities. The paper shows the software module of the information and analytical model, which makes it possible to quantify the risk. A geo-ecological risk management system has been developed, which makes it possible to determine the distribution zones of the most dangerous processes in the "rock mass – technology –tunnel" system based on forecast calculations. The presented methodology for assessing geo-ecological risks during the operation of metro facilities makes it possible to predict the development of emergency situations and assign monitoring and protective measures based on the establishment of acceptable geo-ecological risk values in each specific case.

Keywords: geoecological risk; metro facilities; management system; emergency; monitoring

1. Introduction

Geoecological risk in underground construction is the probability of adverse events resulting in a disruption of the stability of the existing natural and technical geosystem "rock mass – technology – underground structure" as a result of geotechnical activities.

The levels of geo-ecological risk that must be considered in tunnel construction are as follows:

- negligible geo-ecological risk is the maximum level set by regulatory authorities that requires special measures to eliminate it;
- acceptable geo-ecological risk – the maximum level justified from ecological, geotechnical, socio-economic and ecological positions;
- maximum permissible geo-ecological risk – the maximum level allowed by the policy of a mining and construction organization in the field of environmental safety.

When assessing the geo-ecological risk of operating metro facilities, it is primarily necessary to take into account dangerous hydrogeological (the nature of groundwater migration, its temperature regime, composition and mineralization, hydrostatic and piezometric pressure, etc.) and geological (karst, suffusion-erosion, landslide processes, rock collapse, etc.) processes.

The most obvious type of geological risk assessment, as already noted, is the compilation of geological risk maps and the development of a system of indicators of the level of geological danger for a specific

*Corresponding author: gidrotehnik@inbox.ru (E. Kulikova).

mining area, which is implemented through a matrix of the level of geological risks for various territorial objects, while according to international practice, there are 7 groups, each of which characterizes a certain type of or a significant geological risk factor, for example, suitability for the development of underground space, the presence of tectonic processes., groundwater activity, terrain features, karst activity, etc.

2. Methodology

The level of potential geological risk is determined for each specific situation:

- low level, not requiring managerial decision-making;
- the average level, which determines the recommendatory nature of the applied risk management measures;
- a high level that determines the need to take risk management measures;
- a very high level, which necessarily prescribes the adoption of risk management measures.

The identified level of geological risk determines the nature of filling in the matrix as the basis for drawing up risk maps. The maps show the distribution of the potential geological risk of this type in the considered operational area.

The assessment of geoecological risk also determines the consideration of socio-man-made factors that manifest themselves through non-compliance with the operating regime, violation of the work passport, violation of the ventilation regime, non-compliance with safety regulations and sanitary protection standards, etc. In addition, at the stage of operation are taken into account:

- modification of the heat and mass transfer system between the underground structure and the host rock mass;
- changes in soil composition and structure;
- air pollution of the working area by dust and gases from the operation of equipment or rolling stock;
- depletion and pollution of groundwater, changes in the nature of their migration, temperature regime, composition, etc.;
- geomechanical transformation of the Earth's surface.

The calculation of geoecological risk is carried out in relation to each technological process, while coefficients of significance of the consequences of a particular technological process are introduced:

$$R_i = \frac{N_{ij} \sum k_{ij}}{N_j \sum k_j}, \tag{1}$$

where i – the index of the technological process; j – the index of abnormal consequences from the technological process; N_{ij} и N_j – the number of potential undesirable consequences of the i-th process on the natural and technical system and on the totality of potential consequences, respectively; k_{ij} и k_j – coefficients of significance of the consequences of the i-technological process and all possible j-consequences.

The generalized geo-ecological risk R_0 will be determined from the formula:

$$R_o = \sum_{i}^{j} P_i k_i, \tag{2}$$

where P_i – the probability of the manifestation of the i-th process; k_j – the coefficient of significance of the i-th process within the boundaries of the natural and technical geosystem.

To rank geoecological risks and determine its quantitative characteristics at the stage of operation of metro facilities, an expert method was used, the results of which are shown in Table 1.

The types of geoecological risk indicated in Table 1 can be assessed by introducing normalization coefficients that characterize the proportion of the most unfavorable event taken as a unit.

Thus, the geoecological risk during the operation of shallow tunnels can be calculated using the formula:

$$R_g = R_s + R_h + R_a + R_{gw}, \tag{3}$$

where R_s – the risk of geomechanical transformation of the territory; R_h – the risk of changing the heat and mass transfer system between an underground object and the host rock mass; R_a – risk of contamination inside the tunnel atmosphere; R_{gw} – the risk of pollution and depletion of the water basin.

Table 1. Quantitative values of geoecological risks.

No.	Negative environmental processes	The degree of manifestation of the negative process	Code	Coefficient of significance of the negative process indicator
	Shallow tunnels			
1.	Geomechanical transformation of the territory			
	Potential precipitation of the Earth's surface	Small	1	0,3
		Big	2	
	Development of surface forms of karst	Small	1	
		Big	2	
2.	Modification of the heat and mass transfer system between an underground structure and the host rock mass	Small	1	0,2
		Big	2	
3.	Atmospheric pollution	Small	1	0,15
		Big	2	
4.	Pollution and depletion of groundwater			
	Flooding of the territory	Small	1	0,35
		Big	2	
	Changes in temperature conditions and migration patterns	Small	1	
		Big	2	
	Deep-laid tunnels			
1.	Pollution inside the tunnel atmosphere	Small	1	0,1
		Big	2	
2.	Changes in the underground hydrosphere			
	Infiltration into groundwater tunnels	Small	1	0,6
		Big	2	
	Changes in the hydrological regime of groundwater	Small	1	
		Big	2	
3.	Geomechanical transformations of the host rock mass			
	Changing the composition and structure of soils	Small	1	0,3
		Big	2	
	The development of underground forms of karst	Small	1	
		Big	2	

The risk of geomechanical transformation of the territory is determined as follows:

$$R_s = \left(\delta_{ss} q_{ss} + \delta_k q_k\right) p, \tag{4}$$

где δ_{ss} – coefficient of significance of geomechanical transformation of the territory; q_{ss} – the value of the indicator code for geomechanical transformation of the territory; δ_k – coefficient of significance for the development of karst processes; q_k – the value of the karst process development indicator code; p – the normalizing indicator.

The risk of pollution and depletion of a water basin will be defined as:

$$R_{gw} = \left(\delta_f q_f + \delta_r q_r\right) w, \tag{5}$$

где δ_f – coefficient of significance of flooding of the territory; q_f – the value of the territory flooding indicator code; δ_r – coefficient of significance of changes in the regime of groundwater and surface waters; q_r – the value of the indicator code for changes in the regime of groundwater and surface waters; w – the normalizing indicator.

The risk of atmospheric pollution is calculated using the formula:

$$R_a = \delta_a q_a \lambda, \tag{6}$$

where δ_a – coefficient of significance of atmospheric pollution; q_a – the value of the atmospheric pollution indicator code; λ – the normalizing multiplier.

The risk of a change in the heat and mass transfer system between the tunnel and the host array is calculated as follows:

$$R_h = \delta_h q_h m, \tag{7}$$

where δ_h – coefficient of significance of the change in the heat and mass transfer system between the tunnel and the host array; q_h – the value of the indicator code for the change in the heat and mass transfer system between the tunnel and the host array; m is the normalizing multiplier.

The geoecological risk during the operation of deep tunnels can be calculated using the formula

$$R_{ug} = R_m + R_{ua} + R_{ugw}, \tag{8}$$

where R_m – the risk of geomechanical transformation of the host rock mass; R_{ua} – risk of contamination inside the tunnel atmosphere; R_{ugw} – the risk of pollution and depletion of the water basin.

The risk of geomechanical transformation of the host rock mass is determined as follows:

$$R_m = \left(\delta_m q_m + \delta_{uk} q_{uk}\right) p_1, \tag{9}$$

where δ_m – coefficient of significance of changes in soil composition and structure; q_m – the value of the indicator code for changes in soil composition and structure; δ_{uk} – coefficient of importance for the development of underground karst forms; q_{uk} – the value of the indicator code for the development of underground karst formations; p_1 – the normalizing indicator.

The risk of contamination and depletion of the underground hydrosphere is defined as:

$$R_{ugw} = \left(\delta_{inf} q_{inf} + \delta_{hr} q_{hr}\right) w_1, \tag{10}$$

where δ_{inf} – coefficient of importance of infiltration into groundwater tunnels; q_{inf} – the value of the indicator code for infiltration into groundwater tunnels; δ_{hr} – coefficient of significance of changes in the hydrogeological regime; q_{hr} – the value of the hydrogeological regime change indicator code; w_1 – the normalizing indicator.

The risk of contamination inside the tunnel atmosphere is calculated using the formula:

$$R_{ua} = \delta_{ua} q_{ua} \lambda_1, \tag{11}$$

where δ_{ua} – coefficient of importance of pollution inside the tunnel atmosphere; q_{ua} – the value of the tunnel's atmospheric pollution indicator code; λ_1 – the normalizing multiplier.

3. Results

A quantitative analysis of these risks and the establishment of their acceptable values makes it possible to form a geoecological risk control system for the operation of metro facilities (Fig. 1).

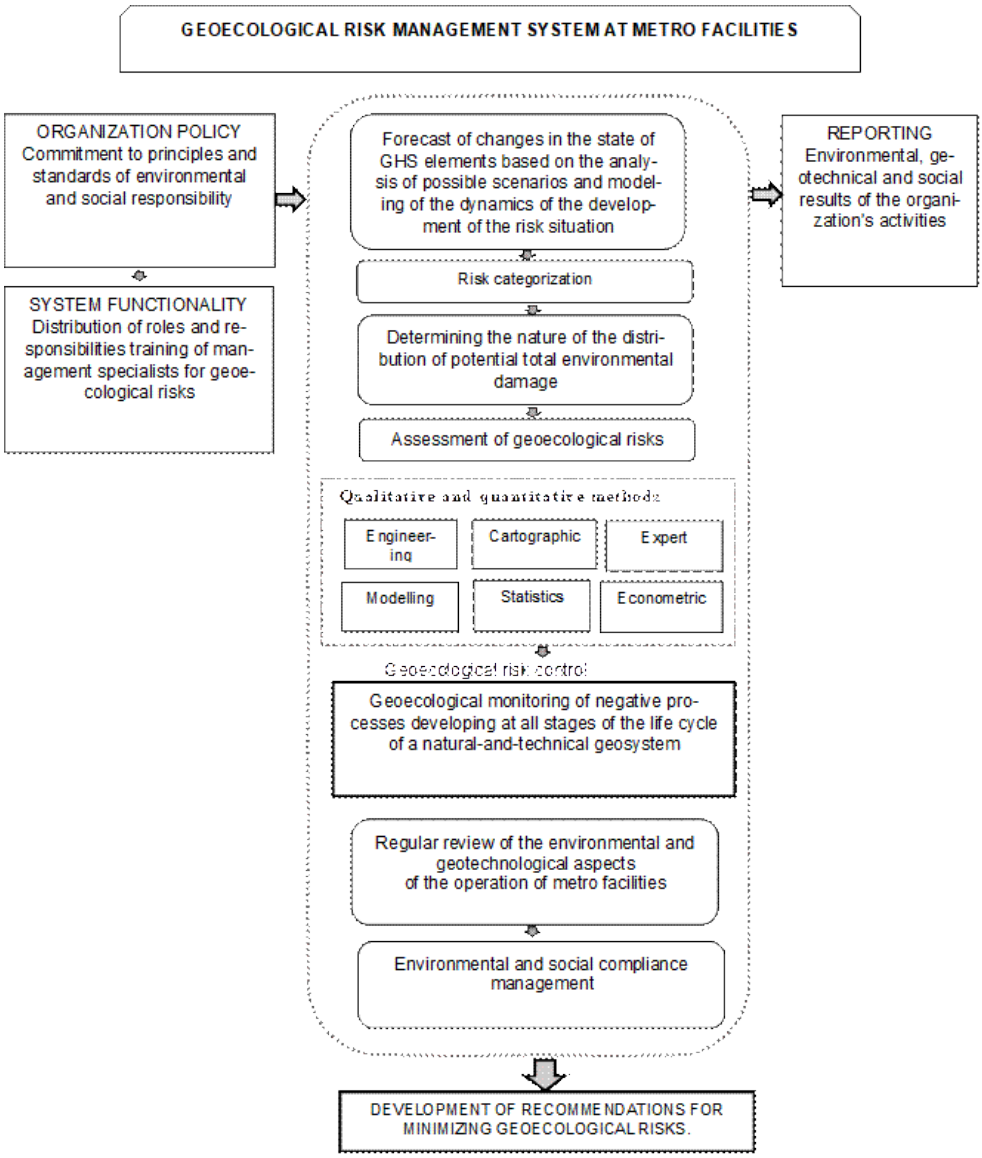

Fig. 1. Geoecological risk management system at metro facilities.

A quantitative risk assessment can be determined based on an information and analytical model, the program module of which is shown in Fig. 2.

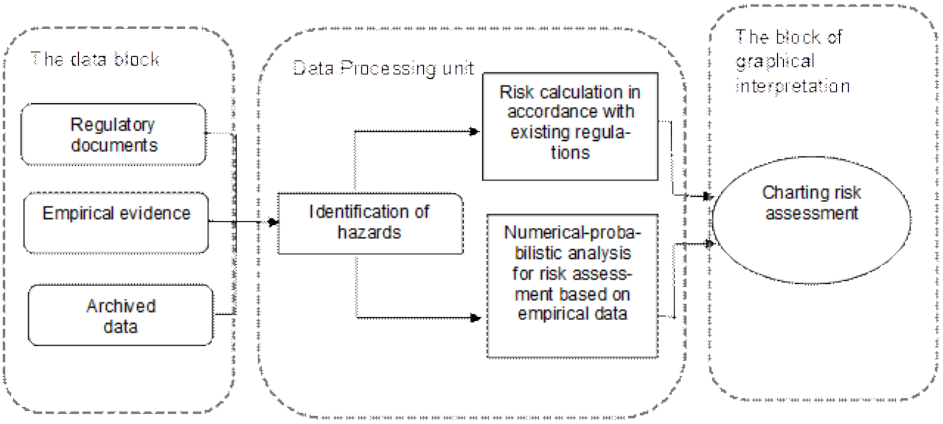

Fig. 2. Functional diagram of the software module.

For a qualitative analysis of the risk level, mapping can be used to identify the zone of maximum damage caused by negative processes caused by technological work during the operation of metro facilities.

The developed geoecological risk control system makes it possible to determine the distribution zones of the most dangerous processes in the rock mass – technology – tunnel system based on forecast calculations.

The presented methodology for assessing geoecological risks during the operation of metro facilities makes it possible to predict the development of emergency and assign monitoring and protective measures based on the establishment of acceptable geoecological risk values in each specific case.

4. Conclusion

1. For the first time, the question was raised about the concept of acceptable risk at the stage of operation of underground metro facilities, i.e. about the level according to which the threshold levels of acceptable and desired environmental safety are set in each specific case. The concept of acceptable risk is associated with a high probability of reducing the safety of technological processes due primarily to the environmental incompatibility of the methods used with natural factors. Moreover, engineering and geological factors are of primary importance.
2. A methodology for managing geoecological risks during the operation of metro facilities has been developed, which makes it possible, based on forecast calculations, to determine the distribution zones of the most dangerous processes in the "rock mass – technology – underground equipment" system.

References

Bourget ,A.P.F., Chiriotti E., Patrinieri E., 2019. Evolution of risk management during an underground project's life cycle. Tunnels and Underground Cities: Engineering and Innovation meet Archaeology, Architecture and Art – Peila, Viggiani&Celestino (Eds). London, Taylor & Francis Group. pp. 4375 – 4385.

Garber, V.A., 2018. Abnormal situations at underground transport facilities. Podzemnye gorizonty. (16):20–25 [In Russ.].

He, X.C., Xu, Y.S., Shen, S.L., Zhou, A.N., 2020. Geological environment problems during metro shield tunnelling in Shenzhen, China. Arabian Journal of Geosciences. vol. 13(2), art. 87. DOI: 10.1007/s12517-020-5071-z.

Hongjun, W., 2016. Earth human settlement ecosystem and underground space research. Procedia Engineering, vol. 165. pp. 765-781. DOI: 10.1016/j.proeng.2016.11.774.

Konyukhov, D.S., 2022. Analysis of mechanized tunneling parameters to determine the overcutting characteristics. Mining Science and Technology (Russia). 7(1):49-56. DOI: 10.17073/2500-0632-2022-1-49-56

Konyukhov, D.S., 2021. Criteria analysis of modern technologies of underground construction. Geotekhnika. no. 1, pp. 40–55. [In Russ].

Kim, D.Y, Farrokh, E., Song, M.K., Hyun, K.S., 2017. Cutting tool wear evaluation for soft ground TBMs. Proceeding of the World Tunnel Congress 2017. Surface challenges – Underground solutions. 9-15th June 2017, Bergen, Norway. Bergen

Kulikova, E. Yu., 2020. Methodical principles for improving the ecological and technological reliability of urban underground structures. MIAB. Mining Inf. Anal. Bull. (6–1):176-185. [In Russ]. DOI: 10.25018/0236-1493-2020-61-0-176-185

Kulikova, E.Yu., 2021. Safety and risk management in underground construction as a complex information process. MIAB. Mining Inf. Anal. Bull. (2–1):134-143. [In Russ]. DOI: 10.25018/0236-1493-2021-21-0-134-143

Kulikova, E.Yu., Balovtsev, S.V., Skopintseva, O.V., 2023. Complex estimation of geotechnical risks in mine and underground construction. Sustainable Development of Mountain Territories. 15(1):7-16. [In Russ]. DOI: 10.21177/1998-4502-2023-15-1-7-16.

Lebedev, M.O., 2018. Choosing a calculation method for stress-strain of supports and lining of transport tunnels. 16thWorld Conference of the Associated Research Centers for the Urban Underground Space (ACUUS 2018), 5-7 November, Hong Kong, pp. 678-687

Mahdi, S., Gastebled, O., Ningre, H., Senechal, M., 2019. Grand Paris Express, Line 15 East – predictive damage analysis combining continuous settlement trough modeling, risk management, automated vulnerability checks and visualization in GIS. – Tunnels and Underground Cities: Engineering and Innovation meet Archaeology, Architecture and Art – Peila, Viggiani&Celestino (Eds) – London, Taylor & Francis Group, pp. 5855-5864

Merisalu, J., Sundell, J., Rosén L., 2023. Probabilistic cost-benefit analysis for mitigating hydrogeological risks in underground construction. Tunnelling and Underground Space Technology. vol. 131(7): 104815. DOI: 10.1016/j.tust.2022.104815

Potapova, E. V., 2021. Typology of metro structures for the tasks of geotechnical risk classification. Mining Science and Technology (Russia). no. 6, pp. 52-60. [In Russ]. DOI: 10.17073/2500-0632-2021-1-52-60

Xing-Tao, Lin, Ren-Peng, Chen, Huai-Na, Wu, Hong-Zhan Cheng, 2019. Deformation behaviors of existing tunnels caused by shield tunneling undercrossing with oblique angle. Tunneling and Underground Space Technology. vol. 89, pp. 78-90. DOI: 10.1016/j.tust.2019.03.021

Xu, Y.S., Shen, J.S., Zhou, A.N., Arulrajah, A., 2018. Geological and hydrogeological environment with geohazards during underground construction in Hangzhou: a review. Arabian Journal of Geosciences. vol. 11, art. 544. DOI: 10.1007/s12517-018-3894-7.

SETC-2025
BELGRADE

TOPIC 9

IMPACT OF CLIMATE CHANGE ON TUNNEL INFRASTRUCTURE

Southeastern Europe Tunnelling Conference (SETC-2025)
1-3 October 2025, Belgrade, Serbia

DOI: 10.5937/SETC25040S

Enhancing Flood Resilience of Underground Traffic Tunnel through Direct Rainfall 2D Modeling - Case Study of the City of Belgrade

Žarko Sretenović[a], Jelena Batica[a], Miodrag Popović[a], Slobodan Radovanović[a] and Vesna Tripković[a]*

[a] Jaroslav Černi Water Institute LLC Belgrade, Belgrade, Serbia; zarko.sretenovic@jcerni.rs, jelena.batica@jcerni.rs, miodrag.popovic@jcerni.rs, slobodan.radovanovic@jcerni.rs, vesna.tripkovic@jcerni.rs

Abstract: This paper examines the impact of climate change on underground traffic tunnel infrastructure, specifically focusing on the increased pluvial flooding risk associated with changing precipitation patterns and extreme weather events. We are presenting a 2D hydrodynamic model designed to assess and enhance the flood resilience of these tunnels during torrential events. The case study conducted in Belgrade, Serbia, evaluates the effectiveness of proposed flood risk management techniques aimed at safeguarding the city's underground transportation infrastructure from potential flooding.

Using the Direct Rainfall Method (DRM), our model simulates rainfall events with various return periods (e.g., 10, 100, and 500 years) to provide a comprehensive assessment of flood impacts on tunnel infrastructure. Detailed topographical data is utilized to accurately capture the complex geometry of the tunnel system and its urban context, allowing for a thorough investigation of factors such as tunnel portal design, raising entrance to the tunnel, drainage system capacity, surface runoff management, and the implications for traffic flow and emergency response.

The simulations reveal critical insights into water levels, discharge, and inundation zones under differing rainfall scenarios. The findings underscore the necessity for resilient design strategies, including road design adaptations (elevation adjustments), construction of flood barriers, implementation of effective water management systems, and sustainable drainage solutions. Furthermore, future considerations regarding these issues are focused on the integration of green construction practices and energy-efficient designs as strategies to enhance the resilience of tunnel infrastructure in response to climate-related challenges.

By delineating flood-prone areas and proposing targeted drainage improvements, this research contributes to developing effective flood risk management plans. Ultimately, this study emphasizes the importance of integrated and systemic approach that merges planning strategies and structural improvements to bolster the safety and resilience of the Belgrade underground transportation system, solving similar issues on tunnelling projects worldwide.

Keywords: flood resilience; underground traffic tunnels; flood risk management; climate change; 2D hydrodynamic modelling

1. Introduction

Urban underground transportation systems, including metro tunnels, are increasingly exposed to flooding as a consequence of extreme weather events resulting from climate change and rapid urbanization (IPCC, 2021). Intensifying rainfall events and more frequent extreme weather conditions, coupled with growing impervious surface areas, have led to higher volumes of surface runoff, overwhelming existing drainage networks (Nodine et al., 2024). These phenomena pose significant safety hazards, financial losses, and interruptions to urban mobility.

In contemporary engineering practice, the planning and design of underground transportation infrastructure present complex challenges (von der Tann et al., 2020). Stormwater management plays

*Corresponding author: zarko.sretenovic@jcerni.rs (Ž. Sretenović).

a pivotal role in ensuring the operational integrity and safety of these facilities. The risks posed by pluvial and fluvial flooding, as well as by sewer surcharges, require integrated approaches to hazard assessment and mitigation.

Flooding is among the most frequent natural hazards affecting urban environments. It impairs the resilience of city systems, prolongs recovery efforts, and often results in substantial technical and economic consequences (Batica and Gourbesville, 2020). Urban underground networks are particularly vulnerable due to their low-lying locations, limited natural drainage, and often aging infrastructure. Pluvial flooding, which occurs when intense rainfall overwhelms drainage capacity, is especially problematic in urbanized areas where infiltration is minimal and overland flow rapidly accumulates (Yosua et al., 2023).

Globally, over 70% of the population is projected to reside in urban areas by 2050 ("Overview," n.d.), significantly increasing disaster risk due to high population density and asset concentration. It is worth considering that interventions outside the tunnel portals can influence the vulnerability of the urban environment to hydrometeorological hazards (Lyu et al., 2018).

This study focuses on assessing the flood resilience of a planned twin-bore traffic tunnel in Belgrade, Serbia, using advanced two-dimensional (2D) hydrodynamic modeling techniques. The objective is to simulate flood scenarios based on various return periods and to evaluate terrain modifications and infrastructure enhancements that can mitigate flood risks. The research contributes to a growing body of work emphasizing proactive and adaptive strategies for urban flood risk management in the context of climate variability.

2. Case Study

Belgrade, the capital of Serbia, is situated at the confluence of the Sava and Danube rivers, a strategic location that has shaped its history and urban development. As part of a broader traffic and urban transformation strategy, a twin-bore urban traffic tunnel has been designed to connect the Sava and Danube slopes in central Belgrade. The tunnel alignment establishes a direct underground connection between Karađorđeva Street (on the Sava side) and Bulevar Despota Stefana (on the Danube side), aiming to reduce traffic congestion in the city center and improve environmental conditions.

The tunnel consists of two separate tubes, each carrying two traffic lanes, with cross-passages. The total length of the traffic route, including access ramps and transitional structures, is approximately 2.6 km. According to the planned project concept, the traffic lanes descend from Karađorđeva Street through the Luka Ćelović Park toward the Savska Slope portal. The approach road passes underneath Gavrila Principa Street and continues to descend into the tunnel, reaching its lowest point approximately at the tunnel midpoint, after which it ascends toward the Danube Slope portal. The portal is connected to Despot Stefan Boulevard via a dedicated ascending ramp, bringing the alignment back to street level. This longitudinal profile was determined by the presence of existing underground sewer collectors and the planned metro corridor, both of which imposed stringent spatial and engineering constraints. As a result, the adopted tunnel gradient could not be avoided and represents the only feasible engineering solution within the urban context.

The tunnel portals are located in low-lying urban areas along the Sava and Danube rivers. These regions, including the Savska padina (Sava slope) and Dunavska padina (Danube slope), have a history of flooding because of their closeness to the rivers and limited natural drainage. Moreover, the central Belgrade sewer system functions as a combined network, carrying both stormwater and sewage through the same pipelines. During heavy rainfall events exceeding the 2-year return period, the system becomes overwhelmed, causing water to overflow and spill onto the streets. This excess water naturally moves toward lower areas, significantly raising the flood risk at the tunnel portal zones.

The planned tunnel connection from Karađorđeva Street to the Danube slope is susceptible to flooding during intense rainfall events or other extreme hydrological conditions. This vulnerability is further amplified by the effects of extreme weather conditions, which are contributing to more frequent and

intense precipitation over shorter durations. As a critical component, the tunnel must be comprehensively protected against external floodwaters that could interrupt traffic, compromise structural integrity, and cause significant economic, operational, and safety-related consequences.

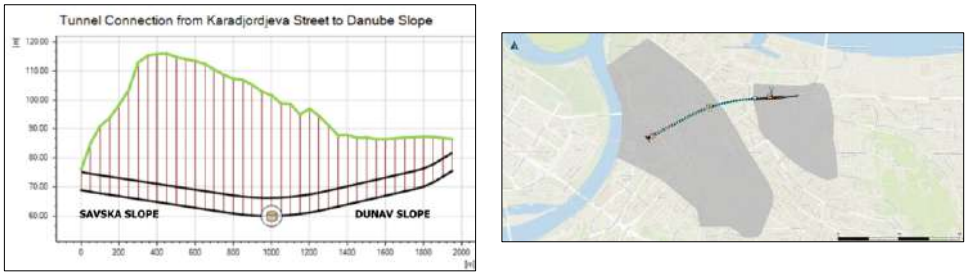

(a) **(b)**

Fig. 1. (a) Longitudinal profile of the traffic Tunnel Connection from Karađorđeva Street to Danube Slope; (b) Location of the planned tunnel alignment between the Sava and Danube slopes with delineated catchment areas contributing to each tunnel portal.

3. Methodology

Accurate topographic data are essential for reliable urban flood modelling, enabling precise simulation of flow distribution, directions, and surface velocities. In this study, a LiDAR-derived point cloud was processed to produce a bare-earth Digital Elevation Model (DEM) at 1×1 meter resolution, eliminating vegetation, buildings, and anomalies. This high-resolution DEM accurately depicted local depressions, infrastructure features (e.g., curbs, ramps), and micro-catchment flow paths near tunnel portals. The DEM was iteratively updated as the tunnel design and terrain evolved, ensuring consistency throughout simulations. Results indicated that minor elevation changes (30 – 50 cm) significantly influence runoff behavior, emphasizing the importance of terrain modifications for flood mitigation.

The study employed the Direct Rainfall Methodology (DRM), which applies precipitation directly to the 2D model grid to simulate overland flow using shallow water equations. This approach treats each cell as a micro-catchment, dynamically generating runoff based on parameters such as cell area, rainfall intensity and duration, Manning's roughness, slope, and infiltration losses. Using synthetic hyetographs based on the Chicago Design Storm (CDS) and Intensity-Duration-Frequency (IDF) curves tailored to Belgrade, simulations for return periods of T = 10, 100, and 500 years were performed using the approach Keifer and Chu (1957). Net rainfall, accounting for drainage system losses, was applied to capture realistic runoff from the terrain, enabling detailed analysis of flood risks and terrain-based interventions.

An integrated modeling framework was developed to evaluate the flood resilience of the tunnel system by combining multiple hydraulic components: two-dimensional (2D), one-dimensional/two-dimensional (1D/2D), and one-dimensional (1D) simulations. The 2D models represented the Sava and Danube slope catchments, which naturally drain toward the tunnel's descending ramps. These models simulated overland flow across a bare-earth DEM, enabling detailed analysis of terrain-runoff interactions in the presence of planned infrastructure. The Sava slope model covered approximately 411 hectares with 4.4 million grid cells, requiring 38 hours per simulation, while the Danube slope model spanned 120 hectares with 1.6 million cells and typically took 6 hours to run. Cross-sections placed at the bottom and top of the tunnel ramps were used to extract hydrographs (flow rates and volumes), which were then applied as inflow boundary conditions for the 1D/2D simulations. The 1D/2D model combined the tunnel drainage pipe network with overland surface flow, allowing assessment of water levels, velocities, flood extents, and pump discharge needs during extreme rainfall events. The 1D model mainly generated longitudinal water surface profiles along the tunnel axis for

various return periods. In this configuration, the tunnel was modeled as a closed conduit with cross-sectional geometry and dimensions matching the actual tunnel design.

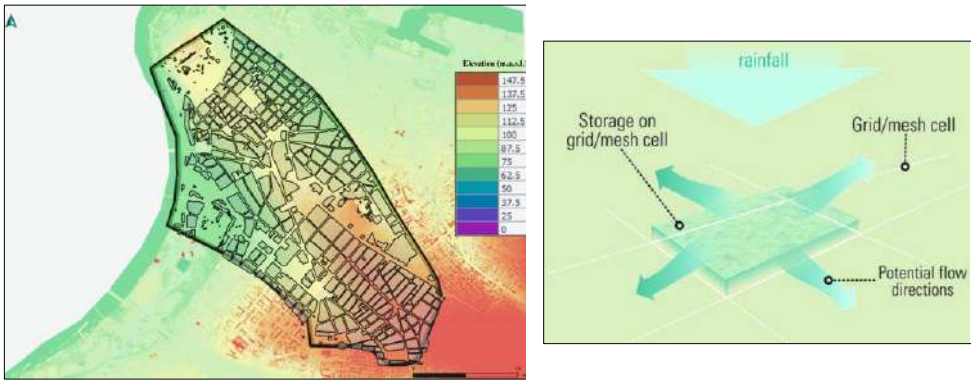

(**a**) (**b**)

Fig. 2. (a) Digital elevation model (DEM) of the Sava slope catchment area with defined 2D computational domain (b) Conceptualisation of Direct Rainfall (ARR, Project 15, Figure 11-1).

Iterative simulations were used to test and optimize grading strategies near tunnel portals. These adjustments included localized elevation increases and protective grading patterns aimed at diverting overland flow. The simulations confirmed that small topographical interventions could substantially influence flood exposure and dewatering times, supporting evidence-based infrastructure design.

3.1. Key Parameters Evaluated

The hydraulic model facilitated a comprehensive assessment of critical parameters influencing flood risk within and around the tunnel area, with particular focus on the sensitivity of runoff dynamics to small elevation changes near the portals. Emphasis was placed on the sensitivity of overland flow to small-scale intervention changes near the tunnel portal. The results demonstrated that even minor topographic modifications, such as elevation increases of 30 to 50 cm, had a measurable impact on flow pathways and flood extents.

The broader context of urban flood risk was considered within the tripartite framework of hazard, exposure, and vulnerability (Zhang et al., 2024). Hazard refers to the frequency and intensity of rainfall events; exposure denotes the spatial distribution of assets at risk, including tunnel portals and electrical systems; vulnerability reflects the capacity of systems to resist and recover from flood impacts.

Effective flood mitigation in dense urban environments requires both horizontal and vertical planning. Horizontally, interventions such as terrain regrading, drainage enhancement, and protective barriers reduce flood hazards across the spatial extent. Vertically, coordination across governance levels is crucial for integrating institutional responsibilities for climate adaptation, land use management, and infrastructure resilience (Yu et al., 2015; Qiu, 2017).

Within the study, it is revealed that a complex interplay of physical infrastructure, spatial configuration, and hydrometeorological variability influences localized flood risk. Thus, integrated strategies are essential for improving the robustness and adaptability of underground traffic systems facing growing climatic uncertainties.

3.2. Flood Risk in the Context of Underground Structures

Underground systems are inherently vulnerable to flooding due to their subterranean location and limited capacity for passive drainage (He et al., 2024). During high-intensity rainfall or elevated water table events, such systems face substantial risks, including operational disruption, structural damage, and compromised passenger safety. Vulnerability extends beyond the physical integrity of tunnels to encompass drainage system performance, passenger safety, emergency access, and response capabilities.

A comprehensive flood risk assessment requires an evaluation of hydrological patterns, historical flood data, and existing drainage network capacity. Sensitivity factors influence system resilience, such as construction material conditions, the effectiveness of existing drainage solutions, and the ability to deploy rapid response measures.

Conducting comprehensive flood risk analyses enables targeted design modifications, infrastructural improvements, and community engagement to strengthen system robustness. Such proactive measures are critical for safeguarding urban mobility and supporting sustainable urban development amid increasing climate variability. Ultimately, enhancing flood resilience involves quantifying risks and implementing mitigation strategies, understanding that resilience is defined as the capacity of an urban system to adapt and maintain functionality when exposed to hazards (UN/ISDR, 2004).

Resilience in this context refers to the capacity of the tunnel system and its associated infrastructure to maintain or rapidly restore function following a disruptive flood event. This necessitates quantifying potential hazards and systematically reducing risk through both structural interventions and institutional adaptation strategies. Ultimately, an effective flood risk management approach for underground transportation systems combines engineered defenses with adaptive operational planning, ensuring long-term safety and service continuity among evolving climate threats.

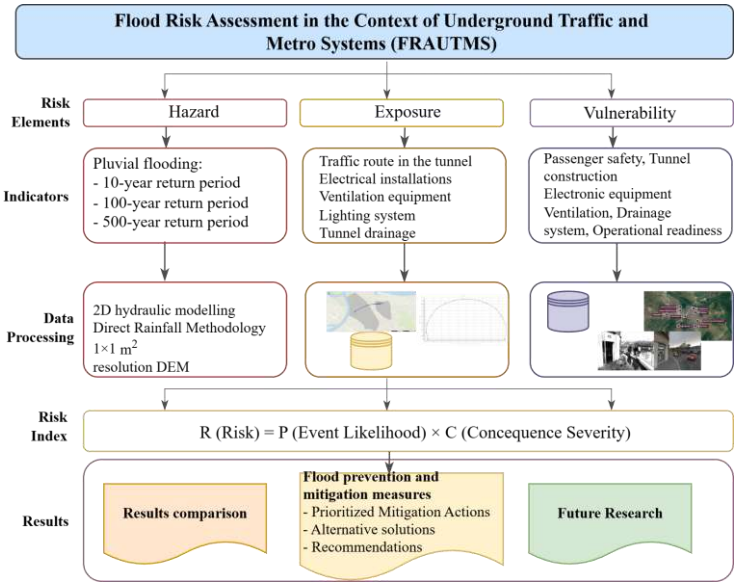

Fig. 3. Flood Risk Assessment of Underground Traffic and Metro Systems Scheme.

The flowchart presents a structured framework for flood risk assessment in underground traffic and metro systems. It begins with the evaluation of hazards, exposure, and vulnerability. These inputs feed into the development of a flood risk model, leveraging tools such as hydraulic simulations and historical data analysis. The model's findings inform flood prevention and mitigation strategies, including both

prioritized actions and alternative solutions. The results are compared to baseline scenarios to assess the effectiveness of proposed measures. This process informs future research directions, ensuring continuous improvement and adaptation of strategies. The integrated approach aims to enhance resilience and safeguard urban infrastructure against flood risks.

3.3. Quantitative Risk Assessment

Quantifying flood risk to underground traffic and subway systems involves a structured evaluation of hazard, exposure, and vulnerability components (Forero-Ortiz, et al., 2020). Hazard assessment comprehends estimating the probability and severity of flood events such as pluvial or river flooding using historical data, hydrological models, and climate projections. Exposure assessment then characterizes the spatial extent and value of assets at risk, including tunnel entrances, electrical and signaling infrastructure, and surrounding landforms that influence flood dynamics. Vulnerability quantifies the system's susceptibility, considering factors like structural integrity, drainage capacity, and redundancy. To facilitate the prioritization of mitigation efforts, a probabilistic risk metric is applied. This approach multiplies the annual probability of occurrence (P) by a severity score (C), producing a composite risk index (R = P × C). Severity scores are assigned based on predefined impact criteria, ranging from negligible service delays to catastrophic infrastructure failure.

$$R = P(Event\ likelihood)xC(consequence\ severity) \quad (1)$$

The range is provided as:

Table 1. Standardized severity scale used in this study.

Severity Score	Description	Example Impacts
1	Negligible	Minor traffic delays, slight wear of equipment, and minimal operational impact
2	Very Low	Slight inconvenience, minor repair needs, limited-service disruption
3	Low	Localized flooding, minor infrastructure impact, manageable repairs
4	Moderate	Noticeable flooding affecting operation, minor structural damage, manageable recovery
5	Significant	Disruption to operations in affected areas, moderate infrastructure damage
6	High	Major service interruptions, structural damage requiring extensive repairs
7	Very High	Large-scale flooding, significant safety hazards, and substantial economic impact
8	Severe	Widespread infrastructure failure, serious safety risks, and long-term disruption
9	Critical	Catastrophic damage, loss of service, and significant safety hazards
10	Catastrophic	Extreme impact, including loss of life, total infrastructure failure, extensive economic and social consequences

This framework empowers an evidence-based understanding of the risk landscape associated with underground tunnel systems. By ranking scenarios from high to low risk based on modelled probabilities and potential impacts, decision-makers can allocate resources more effectively, prioritizing interventions that yield the greatest resilience gains. The use of quantitative risk indices supports transparent communication of risks and enhances coordination across engineering, planning, and emergency response domains.

4. Flood Risk Profile for the Traffic Tunnel

The entrance portals of the Tunnel Connection from Karađorđeva Street to the Danube Slope are located at the lowest points along the alignment. Moreover, the natural slopes of surrounding urban areas, such as Kalemegdan, Kosančićev Venac, Terazije, and Nemanjina Street on the Sava Slope, and Bogoslovija

and Cvijićeva Street on the Danube Slope, concentrate surface runoff toward the tunnel entrances, significantly increasing flood exposure.

Savska Slope portal of Tunnel Connection from Karađorđeva Street to Danube Slope is strategically located adjacent to the right bank of the Sava River, with an elevation of approximately 75-78 meters a.s.l. This positioning makes it only 2 to 4 m above average river flow, increasing its vulnerability to flood. The flood risk in the Sava zone near Belgrade is projected to increase, according to analysis by the World Bank (WB, 2015, 2025). This increase is driven by the impacts of extreme weather events, which is expected to lead to more severe and frequent storm events, as well as increasing property values in the Belgrade Waterfront area, which heightens the potential vulnerability.

To address these vulnerabilities, targeted mitigation measures are essential. These include improving drainage systems around the portal to effectively intercept and divert surface runoff, building barriers or flood gates at the tunnel entrance to block water ingress during floods, and installing early warning systems for river flooding or severe storm. Enhancing the tunnel's waterproofing and sealing infrastructure, properly sizing and conducting routine maintenance of drainage and pumping systems, and integrating flood resilience features into the new tunnel are essential strategies to mitigate flood hazards and ensure the continued operational safety and integrity of the infrastructure.

Additionally, ongoing urban development in Belgrade has led to a significant increase in surface runoff. The runoff coefficient, which was historically below 0.4, has now risen to over 0.8 in some areas due to extensive paving and construction. This doubling of the runoff coefficient results in a substantial increase in peak flow during storm events, further exacerbating flood risks and stressing drainage systems in the area.

Hazard identification in this context includes both natural and infrastructural risks. Pluvial flooding, driven by high-intensity short-duration rainfall, represents the most probable hazard. Riverine flooding, while less frequent, poses significant risks due to backwater flooding. Infrastructure-related hazards include sewer surcharge during peak flows, pump station failure due to power outages or mechanical failures, drainage blockages from debris or ice, and elevated river water levels. The hazards include pluvial flooding caused by localized, high-intensity downpours with rates of at least 50 mm/h, occurring with return periods from 10 to 100 years. River flooding is a significant threat due to elevated water levels in the Sava River, which has a flow rate of 6,500 m^3/s as documented in Q100. There is also a risk of combined sewer surcharge, where stormwater mixed with fecal waste backflows during heavy rains, and drainage system failures caused by pump breakdowns or clogged drains that hinder flood management.

The tunnel portals are located at the lowest points of the old city center, in areas highly exposed to concentrated surface runoff from surrounding slopes. Their close proximity to both the Sava and Danube rivers further increases their vulnerability to flooding. The infrastructure is highly valuable, supporting critical transportation functions such as electrical and signaling equipment located in the roadway zone. Vulnerability stems from the tunnel entrance's design, which lacks a natural overflow or protective barrier, making it prone to flooding.

The system depends heavily on the continuous operation of pumps and functioning backflow valves, creating reliance on mechanical components that may fail. Additionally, the sewer infrastructure is relatively old, dating back to the early 20th century, with limited capacity to manage increased loads. The surrounding area also demonstrates low capacity for sustainable drainage solutions, leading to insufficient rainfall retention and management, which heightens overall flood risk.

5. Results on Modelling Outcomes and Risk Assessment

Comprehensive 2D hydrodynamic simulations were conducted to evaluate the flood vulnerability of the planned tunnel between Karađorđeva Street and the Danube slope. These simulations tested chosen return periods and informed the development of integrated flood mitigation strategies.

5.1. Terrain Elevation and Grading near Tunnel Portals

Iterative simulations optimized terrain grading and elevation around the tunnel portals to minimize surface runoff and stormwater inflow. Results revealed high sensitivity of overland flow to small elevation changes, enabling precise design adjustments. For the Savska slope, the terrain was raised to a maximum of 75.3 m a.s.l., constrained by the access roundabout. Despite this, some upstream runoff during a 10-year rainfall event still reached the tunnel, producing manageable inflows, while a 100-year storm caused significant inundation. Protective walls about 1 m high were constructed along adjacent streets to mitigate lateral inflow. Conversely, the Danube slope was elevated to 87.5 m a.s.l., effectively isolating the portal from the catchment and redirecting surface runoff to natural detention zones. An independent drainage system, including high-capacity inlets, was installed, complemented by lateral barriers along Despot Stefan Boulevard to prevent uncontrolled inflows during extreme events.

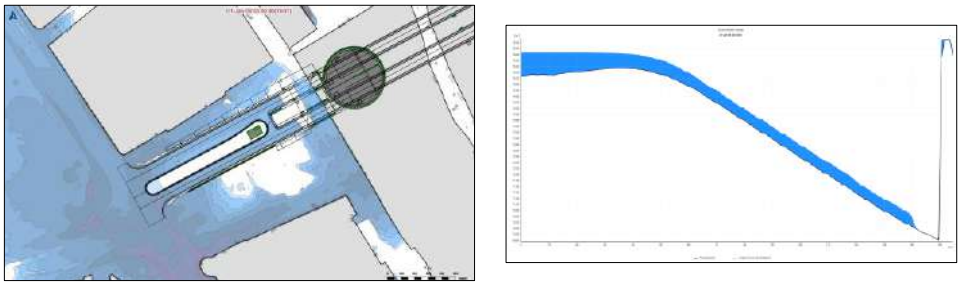

(a) **(b)**

Fig. 4. (a) The flood simulation result near the Sava tunnel portal presents the modelled flood extent and water depth in the area surrounding the tunnel entrance on the Sava slope during a 100-year rainfall event. Blue shading indicates areas with surface water accumulation, highlighting potential inflow zones toward the tunnel. (b) The profile of the approach road and descending ramp toward the tunnel portal on the Sava slope under a 100-year rainfall event. The blue water surface profile indicates that the runoff overtops the elevated terrain in front of the tunnel and enters the tunnel infrastructure. The maximum recorded water depth on the ramp reaches approximately 0.4 m.

5.2. Drainage System and Pumping Stations Design

Drainage and pump capacities were dimensioned based on runoff hydrographs for a 10-year rainfall event. The Savska portal pump station was designed for approximately 100 l/s, and the Danube portal for 150 l/s, each with standby pumps for redundancy. Shaft pumps at each tunnel end, capable of over 250 l/s, serve to evacuate internal runoff under normal and extreme conditions, ensuring full dewatering within a reasonable timeframe and enhancing resilience. The adopted drainage pump capacities are more than double compared to the sizing of fire event pumps in tunnels as required by NFPA 502.

5.3. Risk Matrix Evaluation

A quantitative risk matrix was used to evaluate flood scenarios by combining event probability (P) and consequence severity (C), yielding a risk index ($R = P \times C$). Key modelled scenarios are summarized in Table 2.

This analysis reinforces the importance of a layered mitigation strategy: topographic barriers, independent drainage systems, robust pumping infrastructure, and operational redundancies. It also illustrates the utility of risk indexing for strategic investment and emergency planning. Proposed mitigation measures for the considered demonstration site are listed in the table below, focusing on both prioritized and alternative solutions.

Table 2. Results of risk levels based on the results of hydraulic 2D modelling for the tunnel infrastructure.

Risk	Event Probability (P)	Consequences (C)	Risk Index (R = P × C)	Risk Level
Pluvial Flood (T = 1/10 yr)	0.1	5 (traffic disruption and damages)	0.50	High Risk
Pluvial Flood (T = 1/100 yr)	0.01	9 (full evacuation, huge damage)	0.09	Medium Risk
River Flood (Q100 = 6500 m³/s)	0.01	8 (water entering the tunnel, long reparation period)	0.08	Medium Risk
Sewer Surcharge (in the tunnel)	0.05	4 (local flooding, pollution)	0.20	Medium Risk
Pump Station Failure During Rain	0.03	7 (fast charging tunnel with water)	0.21	Medium to High Risk
Drain Clogging	0.20	3 (local flood waves)	0.60	High Risk
Groundwater Leakage	0.01	5 (construction degradation)	0.05	Low to Medium Risk

Table 3. Proposed key mitigation measures for the flooding of the tunnel infrastructure

Key Mitigation Measures	Description
Prioritized Mitigation Actions	
Portal elevation and grading	Elevate terrain and install protective side walls to redirect surface runoff and minimize direct inflow
Redundant pumping systems (N+1 configuration)	Pump stations are equipped with backup pumps and a diesel/UPS power supply for uninterrupted operation.
High-capacity linear drainage channels	Deployment of clog-resistant drains across the portal width, connected to an independent collector system.
Elevation of electrical equipment	Positioning critical electrical and signaling infrastructure above the design flood level to prevent damage
Alternative solutions	
Flood gates and portable barriers	Implementation of manually deployable or remotely monitored gates for sealing tunnel portals during extreme events
Increased monitoring capacity	Use integrated hydrometeorological sensors and systems to automate responses
Integrated urban catchment management	Improve upstream stormwater control with Low Impact Development (LID) techniques such as detention zones and surface infiltration techniques
Rain forecasting	Coordination with the national hydrometeorological service (RHMZ) to manage runoff from steep urban slopes (e.g., Kosanciceva) ahead of major storms.

6. Recommendation

Based on the findings of hydraulic modeling and technical evaluations, a set of recommendations is proposed to enhance flood resilience for the tunnel infrastructure:

- Elevation of terrain at tunnel portals to divert runoff and minimize inflow from surrounding catchments, considering both functional and spatial constraints.
- Implementation of protective side walls at vulnerable locations to prevent lateral inflows during extreme events.
- Dedicated point drainage systems are designed independently from the main urban network, enabling rapid collection and redirection of runoff.

- Redundantly configured pumping stations with sufficient capacity to handle both basic and emergency scenarios, including backup pumps to ensure reliability.

In the cases where the risk of tunnel flooding cannot be eliminated, advanced traffic signaling systems are essential for ensuring user safety. These systems should:

- Deliver clear and timely warnings to drivers through signage installed along access roads and directly in front of tunnel portals.
- Enable traffic rerouting or tunnel closure in response to real-time flood risks.
- Be integrated with automated water level detection systems and the extensive urban emergency response network.

To preserve the functionality of pumping stations during flooding, it is essential to ensure an uninterrupted power supply. This requires:

- Elevated positioning of transformer stations and backup diesel generators above the design flood level (e.g., above 64 m a.s.l. for the 100-year rainfall scenario).
- Physical protection of electrical components from water ingress through sealed enclosures and raised platforms.

This measure ensures the continuous operation of drainage systems even under catastrophic conditions, minimizing tunnel downtime and structural damage.

To ensure readiness for the most critical scenarios, the drainage system must be sized to accommodate the worst governing event, considering both flooding and fire-related water ingress. This requires designing capacity based on peak runoff from a 100-year rainfall event, with additional margins to account for extreme events. The system should also be capable of handling the volume of water used during fire suppression activities, such as firefighting water, which can significantly increase the water load within the tunnel.

7. Effectiveness of the proposed flood risk management approach

To assess the effectiveness of proposed flood risk management measures for Belgrade's underground traffic system, a comprehensive, multi-criteria approach is recommended. Initially, advanced 2D hydrodynamic modelling, such as the Direct Rainfall Method (DRM), should be employed to simulate diverse rainfall scenarios and evaluate the tunnel's response to mitigation strategies. This includes analysing flood levels, flow velocities, and inundation extents before and after measures like portal elevation and drainage improvements. Subsequently, a probabilistic risk assessment should be conducted, involving hazard characterization, exposure evaluation (including populations and infrastructure), and vulnerability analysis. The resulting risk index helps prioritize interventions by quantifying their potential to reduce flood likelihood and impact severity.

Sensitivity testing and gap analysis through iterative simulations are crucial for refining designs, identifying weaknesses, and determining the most effective measures, such as pump capacity and barrier height under various flood conditions. Real-time hydro-meteorological monitoring should be deployed during rainfall events to enable dynamic feedback and model validation, enhancing response reliability. Stakeholder engagement, including authorities, emergency services, and local communities, is vital to ensure measures are practically effective, acceptable, and capable of operational optimization. Finally, post-event reviews should be conducted after major storms to evaluate performance, adapt strategies, and incorporate emerging insights and technologies to sustain or improve flood resilience over time.

8. Conclusion

The Karađorđeva Street tunnel is situated in a flood-prone area featuring three primary vulnerabilities: proximity to the Sava River, concentrated surface runoff from the steep slopes of Stari Grad, and an

aging or limited-capacity combined sewer system. While pluvial flooding presents the most statistically probable scenario, river flooding and hydraulic backpressure pose the highest potential failure costs. Therefore, a holistic mitigation strategy integrating structural measures such as portal elevation, enhanced pumping systems, and retention structures with operational strategies like early warning systems and routine maintenance is essential to reduce risk to an acceptable level corresponding to a 1% annual probability (T = 1/100).

The hydrodynamic modelling and risk analysis confirmed that mitigation must address a combination of hydrometeorological hazards and infrastructural vulnerabilities intensified by climate change and urbanization. The findings support a resilience-based approach, emphasizing the importance of redundancy, real-time response systems, and climate-adaptive planning.

Proactive flood management also relies on advanced early detection, real-time monitoring, and automated response systems to ensure continuous safety and operation during extreme events. Integrating these technical solutions with strong institutional coordination, contingency planning, and adaptive management practices strengthens system resilience against current and future hydrometeorological hazards. Lessons from the Karađorđeva Danube tunnel case study advocate for best practices such as extensive 2D hydrodynamic modelling with direct rainfall input to evaluate terrain sensitivity and runoff pathways; designing with redundancy to handle failure scenarios; and adopting cross-sectoral planning that aligns tunnel flood protection with broader urban drainage, transportation safety, and climate resilience strategies.

Acknowledgements

The support and insights provided during the development of this research are built upon the findings of the study “Project of the Tunnel Connection from Karađorđeva Street to the Danube Slope, Including Access Roads, Park Areas, and Infrastructure,” conducted by Jaroslav Černi Water Institute LLC, Belgrade.

References

Batica, J., and Gourbesville, P., 2020. From Catstrophe to Resilience. In Advances in Hydroinformatics: SimHydro 2019-Models for Extreme Situations and Crisis Management, pp. 121-133. Springer Singapore.

Forero-Ortiz, E., Martínez-Gomariz, E., Cañas Porcuna, M., Locatelli, L., 2020. Flood risk assessment in an underground railway system under the impact of climate change—A case study of the Barcelona Metro. Sustainability, 12(13), 5291. https://doi.org/10.3390/su12135291

He, R., Tiong, R.L.K., Yuan, Y., Zhang, L., 2024. Enhancing resilience of urban underground space under floods: Current status and future directions. *Tunnelling and Underground Space Technology,* 147: 105674. https://doi.org/10.1016/j.tust.2024.105674

IPCC. (2021). Climate Change, The Physical Science Basis. Contribution of Working Group I to the Sixth Assessment Report of the Intergovernmental Panel on Climate Change (Masson-Delmotte, V. et al., Eds.). Cambridge University Press. https://www.ipcc.ch/report/ar6/wg1/

Keifer, C.J., Chu, H.H., 1957. Synthetic storm pattern for drainage design, *Journal of the Hydraulics Division*, 83(4), 1–25.

Lyu, H-M, Shen J.S., Arulrajah, A. 2018. Assessment of Geohazards and Preventative Countermeasures Using AHP Incorporated with GIS in Lanzhou, China. *Sustainability.* 10(2):304.

Nodine, T.G., Conley, G., Riihimäki, C.A., Holland, C., Beck, N.G., 2024. Modeling the impact of future rainfall changes on the effectiveness of urban stormwater control measures. *Scientific Reports*, 14(1), 4082. https://doi.org/10.1038/s41598-024-53611-1

Qiu, L., 2017. Vertical Urban Planning and Flood Control and Drainage Using Gis Technology. Open House International, Vol. 42 No. 3, pp. 10-14. https://doi.org/10.1108/OHI-03-2017-B0003

UN/ISDR. 2004. Living with Risk: A Global Review of Disaster Reduction Initiatives. United Nations International Strategy for Disaster Reduction Secretariat. Geneva, Switzerland.

Von der Tann, L., Sterling, R., Zhou, Y., Metje, N., 2020. Systems approaches to urban underground space planning and management – A review. *Underground Space*, 5(2), 144–166. https://doi.org/10.1016/j.undsp.2019.03.003

Wang, Y., Zhang, Q., Lin, K., Liu, Z., Liang, Y.-s., Liu, Y., Li, C., 2024. A novel framework for urban flood risk assessment: Multiple perspectives and causal analysis. *Water Research*, 256, 121591. https://doi.org/10.1016/j.watres.2024.121591

WB. World Bank Group. 2015. Water and Climate Adaptation Plan for the Sava River Basin: Annex 2. Guidance Note on Adaptation to Climate Change for Flooding. World Bank. Available via Open Knowledge Repository.

WB. World Bank. (n.d.). Urban development — overview. Available online: https://www.worldbank.org/en/topic/urbandevelopment/overview (accessed on 05 May 2025).

Yosua, H., Kusuma, M.S.B., Nugroho, J., 2023. Study of flood mitigation system for improving the resilience of pluvial flood control of South Jakarta (Case study: Ciledug Raya, Cipulir). *IOP Conference Series: Earth and Environmental Science*, 1169(1), 012036. https://doi.org/10.1088/1755-1315/1169/1/012036

Yu, K., Li, D., Yuan, H., Fu, W., Qiao, Q., Wang, S., 2015. "Sponge City": Theory and practice. City Planning Review, 39(6), 26-36.